

WRDC-TR-89-2097



AD-A216 444

**PRODUCTION OF HIGH DENSITY AVIATION FUELS
VIA NOVEL ZEOLITE CATALYST ROUTES**

*Dr Francis V. Hanson
Associate Professor of Fuels Engineering
Department of Fuels Engineering
University of Utah
Salt Lake City, Utah 84112-1183*

23 OCTOBER 1989

Final Report for Period December 1985 to May 1987

Approved for public release; distribution unlimited.

**AERO PROPULSION AND POWER LABORATORY
WRIGHT RESEARCH AND DEVELOPMENT CENTER
AIR FORCE SYSTEMS COMMAND
WRIGHT-PATTERSON AIR FORCE BASE, OHIO 45483-6563**

**DTIC
ELECTE
DEC 12 1989
S B D**

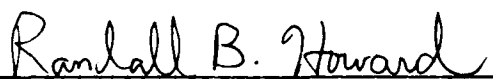
89 12 11 0 27

NOTICE

When Government drawings, specifications, or other data are used for any purpose other than in connection with a definitely Government-related procurement, the United States Government incurs no responsibility or any obligation whatsoever. The fact that the Government may have formulated or in any way supplied the said drawings, specifications, or other data, is not to be regarded by implication, or otherwise in any manner construed, as licensing the holder, or any other person or corporation; or as conveying any rights or permission to manufacture, use, or sell any patented invention that may in any way be related thereto.

This report is releasable to the National Technical Information Service (NTIS). At NTIS, it will be available to the general public, including foreign nations.

This technical report has been reviewed and is approved for publication.

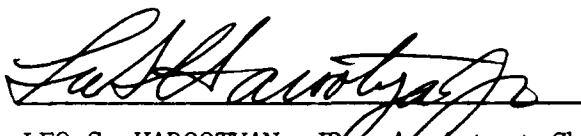


RANDALL B. HOWARD, 1Lt, USAF
Fuels Branch
Fuels and Lubrication Division
Aero Propulsion and Power Laboratory



CHARLES L. DELANEY, Chief
Fuels Branch
Fuels and Lubrication Division
Aero Propulsion and Power Laboratory

FOR THE COMMANDER



LEO S. HAROOTYAN, JR., Assistant Chief
Fuels and Lubrication Division
Aero Propulsion and Power Laboratory

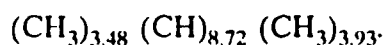
If your address has changed, if you wish to be removed from our mailing list, or if the addressee is no longer employed by your organization, please notify WRDC/POSF, WPAFB OH 45433-6563 to help us maintain a current mailing list.

Copies of this report should not be returned unless return is required by security considerations, contractual obligations, or notice on a specific document.

REPORT DOCUMENTATION PAGE				Form Approved OMB No. 0704-0188		
1a. REPORT SECURITY CLASSIFICATION UNCLASSIFIED			1b. RESTRICTIVE MARKINGS NONE			
2a. SECURITY CLASSIFICATION AUTHORITY N/A			3. DISTRIBUTION / AVAILABILITY OF REPORT Approved for public release; distribution is unlimited.			
2b. DECLASSIFICATION / DOWNGRADING SCHEDULE N/A						
4. PERFORMING ORGANIZATION REPORT NUMBER(S) N/A			5. MONITORING ORGANIZATION REPORT NUMBER(S) WRDC-TR-89-2097			
6a. NAME OF PERFORMING ORGANIZATION The University of Utah		6b. OFFICE SYMBOL (if applicable)	7a. NAME OF MONITORING ORGANIZATION Aero Propulsion and Power Laboratory(WRDC/POSF) Wright Research and Development Center			
6c. ADDRESS (City, State, and ZIP Code) Department of Fuels Engineering Salt Lake City, Utah 84112-1183			7b. ADDRESS (City, State, and ZIP Code) Wright-Patterson AFB, OH 45433-6563			
8a. NAME OF FUNDING / SPONSORING ORGANIZATION		8b. OFFICE SYMBOL (if applicable)	9. PROCUREMENT INSTRUMENT IDENTIFICATION NUMBER F33615-85-C-2567			
8c. ADDRESS (City, State, and ZIP Code)			10. SOURCE OF FUNDING NUMBERS			
			PROGRAM ELEMENT NO. 62203F	PROJECT NO. 3048	TASK NO. 05	WORK UNIT ACCESSION NO. 55
11. TITLE (Include Security Classification) Production of High Density Fuels via Novel Zeolite Catalyst Routes						
12. PERSONAL AUTHOR(S) Dr Francis V. Hanson						
13a. TYPE OF REPORT Final		13b. TIME COVERED FROM Dec 85 to May 87		14. DATE OF REPORT (Year, Month, Day) 1989 October 23		
15. PAGE COUNT 484						
16. SUPPLEMENTARY NOTATION NONE						
17. COSATI CODES			18. SUBJECT TERMS (Continue on reverse if necessary and identify by block number) High Density Fuels, Catalysis, Zeolite, Aviation Fuels			
FIELD	GROUP	SUB-GROUP				
21	04					
19. ABSTRACT (Continue on reverse if necessary and identify by block number) The production of high density aviation fuels from reliable, domestic fossil fuel sources is of considerable importance to the United States Air Force. The production of high density aviation fuels can be achieved by a number of alternative process sequences, for example, shape selective cracking of normal paraffins from an appropriate boiling range fraction of a naphthenic crude; saturation of an aromatic FCC cycle stock of the appropriate boiling range; saturation of an appropriate boiling range fraction from a hydrocracker recycle stream when the feed to the hydrotreater is aromatic in nature; synthesis of the appropriate boiling range aromatic species from oxygenates over crystalline aluminosilicates followed by hydrogenation of the aromatic species; and direct synthesis of the aromatic hydrocarbons from hydrogen and carbon monoxide over crystalline aluminosilicate-supported metal catalysis followed by hydrogenation of the aromatic species. This report summarizes a research program aimed at developing catalyst and processing concepts for the production of high density aviation turbine fuels via novel zeolite catalyst routes. (7U)						
20. DISTRIBUTION / AVAILABILITY OF ABSTRACT <input type="checkbox"/> UNCLASSIFIED/UNLIMITED <input checked="" type="checkbox"/> SAME AS RPT <input type="checkbox"/> DTIC USERS				21. ABSTRACT SECURITY CLASSIFICATION UNCLASSIFIED		
22a. NAME OF RESPONSIBLE INDIVIDUAL RANDALL B. HOWARD, 1Lt, USAF				22b. TELEPHONE (Include Area Code) (513) 255-7423		
				22c. OFFICE SYMBOL WRDC/POSF		

SYNOPSIS

The production of high density aviation turbine fuels from reliable, domestic fossil fuel resources is of considerable importance to the United States Air Force. The initial benchmark high density aviation turbine fuel which led to establishment of the various United States Air Force research programs was the high density Soviet aviation turbine fuel acquired during the mid 1970s. Detailed analysis of this fuel indicated an average molecular structure consisting of a two-ring naphthene containing four substituent methyl groups. The average empirical formula of this high density fuel was determined to be:



The production of turbine fuels of this average structure can be achieved by a number of alternative process sequences, for example, shape selective cracking of normal paraffins from an appropriate boiling range fraction of a naphthenic crude; saturation of an aromatic FCC cycle stock of the appropriate boiling range; saturation of an appropriate boiling range fraction from a hydrocracker recycle stream when the feed to the hydrotreater is aromatic in nature; synthesis of the appropriate boiling range aromatic species from oxygenates over crystalline aluminosilicates followed by hydrogenation of the aromatic species; and direct synthesis of the aromatic hydrocarbons from hydrogen and carbon monoxide over crystalline aluminosilicate-supported metal catalysts followed by hydrogenation of the aromatic species.

Accession For	
NTIS GRA&I	<input checked="checked" type="checkbox"/>
DTIC TAB	<input type="checkbox"/>
Unannounced	<input type="checkbox"/>
Justification	
By _____	
Distribution/	
Availability Codes	
Dist	Avail and/or Special
A-1	

A research program (contract number F33615-85-C-2567) aimed at developing catalyst and processing concepts for the production of high density aviation turbine fuels via novel zeolite catalyst routes was initiated in the Department of Fuels Engineering at the University of Utah during November of 1985.

The original, primary objectives of the program were as follows:

1. to design and fabricate an automated laboratory catalyst testing unit capable of continuous operation and of conducting catalyst screening/evaluation studies and process variable/catalyst aging investigations;
2. selective synthesis of methyl-substituted mono- and dicyclic aromatic hydrocarbons in the aviation turbine fuel boiling range;
3. hydrogenation of alkyl-substituted mono- and dicyclic aromatic hydrocarbons and selected aromatic feedstocks to the corresponding mono- and dicyclic naphthenes in the aviation turbine fuel boiling range; and
4. to conduct an exhaustive survey of the technical and patent literature related to the specific research tasks to be performed under this contract.

The aromatics hydrogenation studies were deemphasized at the instruction of the Technical Project Officer since it was determined that those aspects of the Air Force high density aviation turbine fuel research problem could be accomplished under other sponsored research programs, whereas the zeolite work could only be accomplished as part of the University of Utah program.

The accomplishments of the program through the termination of United States Air Force funding included the following:

- The procedures for the reproducible laboratory synthesis of crystalline aluminosilicates of the ZSM class of zeolites were developed and proven.

- ZSM-5 (methyl-substituted monoaromatics hydrocarbon selectivity) was successfully prepared and characterized in the laboratory. Selectivity and activity data for the conversion of alcohol feedstocks were obtained.
- ZSM-48 (low molecular weight olefin selectivity) was successfully prepared and characterized in the laboratory. Selectivity and activity data for the conversion of methanol were obtained.
- A processing scheme involving the utilization of both ZSM-48 and ZSM-5 was devised for the production of methyl-substituted dicyclic aromatic hydrocarbons and preliminary evaluation of the process concept was carried out in the catalyst testing unit.
- The catalyst testing unit was designed, constructed, and used in the evaluation of catalysts and processing schemes.
- A BET surface area apparatus was designed and fabricated. The operating procedures were developed and tested for a variety of high surface area oxide materials and zeolites, including the ZSM class of zeolites.
- A literature survey database and retrieval system were developed and the assembly of pertinent citations was initiated.

Subsequent to the termination of funding by the United States Air Force an attempt was made to complete the studies in part by using other sources of funding; in particular, unrestricted development funds and grants from industrial research laboratories were used to complete the dissertation studies of Dr. H.P. Wang and the thesis studies of Mr. D.C. Longstaff. Unfortunately, it was not possible to complete all aspects of an anticipated three year research program with limited private sector funds available in the second and third years of the program. Hydrodewaxing studies were incorporated into the program and completed after the discontinuance of the United States Air Force Funding.

The project status and the results of the various elements of the original and expanded research program are discussed in detail in the body of the report.

TABLE OF CONTENTS

<u>Title</u>	<u>Page</u>
SECTION I: INTRODUCTION	1
Aviation Turbine Fuels	1
Possible Processing Schemes for the Production of High	
Density Aviation Turbine Fuels	7
Hydrogenation of Aromatic Refining Feed Streams	8
Removal of Normal Paraffins from Naphthenic Refinery Feed Streams	8
Solvent Extraction	8
Shape Selective Catalytic Dewaxing	10
Shape Selective Formation of Aromatic Hydrocarbons, Followed	
by Hydrogenation to the Corresponding Naphthene	13
SECTION II: ANALYSIS OF AVIATION TURBINE FUEL SAMPLES	15
Analysis of the High Density Aviation Turbine Fuel	17
Analysis of Conventional Aviation Turbine Fuels and Pyrolysis Oils	26
Analysis of the Aromatic 2040 Solvent	26
SECTION III: SHAPE SELECTIVE CATALYSIS	41
Introduction	41
Zeolite Catalysts	42
General Concepts Related to Zeolite Synthesis	43
Characteristic Structures of Catalytically Important Zeolites	45
Large Pore Zeolites	45
Small Pore Zeolites	46
Pentasil Zeolites and Molecular Sieves	47
Shape Selective Zeolite Catalysis and Catalysts	49
Preparation of Shape Selective Zeolites	49
Synthesis of ZSM-type Zeolites	49
Synthesis of Zeolite ZSM-5	50
Synthesis of Zeolite ZSM-48	54
Factors Affecting the Synthesis of the ZSM Family of Zeolites	55
Substitutes in the Framework of the ZSM Family of Zeolites	56
Modification of Shape Selective Zeolites for Catalytic Use	56
Ion Exchange	56
Thermal Treatment	57
Chemical Modification	57
Metal Loading	58
Characterization of Zeolites	59
X-ray Diffraction	59
Microanalysis	59
Thermal Desorption	61

TABLE OF CONTENTS (Continues)

	<u>Page</u>
Vibrational Spectroscopy	62
Solid State NMR	64
Kinetic Characterization	65
Intracrystalline Diffusion in Zeolites	66
Shape Selective Zeolite Catalysis	67
Types of Shape Selective Zeolite Catalysts	67
Coking on Shape Selective Zeolite Catalysts	69
Applications of Shape Selective Zeolite Catalysts in Industrially Significant Processes ...	70
Methanol-to-Gasoline Process	70
Methanol-to-Olefins and Distillates	71
Middle Distillate and Lube Oil Dewaxing	72
M-Forming Process	73
Alkylation of Aromatics	73
Benzene Alkylation	73
Toluene Alkylation	74
Toluene Disproportionation	74
Xylene Isomerization	75
Preparation of Zeolites ZSM-5 and ZSM-48	75
Preparation of Zeolite ZSM-5	75
Preparation of Zeolite ZSM-48	78
Characterization of Synthetic Zeolites	83
Elemental Analysis of Synthetic Zeolites	83
X-ray Diffraction	83
Thermal Desorption	84
Infrared Spectroscopy	84
SEM and the Morphology of Zeolites	87
Channel Structure	87
Acidity	87
Surface Area	88
Reactivity of Methanol and Higher Alcohols over Zeolites	88
Chemical Supplies	90
SECTION IV: SELECTIVE SYNTHESIS OF AROMATIC HYDROCARBONS	
OVER ZEOLITE CATALYSTS	93
Laboratory Preparation of ZSM-5 and ZSM-48 Zeolites	93
Synthesis of ZSM-5	93
Synthesis of ZSM-48	99
Chemical Composition	116
Summary	120
Characterization of Synthesized Zeolites	120
Thermal Desorption	120
Infrared Spectroscopy	125

TABLE OF CONTENTS (Continues)

	<u>Page</u>
Catalytic Cracking of n-Hexane	131
Isomerization of Isobutane	134
Surface Area Measurement	136
Summary	142
Reaction of Alcohols over Zeolites	143
Summary	156
Preliminary Methanol Conversion Process Study	158
Methanol Conversion over ZSM-5 and ZSM-48	159
Pressure Effect	164
Temperature Effect	164
Reaction Index	164
Dual-Reactor Study	168
SECTION V: SELECTIVE HYDROGENATION OF AROMATIC	
HYDROCARBONS	173
Supported Metal Catalyst Preparation	173
Catalyst Characterization by Hydrogen Chemisorption	174
Measurement of Sites	174
Constant Volume Adsorption Apparatus	176
Vacuum System and Handling Apparatus	183
Vacuum System	183
Gas Handling and Purification System	184
Operating Procedures	184
Catalyst Loading	184
Catalyst Pretreatment	185
Adsorption Isotherm Procedure	186
Adsorption Isotherm Calculation Procedure	188
Doser Volume Calibration	189
Calculation of the Cell Volume	190
Adsorption Isotherm Calculation	192
Hydrogenation of Toluene	203
Hydrogenation of Naphthalene	203
SECTION VI: SELECTIVE CATALYTIC CRACKING OF NORMAL PARAFFINS	
IN KEROSENE BOILING RANGE FEEDSTOCKS OVER ZSM-5	206
Introduction	206
Experimental Apparatus	207
Description of the Components of the System	207
Gas Feed System	207
Liquid Feed System	209
Reactor	210

TABLE OF CONTENTS (Continues)

	<u>Page</u>
Product Collection System	210
Operating Procedure	210
Catalyst Loading Procedure	211
Mass Balance Procedure	212
Computer Analysis of Results	214
Model Compound Studies	215
Catalyst Preparation	215
Thermal Cracking	216
Hexadecane Cracking at 573 K (300°C)	216
Cracking Reactions as a Function of Residence Time	219
Distillate Fuel Studies	224
Freeze Point Reductions of Kerosene and Diesel Fuels	224
Dewaxing of Kerosene and Diesel to Maximize Density	229
Conclusions	231
SECTION VII: DESIGN AND CONSTRUCTION OF A BET SURFACE	
AREA APPARATUS	233
Introduction	233
Procedure for Surface Area Measurement	234
Experimental Apparatus	235
Adsorption System	236
Vacuum System	241
Gas Storage System	241
Catalyst Pretreatment System	242
Adsorption/Desorption Isotherm Procedure	242
Determination of Sample Cell Dead Volume	242
Determination of the Isotherm	246
Calculation of the Adsorption/Desorption Isotherm	248
Scope of the BET System	250
Results	251
Computer Program	251
Adsorption/Desorption Isotherm for Alumina	252
Adsorption/Desorption Isotherm for ZSM-5	256
Discussion	258
C-Values	258
Isotherm Modeling	264
Hysteresis Loops	269
Conclusions	273
SECTION VIII: DESIGN AND FABRICATION OF THE CATALYST TESTING UNIT	
Reactor Design	274

TABLE OF CONTENTS (Concluded)

	<u>Page</u>
Temperature Controllers	276
Pressure	276
Space Velocity and Mixing Ratio	278
Gas Feed and Mixing Ratio	278
Liquid Feed	278
Gas-Liquid Separator	278
Two-Stage Compressor	279
Gas Recycle Pump	279
Packed Distillation Column	279
Automation of the Reactor System	283
 SECTION IX: LITERATURE SURVEY	 288
Introduction	288
Database File	291
 REFERENCES	 316
 APPENDIX A: Structural FTIR Spectra of Synthesized Zeolites	 335
 APPENDIX B: Product Distribution for Normal-Hexane Cracking Over Synthesized Zeolites	 351
 APPENDIX C: Product Distribution for Alcohol Reactions over Synthesized Zeolites	 353
 APPENDIX D: Interpolation of Capsule Calibration and Chemisorption Isotherm Computer Program	 359
 APPENDIX E: Reactor Mass Balance Computer Programs	 371
 APPENDIX F: Derivation of the BET Equations	 383
 APPENDIX G: BET Surface Area Computer Program	 403
 APPENDIX H: Data Base Management System for the Surveyed Literature from the High Density Aviation Fuel Project	 425

LIST OF FIGURES

<u>Figure</u>	<u>Page</u>
1. Fuel Density vs. Net Heating Value	2
2. Proposed Conventional Route to High Density Aviation Turbine Fuel Hydrogenation of Aromatic FCC Cycle Stocks	9
3. Proposed Conventional Route to High Density Aviation Turbine Fuel Shape Selective Cracking of n-Paraffins in Naphthenic Aviation Turbine Fuel Fraction	11
4. Proposed Conventional Route to High Density Aviation Turbine Fuel Shape Selective Cracking of n-Paraffins in Hydrocracker Aviation Turbine Fuel Fractions	12
5. Proposed Novel Catalytic Route to High Density Aviation Turbine Fuel Oxygenate Conversion to Aromatic Hydrocarbons Followed by Hydrogenation to the Naphthenes	14
6. Simulated Distillation Curves for High Density Fuel (82-POSF-1028)	21
7. Simulated Distillation Chromatogram High Density Fuel (82-POSF-1028)	22
8. Viscosity-Inverse Temperature Plot High Density Fuel (82-POSF-1028)	24
9. Infrared Spectrum of High Density Fuel (82-POSF-1028)	25
10. Arrhenius Temperature Dependence for Aviation Turbine Fuel Viscosities	34
11. Simulated Distillation Curves Aviation Turbine Fuel Analysis	35
12. ZSM-5 Channel System	48
13. Procedure for Synthesis of HZSM-5	76
14. Procedure for the Direct Synthesis of the Hydrogen-Form of ZSM-5	79
15. Procedure for Synthesis of HZSM-48	80
16. Schematic of Temperature-Programmed Desorption (TPD) and Microreactor Apparatus	85

LIST OF FIGURES (Continues)

<u>Figure</u>	<u>Page</u>
17. Diffuse Reflectance FTIR Cell and Optical Layout	86
18. Volumetric Adsorption System for BET Surface Area Measurement	89
19. Reactor Systems for the Study of Methanol Conversion	91
20. X-ray Diffraction Patterns for ZSM-5	94
21. Differential Scanning Calorimetry Pattern for NaZSM-5 Elimination of the ORganic Cation (TPA)	96
22. Scanning Electron Microscope Images of HZSM-5 Effect of Organic Cations on Synthesis	100
23. Scanning Electron Microscope Images of HZSM-5 Effect of SiO ₂ /Al ₂ O ₃ Ratio	101
24. Comparison of the X-ray Diffraction Patterns for ZSM-5 and ZSM-48	103
25. Effect of SiO ₂ /Al ₂ O ₃ Ratio on the Synthesis of ZSM-48	104
26. Scanning Electron Microscope Images of ZSM-48/5 (70) ZSM-48 and ZSM-5	105
27. X-ray Diffraction Patterns for ZSM-48 Prepared with Different Organic Templates	106
28. Differential Scanning Calorimetry (DSC) of NaZSM-48 Elimination of the Organic Cation (C6DN) from Synthesized NaZSM-48	108
29. Differential Scanning Calorimetry Pattern for NaZSM-48 Elimination of the Organic Cation (C8DN) from Synthesized NaZSM-48	109
30. X-ray Diffraction Patterns for NaZSM-48(200). Effect of Calcination Temperature	110
31. X-ray Diffraction Patterns. Effect of C6DN/SiO ₂ on the Synthesis of ZSM-48	111
32. X-ray Diffraction Patterns. Effect of Na/SiO ₂ on the Synthesis of ZSM-48	112

LIST OF FIGURES (Continues)

<u>Figure</u>	<u>Page</u>
33. X-ray Diffraction Patterns of NaZSM-48X. Effect of Calcination Temperature	114
34. Scanning Electron Microscope Images of NaZSM-48X Effect of Calcination Temperature	115
35. Effect of Crystallization Temperature on the Synthesis of ZSM-48	117
36. Scanning Electron Microscope Image of ZSM-48(200).	118
37. Temperature-Programmed Desorption Spectrum of Ammonia Fresh ZSM-5 Catalyst	122
38. Temperature-Programmed Desorption Spectrum of Ammonia Spent ZSM-5 Catalyst	123
39. Temperature-Programmed Desorption Spectrum of Ammonia Zeolite ZSM-48/5(70)	124
40. Temperature-Programmed Desorption Spectrum of Ammonia Zeolite ZSM-48/5(70)	126
41. Temperature-Programmed Desorption Spectra of Alcohols from HZSM-5	127
42. In-Situ Diffuse Reflectance FTIR Study of Methanol Conversion over ZSM-type Zeolites	130
43. Diffuse Reflectance FTIR Study of the Thermal Desorption of Methanol from Zeolite ZSM-5	132
44. Diffuse Reflectance FTIR Study of the Thermal Desorption of Methanol from Zeolite ZSM-48	133
45. Alpha Test - Normal-Hexane Cracking Activity with Crystalline Aluminosilicates	135
46. Possible Model for N ₂ Adsorption on Zeolites with Intermediate Pore Structure	138
47. Product Distribution from Methanol Conversion over Zeolite HZSM-5(70) Helium Carrier Gas	144

LIST OF FIGURES (Continues)

<u>Figure</u>		<u>Page</u>
48.	Product Distribution from Methanol Conversion over Zeolite HZSM-48(200) Helium Carrier Gas	145
49.	Product Distribution from Methanol Conversion over Zeolite HZSM-5(70) Hydrogen Carrier Gas	149
50.	Product Distribution from Methanol Conversion over Zeolite HZSM-48(200) Hydrogen Carrier Gas	150
51.	Product Distribution from Methanol Conversion over HZSM-5(70)	151
52.	Product Distribution from Methanol Conversion over HZSM-48(200)	152
53.	Effect of SiO ₂ /Al ₂ O ₃ Ratio on Aromatic Selectivity for Methanol Conversion over ZSM-5	153
54.	Effect of Organic Ions used in the Synthesis of ZSM-5 on the Aromatic Selectivity for Alcohol Reactions	155
55.	Effect of Channel Structure on the Aromatic Selectivity in Alcohol Reactions	157
56.	Product Distribution from Methanol Conversion Zeolite ZSM-5	160
57.	Product Distribution from Methanol Conversion Zeolite ZSM-48	161
58.	Product Distribution from Methanol Conversion Zeolites ZSM-48/ZSM-5; Single Reactor Mode	162
59.	Product Distribution from Methanol Conversion Zeolites ZSM-5/ZSM-48; Single Reactor Mode	163
60.	Product Distribution from Methanol Conversion Effect of Reaction Pressure; Zeolite ZSM-5	165
61.	Product Distribution from Methanol Conversion Effect of Reaction Temperature; Zeolite ZSM-5	166
62.	Reaction Index from Methanol Conversion	167

LIST OF FIGURES (Continues)

<u>Figure</u>		<u>Page</u>
63.	Product Distribution from Methanol Conversion over Zeolites ZSM-48 and ZSM-5; Dual Reactor Mode	170
64.	Product Distribution from Methanol Conversion over Zeolites ZSM-48 and ZSM-5; Dual Reactor Mode	171
65.	Constant Volume Adsorption Apparatus	177
66.	Constant Volume Adsorption Apparatus, Detail of Doser System	179
67.	Adsorption Cell	182
68.	Hydrogen and Oxygen Adsorption Isotherms 0.53% Pt/SiO ₂ Catalyst	197
69.	Carbon Monoxide Adsorption Isotherm 0.53 Pt/SiO ₂ Catalyst	198
70.	Hydrogen Chemisorption Isotherm for Pt/Al ₂ O ₃	199
71.	Diagram of Catalytic Dewaxing Reactor System	208
72.	Conversion of n-Hexadecane to Primary and Secondary Cracked Products	220
73.	Carbon Number Yield as a Function of Space Time for the Cracking of Normal Hexadecane at 575 K and 200 psia	221
74.	Product Distribution as a Function of Space Time for the Cracking of Normal Hexadecane at 575 K and 200 psia	223
75.	Carbon Number yield for the Cracking of Kerosene and for the Cracking of n-Hexadecane	226
76.	Schematic of the BET System	237
77.	Components of the BET System	238
78.	Adsorption and Gas Handling System	239
79.	Plot of the BET (A) Equation for Alumina	253
80.	Adsorption/Desorption Isotherm for Alumina	255

LIST OF FIGURES (Concluded)

<u>Figure</u>	<u>Page</u>
81. SEM Photomicrographs of ZSM-5M and ZSM-5-6	257
82. Plot of the BET (A) Equation for ZSM-5M	259
83. Adsorption/Desorption Isotherm for ZSM-5M	260
84. Plot of the BET (A) Equation for ZSM-5-6	261
85. Adsorption/Desorption Isotherm for HZSM-5-6	262
86. Adsorption Isotherm for a ZSM-5 Type Adsorbent	266
87. Adsorption Isotherm for a ZSM-48 Type Adsorbent	268
88. BET Apparatus Data Acquisition System	270
89. Circuit Design for Computer-ET Apparatus Interfacing	271
90. Schematic of BET Software Algorithm	272
91. Schematic of Catalyst Evaluation Unit	275
92. Design for Manual and Automatic Control Modes for the Reactor System Pressure	277
93. Design of the High Pressure Gas-Liquid Separator	280
94. Two-Stage Feed Compressor. Safety and Automatic Control Schematic	281
95. Control Circuit Design for the Two-Stage Feed Compressor	282
96. Packed Distillation Column	284
97. Thermocouple Amplifier	285
98. Pressure Transducer Interface	286
99. Relationships Between Functions for the Literature Survey Database Management System	289

LIST OF TABLES

<u>Table</u>	<u>Page</u>
1. Selected Specifications for Aviation Turbine Fuels	4
2. Aviation Turbine Fuel Specifications	5
3. Identification of Aviation Turbine Fuel Samples	16
4. Physical Properties of Soviet High Density Jet Fuel	19
5. Simulated Distillation of Soviet High Density Jet Fuel	20
6. Elemental Analysis of Soviet High Density Jet Fuel	23
7. Specific Gravities of Aviation Turbine Fuel Samples	27
8. Viscosity as a Function of Temperature Aviation Turbine Fuel Samples	28
9. Viscosities of Jet Fuel Samples at 253 K	29
10. Flash Point/Fire Point Data for Jet Fuel Samples	30
11. Gross Heat of Combustion for Jet Fuel Samples	31
12. Simulated Distillation Data	32
13. Elemental Analysis of Aviation Turbine Fuel Samples	33
14. Comparison of Physical Properties of Aviation Turbine Fuels	36
15. Aviation Turbine Fuel Specifications	37
16. Simulated Distillation Analysis of 2040 Solvent	39
17. Selected Physical Properties of 2040 Solvent	40
18. Organic Cations Used in the Synthesis of ZSM-Type Zeolites	51
19. Nomenclature for the Organic Cations Used in the Synthesis of ZSM-Type Zeolites	52
20. Chemical Formulae of the Organic Cations Used in the Synthesis of ZSM-Type Zeolites	53

LIST OF TABLES (Concluded)

<u>Table</u>	<u>Page</u>
21. Composition Ranges in Terms of Mole Ratios for the Synthesis of ZSM-48	82
22. Chemicals Used in Catalyst Preparation	92
23. Degree of Crystallinity of Synthesized ZSM-5 Samples	97
24. Chemical Composition of Synthesized Zeolites	119
25. IR Structural Characteristics of the Zeolite Frameworks	129
26. Isomerization of Isobutane at 623 K Hydrogen/Isobutane Molar Ratio of Four	137
27. Surface Area Measurements of ZSM-5 and ZSM-48	141
28. Product Distribution from Methanol Conversion over ZSM-5 and ZSM-48 in a Microreactor	147
29. Chemisorption Data for Pt/SiO ₂ Catalyst	200
30. Hydrogenation of Naphthalene over Various Catalysts	205
31. Product Distribution from the Cracking of Normal Hexadecane and Kerosene over HZSM-5	227
32. Normal-hexane Cracking over Synthesized Zeolites	352

Section I: INTRODUCTION

Aviation turbine fuels have been traditionally manufactured by distillation of petroleum crudes followed by mild hydrogen treatment to remove organic sulfur and nitrogen species and to impart thermal stability to the fuel. In order to significantly increase the range of volume limited military aircraft, the United States Air Force has contemplated changing over to higher density aviation turbine fuels. The increased range results from increasing the specific gravity of aviation turbine fuels, and, thus, the volumetric heating value as illustrated in Figure 1. Higher density aviation turbine fuels can be produced by expanding the boiling range of the fuel by raising the endpoint; however, increasing the availability of higher density jet fuels through the adjustment of distillation boiling ranges may be limited not only by existing specifications with regard to freeze point but also by the demand for the same boiling range fraction to produce other products.

The past 15 years have revealed the vulnerability of the United States liquid fuels markets to international events. Events beyond the control or influence of the United States have altered the uniform course of domestic economic progress by influencing the availability and cost of traditional energy sources. Thus, it would be desirable to develop stable, domestic sources of the high density aviation turbine fuels.

Aviation Turbine Fuels

Fuels developed for aviation turbine applications must meet certain established specifications. Many of these specifications can be met by the addition of specific compounds or additives to the fuel in low concentrations. However, there are some specifications that cannot be economically met by blending additives and can only be met by adjusting the boiling range of the fuel.

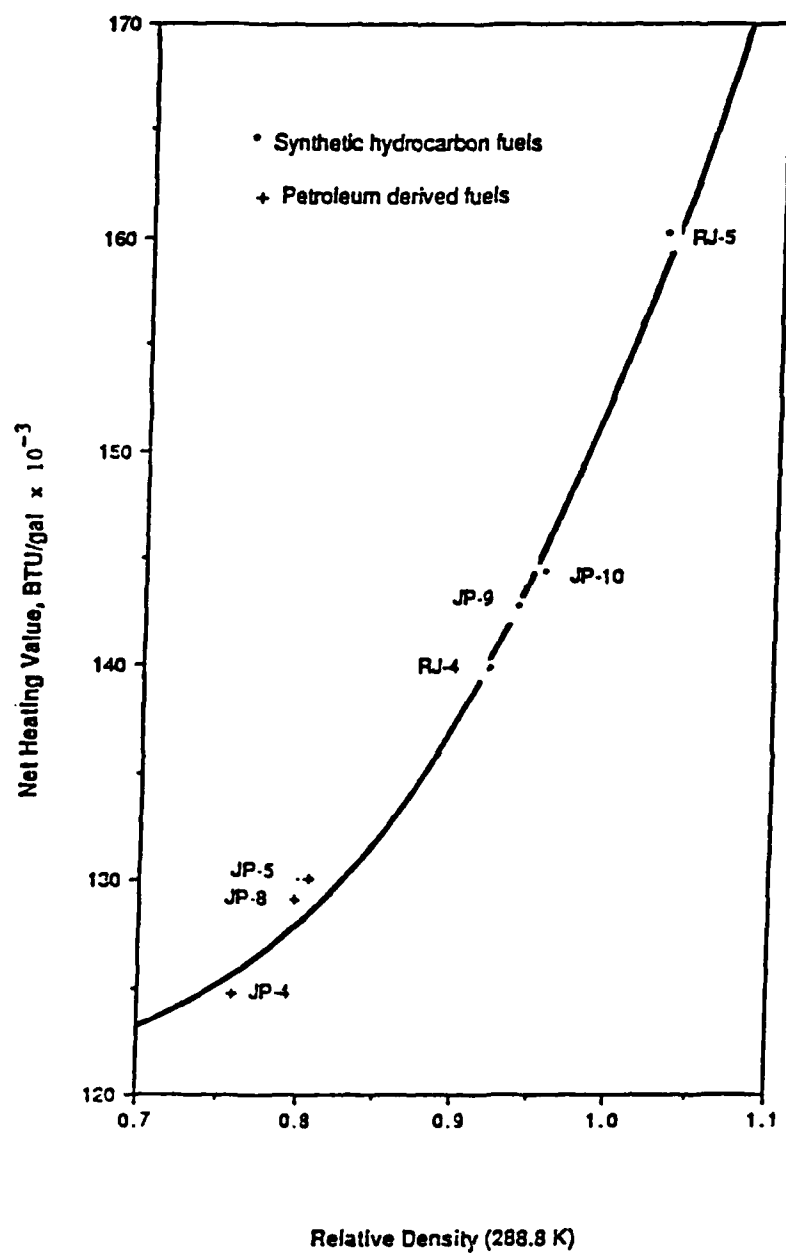


Figure 1. Fuel Density vs. Net Heating Value

A number of the typical specifications for civilian and military jet fuels are listed in Table 1. An indication of the means by which these and other specifications can be met are listed in Table 2; that is, by blending an additive with the straight run fuel or by selecting the proper distillation fraction from an appropriate crude oil.¹

The most critical specifications are those on freeze point, vapor pressure, and aromatics. Fuels for aviation turbines are usually produced from straight run distillation cuts rather than from cracked stocks to meet the specifications on aromatics and olefins. The specification on viscosity is important, but it is only important for very low freeze point fuels which operate at temperatures below 213 K (-60°C). Generally, the low temperature properties of a fuel are defined according to its freeze point, rather than its low temperature viscosity.

Aromatics concentrations must be less than 20 volume percent² because high aromatic fuels produce smoke which excessively heats jet engine components. There exists an added complication for military aircraft related to the visible contrail behind the plane, due to the smoke produced from the combustion of aromatics. Soot in the exhaust gas also makes the jet more vulnerable to heat seeking missiles, due to the higher luminosity of the turbine exhaust gases.

The freeze points of conventional jet fuels range from 233 K to 213 K (-40 to -60°C). If the composition of an aviation turbine fuel is such that the freeze point is too high, then paraffin crystals may form in the fuel stored in the unheated, on-board fuel tanks. These paraffin crystals can deposit in fuel filters and may damage fuel pump components.

Vapor pressure must be low for safety and conservation reasons. However, the vapor pressure must not be too low to avoid aircraft cold starting problems. This is particularly crucial for military jets which are sometimes parked on extremely cold runways.²

Table 1
Selected Specifications for Aviation Turbine Fuels³

Turbine Fuel Property	Civilian Fuels		Military Fuels		
	Jet A	Jet B	JP-4	JP-5	JP-8
Density (g/cm ³)	0.78-0.84	0.75-0.80	0.75-0.85	0.78-0.85	0.78-0.84
Freeze Point (maximum, °F)	-40	-50	-58	-46	-50
Flash Point (minimum, °F)	100	NA	NA	140	100
Aromatics (maximum, vol%)	20	20	25	25	25
Sulfur (maximum, wt%)	0.3	0.3	0.4	0.4	0.4
H ₂ Content (minimum, wt%)	NA	NA	13.6	13.5	13.6
Heat Content (MJ/kg, minimum)	42.8	42.8	42.8	42.6	42.8
Stability Test Temperature (minimum, °F)	473	473	500	500	500

Table 2
Aviation Turbine Fuel Specifications

Specification	Key
Low Aromatic Content	c
Low Freeze Point	c, d
Low Vapor Pressure	c, d
Stability (olefin content)	c, t, a
Sulfur Content	c, t, a
Low Temperature Viscosity	c, d
Water Solubility	a
Electrical Conductivity	a

Key

a - specification can be met by blending of an additive.

c - specification can be met by choice of crude

d - specification can be met by choosing the proper distillation cut

t - specification can be met by chemical treatment of jet fuel

The stability specification for jet fuels requires that the olefin content of the fuel be less than one or two percent. Even though jet fuels are stored in unheated tanks in aircraft, they are used as a coolant for jet engine lubricating oil and the fuel may reach a temperature of 573 K (300°C) or higher in the injection nozzle. For this reason the olefin content must be kept low to avoid polymerization of the olefins and gum formation which can eventually plug some of the fuel injection nozzles.

Aviation turbine fuels need to be low in sulfur and metals because metal sulfates formed in the combustion process can corrode jet engine components. Fuels that contain too much sulfur can be lightly hydrotreated to remove mercaptan sulfur, thus lowering the sulfur content.

Glycol ether is added to the fuels to increase the solubility of water which may condense or freeze in cold fuel tanks. A biocide is also added to restrict the growth of microorganisms at water-hydrocarbon interfaces. This is necessary because microorganisms growing in fuel tanks may form an organic sludge which can plug fuel filters.

Jet fuels can develop static electrical charges during handling and transfer of the fuel from storage tanks to the on-board fuel tanks. If static electrical charges are not dissipated, an electrical arc may occur between the fuel and an electrical ground, thus igniting the fuel vapors. Consequently additives are placed in the fuel to increase its electrical conductivity and to circumvent the build-up of static charge.

The requirement for a low freeze point and low volatility is a dilemma for producers of jet fuels. Only specific cuts of kerosene boiling range materials from specific crudes (which may be of limited availability) can satisfy this dual requirement. Economic considerations dictate that such cuts be either untreated or only lightly hydrogenated to remove nitrogen, sulfur, and olefins.

The requirement that the concentrations of aromatics, olefins, and paraffins be below certain levels limits the possible crudes available for the production of jet fuels to those crudes which have high naphthene content in the 423-523 K (150-250°C) boiling range. These restrictions raise the possibility that the United States could be vulnerable to crude oil supply disruptions during a war involving OPEC oil supplies or an oil embargo. One objective of aviation turbine fuel research and development activities is to produce a naphthenic jet fuel with a normal paraffin content which is low enough so that the freeze point specification will be met. A second objective is to produce these fuels from secure, domestic resources.

Possible Processing Schemes for the Production of High Density Aviation Turbine Fuels

The production of high density aviation turbine fuels can be accomplished by a number of conventional processing schemes^{4,5} as well as by several unconventional schemes. The processing schemes which make use of commercially practiced concepts include the following: shape selective cracking of normal paraffins from an appropriate boiling range fraction of a naphthenic crude; saturation of an aromatic FCC cycle stock of the appropriate boiling range; and saturation of an appropriate boiling range fraction from a hydrocracker recycle stream when the feed to the hydrotreater is aromatic in nature. The unconventional processing schemes include synthesis of the appropriate boiling range aromatic species from oxygenates over crystalline aluminosilicates followed by hydrogenation of the aromatic species; and direct synthesis of the aromatic hydrocarbons from hydrogen and carbon monoxide over crystalline aluminosilicate-supported metal catalysts followed by hydrogenation of the aromatic species.

Hydrogenation of Aromatic Refining Feed Streams

The production of high density aviation turbine fuels could be achieved by the hydrogenation of aromatic FCC cycle stocks⁴ (Figure 2); that is, a naphthenic, high density aviation turbine fuel could be produced from an expanded boiling range jet fuel fraction produced from aromatic petroleum crude oils that have been reacted over conventional fluid zeolite cracking catalysts. The aromatic jet fuel fraction obtained from an FCC liquid recycle stream should be mostly methyl substituted aromatic hydrocarbons which, upon hydrogenation of the aromatic core over a supported noble metal catalyst, would be an excellent high density turbine fuel candidate. The hydrogenation step would also saturate the olefin species and reduce the sulfur and nitrogen heteroatom concentration to comply with the specifications.

Removal of Normal Paraffins from Naphthenic Refinery Feed Streams

An alternate route for the production of high density aviation turbine fuels would be the removal of normal and slightly branched paraffins from an expanded boiling range jet fuel fraction from a naphthenic crude oil or from the second stage recycle stream of a hydrocracker processing an aromatic feed stock composited from various refinery process streams such as coker gas oils, FCC cycle stocks, and/or primary or secondary furfural extracts.

Solvent Extraction

Normal paraffins could be removed by solvent dewaxing from waxy naphthenic distillation cuts of the proper boiling range. Solvent dewaxing consists of chilling the material to be dewaxed in the presence of a solvent to remove normal paraffins.⁶ This process is a step in the manufacture of conventional low pour point lube oils and could be used to selectively remove

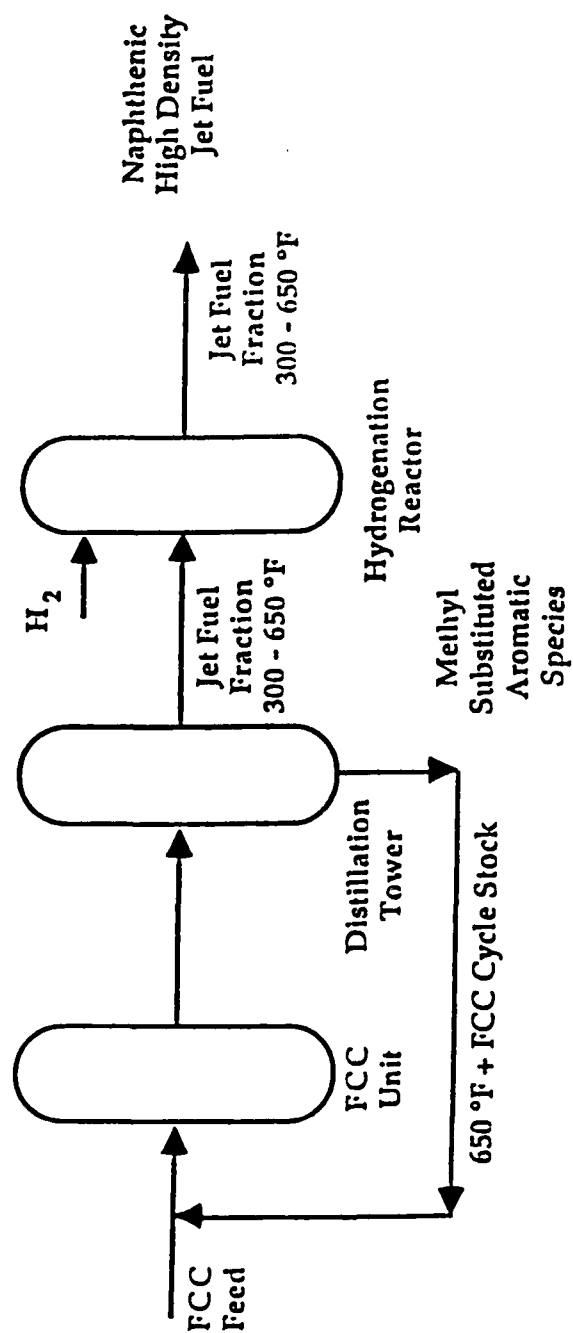


Figure 2. Proposed Conventional Route to High Density Aviation Turbine Fuel
Hydrogenation of Aromatic FCC Cycle Stocks

normal paraffins from these expanded boiling range fractions to reduce the freeze point to meet the fuel specification. The normal paraffins precipitate and the crystals are removed by filtration. This process is expensive due to refrigeration costs.⁷ In the case of dewaxing jet fuels this process would be particularly expensive due to the lower crystallization temperatures of paraffins in the jet fuel boiling range.

Shape Selective Catalytic Dewaxing

An alternative to solvent dewaxing is shape selective cracking of the normal paraffins in an expanded boiling range waxy naphthenic petroleum distillate. The expansion of the boiling range results in an increased freeze point, a larger average ring structure, and a higher density in the jet fuel fraction. The shape selective cracking catalyst will selectively convert the normal paraffins and slightly substituted paraffins to the light and intermediate naphtha boiling range resulting in a reduction of the freeze point. Catalysts suitable for this application include the acid form of ZSM-5⁸⁻¹⁰ and platinum supported on H-Mordenite.¹¹

This process concept can be applied to straight run naphthenic crude oils (Figure 3) or to hydrocracker jet fuel fractions (Figure 4). The cracked naphtha is then distilled to the original initial boiling point of the uncracked feed. If the wax is completely converted to cracked products, only naphthene molecules will remain in the boiling range of the original feed, which would then be suitable as a jet fuel. It is not likely that 100 percent conversion of the normal paraffins will need to be accomplished for the product to meet jet fuel specifications.

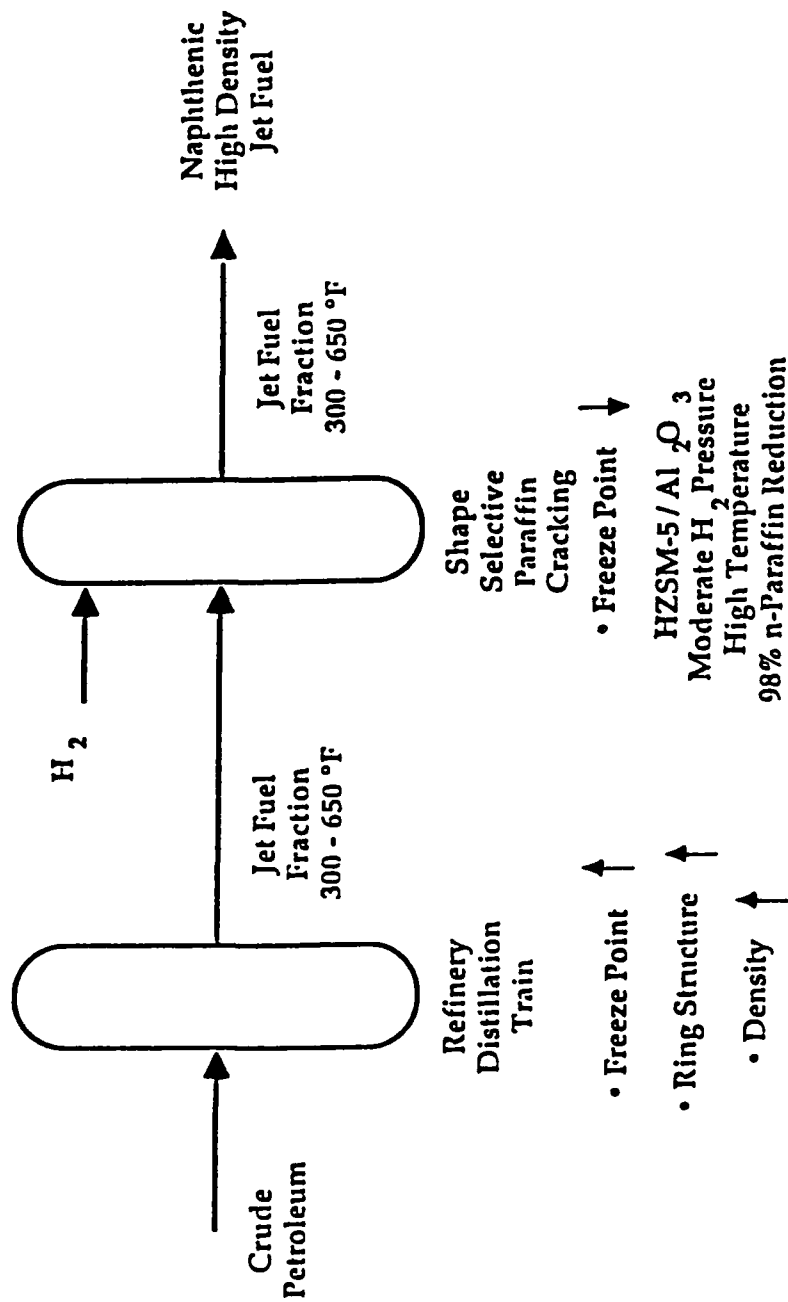


Figure 3. Proposed Conventional Route to High Density Aviation Turbine Fuel. Shape Selective Cracking of n-Paraffins in Naphthenic Aviation Turbine Fuel Fraction.

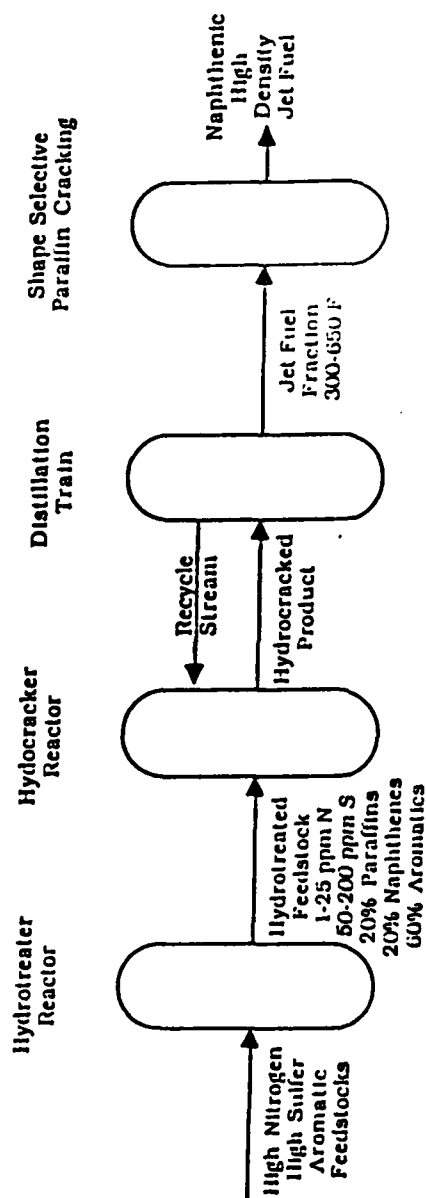


Figure 4. Proposed Conventional Route to High Density Aviation Turbine Fuel.
Shape Selective Cracking of n-Paraffins in Hydrocracker Aviation Turbine Fuel Fractions.

This method of low freeze point jet fuel production requires a shape selective cracking catalyst which will permit normal paraffin and slightly branched molecules to diffuse to active cracking sites but still restrict the diffusion of naphthenic molecules to the active sites. Certain zeolite catalysts such as ZSM-5 exhibit the appropriate shape selective behavior.¹²

Shape Selective Formation of Aromatic Hydrocarbons, Followed by Hydrogenation to the Corresponding Naphthene

An unconventional route to the production of high density aviation turbine fuels involves the use of shape selective catalysts to form the appropriate methyl-substituted aromatic hydrocarbons from oxygenates, followed by hydrogenation of the aromatic core to produce the corresponding naphthene. If feasible, this concept could provide a secure, albeit expensive, domestic source of high density fuels, since the oxygenates can be produced from domestic coal resources via commercially practiced Fischer-Tropsch technology. A schematic of the concept is presented in Figure 5.

A primary objective of this research project was to evaluate the potential of this concept for the production of high density fuels with an emphasis on the aromatic formation reactor system.

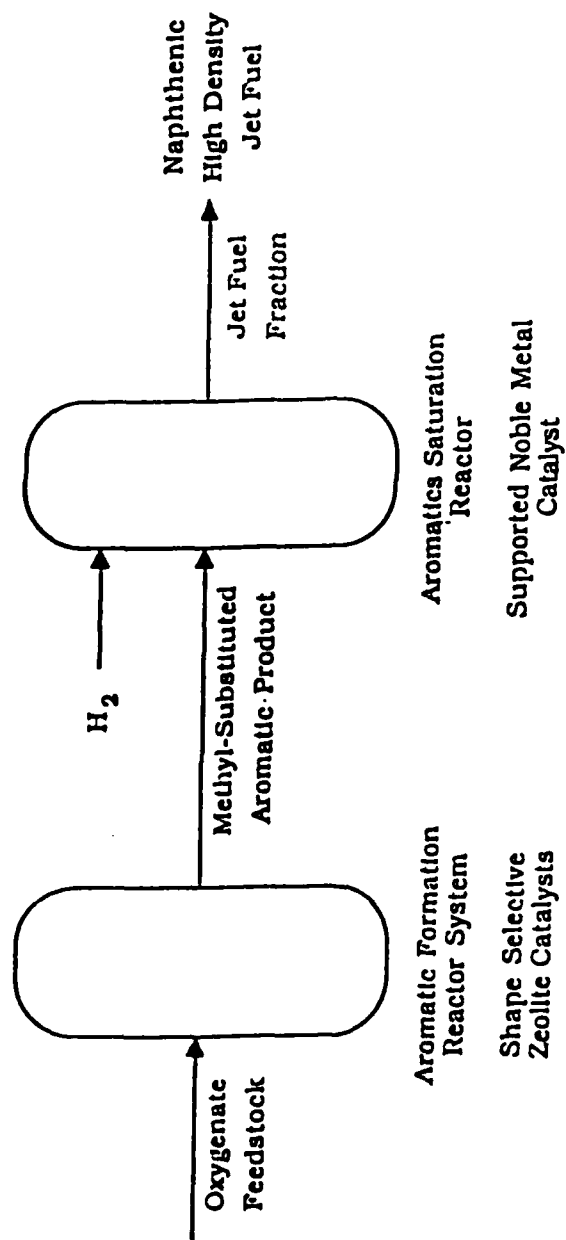


Figure 5. Proposed Novel Catalytic Route to High Density Aviation Turbine Fuel.
Oxygenate Conversion to Aromatic Hydrocarbons Followed by Hydrogenation to the Naphthenes

Section II: ANALYSIS OF AVIATION TURBINE FUEL SAMPLES

**Research Personnel: Chia J. Wang
Graduate Student**

**Hong P. Wang
Graduate Student**

**Francis V. Hanson
Associate Professor**

The initiation of a research program at the University of Utah aimed at producing high density aviation turbine fuels required the development of a data base on aviation turbine fuel properties. This was accomplished by analyzing a series of samples provided by the Air Force Wright Aeronautical Laboratories at Wright-Patterson Air Force Base. The samples included three petroleum-derived fuels, JP-4, JP-5, and JP-8, and a shale oil derived fuel, JP-4. Three samples of a pyrolysis oil product were also included in the analysis program. Since the objective of the research program was to develop catalyst and processing concepts leading to the production of high density aviation turbine fuels, a high density fuel was also incorporated into the analytical program. A secondary objective of the analysis studies was to evaluate the analytical capabilities of the Laboratory of Coal Science, Synthetic Fuels and Catalysis at the University of Utah. The samples provided by the Air Force Wright Aeronautical Laboratories are identified in Table 3. In addition, a sample of an aromatic solvent, 2040 solvent, was analyzed as a potential feedstock for the production of high density aviation turbine fuel by hydrogenation of the aromatic rings.

The analyses performed on the aviation turbine fuel samples, the pyrolysis oils, and the aromatic solvent included both physical and chemical properties, as well as spectroscopic characterization in the case of the high density fuel:

Table 3
Identification of Aviation Turbine Fuel Samples

USAF Sample Code	Sample Identification	Quantity (Quarts)	Color
82-POSF-1028	Soviet MIG 25 Jet Fuel	1	Clear
82-POSF-0541	JP-4 (Petroleum Derived)	2	Faint Yellow
83-POSF-1431	JP-4 (Shale Oil Derived)	3	Clear
83-POSF-1030	JP-5 (Petroleum Derived)	2	Yellow
83-POSF-0462	JP-8 (Petroleum Derived)	2	Clear
82-POSF-0162	Pyrolysis Oil (2%) ^a	1	Slightly Yellow
83-POSF-0801	Pyrolysis Oil (30%) ^b	1	Yellow
84-POSF-1949	Pyrolysis Oil ^c	1	Yellow

^a 2% aromatic hydrocarbons

^b 30% aromatic hydrocarbons

^c 500°F minus cut of 82-POSF-0162 (HDI)

- specific gravity
- viscosity (as a function of temperature)
- flash point
- fire point
- simulated distillation
- heat of combustion
- elemental analysis
 - carbon
 - hydrogen
 - sulfur
 - nitrogen
- infrared spectra
- molecular weight
- nuclear magnetic resonance
 - proton
 - carbon 13

The specific gravities were determined using a vibrating U-tube density meter. The viscosities were measured as a function of temperature using the Wells-Brookfield Model LVT Micro-viscometer. The pour point, flash point, fire point, and the heat of combustion were determined according to the accepted ASTM methods. The elemental analyses and the molecular weights were determined by Galbraith Laboratories of Knoxville, Tennessee. The infrared spectra and nuclear magnetic resonance analysis were performed in the Chemistry Department at the University of Utah.

Simulated distillation data were obtained using a Hewlett-Packard Model 5830A gas chromatograph equipped with a dual flame-ionization detector. The packing material was 3 percent Dexsil 300 on Anakrom Q.

Analysis of the High Density Aviation Turbine Fuel

The high density Soviet aviation turbine fuel was analyzed to provide a basis for the research and development studies on high density fuels. Duplicate tests were performed in each

instance to evaluate and monitor our analytical procedures and to determine the reproducibility of the procedures.

The physical inspections are presented in Table 4, and the simulated distillation analysis is presented in Table 5 and Figure 6. The chromatogram for the high density Soviet jet fuel is reproduced in Figure 7. The elemental analysis and the molecular weight are presented in Table 6. The viscosity is plotted as a function of the inverse temperature in Figure 8.

The Soviet jet fuel had an API gravity of 36.3° API, a pour point of -103°F, a flash point of 175-180°F, and a relatively high volumetric energy content (138,320 Btu/gal). Inspection of the data in Tables 4 and 5 and Figures 6 and 8, indicated that the experimental analytical procedures employed in this project gave excellent reproducibility.

The infrared spectra presented in Figure 9 were run on a PE-283 spectrometer. The spectra exhibited strong bands in the C-H stretch, the C-CH₂ inplane scissor, C-CH₃ in-plane bending, and the CH₂ rocking regions of the spectra. Furthermore, the spectra did not indicate the presence of unsaturated carbon-carbon bonds nor the presence of heteroatoms in this sample. According to Yen et al.,¹² the absorption at 2920 cm⁻¹ attributed to C-H stretching vibrations of methylene groups, whereas the absorption band at 1380 cm⁻¹ is due to C-H symmetric bending vibrations of methyl groups. The absorbance ratio of the 2920 cm⁻¹ to 1380 cm⁻¹ bands was determined, and the value of the ratio was approximately unity indicating a high degree of methyl substitution in the Soviet high density jet fuel.

The proton and carbon-13 nuclear magnetic resonance analysis indicated that the Soviet jet fuel contained essentially no alkanes and no long chain paraffins and only minor amounts of aromatic carbons (<2.4 percent). The majority of the aromatic components are 1-ring structures such as toluene, xylenes, and tetralins. The samples also contained a vanishing small concentration

Table 4
Physical Properties of Soviet High Density Jet Fuel

Physical Property	Run Number 1	Run Number 2
Specific Gravity (60°F/60°F)	0.84334	0.84334
API Gravity, °API	36.3	36.3
Viscosity, cps		
20°C	3.10 ± 0.05	3.12 ± 0.05
30°C	2.50 ± 0.05	2.59 ± 0.05
40°C	2.09 ± 0.05	2.10 ± 0.05
50°C	1.72 ± 0.05	1.74 ± 0.05
Pour Point, °F	-103	-103
Flash Point, °F	179.6	176.0
Fire Point, °F	190.4	186.8
Heat of Combustion		
Kcal g ⁻¹	10.83	11.01
Btu lb _m ⁻¹	19,500	19,810
Btu gal ⁻¹	137,225.5	139,417

Table 5
Simulated Distillation of Soviet High Density Jet Fuel

Distillation Fraction	Run Number 1	Run Number 2
IBP, °F	190.4	185
5	332.6	329
10	376.7	370.4
20	416.3	413.6
30	441.5	438.8
40	463.1	458.6
50	483.8	480.2
60	503.6	500
70	521.6	518
80	545	540.5
90	578.3	578.3
95	599	600.8
99	644	654.8
Gasoline Fraction 125-400°F, wt%	15.7	15.7
Middle Distillate 400-650°F, wt%	83.3	82.5
Heavy Gas Oil 650-1000°F, wt%	1.1	1.8
Residue 1000°F, wt%	0	0
Volatility 1000°F, wt%	100	100

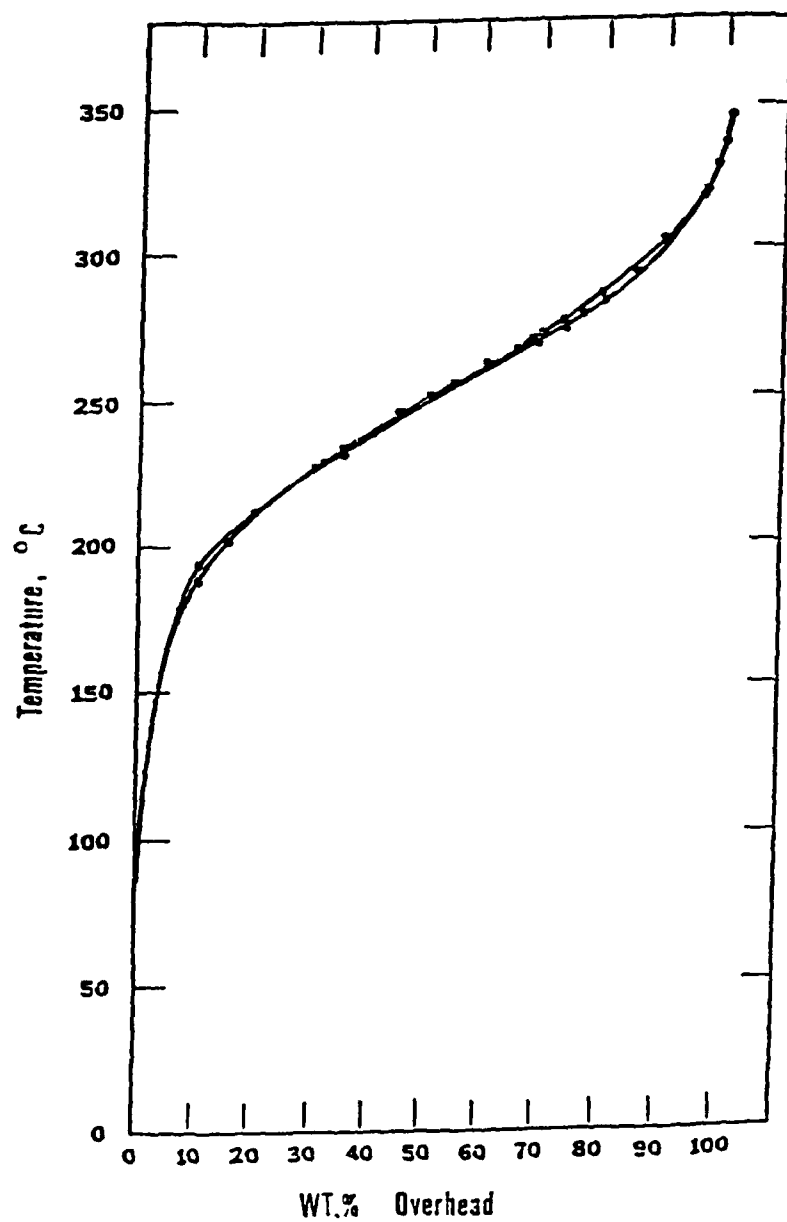


Figure 6. Simulated Distillation Curves for High Density Fuel (82-POSF-1028)

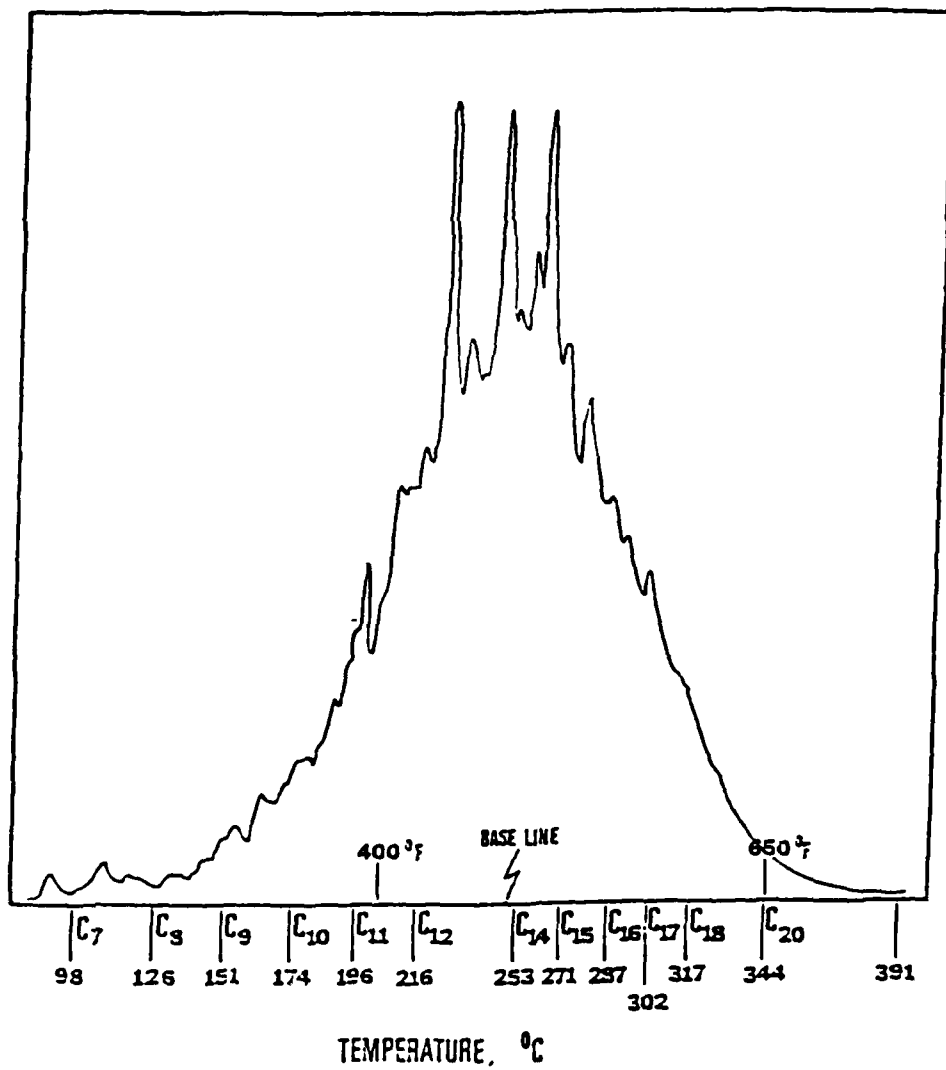


Figure 7. Simulated Distillation Chromatogram
High Density Fuel (82-POSF-1028)

Table 6
Elemental Analysis of Soviet High Density Jet Fuel

Elemental Analysis	
Carbon, Wt%	86.3
Hydrogen, Wt%	13.7
Nitrogen, ppm	6
Sulfur, ppm	16
Atomic Hydrogen/Carbon Ratio	1.89
Molecular Weight, g mol ⁻¹	225

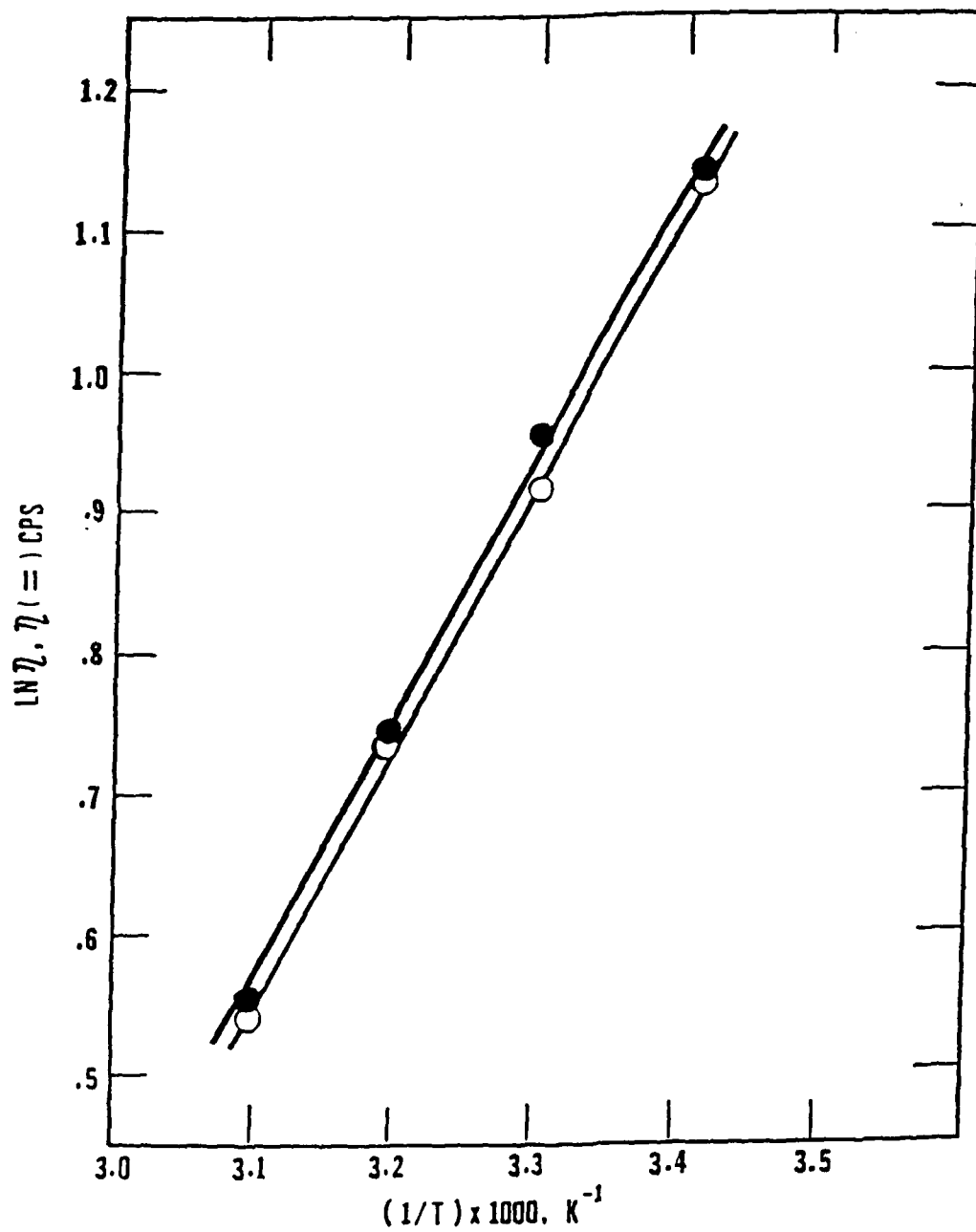


Figure 8. Viscosity-Inverse Temperature Plot
High Density Fuel (82-POSF-1028)

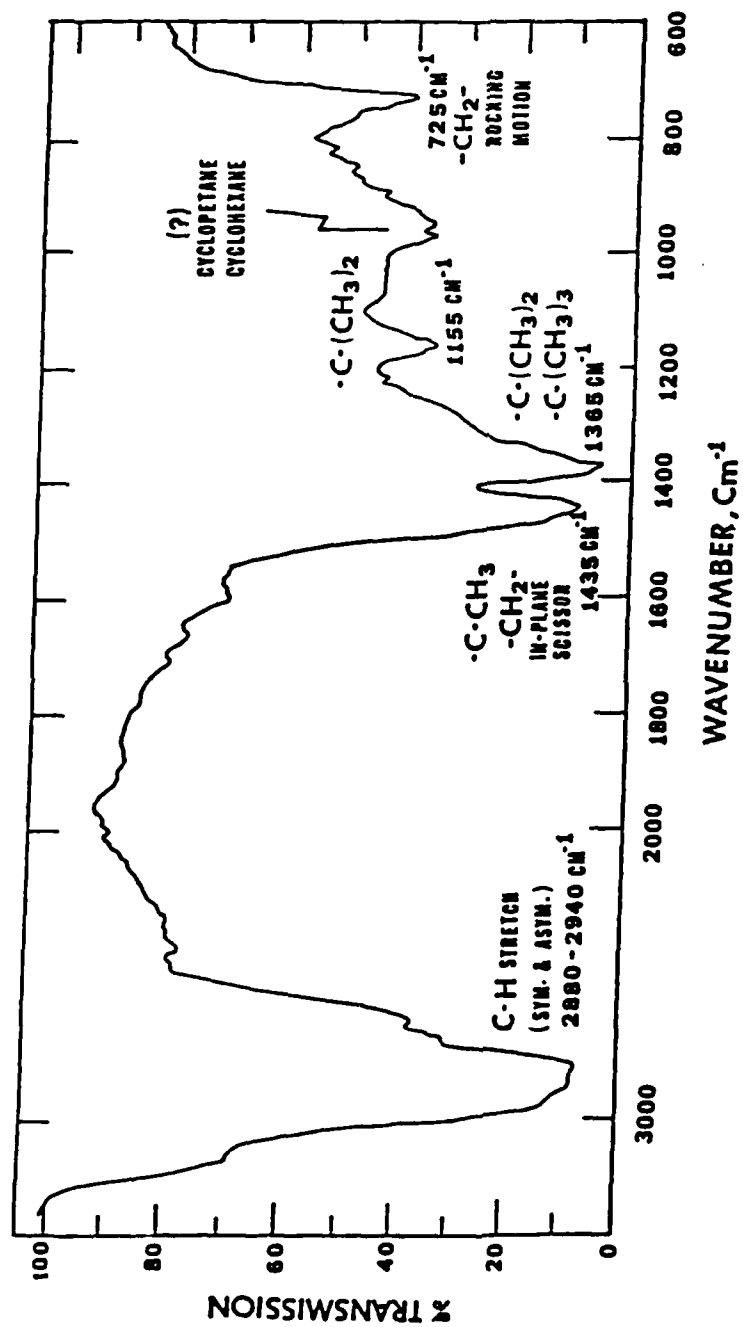
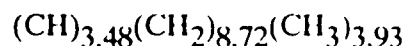


Figure 9. Infrared Spectrum of High Density Fuel (82-POSF-1028)

of 2-ring aromatics. Approximately 35 percent of the protons/hydrogens in the sample were methyl (CH_3) hydrogens. The high degree of methyl substitution was confirmed by the atomic hydrogen to carbon ratio, 1.89, calculated from the elemental analyses. The molecular entities comprising this high density jet fuel are methyl substituted naphthenes (1 and 2 rings), having approximately four methyl groups attached to the fused carbon rings, and isopranes. These species were determined to have an average empirical formula given by



The absence of normal paraffins and the low concentration of aromatics in the Soviet fuel led to the speculation that it might be a hydrogenated catalytic cracker cycle stock or light gas oil,⁴ to which front end specialty hydrocarbon additives had been added.

Analysis of Conventional Aviation Turbine Fuels and Pyrolysis Oils

The results of the physical and chemical analyses of the jet fuel samples are presented in Tables 7 through 13 and in Figures 10 and 11. The standard properties of the aviation turbine fuel samples are compared in Table 14. In general, the data appear to meet the reported specifications¹³ (Table 15) and data from the literature for the various jet fuel samples.

Analysis of the Aromatic 2040 Solvent

A sample of the 2040 solvent was obtained from the Air Force Wright Aeronautical Laboratories for possible use in the aromatics hydrogenation studies. A limited amount of analysis

Table 7
Specific Gravities of Aviation Turbine Fuel Samples

Sample Code	RUN I		RUN II	
	Specific Gravity (60°F/60°F)	API Gravity	Specific Gravity (60°F/60°F)	API Gravity
82-POSF-0162	0.87523	30.2	0.87523	30.2
82-POSF-0541 (JP-4-P)	0.76181	54.2	0.76181	54.2
83-POSF-0462 (JP-8)	0.79605	46.3	0.79605	46.3
83-POSF-0801	0.89652	26.3	0.89652	26.3
83-POSF-1030 (JP-5)	0.81356	42.4	0.81356	42.4
83-POSF-1431 (JP-4-S)	0.76661	53.1	0.76661	53.1
84-POSF-1949 (HD-1)	0.87221	30.7	0.87231	30.7
82-POSF-1028 (SJF)	0.84334	36.3	0.84334	36.3

Table 8

**Viscosity as a Function of Temperature
Aviation Turbine Fuel Samples**

Sample Code	Temperature (°C)	Viscosity (cps)	
		Run I	Run II
82-POSF-0162	20	2.54 ± 0.05	2.52 ± 0.05
	15	2.94 ± 0.05	2.97 ± 0.05
	10	3.32 ± 0.05	3.33 ± 0.05
	5	3.80 ± 0.05	3.85 ± 0.05
82-POSF-0541 (JP-4)	20	0.78 ± 0.05	0.80 ± 0.05
	15	0.82 ± 0.05	0.86 ± 0.05
	10	0.90 ± 0.05	0.90 ± 0.05
	5	0.96 ± 0.05	0.98 ± 0.05
83-POSF-0462 (JP-8)	20	1.18 ± 0.05	1.20 ± 0.05
	15	1.34 ± 0.05	1.37 ± 0.05
	10	1.47 ± 0.05	1.48 ± 0.05
	5	1.65 ± 0.05	1.66 ± 0.05
83-POSF-0801	20	2.62 ± 0.05	2.60 ± 0.05
	15	2.97 ± 0.05	3.01 ± 0.05
	10	3.32 ± 0.05	3.34 ± 0.05
	5	3.85 ± 0.05	3.95 ± 0.05
83-POSF-1030	20	1.74 ± 0.05	2.60 ± 0.05
	15	2.97 ± 0.05	3.01 ± 0.05
	10	3.32 ± 0.05	2.23 ± 0.05
	5	2.54 ± 0.05	2.56 ± 0.05
83-POSF-1431 (JP-4)	20	0.86 ± 0.05	0.89 ± 0.05
	15	0.90 ± 0.05	0.93 ± 0.05
	10	0.98 ± 0.05	0.98 ± 0.05
	5	1.05 ± 0.05	1.10 ± 0.05
84-POSF-1949 (HD-1)	20	2.31 ± 0.05	2.28 ± 0.05
	15	2.63 ± 0.05	2.66 ± 0.05
	10	2.88 ± 0.05	2.92 ± 0.05
	5	3.34 ± 0.05	3.38 ± 0.05
82-POSF-1028 (SJF)	50	1.72 ± 0.05	1.74 ± 0.05
	40	2.09 ± 0.05	2.16 ± 0.05
	30	2.50 ± 0.05	2.59 ± 0.05
	20	3.10 ± 0.05	3.12 ± 0.05

Table 9
Viscosities of Jet Fuel Samples at 253 K

Sample Code	Viscosity ^a	
	(cps)	(cst)
82-POSF-0162	8.3	9.4
82-POSF-0541 (JP-4-P)	1.7	2.2
83-POSF-0462 (JP-8)	3.7	4.7
83-POSF-0801	8.5	9.5
83-POSF-1030 (JP-5)	5.9	7.2
83-POSF-1431 (JP-4-S)	1.9	2.4
84-POSF-1949 (HD-1)	7.9	9.0
82-POSF-1028 (SJF)	8.2	9.7

^aViscosity: temperature data extrapolated to -20°C.

Table 10**Flash Point/Fire Point Data for Jet Fuel Samples**

Sample Code	Flash Point		Fire Point	
	°C	°F	°C	°F
82-POSF-0162	110	230	115	239
82-POSF-0541 (JP-4-P)	--	--	--	--
83-POSF-046 (JP-8)	98	208.4	104	219.2
83-POSF-0801	92	197.6	97	206.6
83-POSF-1030 (JP-5)	109	228.2	115	239
83-POSF-1431 (JP-4-S)	--	--	--	--
84-POSF-1949 (HD-1)	92	197.6	98	208.4
82-POSF-1028 (SJF)	82	179.6	88	190.4

Table 11
Gross Heat of Combustion for Jet Fuel Samples

Sample	Run Number	Heat of Combustion		
		cal/g	Btu/lb	Btu/gal
82-POSF-0162	1	10,720	19,295	140,622
	2	10,679	19,222	140,089
82-POSF-0541 (JP-4-P)	1	10,889	19,601	124,312
	2	10,953	19,715	125,037
83-POSF-0462	1	10,920	19,656	130,276
	2	10,801	19,442	128,856
83-POSF-0801	1	10,613	19,103	142,610
	2	10,509	18,916	141,216
83-POSF-1030 (JP-5)	1	10,776	19,396	131,383
	2	10,613	19,104	129,404
83-POSF-1431 (JP-4-S)	1	11,004	19,807	126,531
	2	11,010	19,818	126,601
84-POSF-1949 (HD-1)	1	10,750	19,351	140,547
	2	10,781	19,406	140,951
82-POSF-1028 (SJF)	1	10,830	19,500	137,226
	2	11,010	19,810	139,417

Table 12
Simulated Distillation Data

Percent Recovered	82-POSF-0162 °C	82-POSF-0162 °F	82-POSF-0541 °C	82-POSF-0541 °F	83-POSF-0462 °C	83-POSF-0462 °F	83-POSF-0801 °C	83-POSF-0801 °F	83-POSF-1030 °C	83-POSF-1030 °F	83-POSF-1431 °C	84-POSF-1949 °C	84-POSF-1949 °F	SOVIET JET FUEL °F
0.5 (IBP)	115	239	<37	<98.6	104	219.2	97	204.6	115	239	<37	<98.6	208.4	190.4
1.0	129	264.2	<37	<98.6	115	239	115	239	129	264.2	<37	<98.6	239	--
5.0	180	356	52.5	126.5	143	289.4	181	357.8	164	327.2	45	113	345.2	332.6
10	186	366.8	76	168.8	155	311	193	379.4	177	350.6	64	147.2	365	376.7
20	200	392	97	204.6	172	341.6	204	399.2	195	383	102	215.6	390.2	416.3
30	205	401	117	242.6	181	357.8	212	413.6	205	401	122	251.6	399.2	441.5
40	213	415.4	128	262.6	191	375.8	223	433.4	217	422.6	142	287.6	413.6	463.1
50	222	431.6	148	298.4	199	390.2	232	458.8	225	437	162.5	324.5	428	483.8
60	229	444.2	171	339.8	208	406.4	241	465.8	237	458.6	179	354.2	438.8	503.6
70	239	462.2	191	375.8	217	422.6	250	482	243	469.4	195	383	453.2	521.6
80	249	480.2	211	411.8	226	438.8	260	500	255	491	210	410	469.4	545
90	262	503.6	230	446	237	458.6	273	523.4	266	510.8	228	442.4	487.4	578.3
95	270	518	239	462.2	243	469.4	280.5	536.9	272	521.6	237	458.6	498.2	599
99	282.5	540.5	251	483.8	251	483.8	290	534	279	534.2	246	474.8	504.5	644
99.5 (FBP)	284	543.2	252	485.6	253	487.4	292	557.6	280	536	249	480.2	507.2	
Gasoline, wt%	26.07			78.39		56.34		19.3		27.83		75.25	25.56	15.7
Middle Distillate, wt%	73.93			21.61		43.66		80.7		72.17		24.75	74.44	83.3
Heavy Gas Oil, wt%	---			---		---		---		---		---	---	1.1
Volatility <1000°F, wt%	100			100		100		100		100		100	100	100

Table 13
Elemental Analysis of Aviation
Turbine Fuel Samples

Sample Code	C (wt%)	H (wt%)	H/C (atomic ratio)
82-POSF-0162	86.96	12.69	1.74
82-POSF-0541 (JP-4-P)	85.77	14.5	2.01
83-POSF-0462 (JP-8)	86.18	13.99	1.93
83-POSF-0801	86.93	12.31	1.69
83-POSF-1030 (JP-5)	85.82	13.44	1.87
83-POSF-1431 (JP-4-S)	85.28	14.41	2.01
84-POSF-1949 (HD-1)	86.81	12.60	1.83
82-POSF-1028 (SJF)	86.3	13.7	1.89

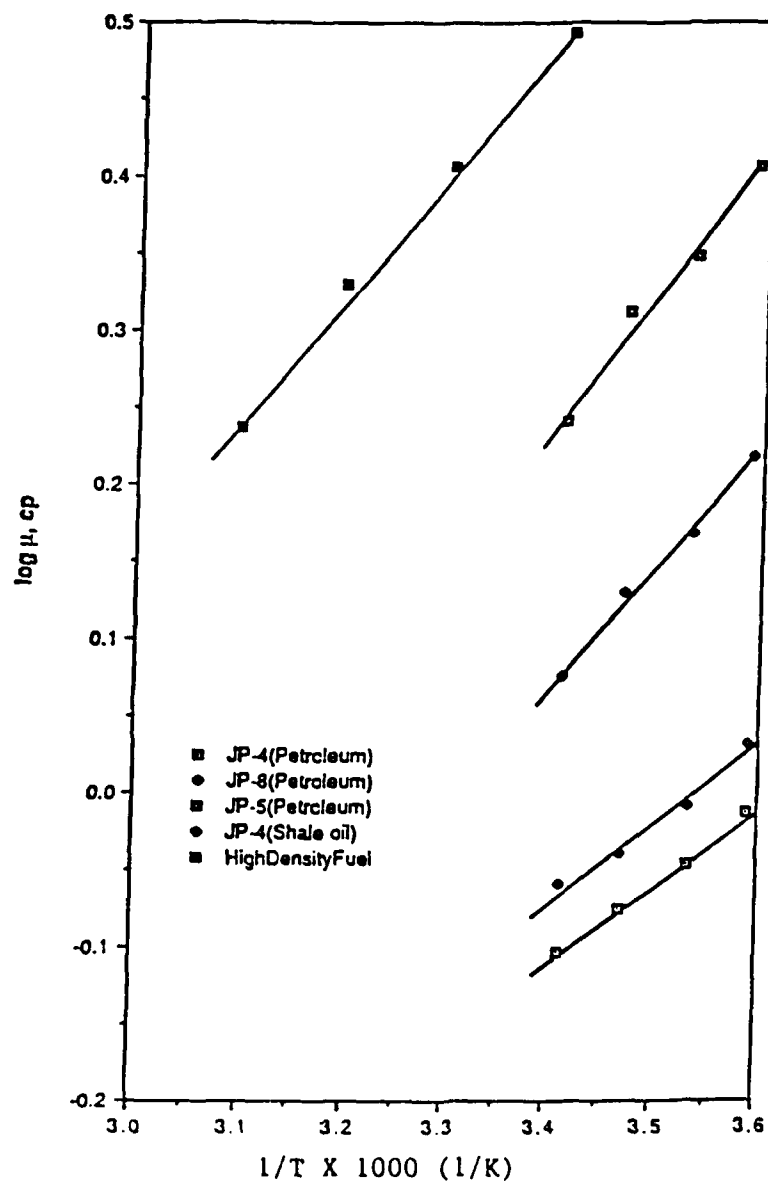


Figure 10. Arrhenius Temperature Dependence for Aviation Turbine Fuel Viscosities

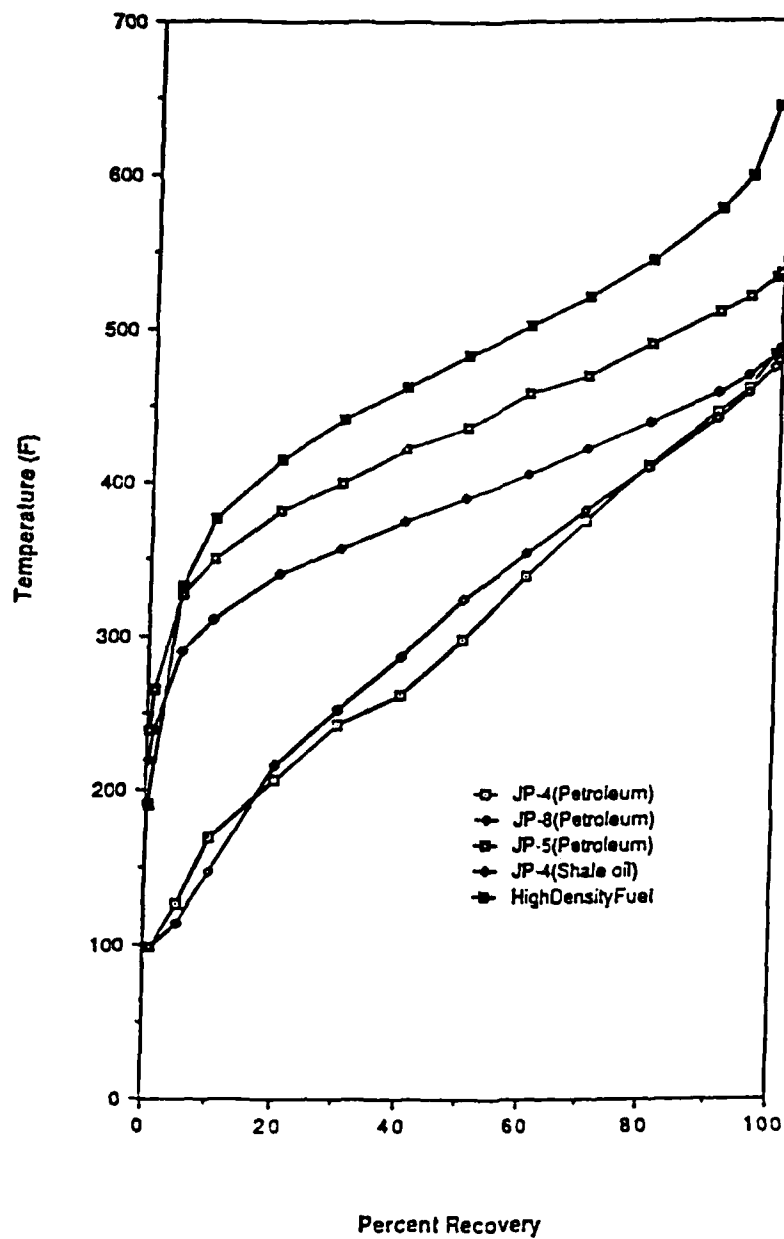


Figure 11. Simulated Distillation Curves
Aviation Turbine Fuel Analysis

Table 14
Comparison of Physical Properties of Aviation Turbine Fuels

Identification	JP-4 Petroleum Derived	JP-4 Shale Derived	JP-5 Petroleum Derived	JP-8 Petroleum Derived	High Density Fuel
CODE	82-POSF-0541	83-POSF-1431	83-POSF-1030	83-POSF-0462	83-POSF-1028
Properties					
Gravity, °API	54.2	53.1	42.4	46.3	36.3
Viscosity @ 253K, cps	2.2	1.9	5.9	3.7	8.2
Simulated Distillation					
Gasoline, wt%	78.4	75.2	27.8	56.3	15.7
Mid Distillate, wt%	21.6	24.8	72.2	43.7	82.8
Gas Oil Fraction, wt%	-	-	-	-	1.5
Flash Point, °F	-	-	228.2	208.4	177.8
Heat of Combustion,					
Btu/gal	124,675	126,556	130,394	129,566	138,320
Atomic H/C Ratio	2.0	2.0	1.87	1.93	1.89

Table 15
Aviation Turbine Fuel Specifications¹³

Fuels Identity	JP-4	JP-5	JP-8
Specifications			
Gravity, °API	45-57	36-48	39-51
Specific Gravity, 60/60°F	0.751-0.802	0.788-0.845	0.775-0.830
Distillation, °F (°C) ^a			
IBP	---	---	---
10% Ovhd	---	400 (204.4)	400 (204.4)
20% Ovhd	290 (143.3)	---	---
50% Ovhd	370 (187.8)	---	450 (232.2)
90% Ovhd	470 (243.3)	---	---
End Point	---	550 (278.8)	550 (278.8)
Flash Point, °F (°C) ^b	---	140 (60)	110 (43.2)
Reid Vapor Pressure, psi	2.0-3.0	---	---
Freeze Point, °F (°C) ^a	-72 (-58)	-51 (-46)	-51 (-46)
Luminometer Number ^b	60	50	45
Smoke Point, mm ^b	---	19.0	25
Net Heat of Combustion, ^b Btu/lbm	18,400	18,300	18,400

^a Maximum permitted values.

^b Minimum permitted values.

was performed on this solvent due to the deemphasis of the aromatics saturation work after receipt of the sample. The 2040 solvent was also considered as a candidate feedstock for a process concept in which an aromatic feedstock would be passed over ZSM-5 in the presence of methanol to produce a permethyl substituted high density aviation turbine fuel. The simulated distillation data are presented in Table 16, and selected, measured properties are reported in Table 17.

Table 16
Simulated Distillation Analysis of 2040 Solvent

% Recovered	°C	°F
0.5 (IBP)	160	320
1.0	164	327
5.0	177	351
10.0	193	379
20.0	212	414
30.0	225	435
40.0	238	460
50.0	242	468
60.0	251	484
70.0	263	505
80.0	273	523
90.0	288	550
95.0	293	559
99.0	334	633
99.5 (FBP)	375	707
Gasoline Fraction 125-400°F, wt%	17.4	
Middle Distillate 400-640°F, wt%	81.4	
Heavy Gas Oil 650-1000°F, wt%	1.2	
Residue 1000°F, wt%	0.0	
Volatility 1000°F, wt%	100.0	

Table 17
Selected Physical Properties of 2040 Solvent

Specific Gravity (15°C)	0.973
API Gravity, °API	13.95
Viscosity, cps	
15°C	2.82
20°C	2.35
Pour Point, °C	-23.0

Section III: SHAPE SELECTIVE CATALYSIS

Research Personnel: Hong P. Wang
Graduate Student

Daniel C. Longstaff
Graduate Student

Francis V. Hanson
Associate Professor

Introduction

The conversion of methanol to aromatic hydrocarbons followed by hydrogenation to the corresponding naphthenes as a route for the conversion of coal or synthetic or natural gas to high density or endothermic jet fuels has at least two advantages. First, high selectivity for a particular product can be achieved by adjusting the catalytic properties of zeolites and/or the process operating conditions. Second, the starting material, methanol, can be produced from alternative nonpetroleum resources via Fischer Tropsch type technologies from domestic coal resources.

It is proposed that high density aviation turbine fuels can be produced by the synthesis of methyl substituted, two-ring aromatic hydrocarbons followed by hydrogenation of the aromatic species to the corresponding naphthene.¹⁴

The advent of shape selective catalysis, first discovered and reported by Weisz and Frillette in the early 1960s,¹⁵ has created new opportunities to direct and control catalytic reactions involving hydrocarbons. Zeolites not only regulate those reactant materials that can diffuse into them but can also regulate those products that can readily diffuse out because of their unique pore structures and shape selectivity, thus controlling the product selectivity.

In the early 1970s, it was found that methanol could be converted to high octane number gasoline over the shape selective zeolite ZSM-5 in excellent yields and with long catalyst cycle

life.¹⁶ Additional research has shown that ZSM-5 can selectively produce specific hydrocarbon classes through variations in operating conditions and by modification of the catalyst preparation scheme.¹⁷⁻¹⁸

The unique catalytic and shape selective properties of ZSM-5 zeolites have been attributed to their crystalline structure. Zeolite ZSM-5 is a pentasil zeolite which possesses pore openings intermediate between those of small pore zeolites such as zeolite A and erionite and large pore zeolites such as faujasite. The 10-membered ring opening of ZSM-5, compared to eight for zeolite A and 12 for the faujasites, permits molecules that are intermediate in size to enter its channels.

A new zeolite designated ZSM-48 was synthesized in the early 1980s.¹⁹ This zeolite, having $\text{SiO}_2/\text{Al}_2\text{O}_3$ ratio >5 , can be used in conjunction with zeolite ZSM-5 for the conversion of methanol or higher alcohols to hydrocarbons in the jet fuel or diesel fuel boiling ranges.

The major objective of this work was to synthesize zeolite catalysts and to evaluate novel processing schemes using these catalysts for the production of methyl-substituted aromatics from oxygenated species. Zeolite structures related to ZSM-5 and ZSM-48 were investigated and explored. An investigation of the reactions of methanol and higher alcohols over synthetic zeolites was also conducted.

Zeolite Catalysts

Zeolites are crystalline, hydrated aluminosilicates. Their chemical composition can be represented by the empirical formula $\text{M}_{2/n}\text{O} \cdot [\text{Al}_2\text{O}_3 \cdot x\text{SiO}_2] \cdot y\text{H}_2\text{O}$, where x is generally equal to or greater than two and n is the valence of the cation M . When M is a proton, the zeolite is a strong Brönsted acid. As x approaches infinity, the framework will, of course, be electronically neutral.

Structurally, zeolites are framework aluminosilicates based on an infinitely extending three-dimensional network of AlO_4 and SiO_4 tetrahedra linked to each other by shared all oxygen atoms. Cations are introduced into the structure to preserve the electronic neutrality since the replacement of tetravalent silicon atoms by trivalent aluminum atoms results in the formation of ionic sites in the vicinity of the aluminum atoms. The cations so introduced are usually readily exchangeable.

Detailed reviews on the structures, physical and chemical properties of the catalytically important zeolites and molecular sieves have been discussed by Breck,²⁰ Rabo,²¹ and Barrer.²² A loose definition of zeolites has been proposed by Smith:²³ a zeolite is an aluminosilicate with a framework structure enclosing cavities occupied by large ions and water molecules, both of which have considerable freedom of movement, permitting ion exchange and reversible dehydration.

In some synthetic zeolites, aluminum cations are replaced by gallium ions, and silicon ions are replaced by phosphorus or germanium ions. The structure of a zeolite after complete dehydration must remain intact to be used as a molecular sieve.

General Concepts Related to Zeolite Synthesis

The most comprehensive early studies on zeolite synthesis were conducted by Barrer and his co-workers. In 1950 the Union Carbide Corporation initiated a systematic study of zeolite synthesis which resulted in the synthesis of about 20 novel synthetic zeolites by the application of a new field of chemistry involving highly reactive alkaline aluminosilicate gel, metastable crystallization, and low temperature, low pressure crystallization.²⁴ Zeolite A, discovered by Breck et al.,²⁵ can be prepared by combining sodium metasilicate and sodium aluminate solutions such that the reaction mixture is aluminum-rich. The powdered crystalline zeolite A can be obtained by refluxing the aluminosilicate gel solution for 3 to 4 hours. Using the same reagents, zeolite X

($\text{SiO}_2/\text{Al}_2\text{O}_3 = 2 - 3$) and zeolite Y ($\text{SiO}_2/\text{Al}_2\text{O}_3 = 3 - 6$)²⁶ can also be synthesized. Both of these zeolites are isostructural with the naturally occurring zeolite, faujasite ($\text{SiO}_2/\text{Al}_2\text{O}_3 = 4.5$).

In 1961, Barrer and his co-workers²⁷ first reported the synthesis of N-A (a siliceous analog of zeolite A) by adding tetramethylammonium cations to sodium aluminosilicate gels. The alkylammonium ion appeared to increase the framework Si/Al ratio, that is, the framework composition was enriched in silicon atoms. Kerr and Kokotailo²⁸ also reported the synthesis of a zeolite designated ZK-4 which was isostructural with zeolite A but whose $\text{SiO}_2/\text{Al}_2\text{O}_3$ ratio was 3.4.

Wadlinger et al.²⁹ received a patent in 1967 which described a new zeolite, designated zeolite beta, and its method of preparation. Zeolite beta was synthesized from silicon-rich reaction mixtures containing tetraethylammonium ions and sodium ions and was the first zeolite to have $\text{SiO}_2/\text{Al}_2\text{O}_3$ ratios greater than 10.

Argauer and Landolt³⁰ patented a preparation procedure that led to the formulation of a medium-pore class of zeolites known as Zeolite Socony Mobil (ZSM-) and more specifically to the zeolite catalyst known as ZSM-5.^{30,31} The discovery of the novel catalytic properties of ZSM-5 during the last decade has been followed by an intensive research effort on the synthesis of other highly siliceous zeolites and catalytic applications of these materials.³²⁻³⁴ ZSM-5 can be prepared from high $\text{SiO}_2/\text{Al}_2\text{O}_3$ ratio reaction mixtures containing sodium and tetrapropylammonium ions and at temperatures above 373 K.³⁰

A new family of molecular sieves has been disclosed having nonaluminosilicate frameworks. An important example of this expansion is the recent discovery of the novel aluminophosphate (AlPO_4) molecular sieves.³⁵⁻³⁷ The structures of several of these materials are analogous to the crystalline aluminosilicate zeolites. These materials represent a new class of microporous inorganic solids that are currently being evaluated in catalytic applications.

Characteristic Structures of Catalytically Important Zeolites

The zeolites that have been widely investigated are those that have achieved industrial applications. These zeolites, namely, X, Y, mordenite, the pentasil types, and erionite, have pore openings characterized by 12-, 10-, and 8-rings of oxygen atoms.

Large Pore Zeolites

Faujasite: Faujasite is a naturally occurring zeolite with chemical composition: $(\text{Na}_2\text{Ca})[\text{Al}_2\text{SiO}_4\text{O}_{12}] \cdot 8\text{H}_2\text{O}$. The synthetic zeolites X and Y have framework structures similar to that of the natural mineral faujasite. The faujasite structure is comprised of truncated octahedra (sodalite cage) interconnected via double six-ring (D6R) units. The three-dimensional framework gives rise to the large supercages approximately 13 Å in diameter. There are eight supercages per unit cell. The supercages are interconnected via 12-membered rings of about 7.4 Å in diameter. The unit cells are cubic with a cell dimension of nearly 25 Å. Each unit cell contains 192 AlO_4 and SiO_4 tetrahedra that are linked through shared oxygen atoms.^{38,39}

The cation sites that exist inside the supercage or close to the wall of the supercages are probably most important for catalytic purposes.⁴⁰ These sites can accommodate hydrogen ions that become framework hydroxyl groups and potential acidic catalytic sites following ion exchange.

Mordenite: Mordenite is a natural, orthorhombic aluminosilicate that has the general formula: $(\text{Na}_2\text{K}_2\text{Ca})[\text{Al}_2\text{SiO}_{10}\text{O}_{24}] \cdot 7\text{H}_2\text{O}$. The mordenite structure contains no large supercages, in contrast, the dehydrated structure has a two-dimensional small-pore channel system. The mordenite structure also contains a one-dimensional pore system (large pore) of parallel elliptical channels defined by 12-membered rings of approximately 6.7 Å diameter.^{38,39} The natural mordenite mineral appears to be a small pore zeolite because the pore system is partially blocked by amorphous impurities or cations resulting in an effective diameter of about 4 Å.³⁸⁻⁴⁰

Mazzite: Mazzite (ZSM-4 or zeolite omega) is a member of the cabazite group. Massite has a one-dimensional system of parallel channels defined by 12-membered rings 7.4 Å in diameter.^{38,39}

Small Pore Zeolites

Erionite: The erionite structure is hexagonal containing double six-membered rings and single six-membered rings that are arranged in parallel planes perpendicular to the hexagonal axis. This arrangement produces supercages supported by columns of cancrinite type cages linked through double six-membered rings. It results in a three-dimensional pore system consisting of cavities with dimensions of 1.5 x 6.3 Å and eight-membered oxygen ring apertures that have dimensions of 3.6 x 5.2 Å.^{38,39}

Erionite is a naturally occurring zeolite having a $\text{SiO}_2/\text{Al}_2\text{O}_3$ ratio of about six (erionite has the general formula: $(\text{Na}_2, \text{Ca}, \text{Mg}, \text{K}_2)\text{O} \cdot [\text{Al}_2\text{O}_3 \cdot \text{SiO}_2] \cdot 6\text{H}_2\text{O}$). It is a thermally stable and acid resistant zeolite. Erionite is commercially used in catalytic cracking and hydrocracking applications. The molecular shape selectivity can be controlled by means of modification of its pore size. The pore system of erionite contains a continuous diffusion path for molecules with a maximum kinetic diameter of 4.3 Å. Thus the structure can adsorb linear hydrocarbons and exclude branched hydrocarbons.⁴⁰

Cabazite: The trigonal structure (possibly triclinic) of cabazite has double six-membered rings linked together through tilted four-membered rings. The framework contains large ellipsoidal cavities, each entered through eight-membered rings. These cavities are joined together via their eight-membered rings to form a three-dimensional channel system having dimensions of 3.6 x 3.7 Å.^{38,39}

Offretite: Offretite is structurally related to erionite except in the sequence of six-membered rings. Intergrowths of offretite and erionite, e.g., ZSM-34 and zeolite T, are observed frequently.³⁸

ZK-5: Zeolite ZK-5 consists of truncated cuboctahedra joined through double six-membered rings in a body-centered structure. The main channel system is defined by eight-membered rings about 3.9 Å in diameter.^{38,39}

Pentasil Zeolites and Molecular Sieves

ZSM-5: The unique catalytic properties of zeolite ZSM-5, as in conversion of oxygenates to hydrocarbon species, have been attributed to its crystal structure.^{41,42}

Zeolite ZSM-5 is comprised of orthorhombic unit cells. The framework consists of a set of sinusoidal channels intersecting with a set of straight channels. The channels (Figure 12) are ellipsoidal with 10-membered ring openings, having the approximate free diameters of about 5.4 x 5.6 Å for straight channels and 5.1 x 5.5 Å for sinusoidal channels.^{30,43,44}

ZSM-11⁴⁴⁻⁴⁶ and silicalite are closely related to ZSM-5 in structure. The ZSM-5 and silicalite have orthorhombic unit cells whereas the unit cell of ZSM-11 is tetragonal. Silicalite-2 and ZSM-11 contain two sets of intersecting straight channels with 10-membered ring openings of about 5.1 x 5.5 Å free dimension.

ZSM-48: Zeolite ZSM-48 was found as an impurity phase in zeolite ZSM-39.⁴⁷ Zeolite ZSM-48 in a form substantially free from impurities was later synthesized hydrothermally by Mobil scientists.⁴⁸ ZSM-48 is a high silica zeolite with orthorhombic or pseudoorthorhombic unit cells. X-ray powder diffraction, electron diffraction, sorption and catalytic characteristics indicate that zeolite ZSM-48 has a framework based on the ferrierite sheet with linear non-interpenetrating

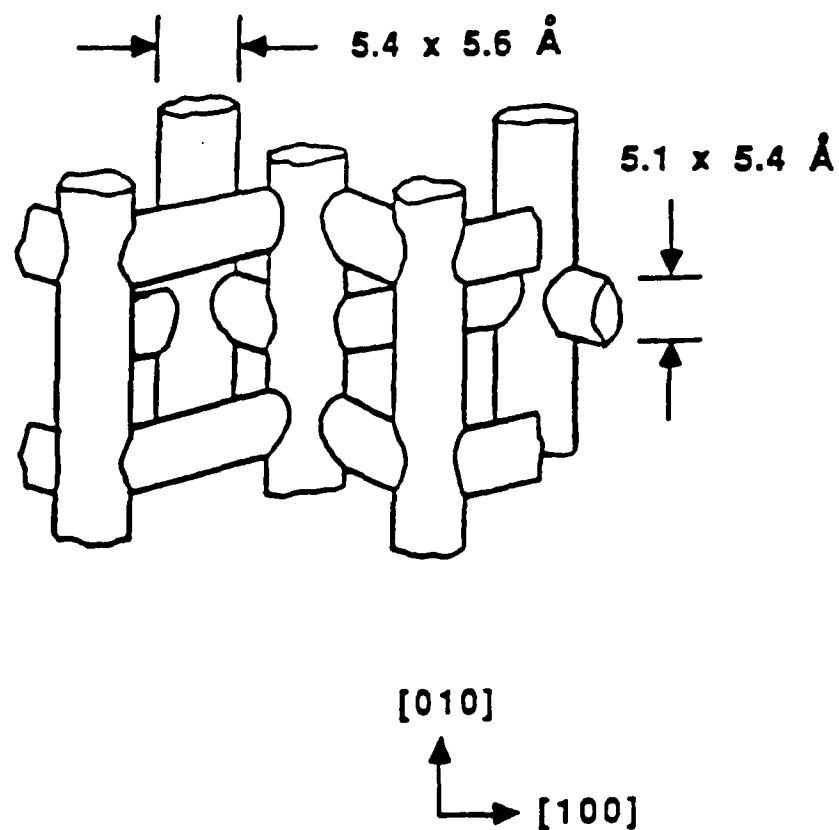


Figure 12. ZSM-5 Channel System

10-membered ring channels (ideal dimensions are $5.3 \times 5.6 \text{ \AA}$) running perpendicular to the sheet. A possible structure for ZSM-48 has been proposed by Schlenker et al.⁴⁹ It is proposed that ZSM-48 has a structure that is based on ferrierite sheets linked via bridging oxygens located in a mirror plane.

Shape Selective Zeolite Catalysis and Catalysts

Preparation of Shape Selective Zeolites

Synthesis of ZSM-type Zeolites

Since the work of Barrer⁴⁰ and Kerr,⁵⁰ a variety of organic cations have been used in the synthesis of zeolites. The major driving force for the use of organic cations was to synthesize a zeolite material with a high $\text{SiO}_2/\text{Al}_2\text{O}_3$ ratio. As the $\text{SiO}_2/\text{Al}_2\text{O}_3$ ratio increases, the acidity, thermal stability and hydrothermal stability also increase.⁵¹ A second objective was to synthesize a zeolite material with a larger intracrystalline pore channel system than those of zeolites X or Y, both of which have been used extensively in catalytic cracking and hydrocracking processes.^{27,52} A wider pore structure zeolite was desirable since it would crack more of the heavy end of the petroleum feed.

The cations used in the synthesis of ZSM-type zeolites are usually members of one of the following classes or types of cation: alkylammonium cations, alkyl-phosphonium cations and organic complexes. Alkylammonium organic cations have been more widely used in the synthesis of zeolites than phosphonium cations. The use of organic cations as templates in the synthesis of zeolites has led to the discovery of many new zeolitic materials.⁵³ The most commercially interesting of these are the ZSM-type zeolites developed by Mobil scientists.^{33,34,54-78} These zeolites are usually synthesized in a reaction mixture containing alkali metal cations in the presence of organic cations or complexes.

The organic cations used in the synthesis of ZSM-type zeolites are identified in Table 18.^{33,34,54-78} The nomenclature and chemical formulae for these organic cations are presented in Tables 19 and 20. Many of these zeolites are structurally related.

Synthesis of Zeolite ZSM-5

Zeolite ZSM-5 was originally prepared from reaction mixtures containing tetrapropylammonium ions.³⁰ Other organic bases, for example, other quaternary ammonium ions,^{79,80} primary and secondary amines,⁸¹ diamines,^{92,93} alcohols⁸⁴ were also used for the preparation of ZSM-5. Numerous other compounds, representative of a wide variety of functional groups,⁸⁵⁻⁸⁸ have been claimed to be effective for preparation of ZSM-5 zeolite under suitable conditions. It is also possible under certain circumstances to crystallize ZSM-5 from reaction mixtures in the absence of an organic base.^{84,87,88}

Zeolite ZSM-5 can also be synthesized in the presence of a tetraureacobalt (II) complex with a specifically defined reaction mixture. Depending on the ratio of tetraureacobalt (II) complex to silica in the zeolite synthesis reaction mixture, the crystalline product consists of highly twinned rectangular prismatic crystals exhibiting extreme uniformity in size from about 5 x 10 microns to about 10 x 20 microns.⁸⁹

Zeolite ZSM-5 can also be prepared containing an outer aluminum-free shell by increasing the hydroxide content or by reducing the organic cation concentrations, i.e., the template ion to SiO₂ ratio. The outer shell is essentially SiO₂ that has crystallized on the zeolite surface in the ZSM-5 type configuration. This preparation technique leads to a more selective catalyst for the production of p-xylene.⁹⁰

Table 18**Organic Cations Used in the Synthesis of ZSM-Type Zeolites**

Zeolite	Cations	Si/Al	Type	Reference
ZSM-4	Na, TMA or P or C	1.5-10		54
ZSM-5	Na, TPA	>6	Pentasil	30,31
ZSM-6	TMACl	13-150		55
ZSM-8	Na, TEA	5-100		56
ZSM-10	K, DDO	2.5-3.5		57
ZSM-11	TBP, BTPP, TBA	10-45	Pentasil	58
ZSM-12	Na, TEA	10-100		59,60
ZSM-18	Na, HMBTP	<50		61
ZSM-20	Na, TEA	3.5-5	Faujasite	62
ZSM-21	Na, ED, P, C	4-25	Ferrierite	63
ZSM-23	Na, P	12-55		64
ZSM-25	Na, TEA	3-5		65
ZSM-34	Na, K, TMA	4-10	Offretite/Erionite	66
ZSM-35	Na, P, ED	4-25	Ferrierite	67
ZSM-38	Na, C	4-25	Ferrierite	68
ZSM-39	TC, P	>20		69
ZSM-43	Cs, C	5-8		70
ZSM-47	TMACl	8-25		71
ZSM-48	Na, C ₃ -C ₁₂ ADA	>75		72-77
ZSM-51	TMPP or DMPP	>30		78

Table 19**Nomenclature for the Organic Cations Used
in the Synthesis of ZSM-Type Zeolites**

TMA	Tetramethylammonium
TPA	Tetrapropylammonium
TEA	Tetraethylammonium
DDO	[1,4-Dimethyl-1,4-diazabicyclo (2,2,2) octane] ²⁺
TBP	Tetrabutylphosphonium
BTPP	Benzyltriphenylphosphonium
TBA	Tetrabutylammonium
HMBTP	1,3,4,6,7,9-Hexahydro-2,2,5,5,8,8-hexamethyl-2H-benzol[1,2-C:3,4-c ¹ ;5-6-C] tripyrolium
ED	Ethylenediamine
P	Pyrrolidine
C	Choline
TC	Tetraurea Co(II)
ADA	n-Alkyl-diamine

Table 20

**Chemical Formulae of the Organic Cations Used
in the Synthesis of ZSM-Type Zeolites**

TMA	$(\text{CH}_3)_4\text{N}^+$
TPA	$(\text{C}_3\text{H}_7)_4\text{N}^+$
TEA	$(\text{C}_2\text{H}_5)_4\text{N}^+$
DDO	$(\text{C}_8\text{H}_{18}\text{N}_2)^{2+}$
TBP	$(\text{C}_4\text{H}_9)_4\text{P}^+$
BTPP	$\text{C}_6\text{H}_5\text{CH}_2(\text{C}_6\text{H}_5)_3\text{P}^+$
TBA	$(\text{C}_4\text{H}_9)_4\text{N}^+$
HMBTP	$\text{C}_6(\text{C}_2\text{H}_4\text{N}(\text{CH}_3)_2)_4^{3+}$
ED	$\text{NH}_2(\text{CH}_2)\text{NH}_2$
P	$\text{NH}(\text{CH}_2)_4$
C	$(\text{CH}_3)_3\text{N}(\text{CH}_2)\text{OH}$
TC	$((\text{NH}_2)_2\text{CO})_4\text{-Co(II)}$
ADA	$\text{NH}_2(\text{CH}_2)_n\text{NH}_2$

Derouane et al.⁹¹ reported two different crystallization processes for the formation of ZSM-5 crystals. In process A, a limited number of ZSM-5 nuclei are formed at the expense of an amorphous aluminum-rich gel phase. The nuclei grow slowly by a liquid-phase ion transport mechanism by incorporating TPA which may serve as a template during the growth process. In process B small X-ray amorphous ZSM-5 aggregates appear very early in the crystallization process followed by formation of X-ray crystalline ZSM-5 due to a solid to solid phase transformation mechanism.

Zeolites having a structure intermediate between ZSM-5 and ZSM-11 can be synthesized in the presence of tetrabutyl-ammonium cation at temperatures of 423 - 448 K.^{56,92} Jablonski et al.⁹³ indicated that ZSM-5/ZSM-11 intergrowth structures can be synthesized from reaction mixtures with the mole oxide ratio: $4.5(\text{TBA})_2\text{O} : 14.7\text{Na}_2\text{O} : \text{Al}_2\text{O}_3 : 173.4\text{SiO}_2 : 2452\text{H}_2\text{O} : 9\text{Br}$. X-ray powder diffraction and selected area electron diffraction were used to identify the intergrowth structures.⁹⁰⁻⁹³

Doelle et al.⁹⁴ reported that the hydrogen form of Zeolite ZSM-5 can be prepared using 1,6-hexanediamine (C6DN) as the organic cation from a sodium-free gel, which after heating in air at 823 K gives the hydrogen form directly without an intermediate ion exchange step.

Synthesis of Zeolite ZSM-48

Zeolite ZSM-48 can be prepared from a reaction mixture containing a source of silica, optionally alumina, alkali metal oxide, water, and RN (RN is a $\text{C}_1\text{-C}_{20}$ organic compound having an amine functional group of $\text{pK}_a \geq 7$).⁷²⁻⁷⁷ In preparing the highly siliceous form of ZSM-48 no alumina is added. Thus the only aluminum present occurs as an impurity introduced into the reactant mixture.

The preparation of crystalline zeolite ZSM-48 requires the silica/alumina mole ratio of reaction mixture to be at least 500 to avoid product contamination with other silicates, notably crystalline silicates ZSM-5 or ZSM-11. Valyocsik⁷⁸ indicated that the silica/alumina mole ratio of the reaction mixture can be much less than 500 (e.g., as low as 180 or less) and still produce relatively pure ZSM-48 if a different organic template (bis(N-methylpyridyl)-ethylinium compound) is used.

High crystallinity zeolite ZSM-48 was prepared from a reaction mixture containing the organic cation, pyrrolidine, by Suzuki et al.⁹⁵ The scanning electron microscope image of the ZSM-48 crystal indicated a rod-like structure 0.2 - 0.4 μm in width and 3 - 5 μm in length.

Factors Affecting the Synthesis of the ZSM Family of Zeolites

Zeolite crystallization is believed to be a nucleation-controlled process from a reaction mixture containing alkaline aqueous gels at temperatures between 353 and 523 K. The primary influences of the reaction mixture compositions in zeolite synthesis were reported by Rollmann:⁹⁶ (1) framework composition is affected by the $\text{SiO}_2/\text{Al}_2\text{O}_3$ ratio; (2) crystallization mechanism is affected by the $\text{H}_2\text{O}/\text{SiO}_2$ ratio; (3) structure and cation distribution are affected by the Na^+/SiO_2 ratio; and (4) framework aluminum content is affected by the $\text{R}_4\text{N}^+/\text{SiO}_2$ ratio. Generally, addition of the organic cation to a reaction mixture used in zeolite synthesis may affect changes on zeolite structure, crystallization rate, chemical composition, and microscopic texture.^{53,96} The organic cation (R_4N^+) is thought to function as a hydroxyl ion donor because of its basicity. The organic cation may also increase the solubility of the aluminate or silicate ions. It has also been postulated that the organic cation serves to organize the water molecules.^{52,53,97-99}

Substitutes in the Framework of the ZSM Family of Zeolites

Introducing other atoms to replace aluminum and silicon in the framework of known zeolites has been widely studied. Such efforts could result in new zeolite structures with unique pore channels and cage systems that could result in the synthesis of new catalyst systems which could promote novel reactions.

Framework substitutes such as B, Ga, Fe, Cr, As, and V in the synthesis of pentasil zeolites have been recently reported.⁵² A number of investigators¹⁰⁰⁻¹⁰⁴ have prepared a material having a ZSM-5 structure in which boron atoms are claimed to be the zeolitic framework. Evidence for this substitution has been given by Taramasso et al.¹⁰⁰ from measurements of the size of the unit cell, and by Gabelica et al.¹⁰⁴ from magic angle spinning NMR (MAS-NMR) data. It should be noted that metal-containing zeolites must be subjected to careful study to identify the location and type of interaction with the zeolite framework structure, that is, to insure that the atom is actually in the framework and not sited on top of an aluminium atom in the framework.

Modification of Shape Selective Zeolites for Catalytic Use

Most industrial reactions are acid catalyzed reactions. Thus it is necessary to modify the synthetic zeolites to introduce the acidic catalytic sites as well as to improve the thermal and chemical properties. The zeolite catalysts can be modified by treatment in the following ways: (1) ion exchange, (2) thermal and hydrothermal treatment, (3) chemical modification, and (4) metal loading.

Ion Exchange

The synthetic routes for preparing zeolites usually result in final products containing a substantial amount of alkali metal ions. The alkali metal cations can be replaced by other cations.

Most zeolite preparation schemes include an ammonium ion exchange if the end result is intended to be a catalyst. The concept is to exchange the alkali cations for ammonium ions and then generate the hydrogen or acidic form of the zeolite by thermal decomposition. The rate and degree of ion exchange strongly depend on factors such as the nature of the zeolite, the type and nature of the cation to be exchanged, and the reaction condition for the ion exchange process. Higher degrees of exchange can usually be obtained by batchwise repetition of the exchange procedure.

Direct proton exchange requires the use of solutions with a higher proton concentration such as dilute acid. However, since most zeolites are acid sensitive, the potential applications of direct proton exchange are limited. The stability of zeolites to acid increases with increasing silica/alumina ratio. Hence high silica zeolites are more suitable for ion exchange with dilute acid.

Thermal Treatment

Ammonium exchange of zeolites and the subsequent thermal decomposition is an important activation procedure for many commercial catalysts. The thermal treatment of the ammonium exchanged zeolites is usually conducted at temperatures ranging from 700 to 950 K.

An informative study on H-form zeolites¹⁰⁵ using differential thermal analysis indicated that the first observation on heating is the loss of physically bound water, resulting in an endotherm near 423 K. Next, an endotherm is observed near 923 K corresponding to final dehydroxylation. High temperature treatments may result in structural collapse.

Chemical Modification

The dealumination of a zeolite without destruction of the zeolite structure by treating with SiCl_4 has been reported by Beyer and Belenykaja.¹⁰⁶ They claimed that the aluminum atoms in

the framework of NaY were replaced by silicon atoms. Klinowski et al.¹⁰⁷ have confirmed this type of dealumination by ^{29}Si -NMR spectroscopy using the sodium-form of mordenite. The dealumination of ZSM-5 with silicon tetrahalides has also been reported by Chang.¹⁰⁸ Namba et al.¹⁰⁹ found that the aluminum atoms on the external surface of ZSM-5 crystallites were removed more selectively than those in the pores by treating NaZSM-5 zeolite with silicon tetrahalide vapors at 723-923 K.¹⁰⁹

Metal Loading

It is often necessary to incorporate additional active components in a catalyst to accomplish the required catalytic transformation from reactants to products in many industrial processes. Such components are frequently metals, metal oxides, or metal sulfides similar to those used in non-zeolite or amorphous oxide catalyst systems. Metals can be loaded in zeolite containing catalysts in several ways including ion exchange of the zeolite from solution, impregnation from solution, adsorption from the gas phase, and comulling during catalyst formation of the solid metal component or its solution.

Metals such as nickel, cobalt, silver, iron, and chromium can be directly exchanged from aqueous solutions of their salts such as nitrates, chlorides, acetates, and the like. Many of these can also be introduced as the amine complex ion. Palladium and platinum that normally exist in solution as negative ions (PdCl_2^{2-}) must be converted into a positive ion before they can be incorporated. Formation of the positively charged tetramine complex from the palladium salts occurs readily in aqueous ammonia to give the $\text{Pd}(\text{NH}_3)_4^{2+}$ ion. Platinum forms a similar complex. When the exchange capacity of the zeolites is low, e.g., high-silica zeolites and molecular sieves such as silicalite and aluminum phosphates, other methods, such as impregnation, must be used.

Characterization of Zeolites

X-ray Diffraction

Crystal structure determination using X-ray powder data has played an important role in the development of the science and technology of zeolite molecular sieves and catalysts since the advent of synthetic zeolites. Crystallization mechanisms, modification processes, molecular sieve properties and catalytic behavior can be properly understood if the complete crystal structure is known.

Identification of zeolites can be carried out on the basis of X-ray diffraction. Powder patterns are the common method by which the crystallinity of a zeolite can be determined.¹¹⁰ If a pattern shows no evidence for crystalline or amorphous contaminants, purity is estimated by the comparison of the intensities of reflections at d-spacings smaller than about six Angstroms with those of a highest purity sample of similar composition and crystal size. Quantitative analyses are much more difficult to conduct because there is no absolute 100 percent crystalline zeolite standard. Thus percent crystallinity can only be compared to an arbitrarily defined standard.

Microanalysis

Many techniques in the field of electron optical instrumentation are available to provide information concerning crystal shape and size and as well as other characteristics of zeolites.^{111,112} One of the most important techniques applied in zeolite research is transmission electron microscopy (TEM). Scanning electron microscopy (SEM) used in conjunction with scanning microprobe analysis yields a great deal of information on zeolites.¹¹³

Scanning Electron Microscopy: In scanning electron microscopy an electron probe is used to scan the surface of a specimen using deflection coils. The interaction between the primary beam

and the specimen produces various signals from back scattered electrons, secondary electrons, X-rays, etc. which may be utilized to form an image of the surface. The appropriate signal is detected, amplified, and displayed on a cathode-ray tube screen scanned synchronously with the beam. One important advantage of SEM is that less stringent specimen preparation requirements are necessary and this permits samples to be examined in a largely unaltered state, since only a conducting surface layer is required. Magnification in the range 20-50000 times is normally available with a resolution down to 100 Å. Zeolite samples are usually covered with a thin film of gold to ensure sufficient electrical conductivity the sample so as to prevent the build-up of a surface charge which leads to distorted image pictures. The gold film also serve to protect heat sensitive samples during analysis.

The back-scattered electrons give a signal varying with the respective atomic number of the probing metal species. Measuring the wavelength of the induced characteristic X-ray radiation with special detectors permits elemental analysis of the surface region upon which the beam is focused. This technique is known as electron microprobe analysis. Ballmoos and Meier¹¹⁴ have studied the distribution of silicon and aluminum in ZSM-5 crystals using the microprobe analysis method. These results are very important in explaining the mechanism of crystallization of the zeolites. The rate of nucleation and crystal growth increases with the silicon content. Furthermore, microprobe analysis has also helped to explain the catalytic activity of zeolites by measuring the number of active centers within the channel system which is a function of the silica-to-alumina ratio.^{114,115}

Transmission Electron Microscopy: Transmission electron microscopy can achieve resolutions of about 3 Å at a magnification of approximately 10^6 . The resolution can be improved by using special imaging techniques known as bright field, dark field, or lattice imaging. The surface scanning technique and the analysis of the characteristic X-ray radiation can also be applied

in the transmission mode, that is, scanning transmission electron microscopy (STEM). This method has the advantage of better resolution as compared with TEM, but has the disadvantage of difficult sample preparation.¹¹³

Lyman et al.¹¹⁶ indicated that particles of ZSM-5 with different silica-to-alumina ratio may have different chemical profiles across the particle. The technique employed was X-ray emission spectroscopy in the STEM. Small particles, silica-to-alumina ratio of 10, indicated either enrichment of silicon near the surface or a near homogeneous composition. Large particles, $\text{SiO}_2/\text{Al}_2\text{O}_3$ ratio of 40, exhibited more aluminium near the particle surface than in the center.

Thermal Desorption

The acid strength of zeolites can be determined by measuring the heat of adsorption or desorption of a suitable probe molecule. Ammonia meets the requirements for such a probe¹¹⁷⁻¹²⁰. Firstly it is small enough to enter all the zeolite pores. Secondly it can react both with the Brönsted and Lewis acid sites. Pyridine is much less suitable with regard to the first requirement. Derouane and co-workers¹¹⁸ have indicated that the concentration of active acidic sites in ZSM-5 is related to the aluminum content of the zeolite and presumed these sites are located at channel intersections. These sites are characterized by an ammonia desorption band near 773 K. Weaker acidic sites are characterized by a desorption band at about 500 K. These weaker sites probably correspond to terminal silanol groups on the external surface of the zeolite or possibly nonzeolitic impurities. However, Haag¹²¹ has reported that a single type of acid site was observed using ammonia temperature-programmed desorption. A single desorption band with a maximum temperature of 673 K was found. If the zeolite is exposed to excess ammonia vapor, three desorption bands are observed and are erroneously thought to indicate the presence of three types of acid sites on zeolite ZSM-5.¹¹⁷⁻¹²⁰

Vibrational Spectroscopy

Vibrational spectroscopic techniques can furnish direct information about the nature of surfaces and adsorbed surface species. These techniques provide information on a molecular level. During the last decade there has been increasing recognition that infrared spectroscopy can yield information not only on short range bond order and characteristics but on long range order in crystalline solids caused by lattice coupling.

Flanigen et al.¹²² have indicated that the mid-infrared vibrations can be classified into two types, named internal and external vibrations. The internal vibrations, including asymmetric stretch ($1250\text{-}950\text{ cm}^{-1}$), symmetric stretch ($720\text{-}650\text{ cm}^{-1}$), and T-O (TO_4 -tetrahedra, T denotes silicon or aluminum atom) bend ($500\text{-}420\text{ cm}^{-1}$), are present in the spectra of zeolites with small changes in absorption frequencies regardless of the type of the framework of the zeolite. The external vibrations depend on the structure of zeolites and are assigned to linkages of the TO_4 -tetrahedra typical for a special framework topology. Groups of this kind are the pore opening ($420\text{-}300\text{ cm}^{-1}$) and double rings ($650\text{-}500\text{ cm}^{-1}$), present in a great variety of zeolites and also the various polyhedral units.

The crystal structure of a ZSM-type zeolite has been studied by X-ray diffraction and infrared spectroscopy. Although the X-ray diffraction pattern of the small ZSM-5 zeolite crystal is characteristic of an amorphous material, the infrared spectra along with catalytic measurements indicated that the material behaved like crystalline ZSM-5.¹²³ The results have been interpreted in terms of the presence of the small ZSM-5 zeolite crystals (diameter less than 80 \AA) in an amorphous matrix.

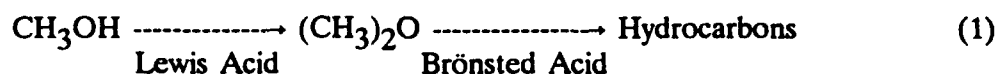
Recently diffuse reflectance spectroscopy has been applied to the study of high silica zeolites. This technique is much more sensitive in comparison with the standard transmittance

infrared spectroscopy. Kanzansky et al.¹²⁴ carried out the measurements on ZSM-5 in the near infrared region, which includes fundamental stretching vibrations of O-H bonds, their overtones and combinations of stretching and bending vibrations. They provided evidence for the similarity of Brönsted and Lewis acidic sites in high silica ZSM-5 and provided an interpretation of the difference in their catalytic activities by shape selectivity effects or by the difference in the concentration of acidic active sites.

Ammonia temperature programmed infrared spectroscopy can provide useful information about the assignment of the different temperature programmed desorption bands. Lok et al.¹²⁵ indicated that the infrared spectrum for ZSM-5 shows two sharp bands at 3740 and 3610 cm^{-1} and a broad band around 3475 cm^{-1} . They noted that the only change in the infrared spectrum during thermal desorption of ammonia from ZSM-5 is the reappearance of a small portion of the 3610 cm^{-1} band. Therefore, the ammonia desorption from ZSM-5 below 528 K is primarily due to physically adsorbed ammonia.

An infrared spectroscopic study of simple alcohols adsorbed on ZSM-5¹²⁶ was in agreement with the results from thermal desorption spectroscopy:¹²⁷ each of the alcohols adsorbs in the vicinity of the aluminium atoms, as evidenced by the disappearance of the hydroxyl band associated with the hydrogen cations.

Furthermore, the comparison of sequences of site populations with observed reactivities on ZSM-5 suggests that Lewis sites are the origin of catalytic activity in the conversion of CH_3OH to $(\text{CH}_3)_2\text{O}$.¹¹⁷ Similar comparisons also indicate that dealuminated Brönsted sites are the principal source of reactivity for the conversion of $(\text{CH}_3)_2\text{O}$ to hydrocarbons.^{128,129} Active acidic sites involving in methanol conversion can be expressed according to the following simplified reaction scheme:



Acid properties of NaHZSM-5 zeolites of various degrees of exchange have been studied by quantitative infrared studies of pyridine adsorption.¹³⁰⁻¹³³ Two kinds of Brönsted acid sites were detected, OH groups vibrating at 3609 cm⁻¹ being strong acid sites and other protonic sites (3740 cm⁻¹) of lower acidity. The concentration of acid sites (determined by infrared spectroscopy) was found to be equal to the concentration of protons introduced into zeolite by ion exchange.^{134,135} These results indicate that the introduction of protons into the zeolite does not acidify weaker sites preexisting in the zeolite before ion exchange.

Solid State NMR

NMR spectra can provide information on the bonding of atoms to the silicon and aluminum in the structure and distinguish between different types of species such as Si-4Si, Si-3Si1Al, Si-2Si2Al, Si-1Si3Al, and Si-4Al in the zeolite lattice and external to the lattice structure. The key is the development of the magic angle (54°44') spinning NMR for the measurement of chemical shift in solid samples. The chemical shift values are characteristic of crystallographically and chemically distinct environments.

Correlations between chemical shift and structure were established,¹³⁶ and used^{137,138} in structural studies of both soluble and insoluble silicates and aluminosilicates. The structure of a wide variety of zeolitic solids has been investigated¹³⁷⁻¹⁴⁹ using ²⁹Si, ²⁷Al and several other nuclei.

Kinetic Characterization

α -Test: The catalytically active centers in the H-form of ZSM-5 are believed to be Brönsted acid sites, i.e., bridging hydroxyl groups associated with framework aluminum atoms. The number of catalytically active acidic hydroxyl groups is equal to the aluminum content, if all the aluminum atoms are in tetrahedral framework positions and if they are not poisoned.

The cracking of n-hexane provides a suitable quantitative test reaction for measuring the acidity of a catalyst. At a given temperature the magnitude of the rate constant, k , is obtained from the equation $k = (1/t) \cdot \ln\{1/(1-\epsilon)\}$, where k is the first order rate constant, ϵ is the fractional conversion and t is the contact time.¹⁵⁰ The rate constant for cracking is expressed in α -units, $\alpha = 1$ being the value of a high activity amorphous $\text{SiO}_2/\text{Al}_2\text{O}_3$.^{151,152} Haag et al.¹²¹ indicated that the hexane cracking activity over HZSM-5 is strictly proportional to the aluminum content over more than three orders of magnitude, extending down to aluminum contents in the parts per million range. Extrapolation of the data on a linear plot gave zero activity at zero aluminum content.^{121,153} A similar linear relationship was also observed between the α -value and the intensity of the NMR signal due to tetrahedral aluminum.¹²¹

Isobutane Isomerization: The isomerization of isobutane which proceeds by a bimolecular mechanism over large-pore zeolites has been used as a probe reaction to study the channel structure of the pentasil zeolites.^{154,155} The product stream contains propane and pentanes in addition to n-butane over mordenite. In zeolite ZSM-5, there is not enough space in the channel intersection for a bimolecular transition state. As a consequence, pentanes are not present in the products of the reaction.¹⁵⁶ This suggests a mono-molecular mechanism. Haag and Dessau¹⁵⁷ indicated this monomolecular transition state involves a pentavalent carbonium ion intermediate.

Surface Area Measurement: Various means have been used to measure surface areas for molecular sieve zeolites including the BET method. However, the BET method gave much lower results than other techniques. The use of the Langmuir isotherm may be the more appropriate method. A simplified method can be used in which V_m (volume of a monolayer of gas adsorbed) is measured at a low relative pressure on the order of 0.02.

External surface area measurements are of importance in understanding the catalytic activity and adsorption properties, since the external surface contributes only to nonselective reaction or adsorption processes.¹⁵⁸ The external surface area of molecular sieve zeolites has been measured by (a) the filled-pore method,¹⁵⁹⁻¹⁶¹ (b) modified BET method using large molecules, or (c) electron microscopy. The shape and size of the zeolite crystals can be measured by SEM; however, the external geometric surface area can be calculated only when the crystals are discrete and relatively homogeneous. Benzene or n-hexane, thought to diffuse freely within the pentasil frameworks, can access all the active surface. Thus the external surface area can be measured by the BET method when the pores are filled with benzene or n-hexane so as to exclude the adsorptive from the internal surface of the zeolite.

Intracrystalline Diffusion in Zeolites

When porous materials are exposed to the gas phase, two well-known regimes are defined in classical diffusion theory. One is the ordinary diffusion regime for which the mean free path of the gaseous molecule is smaller than the pore size of the porous material. It turns out that the diffusivities are equal to the ordinary gaseous diffusion coefficients reduced by the porosity. As the pore size becomes smaller than the molecular mean free path, there is a transition to the Knudsen diffusion regime, where the diffusivity is inversely proportional to the pore dimension.

Crystalline zeolites with their regular, rigid, and defined void structures have introduced a third regime. Weisz¹⁶² has termed it as the configurational diffusion regime. Here, intracrystalline diffusion is affected by the matching of the shape, size, and configuration of the diffusing gas to the corresponding parameters of the zeolite framework. It is believed that this type of intracrystalline diffusion plays a major role in shape selective zeolite catalysis. The rate of the shape selective catalysis might be expected to be controlled by the rate of diffusion rather than by any catalytic phenomenon.^{163,164}

Molecules with sizes similar to or slightly larger than the zeolite pores can usually diffuse through the pore structure due to the molecular vibrations (molecular shape and configuration can change in time) or breaching of the zeolite pores (bond cleavage followed by reconstruction of the bond).²⁰

The size, charge, position in the zeolite framework, and concentration of the exchanged ions may influence the diffusion characteristics of the zeolite framework. The geometry and dimensions of the channel network and crystal shape of the zeolite may also govern diffusion in zeolites.

Shape Selective Zeolite Catalysis

Types of Shape Selective Zeolite Catalysis

Shape selective catalysis using zeolites is based on the locus of active catalytic sites in the intracrystalline pore system, which is very uniform in one or more discrete dimensions. Therefore, shape selectivity may be achieved by virtue of geometric factors, Columbic field interaction, and difference in diffusion rate.¹⁶⁵ Molecular shape selective catalysis can be divided into several major classes: reactant selectivity, product selectivity, restricted transition state selectivity, and molecular traffic control.^{38,155,166,167}

Reactant Selectivity: Reactant or charge selectivity occurs when some of the molecules in a reactant mixture are too large to be able to diffuse freely within the intracrystalline volume of the zeolite because of diffusion constraints, selective sorption, or molecular sieving effects.

Product Selectivity: Product selectivity occurs when the products of the reaction formed within the pores are too bulky to diffuse to the exterior surface of the catalyst where they can be observed. The bulky molecules are either converted to less bulky molecules by cracking or equilibration or deactivate the catalyst by blocking the pores.

Restricted Transition State Selectivity: Restricted transition state molecular shape selectivity occurs when local configuration constraints prevent or limit the formation of a given transition state. Reactions requiring smaller transition states proceed unhindered. Neither reactant nor product molecules is prevented from diffusing through the pores.

An example is the high selectivity of the zeolite ZSM-5 based xylene isomerization process.¹⁵⁵ The ratio of the rate constants for the bimolecular disproportionation to trimethylbenzene and toluene compared with the isomerization to other xylenes ($k_{\text{isom}}/k_{\text{disp}}$) is higher for ZSM-5 than that for HY or H-Mordenite zeolites by 10 - 100 times. It is clear that the narrower pore zeolites restrict the bimolecular reaction due to steric hindrance.

Molecular Traffic Control: The concept of molecular traffic control shape selectivity developed from studies of single component adsorption measurement in ZSM-5 type zeolites.¹⁶⁸ As discussed previously, zeolite ZSM-5 has two types of channel systems, one system is sinusoidal whereas the other is straight. It was observed that molecules such as p-xylene and 3-methylpentane are restricted to the straight channel whereas linear molecules such as n-pentane and n-hexane can diffuse easily through both types of channels. This has led to the proposal that reactant molecules

may enter zeolite ZSM-5 preferentially through one set of channels and the products leave the zeolite by a different set thus minimizing counter diffusion. The general concept of molecular traffic control still requires definitive experimental evidence before it is generally accepted. Reactions that may exhibit molecular traffic control selectivity include benzene alkylation with ethylene and toluene alkylation with methanol over ZSM-5.¹⁶⁹ The higher activity of p-xylene alkylation by methanol in ZSM-11 compared with ZSM-5 may also be due to molecular traffic control.¹⁷⁰

Coking on Shape Selective Zeolite Catalysts

The formation of coke is often acid-catalyzed and it is therefore a major concern when using acidic zeolite catalysts. Understanding the mechanisms that control coking, and its effect on catalytic properties such as selectivity and activity, is essential for catalyst selection and process design.

The low rate of deactivation of ZSM-5 in a number of industrial processes has been attributed to the dimensions of the pores that sterically hinder the formation of coke precursors or intermediates and to the relatively low density of acid sites.¹⁷¹⁻¹⁷⁷ Generally, zeolites with noninterconnecting uniform channels or noninterconnecting nonuniform channels will age more rapidly than their counterparts with interconnecting channels or cages. Interconnected pore networks offer a greater number of pathways to the active sites through which molecules can diffuse randomly, thereby decreasing the number of active sites in the blocked pore. The occurrence of cages in noninterconnecting or interconnecting networks provides room to accommodate initial coke formation without immediate blocking of the pores. These deposits may grow to a size greater than the pore or window aperture, leading to a situation in which the catalyst cannot be regenerated under mild conditions.^{175,176} A qualitative description of aging by

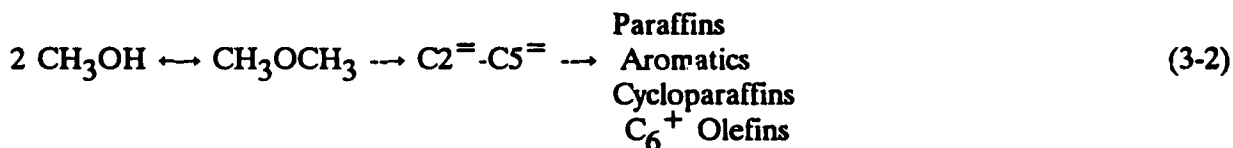
pore blockage has been proposed for the case of increasing coke content.¹⁷⁶ The effect of pore mouth blockage is to reduce the rate of entrance of reactants into the crystallites, to increase the tortuosity of diffusion paths to and from the active sites, and to reduce the intrinsic number of accessible sites.¹⁷⁸ The effects of coking modes, pore mouth restriction and bulk restriction (internal coking) are to reduce the diffusivity of reactant and product molecules as a result of the reduction of the effective diameter of the pore.¹⁷⁵

Applications of Shape Selective Zeolite Catalysts in Industrially Significant Processes

Methanol-to-Gasoline Process

A large variety of acidic catalysts can be used for the conversion of methanol to hydrocarbons.¹⁶ The use of zeolite ZSM-5 as an acid catalyst^{17,38,155,179-202} is particularly attractive as it offers a new and variable route for the direct production of high-grade gasoline from methanol which can be produced from coal or natural gas. The shape selective properties of ZSM-5 catalysts are the basis for the Mobil Methanol-To-Gasoline (MTG) process. Among the advantages of ZSM-5 catalyst are the following: it forms less coke than the other catalysts due to transition state selectivity, and it produces hydrocarbons in a rather narrow compositional range. The MTG processes capable of converting methanol to hydrocarbons and water: the maximum hydrocarbon yield is 44 wt. percent with the balance, 56 wt. percent, being water. Hydrocarbons produced over ZSM-5 include paraffins (60-67 percent), olefins (6-8 percent), and aromatics (27-32 percent).

The methanol reaction over ZSM-5 catalyst involves a series of consecutive steps. Chang and Silvestri¹⁹⁰ proposed that the reaction associated with the production of gasoline boiling range hydrocarbons proceeds according to the following simplified reaction scheme:



Methanol is converted first to dimethylether (DME). This step is very much faster than the subsequent steps. The reaction pathway that accounts for the first C-C bonds formed from methanol or DME, i.e., the creation of a covalent bond between two C₁ units to form a C₂ species, is still unresolved. The species involved in this step is probably a cationic C₁ fragment, and the product is most likely ethylene, or possibly propylene. This initial olefin is further converted to longer aliphatics that later cyclize, dehydrogenate to form aromatics that are alkylated by methanol or shorter olefinic intermediates. These reactions stop at durene because there is no space to form larger polyalkyl-aromatics at ordinary processing conditions. It should be noted that durene formation can be minimized by controlling catalyst and process conditions.²⁰³ Additional research has shown that variations in operating conditions and catalyst modification can selectively produce specific hydrocarbon classes.¹⁶

Methanol-to-Olefins and Distillates

The methanol conversion process can be modified to produce light olefins (MTO) before the C₂ - C₄ olefinic intermediates are converted to higher molecular weight paraffins and aromatics by using a low acidity ZSM-5.²⁰⁴ Pentasil borosilicate zeolites and pentasil aluminosilicates treated with HF have also been reported to be effective in the MTO process.²⁰⁵ The borosilicate catalysts are less active than the aluminosilicate ones and convert methanol to propylene. The fluoridated aluminosilicate pentasil converts methanol to ethylene.

The Mobil Olefins-to-Gasoline and Distillates (MOGD) process converts light olefins to a whole range of liquid products. The products are either gasoline or jet and diesel fuels or even No. 2 fuel oil. Approximately 100 percent high quality gasoline in the "gasoline mode" and 80 - 90 percent jet and diesel fuels plus 10 - 20 percent gasoline in the "distillate" mode can be produced in the MOGD process.²⁰⁶

Middle Distillate and Lube Oil Dewaxing

Middle distillate and lube oil dewaxing processes are based on the principle that long-chain linear and slightly branched hydrocarbons are selectively hydrocracked from the feedstock. Thus the concentration of linear paraffins is reduced and the pour point, cloud point, and freeze point of the product liquids are decreased. The reductions in these properties are related to the fact that linear and slightly branched hydrocarbons have higher melting points than highly branched hydrocarbons and hence give rise to higher pour, cloud and freeze points. Shape selective catalysts can remove the normal paraffins without appreciable conversion of the other components.²⁰⁷

Hydrowaxing processes remove waxy paraffins from intermediate and heavy gas oils (diesel fuel and heating oils) and lube oil base stocks by converting them to gasoline and LPG fractions. The Mobil distillate and lube oil dewaxing processes²⁰⁸⁻²¹¹ use HZSM-5 catalyst. The catalyst may contain a hydrogenation component such as Ni, Zn, or Pt. The catalyst in the similar British Petroleum Process is platinum supported on hydrogen mordenite.²¹²

The middle distillate dewaxing process (MDDW) developed by Mobil is a fixed bed process.²¹⁰ The process decreases the pour point of the product by 30 - 40 K. The by-product gasoline has a relatively high octane number and therefore it may be added to the gasoline pool without further reforming.

Reforming Process

The Mobil Selectoforming process,²¹³ developed in the mid-sixties, introduced an additional processing step to the usual reforming process in which the low octane paraffins are selectively removed by hydrocracking to propane and light gases. The catalyst (erionite) could be placed in the bottom of the last reforming reactor or in a separate reactor.

M-forming,²¹⁴ developed by Mobil Oil Corporation, is more sophisticated than Selectoforming. The process is basically the same with the catalyst being changed from erionite to ZSM-5. The ZSM-5 catalyst can admit singly branched paraffins as well as simple aromatics such as benzene and toluene. The larger channel size permits the removal of the second lowest octane components, the single branched paraffins, by hydrocracking. Furthermore, the aromatic species are alkylated by the olefinic component of the cracked product. The alkylaromatics contribute to octane number and reduce the loss of cracked products to gas, thus increasing the liquid yield.

Alkylation of Aromatics

Benzene Alkylation

Alkylation of benzene with ethylene yields ethylbenzene followed by the dehydrogenation process to produce styrene. The Badger-Mobil vapor phase ethylbenzene process uses ZSM-5 catalyst.²¹⁵ The process relies on the unique shape selective properties of ZSM-5 catalyst. Multiple beds of catalyst are used with benzene and ethylene being added between the beds for temperature control.

Toluene Alkylation

Toluene can be alkylated with ethylene to give ethyl-toluene over ZSM-5 catalyst. The desired p-ethyltoluene is formed preferentially because the catalyst can direct the reaction based on the very small difference in the molecular dimensions either by rate of formation (controlled by transition state selectivity) or rate of diffusion out of the pores.

Techniques for modifying the pore openings of the ZSM-5 catalyst by means of phosphorus,²¹⁶ boron,²¹⁷ and magnesium²¹⁸ have been reported. It is noted that production of o-ethyltoluene, the largest isomer, was essentially eliminated. The selectivity for p-ethyltoluene is significantly improved with these catalysts.

The formation of p-xylene in excess of equilibrium values from toluene alkylation with methanol has been reported over a phosphorus or magnesium modified ZSM-5.^{219,220} Although all three isomers are formed at equilibrium concentrations within the pore structure, the p-xylene can diffuse out of the catalyst approximately 10^4 times faster than the other isomers thus shifting the equilibrium within the catalyst pore structure in favor of p-xylene.

Toluene Disproportionation

Toluene disproportionation, the transalkylation of two moles of toluene to one mole each of xylene and benzene, has been practiced commercially for a number of years.^{211,220-222} The catalyst is ZSM-5. Toluene can be converted with high selectivity to benzene and xylene.²²³ Shape selectivity of the catalyst also helps to minimize coking and the formation of higher molecular weight hydrocarbons.

Xylene Isomerization

The xylene isomerization process is the conversion of m- and o-xylenes to p-xylene.^{224,225} Zeolite ZSM-5 has been applied to this reaction in which it should be possible to influence the direction of the reaction by modifying the pore structure. Modifications of the pore structure by incorporation of boron, magnesium, phosphorus, antimony or by controlled coking can be expected to improve the product distribution due to shape selective effects.^{155,226-228} Improvements on the commercial process by steaming the ZSM-5 or adding alkali ions or by using higher $\text{SiO}_2/\text{Al}_2\text{O}_3$ ratio zeolites have also been reported.²²⁹

Preparation of Zeolites ZSM-5 and ZSM-48

Preparation of Zeolite ZSM-5

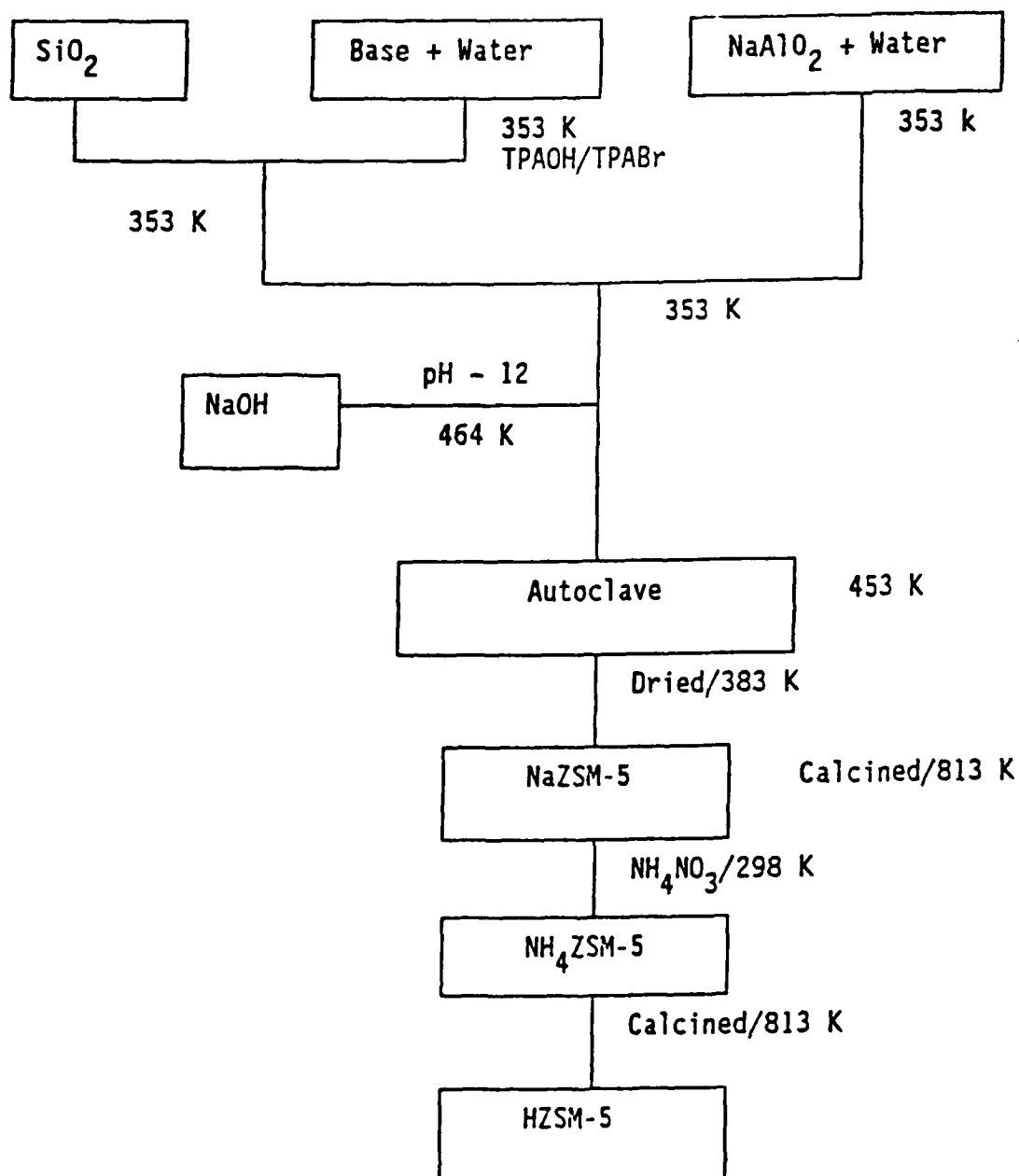
The preparation of the ZSM-5 class of zeolites used in this investigation was based on a method patented by Argauer and Landolt.³⁰ The general preparation scheme used for the synthesis of ZSM-5 is presented in Figure 13. Silica (22.9 g) was partially dissolved in 100 cm³ of 1 N tetrapropylammonium hydroxide (TPAOH) or 2.18 N tetrapropyl ammonium bromide (TPABr) by heating the solution to a temperature of approximately 353 K with magnetic stirring. A solution of sodium aluminate and deionized water was added to the silica solution at 353 K with magnetic stirring. The mixture was placed in a Teflon beaker and heated in an autoclave (capacity 1000 liters) at 453 K (or 433 K) for six days (or 10 days) without stirring. The resultant solid product was filtered, washed with about 1000 cm³ of distilled water and dried at 383 K for 16 hours. A portion of this product was subjected to X-ray diffraction analysis to determine the crystalline nature of the zeolite. The product was then calcined at 813 K in air for 16 hours prior to modification by ion exchange.

- Step 1: The organic cation (TPAOH or TPABr) was dissolved in water at 353 K with magnetic stirring to form Solution A.
- Step 2: Silica was partially dissolved in Solution A at 353 K with magnetic stirring to form Solution B.
- Step 3: Sodium aluminate was dissolved in water at 353 K with magnetic stirring to form Solution C.
- Step 4: Solution B was mixed with Solution C at 353 K with magnetic stirring to form Solution D.
- Step 5: Sodium hydroxide was added to Solution D to adjust the pH value to ~12 at 353 K to form Solution E.
- Step 6: Solution E was transferred to an autoclave and was heated in an oven at 453 K (or 433 K) for 6 days (or 10 days) without stirring to produce the precipitated/crystallized zeolite F.
- Step 7: NaZSM-5, as synthesized, was filtered and washed with distilled water. The sodium-form of ZSM-5 was then dried at 383 K for 16 hours and calcined at 813 K for 16 hours to produce Solid G.
- Step 8: The NaZSM-5 was exchanged using ammonium nitrate to produce the hydrogen-form of ZSM-5.

Figure 13

Procedure for the Synthesis of ZSM-5

PROCEDURE FOR SYNTHESIS OF HZSM-5

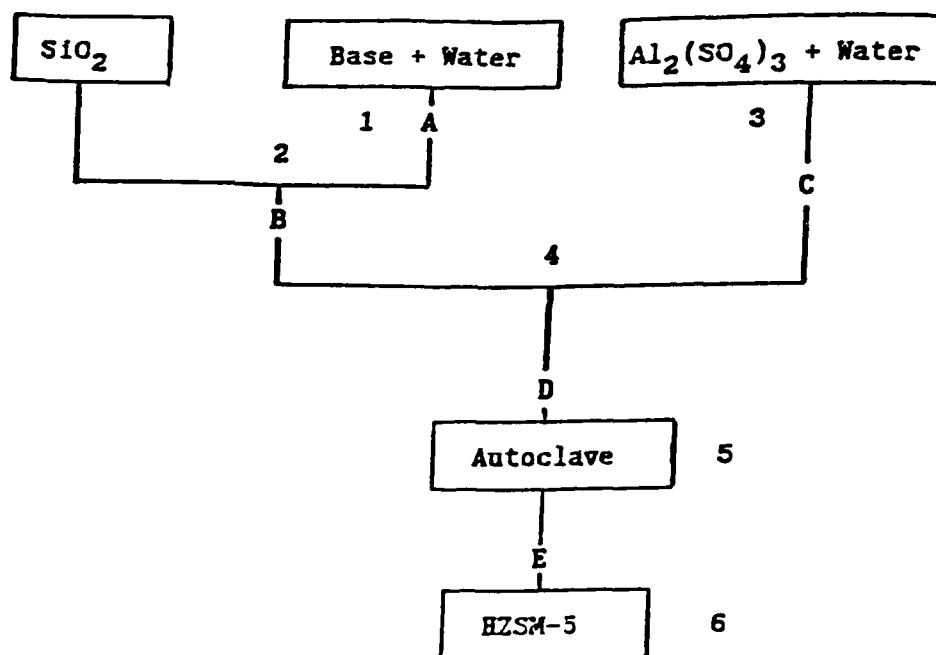


Zeolite ZSM-5 in the hydrogen form was prepared by two procedures. The first method consisted of crystallizing the sodium form of ZSM-5 at 425 K (or 453 K) from a gel containing organic cations (TPABr or TPAOH). The sodium form was subsequently exchanged three times with a 1 N NH_4NO_3 solution at 298 K. The $\text{NH}_4\text{ZSM-5}$ was then heated for 16 hours at 813 K to obtain the hydrogen form of the catalyst, HZSM-5.

A direct method for preparing HZSM-5 with the same structure as indicated by X-ray diffraction patterns has also been investigated. The zeolite crystals are formed using 1,6-diaminohexane (C_6DN) as the organic cation from a sodium-free gel, which after calcination in air at 1023 K directly gives the hydrogen form without an intermediate ion exchange. The procedure for the direct synthesis of the hydrogen form of ZSM-5 is presented in Figure 14. The zeolite obtained in this way is designated as HZSM-5D.

Preparation of Zeolite ZSM-48

ZSM-48 can be prepared from a reaction mixture containing a source of silica, an organic compound (1,6 hexane-diamine (C_6DN), 1,8-diaminooctane (C_8DN) or 1,12-diaminododecane (C_{12}DN)) having an amine functional group with $\text{Pka} > 7$, and an alkali metal oxide (sodium oxide) with or without a source of alumina and water. The procedure for synthesis of ZSM-48 is presented in Figure 15. The composition ranges for the compounds comprising the reaction mixture are presented in Table 21 in terms of the mole ratios of the oxides. The mixture was maintained at 453 K in a stainless-steel autoclave until crystals of ZSM-48 were formed. The sodium-form of ZSM-48 was subsequently exchanged three times with a 1 N ammonium nitrate solution at 298 K. The ammonium-form of ZSM-48 was heated for 16 hours at 1023 K to obtain the hydrogen form of the catalyst.



- Step 1: An organic cation (C6DN) was dissolved in water at 353 K with magnetic stirring to form Solution A.
- Step 2: Silica was partially dissolved in Solution A at 353 K with magnetic stirring to form Solution B.
- Step 3: Aluminium sulfate was dissolved in water at 353 K with magnetic stirring to form Solution C.
- Step 4: Solution B was mixed with Solution C at 353 K with magnetic stirring to form Solution D.
- Step 5: Solution D was transferred to an autoclave and was heated in an oven at 453 K for 2 days without stirring to produce the precipitated/crystallized Zeolite E.
- Step 6: The HZSM-5, as synthesized, was filtered and washed with distilled water. The hydrogen-form of ZSM-5 was then dried at 383 K for 16 hours and calcined at 813 K for 16 hours.

Figure 14

**Procedure for the Direct Synthesis of
the Hydrogen-Form of ZSM-5**

- Step 1: An organic cation (C6DN or C8DN) was dissolved in water at 353 K with magnetic stirring to form Solution A.
- Step 2: Silica was partially dissolved in Solution A at 353 K with magnetic stirring to form Solution B.
- Step 3: Sodium aluminate was dissolved in water at 353 K with magnetic stirring to form Solution C.
- Step 4: Solution B was mixed with Solution C at 353 K with magnetic stirring to form Solution D.
- Step 5: Sodium bromide was added to Solution D to adjust the sodium concentration at a temperature of 353 K with magnetic stirring to form Solution E.
- Step 6: Solution E was transferred to an autoclave and was heated in an oven at 453 K for 2 days without stirring to produce the precipitated/crystallized Zeolite F.
- Step 7: The NaZSM-48, as synthesized, was filtered and washed with distilled water. The sodium-form of ZSM-48 was then dried at 383 K for 16 hours and calcined at 813 K for 16 hours.
- Step 8: The NaZSM-48 was exchanged using ammonium nitrate to produce the hydrogen-form of ZSM-48.

Figure 15

Procedure for the Synthesis of ZSM-48

PROCEDURE FOR SYNTHESIS OF HZSM-48

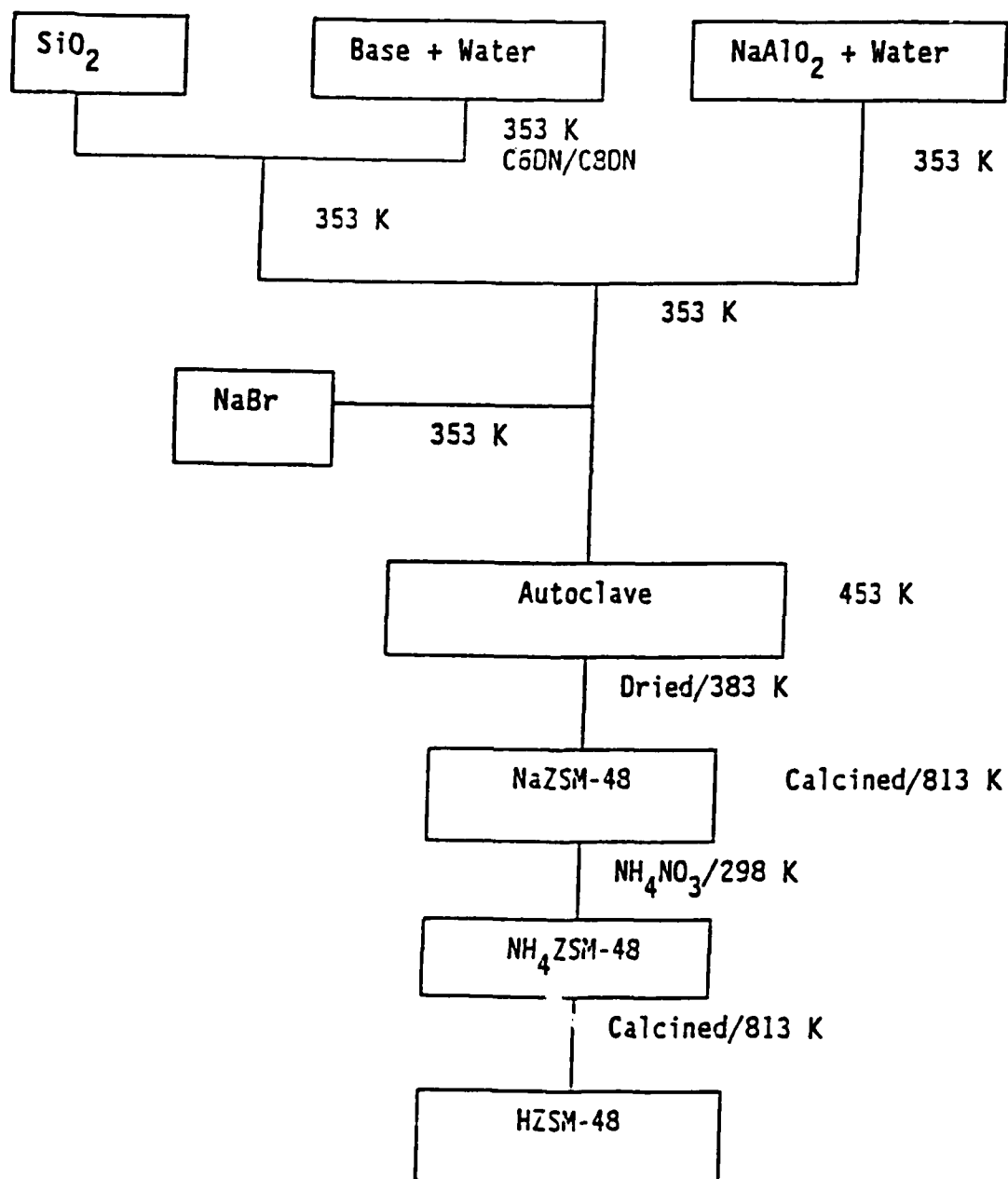


Table 21

**Composition Ranges in Terms of Mole Ratios for
the Synthesis of ZSM-48**

Reactants	Broad⁷⁷	Preferred⁷⁷	This work
$\text{Al}_2\text{O}_3/\text{SiO}_2$	0 - 0.02	0 - 0.01	0.025 - 0.005
Na/SiO_2	0 - 2	0.1 - 1.0	0.6 - 0.3
RN/SiO_2	0.01 - 2.0	0.05 - 1.0	0.3 - 0.1
OH^-/SiO_2	10-100	20-70	40

Characterization of Synthetic Zeolites

Elemental Analysis of Synthetic Zeolites

The elemental analysis of the synthetic zeolites was determined using an electron microprobe method in an EMX-SM Spectrometer (Model-121000, Applied Research Laboratories, Inc.). A wavelength dispersive X-ray detection system (WDS) was used in this microprobe. Lithium fluoride (LiF) crystals with precise d-spacings are used to diffract narrow band X-ray wavelengths into the detector (Extron or Flow). The signals produced are then amplified and counted.

X-ray Diffraction

The structures of the synthetic zeolites were investigated using X-ray diffraction. A Phillips Norelco Electronic Instrument X-ray Diffractometer was used in this study. The incident beam was CuK_α X-ray radiation with a wavelength of 0.15405 nm. The diffracted X-ray was detected by an ionization chamber that could be rotated to determine the angle for constructive interference. The intensity of the diffracted X-ray was measured synchronously as the goniometer of the X-ray diffractometer rotated.

The synthetic zeolites were ground to a fine powder and placed in an aluminum sample holder. X-ray diffraction patterns were measured from 10° to 50° (2θ) at a scanning speed of $2^\circ/\text{min}$. The X-ray diffraction pattern of a ZSM-5 (ammonium-form) sample provided by the Mobil Research and Development Corporation was also determined for comparison with those of the synthetic zeolites prepared for this study.

Thermal Desorption

A schematic of the microreactor system that incorporated a thermo-conductivity detector to monitor feed and product streams is presented in Figure 16. The microreactor/TPD (MCR) apparatus was used to study normal-hexane cracking (α -test), the isobutane isomerization, temperature-programmed ammonia desorption, and alcohols conversion reactions.

Zeolite catalysts were saturated with ammonia by flooding the samples with a flowing stream of 5 percent ammonia/nitrogen for at least 30 minutes at room temperature. The catalysts were then heated at a linear heating rate of 5 K/min in a stream of helium and the amount of ammonia desorbed was continuously monitored by the thermal conductivity detector to give the TPD spectra.

Infrared Spectroscopy

Methanol adsorption and its subsequent reactions on zeolites ZSM-5 and ZSM-48 were studied using a diffuse reflectance infrared cell. The infrared cell (Figure 17) was used in a Digilab FT-IR spectrometer (model FTS-40). Zeolite samples were pretreated in flowing helium at 773 K for two hours. Since the optical path of the cell is very short, the spectra of adsorbed surface species can be measured in the presence of the reactant vapor.

The infrared spectra were measured during reaction and/or after pulse methanol injection with zeolite catalysts. The thermal desorption of methanol from ZSM-5 and ZSM-48 was also studied using the diffuse reflectance FT-IR method.

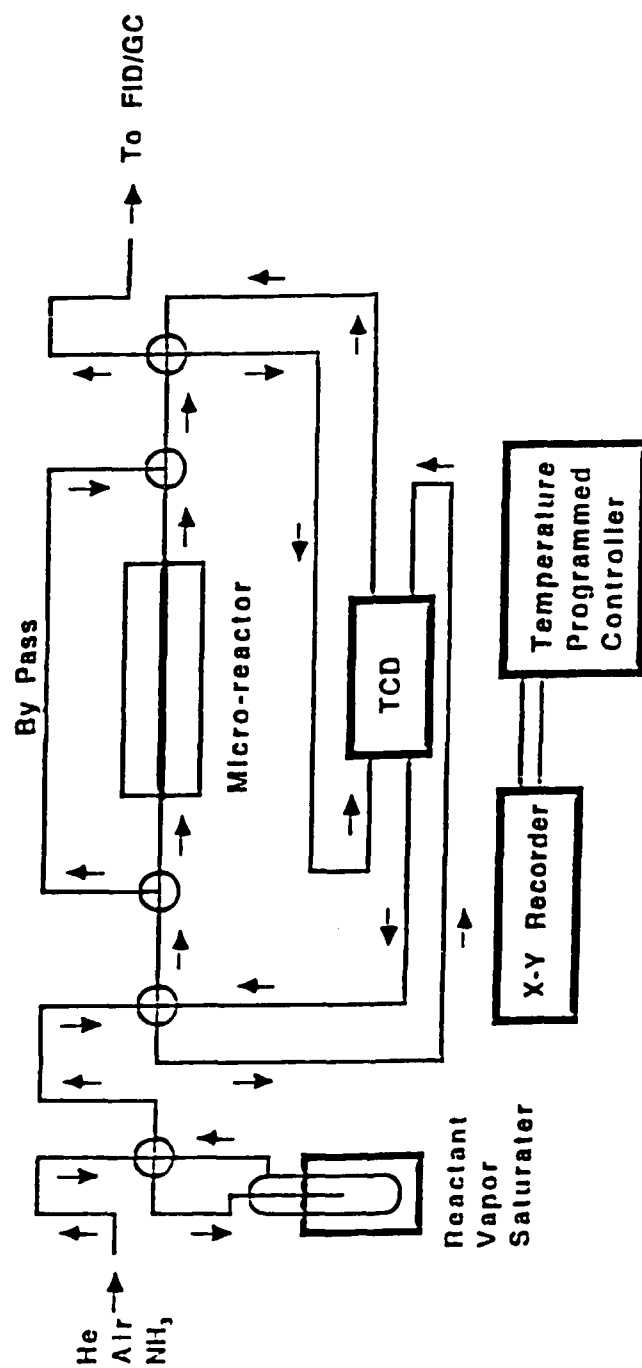


Figure 16. Schematic of Temperature-Programmed Desorption (TPD) and Microreactor Apparatus

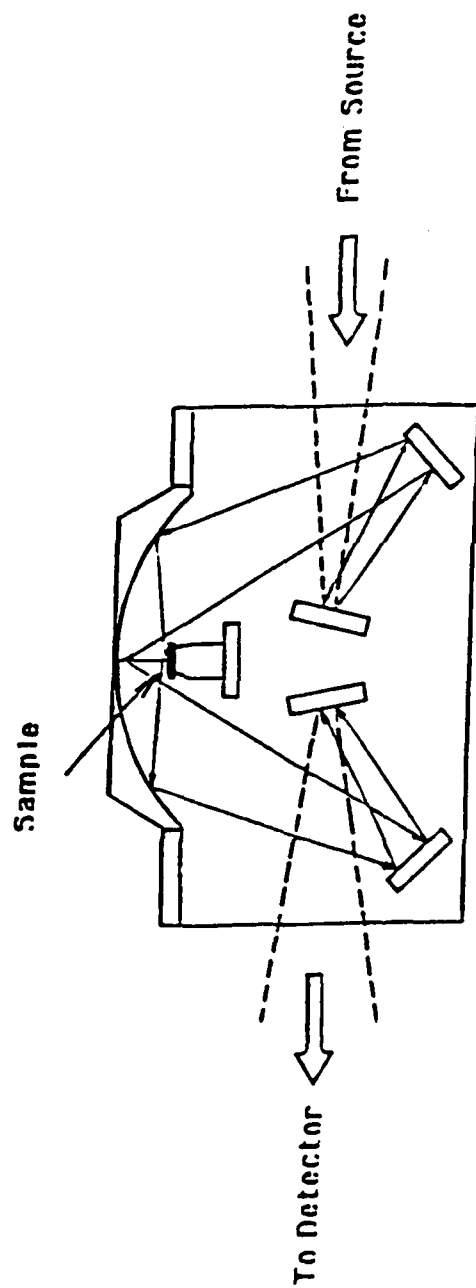


Figure 17. Diffuse Reflectance FTIR Cell and Optical Layout

SEM and the Morphology of Zeolites

The morphology of the zeolites prepared in this investigation was examined with an Hitachi S-530 Scanning Electron Microscope equipped with an X-ray detector (PGT System IV). The vacuum in the specimen chamber was below 5×10^{-6} torr. Samples were mounted on aluminum pegs and coated with a thin film of gold. For small particles analyzed directly on the support, the particle thickness was assumed to be roughly the same as the lateral dimension of the particle.

Energy Dispersive Analysis of X-ray (EDAX) is a rapid semiquantitative method for elemental analysis. Use of this system (PGH System IV) in conjunction with the SEM provides a powerful analytical tool for examining catalyst surfaces.

Channel Structure

The pores of ZSM-5 and ZSM-48 have openings of about 5.5 \AA . They can admit linear and slightly branched paraffins, and simple naphthenes and aromatics. Isomerization of isobutane was studied at 623 K with a hydrogen/isobutane molar ratio of four in the microreactor to investigate the nature of the pore/channel structures of ZSM-5 and ZSM-48.

Acidity

The cracking of n-hexane provides a suitable test reaction for measuring the acidity of the zeolites since n-hexane is free of diffusion limitations for both zeolites ZSM-5 and ZSM-48. Measurements were carried out with n-hexane in a continuous flow microreactor at temperatures at which the conversion is above 5 percent, for accuracy of measurement, and below about 40 percent to avoid complications due to reactant and/or product transport limitations. The hexane cracking activities of crystalline aluminosilicates including HY, ZSM-5, and ZSM-48 were investigated.

Surface Area

The adsorption of nitrogen on the synthesized zeolite catalysts was measured by the volumetric adsorption method in a glass vacuum system (Figure 18). The apparatus consists of a diffusion pump (model PMCS-4B, CVC) backed up with a mechanical vacuum pump (GCA Precision Scientific 225 1/3 hp). The background pressure was monitored with a Penning Vacuum Gauge (Model GPH-320C, CVC) and was of the order of 10^{-4} torr. The pressures during the volumetric adsorption were measured using a MKS Baratron Absolute Pressure Gauge (Type 222B, 0-1000 Torr). A more detailed discussion of surface area measurement, the experimental apparatus, and the treatment of the data are presented in Section VIII and in the Appendices.

The external and internal surface areas of the zeolites were measured using the n-hexane filled-pore method.¹⁵⁹ Calcined zeolite samples were heated in vacuum at 623 K for eight hours. The amounts of adsorbed nitrogen molecules at 77 K were measured both before and after n-hexane filling of the pores of the zeolite samples. The dead volume of the system was measured and calculated from the free expansion of neon at room temperature and 77 K.

Reactivity of Methanol and Higher Alcohols over Zeolites

The activity and selectivity of the synthesized zeolites for alcohol conversion were studied in a stainless steel flow microreactor at a total pressure of one atmosphere and generally at 643 K. The catalysts (one gram reactor charge) were activated in flowing air for four hours at 773 K followed by cooling to the reaction temperature in helium. The reactant mixtures (flow rate of 30 cm³/min) were fed to the reactor in a helium stream that had been saturated by passing the helium through a bubbler containing the alcohols at room temperature. The reactor effluent was analyzed by gas chromatography method in a Hewlett Packard Chromatograph (Model 5830) using an SP-2100 or Chrosorb-102 column.

A fixed-bed flow reactor system (Figure 19) was used to study the reaction of methanol over ZSM-5 and ZSM-48 catalysts. The product from the catalytic reactor was cooled in a high-pressure separator. Light gases were metered through a wet test meter. An X-Y recorder was used to record and measure the temperature of the catalyst bed during reaction. The feed was pure methanol (reagent grade). The liquid products were analyzed using an SP-2100 column while the gaseous products were analyzed using a Chrosorb-102 column. A flame ionization detector was used in both cases.

A dual-stage process (Figure 19) was also studied. The product from the first reactor was conducted to a gas-liquid separator where the light gases were separated from water and liquid product. The light gases were compressed with a Whitey compressor (Model No. SKC49FG1101EX, 1/2 HP) to the inlet pressure of the second reactor where the light gases reacted to form aromatics over ZSM-5.

Chemical Supplies

A listing of the chemicals and materials used in this work is presented in Table 22.

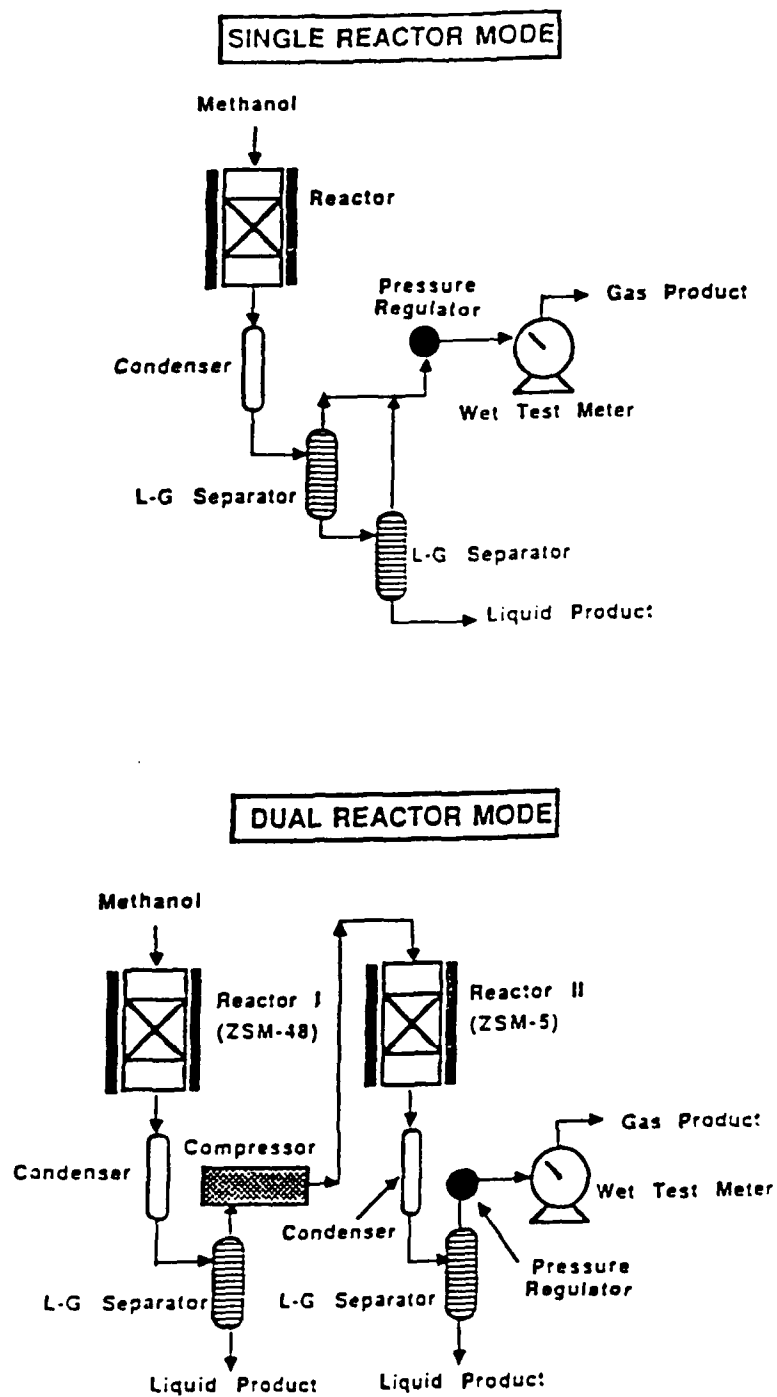


Figure 19. Reactor Systems for the Study of Methanol Conversion

Table 22
Chemicals Used in Catalyst Preparation

Chemical	Application	Purity	Source
Tetrapropylammonium Hydroxide	ZSM-5 prep.	1 M	Aldrich
Tetrapropylammonium Bromide	ZSM-5 prep.	98%	Aldrich
Sodium Aluminate	ZSM-5/48 prep.	pure	Amend
Aluminum Sulfate	ZSM-5 prep.	BG	Baker
Aerosil 200	ZSM-5/48 prep.	-	Degussa
Silica	ZSM-5/48 prep.	G-12	Aldrich
Sodium Bromide	ZSM-48 prep.	GR	EM Sci.
Sodium Hydroxide	ZSM-5 prep.	BG	Baker
Indium Nitrate	ZSM-5/48	99.999%	Aldrich
1,6-Hexanediamine	ZSM-5/48	98%	Aldrich
1,8-Diaminooctane	ZSM-48	98%	Aldrich
1,12-Diaminododecane	ZSM-48	98%	Aldrich
Ammonium Nitrate	Ion exchange	ACS	Aldrich
n-Hexane	α -test	HPLC G.	Mallinckrodt
Isobutane	Isomerization	99.5%	Union Carbide
Ammonium Gas	TPD	5%	Liquid Air
Methanol	TD & Reactions	Spect. G.	Mallinckrodt
Ethanol	Reactions	Spect. G.	Aldrich
n-Propanol	Reactions	Analy. G.	Mallinckrodt
i-Propanol	TGA/TPD	Spect. G.	Fisher
n-Butanol	Reactions	Analy. G.	Baker

Section IV: SELECTIVE SYNTHESIS OF AROMATIC HYDROCARBONS OVER ZEOLITE CATALYSTS

Research Personnel:

Hong Paul Wang
Graduate Student

Francis V. Hanson
Associate Professor

Laboratory Preparation of ZSM-5 and ZSM-48 Zeolites

Synthesis of ZSM-5

ZSM-5-type zeolites were synthesized hydrothermally in this investigation. The crystallization of zeolites from hydrogels includes nucleation and crystallization (crystal growth) processes. The nucleation process is defined to be the formation of the initial crystalline phase. Virtually no information can be found regarding the detailed mechanism of formation of the ultrafine particles (diameters approx. 1-10 nm) in the nucleation process. Thus crystal growth is defined as the process that takes place after 50 percent conversion of the original solution to crystalline material.

The composition of zeolite ZSM-5b in terms of mole oxide ratios of components was $6\text{TPA}\cdot 2\text{Na}_2\text{O}\cdot \text{Al}_2\text{O}_3\cdot 21\text{SiO}_2\cdot 460\text{H}_2\text{O}$. The source of silica was Acrosil (Degussa). The crystal formed after 6 days at a temperature of 423 K and an autogenous pressure of 13 atm was examined using the X-ray diffraction method. The crystalline material was identified as ZSM-5. A comparison of the X-ray diffraction pattern of ZSM-5b to that of Mobil ZSM-5 (ZSM-5M) and amorphous SiO_2 is presented in Figure 20. The patterns indicate that the ZSM-5b synthesized at typical reaction conditions has a crystalline structure similar to ZSM-5M.

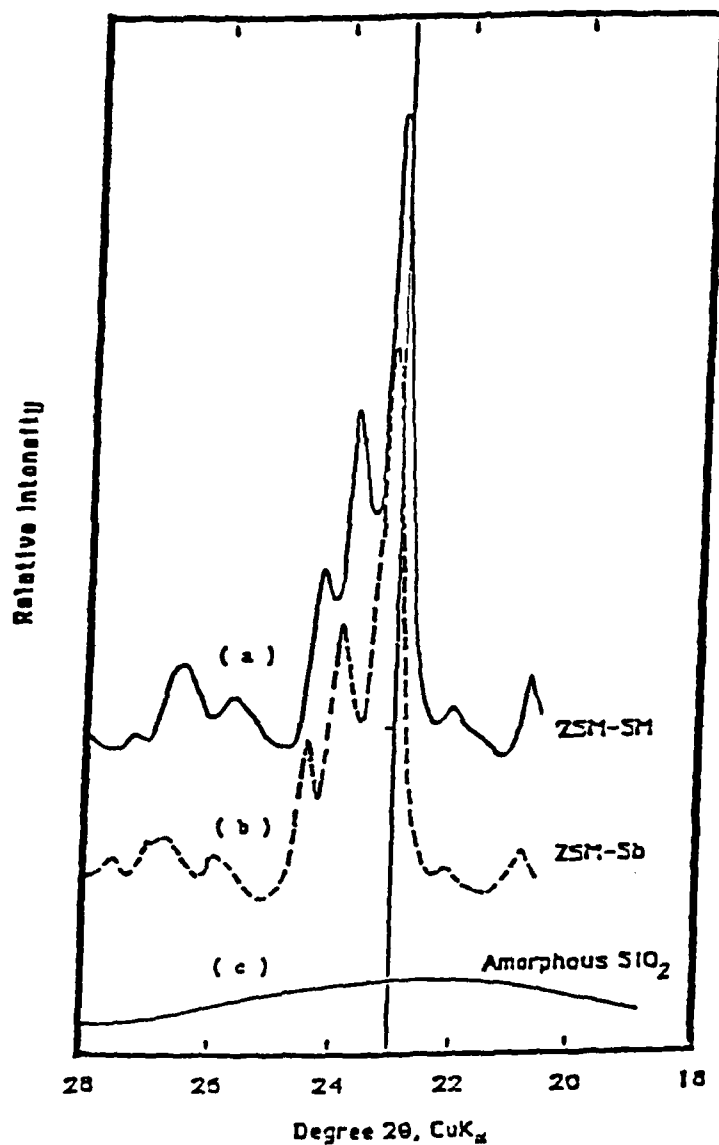


Figure 20. X-ray Diffraction Patterns for ZSM-5
 (a) Mobil Standard ZSM-5
 (b) Synthesized ZSM-5
 (c) Amorphous SiO₂

The elimination of the organic cations such as tetrapropyl ammonium (TPA) ion from ZSM-5 was studied by differential scanning calorimetry (DSC). The DSC pattern obtained in air with the sodium form of ZSM-5b is presented in Figure 21. The broad exotherm between 630 and 820 K in the DSC profile is believed to be associated with the decomposition of the TPA ions. The profile indicates that the minimum temperature necessary to insure complete removal of the TPA ions was around 820 K. Thus it was concluded that the ZSM-5 synthesized in the presence of TPA ions can be activated by calcination at a temperature of 823 K. After calcination at 823 K for 16 hours, the synthetic ZSM-5 was a white crystal.

The influence of synthesis reaction variables on the synthesis of ZSM-5 was also investigated. The X-ray diffraction pattern of the Mobil ZSM-5 sample was used as the standard for characterizing the ZSM-5 zeolites prepared in this investigation. The degree of crystallization (crystallinity) was estimated by comparing the area under the X-ray diffraction bands ($2\theta = 22 - 25^\circ$) to that of ZSM-5M. The ZSM-5M was taken as the standard and was assumed to exhibit 100 percent crystallinity. The crystallinity was calculated from the following relationship:

$$\text{Crystallinity}(\%) = \frac{\text{peak area } (2\theta = 22-25) \text{ of ZSM-5}}{\text{peak area } (2\theta = 22-25) \text{ of ZSM-5M}} \cdot 100 \quad (4-1)$$

The crystallinities of the various ZSM-5 zeolites synthesized in this study are presented in Table 23. It should be noted that the crystallite sizes were about the same (crystallite sizes should be about the same for the two samples if the crystallinity equation is to be valid) for ZSM-5M and zeolites ZSM-5 synthesized by using TPA cations.

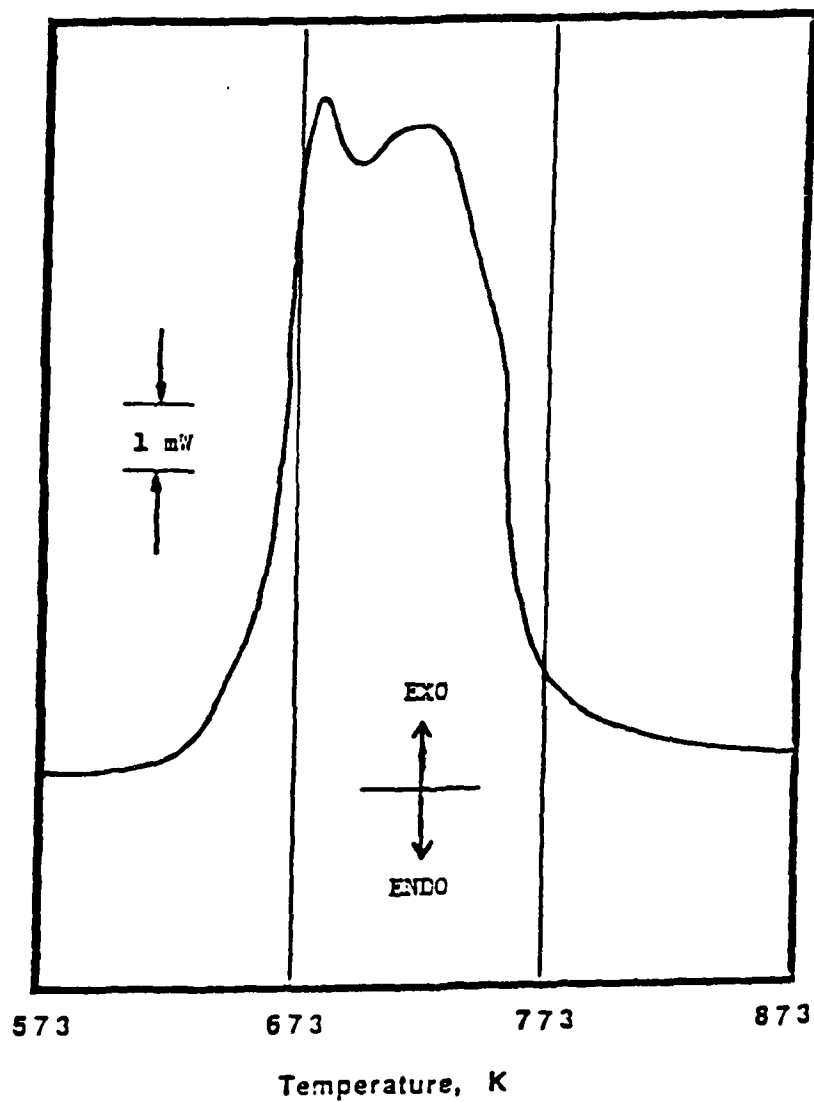


Figure 21. Differential Scanning Calorimetry Pattern for NaZSM-5.
Elimination of the Organic Cation (TPA)

Table 23

Degree of Crystallinity of Synthesized ZSM-5 Samples

Zeolite	Reaction Conditions			Cation ^a	Crystallinity ^b %
	T (K)	P (atm)	Time (days)		
ZSM-5M	-	-	-	-	100
ZSM-5a	425	11	6	TPAOH	86
ZSM-5b	425	11	10	TPAOH	91
ZSM-5c	453	1	6	TPAOH	70
ZSM-5d	453	13	6	TPAOH	99+
ZSM-5e	453	13	6	C6DN	95
ZSM-5D	453	13	6	C6DN	95
ZSM-5(70)	453	13	6	TPABr	99+

- ^a Cation Identities
 TPAOH Tetrapropylammonium hydroxide
 C6DN 1,6-hexane-diamine
 TPABr Tetrapropylammonium Bromide

The composition of synthetic ZSM-5

ZSM-5 a-d	6TPA-2Na ₂ O-Al ₂ O ₃ -21SiO ₂ -46OH ₂ O
ZSM-5 e	6C6DN-2Na ₂ O-Al ₂ O ₃ -21SiO ₂ -46OH ₂ O
ZSM-5D	70C6DN-ONa ₂ O-Al ₂ O ₃ -70SiO ₂ -280OH ₂ O
ZSM-5(70)	18TPA-6Na ₂ O-Al ₂ O ₃ -70SiO ₂ -1400H ₂ O

- ^b Crystallinity computed from the following equation:

$$\text{Crystallinity (\%)} = \frac{\text{peak area (} 2\theta = 22-25 \text{) of ZSM-5}}{\text{peak area (} 2\theta = 22-25 \text{) of ZSM-5M}} \cdot 100 \quad (3)$$

The autogenous pressure, due to the evaporation of the mother liquor that built during the synthesis of ZSM-5c at 453 K, was repeatedly released until atmospheric pressure was attained (> 6 days). The ZSM-5 sample produced in this experiment had a crystallinity of 70 percent. Rollmann⁹⁶ indicated that the initial mole ratio of water-to-silica in the reaction mixture strongly influences the mechanism and rate of crystallization of ZSM-5. It is presumed that the nucleation process was nearly complete during the early stages of the synthesis of ZSM-5c. The subsequent crystallization process may have been retarded due to the lack of hydrolysis in the reaction mixture thus preventing the formation of the ordered, three-dimensional network of ZSM-5.

Digestion time and digestion temperature also influence the structure of the synthesized zeolite. Highly crystalline ZSM-5 was obtained at reaction temperatures of 453 K. Low crystallization temperatures, e.g., 425 K and below, do not favor the formation of high crystallinity ZSM-5. Furthermore, if ZSM-5 remains in prolonged contact with the mother liquor at 425 K, a higher crystallinity ZSM-5 can be obtained in 4 days (Table 23).

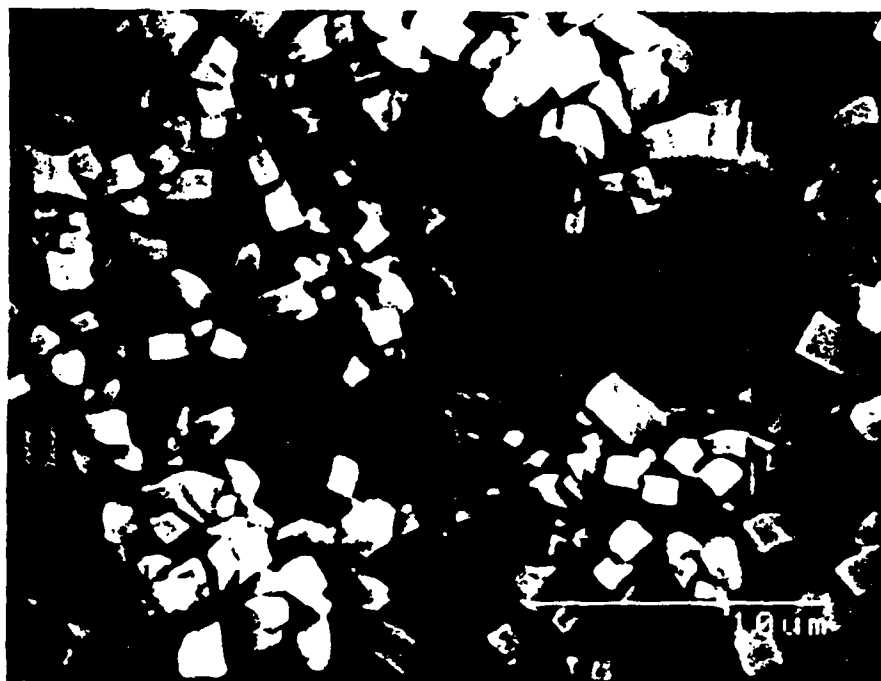
It is believed that the organic content of {Na,TPA}ZSM-5 corresponds to one TPA ion per channel intersection and represents the maximum amount of the ion that can be encapsulated in the ZSM-5 structure. 1,6-Hexane-diamine (C6DN) is smaller and less hydrophobic than TPA. It seems likely that the packing of the C6DN in the ZSM-5 framework is not as highly ordered as that of the TPA ion. The accommodation of the cations in the structure provides little indication of the mechanism by which the organic host species influence the final structure of the zeolite, since both organic cations gave crystalline ZSM-5 (Table 23). However, it is well-known that the TPA ion causes the formation of ZSM-5 with a wide range of reaction mixture compositions and this may indicate that TPA ion is a strong structure directing species. It should be noted that the crystallization of ZSM-5 is determined by factors other than the availability of

a suitable template cation. C6DN seems to have the ability to promote the crystallization of ZSM-5 in the absence of sodium ions. A comparison of the scanning electron microscope (SEM) images of ZSM-5 synthesized in the presence of C6DN and TPABr is presented in Figure 22. The images indicate that the crystallite size ($\sim 4 \mu\text{m}$) of ZSM-5 synthesized with C6DN was larger than that ($\sim 1 \mu\text{m}$) of ZSM-5 synthesized with TPABr since C6DN was found to promote the crystallization of ZSM-5. However, it is not as effective as the TPA ion (crystallinity = 95 percent for ZSM-5D), and it may not be a true template species for ZSM-5.

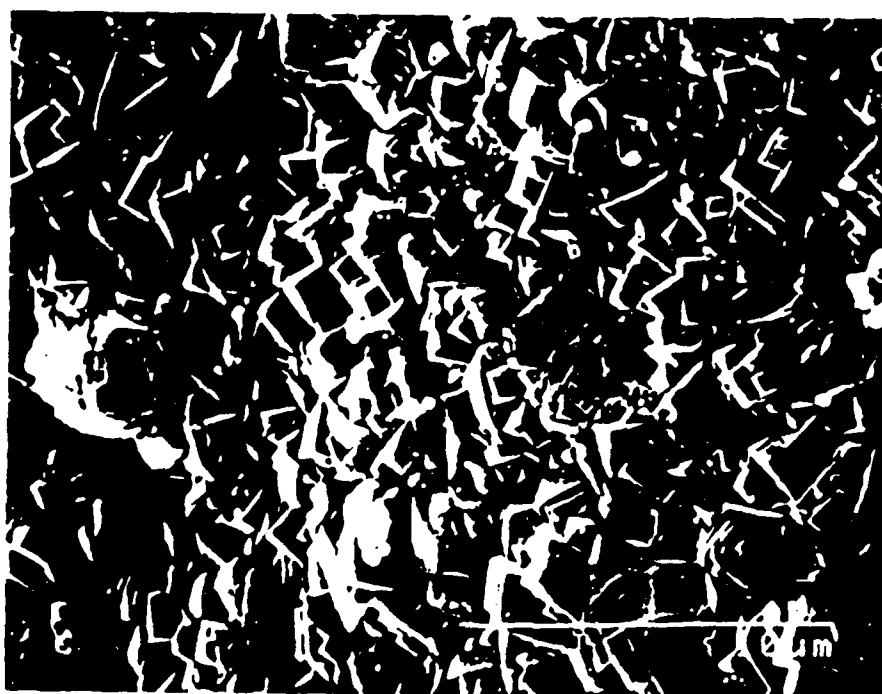
Scanning electron microscope (SEM) micrographs indicated the growth of larger crystals (cubical aggregates in shape and $0.5 - 2 \mu\text{m}$ in size) of ZSM-5 when using a synthesis mixture with a lower aluminum content, as shown in Figure 23. Generally, zeolite crystallization is a nucleation-controlled process occurring in molecularly inhomogeneous, alkaline, aqueous gels. Thus an increase in crystallization rate is expected as the silica-to-alumina ratio is increased due to the fact that the ZSM-5 nuclei is ready to be formed in the high silica content mixture.

Synthesis of ZSM-48

A systematic study of the effects of the organic template and the composition of the reaction mixture on the synthesis of ZSM-48 was also conducted. The synthesis of high-silica ZSM-48 from a reaction mixture in which the only organic ion was C6DN was investigated. The reaction mixture containing C6DN and sodium has shown that the most readily obtained product is ZSM-5 at a low initial molar ratio (IMR) of $\text{SiO}_2/\text{Al}_2\text{O}_3$, although at 453 K when the aluminum content of the reaction mixture was very low (i.e., $\text{SiO}_2/\text{Al}_2\text{O}_3 > 200$) zeolite ZSM-48 crystals were

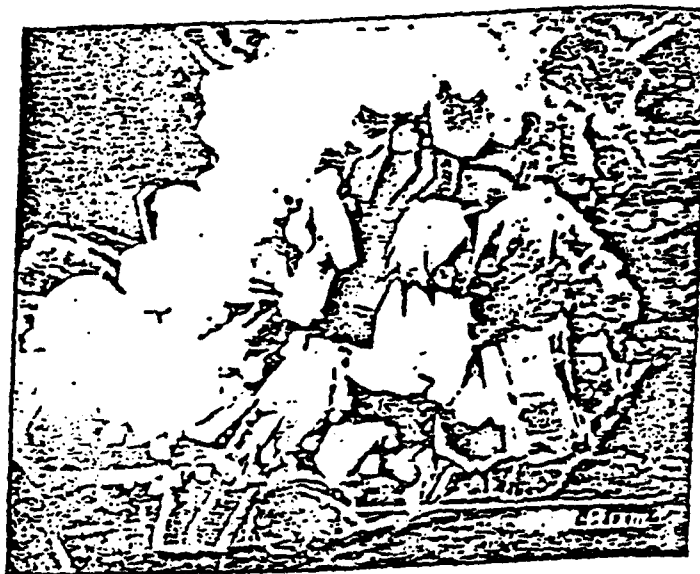


(a) C6DN



(b) TPABr and Exchanged with NH_4NO_3

Figure 22. Scanning Electron Microscope Images of HZSM-5.
Effect of Organic Cations on Synthesis



(a) $\text{SiO}_2/\text{Al}_2\text{O}_3 = 105$



(b) $\text{SiO}_2/\text{Al}_2\text{O}_3 = 35$

Figure 23. Scanning Electron Microscope Images of HZSM-5.
Effect of $\text{SiO}_2/\text{Al}_2\text{O}_3$ Ratio.

formed. The reasons for the transition from pure ZSM-5 to a mixture of ZSM-5 and ZSM-48 to pure ZSM-48 are not understood at present. However, it should be noted that ZSM-48 was initially discovered as an impurity in crystalline ZSM-39.⁴⁹

A comparison of the X-ray diffraction patterns for ZSM-5 with that for ZSM-48 formed using the same organic cation (i.e., C₆DN) are presented in Figure 24. The most intense peaks for the two samples are different. The positions of the two peaks were $2\theta = 23.8$ and $2\theta = 21.2$ for ZSM-5 and ZSM-48, respectively. This difference makes it possible to distinguish between ZSM-5 and ZSM-48.

The effect of the silica-to-alumina ratio on the synthesis of ZSM-48 is shown in Figure 25. It indicates that pure ZSM-48 could be obtained in this investigation only at initial molar SiO₂/Al₂O₃ ratios greater than 200. At an initial molar SiO₂/Al₂O₃ ratios between 25 and 200, a mixture of ZSM-5 and ZSM-48 was produced. The SEM image of ZSM-48/5(70), which is a mixture of ZSM-48 and ZSM-5, is shown in Figure 26. Interpretation of micrograph indicates that the ZSM-5 and ZSM-48 may not be an intergrowth crystal but rather are a physical mixture of the two zeolites.

Different organic cations were also used for the synthesis of ZSM-48. The X-ray diffraction patterns of ZSM-48 zeolites obtained from two different bases, namely, C₆DN (1,6-hexanediamine) and C₈DN (octane 1,8-diamine) are presented in Figure 27. The two samples exhibit almost identical X-ray diffraction patterns. The relative intensities of X-ray diffraction peaks and the diffraction angles of the ZSM-48 synthesized in this investigation are compared with X-ray diffraction patterns for the standard ZSM-48 (data available in reference [72]) which is presented in the insert of Figure 27. The organic cation, C₁₂DN, used in the synthesis of ZSM-48 was not

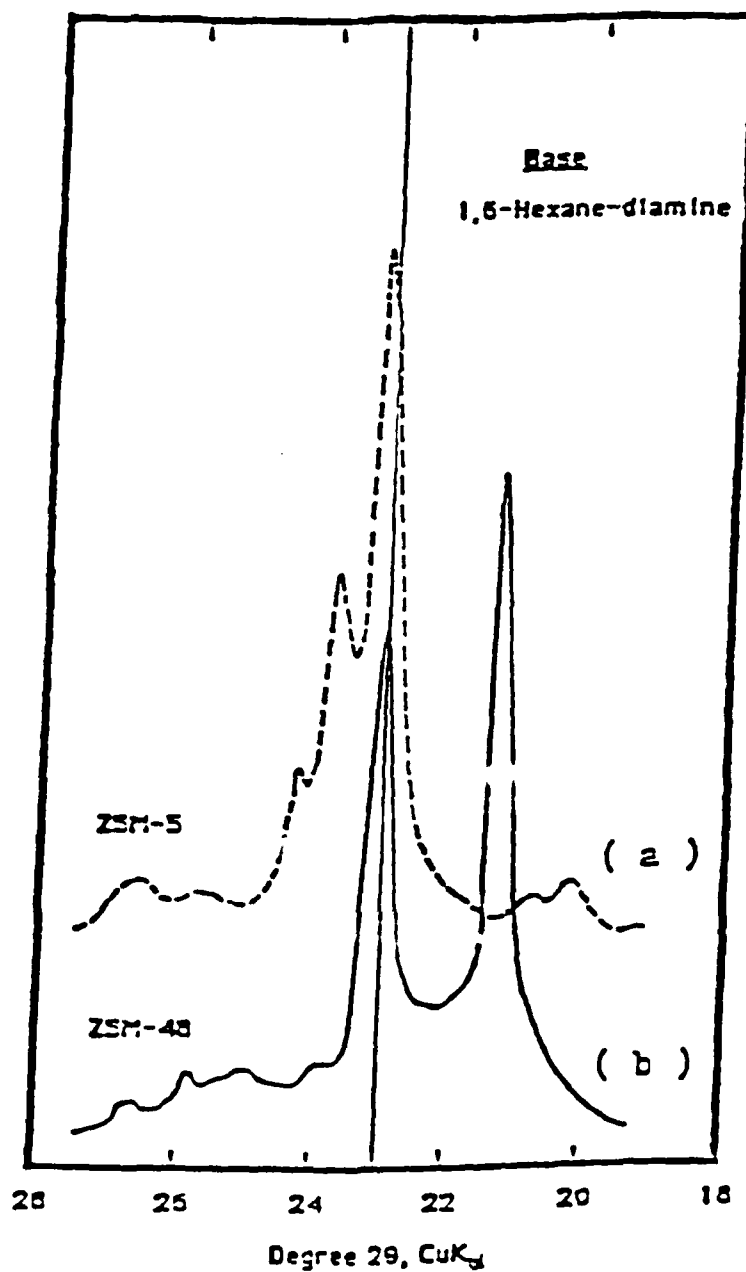


Figure 24. Comparison of the X-ray Diffraction Patterns for ZSM-5 and ZSM-48

(a) ZSM-5

(b) ZSM-48

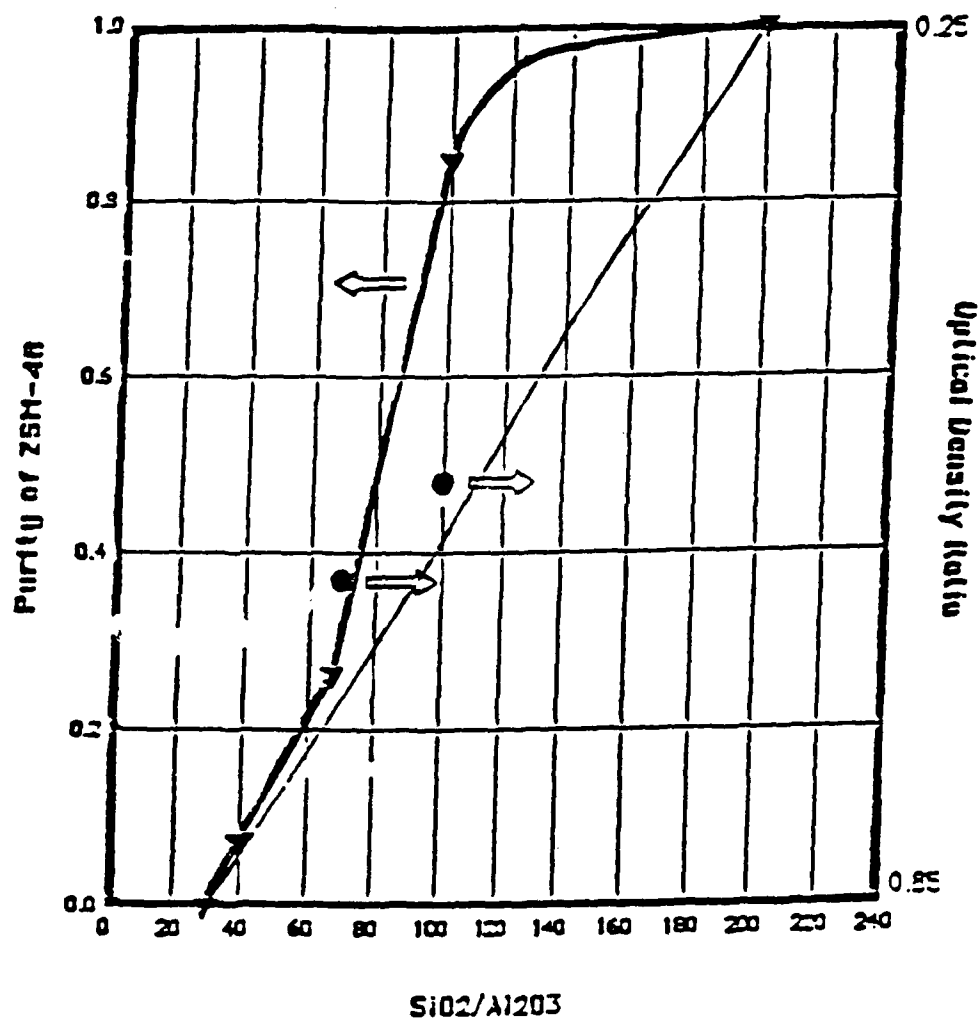


Figure 25. Effect of $\text{SiO}_2/\text{Al}_2\text{O}_3$ Ratio on the Synthesis of ZSM-48.

▲ denote X-ray diffraction crystallinity of zeolites.
● denotes optical density ratio of zeolites.



(a) SEM of HZSM-48/5 (70)



(b) SEM of ZSM-5



(a) SEM of ZSM-48

Figure 26. Scanning Electron Microscope Images of
ZSM-48/5(70)
ZSM-48 and ZSM-5

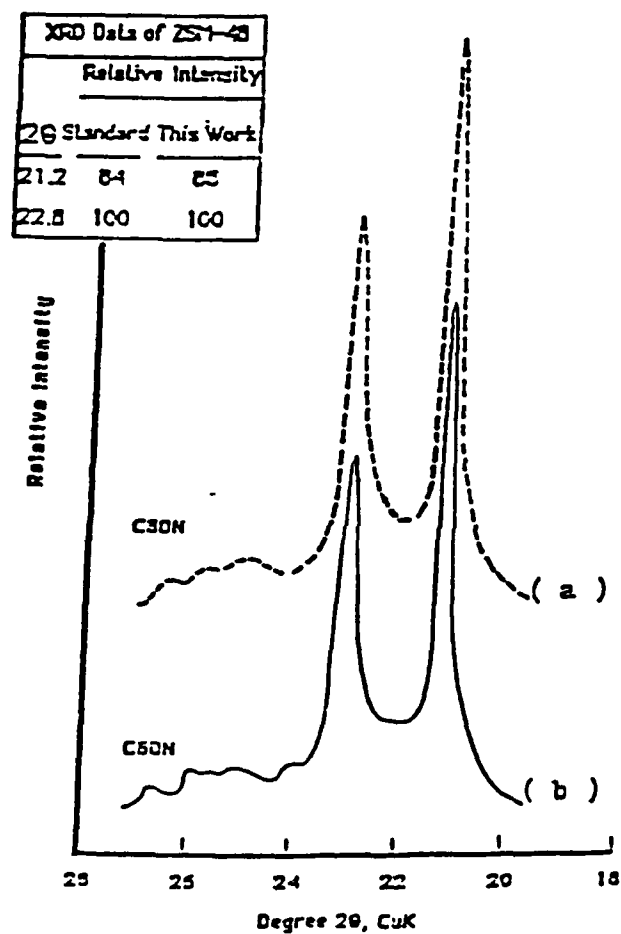


Figure 27. X-ray Diffraction Patterns for ZSM-48 Prepared with Different Organic Templates

(a) C8DN; (b) C6DN

as effective as C6DN or C8DN for synthesis of ZSM-48. It seems likely that the nature of synthesis of ZSM-48 is determined by channel filling by the organic cation at the nucleation stage.

The removal of C6DN and C8DN from the synthesized ZSM-48 was studied by DSC. The DSC patterns for the catalysts prepared with the C6DN and C8DN bases are presented in Figures 28 and 29, respectively. Neither of the organic cations could be completely removed at 873 K. The organic amines in ZSM-48 were eliminated by calcining the samples at 1023 K for 16 hours. White crystal ZSM-48 zeolites were obtained. The effect of calcination temperature on the thermal stability of ZSM-48 is presented in Figure 30. It is clear that the ZSM-48 is a thermally stable zeolite (up to 1323 K).

The organic cations present in a reaction mixture are often the major factor in determining which zeolite structure is obtained. The effect of the C6DN/SiO₂ ratio on the synthesis of ZSM-48 was investigated using X-ray diffraction. The X-ray patterns are presented in Figure 31. At an initial molar C6DN/SiO₂ ratio of 0.1, ZSM-48 could not be produced and the solid appeared to be X-ray amorphous. The ability of the organic ion, C6DN, to alter the course of the nucleation process is apparent. In addition, the effect of the initial molar Na/SiO₂ ratio on the synthesis of ZSM-48, shown in Figure 32, is of interest as a structure-directing function. A structure-unknown crystallite, namely ZSM-48X, was obtained at Na/SiO₂ = 0.45. However, it is very likely that ZSM-48 is one of the components in the ZSM-48X crystallite since all diffraction peaks appearing in the X-ray diffractogram of ZSM-48 are also present in the diffractogram of ZSM-48X.

The cation is said to have a structure-directing function and influences the structure of the zeolite that forms. In early work using alkali and alkaline earth cations, it was suggested that

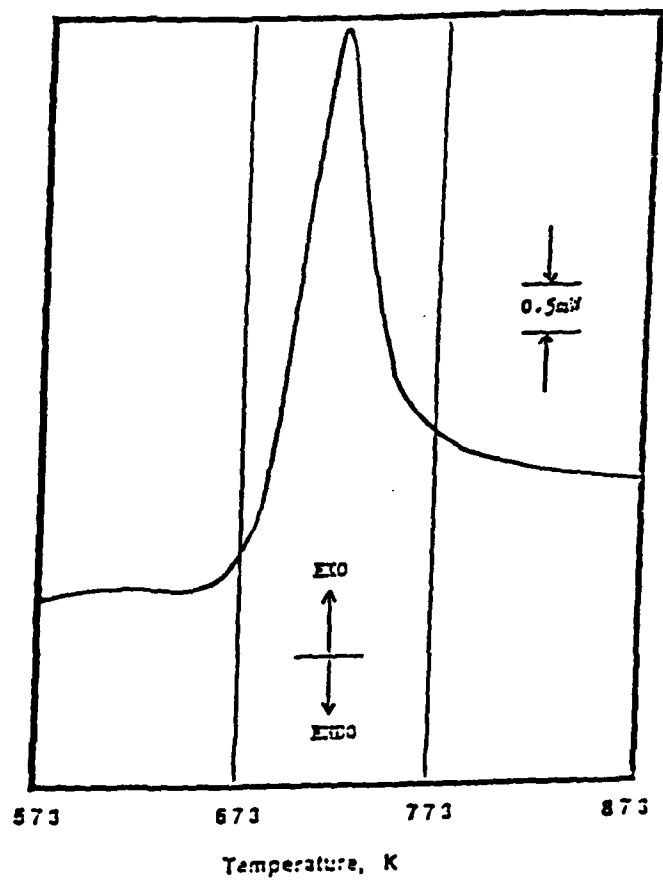


Figure 28. Differential Scanning Calorimetry (DSC) of NaZSM-48.
Elimination of the Organic Cation (C6DN) from Synthesized NaZSM-48

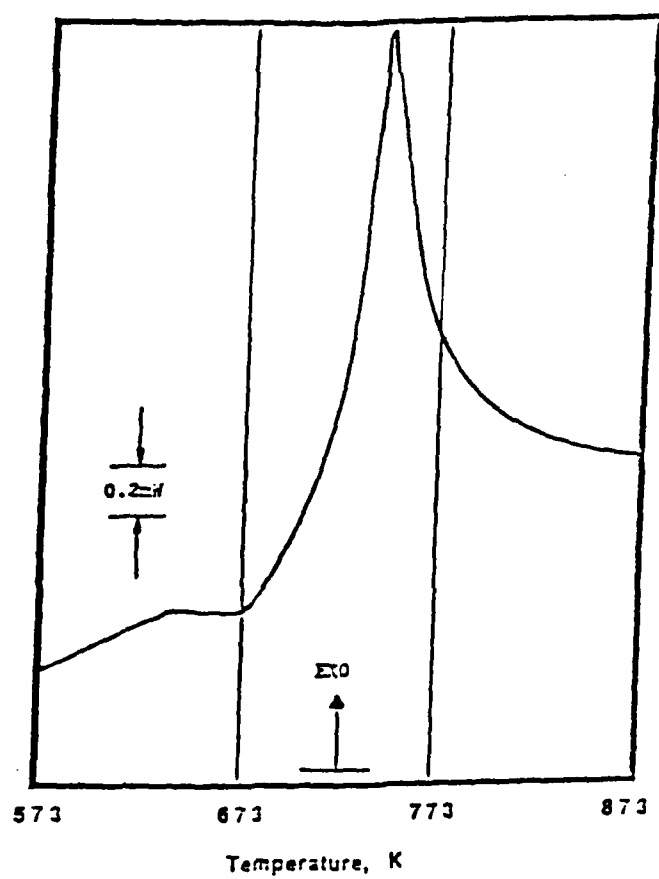


Figure 29. Differential Scanning Calorimetry Pattern for NaZSM-48. Elimination of the Organic Cation (C8DN) from Synthesized NaZSM-48

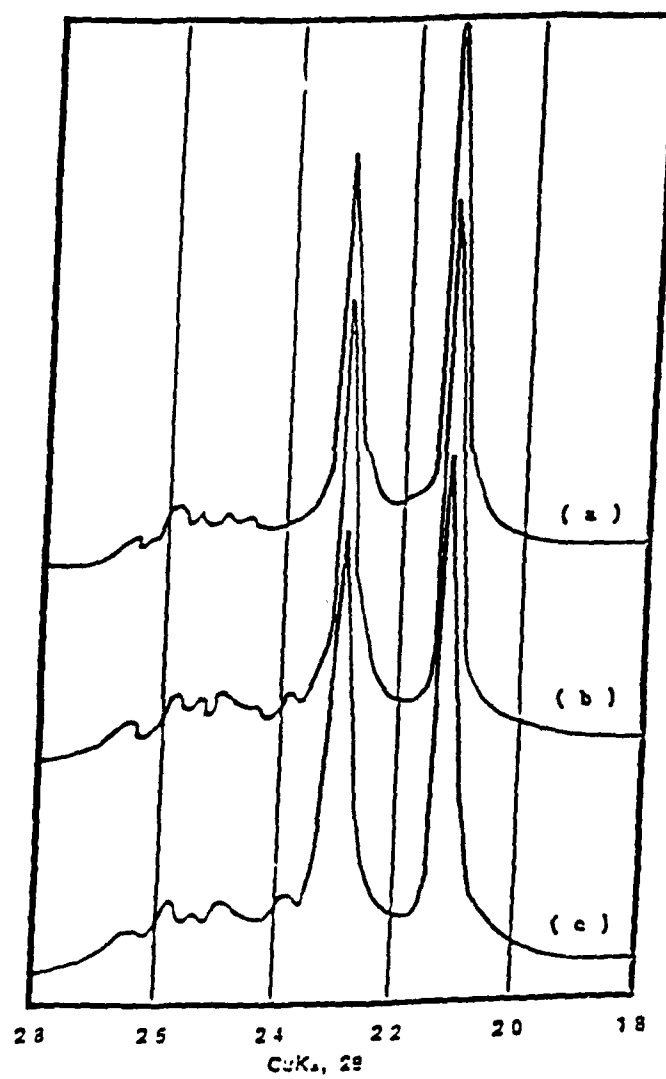


Figure 30. X-ray Diffraction Patterns for NaZSM-48(200).
Effect of Calcination Temperature

- (a) Calcination Temperature = 1323 K
- (b) Calcination Temperature = 1023 K
- (c) Calcination Temperature = 823 K

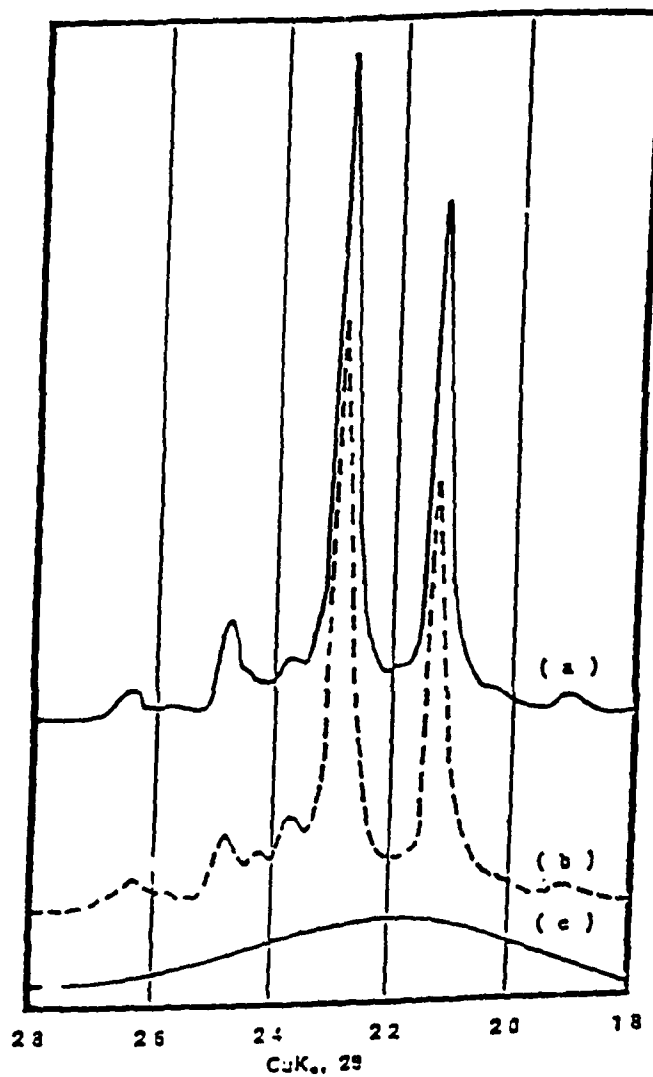


Figure 31. X-ray Diffraction Patterns. Effect of C6DN/SiO_2 on the Synthesis of ZSM-48.

- (a) $\text{C6DN/SiO}_2 = 0.3$
- (b) $\text{C6DN/SiO}_2 = 0.2$
- (c) $\text{C6DN/SiO}_2 = 0.1$

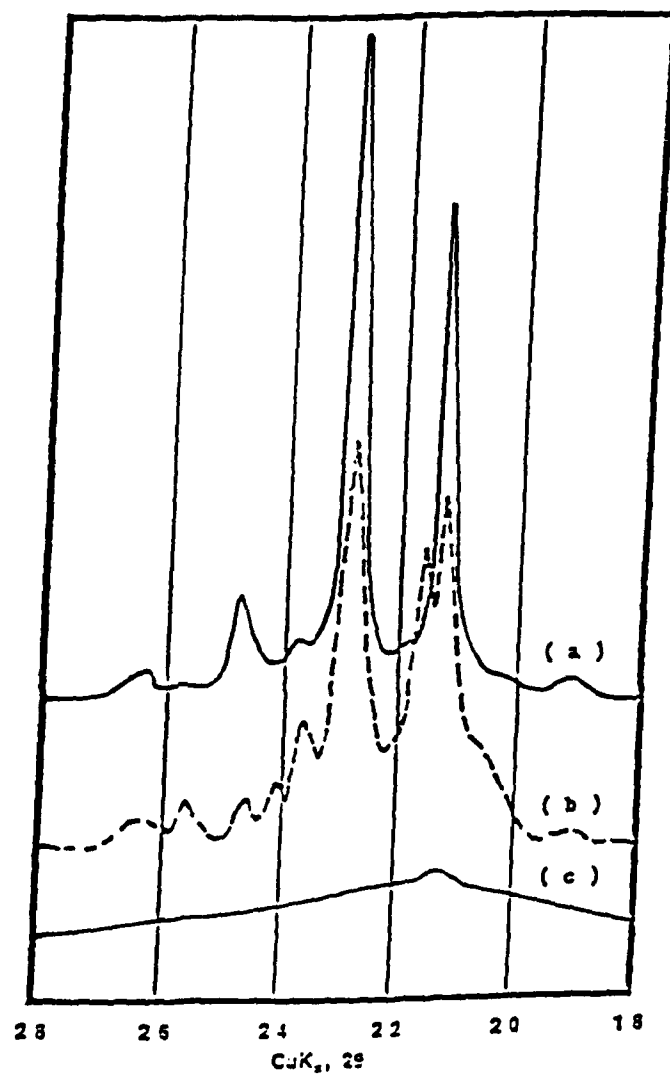


Figure 32. X-ray Diffraction Patterns. Effect of Na/SiO₂ Ratio on the Synthesis of ZSM-48.

- (a) Na/SiO₂ = 0.59
- (b) Na/SiO₂ = 0.45
- (c) Na/SiO₂ = 0.30

the hydrated cation forms the nucleus of certain secondary building units.²⁰ For example, the dehydrated sodium ion influences the formation of a double four ring (D4R) or double six ring (D6R) and the hydrated sodium cation causes the formation of sodalite units. However, the relationship between the cation influence on the structure and the cation influence on gel chemistry is not well-understood. The major complication associated with the use of the cation in the synthesis of ZSM-48 may be that its incorporation results in a specific chemical environment could also affect the nucleation process, and hence the formation, of a particular zeolite, e.g., ZSM-48X.

The initial precipitation of gel and its subsequent conversion to a zeolite may be considered to be an example of Ostwald's rule of successive transformation.²³⁰ According to this rule, the first phase to appear is always thermodynamically less stable than the phase that subsequently replaces it. The first crystals of ZSM-48X to nucleate and grow from the gel having an initial molar Na/SiO₂ ratio equal to 0.45 could not be replaced in the aqueous reaction mixture by another crystalline species such as zeolite ZSM-48. Since the sequence always occurs in the direction of increasing thermodynamic stability, replacement reactions that lead to the less stable zeolite ZSM-48X become possible when it is calcined at high temperatures. The effect of ZSM-48X calcination temperature on the phase transformation is shown in Figure 33. The formation of a thermally stable crystalline species (see Figure 33a) was observed at a calcination temperature of 1323 K. It should be noted that the pure ZSM-48, i.e., ZSM-48(200), was not involved in the phase transformation or structural change at 1323 K (shown in Figure 30a). The SEM images of synthetic ZSM-48X are presented in Figure 34. It should be noted that the topographies of the ZSM-48X calcined at 1323 or 823 K did not change significantly. This may result from a rearrangement of the framework of ZSM-48X (or phase transformation) at high temperatures,

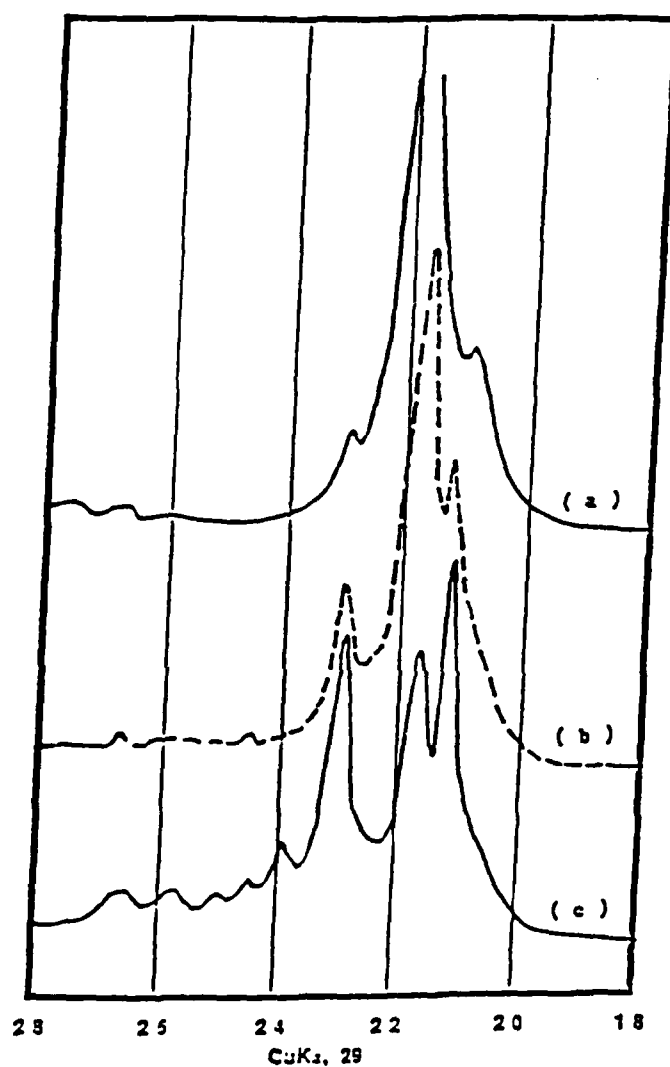
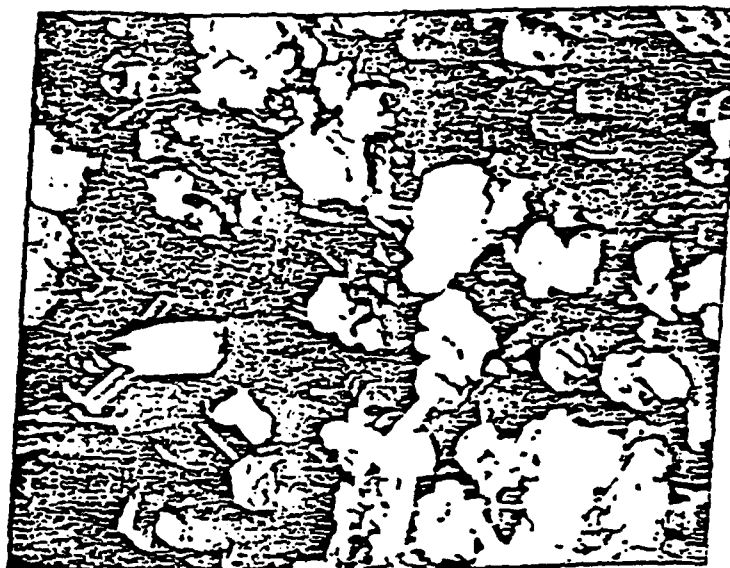


Figure 33. X-ray Diffraction Patterns of NaZSM-48X.
Effect of Calcination Temperature on Phase Transformation.

- (a) Calcination Temperature = 1323 K
- (b) Calcination Temperature = 1023 K
- (c) Calcination Temperature = 823 K



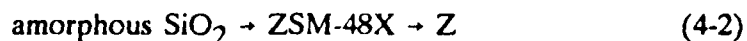
(a) Calcined at $T = 823$ K in air for 16 hours



(b) Calcined at $T = 1323$ K in air for 16 hours

Figure 34. Scanning Electron Microscope Images of NaZSM-48X.
Effect of Calcination Temperature

which may not be distinguished from their topographies directly. A ZSM-48X-type crystalline material was also obtained from a similar reaction mixture at a crystallization temperature of 503 K. The comparison of the X-ray diffraction patterns for the ZSM-48X at zeolite crystallization temperatures of 503 and 453 K is presented in Figure 35. It appears that in the reaction sequence



the system prefers to descend the ladder of relative thermodynamic stabilities in a series of steps rather than in a single step. The symbol Z represents a crystalline material of unknown structure. On the other hand, the necessity of the right gel chemistry in the formation of the zeolite ZSM-48, and the influence of the gel chemistry on the final crystalline material, can not be underemphasized. The structure-directing role of the alkali metal cations in the synthesis of ZSM-48 must also be considered. The crystalline material ZSM-48X was not evaluated catalytically.

The various methods for preparing ZSM-48 result in final products containing substantial amounts of sodium ion. The sodium form was ammonium exchanged to give the hydrogen-form of ZSM-48. A comparison of the SEM images of the hydrogen and sodium forms of ZSM-48 is presented in Figure 36. It was observed that both forms of the ZSM-48 have a similar morphology. The ZSM-48 crystalline material consisted of rod-like crystals with 0.2 - 0.4 μm in width and three-to-five μm in length.

Chemical Composition

The chemical compositions of the zeolites prepared in this study were measured by the electron microprobe analysis (Table 24). In most of the samples, the molar $\text{SiO}_2/\text{Al}_2\text{O}_3$ ratios of

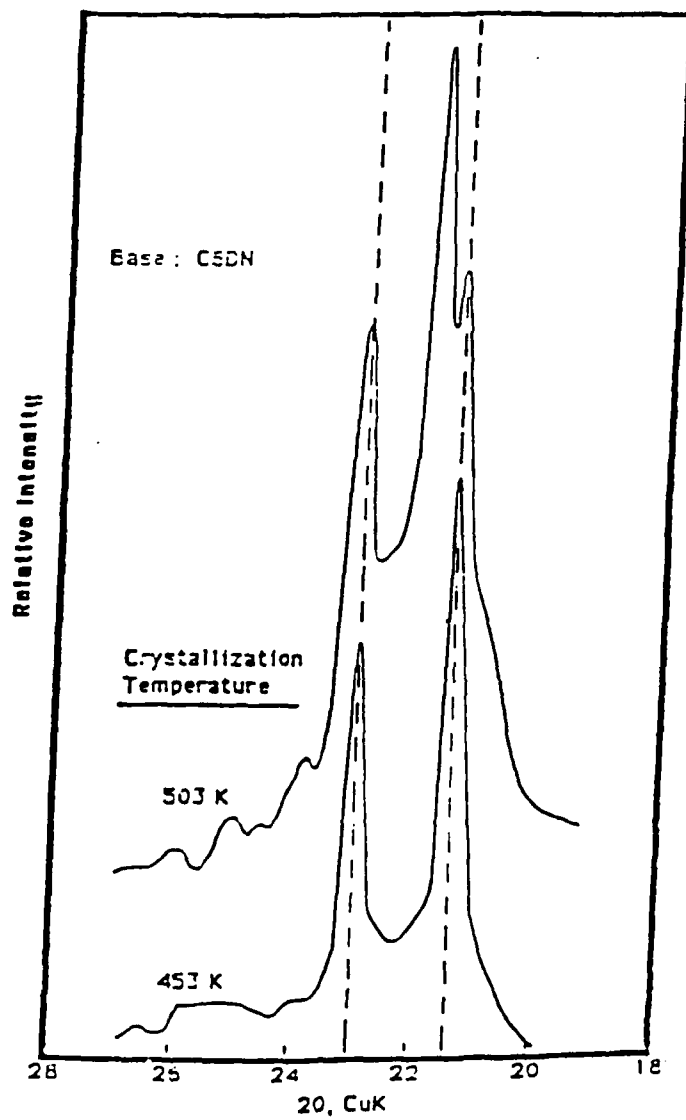


Figure 35. Effect of Crystallization Temperature on the Synthesis of ZSM-48



Sodium-form



Hydrogen-form

Figure 36. Scanning Electron Microscope Image of ZSM-48(200).

Table 24
Chemical Composition of Synthesized Zeolites

Zeolite	IMR SiO₂/Al₂O₃	FMR SiO₂/Al₂O₃
ZSM-5M	N/A	70
ZSM-5D	70	76
ZSM-5(35)	35	40
ZSM-5(70)	70	74
ZSM-5(105)	105	123
ZSM-48(200)	200	239
ZSM-48(100)	100	104
ZSM-48(70)	70	76
ZSM-48(40)	40	49

Note:

IMR: Initial Molar Ratio

FMR: Final Molar Ratio Measured by Electron Microprobe

the crystalline products were higher than the molar $\text{SiO}_2/\text{Al}_2\text{O}_3$ ratios of the parent hydrous gels. Considering the fact that the difference of the $\text{SiO}_2/\text{Al}_2\text{O}_3$ molar ratio between reaction mixture and product is great in these high-silica zeolites, it is presumed that generation of silicon-rich nuclei would be favored during crystallization and that the presence of aluminum in the reaction mixture is not always necessary.

Summary

1. The H-form ZSM-5 can be synthesized directly by the use of diamines as the organic ions.
2. Silicon-rich nuclei of ZSM-5 formed during the initial nucleation process.
3. No direct evidence was obtained to indicate that organic ions function as templates for the synthesis of ZSM-5 or ZSM-48.
4. Zeolite ZSM-48 could only be synthesized at $\text{SiO}_2/\text{Al}_2\text{O}_3 > 200$ at typical reaction conditions in this investigation.
5. A nonintergrowth mixture of ZSM-5 and ZSM-48 formed at $\text{SiO}_2/\text{Al}_2\text{O}_3 = 70$.
6. It is possible that the structure of ZSM-48 was directed highly by sodium ions during the crystallization of the sample.

Characterization of Synthesized Zeolites

Thermal Desorption

Temperature-programmed desorption was used to investigate the acidity of the zeolites prepared in this investigation. The zeolite samples were reacted with ammonia by exposure to ammonia for at least 30 minutes at room temperature. It is believed that the strong acid sites are completely saturated with ammonia since one can determine the excess weakly adsorbed ammonia on the high-silica zeolite surfaces. The excess physisorbed or weakly bonded ammonia

was removed by purging the catalyst with helium. The samples were then heated at a linear rate of (5 K/min) in flowing helium and the amount of ammonia desorbed was continuously monitored with a thermal conductivity detector.

The temperature-programmed desorption (TPD) profiles for ammonia desorption from fresh HZSM-5 ($\text{IMR SiO}_2/\text{Al}_2\text{O}_3 = 70$) and spent HZSM-5 (following the methanol conversion reaction) are presented in Figures 37 and 38, respectively. At least four discrete features at 410, 480, 700, and 830-860 K were observed corresponding to adsorption on Site I, Site II, Site III, and Site IV, respectively. Since the interactions between ammonia and Sites I and II are weak for both of fresh and spent ZSM-5, they are attributed to physisorbed ammonia on ZSM-5 surfaces. The uptakes of ammonia for the fresh ZSM-5 at Site III and Site IV are greater than that for the spent ZSM-5. This indicates that these two sites may be related to the catalytically active centers in ZSM-5 since they have been partially deactivated in the methanol conversion. It is believed that site III and site IV are the Brönsted acid sites and Lewis acid sites, respectively.¹¹⁹

The TPD profile for ammonia desorption from ZSM-48 is presented in Figure 39. The broadening of the desorption band in the temperature range assigned to Type III sites for ZSM-48 may be due to the influence of the channel system of ZSM-48 which could also play a role in molecular traffic control with desorbed ammonia. Furthermore, the differences in the ammonia desorption profiles in the temperature range from 300 to 550 K for ZSM-5 (Figure 37) and ZSM-48 (Figure 39) may also indicate a difference of channel structure for these two types of zeolites. It should be noted that ZSM-48 has an intermediate pore diameter and a two-dimensional non-intersecting channel system.⁴⁹

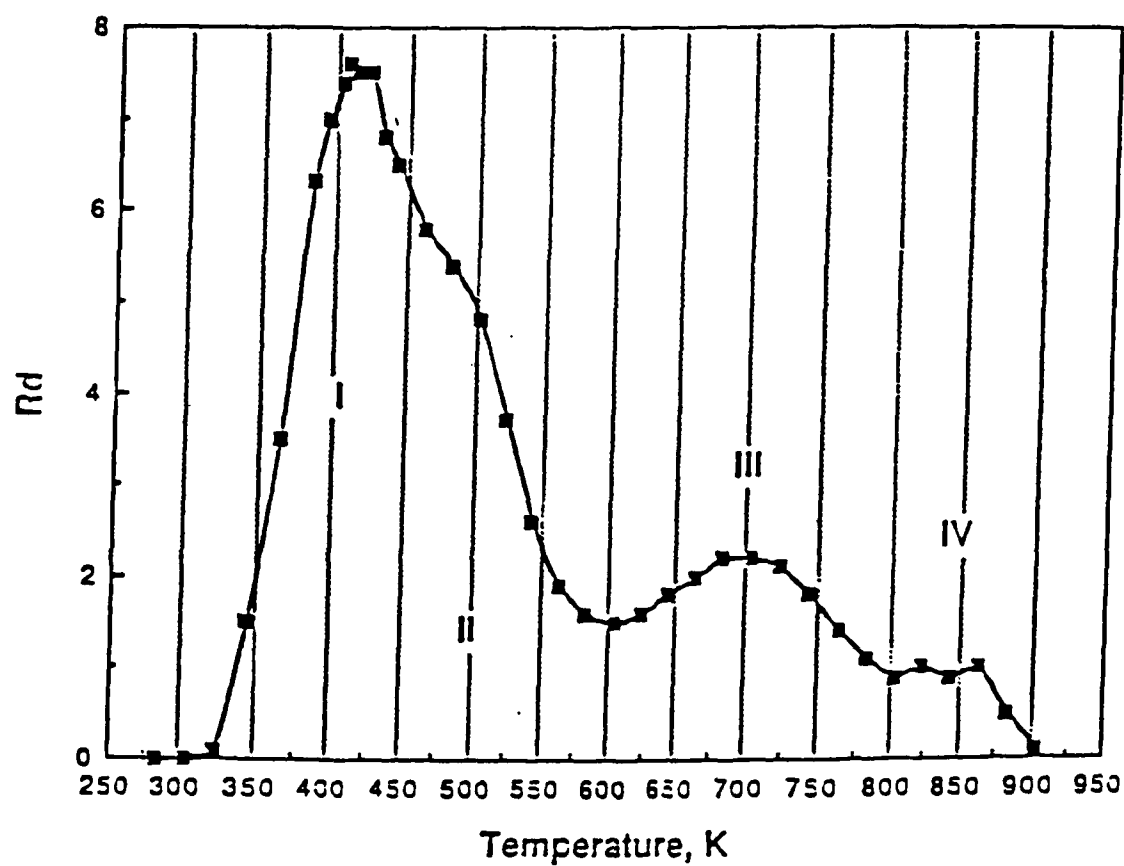


Figure 37. Temperature-Programmed Desorption Spectrum of Ammonia. Fresh ZSM-5 Catalyst

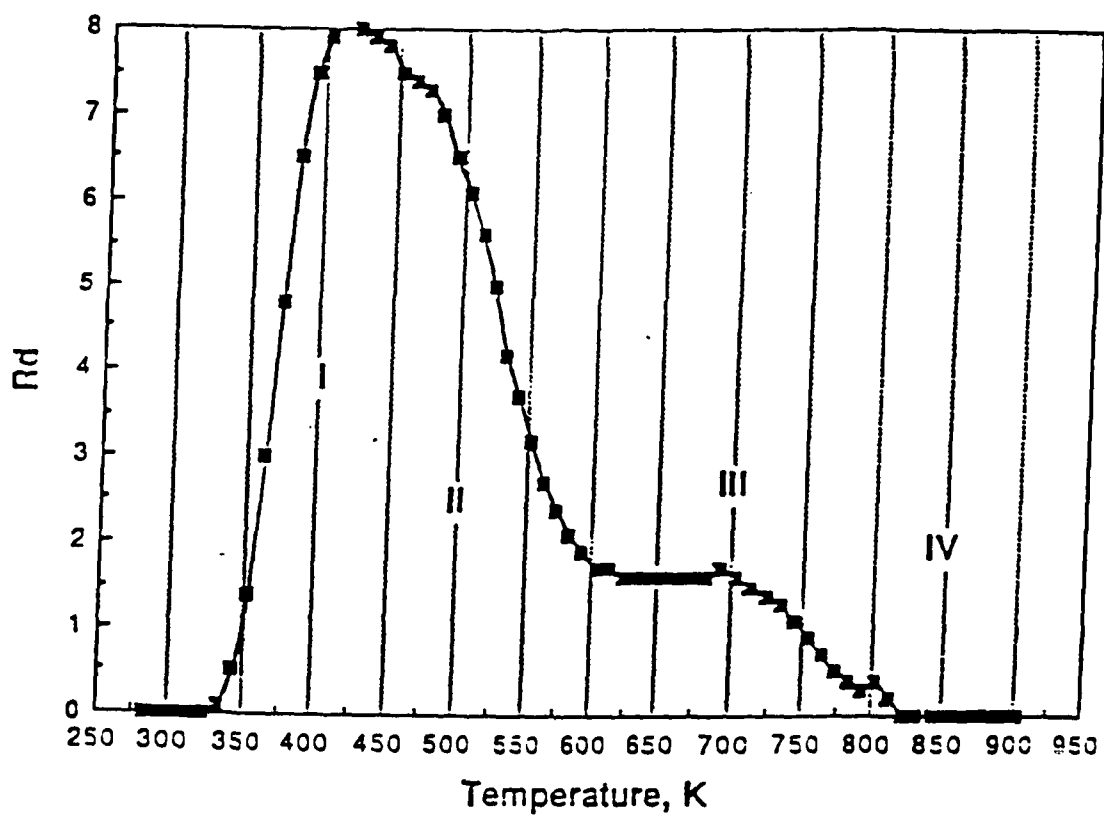


Figure 38. Temperature-Programmed Desorption Spectrum of Ammonia Spent ZSM-5 Catalyst

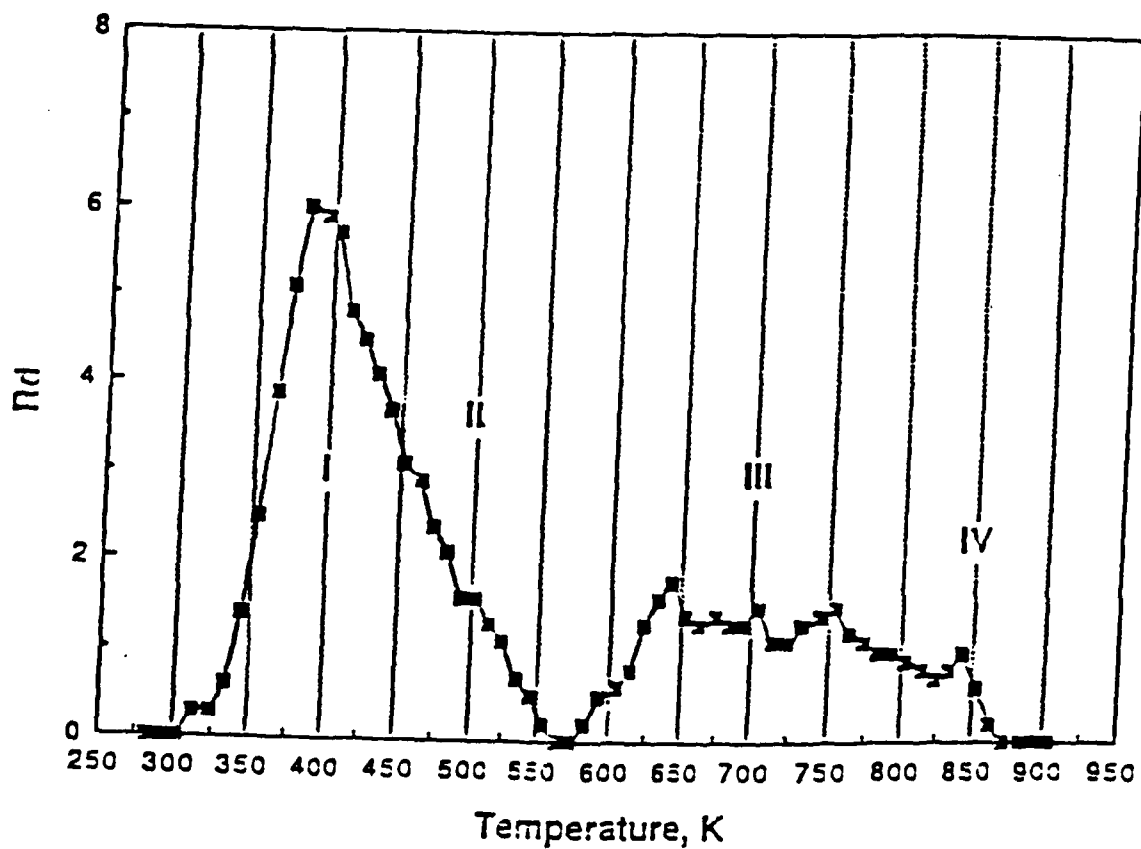


Figure 39. Temperature-Programmed Desorption Spectrum of Ammonia Zeolite ZSM-48/5(70)

The TPD profile for ammonia desorption from HZSM-48/5(70), which has been shown to be a physical mixture of ZSM-5 and ZSM-48, is presented in Figure 40. It is also consistent with the conclusions from the SEM study for zeolite ZSM-48/5(70) (Figure 26) indicating that the zeolite is not an intergrowth mixture of ZSM-5 and ZSM-48. Furthermore, it should be noted that the HZSM-48/5(70) consisted of at least 75 wt. percent of ZSM-5 and 25 wt. percent of ZSM-48 (see Figure 25).

Alcohol desorption from ZSM-5 was studied on a therm-gravimetric analyzer (TGA) equipped with a temperature-programmed controller. The thermal desorption profiles are presented in Figure 41. Physisorbed and chemisorbed methanol were desorbed from ZSM-5 surface in the temperature ranges 323 - 473 K and 473 - 523 K, respectively. Other higher alcohols (C_2 - C_4 normal-alcohols) produced corresponding alcohols, olefins, and oligomers via surface reactions when desorbed from ZSM-5. This indicates that the minimum temperature for the reaction of alcohols over ZSM-5 was around 625 K.

Infrared Spectroscopy

Infrared spectroscopy has been widely used to identify species adsorbed on solid surfaces. During the last decade, there has been increasing use of infrared spectroscopy in structural investigations of zeolites, particularly when the powder X-ray diffraction method may not be suitable for measuring structural information of zeolites with different crystalline sizes. Furthermore, infrared spectroscopy is concerned with short-range order that is only slightly different for zeolites of the same group.

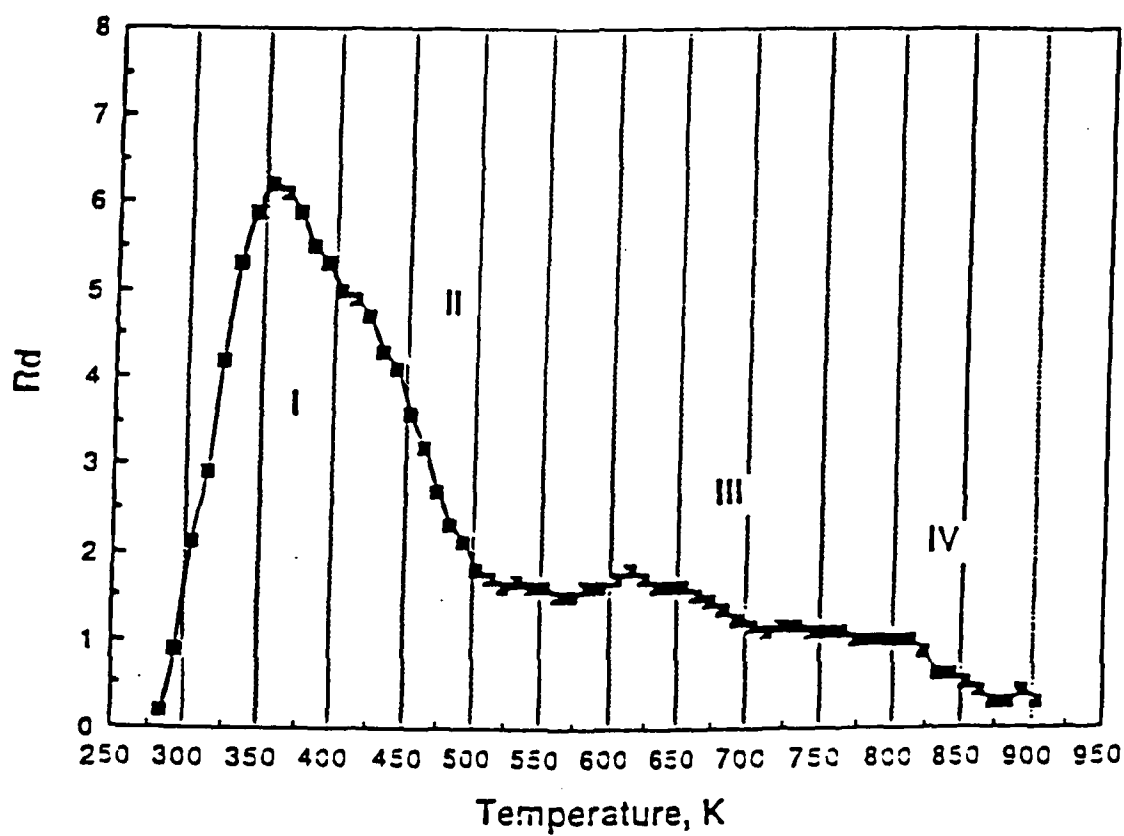


Figure 40. Temperature-Programmed Desorption Spectrum of Ammonia Zeolite ZSM-48/5(70)

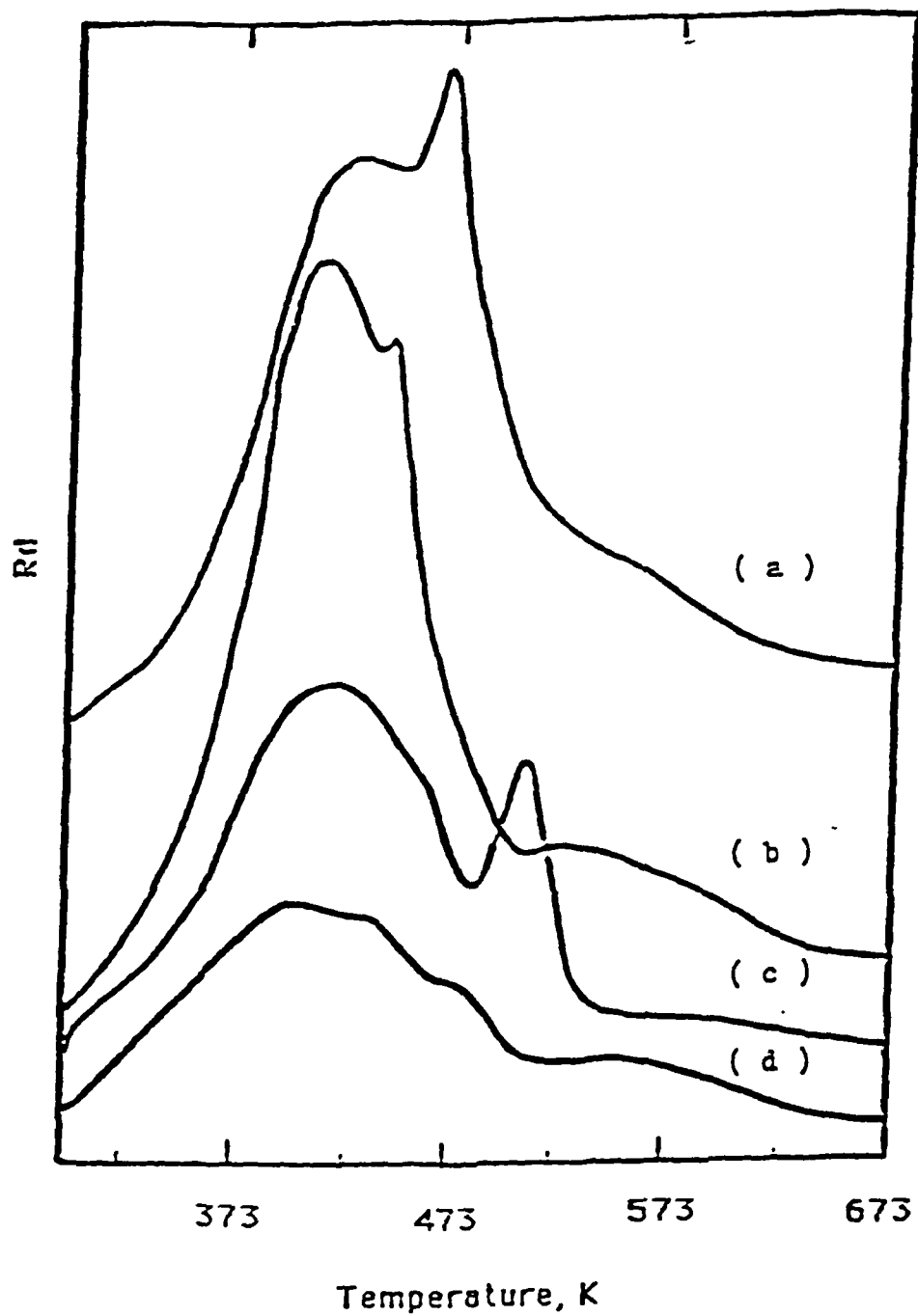


Figure 41. Temperature-Programmed Desorption Spectra of Alcohols from HZSM-5:

- | | | | |
|-----|------------|-----|----------|
| (a) | n-Butanol | (c) | Ethanol |
| (b) | n-Propanol | (d) | Methanol |

The diffuse reflectance FTIR spectra of the zeolites prepared in this investigation are presented in Appendix A. According to the Flanigen-Khatami-Szymanski correlation,²³¹ the 650-550 cm^{-1} band was empirically assigned to the presence of double-rings of tetrahedra in the framework of a zeolite. A band around 500 cm^{-1} , which was not observed in silica, may be attributed to internal vibrations of ZSM-5 or ZSM-48. The optical density ratios of the A ($\sim 600 \text{ cm}^{-1}$) and B ($\sim 500 \text{ cm}^{-1}$) bands determined from normal coordinate calculations are presented in Table 25. It appears reasonable to use the optical density ratio, A/B, as a criterion for determining the structural characteristics of the zeolite frameworks since the ratio depend on the variety of the external vibrations of the zeolites. Thus, one may predict that the A/B ratio increases as the degree of the external vibrations, which are assigned to linkages of the TO_4 -tetrahedra, increases. This is true that for high crystallinity zeolites, the A/B ratio of ZSM-5 is equal to ~ 0.8 and that of ZSM-48 is equal to ~ 0.3 . These data also fit quite well in Figure 25, which shows the effect of the $\text{SiO}_2/\text{Al}_2\text{O}_3$ ratio on the synthesis of ZSM-48. This indicates that infrared spectroscopy also has a potential for offering structural information of zeolite materials.

Infrared spectra were measured using an in situ diffuse reflectance FTIR method during and after pulse methanol reaction with zeolites ZSM-5 and ZSM-48 at 643 K. The difference spectra are shown in Figure 42. The negative features at 3600 and 3745 cm^{-1} observed during methanol reaction may be correlated to the positive feature around 3000 cm^{-1} which is attributed to adsorbed hydrocarbons. The strong broad positive feature between 3000 and 3700 cm^{-1} corresponds to absorption of water (free water plus weakly adsorbed water molecules) produced during methanol reactions. Irreversibly adsorbed hydrocarbons were observed only with ZSM-48 following the methanol reaction.

Table 25

IR Structural Characteristics of the Zeolite Frameworks

Zeolite	Optical Density Ratio, ^a A/B	XRD Crystallinity
HZSM-5M	0.80	100
HZSM-5D	0.81	95
HZSM-5b	0.74	91
HZSM-5(35)	0.84	99 ⁺
HZSM-5(70)	0.83	99 ⁺
HZSM-5(105)	0.82	99 ⁺
H{In}ZSM-5	0.81	99 ⁺
HZSM-48(200)	0.25	ZSM-48
HZSM-48/5(100)	0.51	ZSM-5/ZSM-48
HZSM-48/5(70)	0.65	ZSM-5/ZSM-48
H{In}ZSM-48	0.33	ZSM-48
SiO ₂	0	0

^aOptical Density Ratio, A/B, is defined in the text.

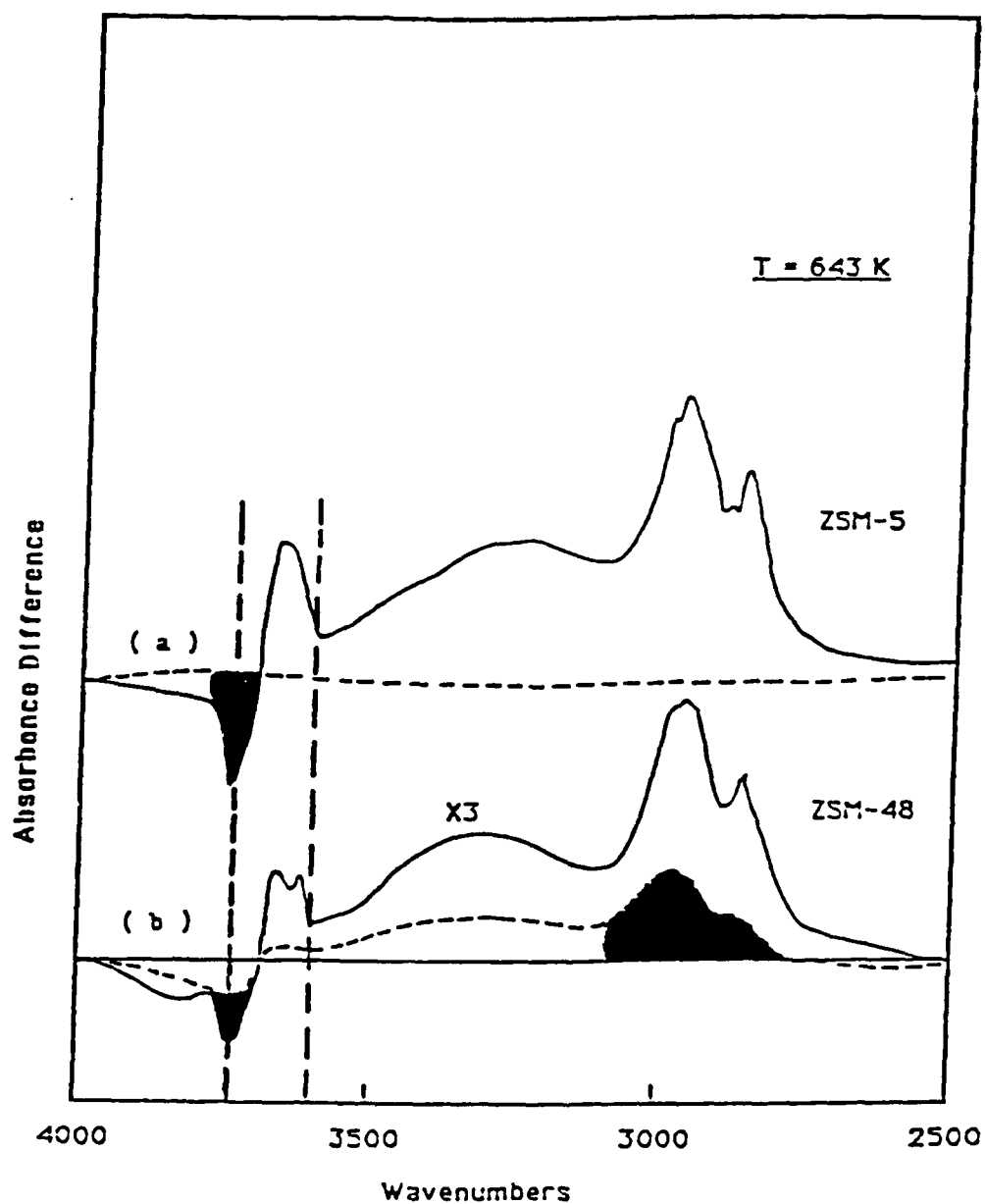


Figure 42. In-situ Diffuse Reflectance FTIR Study of Methanol Conversion over ZSM-Type Zeolites

The thermal desorption of methanol from ZSM-5 and ZSM-48 was also studied using diffuse reflectance FT-IR. The zeolite sample was exposed to methanol vapor at room temperature and heated to the desorption temperatures in the flowing helium. The infrared difference spectra for thermal desorption of methanol from ZSM-5 are presented in Figure 43. The background spectrum was measured on a fresh ZSM-5 sample at room temperature. Methanol interacted with the silanol group at 3710 cm^{-1} and strongly with the hydrogen cation (Brönsted acid site) at 3600 cm^{-1} . Similar results are also observed for ZSM-48 which is presented in Figure 44. However, because of the interference of the hydrogen-bonded hydroxyl groups, the behavior of aluminum-bonded hydroxyl groups (Bronsted sites) could not be observed clearly enough to interpret the difference in the distribution of Brönsted sites between ZSM-5 and ZSM-48 which was observed by ammonia-TPD spectroscopy.

Catalytic Cracking of n-Hexane

The cracking of n-hexane provides a suitable test reaction that is free of diffusion limitations for both intermediate pore size zeolites ZSM-5 and ZSM-48. Primary data (Appendix B) on catalytic cracking activity were obtained from measurements of n-hexane conversion to $C_1 - C_5$ hydrocarbons (mostly C_3 and C_4 aliphatics) in a continuous flow microreactor. A suitable choice of reaction temperature was made for each zeolite so as to maintain conversion within a limited range (5-40 percent) because of the wide range of activities encountered or measured by hexane conversion. At a given temperature the magnitude of the first-order rate constant (k) was obtained from the expression:

$$k = (1/t)\ln[1/(1-\epsilon)] \quad (4-3)$$

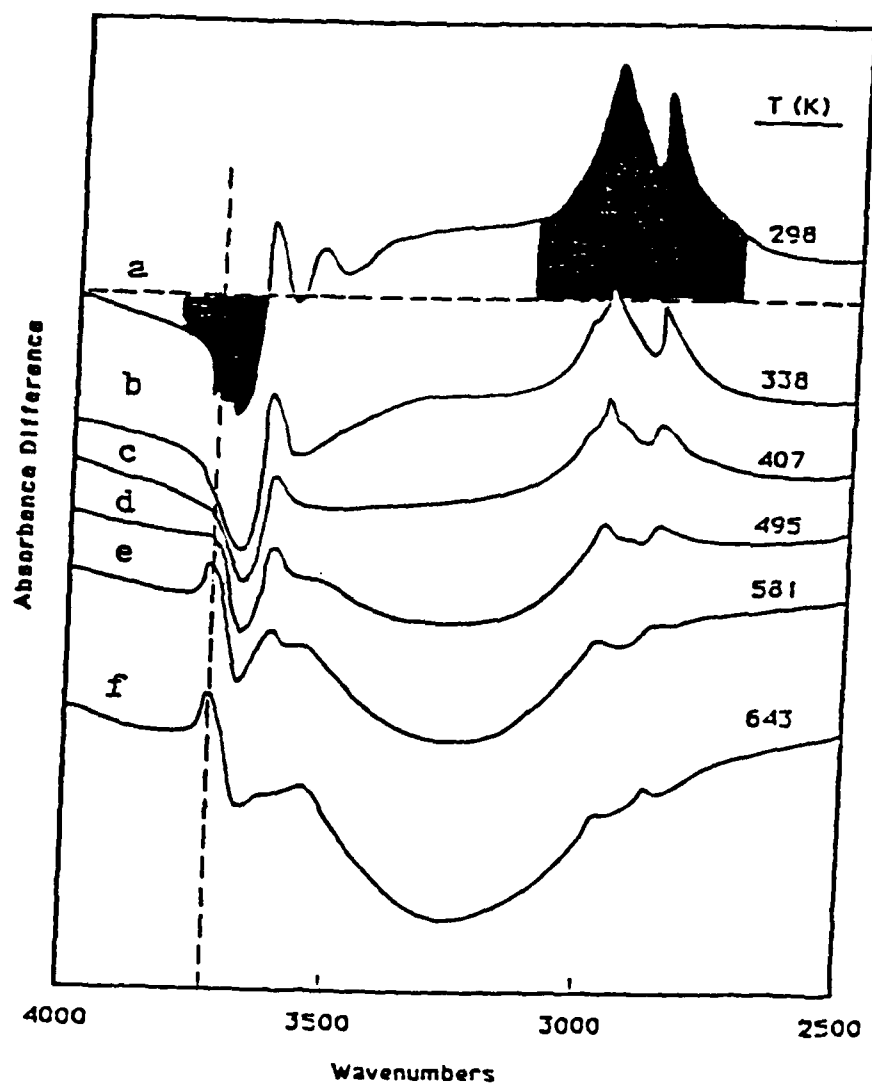


Figure 43. Diffuse Reflectance FTIR Study of the Thermal Desorption of Methanol from Zeolite ZSM-5

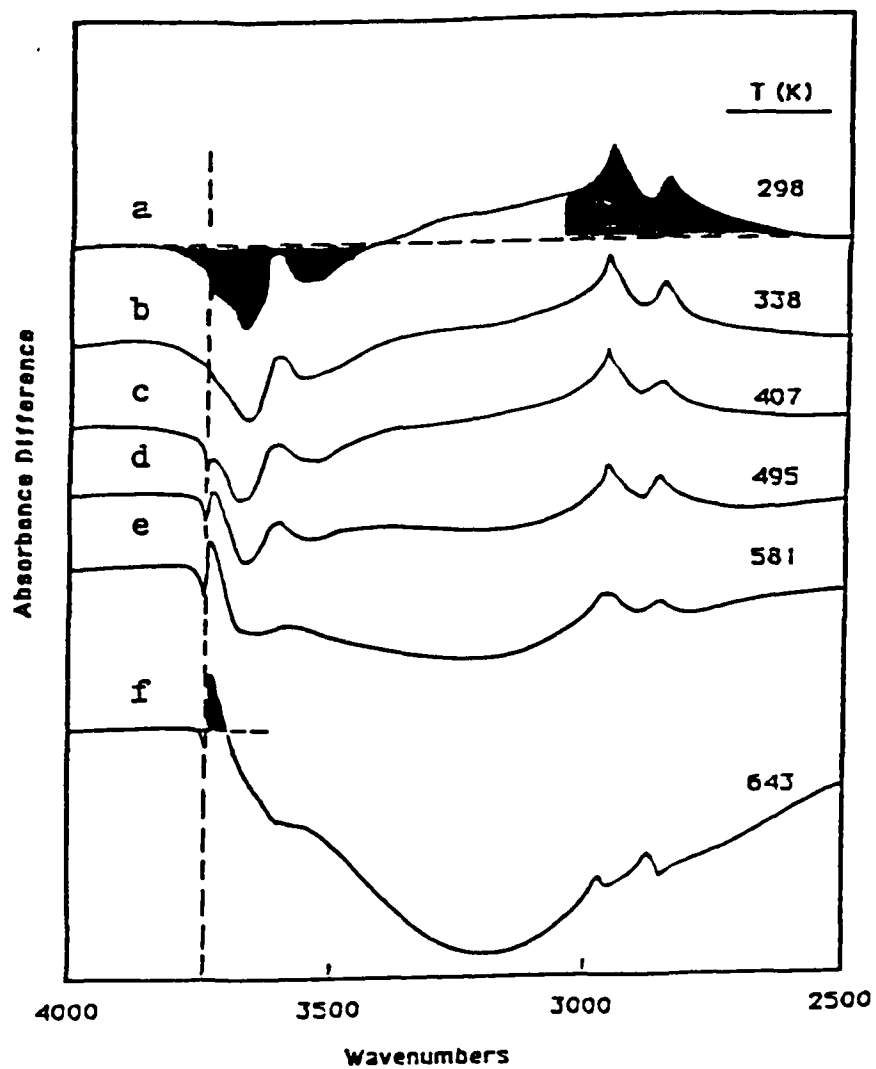


Figure 44. Diffuse Reflectance FTIR Study of the Thermal Desorption of Methanol from Zeolite ZSM-48

where ϵ is the observed fractional conversion and t is the contact time.¹⁵⁰

The results of hexane cracking over crystalline aluminosilicates including HY, ZSM-5, and ZSM-48 are presented in Figure 45. Attainable levels of superactivity of the order of magnitude of $\alpha > 10,000$ (relative to amorphous silica-alumina, $\alpha = 1$) were obtained for both ZSM-5 and ZSM-48. The zeolites Y and ZSM-5 showed a normal apparent activation energy of 30 kcal/mole. Interestingly, a deviation in apparent activation energy from the generally prevailing behavior for the ZSM-48-type zeolites was found. The slopes of the lines in Figure 45 indicate that the apparent activation energy for cracking of n-hexane over ZSM-48/5(70) is approximately one-half of the value (30 kcal/mol) for the ZSM-5 and the HY zeolite. Such a depression of the slope may be expected for a situation where diffusion inhibition corresponds to a utilization factor or Thiele modulus $n < 0.5$. This indicates that the true intrinsic rate constant of the ZSM-48-type zeolites was even greater than measured. The results may be attributed to the two-dimensional channel structure reported for the ZSM-48 which is expected to be different from other zeolites with three-dimensional pore/channel structure.

Isomerization of Isobutane

Product distributions in shape selective catalysis are governed by the size and shape of the pores or channels within the zeolite structure. These pores or channels restrict the diffusion of larger reactant and product species in addition to restricting the formation of larger transition states and hence limiting the size of the molecules that can react or form. The pores of ZSM-5 and ZSM-48 have openings of about 5.5 Å. They can admit linear and slightly branched paraffins, and simple naphthenes and aromatics.

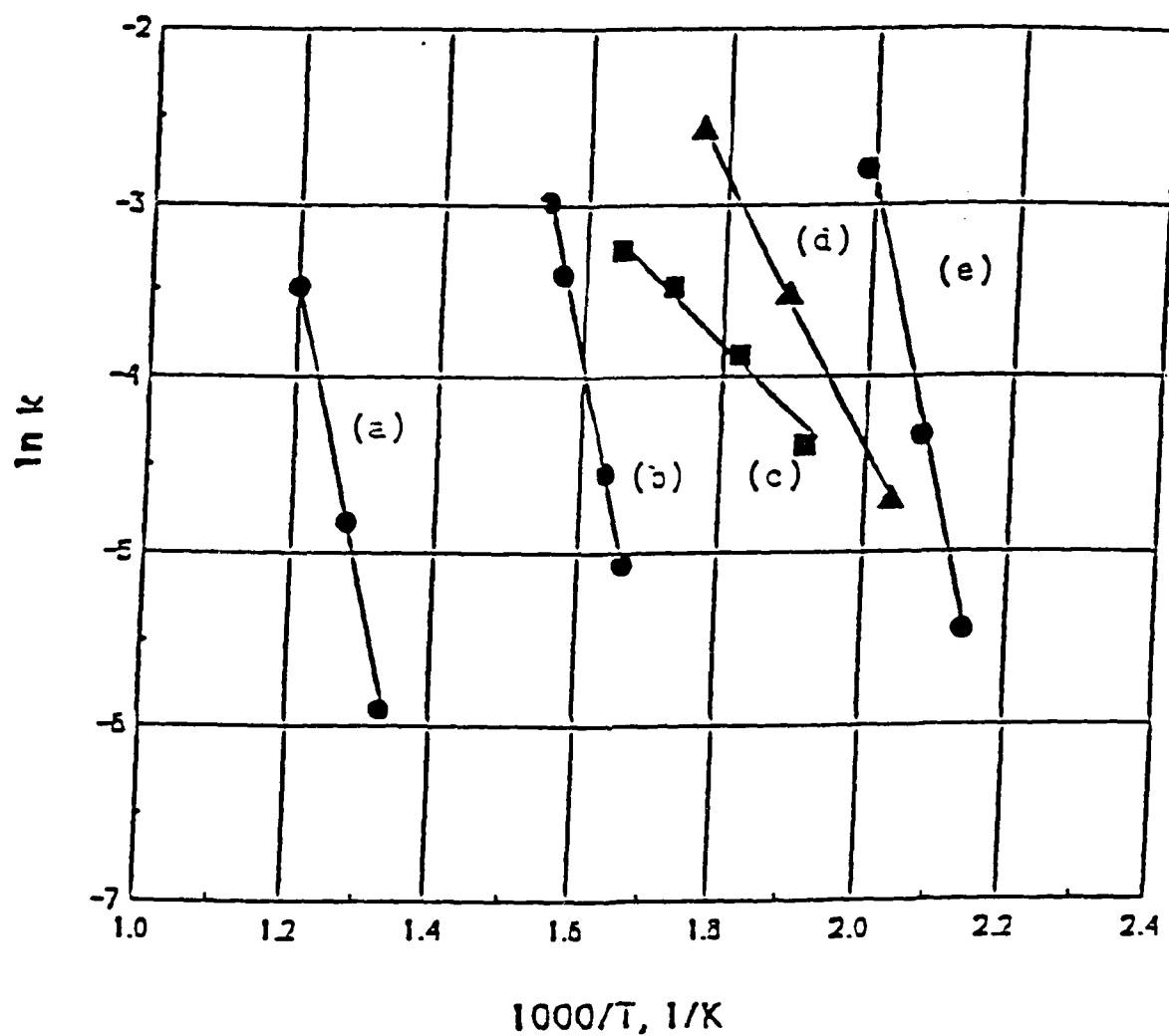


Figure 45. Alpha Test - Normal-Hexane Cracking Activity with Crystalline Aluminosilicates

- (a) Aluminosilica
- (b) HY
- (c) ZSM-48(200)
- (d) ZSM-48/5(70)
- (e) ZSM-5(70)

Isomerization of isobutane was studied at 623 K with a hydrogen/isobutane molar ratio of four in a microreactor to investigate the pore/channel structure of ZSM-5 and ZSM-48. The results are shown in Table 26. Pentanes were absent from the reaction product. This result is in agreement with the conclusion reached by Hilaireau et al.¹⁵⁴ that two isobutane molecules cannot be accommodated simultaneously at the channels intersections of ZSM-5. Thus it also suggests a mono-molecular reaction mechanism for isomerization of isobutane over ZSM-48. In other words, there is not enough space for a bimolecular (isobutane) transition state in the pores of ZSM-5 or ZSM-48.

Surface Area Measurement

The possible modes of nitrogen adsorption on the external and internal (pore system) surface of an intermediate pore zeolite ZSM-5 is illustrated in Figure 46. It also illustrates normal-hexane filling the pore/channel system of a zeolite. Thus, the external surface area can be measured with pores which are filled with normal-hexane. Furthermore, it is noted that it is impossible to form multiple layers of adsorbed nitrogen on the internal surfaces. Thus, even the use of the Langmuir isotherm may not be an appropriate method for the study of adsorption of nitrogen on the surfaces of a microporous (pore diameter $< 20 \text{ \AA}$) zeolite such as ZSM-5 or ZSM-48. A modified Langmuir method combined with a SEM geometrical method was used to investigate the surface area of the synthetic zeolites in this study.

The mean pore diameter for both ZSM-5 and ZSM-48 is believed to be 5.4 \AA . Thus the internal surface area corresponding to a mole of N_2 adsorbed at 77 K in the channel can be calculated as following.

Table 26
Isomerization of Isobutane at 623 K
Hydrogen/Isobutane Molar Ratio of Four

Zeolite	Product Distribution, wt%			Ref.
	Propane	n-Butane	Pentanes	
Mordenite	41	24	11	(128)
HY	7	2	7	This Work
HZSM-5(70)	0	0	0	This Work
HZSM-48(200)	0	0	0	This Work

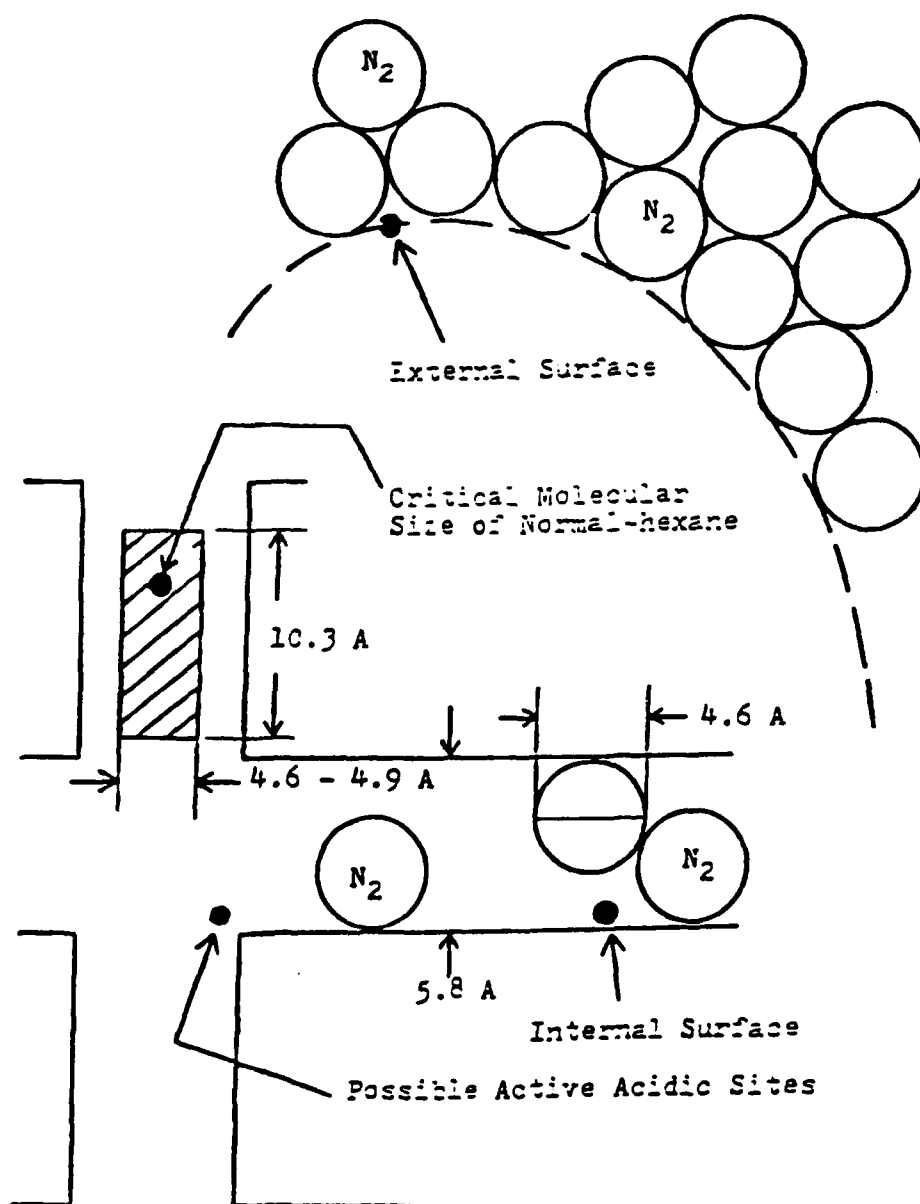


Figure 46. Possible Model for N_2 Adsorption of Zeolites with Intermediate Pore Structure

$$\text{Channel Diameter (Dc)} = 5.4 \times 10^{-10} \text{ m}$$

$$\text{Nitrogen Diameter (Dn)} = 4.6 \times 10^{-10} \text{ m}$$

$$\begin{aligned} \text{Channel Surface Area} &= \pi D_c D_n (6.02 \times 10^{23}) \\ &= 3.14 \times (5.4 \times 10^{-10}) \times (4.6 \times 10^{-10}) \times (6.02 \times 10^{23}) \\ &= 4.7 \times 10^5 \text{ (m}^2\text{/mole N}_2\text{ adsorbed)} \end{aligned}$$

Thus the internal surface area can be calculated.

$$\text{Weight of ZSM-5} = 0.222 \text{ g}$$

$$\text{Weight of ZSM-48} = 0.217 \text{ g}$$

$$\text{Adsorption of N}_2 \text{ at } p/p_0 = 0.63 \text{ and } T = 77 \text{ K}$$

$$\text{Adsorbed N}_2 \text{ on Fresh ZSM-5} = 1.17 \times 10^{-3} \text{ mole}$$

$$\text{Adsorbed N}_2 \text{ on Pore-filled ZSM-5} = 1.00 \times 10^{-3} \text{ mole}$$

$$\text{Adsorbed N}_2 \text{ in the Channel of ZSM-5} = 1.7 \times 10^{-4} \text{ mole}$$

$$\text{Adsorbed N}_2 \text{ on Fresh ZSM-48} = 7.37 \times 10^{-4} \text{ mole}$$

$$\text{Adsorbed N}_2 \text{ on Pore-filled ZSM-48} = 4.76 \times 10^{-4} \text{ mole}$$

$$\text{Adsorbed N}_2 \text{ in the Channel of ZSM-48} = 2.61 \times 10^{-4} \text{ mole}$$

Internal Surface Area of ZSM-5

$$\begin{aligned} &= (1.70 \times 10^{-3}) \times (4.7 \times 10^5) / 0.222 \\ &= 359.9 \text{ (m}^2\text{/g)} \end{aligned}$$

Internal Surface Area of ZSM-48

$$\begin{aligned} &= (2.61 \times 10^{-3}) \times (4.7 \times 10^5) / 0.217 \\ &= 565.3 \text{ (m}^2\text{/g)} \end{aligned}$$

The external surface areas of synthetic zeolites were measured geometrically by SEM images. The SEM pictures of zeolites revealed identifiable cube, sphere, or rod forms. Zeolite ZSM-5 exhibited cubic-like crystals 0.5 - 2 μm in diameter while zeolite ZSM-48 appeared to be a bundle of rod-like crystals. Based on these SEM images, the external geometrical surface area could be calculated as follows.

Calculation of external surface area of ZSM-5

$$D = 1 \times 10^{-6} \text{ m}$$

$$\text{Density } (\rho) = 1.8 \text{ g/cm}^3$$

$$\text{External Surface Area (A)} = 6/RD$$

$$A = 6/[(1 \times 10^{-6}) \cdot (1.8 \times 10^6)] = 3.3 \text{ (m}^2/\text{g)}$$

Calculation of external surface area of ZSM-48

$$D = 3 \times 10^{-7} \text{ m}$$

$$\text{Length (L)} = 4 \times 10^{-6} \text{ m}$$

$$\rho = 1.7 \text{ g/cm}^3$$

$$\text{External Surface Area (A)} = (1 + 4L/D)/\rho$$

$$A = [1 + (4 \times 10^{-6})/(3 \times 10^{-7})] + [(4 \times 10^{-6}) \times (1.7 \times 10^{-6})] = 2.1 \text{ (m}^2/\text{g)}$$

A summary of the surface area measurements for ZSM-5 and ZSM-48 is presented in Table 27. The total surface area measured for ZSM-5 in this work is generally consistent with the reported data.¹⁵⁹ Furthermore, one may expect that zeolite ZSM-48 could be effectively filled with normal-hexane since ZSM-48 has an one-dimensional channel structure while ZSM-5, with three-dimensional channel structure, may not be blocked all its pores by adsorbed normal-hexane.

Table 27
Surface Area Measurements of ZSM-5 and ZSM-48

	<u>Surface Area (m²/g)</u>	
	Internal (Filled-pore Method)	External (SEM Geometrical)
ZSM-5	359.9	3.3
ZSM-48	565.3	2.1

It is true that a higher internal surface area for ZSM-48 than that for ZSM-5 was obtained. In addition, it is believed that most of the active centers of ZSM-5 are located in the interchannel; thus blocking all its pores of ZSM-5 by adsorbed normal-hexane is impossible. A high normal-paraffin (molecular length $> 15 \text{ \AA}$) such as normal-dodecane should be able to block all its pores of ZSM-5 theoretically during surface area measurements.

Summary

1. The Brönsted acid sites of synthesized zeolites were characterized by an ammonia desorption feature near 700 K.
2. For high crystallinity zeolites, the optical density ratio, A/B (a criterion for determining the structural characteristics of the zeolite frameworks), for ZSM-5 is equal to 0.8 and that for ZSM-48 is equal to 0.3.
3. The interactions between active acidic sites and methanol molecules were observed by in situ and thermal desorption FTIR (diffuse reflectance) spectroscopy.
4. Attainable levels of superactivity of the order of magnitude of $\alpha > 10,000$ were observed for ZSM-5 and ZSM-48.
5. It appears that the pore structures of both synthesized ZSM-5 and ZSM-48 have intermediate pore diameters and may not have cages around interchannels.
6. A modified method for measuring the surface area of zeolites with micropores is reported. The relatively low external surface area measured indicates that the catalytic reactions mostly occur on the internal surfaces.

Reaction of Alcohols over Zeolites

Since the development of the process for the conversion of methanol to hydrocarbons by Mobil,³⁰ the reactions of higher alcohols over ZSM-5 catalysis have been widely studied.^{173,181,183} A review of these studies revealed that essentially the same product distribution was obtained for C_1 to C_6 alcohols which indicates that a common reaction network/pathway may be followed.¹⁷³ However, the effect of the channel structure of the ZSM-5 family of zeolites on the selectivity of alcohol reactions has not been described in the literature. The mechanisms of alcohol reactions are not fundamentally different over zeolite catalysts than they would be with any other acidic oxides from a purely chemical standpoint. Zeolites introduce molecular shape selectivity due to pore structure effects. In the course of this work, ZSM-5, ZSM-48, and related zeolites have been used for the systematic study of C_1 - C_4 alcohol reactions. The product distributions are summarized in Appendix III. It should be noted that ZSM-5 and ZSM-48 have similar pore diameters; however, they appear to have different channel structures. Thus these two catalysts were thought to be useful for this type of study.

The alcohol reactions were studied in a fixed-bed continuous flow microreactor operating at atmospheric pressure. Alcohols were fed to the reactor from a saturator by means of helium carrier gas. Reaction product distributions were recorded after 40 minutes on-stream. The most significant aspect of the methanol reaction over both ZSM-5 and ZSM-48 is the cut-off point in the hydrocarbon product distribution at C_{10} aromatics in the reaction temperature range of 594-759 K (shown in Figures 47 and 48, respectively). The aromatic fractions consisted mainly of xylenes and toluene with a smaller amount of benzene, ethylbenzene, and higher alkylated aromatics. The distribution of substituted aromatics is, of course, controlled by the dimensions of

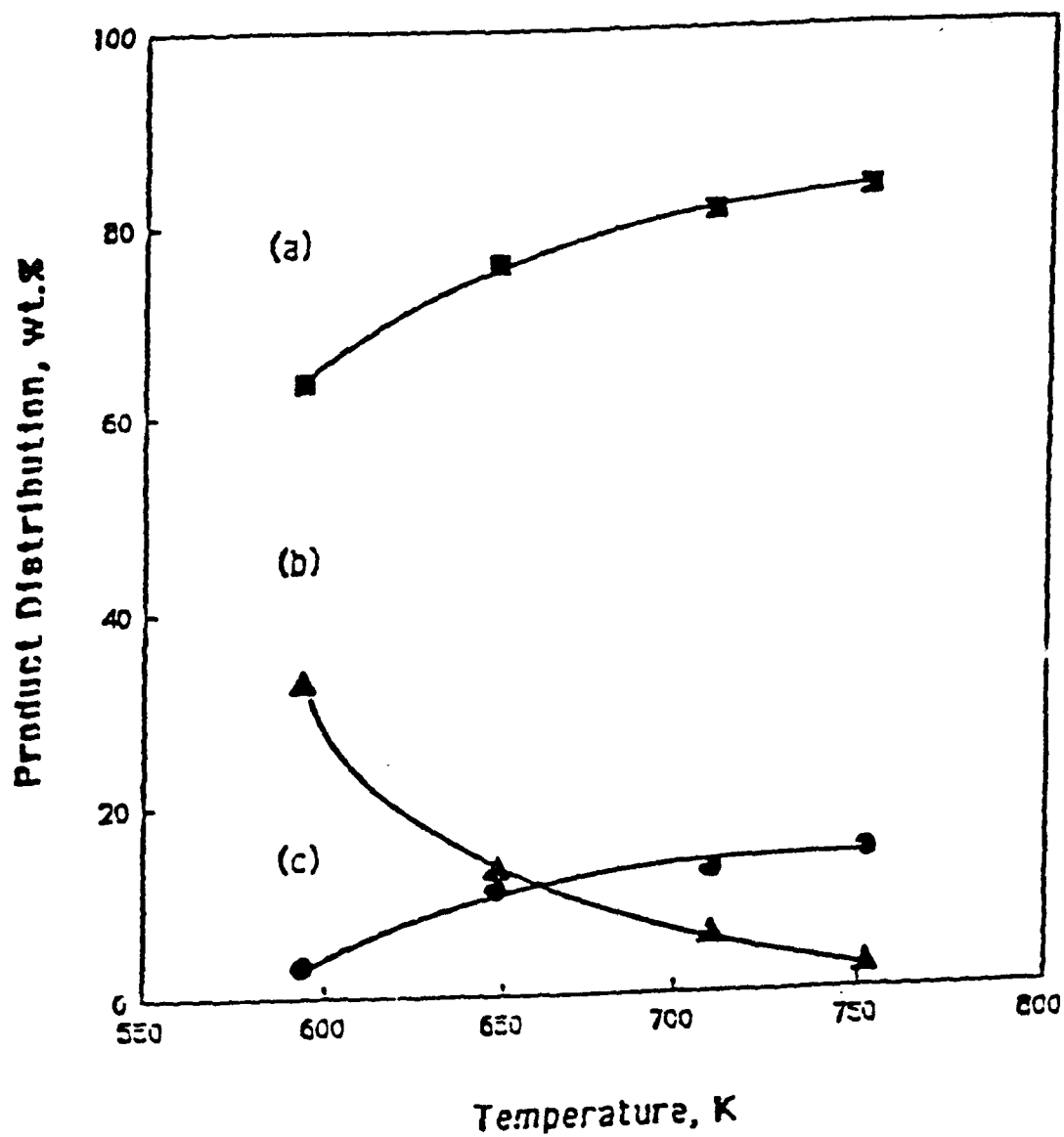


Figure 47. Product Distribution from Methanol Conversion over Zeolite HZSM-5(70) Helium Carrier Gas

(a) $C_1 - C_5$; (b) C_6+ ; (c) Total Aromatics

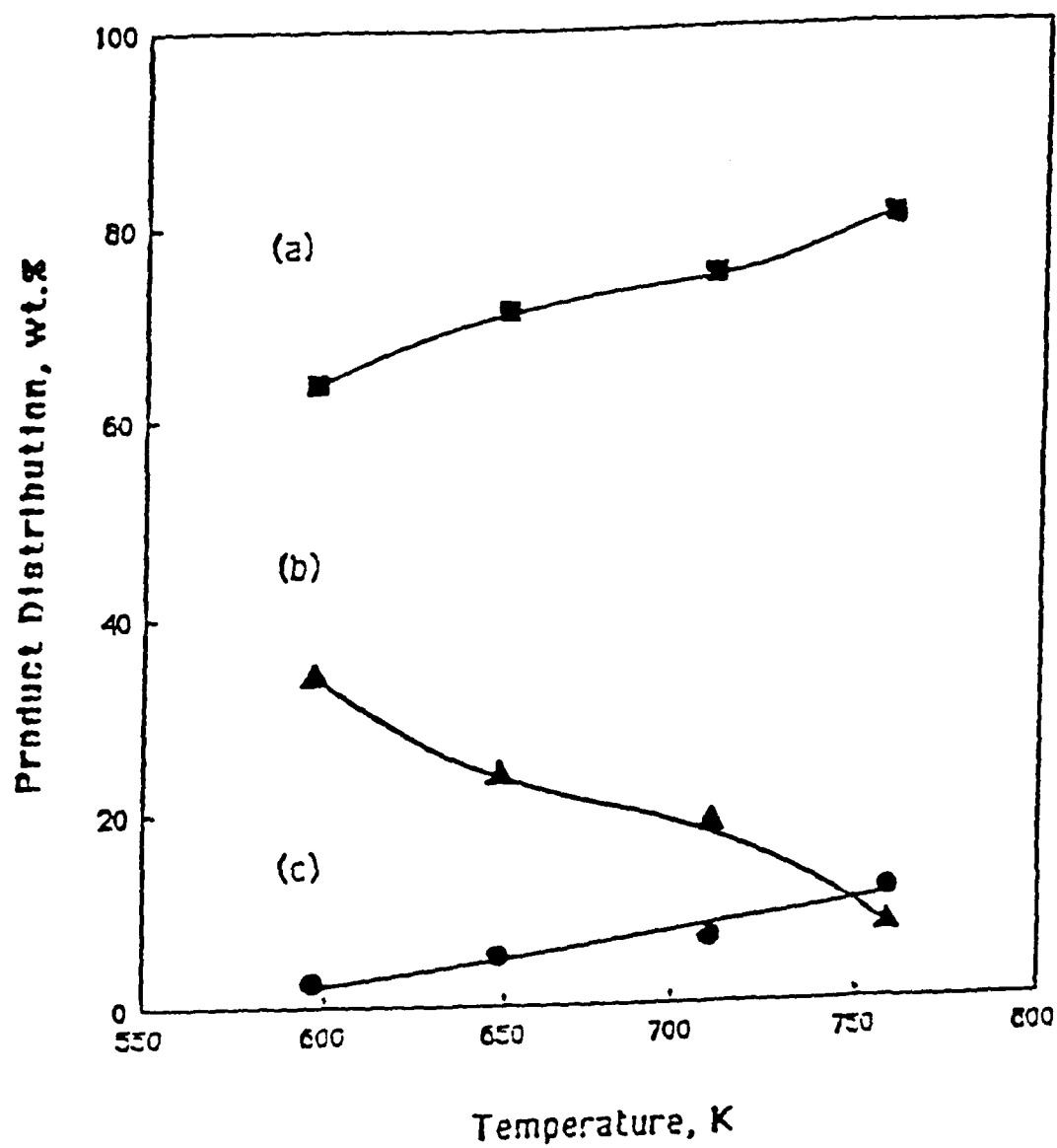


Figure 48. Product Distribution from Methanol Conversion over Zeolite HZSM-48(200) Helium Carrier Gas

(a) $C_1 - C_5$; (b) C_6+ ; (c) Total Aromatics

the intracrystalline pore structure. Catalysis on unconstrained exterior sites would not account for the observed aromatic yields nor for the cut-off at C₁₀ aromatics. Moreover, the surface area of the synthetic zeolites on the exterior is at least two orders of magnitude less than that on the interior (Table 27). Therefore, methanol would be expected to have access to the internal acidic sites and it is likely that most of the conversion to hydrocarbons occurred on these sites.

At a temperature of 594 K the reaction of methanol over ZSM-5 gave a low yield of aromatics, which were mainly xylenes. The main products were C₁ to C₈ aliphatic hydrocarbons. These aliphatics were further converted to aromatics as the temperature was increased up to 648 K; however, as the temperature was increased up to 752 K, the light gas yield increased as a result of secondary cracking. A similar trend was observed with ZSM-48; however, aromatic selectivity was lower (Table 28). The aromatic distribution is believed to be very sensitive to structural differences between the two zeolites. These differences may be attributed to the larger space available at the channel intersections of ZSM-5, which allowed the formation of larger carbonium ion intermediates for further reactions. The size and shape of the channel intersections are essential to explain the effects of transition state selectivity in the conversion of various feedstocks with ZSM-5 catalysts. As noted previously, ZSM-48 does not have channel intersections that permit formation of larger intermediates.⁴⁹ The absence of channel intersections in the intracrystalline pore structure of ZSM-48 could therefore account for the unique shape selective properties of this novel high silica zeolite.

Table 28

**Product Distribution from Methanol Conversion over
ZSM-5 and ZSM-48 in a Microreactor**

(Reaction Temperature = 648 K)

	<u>Product Distribution, wt%</u>	
	ZSM-5	ZSM-48
C ₅ ⁻ aliphatics	56.4	61.0
C ₆ ⁺ aliphatics	32.6	33.7
Aromatics	11.0	5.3

Zeolite channels are generally viewed as spaces where large electrostatic fields and gradients prevail.²³² Such environments can be described as ionic solvents, capable of promoting high energy ionization. It is possible to visualize the formation of carbonium (or carbene) species in this environment; therefore, an investigation of the effect of the presence of hydrogen in the reactant mixture on the yield of unsaturated hydrocarbons was undertaken. Helium was replaced by hydrogen as the carrier gas in this study. Typical hydrocarbon distributions from the reaction of methanol over ZSM-5 and ZSM-48 in the presence of hydrogen are presented in Figures 49 and 50, respectively. Essentially no hydrocarbons above C_{11} were produced and the aromatics are mostly methyl-substituted benzene. We believe that the product distribution is also shape selective in the hydrogen atmosphere. It is clear that hydrogen as well as helium behaved primarily as diluents. This point is illustrated for methanol conversion over ZSM-5 and ZSM-48 in Figures 51 and 52.

It has been noted that the formation of the first C-C bond from methanol requires the participation of Brønsted acid sites stronger than those required for subsequent steps.¹⁶ A series of consecutive steps involving isomerization, oligomerization, cracking, cyclization, and hydrogen transfer are operative after the formation of propylene or of a higher olefin molecule in the initial stages of the reaction. The acidity of ZSM-5 and ZSM-48 was investigated by ammonia-TPD and α -test measurements. The results indicated that both types of zeolite are very acidic in the catalytic sense. The effect of the silica-to-alumina ratio on the aromatic selectivity for the methanol reaction over ZSM-5 is shown in Figure 53. The aromatic selectivities for methanol conversion over ZSM-5 were virtually independent of the silica-to-alumina ratio in the range of silica-to-alumina ratios investigated (35 to 105). The data also indicated that the limited number of active sites at the

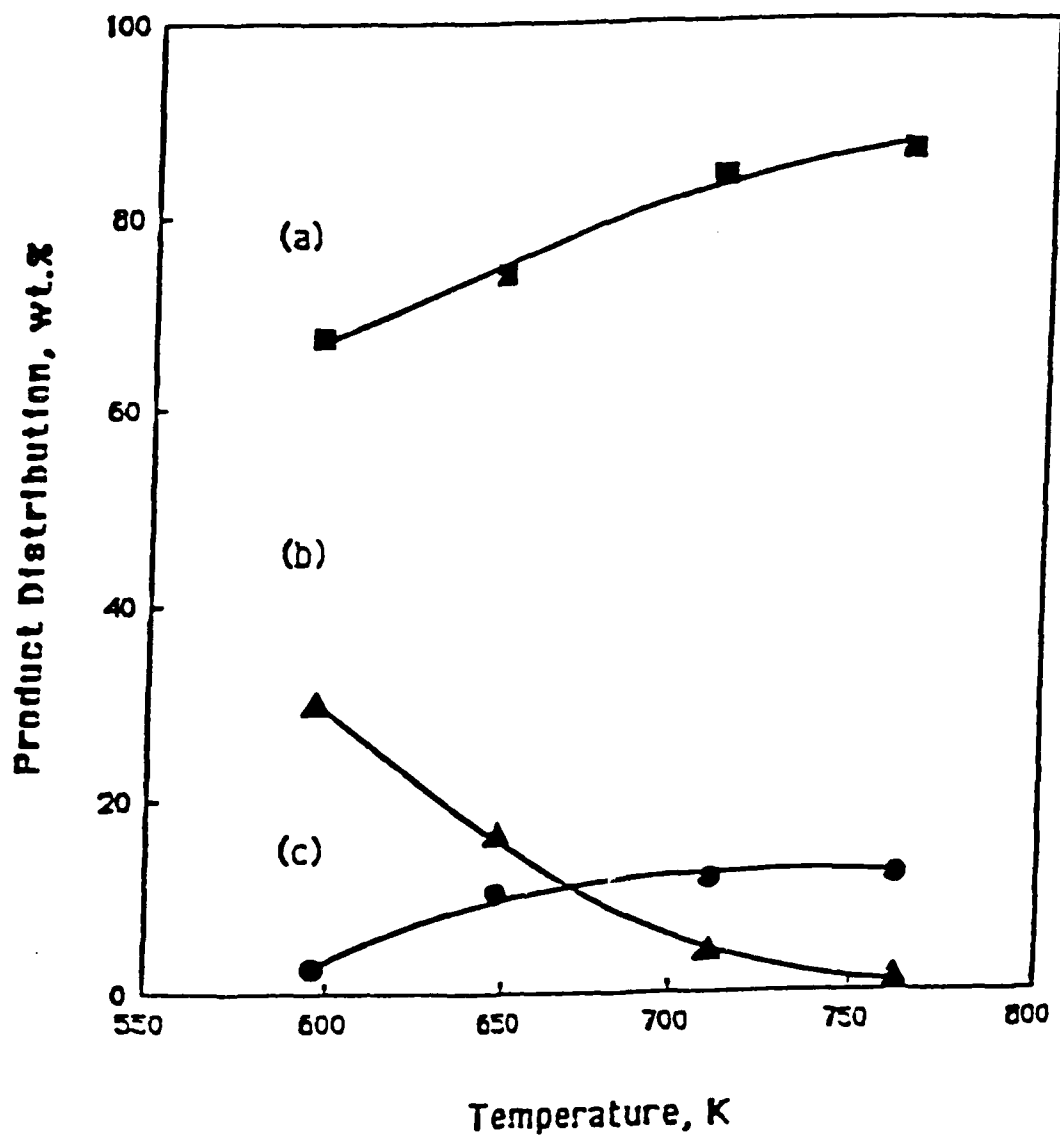


Figure 49. Product Distribution from Methanol Conversion over Zeolite HZSM-5(70)
Hydrogen Carrier Gas
(a) $C_1 - C_5$; (b) C_6+ ; (c) Total Aromatics

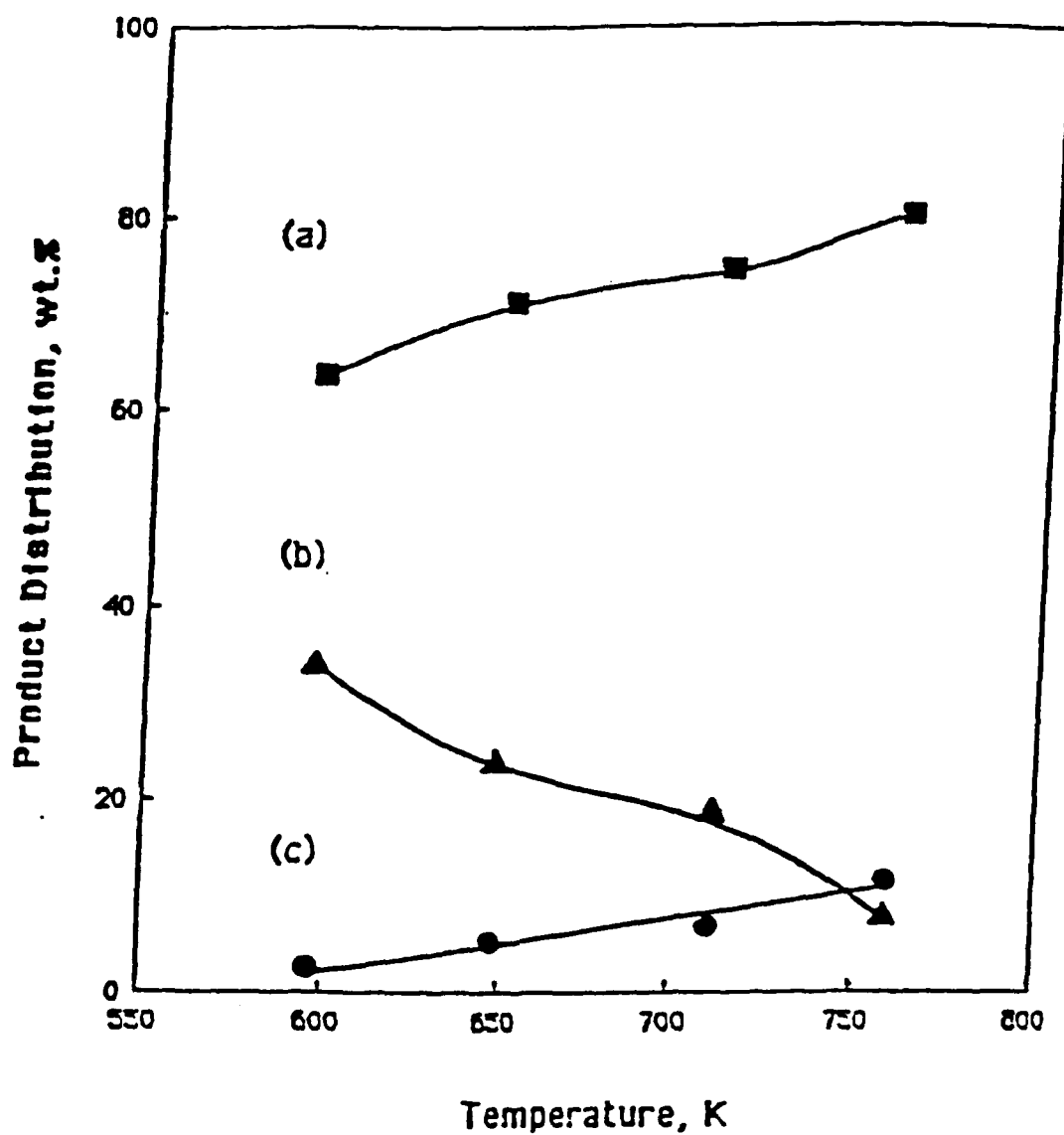


Figure 50. Product Distribution from Methanol Conversion over Zeolite HZSM-48(200) Hydrogen Carrier Gas

(a) $C_1 - C_5$; (b) C_6+ ; (c) Total Aromatics

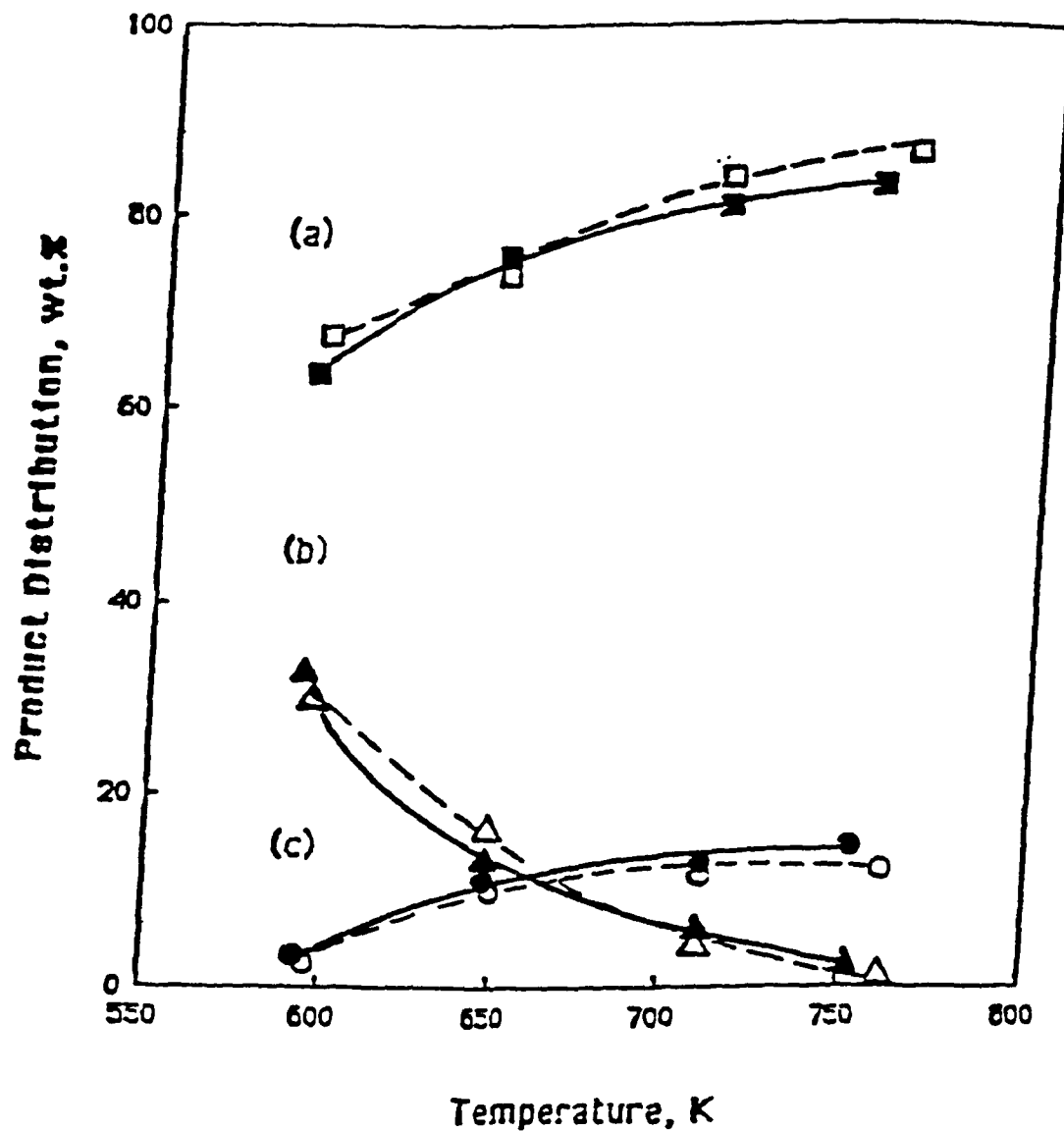


Figure 51. Product Distribution from Methanol Conversion over HZSM-5(70)

(a) $C_1 - C_5$; (b) C_6+ ; (d) Total Aromatics

(Solid lines denote product distribution from methanol conversion in helium carrier gas, and dashed lines denote that in hydrogen carrier gas)

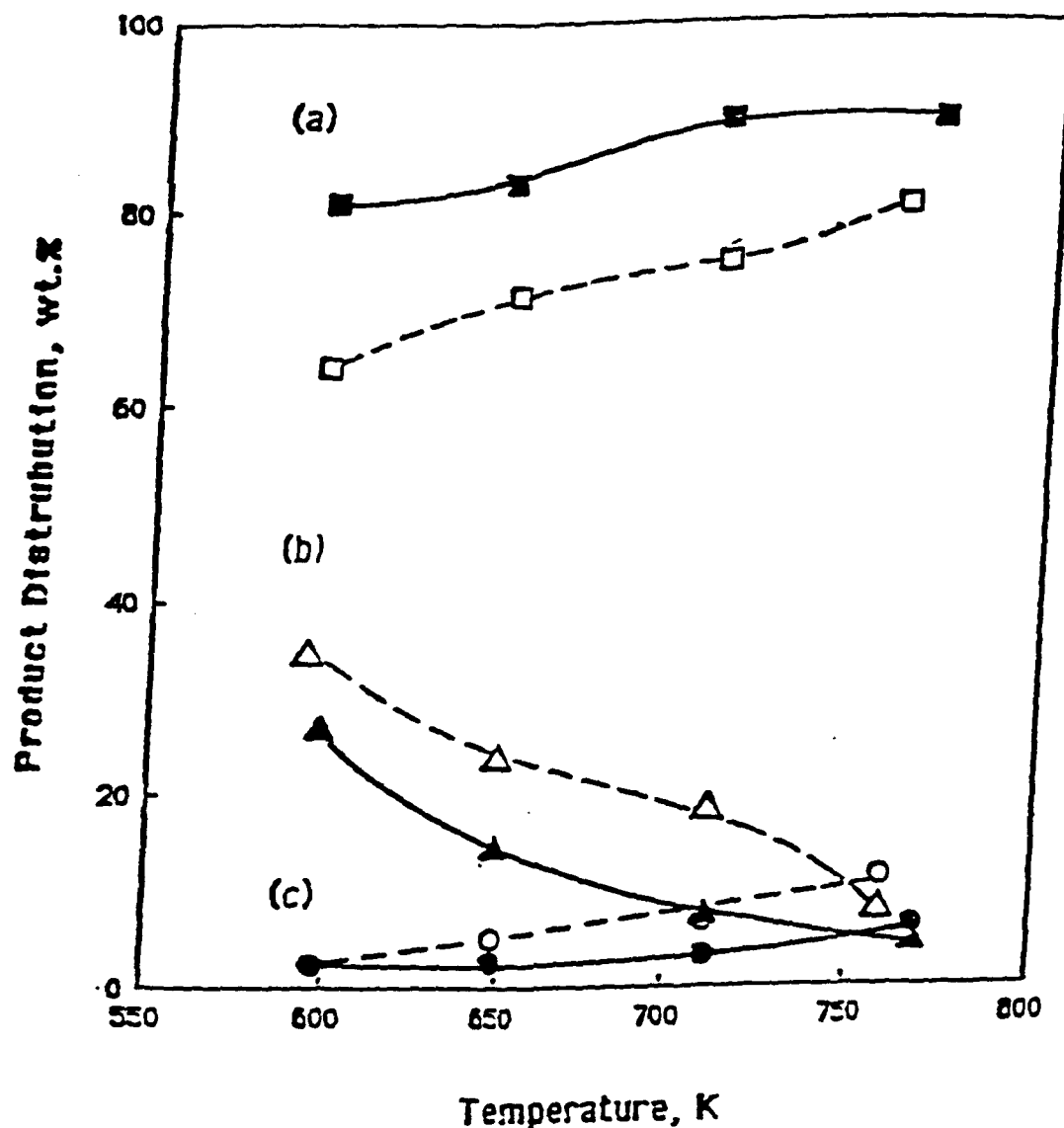


Figure 52. Product Distribution from Methanol Conversion over HZSM-48(200)

(a) $C_1 - C_5$; (b) C_6+ ; (c) Total Aromatics

(Solid lines denote product distribution from methanol conversion in helium carrier gas, and dashed lines denote that in hydrogen carrier gas)

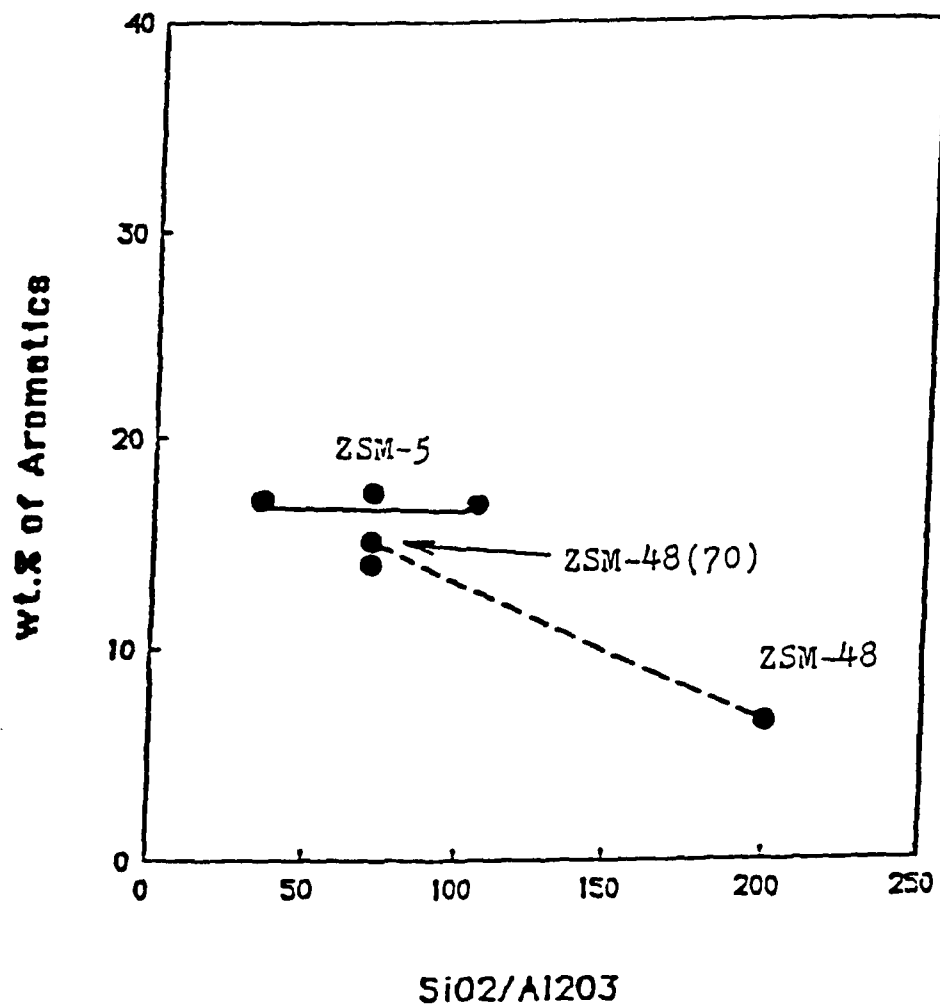


Figure 53. Effect of $\text{SiO}_2/\text{Al}_2\text{O}_3$ Ratio on Aromatic Selectivity for Methanol Conversion over ZSM-5.

channel intersections is essential to explain the observed transition state selectivities. It may be true that the limited number of active acidic sites in the channel intersections are expected since organic cation, such as TPA^+ , may completely occupy the channel intersections of ZSM-5 during the synthesis of the zeolite. It should be noted that methanol was converted first to dimethylether followed by conversion of the dimethylether to olefins. The olefins are transformed into longer chain aliphatics which cyclize and dehydrogenate to form aromatics. The channel intersections of ZSM-5 may provide the necessary space as well as acidity for the formation of aromatics from methanol.

The low aromatic selectivity of ZSM-48 is attributed to local configuration constraints, imposed by the immediate environment of the active centers, which decrease the probability of the formation of the necessary transition state characteristic of the elementary step in the formation of aromatics. The preliminary results reported in the present work may indicate that the difference in the shape-selective properties of a series of pentasil zeolites is due to definitive differences in the zeolite channel structure.

The restricted environment near the active centers may play a distinct role in the ordering of reaction products. The reactions of C_1 - C_4 alcohols over ZSM-5 synthesized in the presence of TPABr (i.e., ZSM-5(70)) or C6DN (i.e., ZSM-5D) were investigated in an attempt to better understand aromatic selectivity. A comparison of their aromatic selectivities is presented in Figure 54. A higher aromatic selectivity is observed for zeolite ZSM-5D as the carbon number of reactant alcohol increases when compared to that for ZSM-5(70). Since both of the zeolites have an identical pore/channel structure, such an observation may result from the difference in the environment of the active centers. In addition, the aromatic selectivity of ZSM-5 during

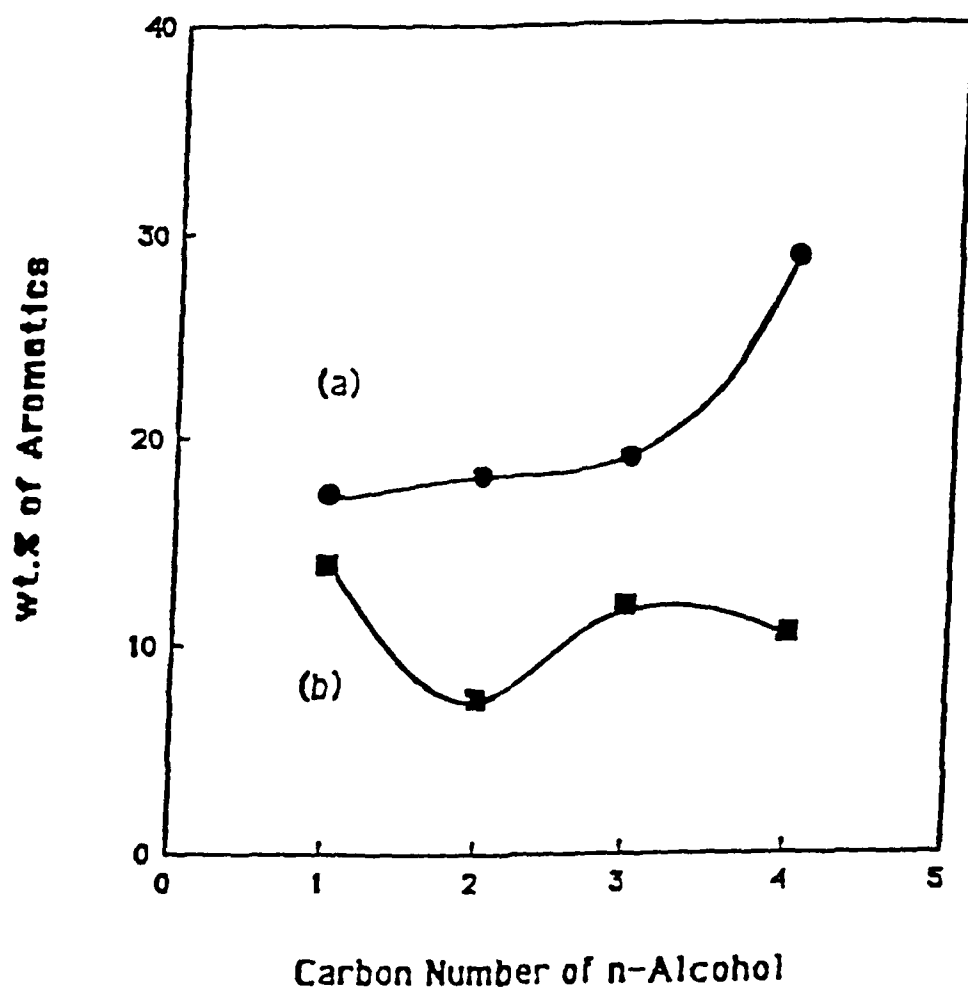


Figure 54. Effect of Organic Ions Used in the Synthesis of ZSM-5 on the Aromatic Selectivity for Alcohol Reactions

(a) C6DN; (b) TPABr

ethanol conversion, which formed ethylene over the ZSM-5 at the initial step in the reaction sequence, was low. This is consistent with other investigations, which indicated that the formation of hydrocarbons may not occur via intermediate ethylene, as free ethylene is less reactive than methanol itself.¹⁶

Thus, as expected, the aromatic selectivities of ZSM-48/5(70), which was determined to be a physical mixture of ZSM-5 and ZSM-48 crystals, were found to lie between those of ZSM-5 and ZSM-48 (shown in Figure 55). Parallel results were also observed in the ammonia-TPD experiments.

Summary

1. The cut-off point in the hydrocarbon product distribution for the methanol reaction over both ZSM-5 and ZSM-48 was found at C₁₀ aromatics.
2. The difference in the shape-selective properties of the pentasil zeolites ZSM-5 and ZSM-48 may be due to differences in the zeolite channel structure.
3. Zeolites synthesized in the presence of different organic ions may induce different environments in the vicinity of active centers even when they have similar pore/channel structure.
4. The restricted environment about the active centers may impose shape selective constraints on the local site reaction mechanism.

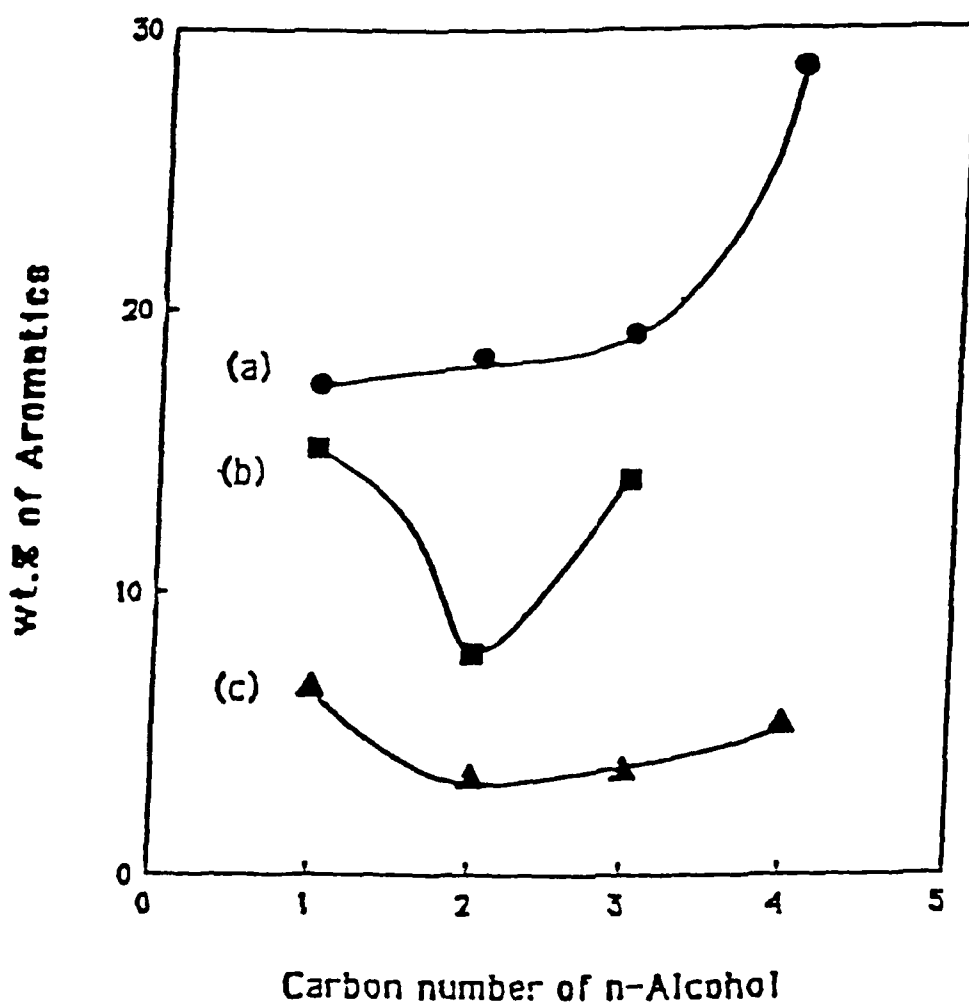


Figure 55. Effect of Channel Structure on the Aromatic Selectivity in Alcohol Reactions
(a) ZSM-5D; (b) ZSM-48/5(70); (c) ZSM-48(200)

Preliminary Methanol Conversion **Process Study**

It was found that ZSM-48 has a high intrinsic selectivity at high conversion for the production of aliphatics (mostly olefins) from methanol. Moreover, the olefins produced from the conversion over ZSM-48 can be converted to a higher boiling distillate by passing the olefins over a ZSM-5-type zeolite catalyst. The product from this process consisted of about 55 wt. percent hydrocarbons boiling between 422 - 616 K (300 - 650°F) which is in the jet fuel boiling range.¹⁹

Olefins are intermediates in the conversion of methanol to aromatic hydrocarbons over shape selective zeolites such as ZSM-5. The problem at hand is to suppress or minimize the final aromatization step to single ring aromatics in the first stage of the dual-stage process. The simplest strategy is to use a ZSM-48 catalyst for producing olefins in the first step followed by conversion of the olefins to jet fuel boiling range aromatics over a suitable catalyst. As indicated, aromatic selectivity could be greatly enhanced (see Figure 55) by conversion of the olefins over ZSM-5. The carbon product distribution from these reactions is, of course, related to zeolite pore/channel geometry.

A fixed-bed continuous flow reactor system that could operate in either a single or dual reactor mode was used to study the conversion of methanol to methyl-substituted aromatics in the jet fuel boiling range. Methanol was charged to the system with a positive displacement pump. A J-type thermal couple was inserted in the center of a five cm³ zeolite catalyst bed for both measuring and controlling temperature.

Methanol Conversion over ZSM-5 and ZSM-48

The typical product distribution from the methanol reaction over ZSM-5 after 24 hours on stream is shown in Figure 56. The reaction was carried out at 643 K, 1 hr⁻¹ LHSV, and atmospheric pressure. At this stage of reaction, the conversion of methanol is essentially complete up to 64 hours on stream. The hydrocarbons span a relatively narrow range of molecular weights, terminating at about C₁₀ as expected. The catalyst gave high selectivity to methyl-substituted aromatic hydrocarbons that is consistent with reported data.¹⁶ The shape selectivity is generally similar to that observed i.e. the microreactor at relatively low space velocity.

The results obtained for the conversion of methanol in the presence of ZSM-48 at 643 K, 1 LHSV, and atmospheric pressure are shown in Figure 57. The high selectivity of ZSM-48 toward olefins at the moderate operating conditions can be readily seen and it is worth noting the absence of aromatic hydrocarbons in the product slate.

It was reported that the olefins produced from the conversion of methanol over ZSM-48 can be converted to higher aromatics by passing the olefins produced over a ZSM-5 zeolite catalyst in a second reactor.¹⁹ In the investigation of the aromatization of olefins, the first experiment involved the reaction of methanol over ZSM-48 in the upper bed followed by conversion of the olefinic product in a second bed containing ZSM-5 in a lower zone of the reactor. The reaction was conducted at 643 K, 1 atm, and 1 LHSV. The results of this experiment (see Figure 58) indicated that the product distribution does not shift to higher hydrocarbons. The reverse loading sequence (ZSM-5 followed by ZSM-48) was also investigated. The product distribution of this process is shown in Figure 59. It should be noted that the results are similar to those of methanol conversion over ZSM-5 (Figure 56).

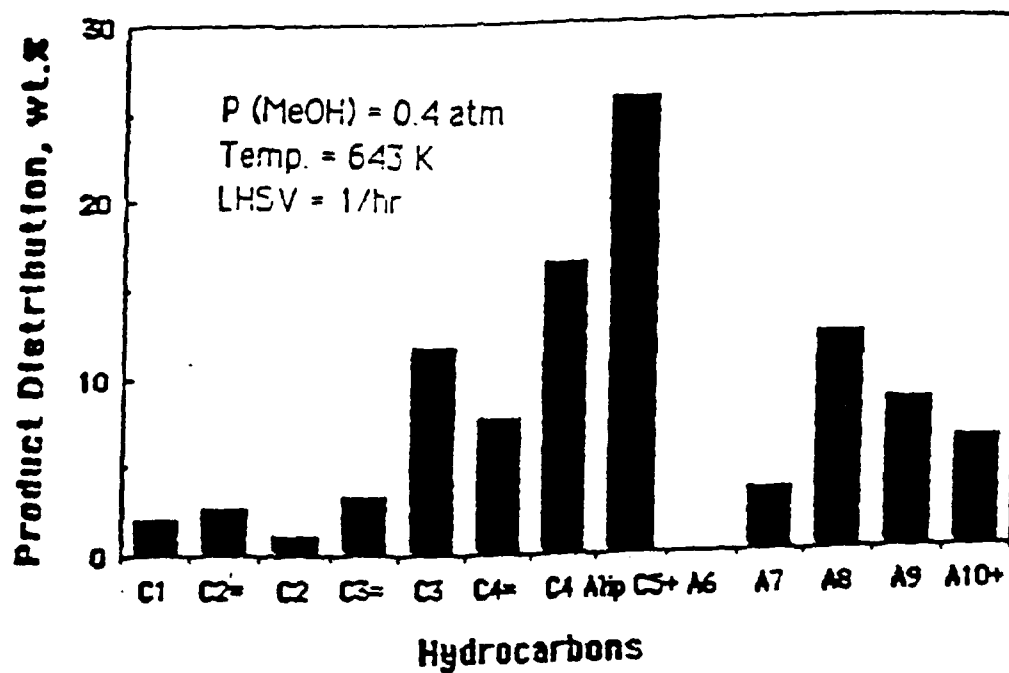


Figure 56. Product Distribution from Methanol Conversion
Zeolite ZSM-5

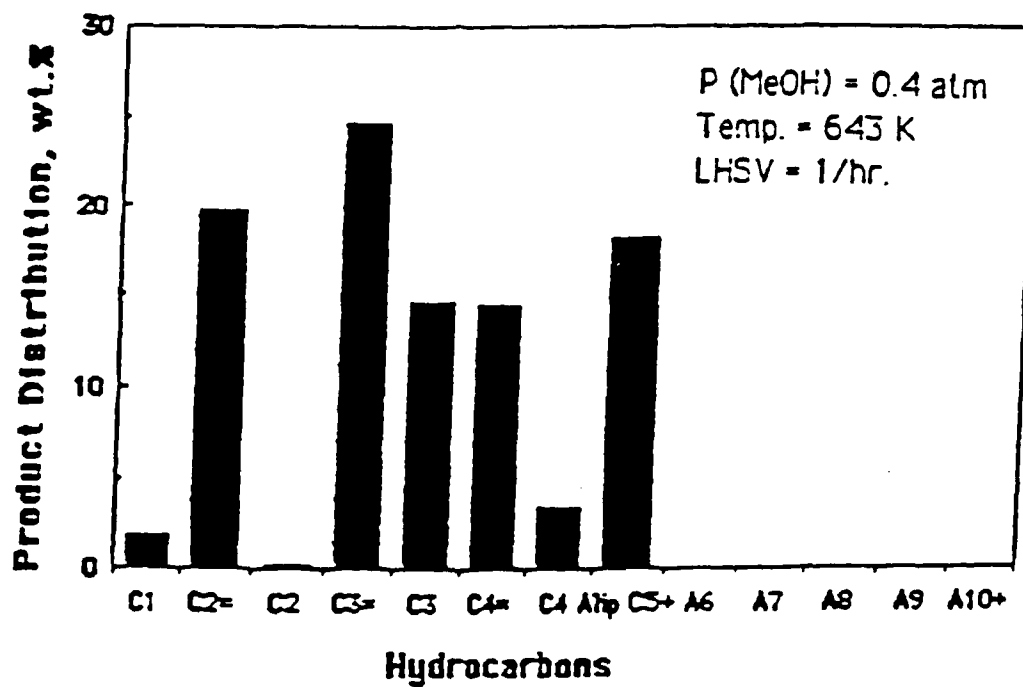


Figure 57. Product Distribution from Methanol Conversion
Zeolite ZSM-48

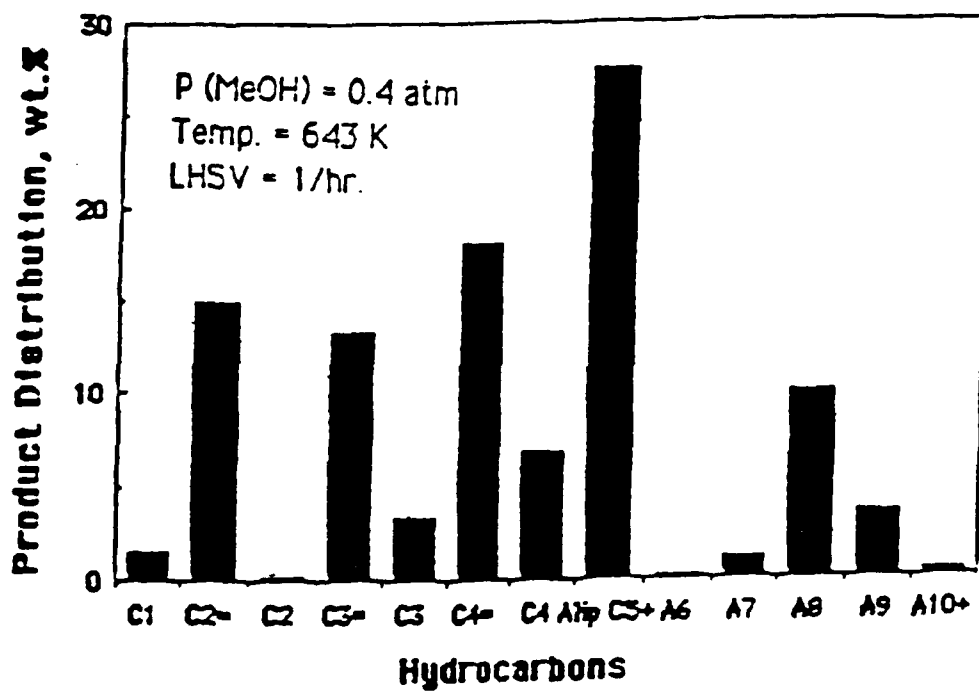


Figure 58. Product Distribution from Methanol Conversion
 Zeolites ZSM-48/ZSM-5
 Single Reactor Mode

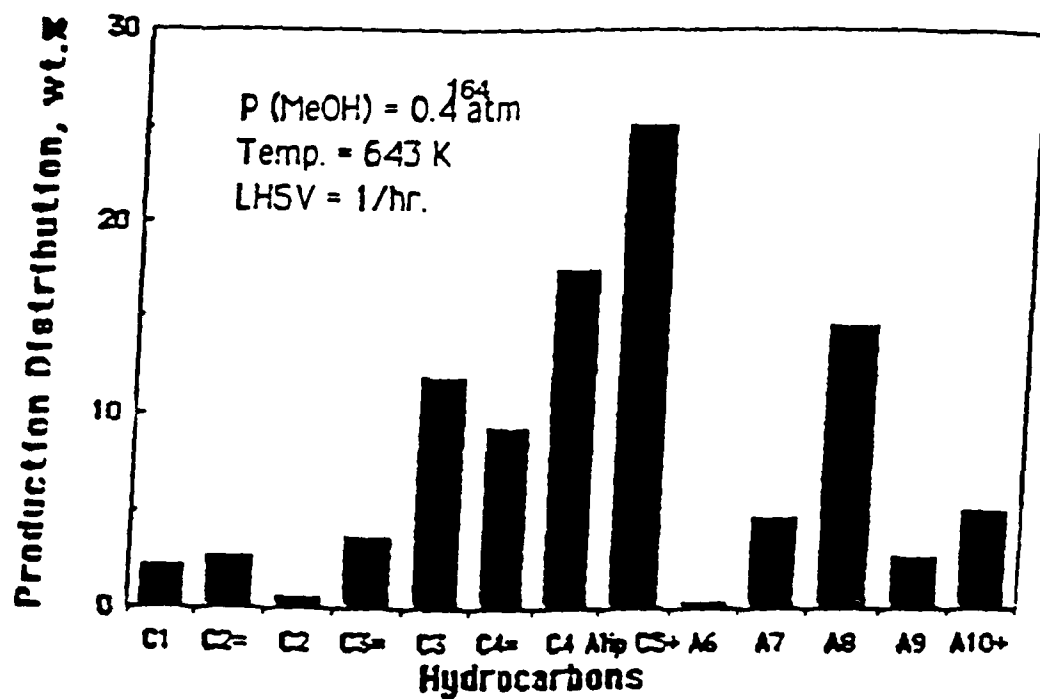


Figure 59. Product Distribution from Methanol Conversion
 Zeolites ZSM-5/ZSM-48
 Single Reactor Mode

It seems that ZSM-5 catalyst is the key to the aromatization reaction. The influence of pressure and temperature on methanol conversion over ZSM-5 was also investigated and the reaction index (RI) was used to describe the performance of the catalysts.

Pressure Effect

The pressure effect on methanol conversion over ZSM-5 is presented in Figure 60. Decreasing the pressure tends to decouple the formation of aliphatics. Increasing pressure results in an increase in the degree of aromatic substitution. Although not favored by thermodynamics, their formation can be attributed to the zeolite shape selectivity.

Temperature Effect

The effect of temperature on the methanol conversion is shown in Figure 61. The yields of xylenes show a maximum at a temperature of 643 K, at atmospheric pressure. It is worth noting that an increase in secondary alkylation occurred at higher temperature. Increasing temperature also results in an increase in the yield of aliphatics.

Reaction Index

In the simplified methanol conversion scheme, the light olefins react reversibly to heavier olefins, which convert further to aromatics and paraffins. The extent of reaction is monitored by a "reaction index," which is the propane/propene ratio. In the simplified scheme $A \rightarrow B \rightarrow C$, reaction index is proportional to the C/B ratio.¹⁶ The reaction index for methanol conversion over ZSM-5 at 0.4 atm methanol partial pressure is presented in Figure 62. The reaction index decreased with increasing time on-stream. In other words, the aromatization reaction may be

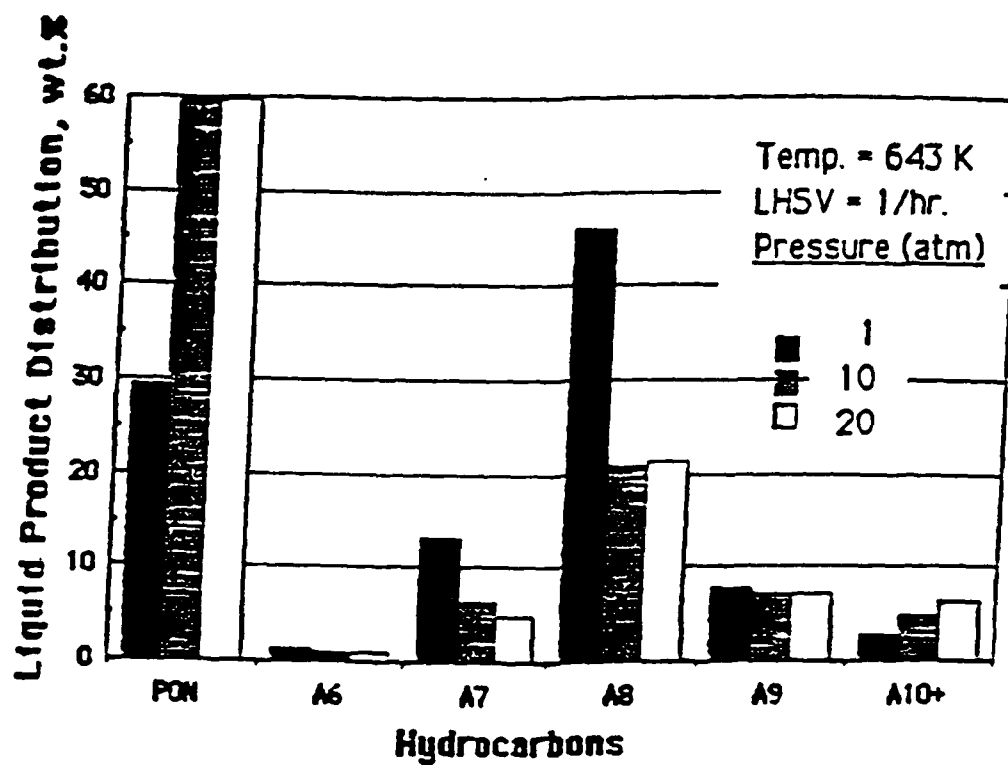


Figure 60. Product Distribution from Methanol Conversion
Effect of Reaction Pressure
Zeolite ZSM-5

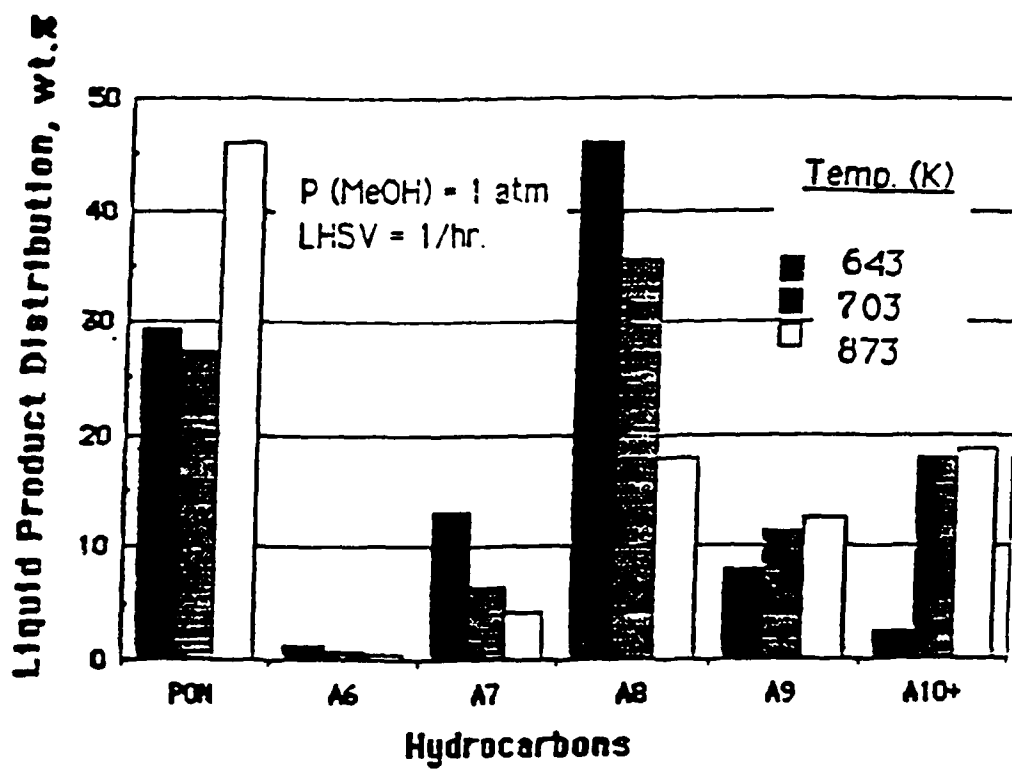


Figure 61. Product Distribution from Methanol Conversion
 Effect of Reaction Temperature
 Zeolite ZSM-5

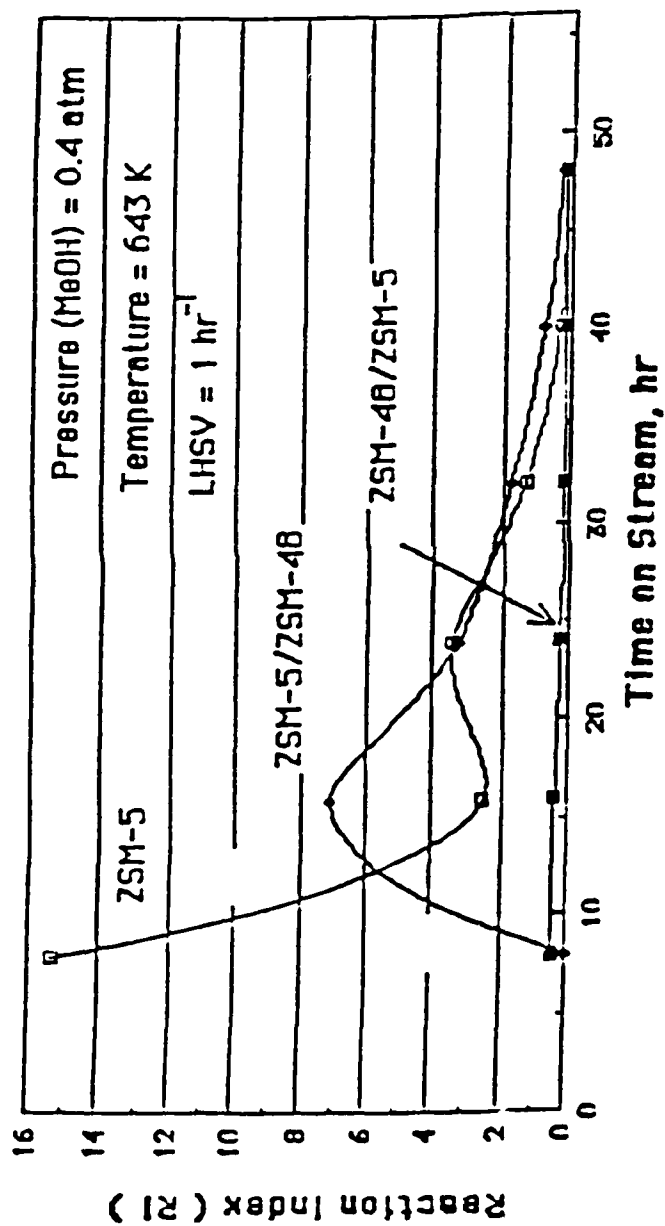


Figure 62. Reaction Index from Methanol Conversion

- (a) ZSM-5
- (b) ZSM-5/ZSM-48
- (c) ZSM-48/ZSM-5

inhibited for an aged ZSM-5 catalyst, which has been deactivated by the formation of coke or by the partial destruction of the zeolite structure by steaming. The reaction index for methanol conversion over ZSM-5/ZSM-48 and ZSM-48/ZSM-5 is also shown in Figure 62. The various combinations and sequences of ZSM-5 and ZSM-48 in a single reactor for methanol conversion do not favor the formation of high molecular weight hydrocarbons. It may be due to high concentration of steam fed to the second bed of catalyst in the lower section of the reactor. Furthermore, it was believed that high molecular weight hydrocarbons could be produced from methanol over ZSM-48 and ZSM-5 at elevated reaction pressures in a dual reactor system.¹⁹

In the first stage, methanol was reacted over a ZSM-48 catalyst that had a high selectivity for olefins. The product from the first reactor was passed through a gas-liquid separator where the light aliphatics were separated from water and liquid phase hydrocarbons. The light olefins were compressed to the inlet pressure of the second reactor where the olefins can react to form aromatics over ZSM-5. Alternatively, the light olefins can be condensed, pressurized and pumped into the second stage reactor.

Dual-Reactor Study

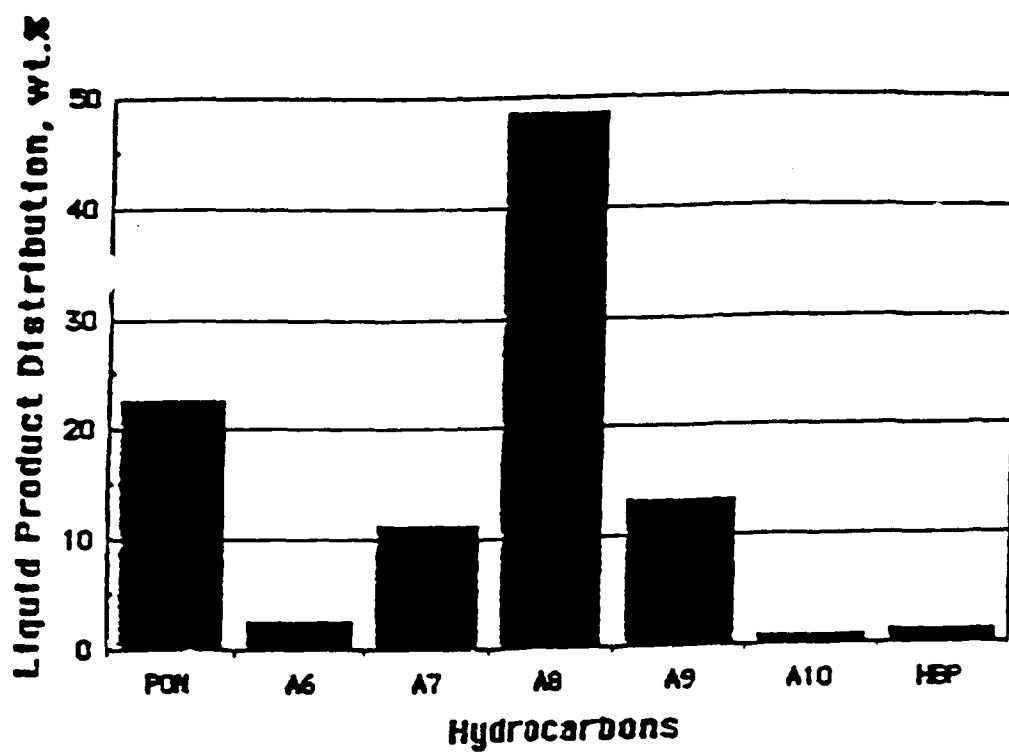
A schematic of the dual-reactor catalyst testing system is presented in Figure 19. The apparatus consisted of a reactor containing ZSM-48 in which olefins were produced, followed by the aromatics-forming reactor containing ZSM-5. The pressure of the second reactor could be increased to ~ 7 atm by a compressor. It should be noted that higher pressures (> 7 atm) in the second reactor could not be obtained due to the liquefaction of light gases in the compressor at pressures > 7 atmospheres. Furthermore, a minimum inlet pressure of five atmospheres was

necessary for operating the compressor. Thus it may not be suitable for compressing olefins such as butenes to or above its critical pressure point ($P_c = 40$ atm). It was not possible to develop a cryogenic pumping system to transfer the olefin produced over ZSM-48 from the outlet pressure of the first reactor to 100 atm. The operating conditions for these exploratory dual reactor fixed-bed process studies were as follows:

	<u>First Reactor</u>	<u>Second Reactor</u>
Catalyst	ZSM-48	ZSM-5
Temperature, K	643	573
Pressure, atm	5	7
LHSV, 1/hr	6	-

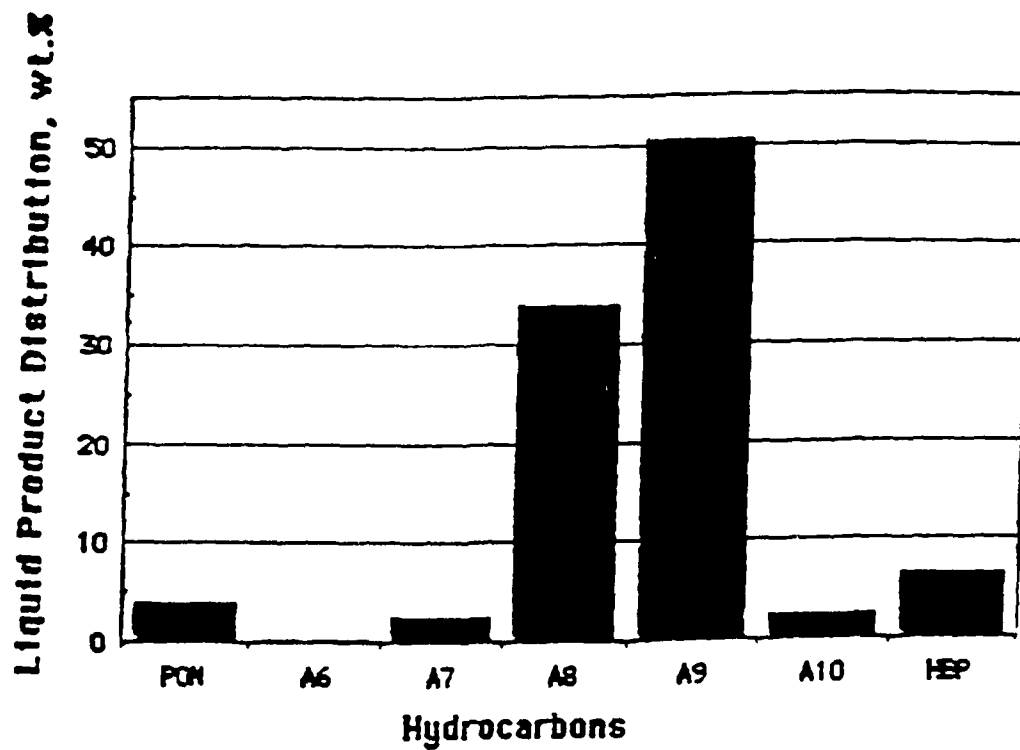
About 7 wt. percent of high boiling point ($>$ B.P. of naphthalene) hydrocarbons was obtained from the conversion of methanol in this system (see Figure 63). High yields of trimethyl-benzenes and low yields of paraffins, olefins, and naphthene (PON) indicate that a high degree of aromatization occurred. The major products of the olefin reaction at 773 K were xylenes (see Figure 64).

The yields of higher molecular weight hydrocarbons were low since the maximum attainable pressure in the second stage (ZSM-5 reactor) was about seven atmospheres and high hydrocarbons could be obtained only at elevated pressures such as 100 atm. The olefins produced in the first stage would condense in the compressor when compressed to a pressure higher than seven atmospheres. The condensed olefins can be collected cryogenically and pump with a liquid feed pump to pressurize to about 100 atm in the second stage.



Reactor I	Reactor II
ZSM-48	ZSM-5
T = 643 K	T = 573 K
P = 5 ATM	P = 7 ATM

Figure 63. Product Distribution from Methanol Conversion over Zeolites ZSM-48 and ZSM-5 Dual Reactor Mode



Reactor I	Reactor II
ZSM-48	ZSM-5
T = 643 K	T = 773 K
P = 5 ATM	P = 7 ATM

Figure 64. Product Distribution from Methanol Conversion over Zeolites ZSM-48 and ZSM-5 Dual Reactor Mode

The difficulties experienced in transferring low molecular weight olefins (C_2 - C_4) from low pressures (1 to 5 atmospheres) to high pressures (100 atmospheres) have slowed the demonstration of the dual reactor concept for the production of dicyclic aromatic hydrocarbons in the aviation turbine fuel boiling range. However, we believe that at 100 atmospheres the yield of these species could be substantial. The dual reactor study has been placed on inactive status until an appropriate method can be developed to operate the ZSM-48 reactor at low pressures and the ZSM-5 reactor at high pressures in series.

Section V: SELECTIVE HYDROGENATION OF AROMATIC HYDROCARBONS

Research Personnel: Lei-Yea Cheng
Graduate Student

Nabin K. Nag
Assistant Research Professor

Kien-Ru Chen
Postdoctoral Fellow

Francis V. Hanson
Associate Professor

Supported transition metals possess good activity for the catalytic hydrogenation of aromatic hydrocarbons.²³³ Under the framework of this project, it was intended to synthesize various one- and two-ring aromatic hydrocarbons via methanol ZSM-5 route and then hydrogenate these aromatic species to fully-saturated naphthenic compounds that are reported to be the major components of high-density jet fuels.²³⁴ The present section is devoted to the efforts toward preparation, characterization, and testing of some supported metal catalysts; however, it should be recognized that this component of the research program was discontinued upon instruction from the Technical Project Officer.

Supported Metal Catalyst Preparation

The incipient wetness or "dry impregnation" method was used to prepare γ -Al₂O₃-supported Ni, Ru, and Pd catalysts.²³⁵ The basic concept involves saturating an appropriate support with that volume of impregnating solution corresponding exactly to the total pore volume of the support and containing the stoichiometric amount of the metal cation to be impregnated. The γ -Al₂O₃ support was purchased from Akzo Chemie, Holland, and its reported specific surface area and pore volume were 209 m²g⁻¹ and 0.6 cm³g⁻¹, respectively. The support was calcined to 500°C overnight before

impregnation. The preparation procedure for a typical nickel catalyst is described in the subsequent discussion. The alumina sample was received in the form of extrudates which were crushed and sieved (35-48 mesh size) to get particles of the size 300-425 μ m. This material was calcined overnight at 500°C; 4.125 g of $\text{Ni}(\text{NO}_3)_2 \cdot 6\text{H}_2\text{O}$ was dissolved in 50 cm^3 water, and 10.584 g of calcined alumina were impregnated with 6.35 cm^3 of this solution by dropwise addition and constant stirring. The impregnated sample was dried at 393 K for 16 hours followed by calcination at 773 K for 16 hours. After reduction, the final catalyst composition was: 1 wt percent Ni on alumina (designated as 1 percent $\text{Ni}/\text{Al}_2\text{O}_3$).

The following catalysts were prepared using the incipient wetness technique:

- a. 0.1 percent $\text{Ni}/\text{Al}_2\text{O}_3$
- b. 1.0 percent $\text{Ni}/\text{Al}_2\text{O}_3$
- c. 2.0 percent $\text{Ni}/\text{Al}_2\text{O}_3$
- d. 2.5 percent $\text{Ru}/\text{Al}_2\text{O}_3$
- e. 2.5 percent $\text{Pd}/\text{Al}_2\text{O}_3$

$\text{Ru}(\text{NO})(\text{NO}_3)_3$ and $\text{Pd}(\text{NO}_3)_2 \cdot x\text{H}_2\text{O}$ (both from Alfa Products) were used as sources for ruthenium and palladium respectively. This series of catalysts, and others to be prepared in the course of this research program were intended to be fully characterized and tested for hydrogenation reactions.

Catalyst Characterization by Hydrogen Chemisorption

Measurement of Sites

The concept of the active sites in heterogeneous catalysis was formulated first by Taylor in 1925 when he suggested that catalyst surfaces might contain some sites particularly active for chemisorption and catalysis.²³⁶ He also pointed out: "...the amount of surface which is catalytically

active is determined by the reaction catalyzed. There will be all extremes between the case in which all the atoms in the surface are active and that in which relatively few are so active." This non-uniformity of the catalytic surface has been confirmed by chemisorption studies in which the heat of adsorption (i.e., heat of formation of adsorption complexes²³⁷ has been shown to vary significantly with surface coverage). Surface heterogeneity has also been confirmed in kinetic studies in which small concentrations of a selective poison significantly suppress catalytic activity. Catalyst poisons are known to affect both catalytic activity and chemisorption capacity; however, the reduction in catalytic activity is more severe than the reduction in chemisorption capacity. Thus, not all sites on which chemisorption occurs act as catalytic sites.

Chemisorption has long been used to characterize catalytically active materials.²³⁸ The number of sites available for chemisorption is determined from the amount of adsorptive required to saturate the surface. The method assumes that a simple relationship exists between the number of molecules or atoms adsorbed at saturation and the number of surface atoms. The catalytic activity of supported metal catalysts, expressed as the turnover number, is related to the total number of surface metal atoms as determined from the selective chemisorption of hydrogen²³⁹⁻²⁴⁵ or from the titration of preadsorbed oxygen with hydrogen.²⁵⁶⁻²⁵⁰ If the reaction occurs on a fraction of the surface metal atoms, the turnover number based on the total number of surface metal atoms will define the lower limit of the turnover number for the reaction under investigation. When comparing the activities of a series of catalysts having the same active component (i.e., metal), the relative activities will be insensitive to the site concentration on which the turnover numbers are calculated. Thus, both the true site density (usually unknown) and the limiting site density (determined by selective chemisorption) provide a viable means of comparing catalyst performance for a chosen reaction.

Constant Volume Adsorption Apparatus

A constant adsorption apparatus was constructed to determine adsorption isotherms for the supported metal catalysts used in the aromatics synthesis, aromatic hydrogenation, and hydrodewaxing studies sponsored by the United States Air Force. The isotherms were obtained by expanding an adsorbate from a calibrated doser volume into an adsorption cell which contained the sample. The amount of the gas adsorbed was calculated from the known doser and cell volumes and the pressures and ambient temperatures before and after expansion of the adsorbate. A schematic of the apparatus is presented in Figure 65. Since this apparatus has not been described previously, it will be discussed in considerable detail.

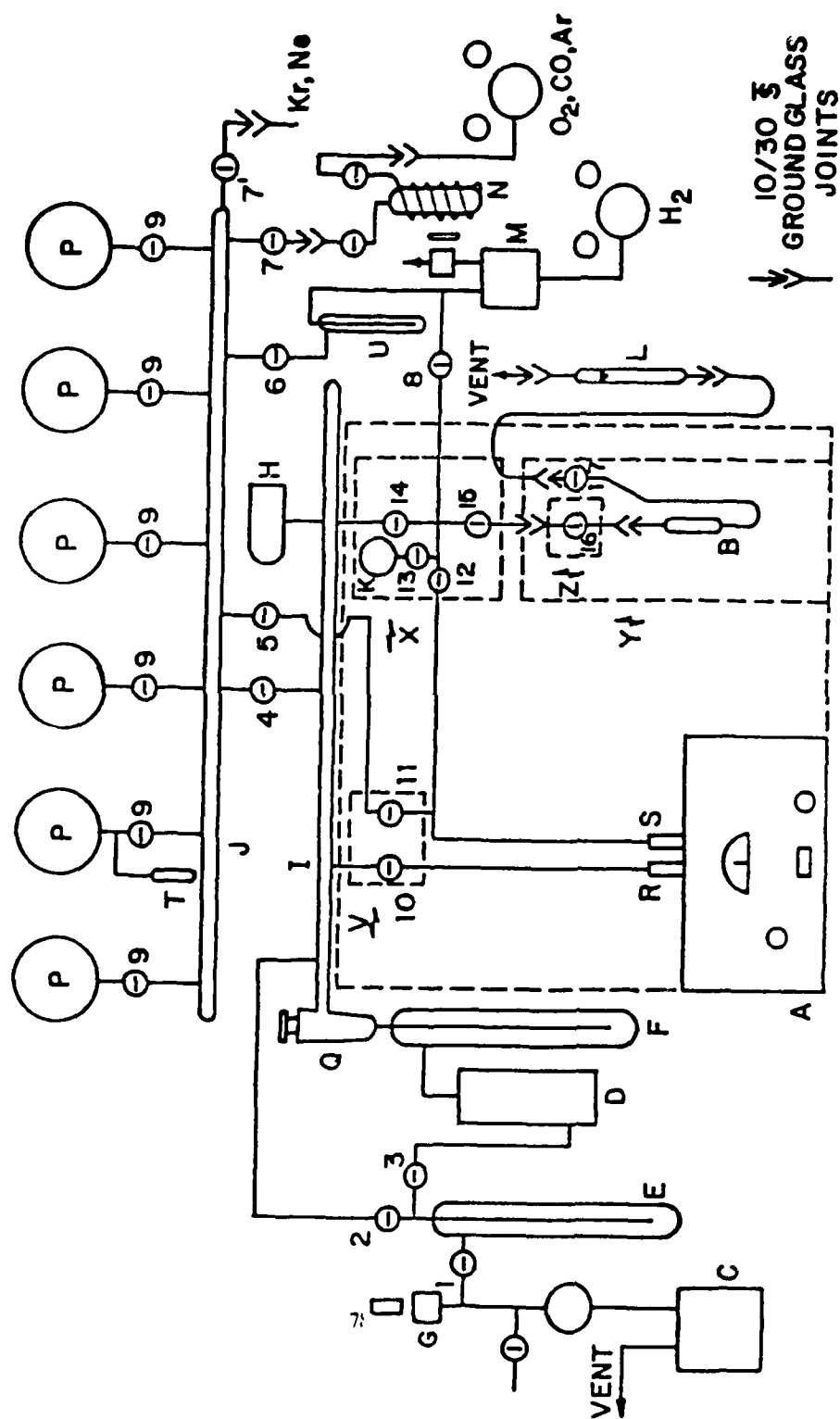
Adsorption System

The adsorption system is depicted in the section of Figure 65 enclosed by the large dashed rectangle. The pressure was measured with a precision pressure gauge (A), model 145 servo-nulling read-out unit, manufactured by Texas Instruments, Inc., Houston, Texas. The pressure sensing device was a Type 5, fused quartz Bourdon capsule. The Bourdon tube was in the form of a spiral, to which a reflecting platinum mirror was attached (see Figure 66). An optical transducer was mounted on a gear that traveled concentrically around the capsule. The deflection of the pressurized Bourdon tube was found by rotating the gear until the light reflected from the tube mirror fell with equal intensity on a pair of matched photocells. The deflection of the tube was then read on the digital counter and the pressure was determined from the counter reading by means of a calibration table. The Type 5 Bourdon capsule had a resolution of 0.001° (corresponding to a minimum measurable deflection of 0.008 Torr). The apparatus was superior to conventional volumetric systems because of the high precision of the gauge, the absence of hysteresis, and the elimination of the need for mercury in the system. The reference side of the

A - Texas Instruments Precision Pressure Gage; B - adsorption cell; C - mechanical vacuum pump; D - oil diffusion pump; E,F - high vacuum cold traps; G - thermocouple vacuum gauge; H - ionization vacuum gauge; I - vacuum manifold; J - gas handling manifold; K - calibrated bulb; L - hydrogen reduction rotameter; M - palladium thimble hydrogen diffuser; N - 13X molecular sieve trap; P - 5 liter gas storage bulbs; R - reference port on fused quartz Bourdon capsule; S - measuring port on capsule; T - cold finger; U - cold trap; V,X,Y,Z - sliding doors on Plexiglas enclosure. All stopcocks are of the high vacuum type and the numbers identify the stopcocks discussed in the text.

Figure 65

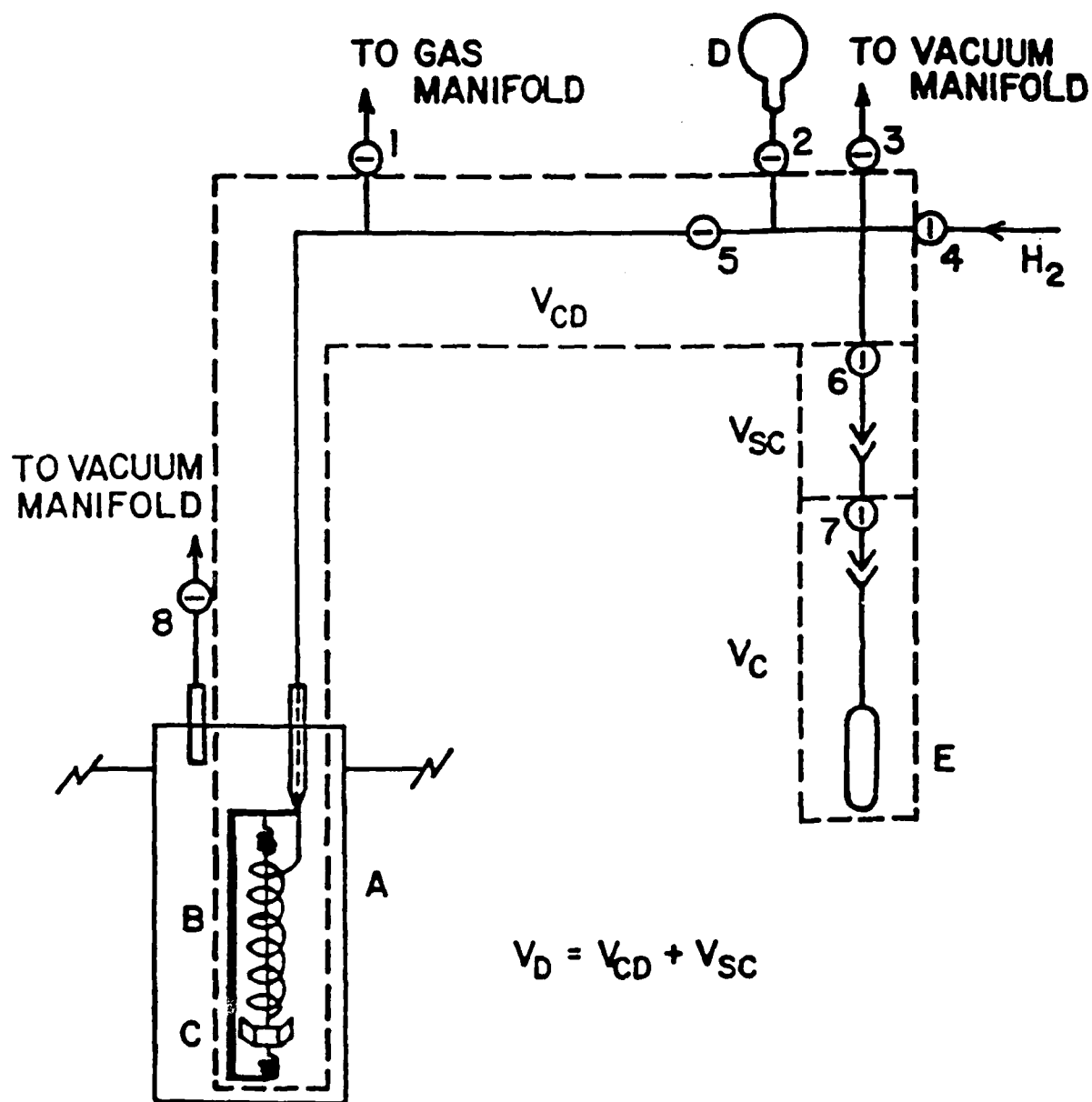
Constant Volume Adsorption Apparatus



A - fused quartz Bourdon capsule; B - quartz spiral;
C - platinum reflecting mirror; D - calibrated bulb
($V_B = 49.055 \text{ cm}^3$); E - adsorption cell; V_{CD} - cali-
brated doser volume; V_{SC} - connecting stopcock
volume; V_C - cell volume. The numbers identify the
stopcocks discussed in the text. $V_D (=V_{CD} + V_{SC})$ -
doser volume for isotherm determination.

Figure 66

**Constant Volume Adsorption Apparatus
Detail of Doser System**



capsule was connected to the vacuum manifold via stopcock (10) and the measuring side was connected to the doser volume by a graded glass seal.

The doser system was constructed from borosilicate glass capillary tubing to minimize the dead volume. All stopcocks were of the high vacuum type and were lubricated with Apiezon "N" grease. The doser volume was connected to the vacuum manifold via a four mm stopcock (14) and to the gas handling manifold via stopcocks (5) and (11). A calibrated bulb (K) was connected to the doser system via stopcock (3) for calibration of dead volumes in the adsorption system. The volume of the bulb was determined before it was glassblown onto the doser system. The bulb was filled with degassed distilled water and placed in a constant temperature bath. After thermal equilibrium was attained, the bulb was weighed on the Mettler Balance. The volume was calculated to 49.055 cm^3 .

A detailed sketch of the flow adsorption cell (B) is presented in Figure 67. The catalyst chamber was made from eight mm OD borosilicate glass tubing and was 60 mm long. The inlet line was made from six mm OD borosilicate glass tubing 170 mm long and terminated in a 10/30 ground glass joint (inner). The exhaust line was made from Pyrex capillary tubing and contained a two mm capillary stopcock (17). The exhaust line was connected to the vent line by a 10/30 ground glass joint (inner). The cell was connected to the doser volume via a two mm capillary stopcock (16) that had 10/30 ground glass joints (outer) on both ends. The joint that joined the cell to the connecting stopcock (16) was sealed with Apiezon black wax and the joint that connected the assembled cell to the doser system was sealed with Apiezon "T" grease.

The entire adsorption system was enclosed in a borosilicate glass box (740 mm x 990 mm) to stabilize the ambient temperature during the course of an isotherm. The front of the box was equipped with three sliding doors (V, X, Z) which permitted access to the stopcocks in the doser

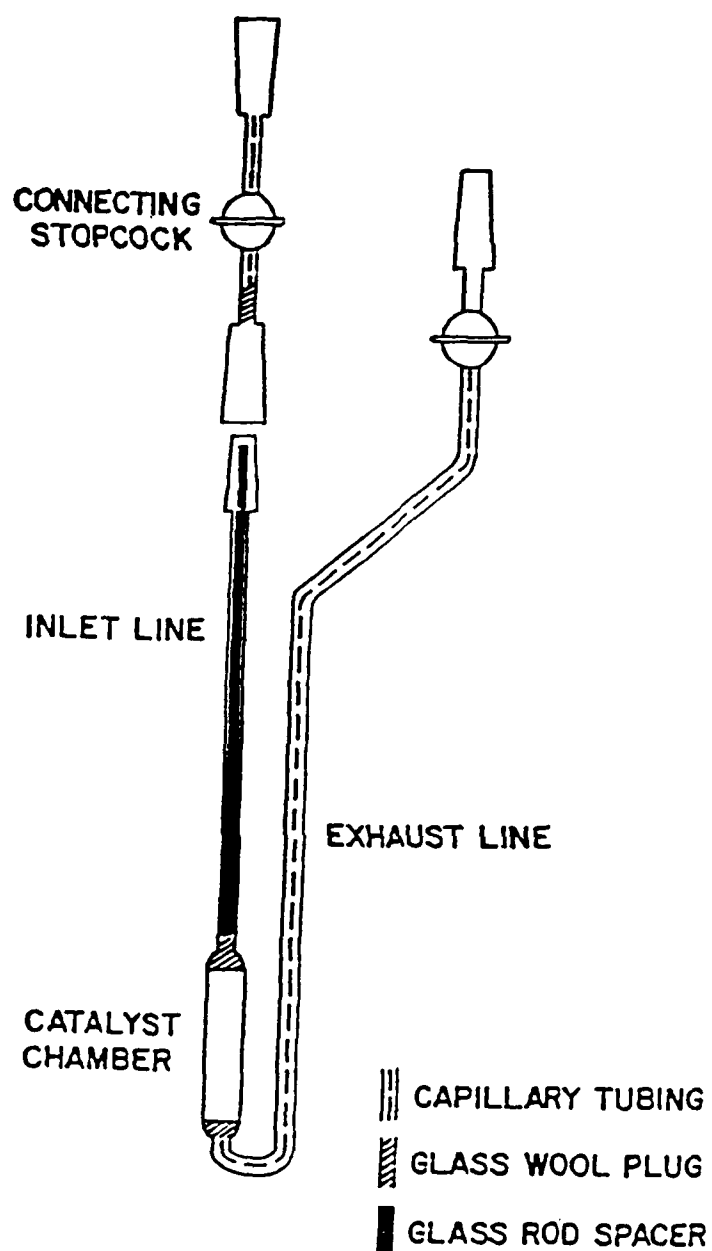


Figure 67. Adsorption Cell

system. The large door (Y) was used when the adsorption cell was changed or when the furnace and constant temperature bath were placed around the cell or were removed. The doors are indicated by the dashed lines in Figure 65 and the arrows indicate the direction each door moved. The box was assembled with machine screws and the front panel could be removed easily for minor repairs or modifications to the doser system or gauge.

VACUUM SYSTEM AND HANDLING APPARATUS

Vacuum System

The vacuum system consisted of a C. V. C. 112 liter per second oil diffusion pump (D), model PMCS-2C, backed by an 0.33 liter per second Precision Scientific mechanical vacuum pump (C), model 25. Dow Corning 704 silicone oil was used in the diffusion pump. The diffusion pump was connected to the vacuum manifold (I) by a 15 mm high vacuum stopcock (Q) which was mounted on top of a 55/50 vacuum cold trap (F). The mechanical pump was isolated from the vacuum manifold by a 40/50 vacuum cold trap to prevent contamination of the adsorbent when the system was rough pumped in the early stages of each evacuation. Both traps were immersed in liquid nitrogen at all times. A C.V.C. thermocouple vacuum gauge (G) was mounted on the mechanical pump side of the trap to monitor the mechanical pump vacuum.

The vacuum manifold was constructed of 25 mm OD borosilicate glass tubing (1050 mm long). The manifold vacuum was measured by a Veeco ionization gauge, model RG 75N, and was read on a C.V.C. ionization gauge controller, type GIC-110A. The ultimate dynamic vacuum of the manifold and adsorption cell was less than 10^{-6} Torr.

Gas Handling and Purification System

The gas handling manifold (J) was also constructed of 25 mm OD borosilicate glass tubing (1200 mm long) and was connected to the vacuum manifold by a 6 mm stopcock (4). Six five-liter gas storage bulbs (P) were connected to this manifold by 4 mm stopcocks (9). One of the bulbs was equipped with a cold-finger (T) for purification of hydrocarbon adsorptives and other condensible gases by repeated freeze-pump-thaw cycles.

All adsorptives, with the exception of hydrogen, were loaded into the gas storage bulbs via stopcocks (7) and (7'). High purity hydrogen (99.93 percent) was used as an adsorptive and was further purified by diffusion through a Milton Roy Company palladium thimble hydrogen purifier (M), model CH-A. The hydrogen also passed through a cold trap (U) at liquid nitrogen temperature before being stored in one of the five-liter bulbs. Matheson research grade oxygen (99.99 percent) was passed through a 13X molecular sieve trap (N) at a dry ice-acetone temperature before being stored in one of the five-liter bulbs, as was the Matheson C.P. grade carbon monoxide (99.5 percent). Matheson research grade neon (99.995 percent) and krypton (99.995 percent) were used without further purification for dead volume determinations. The molecular sieve traps were activated by evacuation at 600 K to a pressure of 5×10^{-4} Torr. A different trap was reserved for purification of each adsorptive.

Operating Procedures

Catalyst Loading

An acid-washed glass wool plug was inserted into the catalyst chamber to serve as a catalyst support grid. The catalyst was weighed without drying and was then loaded into the cell via the inlet line. A second acid-washed glass wool plug was placed on top of the catalyst and a glass rod

was placed in the inlet line to reduce the cell dead volume. The cell was sealed to the connecting stopcock with Apiezon black wax and the assembled adsorption cell was attached to the doser system.

Catalyst Pretreatment

The evacuation was begun by setting stopcocks (Q) and (3) to bypass the diffusion pump and by opening (2) to the vacuum manifold. Stopcock (12) was closed and (14) was opened to the doser system. Stopcock (15) was opened and the connecting stopcock volume was evacuated. When the thermocouple vacuum gauge (G) registered a pressure of $30\text{--}40 \times 10^{-3}$ Torr, stopcock (2) was closed and the evacuation with the diffusion pump was begun. The furnace was placed around the cell (B) and the temperature programmer-controller was started after a one-hour evacuation at room temperature. The sample was evacuated at 423 K for two hours and then cooled to room temperature under evacuation.

The reduction was carried out in the following manner. Stopcock (16) was closed and (12) was opened to the vacuum manifold via stopcock (14). After evacuation of the Bourdon tube, stopcocks (12) and (14) were closed and (8) was opened to admit hydrogen to the doser system. The hydrogen was then slowly admitted to the Bourdon tube by opening stopcock (12). The flare on the hydrogen diffuser (M) was lit, the diffuser heater was turned on, and the hydrogen pressure in the doser system and the cell was allowed to increase. When the pressure was greater than the atmospheric pressure (95° on digital counter), stopcock (17) was opened to the vent line and the flow rate was measured on the rotameter (L). All catalysts were reduced at a space velocity of 0.5-3.0 volumes of hydrogen per unit volume of catalyst per second. After the hydrogen flow was established, stopcock (12) was closed and the hydrogen was evacuated from the measuring side

of the capsule (S) via stopcocks (5) and (11). The furnace was placed around the cell and the temperature programmer-controller was started. All catalysts were heated to the reduction temperature over a period of eight to ten hours and were reduced for four hours. After the reduction, the furnace was removed and the catalyst was cooled to room temperature in flowing hydrogen. Stopcock (17) was closed and the hydrogen diffuser was immediately shut down to prevent overpressuring the cell. Stopcocks (4), (5), (8), and (11) were closed and (14) was opened to the vacuum manifold to evacuate the hydrogen from the cell. Stopcock (12) was opened the doser volume and the adsorption cell were evacuated to a manifold vacuum of less than 10^{-5} Torr. During this evacuation the gauge was zeroed with stopcock (10) open to the vacuum manifold. The furnace was placed around the cell and the catalyst was heated to the final evacuation temperature (723 K) with the programmer-controller system. Usually the catalyst was evacuated for 1-1/2 to 2 hours at this temperature. The furnace was removed and the catalyst was quickly cooled to room temperature under evacuation. The constant temperature bath was then placed around the cell and its temperature was adjusted to the desired isotherm temperature. Stopcock (16) was closed to isolate the cell from the doser volume and (14) was closed to isolate the dosing system from the vacuum manifold. The gas to be adsorbed was transferred from its storage bulb to the gas manifold and from there to the dosing system via stopcocks (5) and (11).

Adsorption Isotherm Procedure

The calculation of the adsorption isotherm required a knowledge of the dead volume of the adsorption cell with the constant temperature bath placed around the cell. Neon was used to determine the dead volumes because helium was shown to diffuse through the quartz spiral into the evacuated reference side of the capsule. The cell and the doser system were evacuated and

stopcocks (14), (15), and (16) were closed. The calibrated doser volume (see Figure 65) was filled with neon to a pressure of 600-750 Torr via stopcock (11). The pressure and ambient temperature were recorded after stopcock (11) had been closed. The neon was then expanded into the connecting stopcock volume via stopcock (15). The pressure and temperature were again recorded. Finally, the neon was expanded into the cell by opening stopcock (16). After the final pressure and temperature were recorded, the neon was evacuated and the procedure was repeated. The dead volume was usually determined three to six times for each catalyst loading. The pressure and ambient temperature were recorded at 120-second intervals over 600 seconds, and the ratio P (degrees)/ T (K) was computed for each point. The system was assumed to be equilibrated when the ratios for two successive points agreed to within five in the fifth significant figure.

Stopcocks (4) and (14) were opened to the vacuum manifold and the neon was evacuated from the doser system, the adsorption cell, and the gas handling manifold. Stopcocks (5) and (11) were also opened to evacuate the neon from the transfer line. The system was evacuated to less than 10^{-5} Torr and stopcocks (4), (11), (14), and (16) were then closed. After the adsorptive was expanded from its gas storage bulb into the gas handling manifold and the transfer line, stopcock (5) was closed. The adsorptive was then admitted to the doser system via stopcock (11) very slowly to avoid excessive vibrations of the Bourdon tube. The initial pressure in the doser system was usually three to four times the final desired pressure after the initial expansion into the cell. Stopcock (11) was closed and the pressure and ambient temperature were recorded. The adsorptive was expanded into the cell via stopcock (16). After the system equilibrated, the pressure and temperature were recorded, and stopcock (16) was closed. This first point was equilibrated for 3600 seconds and the ratio P (degrees)/ T (K) was calculated every 300 seconds. The pressure in the doser system was increased by adding adsorptive from the gas handling manifold via stopcock

(11). The pressure and the temperature were recorded and the adsorptive was expanded into the cell. The system was equilibrated for 720 seconds and the pressure and temperature were read. This sequence of steps was repeated five or six times to complete the isotherm.

When carbon monoxide was used as the adsorptive, stopcock (12) was closed after the final point of the isotherm was taken, and the cell was evacuated for 120 seconds via stopcock (14). Stopcocks (14) and (16) were closed and a second isotherm was obtained to determine the amount of physically adsorbed carbon monoxide.

The procedure for the hydrogen-titration isotherms varied from isotherm to isotherm in the surface reconstruction studies. For the case of the high temperature (673 K) reduction isotherm, the cell was cooled to room temperature in flowing hydrogen following the reduction. The hydrogen diffuser was shut down and the hydrogen was evacuated as described in the preceding section. Oxygen was transferred from its storage bulb to the doser volume via stopcocks (5) and (11). Stopcock (11) was closed and the oxygen was expanded into the cell to a pressure of 500-600 Torr by opening stopcock (16). The stopcock was closed and the oxygen was evacuated from the system. After 3600 seconds, the oxygen was evacuated from the cell at room temperature for 3600 seconds. The hydrogen-titration isotherm was then obtained in the manner described above.

Adsorption Isotherm Calculation Procedure

The adsorption isotherm calculation outlined below was based on the procedure for the determination of adsorption isotherms that was discussed previously. The volumes and stopcocks mentioned in the subsequent discussion refer to Figure 66. The volumes were defined as follows: the cell volume, V_C , was the volume of the adsorption cell and included the bore of stopcock (7); the connecting stopcock volume, V_{SC} , was the volume between stopcocks (6) and (7) and included

the bore of stopcock (6); the calibrated doser volume, V_{cd} , was the volume enclosed by stopcocks (1), (2), (3), (4), and (6), and included the volume of the quartz Bourdon spiral (B); and the doser volume, V_D , was the sum of V_{CD} and V_{SC} . It was necessary to use neon for the calibration because it was shown that helium diffused through the quartz spiral into the evacuated reference side of the capsule (A).

Doser Volume Calibration

The standard bulb (D) was calibrated in the following manner before it was attached to the doser volume. The bulb plus stopcock was weighted, evacuated, and filled with degassed, distilled water. After the bulb filled with water and had been equilibrated for 16 hours, it was removed from the constant temperature bath and weighed a second time. The volume was calculated from the mass and the specific gravity of water at the bath temperature. This procedure was repeated five times and the volume of the bulb ($V_{CB}=49.055 \text{ cm}^3$) was determined from the average of the measurements.

The calibrated bulb and the doser volume to be calibrated, V_{CD} , were filled with neon and initial pressure, P_1 , and the ambient temperature, T_1 , were recorded. Stopcock (2) was closed and the dose volume was evacuated via stopcock (3) to 10^{-5} torr. Stopcock (3) was closed, (2) was opened, and the neon was expanded from the bulb into the doser volume. The final pressure, P_2 , and the ambient temperature, T_2 , were recorded after equilibration. The neon was assumed to behave as an ideal gas; thus

$$\frac{P_1 V_{CB}}{T_1} = \frac{P_2 V_{CB}}{T_2} + \frac{P_2 V_{CD}}{T_2} . \quad (5-1)$$

This equation was rearranged to express the calibrated doser volume as

$$V_{CD} = \left(\frac{P_1}{T_1} - \frac{P_2}{T_2} \right) \left(\frac{T_2}{P_2} \right) V_{CB} \quad (5-2)$$

The values of P_1/T_1 and P_2/T_2 were determined in 25 sets of measurements, of which ten were discarded on the basis of the 4d and 2.5d rules. The range of initial pressures was 150 to 450 torr and the corresponding range of final pressures was 130 to 400 Torr. There was no systematic variation in the value of V_{CD} as a function of the initial pressure, P_1 . The calibrated doser volume was 6.2890 cm^3 with a standard deviation of 0.018 and a 95 percent confidence level that the volume was between 6.279 and 6.299 cm^3 .

Calculation of the Cell Volume

The volumes of the connecting stopcock, V_{SC} , and the adsorption cell, V_C , were determined by filling the calibrated doser volume, V_{CD} , with neon and expanding the neon sequentially into the connecting stopcock and the cell which had been previously evacuated. The cell volume was determined the cell at the ambient temperature or with the cell immersed in the thermostated bath at the isotherm temperature. The equations were derived for the case with the cell immersed in the bath.

If

$$V_1 = V_{CD}$$

$$V_2 = V_{CD} + V_{SC}$$

$$V_3 = V_{CD} + V_C = V_2 + V_C$$

and P_1 , P_2 , and P_3 were equilibrium pressures of the neon in the volumes V_1 , V_2 , and V_3 , respectively, measured at the ambient temperatures T_1 , T_2 , and T_3 in the Plexiglas enclosure, then, from the ideal gas law,

$$\frac{P_1 V_1}{T_1} = \frac{P_2 V_2}{T_2} = \frac{P_3 V_2}{T_3} + \frac{P_3 V_C}{T_C} . \quad (5-3)$$

The connecting stopcock was calculated from the first two terms of Equation (5-3); that is,

$$\frac{P_1 V_{CD}}{T_1} = \frac{P_2 (V_{CD} + V_{SC})}{T_2} \quad (5-4)$$

which gave

$$V_D = V_{SC} + V_{CD} . \quad (5-5)$$

The doser volume was then calculated from

$$V_D = V_{SC} + V_{CD} .$$

The cell volume was calculated from the second two terms of the Equation (5-3); that is,

$$\frac{P_2 V_D}{T_2} = \frac{P_3 V_D}{T_3} + \frac{P_3 V_C}{T_C}$$

which was rearranged to give

$$V_C = \left(\frac{P_2}{T_2} - \frac{P_3}{T_3} \right) \left(\frac{T_C}{P_3} \right) V_D . \quad (5-6)$$

If the cell was at the ambient temperature, the expression for the cell volume was

$$V_C = \left(\frac{P_2}{T_2} - \frac{P_3}{T_3} \right) \left(\frac{T_3}{P_3} \right) V_D . \quad (5-7)$$

Adsorption Isotherm Calculation

Adsorption isotherms were determined in the following manner. The adsorption cell and the doser volume were evacuated to less than 10^{-5} Torr and stopcock (7) was closed. The doser volume was filled with adsorptive to pressure P_1 (1) at the ambient temperature TR_1 (1). Stopcock (7) was opened and the adsorptive was admitted to the cell. The equilibrated pressure P_2 (1) at the ambient temperature T_2 (1) was recorded after one hour.

A material balance on the doser volume and the adsorption cell gave

$$n_{D,1}(1) = n_{D,2}(1) + n_{C,2}(1) + n_{a,2}(1) \quad (5-8)$$

where $n_{D,1}(1)$ was the moles of adsorptive in the doser volume at the initial conditions for the first isotherm point; $n_{D,2}(1)$ was the moles of adsorptive in the doser volume at the final conditions for the first isotherm point; $n_{C,2}(1)$ was the moles of adsorptive in the gas phase in the cell at the final conditions for the first isotherm point, and $n_{a,2}(1)$ was the moles of adsorbate at the final conditions for the first isotherm point. The amount adsorbed, assuming the adsorptive obeyed the ideal gas law, was given by

$$n_{a,2}(1) = \frac{P_1(1) V_D}{R T_1(1)} - \frac{P_2(1) V_D}{R T_2(1)} - \frac{P_2(1) V_C}{R T_C} \quad (5-9)$$

or

$$n_{a,2}(1) = \left(\frac{P_1(1)}{T_1(1)} - \frac{P_2(1)}{T_2(1)} \right) \frac{V_D}{R} - P_2(1) \frac{V_C}{R T_C} . \quad (5-10)$$

The amount adsorbed was expressed as

$$n_{a,2}(1) = \frac{P_S V_a(1)}{R T_S} \quad (5-11)$$

where P_S was 760 Torr, T_S was 273.16 K, and $V_a(1)$ was the volume of adsorbate at the standard temperature and pressure. Substituting Equation (5-11) into (5-10), an expression was obtained for the amount of adsorbate for the first isotherm point in PV units, that is

$$P_S V_a(1) = \left(\left(\frac{P_1(1)}{T_1(1)} - \frac{P_2(1)}{T_2(1)} \right) V_D - P_2(1) \frac{V_C}{R T_C} \right) T_S \quad (5-12)$$

The cell was isolated from the doser volume after equilibrium of the first isotherm point by closing stopcock (7). Adsorptive was added to the doser volume and the initial pressure for the second isotherm point, $P_1(2)$ at $T_1(2)$, was recorded. Stopcock (6) was opened, the adsorptive was expanded into the cell and the equilibrated pressure $P_2(2)$ and $T_2(2)$ was recorded. A second material balance gave

$$n_{D,1}(2) + n_{C,2}(1) + n_{a,2}(1) = n_{D,2}(2) + n_{C,2}(2) + n_{a,2}(1,2) \quad (5-13)$$

where $n_{D,1}(2)$ was the moles of adsorptive in the doser volume at the initial conditions for the second isotherm point, $n_{D,2}(2)$ was the moles of adsorptive in the doser volume at the final conditions for the second isotherm point, $n_{C,2}(2)$ was the moles of adsorptive in the gas phase in the cell at the final conditions for the second isotherm point, and $n_{a,2}(1,2)$ was the total moles of adsorbate at the final conditions for the second isotherm point. The total moles of adsorbate, the sum of the moles adsorbed after each expansion into the cell, was given by

$$n_{a,2}(1,2) = n_{a,2}(1) + n_{a,2}(2) \quad (5-14)$$

where $n_{a,2}(2)$ was the moles of adsorptive that adsorbed at the final conditions for the second isotherm point as a result of the second dose. Equation (5-14) was substituted into (5-13) and the amount adsorbed, $n_{a,2}(2)$, was given by

$$n_{a,2}(2) = \frac{P_1(1)}{R T_1(2)} + \frac{P_2(1) V_C}{R T_C} - \frac{P_2(2) V_D}{R T_2(2)} - \frac{P_2(2) V_C}{R T_C} \quad (5-15)$$

or in terms of volume adsorbed,

$$P_S V_a(2) = \left(\frac{P_1(2)}{T_1(2)} - \frac{P_2(2)}{T_2(2)} \right) V_D = (P_2(2) - P_2(1)) \frac{V_C}{T_C} T_S. \quad (5-16)$$

The procedure was repeated for the third isotherm point. The initial pressure, $P_1(3)$ at $T_1^*(3)$, was recorded, and the adsorptive was expanded into the cell, after which the equilibrated pressure $P_2(3)$ at $T_2(3)$ was recorded. The material balance gave

$$n_{D,1}(3) + n_{C,2}(2) + n_{a,2}(1,2) = n_{D,2}(3) + n_{C,2}(3) + n_{a,2}(1,2,3) \quad (5-17)$$

where $n_{D,1}(3)$ was the moles of adsorptive in the doser volume at the initial conditions for the third isotherm point, $n_{d,2}(3)$ was the moles of adsorptive in the doser volume at the final conditions for the third isotherm point, $n_{C,2}(3)$ was the moles of adsorptive in the gas phase in the cell at the final conditions for the third isotherm point and $n_{a,2}(1, 2, 3)$ was the total moles of adsorbate at the final conditions for the third isotherm point. The total moles of adsorbate after the third dose was

$$n_{a,2}(1,2,3) = n_{a,2}(1) + n_{a,2}(2) + n_{a,2}(3) \quad (5-18)$$

where $n_{a,2}(3)$ was the amount of adsorptive that was adsorbed as a result of the third expansion of adsorptive into the cell. The amount adsorbed was given by

$$P_S V_a(3) = \left(\left(\frac{P_1(3)}{T_1(3)} - \frac{P_2(3)}{T_2(3)} \right) V_D - (P_2(3) - P_2(2)) \frac{V_C}{T_C} \right) T_S \quad (5-19)$$

The expression for the n th isotherm point was obtained after inspection of Equations (5-12), (5-16), and (5-19); that is,

$$P_S V_a(n) = \left(\left(\frac{P_1(n)}{T_1(n)} - \frac{P_2(n)}{T_2(n)} \right) V_D - (P_2(n) - P_2(n-1)) \frac{V_C}{T_C} \right) T_S \quad (5-20)$$

where $V_a(n)$ was the amount of adsorptive that adsorbed at the final pressure $P_2(n)$ as a result of the n th expansion of adsorptive into the cell and $P_2(n-1)$ was zero when $n=1$. The amount of adsorptive that was adsorbed per gram of catalyst was a result of the n th expansion was given by

$$V_a(n) = \frac{P_S V_a(n)}{(760 \text{ Torr}) (\text{mass catalyst, g})} \quad (5-21)$$

or, in μmol per gram of catalyst,

$$n_a(n) = \frac{V_a(n)}{0.22414 \text{ cm}^3 \mu\text{mol}^{-1}} \quad (5-22)$$

The total amount of adsorbate at the equilibrium pressure $P_2(n)$ for the n th isotherm point was

$$n_a (\mu\text{mol g}^{-1}) = \sum_{i=1}^n n_a(i). \quad (5-23)$$

The value of n_a ($\mu\text{mol g}^{-1}$) for each $P_2(n)$ was plotted versus $P_2(n)$. The best straight line through the n isotherm points was extrapolated to zero pressure, and this intercept was taken as the amount of adsorptive taken up by the supported metal.

A series of typical isotherms are presented in Figures 68 and 69 for hydrogen, oxygen, and carbon monoxide chemisorption on an 0.53 weight percent platinum on silica hydrogenation catalyst.

A second platinum hydrogenation catalyst 0.56 percent Pt/ Al_2O_3 (obtained from a different source) was used for additional testing of the apparatus. The catalyst was reduced in-situ in flowing of hydrogen at 450°C for four hours prior to chemisorption experiments which were conducted at room temperature (25°C). The reduced catalyst was evacuated (down to 10^{-5} torr) at 50 percent above the temperature of reduction for 1-1/2 hours in order to remove any residual hydrogen before hydrogen chemisorption. A double isotherm method was used to ascertain the hydrogen uptake values (Figure 70). The first isotherm represented both chemisorbed and physisorbed hydrogen. After this, the sample was evacuated at room temperature to remove the physisorbed fraction of hydrogen and then the second isotherm, representing only physisorbed hydrogen, was generated. As shown in Figure 70, the isotherms were essentially parallel. The amount of chemisorbed hydrogen was obtained by taking the difference in the hydrogen uptake values corresponding to the two isotherms at zero pressure. In this particular case, the amount of hydrogen chemisorbed was found to be $4.019 \mu\text{mol/g}^{-1}$ catalyst. This gave a dispersion of 20.3 percent, which was considered reasonable.

A computer program (listed in Appendix D) was written and used to analyze the chemisorption data. A representative output of this program is included in Appendix D.

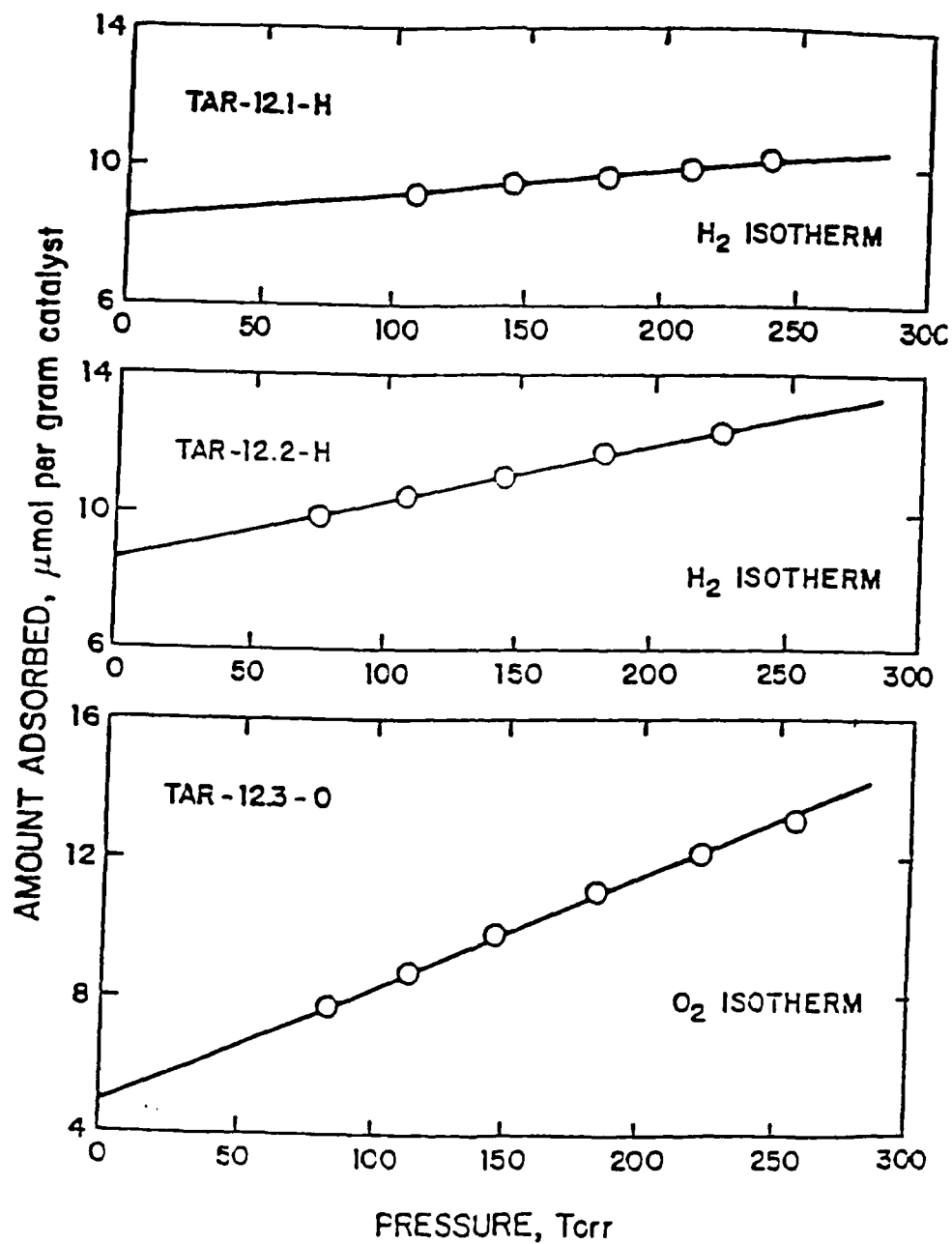


Figure 68. Hydrogen and Oxygen Adsorption Isotherms
0.53% Pt/ SiO_2 Catalyst

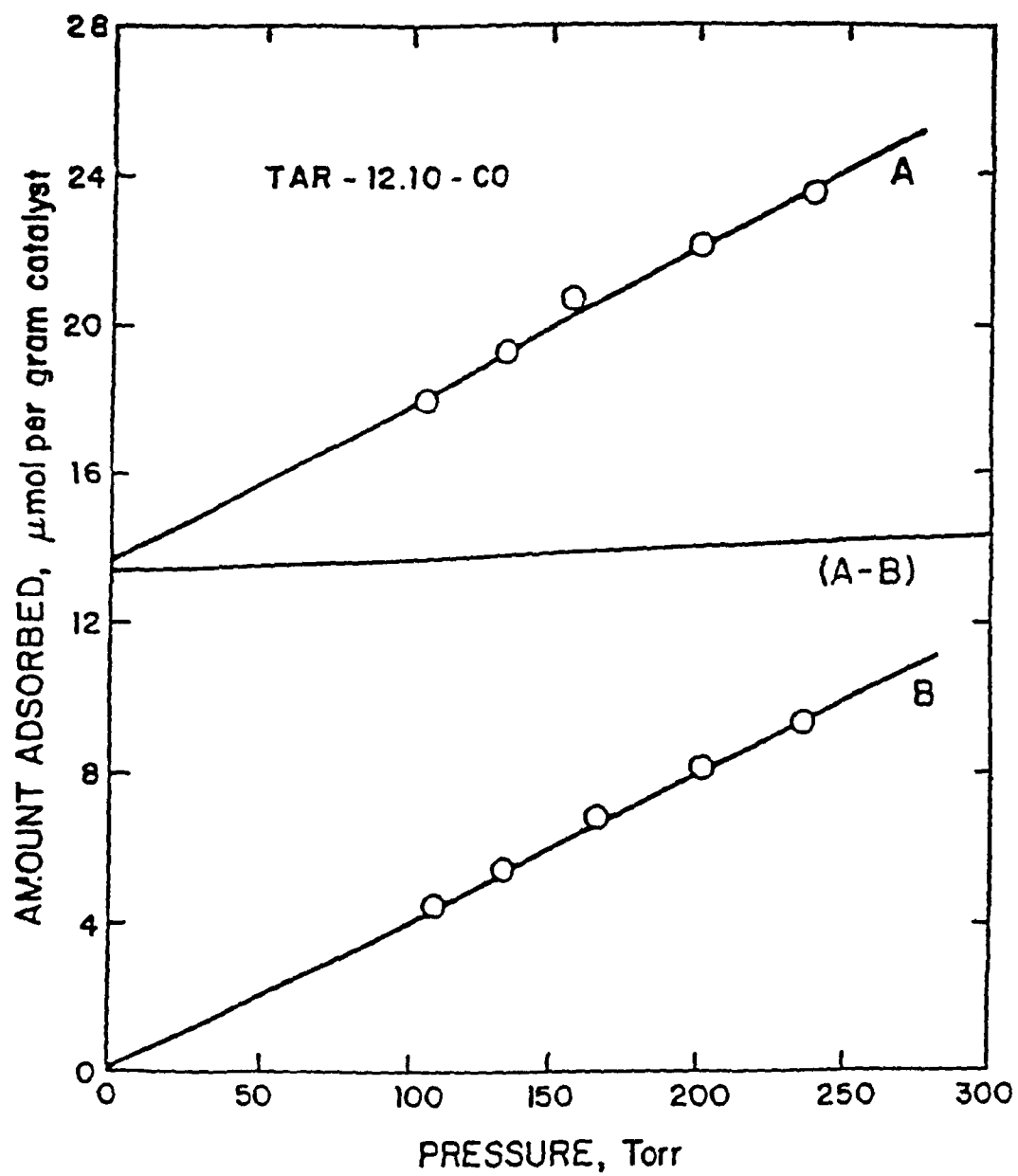


Figure 69. Carbon Monoxide Adsorption Isotherm
0.53 Pt/SiO₂ Catalyst

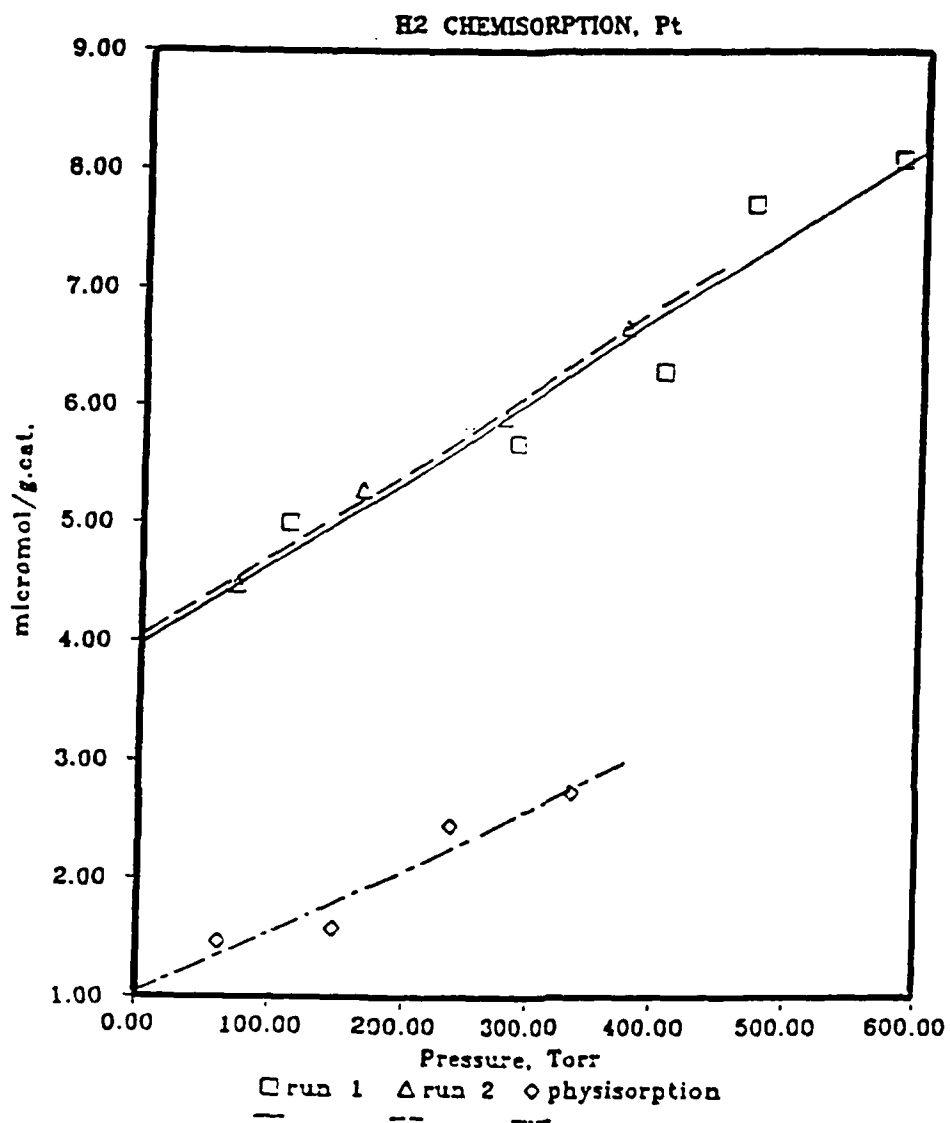


Figure 70. Hydrogen Chemisorption Isotherm for Pt/Al₂O₃

Table 29

Chemisorption Data for Pt/SiO₂ CatalystTAR-12

Catalyst:	0.53 percent Pt/SiO ₂
Catalyst loading:	2.0078 g (wet) 54.55 μmol total Pt
Cell temperature:	293 K
Cell volume:	10.4403 cm ³
Doser volume:	6.8593 cm ³

TAR-12.1-II (Hydrogen Isotherm)

P ₁ (Torr)	T ₁ (K)	P ₂ (Torr)	T ₂ (K)	n _a ($\mu\text{mol g}^{-1}$)
326.6	300.7	107.8	300.8	9.20
209.0	300.8	146.6	300.8	9.53
232.6	300.9	179.8	300.9	9.75
260.4	300.8	210.8	300.8	9.93
284.4	300.7	239.0	300.7	10.19

catalyst pretreatment: evacuation, 423 K, 2 h
reduction, 673 K, 4 h
evacuation, 723 K, 1-1/2 h
intercept: 8.54 $\mu\text{mol g}^{-1}$ H₂ uptake

Table 29 (con't)

Chemisorption Data for Pt/SiO₂ CatalystTAR-12.2-H (Hydrogen Isotherm)

P_1 (Torr)	T_1 (K)	P_2 (Torr)	T_2 (K)	n_a ($\mu\text{mol g}^{-1}$)
244.6	301.5	74.2	301.7	9.90
162.4	301.8	107.6	301.8	10.46
205.7	301.8	144.5	301.8	11.06
243.7	301.6	181.8	301.5	11.71
293.1	301.5	223.9	301.3	12.27

catalyst pretreatment: evacuation, 573 K, 1-1/2 h
 intercept: 8.67 $\mu\text{mol g}^{-1}$ H₂ uptake

TAR-12.3-O (Oxygen Isotherm)

P_1 (Torr)	T_1 (K)	P_2 (Torr)	T_2 (K)	n_a ($\mu\text{mol g}^{-1}$)
253.8	300.3	82.7	300.6	7.70
166.4	300.7	113.4	300.8	8.64
205.7	300.9	146.9	300.9	9.79
245.6	301.0	182.8	300.9	11.03
284.6	300.9	220.1	300.9	12.13
318.4	300.8	256.3	300.8	13.14

catalyst pretreatment: evacuation, 723 K, 2 h
 intercept: 5.0 $\mu\text{mol g}^{-1}$ O₂ uptake

Table 29 (concluded)

Chemisorption Data for Pt/SiO₂ CatalystTAR-12.10-CO (Carbon Monoxide Isotherm)

P_1 (Torr)	T_1 (K)	P_2 (Torr)	T_2 (K)	n_a ($\mu\text{mol g}^{-1}$)
363.4	296.7	104.8	296.7	18.00
183.0	297.0	132.9	298.2	19.24
223.4	298.5	165.3	298.7	20.72
265.3	298.8	201.5	299.0	22.16
303.8	299.1	238.7	299.3	23.51

catalyst pretreatment: reduction, 673 K, 4 h
evacuation, 723 K, 1-1/2 h

P_1 (Torr)	T_1 (K)	P_2 (Torr)	T_2 (K)	n_a ($\mu\text{mol g}^{-1}$)
298.9	299.5	107.5	299.8	4.48
182.8	299.9	134.7	300.0	5.53
223.7	300.2	166.7	300.2	6.84
265.4	300.3	202.5	300.4	8.16
295.9	300.5	236.4	300.5	9.34

catalyst pretreatment: evacuation, 293 K, 120 s
intercept: 13.45 $\mu\text{mol g}^{-1}$ net CO uptake

Hydrogenation of Toluene

A high-pressure flow reactor was used to make an exploratory hydrogenation reaction run with toluene as feed and 2 percent Ni/Al₂O₃ as catalyst. The reactor system was available and was used for these preliminary experiments. The experimental conditions were as follows:

Catalyst:	2 percent Ni/Al ₂ O ₃ (6.5 cm ³)
Temperature:	300°C
Pressure:	370 Psig
Toluene LHSV:	15.2 cm ³ /hr cm ³ cat.
Hydrogen GHSV:	0.21 cm ³ /hr cm ³ cat.
Reaction Time:	4 h.

The catalyst was secured between two layers of inert 'Denstone' and separated by two stainless steel mesh cloths. A thermocouple was placed through a thermowell so that the tip of it was exactly at the center of the catalyst bed. The calcined catalyst was reduced in-situ in flowing hydrogen (at 1 atm and at 37 cm³/min) for four hours at 450°C. After reduction, the reactor was cooled down to 300°C and the toluene flow was started. A sample was taken after 4 hours of run and analyzed. The conversion was found to be about 10 percent and the products were mainly methyl cyclohexane. A GC column (10 percent OV-17 on chromwax, 12") was purchased and tested for analysis. This is capable of analyzing aromatic hydrocarbons and naphthenes and naphthenoaromatics containing up to at least 14 carbon atoms.

Hydrogenation of Naphthalene

A series of experiments was conducted with a variety of metals supported upon alumina. The metals included ruthenium, rhodium, palladium, and rhenium. At high temperatures (>275°C),

the predominant reaction pathway was cracking, whereas at low temperatures ($<230^{\circ}\text{C}$), the cracking reactions were suppressed and the hydrogenation pathway was dominant. The preliminary results are summarized in Table 30. The reported data were obtained at a hydrogen partial pressure of 2300 psig with a 0.5 wt percent naphthalene in normal heptane feedstock. The duration of each run was 2.5 hours. The catalysts were reduced in-situ in flowing hydrogen ($40\text{ cm}^3\text{ min}^{-1}$) at 500°C for six hours. As indicated previously, this work was deemphasized and placed on inactive status at the direction of the Technical Project Officer.

Table 30

Hydrogenation of Naphthalene over Various Catalysts

Run #	Catalyst	Temp, °C	percent Conversion		percent Selectivity	
				Tetralin	Decalins	Cracking
1.	2.5 percent Ru/Al ₂ O ₃	300	100	0	11.0	89.0
2.	2.5 percent Ru/Al ₂ O ₃	225	100	0	97.0	3.0
3.	2.5 percent Ru/Al ₂ O ₃	125	100	0	100.0	0.0
4.*	2.5 percent Ru/Al ₂ O ₃	300	90	--	10.0	90.0
5.	2.5 percent Rh/Al ₂ O ₃	300	100	trace	95.0	4.9
6.	2.5 percent Pd/Al ₂ O ₃	300	100	trace	99.0	--
7.	5.0 percent Re/Al ₂ O ₃	300	82	29.5	65.5	5.0

*This run was made with decalin as feed.

**Section VI: SELECTIVE CATALYTIC CRACKING OF NORMAL PARAFFINS
IN KEROSENE BOILING RANGE FEEDSTOCKS OVER ZSM-5**

Research Personnel:

**Daniel C. Longstaff
Graduate Student**

**Francis V. Hanson
Associate Professor**

Introduction

The research activities reported in this section were primarily concerned with producing higher density aviation turbine fuel from waxy naphthenic crudes. The method proposed to produce a high density fuel was to expand the boiling range of the fuel by increasing the end-point of the kerosene fraction of a naphthenic crude. The expansion of the boiling range will result in a higher density kerosene; however, it will also have an undesirably high freeze point. Dewaxing will reduce the freeze point of the kerosene so it can meet aviation turbine fuel specifications while having a higher density.

Normally jet fuels are not subjected to any catalytic treatment other than perhaps a mild catalytic hydrogenation to reduce the sulfur content when the sulfur content exceeds specifications or a mild catalytic oxidation to oxidize mercaptan sulfur so it can be removed more easily by a caustic wash. Catalytic dewaxing would represent a new processing step in the production of aviation turbine fuels and would increase the cost of producing jet fuels. However, it would also broaden the range of acceptable crudes for the production of standard and high density aviation turbine fuels to include the use of certain waxy naphthenic crudes.

A secondary effect would be the stabilization of crude availability for aviation turbine fuel manufacture, particularly during an oil shortage or in wartime.

Experimental Apparatus

Commercial catalytic dewaxing of lubricating oils is carried out in a fixed bed reactor system. A fixed bed reactor system was modified for this investigation.

The modifications included the following:

1. a liquid feed reservoir and pump were added to the apparatus;
2. the gas feed system was modified to handle a single gas; and
3. a reactor by-pass line was added to facilitate operation of the system.

Description of the Components of the System

A schematic of the apparatus is presented in Figure 71. The reactor system consisted of four main components:

1. the gas feed system;
2. the liquid feed system;
3. the reactor; and
4. the product collection system.

Gas Feed System

The gas feed system was designed to regulate and monitor the flow of the diluent gas to the reactor. The pressure of the gas exiting the reactor was controlled by a Mity Mite Inc. back pressure control valve (BPCV) which was rated to 2000 psig. The BPCV was pressurized to the desired operating pressure with nitrogen. The gas flow rate to the reactor was controlled by a Union Carbide Mass Flowmeter Model FM-12C.

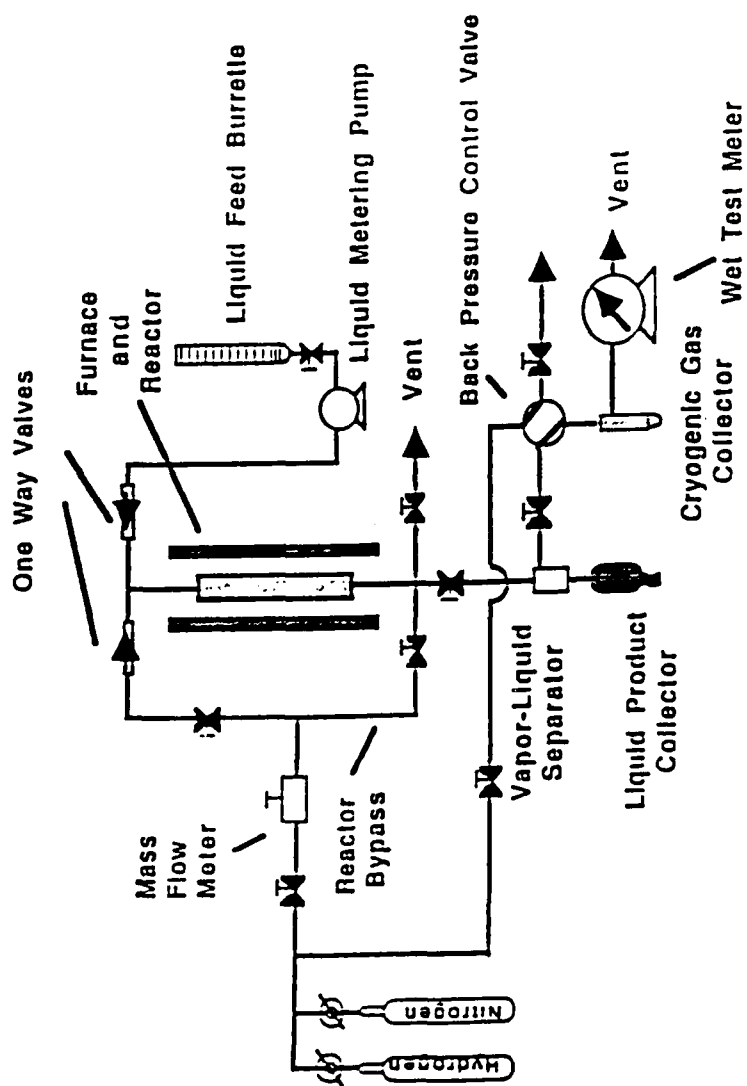


Figure 71. Diagram of Catalytic Dewaxing Reactor System

The system was protected from overpressuring by a Swagelok, Inc., model SS-4R3A-C, pressure relief valve which could be set to open at pressures between 750 and 1500 psig. The pressure relief valve was usually set to open at 970 psig which was 30 psig below the maximum pressure rating of the liquid feed pump.

A bypass line made it possible to flush the product collection system without passing the gas through the reactor. The gases used in the gas feed system were hydrogen and nitrogen. Hydrogen was used as the diluent in most experiments and nitrogen was used to flush the reactor or to pressurize the BPCV.

Liquid Feed System

The liquid feed system was designed to control and monitor the flow of liquid into the reactor. The main component of the system was a Milton Roy model DB-1-60R metering liquid feed pump. The volume pumped could be controlled by adjusting a dial on the pump which controlled the stroke length of the pump piston. The minimum steady state pump rate was such that a weight hourly space velocity (WHSV) of 1-3 g of feed/(g of catalyst)(h) could be maintained over a two gram sample of catalyst. The maximum operating pressure of the pump was 1000 psig. In order to avoid the possibility of damaging the pump by overpressurizing, a pressure relief valve was connected to the liquid feed line. The Swagelok Inc. model SS-4R3A-C pressure relief valve could be set to open between 750 and 1500 psig. During normal operation the valve was set to open at 970 psig.

A valve was connected to the liquid feed line so that the pump could be primed prior to operating at elevated pressures. The liquid feed passed into the gas-liquid mixing zone through a one way valve to prevent the flow of gas into the liquid feed system.

Reactor

The reactor consisted of a 1/2 inch inside diameter stainless steel tube encased in a cylindrical copper block which acted as a heat sink to evenly distribute the heat from the furnace. The intent was to prevent large localized heat variations in the reactor due to hot or cold spots in the electrical furnace. A 1/8 inch OD thermowell was located on the axis through the reactor tube to monitor the temperature profiles in the catalyst bed.

The reactor tube had a flange threaded onto each end of it. These flanges could be connected to matching flanges through which feed or products could flow. The reactor was sealed by stainless steel o-rings.

Product Collection System

The effluent stream from the reactor passed into a vapor-liquid separator which also served as a liquid collector. The non-condensable vapor stream was vented through the BPCV.

The cryogenic gas collector consisted of a vaporizer test tube that was packed with shredded cellulose submerged in a liquid nitrogen bath to condense all the condensibles into a vessel which could be weighed to determine the mass of material collected.²⁵¹ This method usually provided a mass balance of 100 ± 0.5 -2 percent.

The composition of the gases condensed were determined by gas chromatography. The volume of the gas that passed through the cryogenic gas collector was determined with a wet test meter.

Operating Procedure

The acquisition of meaningful data required that the following be observed:

1. the reaction conditions must remain constant, that is the temperature, pressure, catalyst activity and liquid and gas feed rates should not change during the time period when a material balance is made; and
2. a complete mass balance must be obtained on the hydrocarbon feed.

The experimental operating procedures were developed to maintain the reaction conditions constant and to enable collection and measurement of the liquid and gas products of the reaction.

Catalyst Loading Procedure

The catalyst bed was located between two sections of inert packing. The inert packing serves to support the catalyst as well as providing a surface for heating the reactant mixture. The catalyst was loaded into the reactor according to the following procedure. The top flange was secured to the reactor. The thermowell was connected to the top flange and positioned along the axis of the reactor. The reactor was clamped upside down in a vise. A plug of nitric acid washed glass wool was inserted in the reactor without pushing it through the top flange. Alundum that had been soaked in hot nitric acid, rinsed with deionized water and dried was then poured into the reactor to within 1/2 inch of the point along the entered thermowell where the catalyst bed was to be placed. Distances in the thermowell were gauged by means of a rod that was slid into the reactor to determine the depth of the alundum bed. After the alundum was packed to the appropriate depth a second wad of nitric acid washed glass wool was placed in the reactor and a sample of catalyst was placed on top of the plug of glass wool.

The catalyst was then held in place by a third plug of acid washed glass wool. The glass wool plug was then followed by enough acid washed alundum to fill up the reactor to within 1/2 inch of the top. A fourth and final plug of glass wool was then placed in the reactor to keep particles of alundum from falling out of the reactor.

After the reactor was completely packed the bottom flange was bolted onto the reactor and it was pressure tested with nitrogen. A mixture of silicon carbide and dodecane would be used to polish the o-rings so that they would form a proper seal with the reactor.

The pressure test was done with the reactor in the vise. This facilitated any necessary adjustments. The orientation of the o-rings with respect to the reactor tube was changed if a particular configuration had a tendency to leak. When it was determined that the reactor did not leak it was connected to the reactor system and the standard catalyst pretreatment procedures were followed.

Mass Balance Procedure

Experiments must be conducted so as to obtain complete material balances so that definitive conclusions concerning catalyst activity and selectivity can be drawn. In most cases catalytic runs with complete mass balances were only attempted once a day due to the effort required.

The reactor was always left at reaction temperature to save time and to avoid possible effects on the catalyst resulting from heating and cooling cycles. Prior to making a material balance the feed and diluent gas were passed over the catalyst for a period of time ranging from an hour to several hours to ensure that the catalyst and the system were operating at steady state. The gas flow rate was determined with a wet test meter. The liquid feed pump set point was set so that the correct liquid hourly space velocity was established. The rate of liquid feed was determined by measuring the amount of liquid removed from the liquid feed buret during a given period of time.

During the equilibrated stage of the experiment the liquid accumulated in the vapor-liquid separator was occasionally removed from the separator by means of a valve at the bottom of the

separator. This was always done slowly to minimize the reduction of the pressure in the system. The cryogenic gas collector was not cooled during this period because it was much more difficult to empty than the vapor-liquid separator.

Prior to the start of the material balance a sample of gas leaving the vapor-liquid separator was taken to determine the methane to ethane ratio of the product gas. This was done because the vapor pressure of methane is high enough in the cryogenic liquid separator that most of it escapes to the vent. This does not significantly affect the mass balance because of the small amount of methane that is normally produced but it makes it impossible to accurately correlate data based on methane collected in the cryogenic liquid separator.

At the start of the material balance the vapor-liquid separator was carefully emptied without upsetting the system pressure, the volume of liquid in the buret was recorded, the reading on the wet test meter was set to zero and the timer was started. The cryogenic gas collector was filled with liquid nitrogen and kept filled for the duration of the material balance. During the course of the run the reactor temperature was recorded. A reactor temperature profile was sometimes recorded if it was thought that it might provide useful information about the nature of the reactions taking place in the catalyst bed.

When the material balance was completed the volume of liquid in the buret and the reading on the wet test meter were recorded. The time that had elapsed since the start of the material balance was also noted. The pump was shut off and the valve between the reactor and the vapor-liquid separator was shut off to prevent extra product being collected in addition to the product that was collected during the time period of the material balance. The valve in the reactor bypass was opened so that gas would continue to flow from the gas supply system to the product collecting system while keeping the reactor separated from the rest of the system.

The C₃ and C₄ species dissolved in the liquid product collected in the vapor-liquid separator were weathered into the cryogenic vapor collector. The test tube in the cryogenic vapor collector was removed and weighed to determine the mass of vapor collected.

The test tube from the cryogenic vapor collector was allowed to warm to room temperature and the vapors evolved were collected by water displacement. The gas that was collected in the water bottle was transferred to a gas sampling bottle and a sample was injected into a gas chromatograph to determine the relative amounts of the different hydrocarbons.

While the test tube from the cryogenic vapor trap was warming to room temperature the liquid from the vapor liquid separator was collected and weighed. A sample of the liquid was saved in a glass sample bottle which was then stored in a refrigerator. About 0.05 μ l of the liquid was injected onto a 10 percent Phenylmethyl silicon 10 M X 530 μ m column for gas chromatographic analysis.

The mass balance was determined by comparing the sum of the weight of the gas and liquid products with the weight of liquid feed.

Computer Analysis of Results

If the mass balance was good (100 ± 2 percent), the chromatographs of the gas and liquid products were analyzed for the amounts of different species. A computer program was written to compute the conversions to paraffins, olefins and naphthenes, and aromatics of different carbon numbers. The program is found in Appendix B along with a sample input and output.

Model Compound Studies

Catalyst Preparation

It is accepted that ZSM-5 catalysts exhibit the shape selective properties necessary to selectively crack normal paraffins and isoparaffins in a mixture of kerosene and higher boiling range naphthenes.^{8-10,252,253} However, the optimum parameters that are required for catalyst synthesis, catalyst pretreatment and reaction conditions are not outlined in the literature. The objective of this research was to dewax an expanded boiling range distillate, to produce a high density aviation turbine fuel rather, than to produce a high octane naphtha. Therefore, it was decided to maximize catalyst activity at the expense of high octane cracked products.

Initially it was thought best to study the cracking of a model compound, n-hexadecane, because it is a normal paraffin of approximately the same boiling range as the distillates that were to be catalytically dewaxed. In addition there are several literature references to the cracking of n-hexadecane over HZSM-5²⁵⁴ and Pt/HZSM-5.²⁵⁵

Unfortunately these reports lack details on how the catalysts were activated. It has been reported¹⁶ that the active cracking sites in HZSM-5 are the strong acid tetrahedral aluminum sites which are not fully activated from the ammonium form of the catalyst except by calcination at temperatures above 623-773 K (350-500°C). Care was taken not to heat the catalyst to a temperature higher than that necessary to activate the strong acid sites to avoid the possibility of dehydroxylation of strong Brönsted sites to weaker Lewis base sites²⁵⁶ and the consequent reduction of total cracking activity.

Ammonia TPD indicated that most of the strong acid sites are activated by heating above 773 K (500°C). Therefore it was decided to activate the ZSM-5 catalysts by heating in air to 783 K (510°C) in air at a programmed rate of 5 K/ min. The sample was held at 783 K (510°C) for

10 minutes followed by cooling to room temperature. The catalysts were then loaded in the reactor and heated to the reaction temperature.

Thermal Cracking

In order to establish that the reactor possessed no inherent catalytic cracking activity due to the wall surface or to the inert packing in the reactor a set of blank cracking runs were conducted. The reactor was packed with inert alumina and hexadecane was passed over the alumina at different temperatures to determine the conversion. Five runs were done at 50 K intervals from 573 to 773 K (300 to 500°C). No attempt was made to collect or analyze the gas product. The liquid product was analyzed by gas chromatography.

At 573 K, 623 K, and 673 K (300, 350 and 400°C) there was little or no conversion as evidenced by the lack of chemical species other than normal hexadecane in the liquid product. At 723 K (450°C) a series of equally sized peaks from C_{10} to C_{15} were obtained. These species were believed to have been alpha olefins resulting from the thermal cracking of normal hexadecane. A series of other peaks were also obtained. At 773 K (500°C) a higher yield of the same product slate was obtained. These experiments indicated that the reactor and the inert alumina packing possessed no inherent cracking activity at temperatures below 673 K (400°C). Above 673 K (400°C) the alumina packing may exhibit the ability to catalyze thermal cracking reactions. It was also concluded that at temperatures greater than 673-723 K (400-450°C) the apparent selectivity of the catalyst will reflect nonshape-selective thermal cracking reactions.

Hexadecane Cracking at 573 K (300°C)

A series of experiments were performed at 573 K (300°C) to determine if the cracking product boiling above C_4 could be maximized by the right choice of operating conditions. The

way to achieve this object is to minimize secondary cracking of the primary cracked products. The cracking experiments were performed over a range of WHSV at constant total pressure and temperature.

The temperature at which the cracking of n-hexadecane over ZSM-5 was studied was selected to minimize secondary cracking of the primary products of the reaction. However, low rates of secondary cracking are achieved at the expense of cracking activity. In commercial hydrodewaxing over ZSM-5¹⁰ the initial temperature of reaction is 563 K (290°C) with fresh HZSM-5. As the catalyst deactivates the temperature is gradually raised to 643 K (370°C) over a period of several weeks. The reactor then operates at temperatures between 643 and the end of the cycle temperature, 703 K (430°C) At 703 K (430°C) the catalyst is regenerated.

It is also noted that a study of n-hexadecane cracking on ZSM-5 by Bezouhanova et al.²⁵⁴ indicated that at a LHSV of 1 and a temperature of 643 K (370°C) the primary product obtained with HZSM-5 of varying Si/Al ratios were C₃'s and C₄'s and to a lesser extent aromatics. Therefore it was thought that by lowering the temperature of reaction that the yield of higher boiling products could be increased. A temperature of 573 K (300°C) was chosen to study the rate of formation of secondary and primary cracked products as a function of the space velocity.

A pressure of 200 psig was chosen for the experiments because it was thought that hydrogen pressure would reduce the rate of coke formation and maintain catalyst activity. In commercial dewaxing processes a pressure of 400-800 psig of hydrogen and hydrocarbon is used with HZSM-5¹⁰ and 300-1500 psig with Pt-H-Mordenite.¹¹

The hexadecane was diluted with hydrogen at 200 psia to prevent the condensation of hexadecane in the reactor due to the vapor pressure of hexadecane at 573 K (300°C) (\approx 19 psia).

The ammonium form of the catalyst was pressed into pellets at 90000 psig. The pellets were then crushed and sized between 14 and 35 mesh. Pellets smaller than 35 mesh were crushed into powder and repressed into new pellets. Pellets that were larger than 14 mesh were recrushed. This procedure was followed until all the zeolite was incorporated into granules between 14 and 35 mesh.

The zeolite was 93 percent crystalline and ammonia temperature programmed desorption measurements showed that it had 0.5 mmol/g of Brönsted acid sites. After calcination at 783 K (510°C) two grams of this sample was placed in the reactor according to the procedure described previously.

An initial experiment was conducted to determine how the catalyst activity and product selectivity changes during catalyst utilization.

Hydrogen flow at 200 psig was established over the catalyst and the flow of hexadecane was started. The temperature of the reactor was about 577 K (304°C) initially. The flow rate of hydrogen was 12 l(STP)/(g·cat)(h) and the WHSV of liquid normal hexadecane was 12.

In the first two or three minutes the temperature of the catalyst rose five or ten degrees centigrade and then dropped as an endothermic temperature profile was established.

Samples of liquid flowing between the catalytic reactor and the vapor liquid separator were collected and analyzed every several hours. The first drops of liquid product contained about 35 weight percent normal hexadecane. Liquid product after 45 min was about 50 weight percent normal hexadecane and after two hours the liquid product was about 65 weight percent normal hexadecane and it remained at that level for the duration of the run.

It was shown from this experiment that the ZSM-5 synthesized and utilized for hydrodewaxing required less than two hours to achieve a metastable activity. There is no doubt

from the literature¹⁰ that there is a very slow decline in the total catalytic activity that occurs over weeks and even months. A time period ranging from an hour to several hours was employed for fresh catalyst attenuation in further experiments.

Cracking Reactions as a Function of Residence Time

A series of cracking experiments were done to study the effect of residence time with respect to the formation of different products. Only those experiments in which a mass balance of 100 ± 2.5 percent were considered acceptable.

The fraction of n-hexadecane feed converted and the yields of primary and secondary cracking products as a function of the space time are presented in Figure 72. The yields of each carbon number produced per one hundred moles of normal hexadecane converted for two different space times are presented in Figure 73.

The percentage of feed converted to primary cracked products and to secondary cracking products was determined by the fact that the moles of feed consumed is equal to the moles of primary cracking reactions and to one half the moles of primary products. The difference between the total moles of cracked products and the moles of primary products is the moles of secondary cracking products.

It is also assumed that the average molecular weight of primary cracked products is equal to one half of the molecular weight of the feed and that the average molecular weight of the secondary cracked products is equal to one fourth of the molecular weight of the feed. These relationships were used in the derivation of the mass balance equation to express that the weight percent of feed converted, the weight percent converted to primary cracked products and to secondary cracked products. The data obtained from these experiments was processed and is presented in Figures 72 and 73.

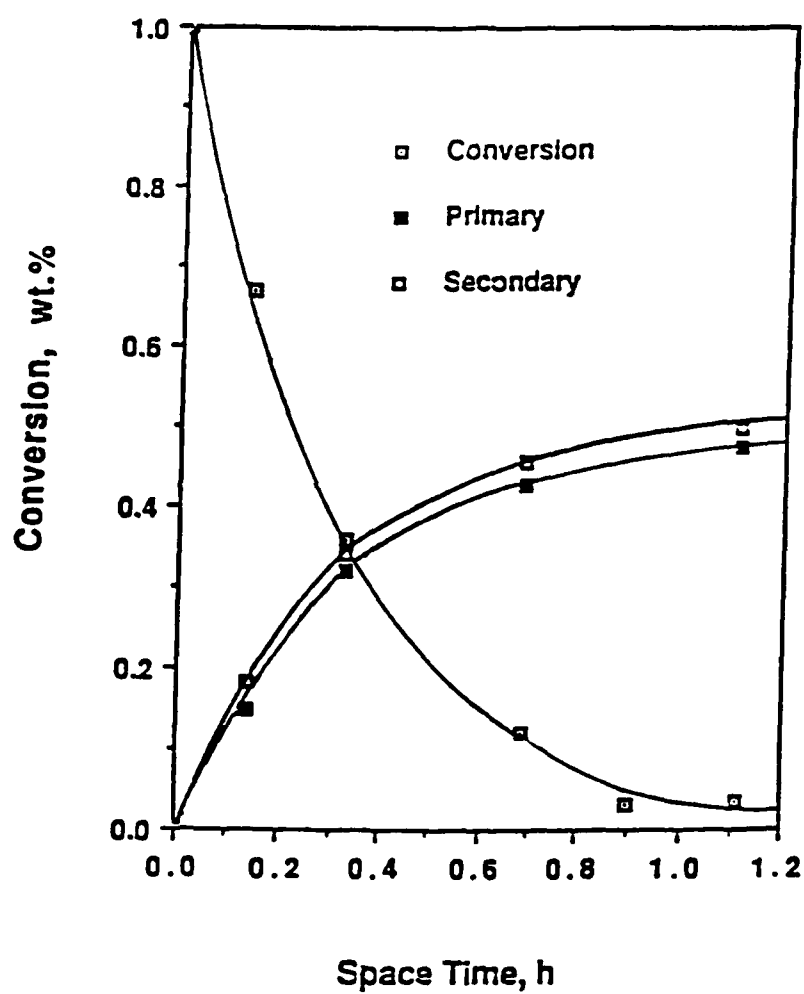


Figure 72. Conversion of n-Hexadecane to Primary and Secondary Cracked Products

Product Distribution

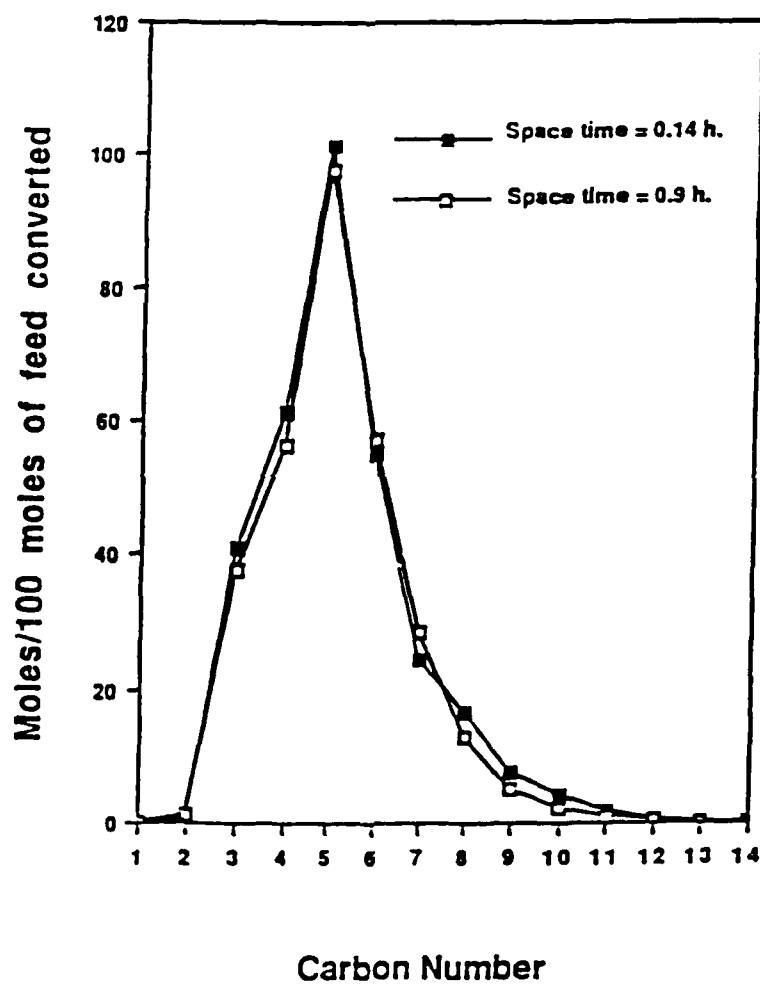


Figure 73. Carbon Number Yield as a Function of Space Time for the Cracking of Normal Hexadecane at 575 K and 200 psia

The conversion of feed, the yield of primary and secondary cracked products as a function of $WHSV^{-1}$ are presented in Figure 72. The secondary cracked products appear to form in parallel with the primary cracked products in Figure 72. This indicates that the lag time between the formation of primary cracked products and the formation of secondary cracked products is very short.

The carbon number yields per 100 moles of feed converted is presented in Figure 73 for two different space times. As in Figure 72, the distribution of product carbon numbers is not a function of space time (or conversion of the feed) indicating that the formation of secondary products from primary cracked products is rapid. It was originally theorized that at lower space times (lower conversions) the products would have significantly more gasoline range boiling material than at longer space times and higher conversions. However at the two space times for which data is presented in Figure 73 there is very little variation in the carbon number yields even though there is a large difference in the two space times.

When the mechanism of cracking is considered it is apparent why the formation of secondary cracked products occurs so rapidly in parallel with the formation of primary cracked products. The rate determining step for the formation of secondary cracked products is the same as the rate determining step for the formation of primary cracked products. The rate determining step for the formation of primary products from hexadecane, as in other catalytic cracking reactions, is the abstraction of a hydride ion to form a carbonium ion.¹¹ The carbonium formed rapidly cracks and to a smaller carbonium ion and an olefin. The carbonium ion formed in the primary cracking reaction can rapidly crack to form secondary products.

Plots of the weight fraction of the feed converted to paraffins, olefins and naphthenes, and aromatics as a function of space time is presented in Figure 74. Aromatics and paraffins are

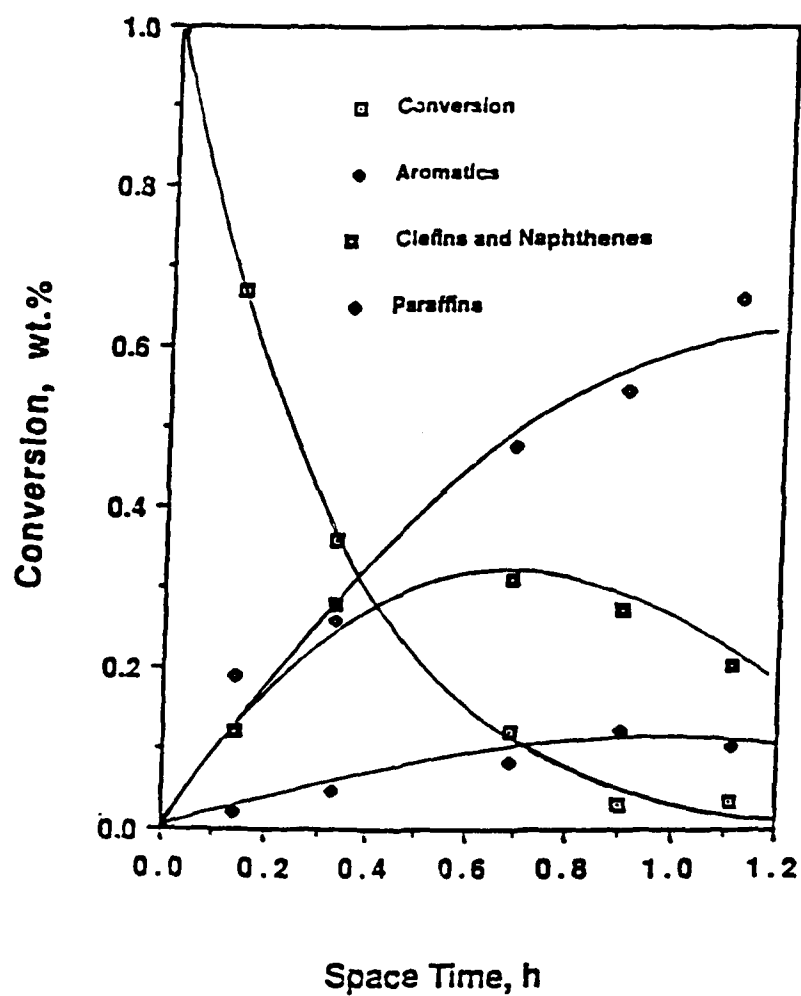


Figure 74. Product Distribution as a Function of Space Time for the Cracking of Normal Hexadecane at 575 K and 200 psia

secondary products formed from olefins (primary products) by hydrogen transfer reactions. There is no lag time in their formation indicating that the secondary reactions of olefins to form aromatics and paraffins occurs more rapidly than the formation of olefins.

These sets of experiments indicated that the ratio of primary to secondary cracked products cannot be varied by varying the retention time of the feed. This is because secondary cracked products are formed so quickly from primary cracked products that the formation of secondary cracked products appears to take place in parallel with the formation of primary cracked products.

It is recognized that the selectivity of the catalyst for the formation of primary products can be adjusted by altering the conditions of catalyst synthesis and pretreatment. However, the objective of this research was not to maximize naphtha production so further investigations concentrated on kerosene freeze point reduction by dewaxing.

Distillate Fuel Studies

Freeze Point Reductions of Kerosene and Diesel Fuels

Samples of kerosene and diesel fuel were obtained from the Flying J Oil Refinery in Salt Lake City. Both were distillate cuts from a blend of Wyoming Sweet and Altamont crudes.

The kerosene cut had an initial boiling point of 411 K (138°C) and an end point of 603 K (330°C). The diesel had an initial boiling point of 456 K (183°C) and an end point of 673 K (400°C). The initial boiling points and endpoints were based on boiling points at normal atmospheric pressure. From the GC analysis it was estimated that the kerosene had an average molecular weight of 182 g/mol.

The kerosene as received had a freeze point of 253 K (-20°C). The diesel had a freeze point of 280.45 K \pm 0.1 K (7.3°C \pm 0.1°C) and a cloud point between 278.15 and 278.95 K (5. and 5.8°C)

A sample of kerosene was cracked over HZSM-5 at a WHSV of 12, a hydrogen/hydrocarbon ratio of 13.5, a temperature at 643 K (370°C) and a total pressure of 200 psia. The reaction was run discontinuously for three days. This was done to collect enough liquid product to have sufficient sample for the determination of the freeze point after distillation of the naphtha fraction. No mass balance was attempted. At the conditions of the experiment 30 percent of the total kerosene feed was converted to cracked products.

The liquid products collected in this run were distilled to 446 K (173°C) to remove the cracked products from the unconverted kerosene boiling range feed. The freeze point of the product boiling above 446 K (173°C) was less than 213 K (-60°C) The density of the kerosene had increased from 0.791 to 0.822 at ambient temperature.

A sample of kerosene was cracked at a WHSV of 11.1, a hydrogen/hydrocarbon ratio of 13.9, a temperature of 642.5 K (369.5°C), and a pressure of 200 psia. A mass balance of 101.1 percent was obtained in this experiment. The purpose of this run was to determine the products obtained from cracking of kerosene on HZSM-5 under approximately the same conditions for which the kerosene based jet fuel was obtained. A plot of the product carbon number yield per 100 moles of converted feed as a function of feed and conditions is presented in Figure 75. These results can be compared to Figure 73 which was obtained for the cracking of normal hexadecane at 575 K (302°C). A list of the different products produced from cracking normal hexadecane at 575 K (302°C) on HZSM-5 and from cracking kerosene on at 643 K (370°C) on HZSM-5 is presented in Table 31. The products per one hundred moles of kerosene cracked were adjusted to the same value as the products per one hundred moles of hexadecane cracked. This was necessary because of the lower molecular weight of the kerosene. The factor by which they were multiplied was the molecular weight of normal hexadecane (226 g./mol.) divided by the average molecular weight of the kerosene (182 g./mol.)

Product Distribution

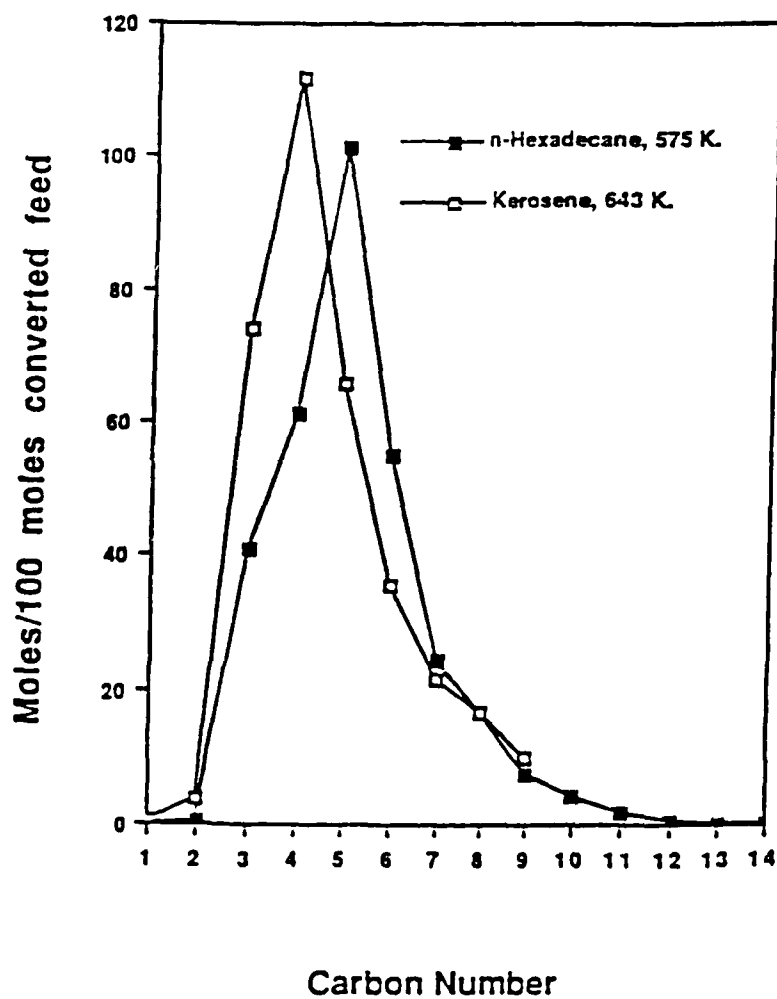


Figure 75. Carbon Number Yield for the Cracking of Kerosene and for the Cracking of n-Hexadecane

Table 31

**Product Distribution from the Cracking of Normal
Hexadecane and Kerosene over HZSM-5**

Feedstock		
	Normal Hexadecane	Altamont & Wyoming Sweet Kerosene
Temperature, K	575	643
Reactor Pressure, psia	200	200
C ₁	-	0.5
C ₂ =	1.0	3.2
C ₂	0.1	0.6
C ₃ =	-	31.4
C ₃	37.5	42.7
i-C ₄	13.5	19.3
n-C ₄	21.7	47.1
C ₄ =	21.2	45.5
i-C ₅	19.3	11.6
n-C ₅	54.4	19.4
C ₅ =	23.8	34.6
C ₆	39.4	12.2
C ₆ *	9.3	20.3
Benzene	6.4	3.2
C ₇ *	14.8	7.4
C ₇ = *	4.2	10.9
Toluene	5.5	3.4
C ₈ *	7.6	4.3
C ₈ = *	4.5	6.6
C ₈ aromatics	4.3	5.5
C ₉ *	2.0	3.1
C ₉ = *	0.9	2.6
C ₉ aromatics	4.4	4.4
+C ₁₀	6.6	-
Total Moles/100 Moles Cracked (adjusted)	302.4	340.3

* olefins and naphthenes

At 643 K (370°C) C_4 is the most abundant product when converting kerosene and that at 573 K (300°C) C_5 is the most abundant product when converting n-hexadecane (Figure 75). The difference is due to temperature rather than to the difference in the molecular weight of the feed. This is confirmed by Corma and co-workers²⁵⁷ who found that C_3 is the major product for cracking normal heptane on HZSM-5 at 723 K (450°C) and by Bezouhanova et al.²⁵⁴ who cracked normal hexadecane on HZSM-5 at 643 K (370°C). They found that at low Si/Al ratios that C_3 was the major product and at higher Si/Al ratios that C_4 was the major product.

On acid catalysts paraffins are cracked by a β -scission mechanism. Traditionally propylene and butenes are thought to be the main product of β -scission.²⁵⁸ This is true for cracking operated at high temperatures but at low temperatures butenes and pentenes are the major products from cracking over HZSM-5. This is probably because carbonium ions are more stable on the fourth or fifth carbon at lower temperatures than on the third and fourth carbons. Because of the predominance of carbonium ions located at higher carbon atoms there is a resulting increase in the formation of C_4 and C_5 .

A sample of diesel fuel was passed over HZSM-5 at a WHSV of 12.5-13 with a hydrogen flow of 15-18 l(STP)/(g•cat)(h) at 643 K (370°C) and a total pressure of 200 psia. The reaction was run continuously for two days. The runtime was extended to two days to produce a reasonable amount of kerosene after distilling out the naphtha. No mass balance was attempted but the conditions of the run were such that 30 percent of the feed was converted.

The total liquid product was distilled to 485 K (212°C) to remove the gasoline product from the unconverted diesel feed. The freeze point of the remaining uncracked diesel was reduced from 280.3 K (7.3°C) to less than 208 K (-65°C) The specific gravity had been increased from 0.81 to 0.835. Even though the diesel had an initially higher freezing point than the kerosene, after

dewaxing both samples had essentially no freezing point whatsoever. Since the unconverted portion of the cracked kerosene and distillate cuts consisted principally of naphthenic molecules there was a vast number of different species and different isomers. Consequently, it is difficult for crystals to form because of the low possibility that molecules of the same species or of the same shape can agglomerate to form crystals. Instead of forming orderly crystal structures unlike molecules bond together by van der Waals' forces and the viscosity of the mixture increases. The result of molecules being held by van der Waals' forces without crystals being formed is the formation of a gel that probably does not form crystals even if cooled to cryogenic temperatures.

This does not mean that the low temperature properties of such a mixture would be suitable for use in aviation turbines simply because the fuel does not freeze. Rather, the low temperature viscosity properties of the fuel become more crucial than its freeze point in aviation turbine fuel applications.

These two experiments showed three things:

1. the freeze point of a waxy naphthenic kerosene and diesel could be reduced to meet jet fuel specifications for freeze points;
2. the freeze point of catalytically dewaxed jet fuels may be replaced by the viscosity of the fuel in setting the low temperature limit in aviation turbine fuel applications; and;
3. the density of a waxy naphthenic distillate is increased by catalytic dewaxing.

Dewaxing of Kerosene and Diesel to Maximize Density

The possibility of increasing the density of the kerosene or diesel cuts by catalytic dewaxing was investigated. The dewaxing of these two samples had not completely removed the paraffins. Since paraffin and isoparaffin molecules reduce the overall density of a distillate, a sample of

kerosene and diesel were submitted to shape selective cracking under such conditions that all or nearly all the paraffins were selectively removed by cracking. These experiments were conducted so that the catalyst operated in a hydrocracking mode induced by hydrogen partial pressures over 900 psia which caused an increase in catalyst activity and selectivity.

The kerosene was cracked at a WHSV of 11, a temperature of 643 K (370°C) and a hydrogen partial pressure of 900 psia. The hydrogen/hydrocarbon pressure ratio was 40. It was kept high to keep the kerosene partial pressure low enough so it would vaporize completely in the reactor. The conditions of the experiment were such that 60 percent of the feed was converted to lighter products.

The liquid product was distilled to 471 K (194°C) to match the initial boiling point of the United States Air Force (USAF) high density JP-8 grade jet fuel. The kerosene feed had a final boiling point of 603 K (330°C) which surpassed the final boiling point of JP-8 grade jet fuel by 30 K. It was assumed that the final boiling point of the kerosene did not change during dewaxing.

The undistilled kerosene was filtered with activated charcoal to remove a light lemon color that developed during distillation. The specific gravity of the liquid was 0.83 at ambient temperature and represented a specific gravity increase of 0.04 above that of the unreacted kerosene and almost 0.01 above the density of the kerosene cracked at less severe conditions.

A sample of diesel was hydrocracked under the same conditions hydrocracking conditions. It was distilled up to 475 K (212°C). The specific gravity of the diesel boiling product was 0.855 and represented a specific gravity increase of 0.045 over the unreacted kerosene and a specific gravity increase of 0.025 over the diesel cracked under less severe conditions.

These two experiments show that the density of a jet fuel can be increased at the expense of the total yield of the product.

There is no doubt that mild hydrodewaxing can increase the yield of jet fuel from the original feed at the expense of the density and still meet the freeze point specifications.

Conclusions

It is possible to reduce the freeze point of jet fuel boiling distillates by shape selective cracking of paraffins in the presence of naphthenes on HZSM-5 catalyst. The freeze point reduction is due to the reactant selectivity of HZSM-5 which allows paraffins and isoparaffins to diffuse to active cracking sites while it restricts the diffusion of bulkier naphthenes into the pore structure. The standard reaction conditions were 643 K (370°C) and 200 psia total hydrogen plus hydrocarbon pressure. The feed rate of hydrogen was such that the hydrocarbon feed to the reactor was in the vapor phase.

The catalytic reactor was operated to crack kerosene and diesel boiling range cuts in the presence of HZSM-5 cracking catalyst. Due to the restricted size of the pores of HZSM-5 catalyst, paraffins were selectively cracked in the presence of bulkier naphthenes. After the distillation of the naphtha formed from the cracking of the paraffins, the resulting distillate had a greatly reduced freeze point. Densities were also increased by several percent due to the selective removal of the less dense paraffins and isoparaffins from the feedstocks.

Under more severe hydrocracking conditions it was possible to produce a kerosene boiling range distillate with very low freeze point and a density of 0.83, which was well within the density requirements (0.775-0.84)³ for the military high density JP-8 fuel. The high density of the fuel was a result of two factors:

1. the high naphthene content of the dewaxed kerosene; and
2. the expanded boiling range of the kerosene (a 30 K higher endpoint than JP-8 grade jet fuel).

Under the same conditions a diesel boiling distillate (485-673 K [212-400°C]) with a very low freeze point and a density of 0.855 could be obtained which surpassed the density range for JP-8 grade jet fuel.

High density jet fuels can be produced by dewaxing expanded boiling range kerosene. The density obtained is a function of the endpoint of the fuel. The dewaxed diesel had a higher endpoint than the dewaxed kerosene and as a consequence, a higher density.

Normally the freeze point sets the low temperature limits of potential jet fuels. If jet fuels can be economically dewaxed to remove paraffins the freeze point of jet fuels will be less of a factor for determining what kinds of feedstocks can be used for jet fuels. The low temperature viscosity will become a more important factor in determining what distillate cuts will be suitable for the production of jet fuels.

Cracking of kerosene and normal hexadecane over HZSM-5 occurs by β -scission. At 573 K (300°C) the activity of the catalyst is low enough so that C_5 is the most abundant product. At 643 K (370°C) C_4 is the main product. It is anticipated that at temperatures over 673-723 K (400-450°C) that C_3 would be the main product. Higher temperatures result in smaller fragments from β -scission cracking.

Secondary cracking and aromatization reactions appear to be occurring parallel to primary cracking reactions. This is because the rate determining step for primary cracking, secondary cracking and aromatization reactions is the same, the abstraction of an hydride from a paraffin to form a carbonium ion which can crack and re crack, or crack and abstract an hydride from a naphthene or another feed molecule. At conversions higher than maybe a few percent the product yield is not a function of conversion and residence time, it is a function of other variables like the temperature, the Si/Al ratio and the method of catalyst pretreatment.

Section VII: DESIGN AND CONSTRUCTION OF A BET SURFACE AREA APPARATUS

Research Personnel: Daniel C. Longstaff
Graduate Student

Kien-Ru Chen
Postdoctoral Fellow

Francis V. Hanson
Associate Professor

Introduction

Catalytic activity is related to the number of active sites that are distributed over the surface of the catalyst. It is generally assumed that the number of catalytic sites per unit mass of catalyst will increase as the surface area of the catalyst increases. During catalyst pretreatment or use changes in the catalyst may occur that could result in an increase or decrease in the total catalyst surface area. If the pretreatment of a porous oxide catalyst includes a calcination procedure caution must be exhibited to insure that the calcination temperature does not induce collapse of the pore structure of the catalyst. When the calcination temperature is too high the collapse of the pore structure will cause a significant reduction in the surface area of the catalyst with a loss of active sites and a concomitant loss of activity. Sintering of the metal crystallites in supported metal catalysts during calcination or reduction will also be accompanied by a significant loss in catalytic activity.

The surface area of porous catalysts can also be affected by chemical processes which take place during the course of the reaction such as the deposition of carbonaceous residues. For example, in zeolite cracking catalysts such as ZSM-5 there are two types of catalyst deactivation due to coke deposition. Coke or organic residue may deposit either (1) directly on the catalytically active site, or (2) at the pore mouths of the catalyst (pore mouth plugging).

If the zeolite catalyst deactivation occurs via mechanism 1, large losses in catalyst activity would be accompanied by small losses in catalyst surface area. In the case of mechanism 2, large losses in catalyst activity are accompanied by large losses in accessible catalyst surface area. Thus a knowledge of the surface area of fresh, equilibrated, and deactivated catalysts is necessary for the complete evaluation of catalyst performance.

In addition to surface area changes the adsorption and desorption of an adsorptive such as nitrogen can provide important information regarding the pore structure of a catalyst.

The most widely applied technique for the determination of the surface areas and pore sizes for porous materials is the BET method.²⁵⁹ Thus, a BET surface area measurement system was designed and fabricated for use in the determination of surface areas of laboratory prepared samples of the ZSM-family of zeolites.

Procedure for Surface Area Measurement

Surface areas of porous adsorbents and catalysts are calculated by determining the amount of an adsorptive that forms a monolayer on the surface of the adsorbent. The amount of an adsorptive that is required to form a monolayer on a catalyst can be determined by either of two methods:²⁶⁰

1. the volumetric method, and
2. the gravimetric method.

The volumetric method consists of determining the pressure of a quantity of the adsorptive in the presence of the solid. The amount adsorbed is calculated by taking a mass balance over the system. An adsorption isotherm is determined by measuring the amount adsorbed for a series of different pressures at a specified temperature.

In the gravimetric method the amount of gas adsorbed on the solid is directly measured by weighing the sample on a microbalance. The weight of the clean catalyst is determined in a vacuum. The weight of the catalyst is then determined after it has come to equilibrium with the adsorptive at a known pressure and temperature. The volumetric method was used in this investigation and a volumetric adsorption apparatus was designed and constructed.

Monolayer coverage cannot be directly determined for physisorption because multiple layers of adsorptive molecules are formed on the catalyst surface. However, the BET equation²⁵⁹ may be used to calculate the volume of a gas adsorbed at the temperature and pressure required to form a monolayer on a catalyst surface. The BET equation is based on the concept that the second and higher monolayers of physisorbed adsorptive are a liquid phase, while the first monolayer exists as a physisorbed phase on the bare surface. The BET equation, which is derived in Appendix A, provides a relationship between the volume of gas adsorbed on a surface and the pressure at which it is adsorbed. The monolayer volume, v_m , appears in the equation and can be calculated if the volumes adsorbed at different pressures and a single temperature are known.

Experimental Apparatus

The BET system constructed for this investigation consisted of four parts:

1. an adsorption system for the determination of adsorption and desorption isotherms;
2. a vacuum system to properly evacuate all parts of the system prior to the determination of the isotherms;
3. a gas supply system to properly store and handle gases used in the system without contamination; and
4. a catalyst pretreatment system to prepare the catalyst samples.

A schematic of the BET system is presented in Figure 76. All the major components are labelled. The BET system was constructed so that dynamic pressures of 10^{-6} torr could be attained. Consequently, the BET system was constructed with Pyrex glass tubing and high vacuum Pyrex glass joints lubricated with high vacuum grease. The system's small volume in relation to the capacity of the diffusion and mechanical vacuum pumps minimized the system evacuation time.

Adsorption System

The adsorption and gas handling system is the dashed rectangle labelled I in Figure 77. A more detailed diagram of the adsorption system and the gas supply system is shown in Figure 78. The adsorption system consists of:

1. a calibrated doser manifold of known volume, V_D , to introduce the adsorptive into the sample cells;
2. two sample cells to hold the catalyst sample cells during the determination of adsorption/desorption isotherms;
3. a pressure gauge to determine pressure in the doser volume and in the sample cell during adsorption experiments; and
4. a calibration bulb of known volume to determine the dead volume and to supplement the dosing volume when needed.

The pressure gauge was an MKS Baratron Type 222B Absolute Pressure Gauge. It consisted of a capacitor positioned between the system and a volume evacuated to 10^{-7} torr. The capacitor was connected to an electronic signal conditioner which converts electronic frequencies to voltage outputs, and sends a signal to an MKS Brand 200/400 Series PDR-D-1 Power Supply and Digital Readout. The Baratron gauge operates as a result of the deflection of a metal diaphragm which serves as one side of the capacitor. When the pressure causes the diaphragm to

1. Storage bottle
2. Supply manifold
3. Capillary manifold
4. Calibration bulb of known volume
5. Sample cells
6. Baritron pressure gauge
7. Main manifold
8. Sample pretreatment connection
9. Penning high vacuum gauge
10. Diffusion pump cold trap
11. Diffusion pump
12. Diffusion pump bypass
13. Mechanical pump cold trap
14. Mechanical pump

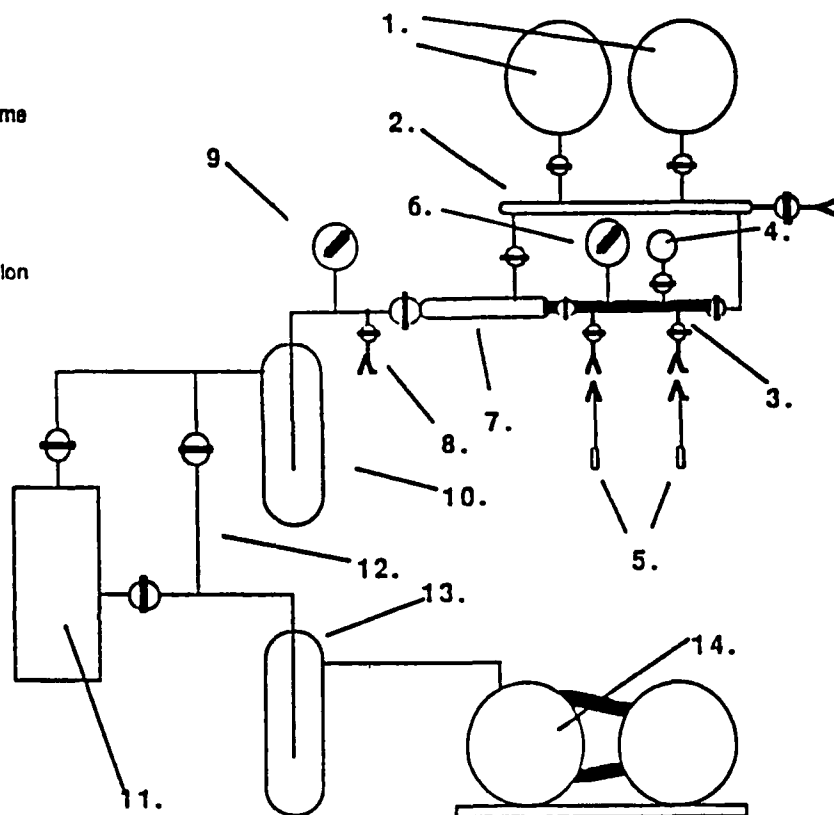


Figure 76. Schematic of the BET System

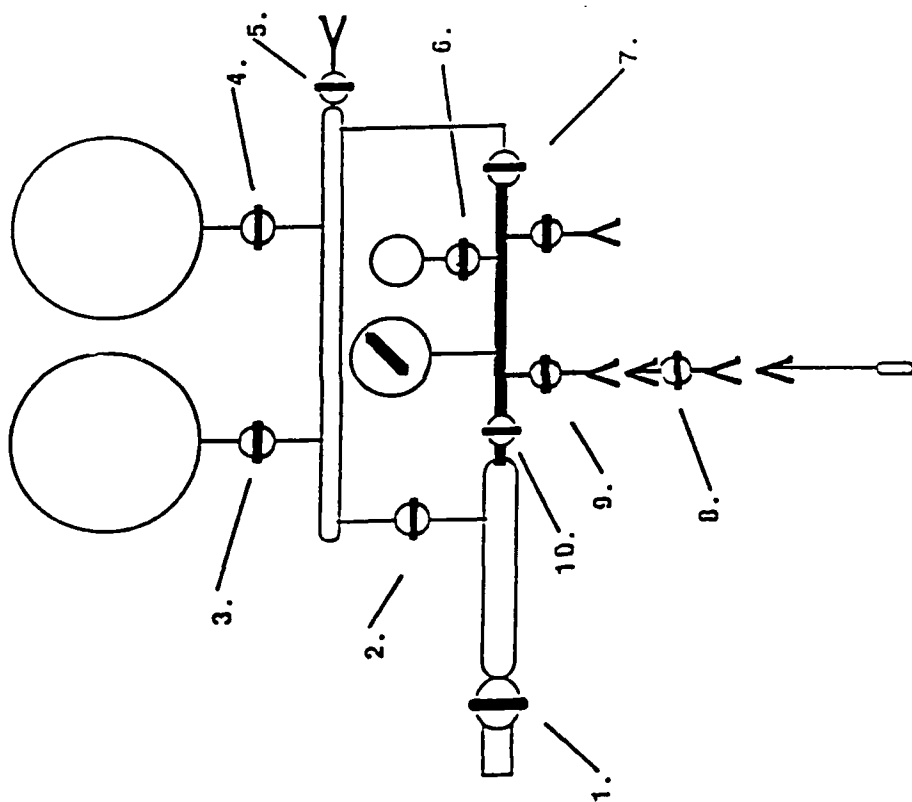


Figure 78. Adsorption and Gas Handling System

deflect, the capacitance of the capacitor changes. This change in the capacitance is measured electronically, recorded, and displayed. The Baratron pressure gauge was connected to the capillary manifold by a 1/2 inch Cajon Ultratorr union. The doser system had a suitable connection which allowed the Baratron gauge to be mounted in a vertical position to prevent contamination of the diaphragm.

The doser system was constructed from two mm inside diameter Pyrex tubing to minimize its volume. The volume of the doser system was determined by calibration with a calibration bulb of known volume. The volume of the calibration bulb was determined prior to the construction of the gas adsorption system. A glass bulb was blown and connected to a two mm stopcock which allowed the bulb to be sealed. The bulb was evacuated with a vacuum pump, then weighed on a laboratory balance capable of reading to 10^{-5} g. The bulb was filled with degassed distilled water. The bulb and the water were allowed to come to thermal equilibrium in a calorimeter. The temperature of the water was determined and the stopcock was shut. The exterior of the bulb was dried and the bulb and water were weighed. The volume of the bulb was calculated from the density and weight of the water. This procedure was repeated nine times and the volume of the bulb was determined to be $51.26 \text{ cm}^3 \pm 0.011 \text{ cm}^3$.

In order to connect the sample cells to the doser volume, the doser volume was outfitted with two connections which consisted of a two mm stopcock and a 10/30 female connection.

The cells consisted of two parts, the actual cell itself which consisted of an oblong bulb. The oblong bulb contained a thermowell for temperature measurement. This bulb was connected to a 12/30 ground glass male joint by a 10 inch long neck. This allowed the cell to be fairly well submerged in a liquid nitrogen bath. The other portion consisted of a two mm stopcock with a 12/30 ground glass female joint to which the cell was connected, and a 10/30 ground glass male

joint which allowed the stopcock and cell to be connected to the doser manifold. This arrangement permitted the transfer of the catalyst sample from the sample pretreatment connector to the doser volume connector without exposing the catalyst sample to the atmosphere.

Vacuum System

The vacuum system is indicated by the dashed box labelled II in Figure 77. The vacuum system permitted the evacuation of the adsorption cell pressure to less than 10^{-4} torr without the back migration of oil vapors into the system. It consisted of a CVC PMCS-4B diffusion pump backed by a GCA Precision Scientific D25 mechanical vacuum pump. Dow-Corning 704 diffusion pump fluid was used in the diffusion pump.

The adsorption system was isolated from the vacuum pumps by liquid nitrogen cold traps to prevent back streaming of the pump oils. These cold traps were kept filled with liquid nitrogen in normal operation. One cold trap was placed between the dosing and gas storage manifolds and the vacuum system, and the other was between the mechanical pump and the diffusion pump. The pumps could be isolated from one another and from the system by three 25 mm glass stopcocks.

The system vacuum was monitored with a CVC brand GPH-320C Penning Vacuum Gauge mounted between the vacuum system and the supply manifold. The gauge was capable of measuring pressures in the range 10^{-7} to 0.25 torr.

Gas Storage System

The gas storage system is indicated by the dashed box labelled III in Figure 77. Nitrogen was most frequently used as an adsorptive in determining isotherms. Neon²⁶¹ was used for determining cell dead volumes because at ambient temperature it does not physisorb on catalysts or adsorbents and it does not diffuse through glass like helium. The gas storage system consisted

of a gas supply manifold connected to two 5000 cm³ glass bulbs by high vacuum stopcocks. One bulb was used to store nitrogen. The other was used to store neon. Gas was added to the supply manifold and storage bulbs through a four mm stopcock connected to a 12/30 female joint. The supply manifold was constructed of 25 mm i.d. Pyrex tubing. The supply manifold was connected to the vacuum manifold and to the doser volume by means of a four mm stopcocks.

Catalyst Pretreatment System

The catalyst pretreatment system is indicated by the dashed box labelled IV in Figure 77. It was connected to the cell by Pyrex tubing which was placed below the diffusion pump bypass on the BET system. The cell was heated with a 1200 watt Autoclave Engineer's brand furnace controlled by a Variac.

Adsorption/Desorption Isotherm Procedure

Determination of Sample Cell Dead Volume

In the volumetric method for determining BET isotherms and hysteresis curves, it is necessary to know the total cell dead volume and the cell volume at the isotherm temperature. This made it necessary to determine the total cell dead volume, V_C , and the cryogenic cell volume, V_{CC} , prior to putting the catalyst into the cell. Before initiating the BET isotherm the cell volume is again measured with the catalyst in the cell. The reduction in the total volume is assumed to be totally due to the volume of catalyst in the cell and is subtracted from the cryogenic cell volume that was originally measured when the cell was empty.

The procedure for determining the cell volumes consisted of the following steps. An acid washed glass wool plug was placed in the top of the cell and the cell and stopcock assembly were connected to the doser volume. The cell system was evacuated to less than 10^{-4} torr. Stopcock

(8) (Figure 78) was shut to separate the doser volume from the cell. Neon was admitted to the doser volume and the pressure indicated on the Baratron gauge was recorded. Stopcock (8) was then opened and the neon allowed to enter the cell. This procedure was repeated several times to insure reproducibility. The cell volume was then calculated from Equation (7-1), which assumes that the temperature of the doser manifold and the empty cell are equal.

$$V_C = V_D \left(\frac{P_1 - P_2}{P_2 - P_0} \right) \quad (7-1)$$

where

P_0 is the original pressure in the cell, torr;

P_1 is the original pressure in the doser volume, torr;

P_2 is the pressure in the cell and doser volume after the stopcock is opened, torr;

V_D is the doser manifold volume, torr; and

V_C is the total dead cell volume, cm^3 .

After the cell dead volume had been determined, the cell was immersed in liquid nitrogen up to a specific level. The above procedure was repeated to determine the cryogenic cell volume. The cryogenic cell volume was calculated from Equation (7-2):

$$V_{CC}^I = (V_C + V_D) \frac{T_C}{(T_H - T_C)} \frac{(P_2 - P_0)}{(P_1 - P_2)} \quad (7-2)$$

where:

V_{CC}^I is the cell volume at the cryogenic temperature, cm^3 ;

T_C is the temperature of the liquid nitrogen bath, K; and

T_H is the ambient temperature, K.

The cell volume at ambient temperature is calculated from Equation (7-3).

$$V_{CH} = V_C - V_{CC} \quad (7-3)$$

where:

V_{CH} is the cell volume at ambient temperature, cm^3 .

Once the total cell volume and the cell volume at cryogenic temperature were determined, the cell and stopcock were removed from the doser volume. The glass wool plug was removed from the cell and saved. A weighed amount of catalyst was placed into the cell and the glass wool plug was reinserted into the cell.

The sample was then ready for degassing. The purpose of degassing is to remove any adsorbed species from the catalyst surface. Water is usually the main adsorptive that needs to be removed. The temperature and total time of degassing were a function of the catalyst. For ZSM-5, holding the sample of ZSM-5 at 623 K (350°C) for several hours under the diffusion pump vacuum was more than sufficient. ZSM-5 is a hydrophobic material and almost all the water is desorbed below 523 K (250°C).²⁶² A 10/30 female connector and stopcock were available on the BET vacuum system for degassing samples. The position of the degassing connector allowed samples to be degassed while the adsorption isotherms were being determined for other samples. Once the degassing was completed, the stopcock on the cell was shut to maintain the sample under vacuum. The stopcock and cell were transferred to the doser volume manifold to obtain the isotherm.

Prior to the determination of the adsorption isotherm, it was always necessary to redetermine the total cell dead volume with the sample in the cell. This was done with the dosing volume and the cell at ambient temperature. The procedure described above was used to

determine the dead volume of the catalyst-cell system. The difference in the cell volume before and after putting the sample in was assumed to be the volume of the sample, and this volume was subtracted from V_{CC}^I , the volume of the empty cell at the isotherm temperature. This volume was denoted V_{CC} and represented the dead volume of the cell at the cryogenic temperature of liquid nitrogen. V_{CH} , the dead volume of the cell at ambient temperature, did not change even though the cell contained a sample, because the sample was positioned in the portion of the cell that was submerged in liquid nitrogen during the determination of the adsorption isotherm. The difference between the total cell volume and the volume at liquid nitrogen temperatures was denoted V_{CH} and appears in the mass balance.

An alternate and more efficient method requires helium to be used as the gas to determine the cell dead volume. The first step is to load the catalyst into the cell before determining the cell's dead volume, and then degas the sample. After degassing, the cell is connected to one of the sample ports on the dosing manifold, the system is evacuated, and the sample cell is submerged in liquid nitrogen to the level at which it is submerged during the determination of the BET surface area. The procedure is then followed for determining the cell's dead volume at ambient temperature, but helium is used instead of neon because it is expected that helium will not physisorb on the adsorbent. The volume is then calculated from Equation (5-23), and a revised form of the mass balance is used when the adsorption/desorption isotherm is calculated. The volume determined by this method will be several times larger than the actual dead volume because the helium will be concentrated in the portion of the cell held at cryogenic temperatures. This method was never used but it is recommended because of its simplicity as compared with the method outlined previously. One attempt was made to do this procedure with neon, but it was unsuccessful because neon will physisorb on zeolite at liquid nitrogen temperatures, even though

the temperature of liquid nitrogen is well above the critical temperature of neon (boiling point of nitrogen @ 650 torr = 76.1 K, critical temperature of neon = 44.4).²⁶³

Determination of the Isotherm

The actual adsorption isotherm was determined according to the following procedure. The gas supply manifold, the dosing volume and the cell were all evacuated to 10^{-7} torr. The cell was immersed in a liquid nitrogen bath to the same level at which the cryogenic cell volume had been determined. Then stopcocks (1), (2), (6), (7), (9), and (10) were shut to separate each part of the system from every other part. Stopcock (4) on the nitrogen storage bulb was opened to admit nitrogen into the storage manifold. Stopcock (7) between the supply manifold and the dosing volume was opened, and nitrogen was admitted to the dosing volume. The nitrogen initial pressure in the dosing volume was adjusted by withdrawing a small amount of the nitrogen into the calibration bulb until the pressure reached the desired level. The gas in the calibration bulb was then available for further use.

The appropriate initial doser volume pressure is critical in order to have the desired amount of adsorption on the catalyst. During the determination of the adsorption isotherms, the pressure in the doser volume must be greater than the pressure in the sample cell at each step. During the determination of the desorption isotherms, the pressure in the dosing manifold must be less than the pressure in the sample cell. The pressure in the doser volume was recorded as P_1 . Stopcock (9) on the cell was opened, and nitrogen flowed into the cell and was adsorbed by the sample. The pressure in the doser volume-sample cell-catalyst system usually required up to 30 min for the pressure to equilibrate. The greater the amount of nitrogen adsorption, the longer it took for the system to come to equilibrium. After equilibrium was established, the pressure (P_2) was recorded. Stopcock (9) on the cell was shut and additional nitrogen was admitted to the doser volume. This

procedure was continued for as many isotherm points as was deemed necessary. If the surface area of ZSM-5 was being determined, data was taken up to a value of p/p_0 of 0.15. If a complete adsorption/desorption isotherm was being determined, the procedure was continued until the pressure had reached the saturation pressure of nitrogen vapor at the temperature of the sample followed by reduction of the pressure to a few torr.

When the complete adsorption/desorption isotherm was determined, the adsorption portion of the isotherm was terminated after the pressure in the cell had reached the vapor pressure of nitrogen at the temperature of the catalyst in the cell. This pressure was usually a few torr above the ambient pressure. This was because the ambient pressure regulates the temperature of the boiling liquid nitrogen bath which was always slightly above the boiling temperature of pure nitrogen at the ambient pressure due to the presence of condensed oxygen in the liquid nitrogen bath. At the maximum pressure, care was taken to insure that the pressure in the cell had indeed attained equilibrium. If this caution is not observed, desorption will cause a deviation in the adsorption isotherm at pressures below the hysteresis pressure. Therefore the adsorption isotherm was usually stopped a few torr below the actual vapor pressure of nitrogen.

In determining the isotherm it was important to always maintain the level of liquid nitrogen in the bath around the cell at the same level at which the value of V_{CC}^I was measured to reduce the possibility of measurement errors.

Whenever nitrogen was admitted to the doser volume prior to opening the stopcock on the cell it was useful to estimate the appropriate P_1 in the doser volume to give the desired value of P_2 in the cell and doser volume after the pressure had been allowed to equilibrate. A semiquantitative method for estimating P_1 was developed. The quantity β was defined according to Equation (7-3):

$$\beta = \frac{(P_1 - P_2)}{(P_2 - P_o)} \quad (7-4)$$

The ratio of pressures also appears in Equation 3-1 and β is a function of position on the adsorption isotherm, and gradually changes as a function of p/p_o . It gave good predictions of the value of P_1 to give a desired value for P_2 . The procedure was to determine β for the point corresponding to P_n on the adsorption isotherm and then use Equation (7-5) to calculate the desired P_1 for the point corresponding to P_{n+1} .

$$P^1_1 = P^1_2 + \beta(P^1_2 - P^1_o) \quad (7-5)$$

where:

P^1_1 is the predicted pressure of the doser volume, torr;

P^1_2 is the desired equilibrium pressure, torr; and

P^1_o is the pressure in the sample cell, torr.

The pressure, P^1_1 , in the doser volume required to raise the pressure in the sample cell from P^1_o to P^1_2 after stopcock (9) was opened was calculated from Equation (7-5). This method can calculate values for P_1 such that there is a very even spacing between consecutive points on the adsorption/desorption isotherm.

Calculation of the Adsorption/Desorption Isotherm

After sufficient data points had been taken, the mass balance was used to calculate the amount of nitrogen gas adsorbed on the catalyst for each set of data points. The mass balance equation used to calculate the volume adsorbed can be derived from the gas law and is given by:

$$V_{ads} = V_{ads,o} + \frac{T_{STP}}{P_{STP}} \frac{V_D}{T_H} (P_1 - P_2) - \frac{T_{STP}}{P_{STP}} \frac{V_{CH}}{T_H} (P_2 - P_o) + \frac{V_{CC}}{T_C} (P_2 - P_o) \quad (7-6)$$

where:

V_{ads} is the volume of gas at STP adsorbed, cm^3 ;

$V_{ads,o}$ is the volume of gas at STP adsorbed at the previous data point, cm^3 ;

P_{STP} is the standard pressure, 760 torr; and

T_{STP} is the standard temperature, 273.15 K.

After the amount of gas adsorbed on the sample for each P_{n+1} was calculated the linear form of the BET equation²⁵⁹ was used to calculate $V_{ads,m}$, the monolayer volume of the adsorptive at the standard temperature and pressure that is required. The linear form of the BET equation is given in Equation (7-7). Equation (7-7) is also referred to as the BET (A) equation.

$$\frac{p}{V_{ads}(p_o - p)} = \frac{1}{V_m c} + \frac{(c-1)}{V_m c} \left(\frac{p}{p_o} \right) \quad (7-7)$$

where:

V_m is the monolayer volume, cm^3 ;

V_{ads} is the volumes (STP) which adsorbed at a pressure p , cm^3 ;

p is the equilibrium pressure, torr;

p_o is the vapor pressure of adsorptive at the sample temperature, torr; and

c is the 'c-value'.

If p/p_o is plotted versus $p/V_{ads}(p_o - p)$ a straight line of slope $(c-1)/V_m c$ and intercept of $1/V_m c$ should be obtained. The slope and intercept can be solved to give V_m and c . V_m would then be used in Equation (7-8) to calculate S , the surface area of the catalyst or adsorbent per unit mass.

$$S = \frac{V_m}{22,400} \frac{N_{av}}{m} A \quad (7-8)$$

where:

S is the surface area of sample g/cm^3 ;

V_m is the monolayer volume, cm^3 ;

m is the mass of sample in cell, g;

N_{av} is Avogadro's Number; and

A is the area covered by a single molecule of adsorptive, m^2 .

The area covered by a single molecule of adsorbed nitrogen is $16.2 \times 10^{-20} \text{ m}^2$.

The variable c is related to the heat of adsorption of the adsorptive on the sample by Equation (7-9).

$$c = A_o \exp\left(\frac{(E_1 - E_L)}{RT}\right) \quad (7-9)$$

where:

E_1 is the heat of adsorption of the first monolayer, cal/mol;

E_L is the heat of adsorption of further layers, assumed to be equal to the latent heat of condensation, cal/mol;

R is the Universal gas constant, cal/mol/K;

T is the absolute temperature of sample, K; and

A_o is the pre-exponential factor.

The relationship between A_o and the pore size is discussed in a subsequent section.

Scope of the BET System

In addition to being used to determine surface areas of catalysts and adsorbents the BET system can be used to investigate the deactivation of catalysts. For example, if ZSM-5 is heated

to 973 K (700°C) followed by contact with water vapor at 923 K (650°C) there is a 75 percent reduction in the number of strong acid sites; however, the reduction in surface area was only 10 percent. Thus the combinations of heat and water vapor did not appear to collapse the significantly collapse the crystalline structure, however it did selectively destroy the strong acid sites.

The shape selectivity of ZSM-type zeolites becomes less effective as the crystallite size is reduced because of a corresponding increase in the external crystallite surface area and active sites on the external surface of the crystallite. These external sites are not shape selective relative to the sites located inside the zeolite micropores. Two techniques have been developed to determine the external surface area of ZSM-5 crystallites²⁶⁴ by adsorption techniques. The first method consists of adsorbing propane or butane vapor in the pores of the sample and then cooling the sample cell in liquid nitrogen. An adsorption isotherm is determined and since the pores are filled with frozen propane or butane the only adsorption is on the external surface of the crystallite. The second method is more involved because it involves the rate of the adsorption of neopentane on ZSM-5. Because of the large size of neopentane molecules with respect to the pores of ZSM-5, neopentane adsorbs more slowly onto the interior surface of ZSM-5 crystallites than onto the external crystallite surface area. The amount of adsorptive adsorbed on the external crystallite surface can be determined from a plot of the amount of adsorptive adsorbed with respect to time raised to the 0.5 power.

Results

Computer Program

A computer program was developed to process the data produced from the BET system. It appears in Appendix G along with a sample input and output.

Adsorption/Desorption Isotherm for Alumina

After the BET system was completed a series of surface area measurements were made using alumina as the adsorbent to determine the reproducibility of the system and to develop a proper technique for the efficient and accurate determination of isotherms. These results are included to provide a contrast between the physisorption properties of a macroporous solid like alumina with the physisorption properties of a microporous solid such as ZSM-5 zeolite.

A sample of Ketjen alumina was provided by Dr. Nabin K. Nag. The Ketjen company reported a surface area of $210 \text{ m}^2/\text{g}$ and a pore volume of $0.6 \text{ cm}^3/\text{g}$ for the sample. The alumina was calcined and then put in the adsorption cell. The alumina was degassed at 573 K (200°C) at 0.5 Torr followed by evacuation at 623 K (350°C) until the pressure in the adsorption cell was less than 10^{-3} torr . The sample cell was then cooled to the ambient temperature and transferred to the doser volume (without exposing the alumina to the atmosphere or moisture). The doser manifold and the volume of the sample cell were determined using the calibration bulb attached to the doser manifold. The sample cell volume was determined by expanding the neon from the doser volume into the sample cell. The average volumes and the standard deviation of the volume were then determined from the pressure-temperature data.

Several BET adsorption isotherms were determined. The first two runs did not give satisfactory results, due to lack of operating experience which resulted in unevenly spaced data and due to inappropriate operating procedures. The third run was an attempt at generating an adsorption/desorption isotherm which failed due to an operating mistake. However, enough good data was obtained during run number three to obtain a BET surface area for the alumina sample. Run number four consisted of a complete adsorption/desorption isotherm. The BET surface area of the alumina obtained during run number four will be compared with the BET surface area obtained during run number three to show the reproducibility of the data. Figure 79 is a plot of

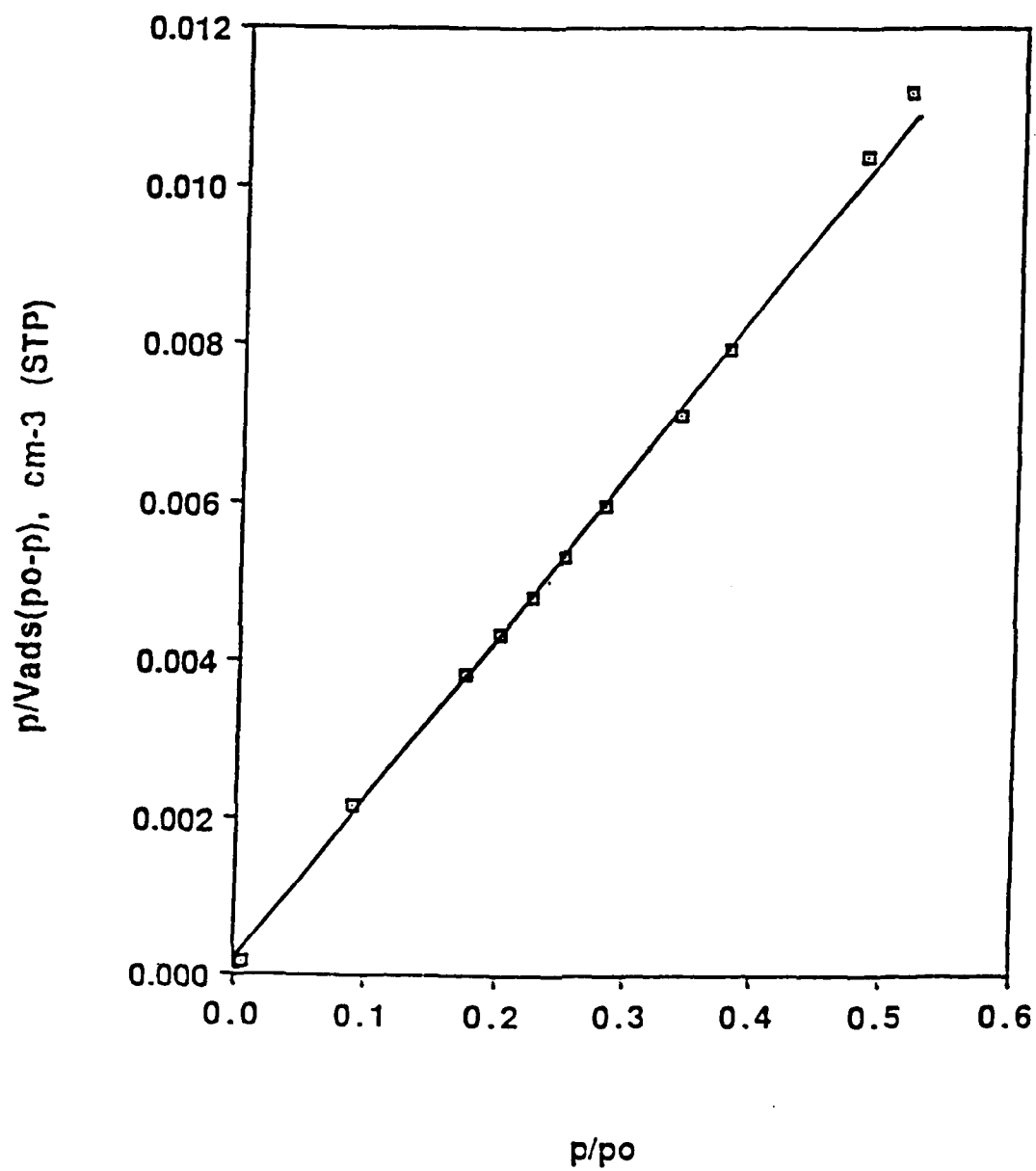


Figure 79. Plot of the BET (A) Equation for Alumina

p/p_0 versus $p/V_{\text{ads}}(p_0 - p)$. The plot is a straight line up to about $p/p_0 = 0.35$ which is where the BET (A) equation starts to break down. The reduction in the amount of accuracy of adsorption at increased p/p_0 is related to the filling of the smallest pores of the sample. In the derivation of the BET (A) equation it was assumed that adsorption of the sample took place on a flat surface such that an unlimited number of adsorbed layers could be formed. At low surface coverages this assumption is reasonable for most porous solids. However, as the pores fill up the adsorbed layers interfere with the adsorption of subsequent layers on opposite sides of the pores. The BET (B) equation relieves this assumption by introducing a quantity n , which is the number of monolayers that can be formed in the pores of an adsorbent. The use of the BET (B) equation on adsorbents of varying pore diameter has been reported to give a close fit of the adsorption isotherm up to a relative pressure of 0.6 to 0.7 for adsorbents with a range of pore sizes²⁵⁹ and as high as a relative pressure of 0.93 for adsorbents of uniform pore size have given straight line fits up to $p/p_0 = 0.93$.²⁵⁹

The adsorption/desorption isotherm for the Ketjen alumina sample is presented in Figure 80. The hysteresis loop obtained with the alumina is known as a type A hysteresis.²⁶⁵ Type A hysteresis is defined as hysteresis where either the adsorption or desorption branches of the hysteresis loop are steep. The data was processed by the computer program that has been previously mentioned and the BET (A) equation was solved by the computer program to give the monolayer volume from which was obtained a surface area of $209 \text{ m}^2/\text{g}$ and a value for (E1-EL) of 725 cal./mol. In determining the BET surface area it is important to use data points up to, but not surpassing the region (usually $p/p_0 > 0.35$) where the BET (A) equation does not apply. The number of data points taken to determine the surface area was determined by calculating a least squares fit of the processed data points to the BET (A) equation up to several relative pressures

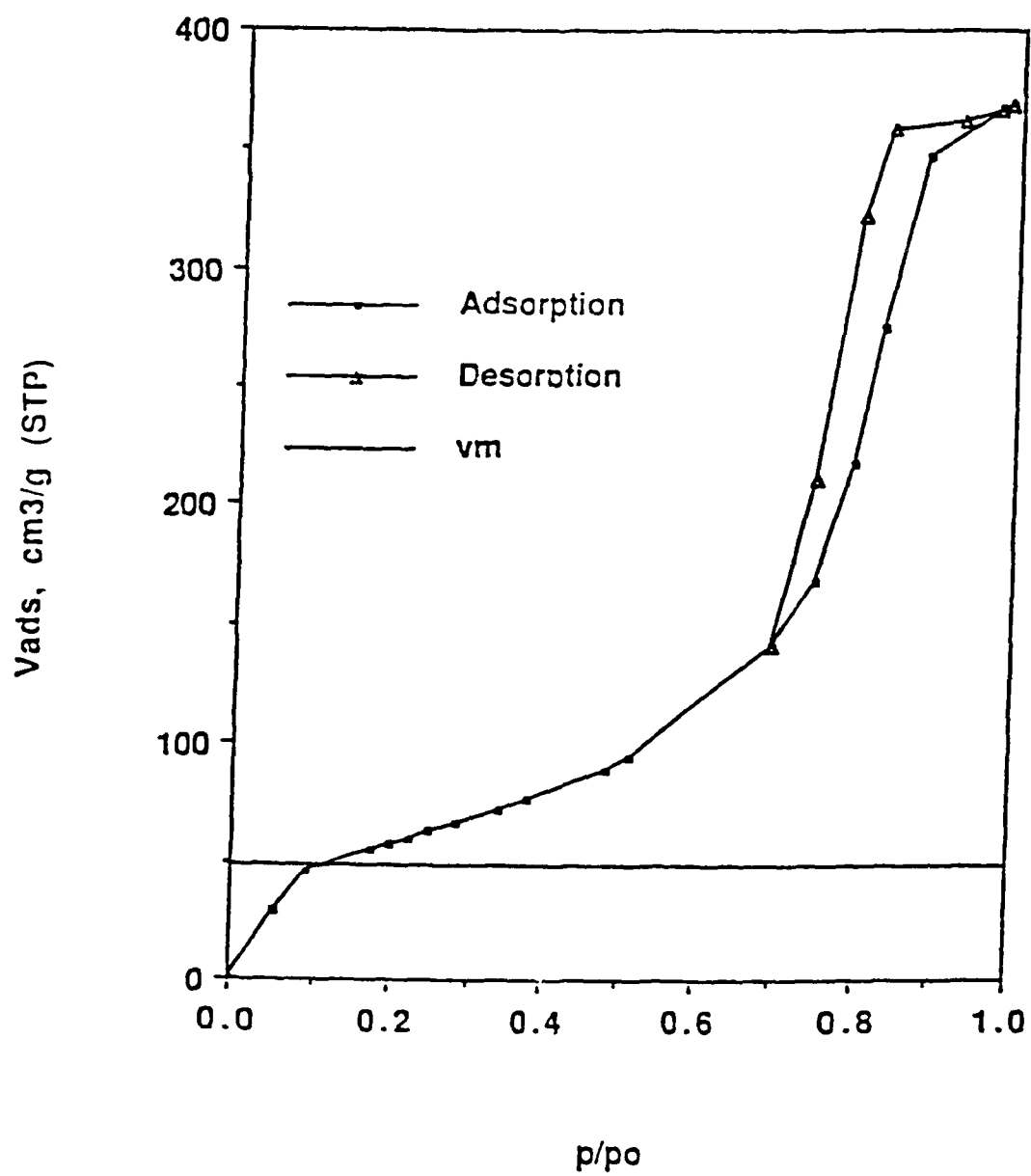


Figure 80. Adsorption/Desorption Isotherm for Alumina

and then taking the set of points that gave the best least squares fit of the data points processed according to the BET (A) equation to a straight line determined by least squares fitting. The BET surface area measured with the BET system during run number three was $209.2 \text{ m}^2/\text{g}$. The BET surface area of the same sample of alumina determined in run number four was $209.0 \text{ m}^2/\text{g}$. The small difference between these two values is just fortuitous and varied by several m^2/g depending on the number of data points used to determine the surface area.

These results correlated closely (within ~ 3 percent) with the surface area reported by Ketjen ($210 \text{ m}^2/\text{g}$). The reproducibility of this technique was determined to be 99 percent.

Adsorption/Desorption Isotherm for ZSM-5

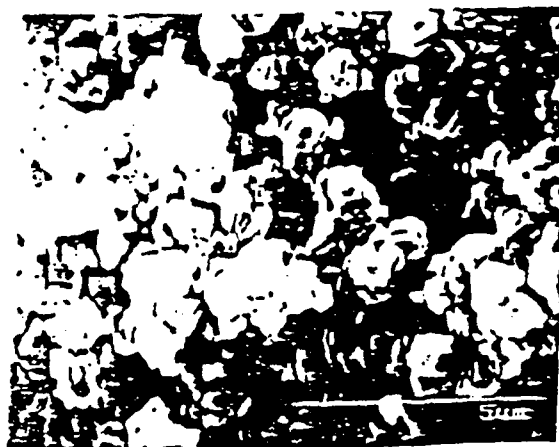
The adsorption/desorption isotherms were determined for several samples of ZSM-5. In particular two samples were carefully examined: A sample of commercially prepared ZSM-5 (ZSM-5M) donated by the Mobil Research and Development Corporation and the hydrogen form of ZSM-5 (HZSM-5-6) that was synthesized as part of this research project. Both of these samples were studied in the powder form.

It is believed that the Mobil sample was manufactured according to the Type B synthesis. Scanning electron micrographs of the HZSM-5M and the HZSM-5-6 samples are presented in Figure 81.

The hysteresis curve obtained with ZSM-5M was the first run in which the quantity β , that was described in the previous section, was used. Its use resulted in very even spacing between consecutive points on the adsorption/desorption isotherm. During the collection of this set of data the calibration volume connected to the doser manifold was used to increase the dosing volume when the adsorption isotherm curve became quite steep as the intercrystalline voids filled with liquid nitrogen.



SEM Photomicrograph of ZSM-5M



SEM Photomicrograph of ZSM-5-6

Figure 81. SEM Photomicrographs of ZSM-5M and ZSM-5-6.

A plot of p/p_0 versus $p/(V_{\text{ads}}(p_0-p))$ is presented in Figure 82 for the ZSM-5M sample. It is clear that the line starts to curve upward at a relatively low value of p/p_0 , that is, 0.12.

The adsorption/desorption isotherm for ZSM-5M is presented in Figure 83 and exhibited a Type B hysteresis. Type B hysteresis is defined as hysteresis where the adsorption branch of the adsorption isotherm occurs at a relative pressure of unity and where the desorption branch occurs at relative moderate pressures.

A plot of p/p_0 versus $p/V_{\text{ads}}(p_0-p)$ for HZSM-5-6 is presented in Figure 84. The data for ZSM-5M and HZSM-5-6 appear to be similar (Figures 82 and 83).

The adsorption/desorption isotherm for HZSM-5-6 is presented in Figure 85. ZSM-5-6 also displays Type B hysteresis.

The y-intercepts and the slopes of the lines in Figures 82 and 84 were determined and used to compute the monolayer volumes, v_m , and the c-values. The monolayer volumes were used to calculate the surface areas of the respective samples. The surface area of the ZSM-5M was 416 m^2/g and the surface area of ZSM-5-6 was 413 m^2/g . The agreement in the surface areas for the ZSM-5M and ZSM-5-6 indicate that the ZSM-5 preparation techniques employed in this study were capable of producing catalyst specimens similar to those prepared by commercial techniques.

Discussion

C-Values

The quantity (E_1-E_L) , is the difference between the heat of adsorption of the first monolayer and the heat of adsorption of the first monolayer and the heat of adsorption of subsequent monolayers, may be calculated from the data. The BET (A) equation assumes that molecules in the second and higher monolayers have the same properties as molecules in the liquid phase, consequently the heat of adsorption of the second and higher monolayers should be

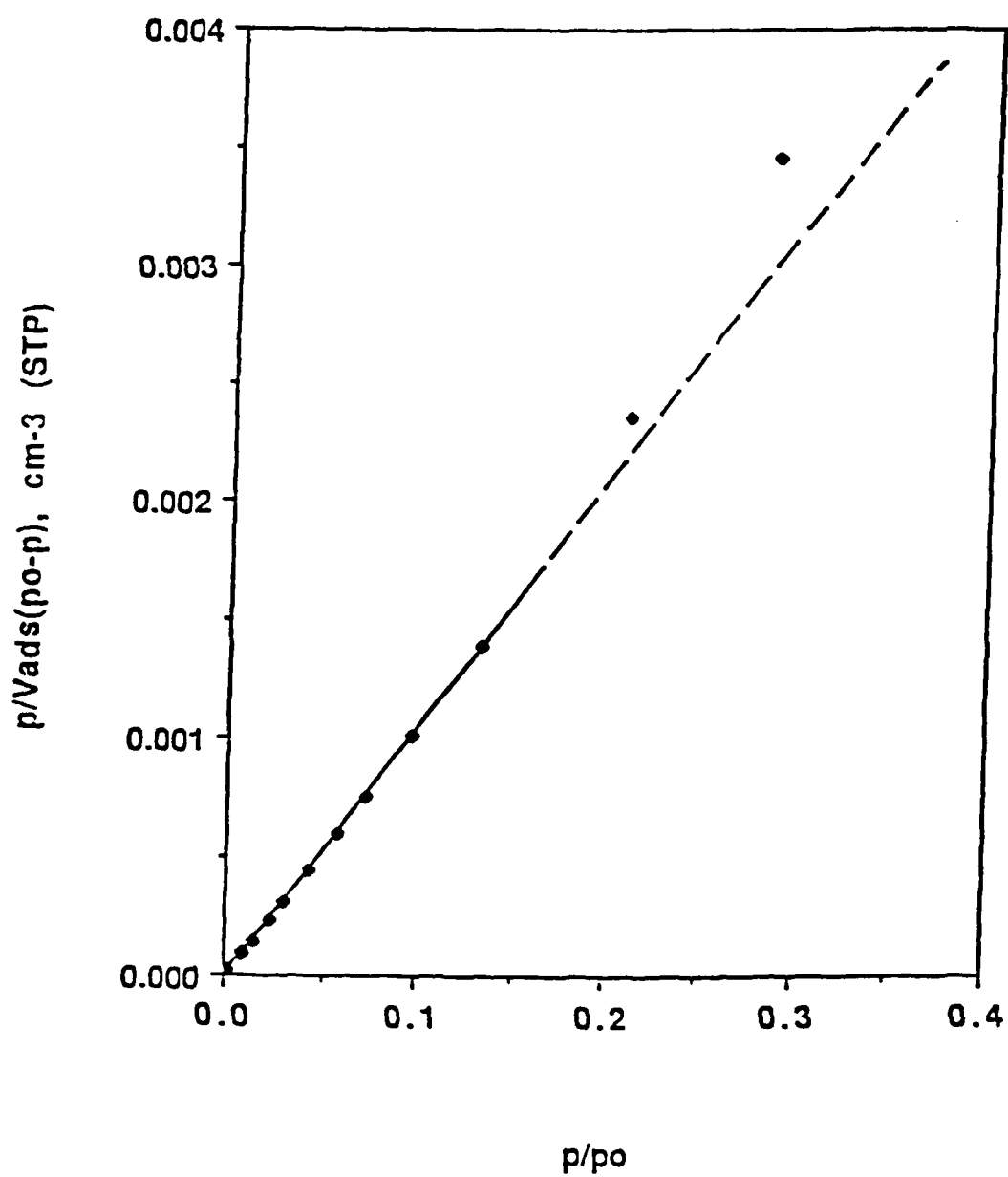


Figure 82. Plot of the BET (A) Equation for ZSM-5M

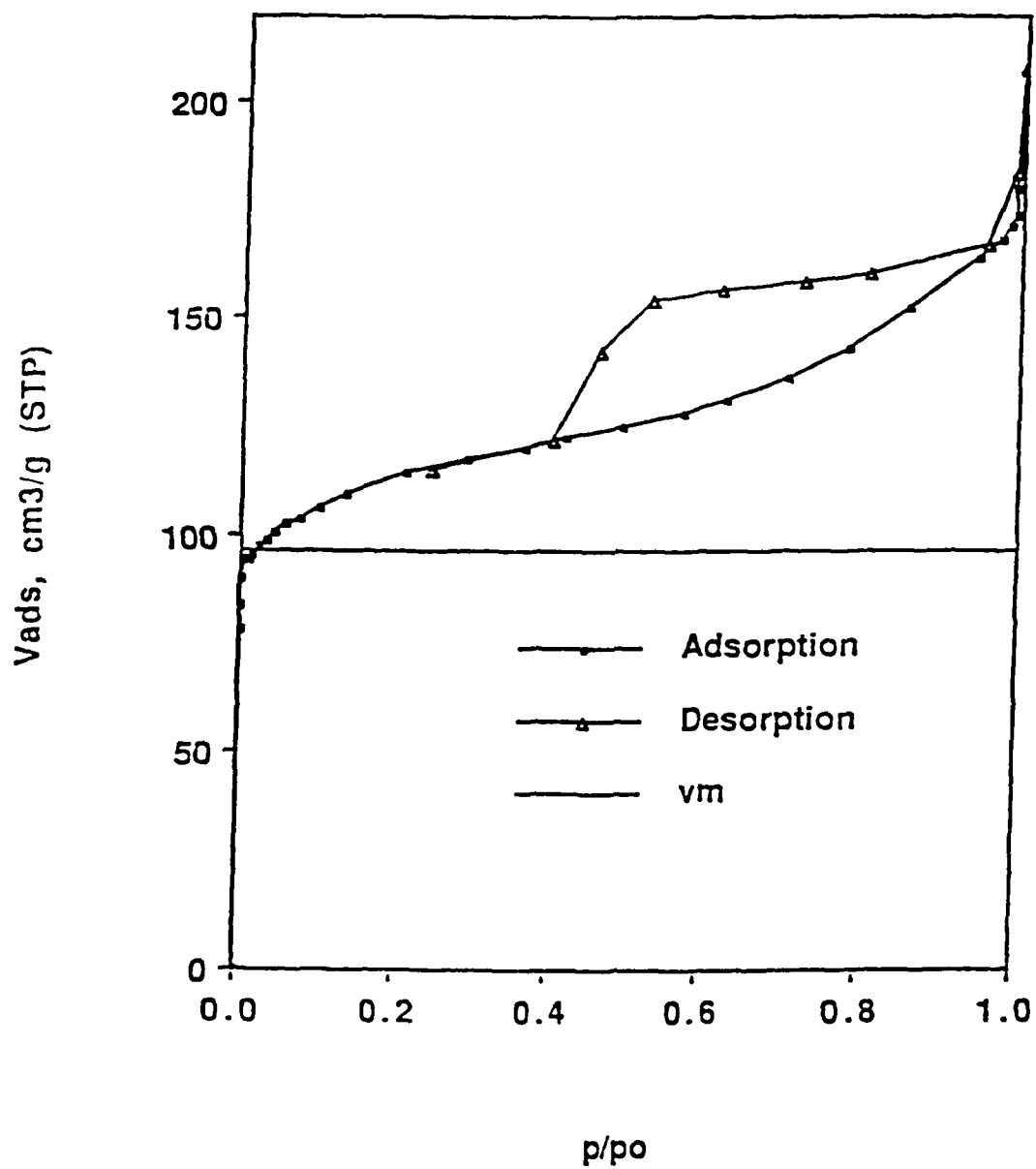


Figure 83. Adsorption/Desorption Isotherm for ZSM-5M

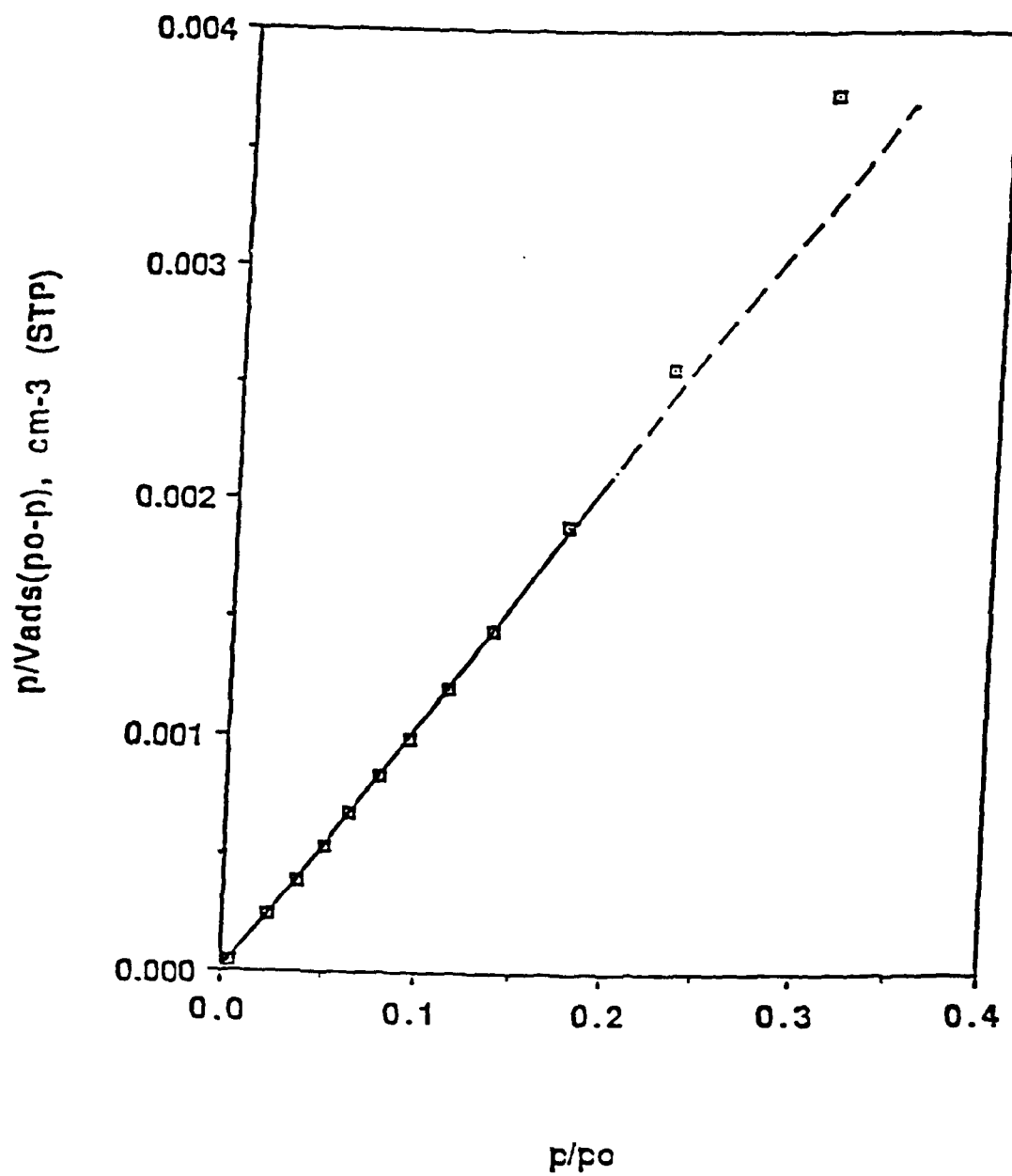


Figure 84. Plot of the BET (A) Equation for ZSM-5-6

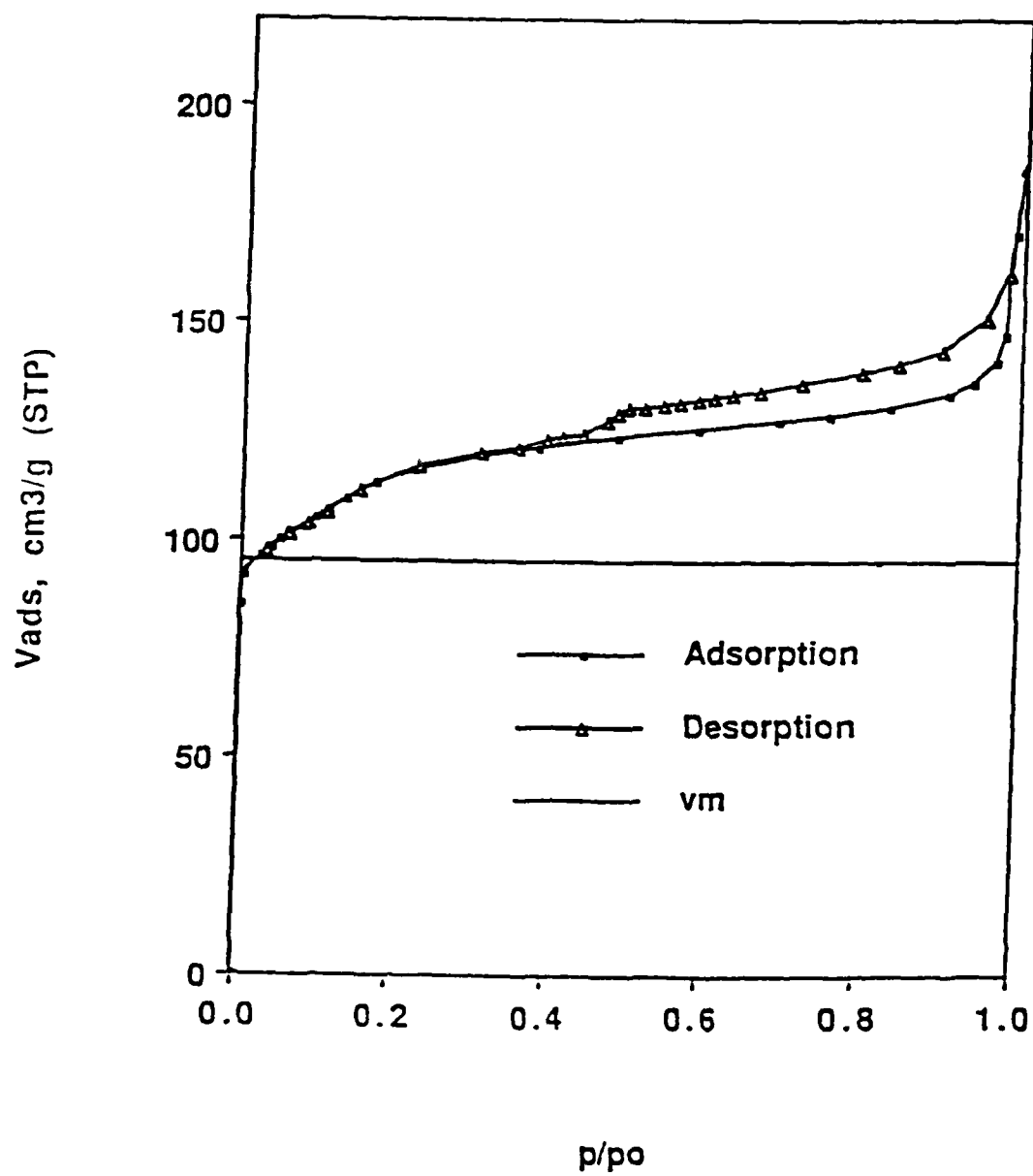


Figure 85. Adsorption/Desorption Isotherm for HZSM-5-6

equivalent to the latent heat of condensation of the adsorptive. Brunauer, Emmett and Teller²⁵⁹ reported that $(E_1 - E_L)$ is fairly constant for the same gas on different adsorbents. They found that for nitrogen $(E_1 - E_L)$ is about 840 ± 50 cal/mol. They also pointed out that the value of the pre-exponential factor should be approximately unity. This is apparent from the nature of the pre-exponential factor, A_o , which is defined in Equation (7-10)

$$A_o = \left(\frac{a_1}{b_1} \right) \left(\frac{b_2}{a_2} \right) \quad (7-10)$$

where:

- a_1 is the frequency factor for condensation in the first monolayer;
- a_2 is the frequency factor for condensation into the second monolayer;
- b_1 is the frequency factor for desorption from the first monolayer; and
- b_2 is the frequency factor for desorption from the second monolayer.

The similarity in the nature of these two sets of frequency factors indicates that the ratios should be unity.

The values of $(E_1 - E_L)$ were calculated for ZSM-5M and ZSM-5-6 based on the assumption that the A_o 's were unity. $(E_1 - E_L)$ for physisorption on these two samples was 1400-1500 cal/mol. Thus the c-value obtained from the BET (A) equation is about 50 times greater than the c-value reported for nitrogen physisorption on silica gel by Brunauer et al.²⁵⁹ Generally high c-values are characteristic of microporosity.²⁶⁶

The higher c-values may be a result of an increase in the pre-exponential factor rather than some unknown effect which causes a fifty percent increase in the heat of adsorption of the first monolayer. The pre-exponential factor contains the ratios of the adsorption frequency factors and the desorption frequency factors. These frequency factors are a function of the geometry of adsorptive molecules and of the geometry of the surface and the pore. In ZSM-5 the pore spaces

are very restricted and the opportunity for a desorbed nitrogen molecule to pass out of the pore without resorbing on the opposite side of the pore is greatly reduced. The frequency factor for desorption from the first monolayer, b_1 , appears in the denominator of the expression for A_0 , as a result of the greatly reduced value for b_1 , there is a large increase in the term A_0 for physisorption in ZSM-5.

Another effect of the small pore size is the deviation of the data from linearity in the plot of the BET (A) equation at low dimensionless pressures, p/p_0 . In Figures 82 and 84, which were plots of data obtained for ZSM-5M and ZSM-5-6, respectively, the deviation from linearity starts at about $p/p_0 = 0.10$. Usually the BET (A) equation applies past $p/p_0 = 0.30$. The deviation at low values of p/p_0 is related to the number of adsorbed layers that can form in the pores of the adsorbent. The smaller the pore diameter the fewer the adsorbed layers that can be accommodated in the pore and the lower the value p/p_0 at which the deviation from linearity occurs.

Isotherm Modeling

The BET (B) equation relieves the assumption of the BET (A) equation that an infinite number of monolayers can be formed on the surface of the catalyst or adsorbent. It accomplishes this by introducing a quantity, n , which is the number of monolayers that can be formed in a pore. The BET (B) equation is applicable for an adsorbent or catalyst with a uniform pore size distribution. However, if an adsorbent has a range of pore sizes the BET (D) equation, which is a modified form of the BET (B) equation, can describe adsorption on such a material. The BET (B) and BET (D) equations are derived in Appendix F.

The BET (B) and/or the BET (D) equations are used by first determining the monolayer volume, v_m , and the heat of adsorption term, $(E_1 - E_L)$, for an adsorbent or catalyst. Then use v_m

and $(\tau - 1)$ in the BET (B) or the BET (D) equation for various values of n_i (where n_i is the number of monolayers that will form in a type i pore, different types of pores varying by pore diameter only). The combination of n_i 's that give the best fit of the adsorption isotherm are taken to be the best description of the pore size distribution.

A modified form of the BET (D) equation was derived to account for the variation in 'c-values' that is observed in micropores. A Fortran language program, BETD, was written to model adsorption isotherms with an input value of v_m , $(E_1 - E_L)_i$ and β_i .

The program BETD was used to model adsorption isotherms for a ZSM-5 type adsorbent, which is displayed in Figure 86, and a ZSM-48 type adsorbent, which is displayed in Figure 87. The combination of data used to generate Figure 86 does not represent a computer optimization to fit an adsorption isotherm of ZSM-5. This data results from estimates of noncrucial values and a rough optimization of the more crucial values. A ZSM-5 type adsorbent differs from a ZSM-48 type adsorbent in that ZSM-5 zeolite contains 5-6 Å pores and pore intersections while ZSM-48 zeolite contains 5-6 Å pores and no pore intersections.

The data used to obtain Figure 86, the adsorption isotherm for a ZSM-5 type adsorbent are $v_m = 100 \text{ cm}^3/\text{g}$, with three types of pores, being characterized as follows:

- Type (1) $n_1 = 1.2$; $(E_1 - E_L)_1 = 1500 \text{ cal./g}$; $\beta_1 = 0.47$; pores corresponding to the actual pores of ZSM-5;
- Type (2) $n_2 = 1.95$; $(E_1 - E_L)_2 = 900 \text{ cal./g}$; $\beta_2 = 0.50$; pores corresponding to the pore intersections of ZSM-5; and
- Type (3) $n_3 = 30$; $(E_1 - E_L)_3 = 800 \text{ cal./g}$; $\beta_3 = 0.03$; pores corresponding to intercrystalline mesopores of ZSM-5.

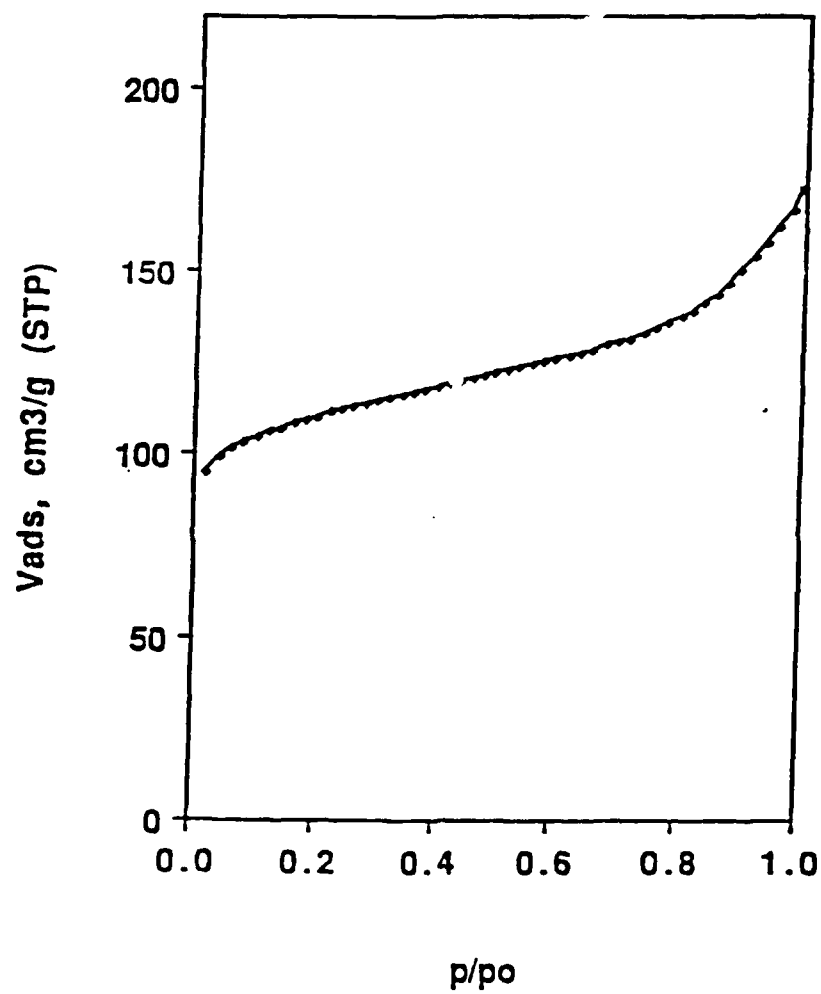


Figure 86. Adsorption Isotherm for a ZSM-5 Type Adsorbent

The variables defined here are the variables in the BET (D) equation. The number of monolayers formed in type i pores is n_i ; $(E_1 - E_L)_i$ is the heat of adsorption term for the 'c-value' for adsorption in pore type i ; and β_i is the fraction of the surface area contained in type i pores. The quantity β_1 is approximately equal to β_2 which means to say that the surface area of pore intersections in ZSM-5 zeolite is approximately equal to the pore surface area in ZSM-5 zeolite. Consequently the selectivity and activity of reactions in ZSM-5 zeolite is as much a result of reactions in the pore intersections as in the pores themselves. Comparisons of Figure 86 with the adsorption isotherms of Figures 83 and 85 will show the relative similarity between the measured isotherms and the calculated isotherm.

An adsorption isotherm of a ZSM-48 type adsorbent is displayed in Figure 87. It differs from the adsorption isotherm for a ZSM-5 type adsorbent in that ZSM-48 has no pore intersections and ZSM-5 does. The data used to obtain Figure 87 are $v_m = 100 \text{ cm}^3/\text{g}$, with two types of pores, being characterized as follows:

Type (1) $n_1 = 1.2$; $(E_1 - E_L)_1 = 1500 \text{ cal/g}$; $\beta_1 = 0.97$, pores corresponding to the pores of ZSM-48; and

Type (2) $n_2 = 30$; $(E_1 - E_L)_2 = 800 \text{ cal/g}$; $\beta_2 = 0.03$, pores corresponding to the intercrystalline mesopores of ZSM-48.

The difference between the data used to obtain Figure 86 and the data used to obtain Figure 87 is simply that pore type 2 in the data used to obtain Figure 86 has been combined with pore Type 1.

The differences in Figure 86 and Figure 87 is because Figure 87 is the adsorption isotherm of a ZSM-48 type adsorbent which lacks pore intersections like a ZSM-5 type adsorbent. Consequently any differences arising between the selectivity and activity of reactions over ZSM-5

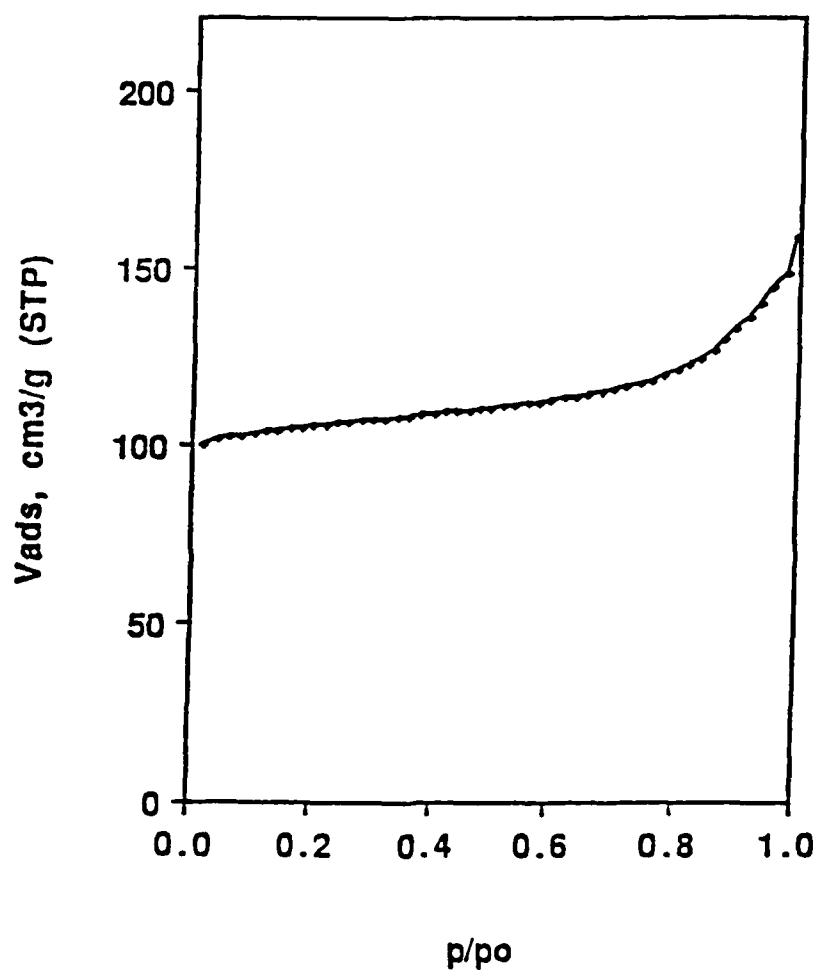


Figure 87. Adsorption Isotherm for a ZSM-48 Type Adsorbent

and over ZSM-48 results partly from the absence of pores in ZSM-48. This has been shown to be the case. The dehydration of methanol on ZSM-5 results in the production of olefins which oligomerize and transfer hydrogen to form aromatics and paraffins. However, the dehydration of methanol on ZSM-48 produces just olefins.²⁶⁷ This is because ZSM-48 lacks pore intersections which are able to contain the bimolecular hydrogen transfer state necessary for the formation of aromatics.

The BET data outputs, temperature and adsorptive pressure, are sent directly to the computer and analyzed. The BET data acquisition scheme and the circuit design for interfacing the computer and the BET apparatus are presented in Figures 88 and 89, and the BET software algorithm is presented in Figure 90.

Hysteresis Loops

Breck²⁶¹ has reported that zeolites do not exhibit hysteresis loops. The reason is that hysteresis is only possible in pores where the radius of the pore is twice the diameter of the adsorbed molecules.²⁶⁸ The pores of ZSM-5 have a diameter between 5.0 and 6.0 Å. A molecule of nitrogen has a diameter of 3.8 Å which is five or six times smaller than the minimum diameter for hysteresis in a pore of ZSM-5. This is an apparent contradiction with the data that is presented in Figures 82 and 84 where a clear hysteresis loop for each sample of ZSM-5 is observed. The following observations were made regarding the adsorption desorption isotherms:

1. hysteresis loops were obtained for both samples of ZSM-5;
2. the hysteresis loop for the ZSM-5M differs somewhat from the hysteresis loop of ZSM-5-6, in that the difference between the adsorption and desorption branches of the hysteresis loop are more pronounced in ZSM-5M than in ZSM-5-6;

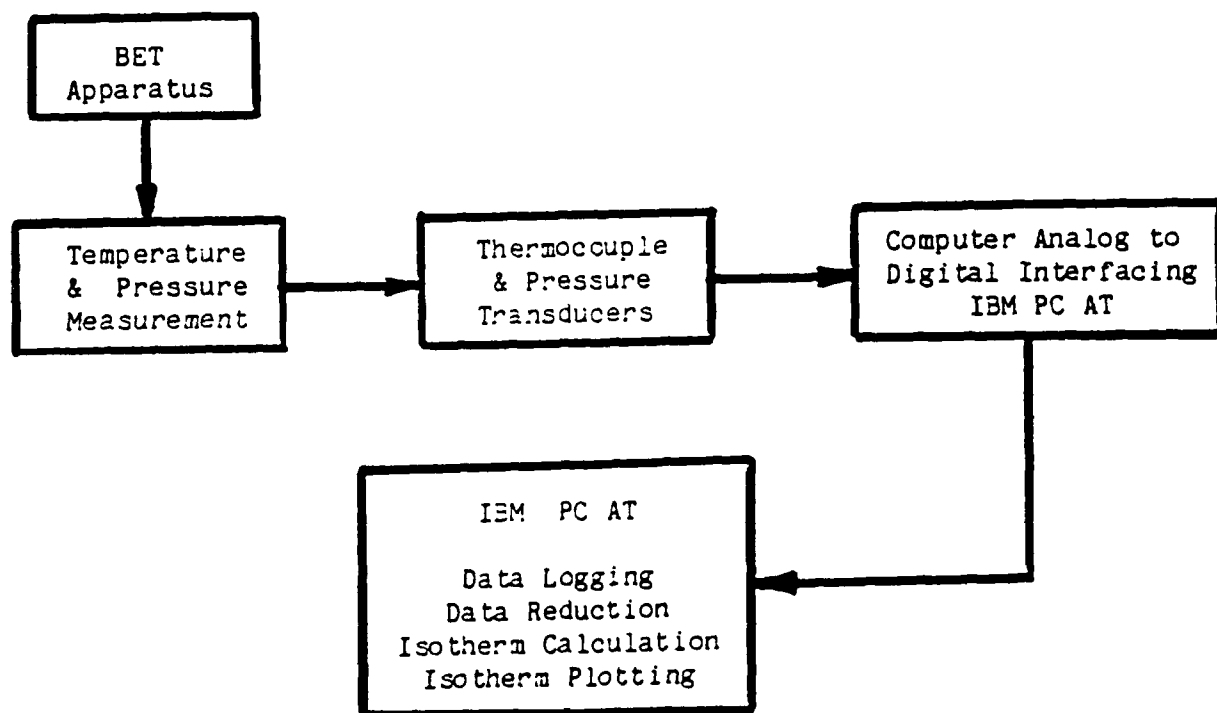
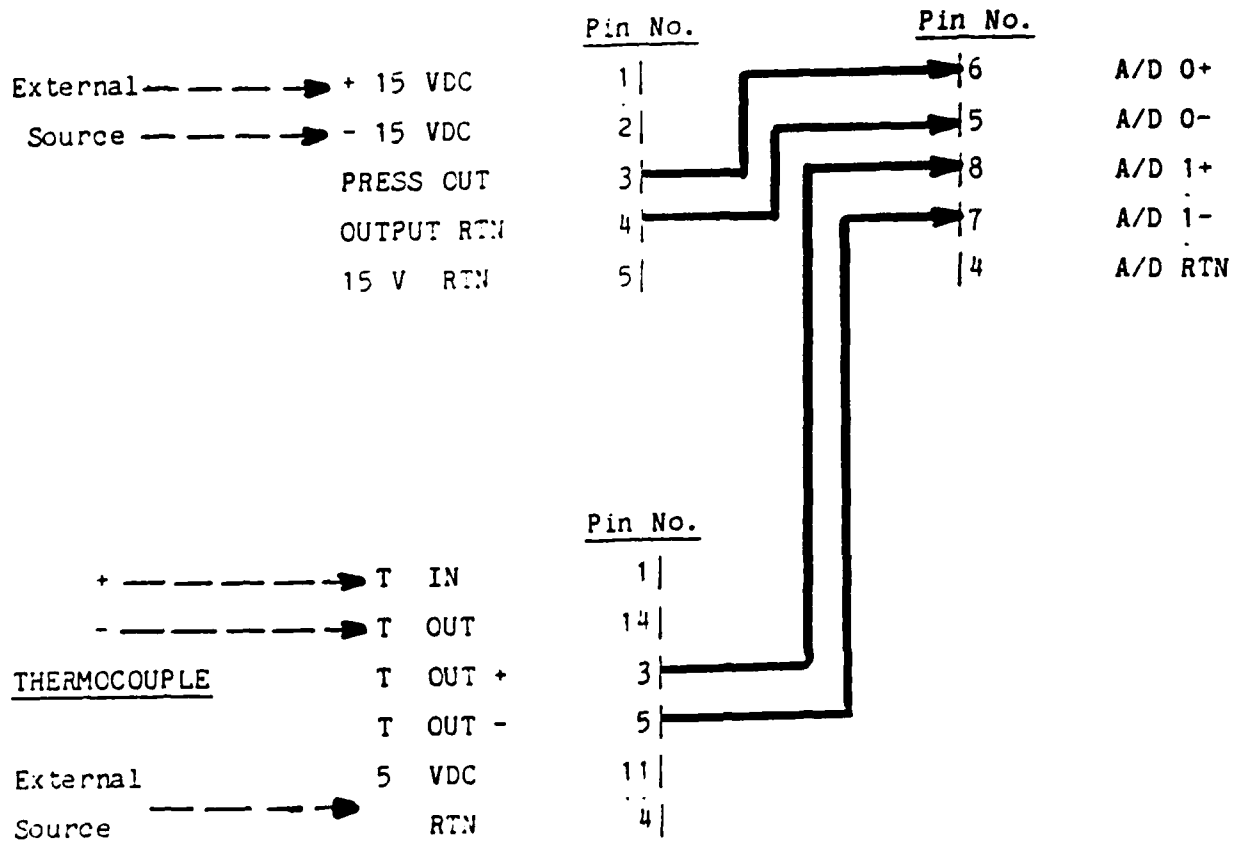


Figure 88. BET Apparatus Data Acquisition System

BARATRON GAUGE

IBM DA SYSTEM



AD594

Figure 89. Circuit Design for Computer-BET Apparatus Interfacing

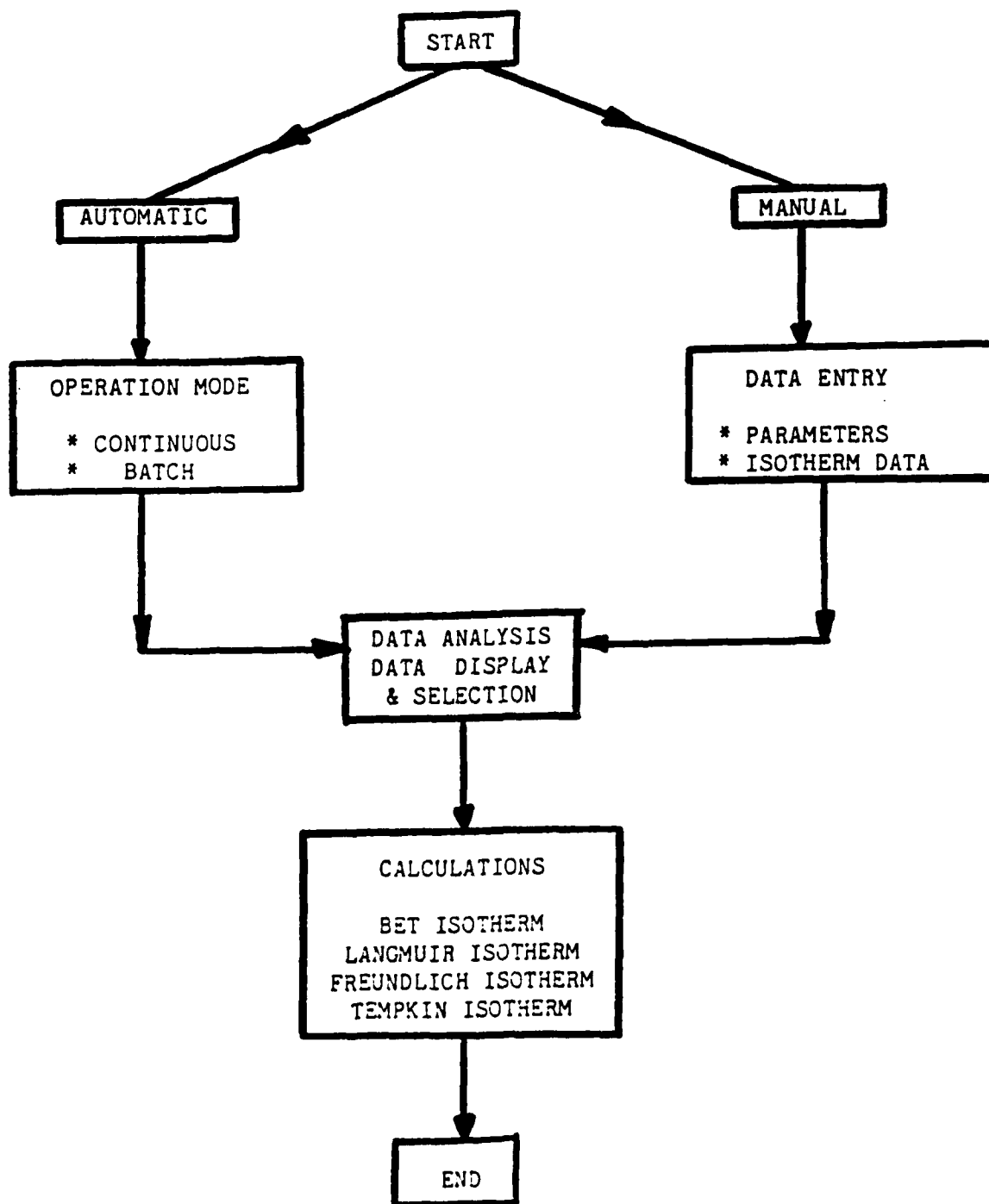


Figure 90. Schematic of BET Software Algorithm

3. the intercrystalline pore structure of the ZSM-5-6 differs from that of ZSM-5-6, in that the crystallites of ZSM-5M consist of smaller and more discrete crystallites than the crystallites of ZSM-5-6 which are larger and agglomerated together in 10 μm to 50 μm clusters; and
4. both hysteresis loops show hysteresis effects occurring in a broad size range of pores, from angstrom size pores up to micron size pores.

These four observations led to the conclusion that the hysteresis loops observed here on ZSM-5 are a result of hysteresis effects in intercrystalline mesopores and not in the intracrystalline micropores. It is expected that an adsorption/desorption isotherm of a single large crystal of ZSM-5 would not display hysteresis because of the lack of an intracrystalline pore structure.

Conclusions

In order to study the surface and pore properties of ZSM-5 a BET system was constructed and experiments, were developed for the reproducible determination of adsorption/desorption isotherms. ZSM-5 displayed two outstanding features:

1. higher c-values probably as a result of ZSM-5's microporosity; and
2. hysteresis loops which represent filling and emptying of intercrystalline pores.

Because of the differences in the hysteresis loops of different samples of ZSM-5 it should be possible to correlate different crystallite structures and arrangements with differences in hysteresis loops.

Section VIII: DESIGN AND FABRICATION OF THE CATALYST TESTING UNIT

Research Personnel:

Kien-Ru Chen
Postdoctoral Fellow

Jerald W. Wiser
Undergraduate Research Associate

Francis V. Hanson
Associate Professor

The screening and evaluation of candidate catalysts and the process variable studies to be conducted for both the aromatics formation step and the aromatics hydrogenation step required the design and fabrication of a bench scale catalyst testing unit. The unit was designed to be capable of conducting all the investigations outlined in the research proposal and for maximum flexibility with regard to process operating variables and process configurations.

Reactor Design

A schematic of the high pressure flow reactor system for aviation turbine fuel synthesis is presented in Figure 91. The reactor was designed on the assumption that it would operate as a fixed or packed bed reactor. Four critical process operating variables were selected to establish the design basis: temperature, pressure, gas and liquid space velocities, and feed ratios. It was required that all process variables must be capable of being monitored and adjusted in both the manual and automatic control operating modes. The ranges of the process operating conditions selected in the design process were as follows:

Catalyst Volume: 10-100 cm³

Temperature: 373-773 K

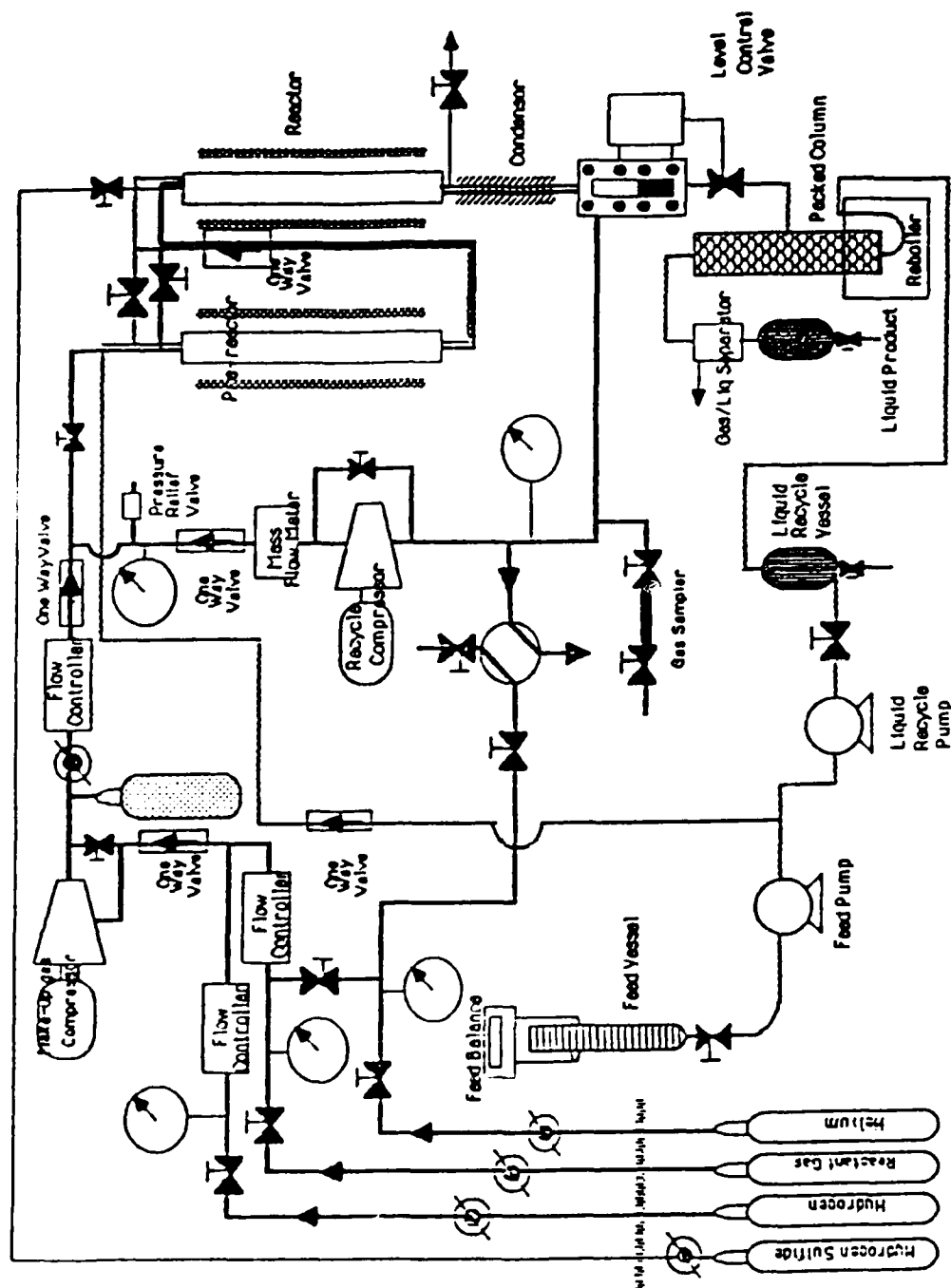


Figure 91. Schematic of Catalyst Evaluation Unit

Pressure:	0-3000 psig
Liquid Feed:	0-500 cm ³ /h
LHSV:	0.1-50 h ⁻¹
Gas Feed:	2-60 l/h
GHSV:	20-5000 h ⁻¹

The reactor was fabricated with flanged entrance and exit regions to facilitate cleaning and catalyst loading procedures.

Temperature Controllers

The reactor furnace temperature controllers, capable of operating in both the manual and automatic control modes, can be provided by several controller manufacturers such as Love Control, Omega, and Barber-Coleman. Four Love temperature controllers were installed for the initial manual control operating phase and will be converted to automatic control mode at the appropriate time.

Pressure

High-pressure controllers (up to 3000 psig) for small-scale testing units were not commercially available. Therefore, one back-pressure regulator from Mity-Mite Inc., and two high-pressure gas solenoid valves from Atkomatic Valve Inc. coupled with capillary tubes were used to control the system pressure. A schematic of the circuit for the manual and automatic control modes for the reactor system pressure is presented in Figure 92. Helium was supplied to the control loop as the instrument gas. The pressure reading obtained from the pressure transducer is used to activate the solenoid valves depending on whether the system pressure needs to be

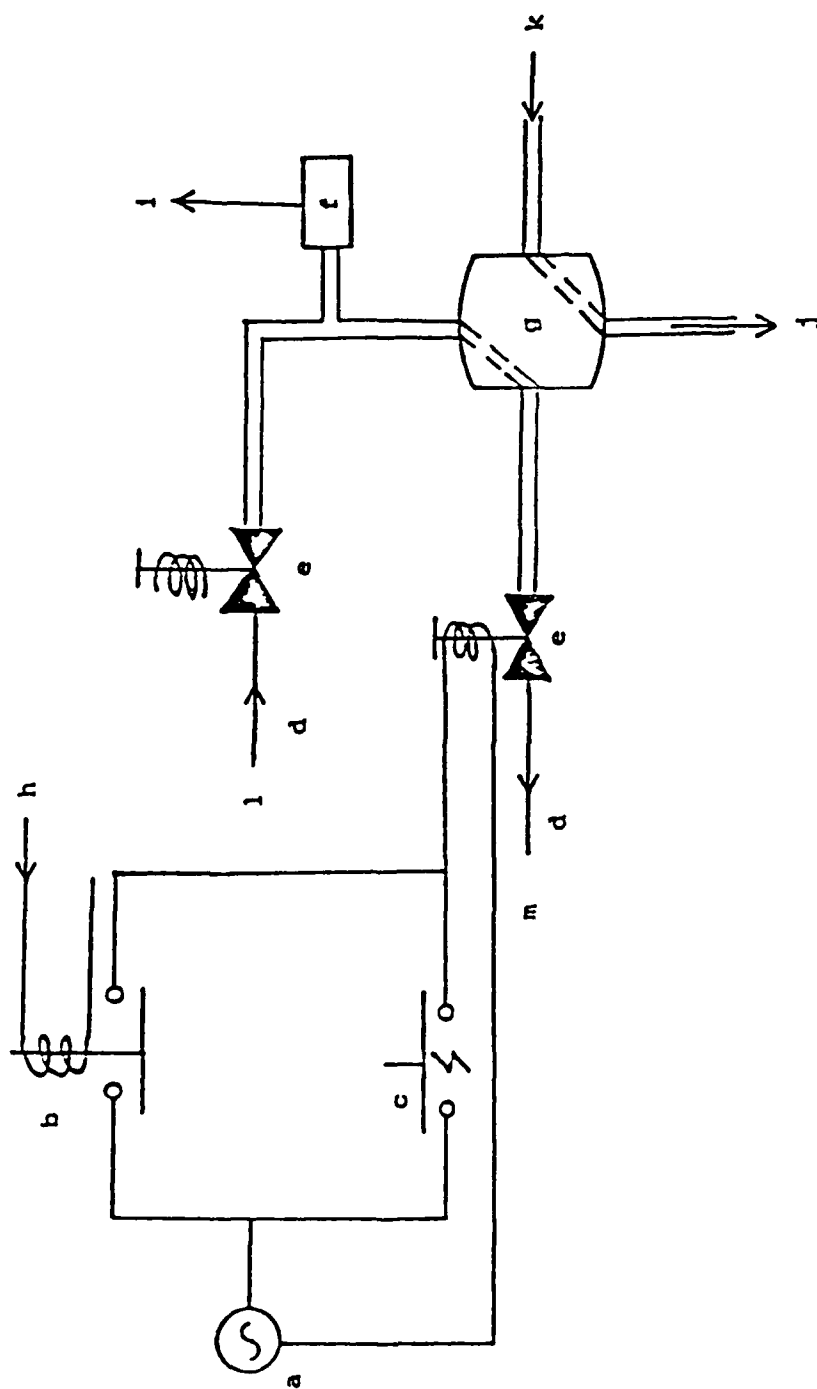


Figure 92. Design for Manual and Automatic Control Modes for the Reactor System Pressure

(a) Electrical Source; (b) Relay; (c) Push Button Switch; (d) Capillary Tube; (e) High Pressure Gas Solenoid Valve; (f) Pressure Transducer; (g) Back Pressure Regulator; (h) Signal from Microcomputer; (i) Signal into Microcomputer; (j) System Pressure; (k) System Outlet; (l) Instrument Gas Inlet; (m) Instrument Gas Outlet

increased or decreased. For instance, if the pressure transducer reading is low compared to the set point pressure, the upstream solenoid valve is opened and the pressure in the control loop is increased, resulting in an increase in the system pressure. The capillary tubes were used in order to obtain a slow rate of change of pressure during pressure adjustment. The unit can be operated in both manual and automatic control modes.

Space Velocity and Mixing Ratio

Gas Feed and Mixing Ratio

The gases flowing into the reactor system (Figure 91) are controlled by Linde mass flow meters and controllers. Mixing of up to four different gases can be controlled and monitored at the same time with the manual and automatic control functions. The control range for gas flow rates is 0-3000 cm³/min.

Liquid Feed

The liquid feed to the reactor system is supplied by the Milton Roy high pressure metering pump. The rated capacity of this pump is 1000 cm³/hr at a pressure of 5000 psig. However, the automatic control mode is not commercially available for this pump, and a step motor from Thurst Inc. can be installed and used to control the liquid feed pump in the automatic control mode.

Gas-Liquid Separator

A gas-liquid separator, located downstream of the reactor, is used to separate the gas and liquid products into two streams. A Brooks high pressure (up to 3000 psig) site glass served as the gas-liquid separator, and it can be modified for both manual and automatic control operating

modes. A high-pressure liquid solenoid valve from Atkomatic Inc. and two high-pressure liquid level sensors from FCI were utilized to achieve the liquid level control in the gas-liquid separator. The design of a high-pressure gas-liquid separator is presented in Figure 93.

Two-Stage Compressor

A two-stage compressor from PPI, Inc., was acquired to compress the low-pressure gas feed (70 psig) into the high pressure gas storage cylinder (maximum 5000 psig) (see Figure 91). The reactor system can be economically operated with this compressor whenever high gas space velocity or high pressure reaction conditions are required. The preliminary design for make-up compressor system is presented in Figure 94. The control circuit for this two-stage compressor system is presented in Figure 95.

Gas Recycle Pump

A Whitney laboratory compressor was purchased for use as a gas recycle pump whenever the recycle mode of operation is required. The rating of this pump is: a discharge pressure of 5000 psig and gas flow capacity of 10,000 cm³/hr. The compressor can be operated in both the manual and automatic control modes.

Packed Distillation Column

The column was made from a two-foot long, two-inch I.D. stainless steel tube. The inside of both ends of the tube are threaded for pipe plugs. Two holes were drilled and threaded with 1/4 inch NPT 2 and 10 inches down from the top. Drilling through Swagelock fittings placed in

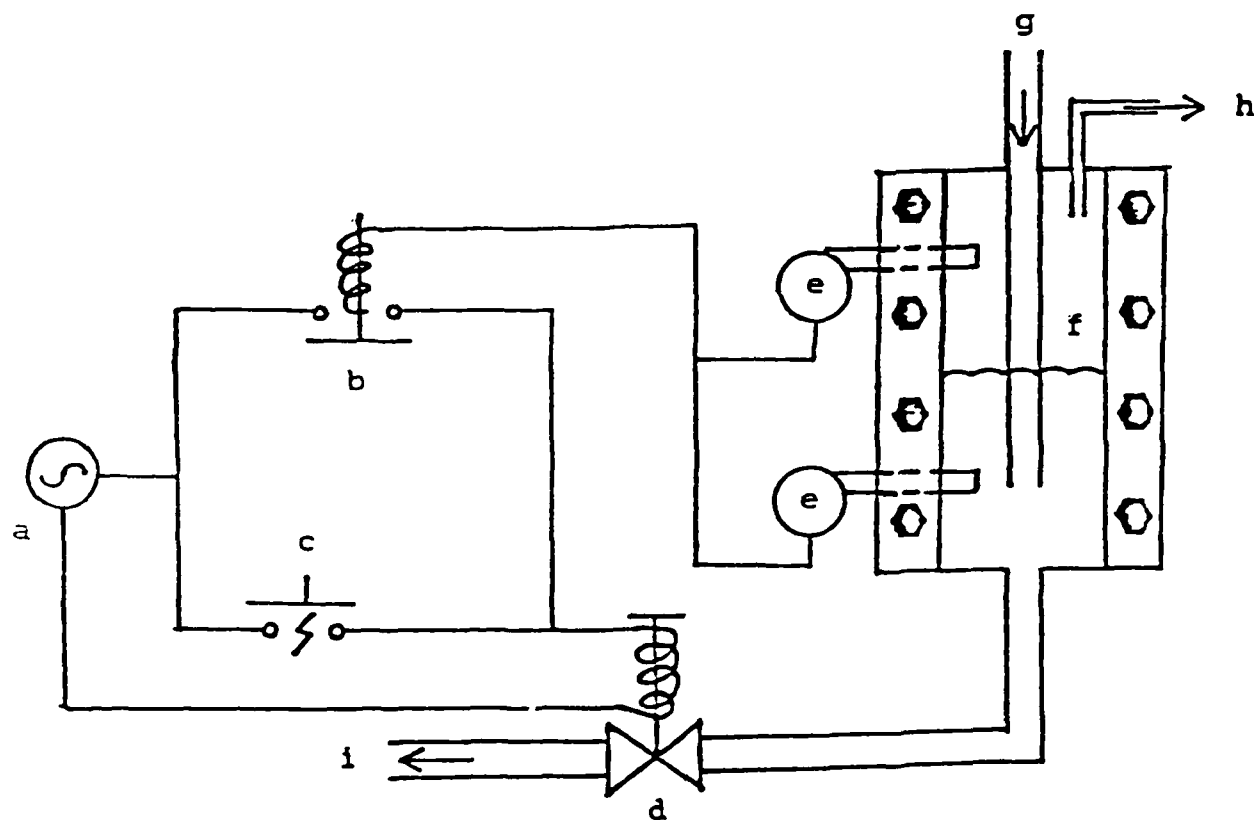
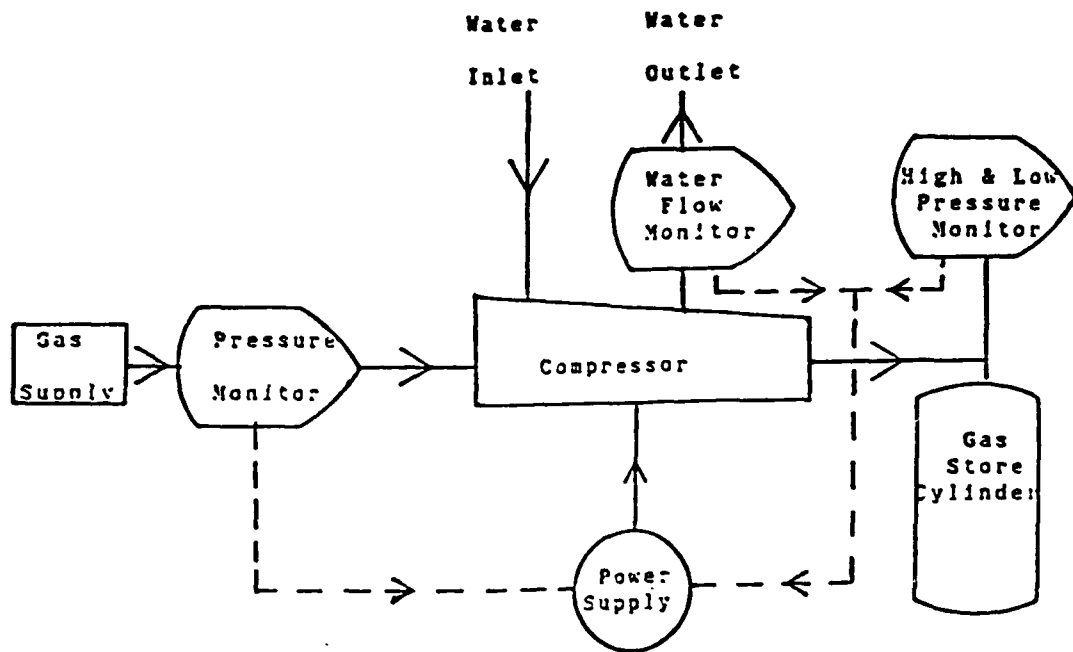


Figure 93. Design of the High Pressure Gas-Liquid Separator

(a) Electrical Source; (b) Relay; (c) Push Button Switch; (d) High Pressure Liquid Solenoid Valve; (e) High Pressure Liquid Level Sensor; (f) High Pressure Brooks Site Glass; (g) Reactor Effluent; (h) Gas Product Outlet; (i) Liquid Product Outlet



Signal Condition

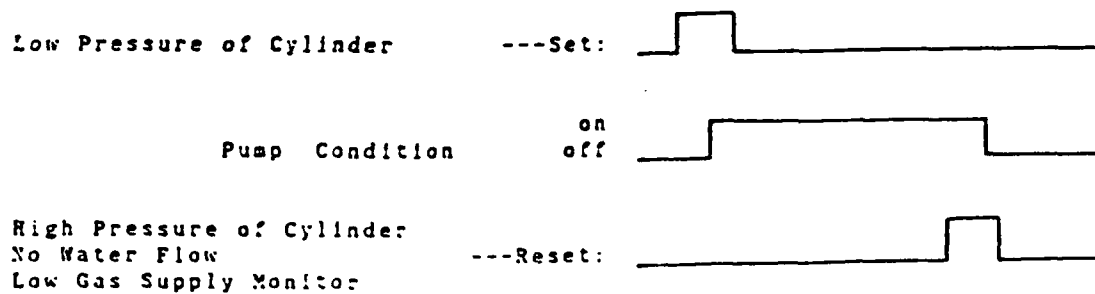


Figure 94. Two-State Feed Compressor Safety and Automatic Control Schematic

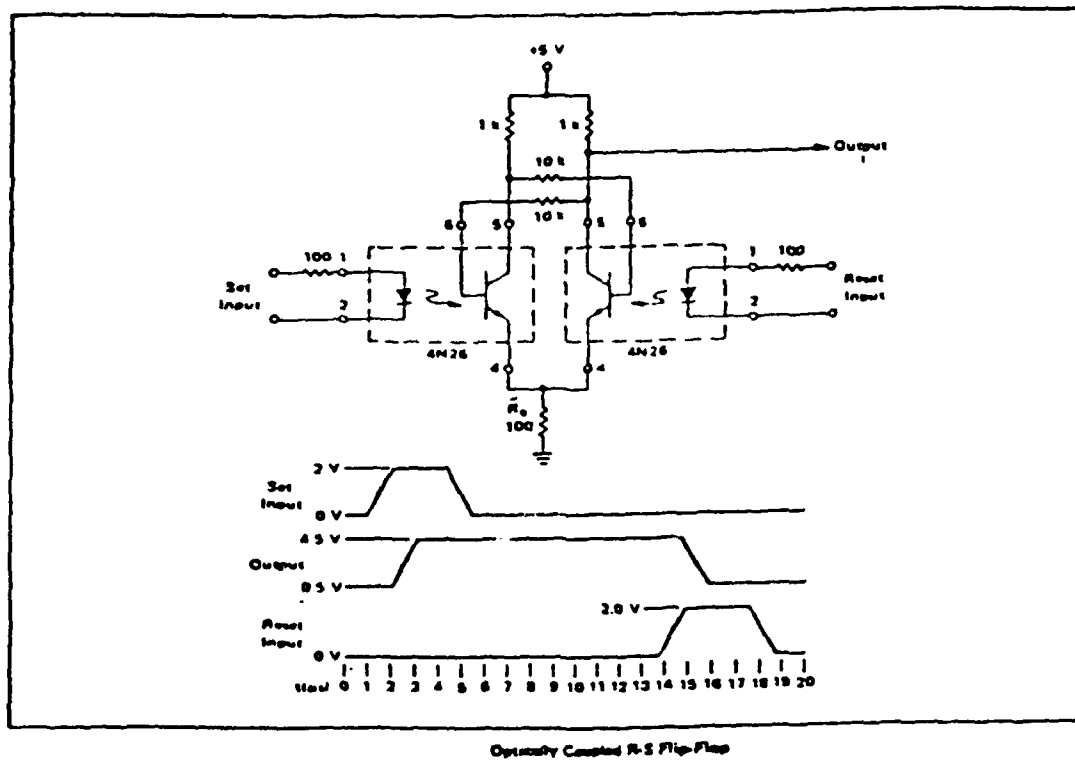


Figure 95. Control Circuit Design for the Two-State Feed Compressor

these taps secured the feed and recycle lines, and the pipe plugs on each end are machined to receive fittings for the vapor and liquid effluent streams. The recycle ratio is controlled by positioning a valve which allows flow back to the column. This can be adjusted, based on input from various sources throughout the system, by the computer. Temperature is controlled by two controllers, one for the reboiler and the other for the column itself. The column is heated with a single layer of heating tapes and insulation, giving a maximum operating temperature of approximately 350°C.

The packing material is stainless steel coils approximately 1/4 inch in diameter and 3/8 inch long. The reboiler section is created by a three-inch vertical rise of the exit stream. This is a 1/8 inch tube which passes under the heat tapes which surround the reboiler section of the column. A schematic of the distillation column is presented in Figure 96. The reactor system operated at the proposed specifications without significant problems.

Automation of the Reactor System

The following electronic circuit designs were completed for use in the automation of the apparatus and underwent preliminary testing:

Thermocouple Amplifier (Figure 97).

Pressure Transducer Interface (Figure 98).

Software Program (Appendix H) for Translation Technique for the Digital to Analog Converter and Analog to Digital Converter. Fourth-order polynomial equations are used to correlate the relationship between temperature and millivoltage for J-type thermocouples:

$$T(\text{mV}) = C_1 + C_2 * \text{mV} + C_3 * \text{mV}^2 + C_4 * \text{mV}^3 + C_5 * \text{mV}^4 \quad (8-1)$$

$$\text{mV}(T) = C_1 + C_2 * T + C_3 * T^2 + C_4 * T^3 + C_5 * T^4 \quad (8-2)$$

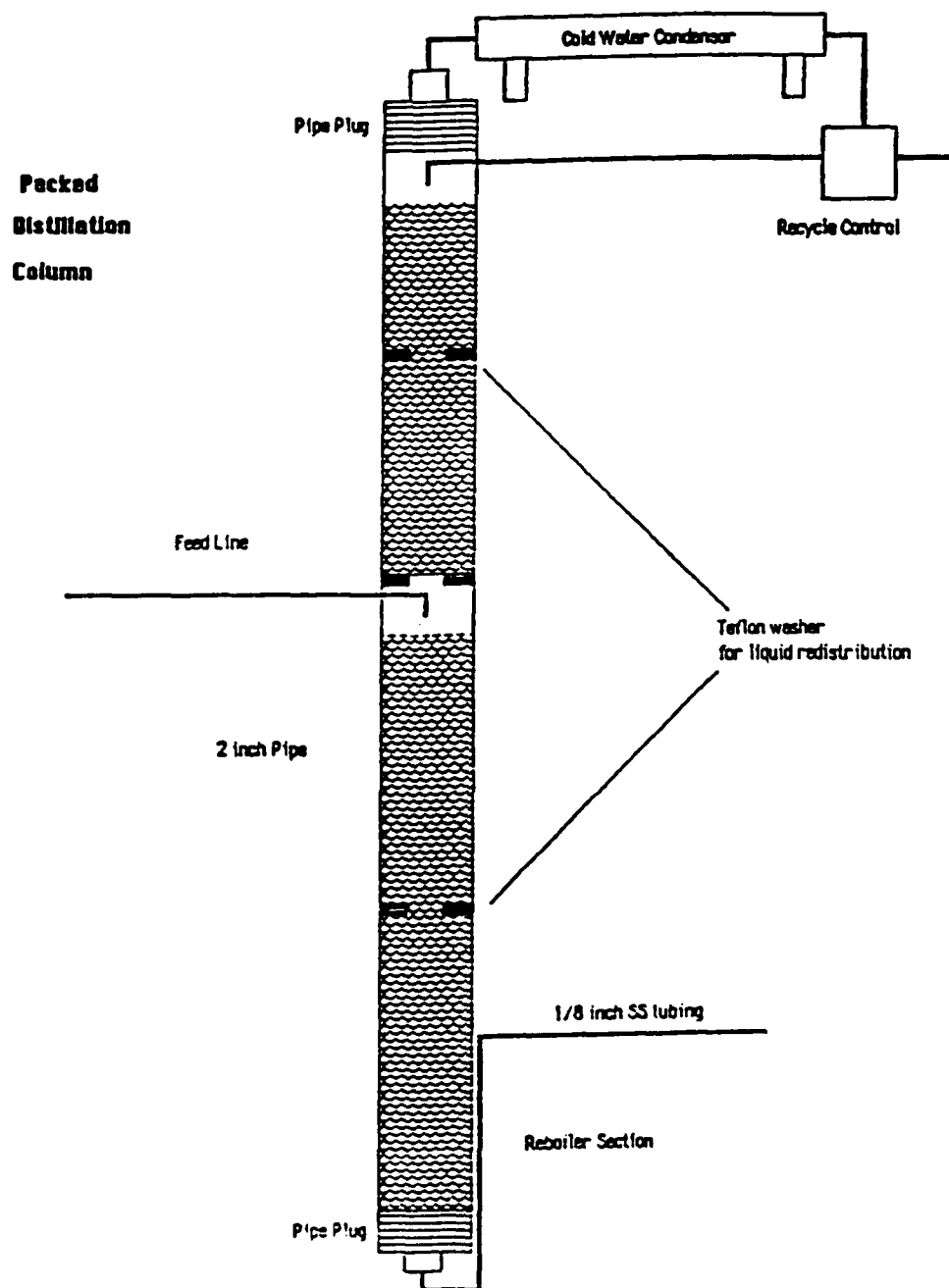


Figure 96. Packed Distillation Column

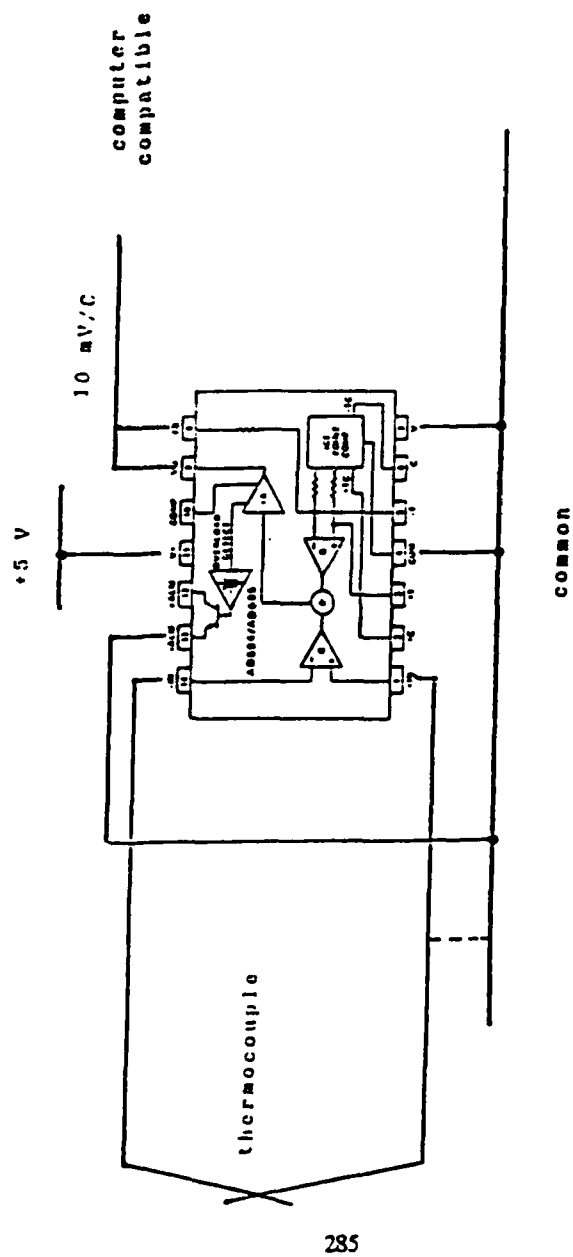


Figure 97. Thermocouple Amplifier

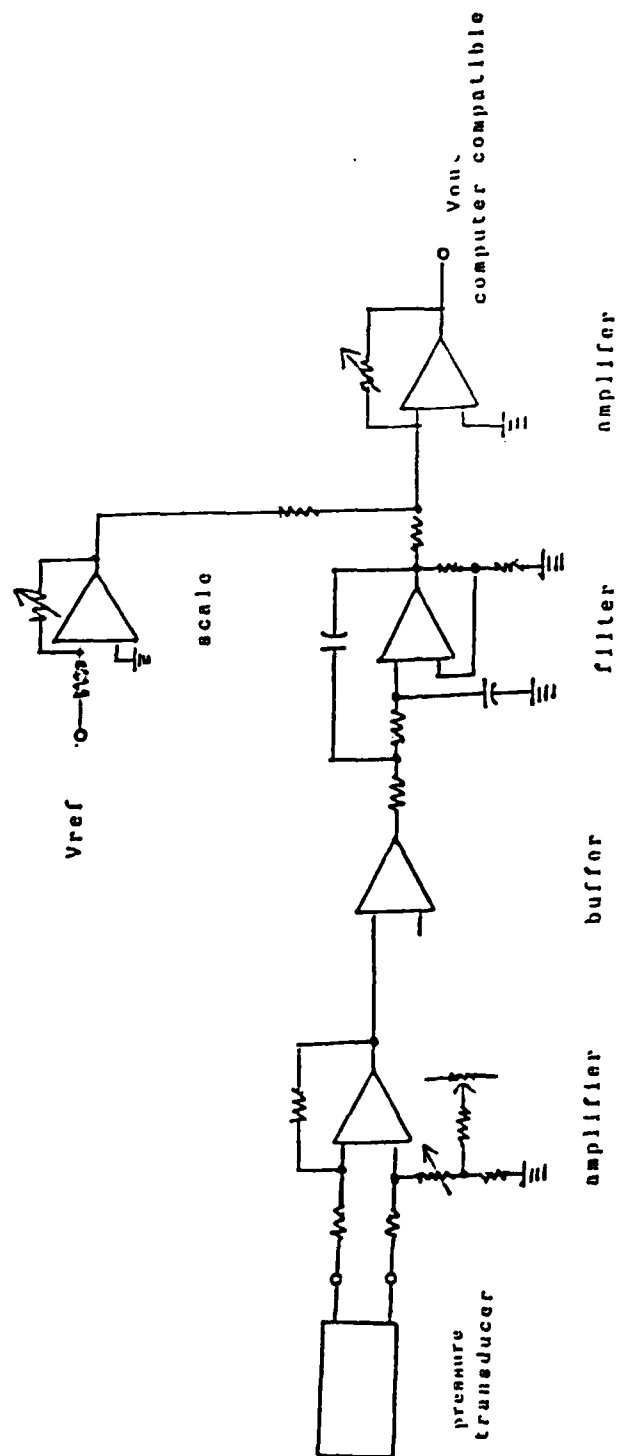


Figure 98. Pressure Transducer Interface

Equations (8-1) and (8-2) are applied to the A/D and the D/A translations, respectively. The program, named fit.c (Appendix H), for data fitting can treat the millivoltage as a function of temperature for J-type thermocouples and the temperature as a function of millivoltage for J-type thermocouples.

Section IX: LITERATURE SURVEY

Research Personnel:	Lei-Yea Cheng Graduate Student
	Daniel Longstaff Graduate Student
	H. Paul Wang Graduate Student
	Kien-Ru Chen Postdoctoral Fellow
	Nabin K. Nag Assistant Research Professor
	Francis V. Hanson Associate Professor

INTRODUCTION

The literature survey to be conducted in conjunction with the high-density aviation turbine fuel research project was designed to be readily accessible to the University of Utah research team and to the personnel at the Wright Aeronautical Laboratories. A database management system based on the concept of "Information Automation" was set up on the IBM PC-AT and consisted of the following components:

1. Literature database files;
2. Data Transition: Addition, Edit, and Deletion; and
3. Data File Searching and Maintenance.

The relationship between these procedures is illustrated in Figure 99.

The database files are structured to record up to six authors, the journal reference, the volume, page numbers, year of publication, and title of the article. The field also contains eight (8) indices which permit classification and retrieval of information/key words related to each entry

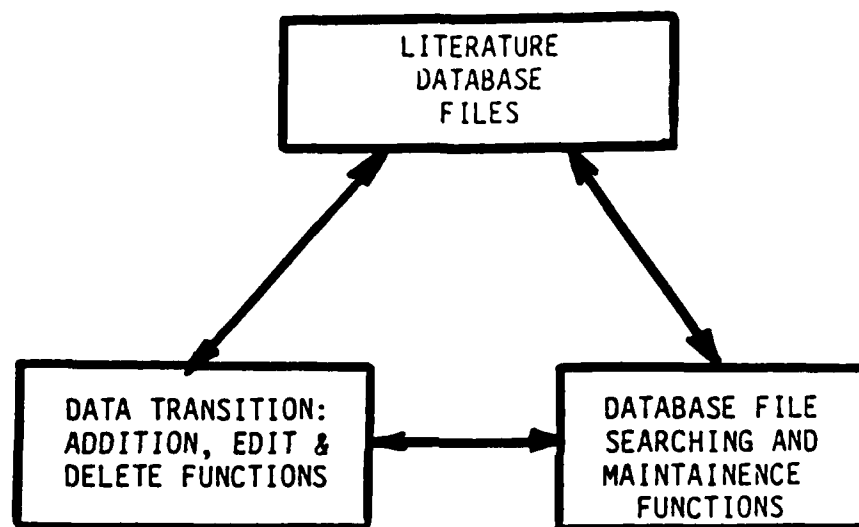


Figure 99. Relationships Between Functions for the Literature Survey Database Management System

in the database file. The search routine is capable of both single entry and multiple entry searches of the database file.

The technical subjects which were intended to be covered included the following:

1. shape selective catalysis;
2. zeolite catalyst preparation, characterization, and evaluation;
3. reactions of oxygenates over solid oxide materials;
4. supported metals catalysis;
5. preparation, characterization, and evaluation of supported metal catalysts;
6. hydrogenation of aromatic hydrocarbons and feedstocks; and
7. design concepts in catalytic reactor systems.

A printout of the database file as it had evolved at the termination of funding by the Air Force Wright Aeronautical Laboratories of the United States Air Force is included for record purposes.

Database File

PAPER NUMBER: 1

Weitkamp, A. W., 'Stereochemistry and Mechanism of Hydrogenation of Naphthalenes on Transition Metal Catalysts and Conformational Analysis,' Adv. Catal., 18, 1, 1968

PAPER NUMBER: 2

Indyukov, M. K., Danielyan, M. K., Kudinov, A. A., and Mamedova, A. I., 'Production of High Density Fuel from Aromatic Petroleum Cuts,' , 185, 1985

PAPER NUMBER: 3

Boudart, M. , 'Catalysis by Supported Metals ,' Adv. Catal., 20, 153, 1969

PAPER NUMBER: 4

Bond, G. C., and Burch, R. , 'Strong Metal-Support Interactions ,' Catalysis-A Specialist Periodic Report, 6, 27, 1982

PAPER NUMBER: 5

Wilson, M. F., Fisher, I. P., and Driz, J. F. , 'Hydrogenation of Aromatic Compounds in Synthetic Crude Distillates Catalyzed by Sulfided Ni-W/Alumina ,' J. Catal., 95, 155, 1985

PAPER NUMBER: 6

Vedrine, J., Auroux, A., Dejaive, P., Ducarme, V., Hoser, H., and Shuibao, Z. , 'Catalytic and Physical Properties of Phosphorus Modified ZSM-5 Zeolite ,' J. Catal., 73, 147, 1982

PAPER NUMBER: 7

Csicsery, S. , 'Shape Selective Catalysis in Zeolites ,' ACS Fuels Chem. Div., 28(2), 116,

PAPER NUMBER: 8

Donnelly, S. P., and Green, J. R. , 'Catalytic Dewaxing Process Improved ,' Oil & Gas J., 10/27/80, 77, 1980

PAPER NUMBER: 9

Chen, N. Y., and Garwood, W. E. , 'Some Catalytic Properties of ZSM-5, a New Shape Selectivity Zeolite ,' J. Catal., 52, 453, 1978

PAPER NUMBER: 10

Gorring, R. I. , 'Diffusion of Normal Paraffins in Zeolite T: Occurrence of Window Effect ,' J. Catal., 31, 17, 1973

PAPER NUMBER: 11

Chen, N.Y., Kaeding, W.W., and Dwyer, F.G., 'Para-Directed Aromatic Reactions over Shape-Selective Molecular Sieve Zeolite Catalysts ,' J. Amer. Chem. Soc., 101, 6783,

PAPER NUMBER: 12

Nag, N. K. , 'On the Mechanism of Hydrogenation Reactions Occurring Under Hydroprocessing Conditions,' Appl. Catal., 10, 53, 1984

PAPER NUMBER: 13

Rubin, M.K., Cynwyd, B., Plank, C.E., and Rosinski, E.J., 'Synthesis of Zeolite ZSM-4,' U.S. Patent, 4,021,447, 1977

PAPER NUMBER: 14

Argmer, R.J., and Landolt, G.R., 'Crystalline Zeolite ZSM-5 and Method of Preparing the Same,' U.S. Patent, 3,702,886, 1972

PAPER NUMBER: 15

Peirine, B.P., 'Synthesis of Zeolite ZSM-5,' U.S. Patent, 4,100,262, 1978

PAPER NUMBER: 16

Rollmann, L.D., 'ZSM-5 Particle Containing Aluminum-Free Shells on Its Surface,' U.S. Patent, 4,148,713, 1979

PAPER NUMBER: 17

Acres, G.J.K., Bird, A.J., Jenkins, J.W., King, F., Kemball, C. (Ed.), and Dowden, D.A. (E , 'The Design and Preparation of Supported Catalysts(A Review of the Recent Literature Published up to mid-1980,' A Specialist Periodical Report: Catalysis, 4(1), 1, 1980

PAPER NUMBER: 18

Kokotailo, G.T., 'Crystalline Zeolite Product Constituting ZSM-5/ZSM-11 Intermediates ,' U.S. Patent, 4,229,424, 1980

PAPER NUMBER: 19

Kokotailo, G.T., 'Catalytic Conversion with Crystalline Zeolite Product Constituting ZSM-5/ZSM-11 Intermediates ,' U.S. Patent, 4,289,607, 1981

PAPER NUMBER: 20

Chen, N.Y., Lucki, S.J., and Garwood, W.E., 'Dewaxing of Oils by Shape Selective Cracking and Hydrocracking over Zeolites ZSM-5 ,' U.S. Patent, 3,700,585, 19

PAPER NUMBER: 21

Ciric, J., 'Crystalline Zeolite ZSM-10,' U.S. Patent, 3,692,470, 1972

PAPER NUMBER: 22

Chu, P., 'Crystalline Zeolite ZSM-11,' U.S. Patent, 3,709,979, 1973

PAPER NUMBER: 23

Rosinski, E.J., Rubin, M.K., and Cynwyd, Bala, 'Hydrocarbon Conversion with ZSM-12,' US Patent, 3,970,544, 1976

PAPER NUMBER: 24

Dessau, R.M., 'Hydrogenation and Oxidation Using ZSM-5,' J. Catal., 77, 304, 1982

PAPER NUMBER: 25

Hargrove, J.D., Elkes, G.J., and Richardson, A.H., 'New Dewaxing Process Proven in Operations,' Oil and Gas J., 77(3), 103, 1979

PAPER NUMBER: 26

Akimoto, O., Iwamoto, Y., Kodama, S., and Takeuchi, C., 'Pilot Plant Automation for Catalyst Hydrotreating of Heavy Residual,' ACS. Petro. Chem. Div. Prep., August, 1010, 1983

PAPER NUMBER: 27

Zilora, K.S., and Erskine, W., 'A System for Integrating Pilot Plant Operating Data and Analytical Data,' ACS. Petro. Chem. Div. Prep., August, 973, 1983

PAPER NUMBER: 28

Johnson, H.D., Hogon, R.J., and McMurtrie, D.E., 'An Integrated Testing Facility for Bench Scale Catalyst Research,' ACS. Petro. Chem. Div. Prep., August, 960, 1983

PAPER NUMBER: 29

Rosinski, E.J., and Rubin, M.K., 'Crystalline Zeolite ZSM-12,' US Patent, 3,832,449, 1974

PAPER NUMBER: 30

Plank, C.J., Rosinski, E.J., and Givens, E.N., 'Converting Low Molecular Weight Olefins over Zeolites,' U.S. Patent, 4,021,502, 1977

PAPER NUMBER: 31

Ciric, J., 'Organic Compound Conversion by Zeolite ZSM-20 Catalysts,' US Patent, 4,021,331, 1977

PAPER NUMBER: 32

Plank, C.J., and Rosinski, J., 'Crystalline Zeolite and Method of Preparing Same,' US Patent, 4,046,859, 1977

PAPER NUMBER: 33

Rubin, M.K., Rosinski, E.J., and Plank, C.J., 'Crystalline Zeolite ZSM-34 and Method of Preparing the Same,' US Patent, 4,086,186, 1978

PAPER NUMBER: 34

Plank, C.J., and Rosinski, E.J., 'Crystalline Zeolite and Method of Preparing Same,' US Patent, 4,016,245, 1977

PAPER NUMBER: 35

Plank, C.J., and Rubin, M.K., 'Hydrocarbon Conversion over ZSM-38,' US Patent, 4,105,541, 1978

PAPER NUMBER: 36

Kokotailo, G.T., and Sawruk, S., 'Method for Improving Organic Cation-Containing Zeolites,' US Patent, 4,187,283, 1980

PAPER NUMBER: 37

Chu, C., 'Shape Selective Reactions with Group via Modified Zeolite Catalysts,' US Patent, 4,259,537, 1981

PAPER NUMBER: 38

Grose, R.W., and Flanigen, E.M., 'Crystalline Silica,' US Patent, 4,061,724, 1977

PAPER NUMBER: 39

Chang, C.D., 'Hydrocarbons from Methanol,' Catal. Rev. -Sci. Eng., 25(1), 1-18, 1983

PAPER NUMBER: 40

Chuang, S.C., Goodwin, Jr, J.G., and Wender, I., 'The Effect of Alkali Promotion on CO Hydrogenation Over Rh/TiO₂,' J. Catal., 95, 435-446, 1985

PAPER NUMBER: 41

Prasad, K.H.V., Prasad, K.B.S., Mallikarjunan, M.M., and Vaidyeswaran, R., 'Self-Poisoning and Rate Multiplicity in Hydrogenation of Benzene,' J. Catal., 84, 65-73, 1984

PAPER NUMBER: 42

Inu, T., and Okazumi, F., 'Propane Conversion to Aromatic Hydrocarbons on Pt/H-ZSM-5 Catalysts,' J. Catal., 90, 366-367, 1984

PAPER NUMBER: 43

Takeuchi, K., Matsuzaki, T., Arakawa, H., and Sugi, Y., 'Synthesis of Ethanol from Syngas Over Co-Re-Sr/SiO₂ Catalysts,' Appl. Catal., 18, 325-334, 1985

PAPER NUMBER: 44

Tagawa, T., Pleizier, G., and Amenomiya, Y., 'Methanol Synthesis from Co₂+H₂. I. Characterization of Catalysts by TPD,' Appl. Catal., 18, 285-293, 1985

PAPER NUMBER: 45

Inui, T., Medhanavin, D., Praserthdam, P., Fukuda, K., Ukawa, T., Sukamoto, A., and Miyamoto, A., 'Methanol Conversion to Hydrocarbons on Novel Vanadosilicate Catalysts,' Appl. Catal., 18, 311-324, 1985

PAPER NUMBER: 46

Foster, N.R., 'Direct Catalytic Oxidation of Methane to Methanol - A Review,' Appl. Catal., 19, 1-11, 1985

PAPER NUMBER: 47

Knozinger, H., and Ratnasamy, P., 'Catalytic Aluminas: Surface Models and Characterization of Surface Sites,' Catal. Rev. -Sci. Eng., 17(1), 31-70, 1978

PAPER NUMBER: 48

Miller, Stephen J., and Hughes, R., 'Combination Process for Upgrading Naphtha,' US Patent, 4,190,519, 1980

PAPER NUMBER: 49

Kaeding, W.W., Chu, C., Young, L.B., Weinstein, B., and Butter, S.A., 'Selective Alkylation of Toluene with Methanol to Produce para-Xylene,' J. Catal., 67, 159, 1981

PAPER NUMBER: 50

Yanik, Stephen J., Demmel, Edward J., Humphries, Adrian P., and Campagna, R., 'FCC Catalysts Containing Shape-Selective Zeolites Boost Gasoline Octane Number and Yield,' Oil and Gas J., 83(19), 108, 1958

PAPER NUMBER: 51

Tabak, S.A., and Krambeck, F.J., 'Shaping Process Makes Fuels,' Hydrocarbon Processing, 72(9), 1985

PAPER NUMBER: 52

Weitkamp, Jens, Jacobs, Peter A., and Martens, Johan A., 'Isomerization and Hydrocracking of C9 Through C16 n-Alkanes on Pt/H-ZSM-5 Zeolite,' Appl. Catal., 8, 123, 1983

PAPER NUMBER: 53

Smith, K.W., Starr, W.C., and Chen, N.Y., 'New Process Dewaxes Lube Base Stocks,' Oil & Gas J., 78(21), 75, 1980

PAPER NUMBER: 54

Brunauer, S., Emmett, P.H., and Teller, E., 'Adsorption of Gases in Multimolecular Layers,' J. Amer. Chem. Soc., 60, 317, 1938

PAPER NUMBER: 55

Guisnet, M., and Perot, G., 'Shape Selective Catalysis and Reaction Mechanisms,' J. Amer. Chem. Soc., 28(2), 137, 1983

PAPER NUMBER: 56

Jacobs, P.A., Marten, J.A., Weitkamp, J., and Beyer, J., 'Shape Selectivity in High Silica Zeolites,' Faraday Discussions of the Chemical Society, 72, 353, 1981

PAPER NUMBER: 57

Corma, A., Monton, J.B., and Orchilles, A.V., 'Cracking of n-Heptane on a ZSM-5 Zeolite, the Influence of Acidity and Pore Structure,' Appl. Catal., 16, 59, 1985

PAPER NUMBER: 58

Qin, G., Zheng, L., Xie, Y., and Wu, C., 'On the Framework Hydroxyl Groups of HZSM-5,' J. Catal., 95, 609, 1985

PAPER NUMBER: 59

Derouane, Eric G., Nagy, Janos B., Dejaive, Pierre, Van Hooff, Jan, Vedrine, J.C., and Naccache, C., 'Elucidation of the Mechanism of Conversion of Methanol and Ethanol to Hydrocarbons on a New Type of Synthetic Zeolite,' J. Catal., 53, 40, 1978

PAPER NUMBER: 60

Chu, P., 'Aromatization of Ethane,' U.S. Patent, 4,120,910, , 1978

PAPER NUMBER: 61

Dukek, W.G., 'Aviation and Other Gas Turbine Fuels,' Kirk-Othmer Encyclopedia of Chemical Technology, 3, 328, 1981

PAPER NUMBER: 62

Chu, C., Guenther, H.K., Lago, R.M., and Chang, C.D., 'Isomorphous Substitution in Zeolite Frameworks,' J. Catal., 93, 451, 1985

PAPER NUMBER: 63

Dessau, R.M., 'Shape-Selective Platinum/ZSM-5 Catalysts,' J. Catal., 89, 520, 1984

PAPER NUMBER: 64

Fraenkel, D., Cherniavsky, M., and Levy, M., 'Evidence for the Involvement of Two Sieving Effects in the Catalytic Alkylation of Aromatics over HZSM5-Type Zeolites,' 8th International Congress on Catalysis Proceeding, IV-545, 1984

PAPER NUMBER: 65

Chang, C.D., Chu, C.T., and Socha, R.F., 'Methanol Conversion to Olefins over ZSM-5,' J. Catal., 86, 289, 1984

PAPER NUMBER: 66

Fort, A.W., and Davis, B.H., 'Carbon-14 Rearrangement in the Alkylation of Benzene with [1-14C]Ethanol over ZSM-5 Catalyst,' J. Catal., 96, 357, 1985

PAPER NUMBER: 67

Young, L.B., Butter, S.A., and Kaeding, W.W., 'Shape Selective Reactions with Zeolite Catalysts,' J. Catal., 76, 418, 1982

PAPER NUMBER: 68

Dejaive, P., Auroux, A., Gravelle, P.C., and Vedrine, J.C., 'Methanol Conversion on Acidic ZSM-5, Offretite, and Mordenite Zeolites: A Comparative Study of the Formation and Stability of Coke Deposits,' J. Catal., 70, 123, 1981

PAPER NUMBER: 69

Kagi, D., 'In Re: Mechanism of Conversion of Methanol over ZSM-5 Catalyst,' J. Catal., 69, 242, 1981

PAPER NUMBER: 70

Dejaive, P., Vedrine, J.C., Bolis, V., and Derouane, E.G., 'Reaction Pathways for the Conversion of Methanol and Olefins on HZSM-5 Zeolite,' J. Catal., 63, 331, 1980

PAPER NUMBER: 71

Andersson, J.R., and Christov, V., 'Mechanism of Some Conversion over ZSM-5 Catalyst,' J. Catal., 61, 477, 1980

PAPER NUMBER: 72

Kaeding, W.W., and Butter, S.A., 'Production of Chemicals from Methanol. I. Low Molecular Weight Olefins,' J. Catal., 61, 155, 1980

PAPER NUMBER: 73

Chang, C.D., and Silvestri, A.J., 'The Conversion of Methanol and Other O-Compounds to Hydrocarbons over Zeolites Catalysts,' J. Catal., 47, 240, 1977

PAPER NUMBER: 74

Gregg, S.J., and Sing, K.S.W., 'Chemisorption,' Adsorption, Surface Area and Porosity, Chap. 6, 252, 1967

PAPER NUMBER: 75

Meisel, S.L., McCullough, J.P., Lechthaler, C.H., and Weisz, P.B., 'Gasoline from Methanol in One Step,' Chemtech, February, 86, 1976

PAPER NUMBER: 76

Haag, W.O., 'Acid Catalyst with Medium Pore Zeolites,' The Sixth International Zeolite Conference, 466, 1984

PAPER NUMBER: 77

Sinfelt, J.H., 'Bifunctional Catalysis,' Adv. Chem. Eng., 37, 1964

PAPER NUMBER: 78

Mucka, V., Ostrihonova, A., Kopernicky, I., and Mikula, O., 'Dearomatization of Jet Fuel on an Irradiated Supported-Platinum Catalyst,' Radiat. Phys. Chem., 21, 481, 1983

PAPER NUMBER: 79

Dubovkin, N.F., Tararyshkin, M.E., and Abashina, L.D., 'Vapor Pressure and Critical Parameters of Jet Fuels,' Chem. & Tech. of Fuels and Oils (Russ.), (4), 207, 1981

PAPER NUMBER: 80

Krasnaya, L.V., Postnikova, N.G., and Zrellov, V.N., 'Chromatographic Method for Determination of Content of Aromatic Hydrocarbons in Aviation Gasolines,' Chem. & Tech. of Fuels and Oils (Russ.), (2), 100, 1985

PAPER NUMBER: 81

Narita, E., Sato, K., and Okabe, T., 'A Convenient Method for Crystallization of Zeolite ZSM-5 by Using Seed Crystals in Acetone/Water Mixture System,' Chemistry Letters, 1055, 1984

PAPER NUMBER: 82

Solash, Jeffrey, Hazlett, Robert N., Burnett, Jack C., Beal, Erna, and Hall, James M., 'Relation Between Fuel Properties and Chemical Composition, Chemical Characterization of U.S. Navy Shale-Oil Fuels,' ACS Symp. Ser., 163, 237, 1981

PAPER NUMBER: 83

Solash, Jeffrey, Hazlett, Robert N., Burnett, Jack C., Beal, Erna, and Hall, James M., 'Relation Between Fuel Properties and Chemical Composition, Physical Properties of U.S. Navy Shale-Oil Fuels,' ACS Symp. Ser., 163, 253, 1981

PAPER NUMBER: 84

Solash, Jeffrey, Hazlett, Robert N., Burnett, Jack C., Beal, Erna, and Hall, James M., 'Relation Between Fuel Properties and Chemical Composition, Stability of Oil Shale-Derived Jet Fuel,' ACS Symp. Ser., 163, 267, 1981

PAPER NUMBER: 85

Narita, E., Sato, K., Yatabe, N., and Taijiro, O., 'Synthesis and Crystal Growth of Zeolite ZSM-5 from Sodium Aluminosilicate System Free of Organic Templates,' Ind. Eng. Chem. Product Res. Dev., 24, 507, 1985

PAPER NUMBER: 86

Harrison, I.D., Leach, H.F., and Whan, D.A., 'Correlation Between the Sorptive and Catalytic Properties of a Series of Pentasil Zeolites,' The Sixth International Zeolite Conference, 479, 1984

PAPER NUMBER: 87

Van Hooft, J.H.C., Van den Berg, J.P., Wolthuisen, J.P., and Volmer, A., 'The Reaction Mechanism of the First C-C Bond Formation in the Methanol to Gasoline Process,' The Sixth International Zeolite Conference, 489, 1984

PAPER NUMBER: 88

Vedrine, J.C., Auroux, A., Coudurier, G., Engelhard, P., Gallez, J.P., and Szabo, G., 'Shape Selectivity and Acidity of ZSM-5 and ZSM-11 Type Zeolites,' The Sixth International Zeolite Conference, 497, 1984

PAPER NUMBER: 89

Sosa, R.C., Nitta, M., Beyer, H.K., and Jacobs, P.A., 'Shape-Selectivity of Pentasil-type Zeolites in the Bifunctional Conversion of Ethylbenzene and Propylbenzene,' The Sixth International Zeolite Conference, 508, 1984

PAPER NUMBER: 90

Lazarenko, V.P., Shirokova, G.B., Ermakova, T.I., and Sablina, Z.A., 'Modern Methods for Evaluating Jet Fuel Properties,' Chem. & Tech. of Fuels and Oils, (6), 480, 1976

PAPER NUMBER: 91

Gorenkov, A.F., 'Comparative Evaluation of Jet Fuel Quality Level,' Chem. & Tech. of Fuels and Oils, (12), 762, 1980

PAPER NUMBER: 92

Dubovkin, N.F., and Malanicheva, V.G., 'Density and Viscosity of Jet Fuels,' Chem. & Tech. of Fuels and Oils, (8), 543, 1980

PAPER NUMBER: 93

de Gaudemaris, G., Franck, J.P., Lepage, J.F., and Bonnifay, P., 'Hydrogenate for Better Jet Fuel,' Hydrocarbon Process., 56(11), 287, 1977

PAPER NUMBER: 94

Ostrihonova, Alica, Kopernicky, Ivan, Mikula, Oldrich, and Mucka, Viliam, 'Dearomatization of a Jet Fuel Fraction on a Platinum Catalyst,' Collect. Czech. Chem. Commun., 47(11), 2858, 1982

PAPER NUMBER: 95

Post, M.F.M., Amstel, J.V., and Kouwenhoven, H.W., 'Diffusion and Catalytic Reaction of 2,2 Dimethylbutane in ZSM-5 Zeolite,' The Sixth International Zeolite Conference, 517, 1984

PAPER NUMBER: 96

Heering, J., Riekert, L., and Marosi, L., 'Sorption and Catalytic Reaction in Different Preparation of Zeolite H-ZSM-5,' The Sixth International Zeolite Conference, 528, 1984

PAPER NUMBER: 97

Oudejans, J.C., Van der Gaag, F.J., and Van Bekkum, H., 'Ammoxidation of Toluene and Related Aromatics over Zeolite ZSM-5. A New Application of Zeolite ZSM-5,' The Sixth International Zeolite Conference, 536, 1984

PAPER NUMBER: 98

Holderich, W., Eichhorn, H., Lehnert, R., Marosi, L., Mross, W., and Reinke, R., 'Aluminosilicate and Borosilicate Zeolites and Their Use in the Conversion of Methanol to Olefins,' The Sixth International Zeolite Conference, 545, 1984

PAPER NUMBER: 99

Occelli, M.L., Innes, R.A., Apple, T.M., and Garstein, B.C., 'Surface Properties of Offretite and ZSM-34 Zeolites,' the Sixth International Zeolite Conference, 674, 1984

PAPER NUMBER: 100

Soxhoorn, G., van Santen, R.A., van Erp, W.A., Hays, G.R., Alma, N.C.M., and Huis, R., 'A High-Resolution Solid-State ¹³C NMR Investigation of Occluded Templates in Pentasil-Type Zeolites: Some ²⁹Si Solid-State NMR Charact. ZSM5,' The Sixth International Zeolite Conference, 694, 1984

PAPER NUMBER: 101

Taylor, W.F., 'Kinetics of Deposit Formation from Hydrocarbons. III. Heterogeneous and Homogeneous Metal Effects,' J. Appl. Chem., 18, 251, 1968

PAPER NUMBER: 102

Robertson, A.G., and Williams, R.E., 'Jet Fuel Specifications: The Need for Change,' Shell Aviation News, 435, 1976

PAPER NUMBER: 103

Hsieh, B.C.B., Wood, R.E., and Anderson, L.L., 'Fractionation of Low Temperature Coal Tar by Gel Permeation Chromatography,' Anal. Chem., 41, 1066, 1969

PAPER NUMBER: 104

Dalling, Don K., Brent, Brent K., and Pugmire, Ronald J., 'Carbon-13 and Proton Nuclear Magnetic Resonance Analysis of Shale-derived Refinery Products and Jet Fuels,' NASA Contractor Report 174761, Sep., , 1984

PAPER NUMBER: 105

Chang, C.D., Chu, C.T., and Socha, R.F., 'Methanol Conversion to Olefins over ZSM-5,' J. Catal., 86, 289, 1984

PAPER NUMBER: 106

Young, L.B., Butter, S.A., and Kaeding, W.W., 'Shape Selective Reactions with Zeolite Catalysts,' J. Catal., 76, 418, 1982

PAPER NUMBER: 107

Dejaifve, P., Auroux, A., Gravelle, P.C., and Vedrine, J.C., 'Methanol Conversion on Acidic ZSM-5, Offretite, and Mordenite Zeolites: A Comparative Study of the Formation and Stability of Coke Deposits,' J. Catal., 70, 123, 1981

PAPER NUMBER: 108

Chang, C.D., 'Mechanism of Conversion of Methanol over ZSM-5 Catalyst,' J. Catal., 69, 242, 1981

PAPER NUMBER: 109

Dejaifve, P., Vedrine, J.C., Bolis, V., and Derouane, E.G., 'Reaction Pathways for the Conversion of Methanol and Olefins on HZSM-5 Zeolite,' J. Catal., 63, 331, 1980

PAPER NUMBER: 110

Anderson, J.R., Mole, T., and Christov, V., 'Mechanism of Some Conversions over ZSM-5 Catalyst,' J. Catal., 61, 477, 1980

PAPER NUMBER: 111

Kaeding, W.W., and Butter, S.A., 'Production of Chemicals from Methanol,' J. Catal., 61, 155, 1980

PAPER NUMBER: 112

Chang, C.D., and Silvestri, A.J., 'The Conversion of Methanol and Other O-Compounds to Hydrocarbons over Zeolite Catalysts,' J. Catal., 47, 240, 1977

PAPER NUMBER: 113

Liederman, D., Yurchak, S., Kuo, J.C.W., and Lee, W., 'Mobil Methanol-to-Gasoline Process,' J. Energy, 6, 340, 1982

PAPER NUMBER: 114

Miesel, S.L., McCullough, J.P., Lechthaler, C.H., and Weisz, P.B., 'Gasoline from Methanol in One Step,' CHEMTECH, Feb., 86, 1976

PAPER NUMBER: 115

Wise, J.J., and Voltz, S.E., 'Conversion of Methanol to High-Octane Gasoline,' Contractor Report, ,

PAPER NUMBER: 116

Hochevar, S., Bochevskii, G.V., Drzaj, B., and Ione, J.G., 'Methanol-Based Synthesis of Hydrocarbons on Bifunctional Y-type Zeolites,' React. Kinet. Catal. Lett., 13(4), 425, 1980

PAPER NUMBER: 117

Sayed, M.B., Kydd, R.A., and Cooney, R.P., 'A Fourier-Transform Infrared Spectral Study of H-ZSM-5 Surface Sites and Reactivity Sequences in Methanol Conversion,' J. Catal., 88, 137, 1984

PAPER NUMBER: 118

Gilson, J.P., and Derouane, E.D., 'On the External and Intracrystalline Surface Catalytic Activity of Pentasil Zeolites,' J. Catal., 88, 538, 1984

PAPER NUMBER: 119

Yopsoe, N., Pedersen, K., and Derouane, E.G., 'Infrared and Temperature-Programmed Desorption Study of the Acidic Properties of ZSM-5-Type Zeolites,' J. Catal., 70, 41, 1981

PAPER NUMBER: 120

Grady, M.C., and Gorte, R.J., 'Adsorption of 2-Propanol and Propene on H-ZSM-5: Evidence for Stable Carbonium Ion Formation,' J. Phys. Chem., 89, 1305, 1985

PAPER NUMBER: 121

Jacobs, P.A., 'Framework Hydroxyl Groups of H-ZSM-5 Zeolites,' J. Phy. Chem., 86, 3050, 1982

PAPER NUMBER: 122

Gilbert, John B., and Henry, H. Clarke, 'Process for the Hydrogenation of Olefins and Aromatic Compounds,' U.S. Patent, 4,240,900, 1980

PAPER NUMBER: 123

Fisher, Dennis H., 'High Energy Fuel Compositions,' U.S. Patent, 4,394,528, 1983

PAPER NUMBER: 124

Brunn, Louis W., and Lopez, Jaime, 'Production of Jet and Diesel Fuels from Highly Aromatic Oils,' U.S. Patent, 4,427,534, 1984

PAPER NUMBER: 125

Hamner, Glen P., 'Production of Jet and Diesel Fuels,' U.S. Patent, 4,501,653, 1985

PAPER NUMBER: 126

Cooper, J.R., and Taylor, L.T., 'GC/FT-IR Experimental Considerations in the Separation of Complex Hydrocarbon Mixtures Using Fused Silica Columns,' Applied Spectroscopy, 38, 366, 1984

PAPER NUMBER: 127

Cookson, David J., Latten, Jozef L., Shaw, Ian M., and Smith, Brian E., 'Property-Composition Relationships for Diesel and Kerosene Fuels,' Fuel, 64, 509, 1985

PAPER NUMBER: 128

Pope, C.G., 'Sorption of Benzene, Toluene, and P-xylene on Silicate and H-ZSM-5,' J. Phys. Chem., 90, 835, 1985

PAPER NUMBER: 129

Dessau, R.M., 'On the H-ZSM-5 Catalyzed Formation of Ethylene from Methanol or Higher Olefins,' J. Catal., 99, 111, 1986

PAPER NUMBER: 130

Anunziata, O.A., Orio, O.A., Herrero, E.R., Lopez, A.F., Perez, C.F., and Suarez, A.R., 'Conversion of Fermentation Products to Aromatic Hydrocarbons Over Zeolite-Type HZSM-5 In One Step,' Appl. Catal., 15, 235-245, 1985

PAPER NUMBER: 131
Chow, Ming, Park, S.H., and Sachtler, W.M.H., 'Ring Enlargement and Ring Opening Over Mono- and Bifunctional Catalysts,' Appl. Catal., 19, 349-364, 1985

PAPER NUMBER: 132
Engelen, C.W.R., Wolthuisen, J.P., and van Hooff, J.H.C., 'Reactions of Propane Over a Bifunctional Pt/H-ZSM-5 Catalyst,' Appl. Catal., 19, 153-163, 1985

PAPER NUMBER: 133
Bezouhanova, C.P., Dimitrov, Chr., Nenova, V., Dimitrov, L., and Lechert, H., 'Cracking of Paraffins On Pentasils With Different Si/Al Ratios,' Appl. Catal., 19, 101-108, 1985

PAPER NUMBER: 134
Scholle, K.F.M.G.J., Veeman, W.S., Frenken, P., and van der Walden, 'Characterization of Intermediate TPA-ZSM-5 Type Structures During Crystallization,' Appl. Catal., 17, 233-259, 1985

PAPER NUMBER: 135
Van Der Gaag, F.J., Jansen, J.C., and Van Bekkum, H., 'Template Variation In The Synthesis of Zeolite ZSM-5,' Appl. Catal., 17, 261-271, 1985

PAPER NUMBER: 135
Ducarme, Valentin, and Vedrine, Jacques, 'ZSM-5 and ZSM-11 Zeolites: Influence Of Morphological and Chemical Parameters On Catalytic Selectivity And Deactivation,' Appl. Catal., 17, 175-184, 1985

PAPER NUMBER: 137
Mole, T., Anderson, J.R., and Creer, G., 'The Reaction of Propane Over ZSM-5-H and ZSM-5-Zn Zeolite Catalysts,' Appl. Catal., 17, 141-154, 1985

PAPER NUMBER: 138
Corma, A., Monton, J.B., and Orchilles, A.V., 'Cracking of N-Heptane On A HZSM-5 Zeolite. The Influence of Acidity and Pore Structure,' Appl. Catal., 16, 59-71, 1985

PAPER NUMBER: 139
Chu, Chin-Chiun, 'Selective Production of Para-Xylene,' U.S. Patent 4,250,345, 1981

PAPER NUMBER: 140
Fraenkel, D., Cherniavsky, M., and Levy, M., 'Evidence For The Involvement of Two Sieving Effects in the Catalytic Alkylation of Aromatics over HZSM5-Type Zeolites,' 8th Internatl. Con. on Catal. Proc., DEHEMA, IV, 545-554, 1984

PAPER NUMBER: 141

Burwell, R.L., 'Supported Pt, Pd, and Ru Catalysts,' *Langmuir*, 2, 2, 1986

PAPER NUMBER: 142

McLellan, G.D., and Howe, R.F., 'J. Catal.', 99, 486, 1986

PAPER NUMBER: 143

Rieck, J.S., and Bell, A.T., 'Studies of the Interaction of H₂ and CO with Pd/TiO₂ and TiO₂-promoted Pd/SiO₂,' *J. Catal.*, 99, 262, 1986

PAPER NUMBER: 144

Rieck, J.S., and Bell, A.T., 'Studies of the Interaction of H₂ and CO with Pd/SiO₂ Promoted with La₂O₃, CeO₂, Pr₆O₁₁, Nd₂O₃ and Sm₂O₃,' *J. Catal.*, 99, 278, 1986

PAPER NUMBER: 145

Santill, D.S., 'The Mechanism of Aromatic Transalkylation in ZSM-5,' *J. Catal.*, 99, 327, 1986

PAPER NUMBER: 146

Santill, D.S., 'Pore Probe: A New Technique for Measuring the Concentration of Molecules Inside Porous Materials at Elevated Temperatures,' *J. Catal.*, 99, 335, 1986

PAPER NUMBER: 147

Viswanathan, B., andopalakrishna, V., 'Effect of Support and Promoter in Fischer-Tropsch Cobal Catalysts,' *J. Catal.*, 99, 342, 1986

PAPER NUMBER: 148

Smith, K.J., and Everson, R.C., 'Fischer-Tropsch Reaction Studies with Supported Ruthenium Catalysts. II. Effect of Oxidative Pretreatment at Elevated Temperatures,' *J. Catal.*, 99, 349, 1986

PAPER NUMBER: 149

Yamashita, H., Yoshikawa, M., Funabiki, T., and Yoshida, S., 'Catalysis by Amorphous Metal Alloys. V. Hydrogenation of Carbon Monoxide Over Amorphous Ni₇₈P₁₉La₃ Ribbon Alloys,' *J. Catal.*, 99, 375, 1986

PAPER NUMBER: 150

Van Tiep, L., Bureau-Tardy, M., Bugli, G., Djega-Mariadas, sou, G., Che, M., and Bond, G.C., 'The Effect of Reduction Conditions on the Chloride Content of Ir/TiO₂ Catalysts and Their Activity for Benzene Hydrogenation,' *J. Catal.*, 99, 449, 1986

PAPER NUMBER: 151

Lee, C., Schmidt, L.D., Moulder, J.F., and Rusch, T.W., 'Effects of Particle Structures on CO Hydrogenation on Ni on SiO₂,' J. Catal., 99, 472, 1986

PAPER NUMBER: 152

Dessau, R.M., 'On the H-ZSM-5 Catalyzed Formation of Ethylene from Methanol or Higher Olefins,' J. Catal., 99, 111, 1986

PAPER NUMBER: 153

Fleisch, T.H., Meyers, B.L., Ray, G.J., Hall, J.B., and Marshall, C.L., 'Hydrothermal Dealumination of Faujasites,' J. Catal., 99, 117, 1986

PAPER NUMBER: 154

Presland, A.E.B., Price, G.L., and Trimm, D.L., 'Particle Size Effects During the Sintering of Silver Oxidation Catalysts,' J. Catal., 26, 313, 1972

PAPER NUMBER: 155

Williams, A., Butler, G.A., and Hammonds, J., 'Sintering of Nickel-Alumina Catalysts,' J. Catal., 24, 352, 1972

PAPER NUMBER: 156

Clay, R.D., and Petersen, E.E., 'Catalytic Activity of an Evaporated Platinum Film Progressively Poisoned with Arsine,' J. Catal., 16, 32, 1970

PAPER NUMBER: 157

Goldstein, M.S., and Morgan, T.R., 'Quinoline Titration of Cumene-Cracking Activity on Type-Y Molecular Sieve Catalysts,' J. Catal., 16, 232, 1970

PAPER NUMBER: 158

Hughes, T.R., Houston, R.J., and Sieg, R.P., 'Flow Adsorption Method for Catalyst Metal Surface Measurements,' Ind. Eng. Chem. (Proc. Des. Devel.), 1, 96, 1962

PAPER NUMBER: 159

Eberly, P.E., Kimberlin, C.N., Miller, W.H., and Drushel, H.V., 'Coke Formation on Silica-Alumina Cracking Catalysts,' Ind. Eng. Chem. (Proc. Des. Devel.), 5, 193, 1966

PAPER NUMBER: 160

Voorhies, A., 'Carbon Formation in Catalytic Cracking,' Ind. Eng. Chem., 37, 318, 1945

PAPER NUMBER: 161

Herrmann, R.A., Adler, S.F., Goldstein, M.S., and Debaun, R.M., 'The Kinetics of Sintering of Platinum Supported on Alumina,' J. Phys. Chem., 65, 2189, 1961

PAPER NUMBER: 162

Pines, H., and Haag, W.O., 'Alumina: Catalyst and Support. I. Alumina, its Intrinsic Acidity and Catalytic Activity,' J. Amer. Chem. Soc., 82, 2471, 1960

PAPER NUMBER: 163

Rudershausen, C.G., and Waston, C.C., 'Variables Affecting Activity of Molybdena-Alumina Hydroforming Catalyst in Aromatization of Cyclohexane,' Chem. Eng. Sci., 3, 110, 1955

PAPER NUMBER: 164

Haldeman, R.G., and Botty, M.C., 'On the Nature of the Carbon Deposit of Cracking Catalysts,' J. Phys. Chem., 63, 489, 1959

PAPER NUMBER: 165

Aga, R.L., Debus, H.R., and Allen, E.R., 'Arofining Improves Jet Fuels,' Hydrocarbon proc., April, 153, 1971

PAPER NUMBER: 166

Haggin, J., 'Dual Role in Chemicals, Fuel Enhances Methanol's Importance,' C&EN, August, 24, 1986

PAPER NUMBER: 167

Sedran, U.S., and Figoli, N.S., 'Relation Between Acidity and Activity During the Transformation of Methanol to Hydrocarbons on Amorphous Silica-Alumina,' Appl. Catal., 19, 317, 1985

PAPER NUMBER: 168

Prasad, Y.S., and Bakhshi, N.N., 'Effect of Pretreatment of HZSM-5 Catalyst on its Performance in Canola Oil Upgrading,' Appl. Catal., 18, 71, 1985

PAPER NUMBER: 169

Chantal, P.D., Kaliaguine, S., and Grandmaison, J.L., 'Reactions of Phenolic Compounds Over ZSM-5,' Appl. Catal., 18, 133, 1985

PAPER NUMBER: 170

Corma, A., Monton, J.B., and Orchille, A.V., 'Cracking of n-Heptane on a HZSM-5 Zeolite. The Influence of Acidity and Pore Structure,' Appl. Catal., 17, 59, 1985

PAPER NUMBER: 171

Mole, T., Anderson, J.R., and Creer, G., 'The Reaction of Propane Over ZSM-5-H and ZSM-5-Zn in Zeolite Catalysts,' Appl. Catal., 17, 141, 1985

PAPER NUMBER: 172

Ducarme, V., and Vedrine, J.C., 'ZSM-5 and ZSM-11 Zeolites: Influence of Morphological and Chemical Parameters on Catalytic Selectivity and Deactivation,' Appl. Catal., 17, 175, 1985

PAPER NUMBER: 173

Van der Gaag, F.J., Jansen, J.C., and Van Bekkum, H., 'Template Variation in the Synthesis of ZSM-5,' Appl. Catal., 17, 261, 1985

PAPER NUMBER: 174

, , , ,

PAPER NUMBER: 175

Borade, R.B., Hegde, S.G., Kulkarni, S.B., and Ratnasamy, P., 'Active Centres Over HZSM5 Zeolites For Paraffin Cracking,' Appl. Catal., 13, 27, 1984

PAPER NUMBER: 176

Gabelica, Zelimir, Blom, Niels, and Derouane, Eric G., 'Synthesis and Characterization of ZSM-5 Type Zeolites. III. A Critical Evaluation of the Role of Alkali and Ammonium Cations,' Appl. Catal., 5, 227, 1983

PAPER NUMBER: 177

Gabelica, Zelimir, Derouane, Eric G., and Blom, Niels, 'Synthesis and Characterization of Pentasil Type Zeolites. II. Structure-Directing Effect of the Organic Base or Cation,' Appl. Catal., 5, 109, 1983

PAPER NUMBER: 178

Chandawar, K.H., Kulkarni, S.B., and Ratnasamy, P., 'Alkylation of Benzene With Ethanol Over ZSM5 Zeolites,' Appl. Catal., 4, 287, 1982

PAPER NUMBER: 179

Babu, G.P., Hegde, S.G., Kulkarni, S.B., and Ratnasamy, P., 'Active Sites over HZSM5 Zeolites. I. Xylene Isomerization,' J. Catal., 81, 471, 1983

PAPER NUMBER: 180

Jaras, Sven, 'Rapid Methods of Determining the Metals Resistance of Cracking Catalysts,' Appl. Catal., 2, 207, 1982

PAPER NUMBER: 181

Saha, N.C., and Wolf, E.E., 'CO Methanation Activity and XPS Studies of Pd Supported On ZSM5 and Y Zeolites,' Appl. Catal., 13, 101, 1984

PAPER NUMBER: 182

Hidalgo, Carmela V., Itoh, Hirofumi, Hattori, Tadashi, Niwa, Miki, and Murakami, Y., 'Measurement of the Acidity of Various Zeolites by Temperature Programmed Desorption of Ammonia,' J. Catal., 85, 362, 1984

PAPER NUMBER: 183

Prasad, Y.S., and Bakhshi, N.N., 'Effect of Pretreatment of HZSM-5 Catalyst On Its Performance in Canola Oil Upgrading,' Appl. Catal., 18, 71, 1985

PAPER NUMBER: 184

Vedrine, Jacques C., Aurous, Zline, Bolis, Vera, Dejaifve, P., Derouane, Eric, and Nagy, Janos, 'Infrared, Microcalorimetric, and Electron Spin Resonance Investigations of the Acidic Properties of the H-ZSM-5 Zeolite,' J. Catal., 59, 248, 1979

PAPER NUMBER: 185

Balkrishnan, I., Rao, B.S., Hegde, S.G., Kotasthane, A., Kulkarni, S.B., and Ratnaswamy, P., 'Catalytic Activity and Selectivity in the Conversion of Methanol to Light Olefins,' J. Molec. Catal., 17, 261, 1982

PAPER NUMBER: 186

Balsama, S., Beltrame, P., Beltrame, P.L., Carniti, P., Forni, L., and Zuretti, G., 'Alkylation of Phenol With Methanol Over Zeolites,' Appl. Catal., 13, 161, 1984

PAPER NUMBER: 187

Nelson, Harold C., Lussier, Roger J., and Still, Margaret E., 'An Estimate of Surface Acidity in Amorphous Catalysts From Temperature-Programmed Desorption Measurements. A Simple Tool For Catalyst Charac,' Appl. Catal., 7, 113, 1983

PAPER NUMBER: 188

Chang, C.D., Chu, C.T.W., Perkins, D.P., and Valyocsik, E.W., 'Olefins from Methanol and/or Dimethyl Ether,' U.S. Patent, 4,476,338, , 1984

PAPER NUMBER: 189

Chang, C.D., and Lang, W.H., 'Conversion of Methanol to Gasoline with Minimum Durene Production,' U.S. Patent, 4,013,732, , 1977

PAPER NUMBER: 190

Rubin, M.K., Plank, C.J., and Rosinski, E.J., 'Organic Compound Conversion over ZSM-23,' US Patent, 4,104,151, , 1978

PAPER NUMBER: 191

Olson, D.H., and Haag, W.O., 'Xylene Isomerization,' US Patent, 4,159,282, , 1979

PAPER NUMBER: 192

Grose, R.W., and Flanigen, E.M., 'Novel Zeolite Compositions and Processes for Preparing and Using Same,' US Patent, 4,257,885, , 1981

PAPER NUMBER: 193

Rollmann, L.D., and Valyocsik, E.W., 'Continuous-Stream Method of Preparing Crystalline Zeolites,' European Patent Application, 0021675, , 1980

PAPER NUMBER: 194

Rollmann, L.D., and Valyocsik, E.W., 'Synthesis of Large Crystal Zeolite ZSM-5 and Zeolites so Made,' European Patent Application, 0021674, , 1980

PAPER NUMBER: 195

Doherty, H.G., Rosinsid, E.J., and Plank, C.J., 'Crystalline Zeolites, Synthesis and Use Thereof,' European Patent Application, 0015702, , 1980

PAPER NUMBER: 196

Rodewald, P.G., and Haag, W.O., 'Decomposition of Formic Acid in Very Low Concentration,' US Patent, 4,093,543, , 1978

PAPER NUMBER: 197

Rodewald, P.G., 'Manufacture of Light Olefins,' US Patent, 4,066,714, , 1978

PAPER NUMBER: 198

Kaeding, W.W., and Young, L.B., 'Selective Production of Para-Xylene,' US Patent, 4,034,053, , 1977

PAPER NUMBER: 199

Kaeding, W.W., 'Selective Production of Para-Xylene,' US Patent, 4,029,716, , 1977

PAPER NUMBER: 200

Butter, S.A., 'Selective Production of Para-Xylene,' US Patent, 4,007,231, , 1977

PAPER NUMBER: 201

Dessau, R.M., 'Diels-Alder Cyclization over Low Acidity Large-Pore Zeolites,' US Patent, 4,384,153, , 1983

PAPER NUMBER: 202

Young, L.B., 'ZSM-12 Cycloolefin Dimerization,' US Patent, 4,255,600, , 1981

PAPER NUMBER: 203

Rosinski, E.J., and Rubin, M.K., 'Crystalline Zeolite ZSM-12,' US Patent, 3,832,449, , 1974

PAPER NUMBER: 204

Jenkins, E.E., 'Synthetic Crystalline Zeolite and Preparation Thereof,' US Patent, 3,578,398, , 1971

PAPER NUMBER: 205

Chang, C.D., and Lang, W.H., 'Conversion of Alcohols and Ethers to Hydrocarbons,' US Patent, 3,899,544, , 1975

PAPER NUMBER: 206

Butter, S.A., and Kaeding, W.W., 'Methylation of Toluene,' US Patent, 3,965,208, 1976

PAPER NUMBER: 207

Chu, C., 'Selective Production of Para-Xylene and Catalyst Therefor,' US Patent, 3,965,210, , 1976

PAPER NUMBER: 208

Butter, S.A., 'Process for Manufacturing Hydrocarbons,' US Patent, 3,979,472, , 1976

PAPER NUMBER: 209

Pyke, D.R., Whitney, P., and Houghton, H., 'Chemical Modification of Crystalline Microporous Aluminum Phosphates,' Appl. Catal., 18, 173, 1985

PAPER NUMBER: 210

Lechert, H., and Meyer, A., 'Conversion of Methylcyclopentane on H-ZSM-5 Zeolites,' J. Mol. Catal., 35, 349, 1986

PAPER NUMBER: 211

Ashton, A.G., Batmanian, S., Dwyer, J., Elliott, I.S., and Fitch, F.R., 'The Catalytic Properties of Modified Pentasil Zeolites,' J. Mol. Catal., 34, 73, 1986

PAPER NUMBER: 212

Sayed, M.B., Auroux, A., and Vedrine, J.C., 'Effect of Impregnation of ZSM-5 with H₃BO₃ on its Acidity: A Microcalorimetric Study of NH₃ Adsorption,' Appl. Catal., 23, 49, 1986

PAPER NUMBER: 213

Nayak, V.S., and Riekert, L., 'Catalytic Activity and Product Distribution in the Disproportionation of Toluene on Different Preparations of Pentasil Zeolite Catalysts,' Appl. Catal., 23, 403, 1986

PAPER NUMBER: 214

Suzuki, Isao, Namba, Seitaro, and Yashima, Tatsuaki, 'Determination of External Surface Area of ZSM-5 Type Zeolite,' J. Catal., 81, 485, 1983

PAPER NUMBER: 215

Nakamoto, Hiromi, and Takahashi, Hiroshi, 'Crystallization of Zeolite ZSM-5 From Single Cation System,' Chem. Letters, 1739, 1981

PAPER NUMBER: 216

Erdem, Ayse, and Sand, L.B., 'Crystallization and Metastable Phase Transformations of Zeolite ZSM-5 in the (TPA)₂₀-Na₂₀-K₂₀-Al₂O₃-SiO₂-H₂O System,' J. Catal., 60, 241, 1979

PAPER NUMBER: 217

Chao, Kuei-Jung, Tsai, Tseng Chang, Chen, Mei-Shu, and Wang, Ikai, 'Kinetic Studies on the Formation of Zeolite ZSM-5,' Chem. Soc., Faraday Trans. I, 77, 547, 1981

PAPER NUMBER: 218

Grose, Robert W., and Flanigen, M., 'Novel Zeolite Compositions and Processes For Preparing and Using Same,' U.S. Patent 4,257,885, , 1981

PAPER NUMBER: 219

Valyocsik, E.W., 'Crystalline Silicate ZSM-5,' European Patent Application, EP142,317, May 25, 1985, ,

PAPER NUMBER: 220

Chen, N.Y., Mitchell, T.O., Olson, D.H., and Peirina, B.P., 'Irreversible Deactivation of Zeolite Fluid Cracking Catalyst, 1.,' I. and EC Prod. Res. Dev., 16, 244-247, 1977

PAPER NUMBER: 221

Butt, J.B., Lin, T.-A., and Schwartz, L.H., 'Iron Alloy Fischer-Tropsch Catalysis. VI. Fe Co on ZSM-5,' J. Catal., 97, 261-263, 1986

PAPER NUMBER: 222

Chen, Y.W., Wang, H.T., and Goodwin, J.G., 'Effect of Preparation Methods on the Catalytic Properties of Zeolite-Supported Ruthenium in the Fischer-Tropsch Synthesis,' J. Catal., 83, 415-427, 1983

PAPER NUMBER: 223

Csicsery, S.M., 'Catalyst Activation Process,' U.S. Patent 4,002,578, , 1977

PAPER NUMBER: 224

Chang, C.D., Chu, C.T.W., Perkins, P.D., and Valyocsik, E., 'Olefins from Methanol and/or Dimethyl Ether,' U.S. Patent 4,476,338, , 1984

PAPER NUMBER: 225

Chen, N.Y., Mitchell, T.O., Olson, D.H., and Peirine, B.P., 'Irreversible Deactivation of Zeolite Fluid Cracking Catalyst, 2.,' I. and EC Prod. Res. Dev., 16, 247-252, 1977

PAPER NUMBER: 226

Frilette, V.J., Weisz, P.B., and Golden, R.L., 'Catalysis by Crystalline Aluminosilicates. 1. Cracking of Hydrocarbon Types over Sodium and Calcium 'X' Zeolites,' J. Catal., 1, 301-306, 1962

PAPER NUMBER: 227

Weisz, P.B., Frilette, V.J., and Maatman, R.W., 'Catalysis by Crystalline Aluminosilicates. 2. Molecular-Shape Selective Reactions,' J. Catal., 1, 307-312, 1962

PAPER NUMBER: 228

Richardson, J.T., and Propp, J.L., 'Pore Size Effects on Sintering of Ni/Al₂O₃ Catalysts,' J. Catal., 98, 457-467, 1968

PAPER NUMBER: 229

Vannice, M.A., Hasselbring, L.C., and Sen, B., 'Direct Measurements of Heats of Adsorption on Platinum Catalysts,' J. Catal., 97, 66-74, 1986

PAPER NUMBER: 230

Benson, J.E., and Boudart, M., 'Hydrogen-Oxygen Titration Method for the Measurement of Supported Platinum Surface Areas,' J. Catal., 4, 704-710, 1965

PAPER NUMBER: 231

Benesi, H.A., Curtis, R.M., and Studer, H.P., 'Preparation of Highly Dispersed Catalytic Metals,' J. Catal., 10, 328-335, 1968

PAPER NUMBER: 232

Marcelin, G., Vogel, R.F., and Swift, H.F., 'The Gas-Phase Hydrogenation of Benzene Using Phosphate-Supported Nickel Catalysts,' J. Catal., 98, 64-69, 1986

PAPER NUMBER: 233

Wilson, G.R., and Hall, W.K., 'Studies of the Hydrogen Held by Solids. XIX. H₂ and O₂ Chemisorption on Silica-Supported Platinum,' J. Catal., 24, 306-314, 1972

PAPER NUMBER: 234

Adams, C.R., Benesi, H.A., and Curtis, R.M., 'Particle Size Determination of Supported Catalytic Metals: Platinum on Silica Gel,' J. Catal., 1, 336-344, 1962

PAPER NUMBER: 235

Buotounet, M., Kizling, J., Touroude, R., and Maire, G., 'Monodispersed Colloidal Metal Particles from Non-aqueous Solution: Behaviour for the Hydrogenation of But-1-ene of Platinum Particles,' Appl. Catal., 20, 163-177, 1986

PAPER NUMBER: 236

Trimm, D.L., and Stanislaus, A., 'The Control of Pore Size in Alumina Catalyst Supports: A Review,' Appl. Catal., 21, 215-238, 1986

PAPER NUMBER: 237

Wang, I., Huang, W.H., and Wu, J.C., 'Benzene Hydrogenation over Ni/TiO₂-ZrO₂ Catalyst,' Appl. Catal., 18, 273-283, 1985

PAPER NUMBER: 238

Fouilloux, P., 'The Nature of Raney Nickel, Its Adsorbed Hydrogen and Its Catalytic Activity for Hydrogenation Reactions,' Appl. Catal., 8, 1-42, 1983

PAPER NUMBER: 239

Weilers, A.F.H., Zwolsman, G.J., Van der Grift, C.J.G., and Geus, J.W., 'The Preparation and Characterization of Silica-Supported Pt-Ni Catalysts,' Appl. Catal., 19, 187-202, 1985

PAPER NUMBER: 240

Boitiaux, J.P., Cosyns, J., and Vasudevan, S., 'Hydrogenation of Highly Unsaturated Hydrocarbons over Highly Dispersed Pd Catalyst,' Appl. Catal., 15, 317-326, 1985

PAPER NUMBER: 241

Sarkny, J., and Gonzalez, R.D., 'Effect of Pretreatment on Dispersion and Structure of Silica and Alumina Supported Pt Catalysts,' Ind. Eng. Chem. Prod. Res. Dev., 22, 548-552, 1983

PAPER NUMBER: 242

Yoon, K.J., Walker, P.L., Mulay, L.N., and Vannice, M.A., 'Benzene Hydrogenation over Iron. 1. Specific Activities and Kinetic Behavior over Unsupported Iron and Iron Dispersed on SiO₂, Al₂O₃,' Ind. Eng. Chem. Prod. Res. Dev., 22, 519-526, 1983

PAPER NUMBER: 243

Menon, P.G., Marin, G.B., and Froment, G.F., 'Effect of Sulfur Poisoning on the Hydrogenolysis Activity of Pt in Pt-Al₂O₃ Catalysts,' Ind. Eng. Chem. Prod. Res. Dev., 21, 52-56, 1982

PAPER NUMBER: 244

Sapre, A.V., and Gates, B.C., 'Hydrogenation of Aromatic Hydrocarbons Catalyzed by Sulfided CoO-MoO₃/r-Al₂O₃. Reactivities and Reaction Networks,' Ind. Eng. Chem. Process Des. Dev., 20, 68-73, 1981

PAPER NUMBER: 245

Hopkins, P.D., and Meyers, B.L., 'Thermal and Steam Stability of Commercial Hydroprocessing Catalysts,' Ind. Eng. Chem. Prod. Res. Dev., 22, 421, 1983

PAPER NUMBER: 246

Martin, G.A., and Dalmon, J.A., ',' J. Catal., 75, 233-242, 1982

REFERENCES

1. Dukek, W. G., "Aviation and Other Gas Turbine Fuels," in Kirk-Othmer Encyclopedia of Chemical Technology, 3rd ed.; Grayson, Martin, Ed.; Wiley, New York, 1981, Vol. 3, 328.
2. Robertson, A. G. and Williams, R. E., "Jet Fuel Specifications: The Need For Change," Shell Avia. News, (1976) (435), 10.
3. Treager, I. E., Aircraft Gas Turbine Engine Technology, 2nd Ed.; McGraw-Hill, New York, 1979, p. 202.
4. Indukov, N. M., Danielyan, M. K., Kudinov, A. A. and Mamedova, A. I., "Production of High-Density Fuel from Aromatic Petroleum Cuts," [Khim. Tech. Topliv i Masel #4, 15 (1985)] Chem. Technol. Fuels Oils (Engl. Transl.), (1985), 21, 185.
5. Atwood, M. T., and Smits, C. M., "High Density Jet Fuels from Naphthenic Crudes and from Refinery Hydrocracking Operations," ACS Preprints of Symposium on Structure of Future Jet Fuels, 1987, p. 600.
6. Waddams, A. L., Chemical Processes, 4th ed.; Gulf Publishing Co., Houston, Tx., 1980, p. 47.
7. Gary, James H. and Handwork, Glenn E., Petroleum Refining Technology and Economics, Marcel Dekker, Inc., New York, 1984, p. 241.
8. Chen, N. Y., Lucki, S. J. and Garwood, W. E., "Dewaxing of Oils by Shape Selective Cracking and Hydrocracking Over Zeolites ZSM-5 and ZSM-8," U.S. Patent 3,700,585, 1972.
9. Starr, C. W., Smith, K. W. and Chen, N. Y., "New Process Dewaxes Lube Base Stocks," Oil & Gas J., (1980), 78, (21), 75.
10. Donnelly, J. P. and Green, J. R., "Catalytic Dewaxing Process Improved," Oil & Gas J., (1980), 78, (43), 77.
11. Hargrove, J. D., Elkes, G. J. and Richardson, A. H., "New Dewaxing Process Proven in Operations," Oil & Gas J., (1979), 77, (3), 103.
12. Yen, T.F., and Erdman, G., "Investigation of the Structure of Petroleum Asphaltenes and Related Substances by Infrared Analysis," Am. Chem. Soc. Div. Petr. Chem. Reprints, 7(#1), 5 (1962).
13. Aga, R.L., Debus, H.R., and Allen, E.R., "Arofining Improves Jet Fuels," Hydrocarbon Proc. 50 (#4), 153, (1971).

14. Hanson, F.V., "Future Aviation Turbine Fuels," Presented at High Density Jet Fuels Meeting, Snow Bird, Utah, 1985.
15. Weisz, P. B., and Frilette, V. J., "Intracrystalline and Molecular Shape-selective Catalysis by Zeolite Salts," *J. Phys. Chem.*, (1960), 64, 382.
16. Chang, C. D., "Hydrocarbons from Methanol," *Catal. Reviews*, (1983), 25, 1.
17. Gabelica, Z., "Conversion of Methanol over Zeolites Catalysts: II Industrial Processes," in Zeolites: Science and Technology; Ribeiro, F. R., Rodrigues, A. E., Rollmann, L. D., and Naccache, C., Ed.; NATO ASI Series, Martinus Nijhoff Publishers, Boston, 1984, p. 529.
18. Derouane, E. G., "Conversion of Methanol over Zeolites Catalysts: I Reaction Mechanisms," in Zeolites: Science and Technology; Ribeiro, F. R., Rodrigues, A. E., Rollmann, L. D., and Naccache, C., Ed.; NATO ASI Series, Martinus Nijhoff Publishers, Boston, 1984, p. 515.
19. Chang, C. D., Chu, C. T. W., and Perkins, P. D., "Olefins from Methanol and/or Dimethyl Ether," U.S. Patent 4,476,338, 1984.
20. Breck, D. W., Zeolite Molecular Sieves, Wiley, New York, 1974.
21. Rabo, J. A., Zeolite Chemistry and Catalysis, ACS Monograph 171, American Chemical Society, Washington, D. C., 1976.
22. Barrer, R. M., Zeolite and Clay Minerals as Sorbents and Molecular Sieves, Academic Press, New York, 1978.
23. Smith, J. V., "Definition of a Zeolite," *Zeolites*, (1984), 4, 309.
24. Breck, D. W., Eversole, W. G., and Milton, R. M., "New Synthetic Crystalline," *J. Am. Chem. Soc.*, (1956), 78, 2338.
25. Breck, D. W., Eversole, W. G., Milton, R. M., Reed, T. B., and Thomas, T. L., "Crystalline Zeolite I. The Properties of a New Synthetic Zeolite, Type A," *J. Am. Chem. Soc.*, (1956), 78, 5963.
26. Breck, D. W., "Crystalline Molecular Sieves," *J. Chem. Educ.*, (1964), 41(12), 678.
27. Barrer, R. M., and Denny, P. J., "Hydrothermal Chemistry of the Silicates. IX. Nitrogenous Aluminosilicates," *J. Chem. Soc.*, (1961), 971.
28. Kerr, G. T., and Kokotailo, G. T., "Sodium Zeolite ZK-4, A New Synthetic Crystalline Aluminosilicate," *J. Am. Chem. Soc.*, (1961), 83, 4675.
29. Wadlinger, R. L., Kerr, G. T., and Rosinski, E. J., "A Crystalline Zeolite with Improved Adsorption and Catalytic Properties," U.S. Patent 3,308,069, 1967.

30. Argauer, R. J. and Landolt, G. R., "Crystalline Zeolite ZSM-5 and Method of Preparing the Same," U.S. Patent 3,702,886, 1972.
31. Pelrine, B. P., "Synthesis of Zeolite ZSM-5," U.S. Patent 4,100,262, 1978.
32. Jacobs, P. A., and Martens, J. A., Synthesis of High-silica Aluminosilicate Zeolites, Elsevier, New York, 1987.
33. Weisz, P. B., "Zeolites-New Horizons in Catalysis," CHEMTECH, (1973), 498.
34. Robson, H., "Synthesizing Zeolites," CHEMTECH, (1978), 176.
35. Wilson, S. T., Lok, B. M., and Flanigen, E. M., "Crystalline Metallophosphate Compositions," U.S. Patent, 4,310,440, 1982.
36. Lok, B. M., Messina, A., Patton, R. L., Gajek, R. T., Cannan, T. R., and Flanigen, E. M., "Silico-alumino-phosphate Molecular Sieves: Another New Class of Microporous Crystalline Inorganic Solids," J. Am. Chem. Soc., (1984), 106(20), 6092.
37. Wilson, S. T., Lok, B. M., Messina, C. A., Cannon, T. R., and Flanigen, E. M., "Aluminophosphate Molecular Sieves: A New Class of Microporous Crystalline Inorganic Solids," in Intrazeolite Chemistry; Stucky, G. D. and Dwyer, F. G., Ed.; ACS Symposium series 218, Washington, D. C., 1983, p. 79.
38. Ward, J. W., "Molecular Sieve Catalysts," Appl. Ind. Catal., (1984), 3, 271.
39. Smith, J. V., "Origin and Structure of Zeolites," in Rabo, J. A., Zeolite Chemistry and Catalysis, ACS Monogr. 171, American Chemical Society, Washington, D. C., 1976, p. 3.
40. Barrer, R. M., "Zeolite Structure," in Zeolites: Science and Technology; Ribeiro, F. R., Rodrigues, A. E., Rollmann, L. D., and Naccache, C., Ed.; NATO ASI Series, Martinus Nijhoff Publishers, Boston, 1984, p. 35.
41. Kokotailo, G. T., "Zeolite Crystallography," in Zeolites: Science and Technology; Ribeiro, F. R., Rodrigues, A. E., Rollmann, L. D., and Naccache, C., Ed.; NATO ASI Series, Martinus Nijhoff Publishers, Boston, 1984, p. 83.
42. Michiels, P., and De Herdt, O. C. E., Molecular Sieve Catalysts, Pergamon Press, New York, 1987, Chap. VIII.
43. Olson, D. H., Kokotailo, G. T., Lawton, S. L., and Meier, W. M., "Crystal Structure and Structure-related Properties of ZSM-5," J. Phy. Chem., (1981), 85, 2238.
44. Kokotailo, G. T., Lawton, S. L., Olson, D. H., and Meier, W. M., "Structure of Synthetic Zeolite ZSM-5," Nature, (1978), 272, 437.

45. Kokotailo, G. T., Chu, P., Lawton, S. L., and Meier, W. M., "Synthesis and Structure of Synthetic Zeolite ZSM-11," *Nature*, (1978), 275, 119.
46. Schlenker, J. L., Dwyer, F. G., Jenkins, E. E., Rohrbaugh, W. J., and Kokotailo, G. T., "Crystal Structure of a Synthetic High Silica Zeolite - ZSM-39," *Nature*, (1981), 294, 340.
47. Chu, P., "Zeolite ZSM-48, and its use as Catalyst for Organic Compound Conversion," U.S. Patent 4,397,827, 1981.
48. Rollmann, L. D., and Valyocsik, E. W., "Crystalline Zeolitic Material," U.S. Patent 4,423,021, 1983.
49. Schlenker, J. L., Rohrbaugh, W. J., Chu, P., Valyocsik, E. W., and Kokotailo, G. T., "The Framework Topology of ZSM-48: A High Silica Zeolite," *Zeolites*, (1985), 5(6), 355.
50. Kerr, G. T., "The Synthesis and Properties of Two Catalytically Important Zeolites," *Catal Rev. Sci. Eng.*, (1981), 23, 281.
51. Flanigen, E. M., "Molecular Sieve Zeolite Technology: The First Twenty Five Years," in Zeolites: Science and Technology; Ribeiro, F. R., Rodrigues, A. E., Rollmann, L. D., and Naccache, C., Ed.; NATO ASI Series, Martinus Nijhoff Publishers, Boston, 1984, p. 3.
52. Whyte, T. E., and Dalla Betta, R. A., "Zeolite Advances in the Chemical and Fuel Industries: A Technical Perspective," *Catal. Rev. Sci. Eng.*, (1982), 24(4), 567.
53. Jacobs, P. A., and Martens, J. A., Synthesis of High-silica Aluminosilicate Zeolites, Elsevier Science Publishing Co., New York, 1987, and References therein.
54. Rubin, M. K., Plank, C. J., and Rosinski, E. J., "Synthesis of Zeolite ZSM-4," U.S. Patent 4,021,447, 1977.
55. Kokotailo, G. T., and Sawruk, S., "Improving Organic Cation-containing Zeolites," U.S. Patent 4,187,283, 1980.
56. Chen, N. Y., Lucki, S. J., and Garwood, W. E., "Dewaxing of Oils by Shape Selective Cracking and Hydrocracking over Zeolites ZSM-5 and ZSM-8," U.S. Patent 3,700,585, 1972.
57. Ciric, J., "Crystalline Zeolite ZSM-10," U.S. Patent 3,692,470, 1972.
58. Chu, P., "Crystalline Zeolite ZSM-11," U.S. Patent 3,709,979, 1973.
59. Rosinski, E. J. and Rubin, M. K., "Crystalline Zeolite ZSM-12," U.S. Patent 3,832,449, 1974.
60. Rosinski, E. J. and Rubin, M. K., "Hydrocarbon Conversion with ZSM-12," U.S. Patent 3,970,544, 1976.

61. Plank, C. J., Rosinski, E. J., and Givens, E. N., "Converting Low Molecular Weight Olefins over Zeolites," U.S. Patent 4,021,502, 1977.
62. Ciric, J., "Organic Compound Conversion by Zeolite ZSM-20 Catalysts," U.S. Patent 4,021,331, 1977.
63. Plank, C. J., Kosinski, E. J., and Rubin, M. K., "Crystalline Zeolite and Method of Preparing Same," U.S. Patent 4,046,859, 1977.
64. Plank, C. J., Rosinski, E. J., and Rubin, M. K., "Synthetic Crystalline Aluminosilicate Zeolites," U.S. Patent 4,076,842, 1978.
65. Doherty, H. G., Plank, C. J., and Rosinski, E. J., "Crystalline Zeolite for a Hydrocarbon Conversion Catalyst," U.S. Patent 4,247,416, 1981.
66. Rubin, M. K., Kosinski, E. J., and Plank, C. J., "Crystalline Zeolite ZSM-34 and Method of Preparing the Same," U.S. Patent 4,086,186, 1978.
67. Plank, C. J., Kosinski, E. J., and Rubin, M. K., "Crystalline Zeolite and Method of Preparing Same," U.S. Patent 4,016,245, 1977.
67. Plank, C. J., Rubin, M. K., and Kosinski, E. J., "Hydrocarbon Conversion over ZSM-38," U.S. Patent 4,105,541, 1978.
68. Nanne, J. M., Post, M. F. M., and Stork, W. H. J., "Ferrierite, and Its Use as Catalyst or Catalyst Carrier for Converting Hydrocarbons, and for Separating Hydrocarbons," European Patent 12,473, 1980.
70. Rubin, M. K., Rosinski, E. J., and Plank, C. J., "Aluminosilicates as Catalysts for Organic Compound Conversion," U.S. Patent 4,247,728, 1981.
71. Kokotailo, G. T. and Sawruk, S., "Method Improving Organic Cation-containing Zeolites," U. S. Patent 4,178,283, 1980.
72. Rollmann, L. D., and Valyocsik, E. W., "Crystalline Zeolite Material, Synthesis and Use Thereof," European Patent 15,132, 1980.
73. Rollmann, L. D., and Valyocsik, E. W., "Method of Preparing Silico-crystal ZSM-48," U. S. Patent 4,423,021, 1983.
74. Chu, P., "Method of Preparing Zeolite ZSM-48, the Zeolite so Prepared and its Use as Catalyst for Organic Compound Conversion," European Patent 23,089, 1980.
75. Chu, P., "Silico-crystal ZSM-48 Method of Preparing Same and Catalytic Conversion therewith," U. S. Patent 4,448,675, 1984.

76. Chu, P., "Silico-crystal Method of Preparing Same and Catalytic Conversion therewith," U. S. Patent 4,397,827, 1983.
77. Valyocsik, E. W., "Synthesis of Crystalline Silicate ZSM-48," U.S. Patent 4,585,747, 1986.
78. Valyocsik, E. W., "Zeolite ZSM-51 Composition," U. S. Patent 4,568,654, 1986.
79. Lok, B. M., Cannan, T. R., and Messina, C. A., "The Role of Organic Molecules in Molecular Sieve Synthesis," *Zeolites*, (1983), 3, 282.
80. Kulkarni, S. B., Shiralkar, V. P., Kotasthane, A. N., Borade, R. B., and Ratnasamy, P., *Zeolites*, "Studies in the Synthesis of ZSM-5 Zeolites," (1982), 2, 313.
81. Rubin, M. K., Rosinski, E. J., Plank, C. P., "Synthesizing Low-sodium crystalline Aluminosilicate Zeolites with Primary Amines," U.S. Patent 4,151,189, 1979.
82. Rollmann, L. D., and Valyocsik, E. W., "Synthesis of Zeolite ZSM-11," U.S. Patent 4,108,881, 1978.
83. Rollmann, L. D., and Valyocsik, E. W., "Synthetic Crystalline Aluminosilicate Zeolite," U.S. Patent 4,139,600, 1979.
84. Plank, C. J., Rosinski, E. J., and Rubin, M. K., "Zeolites," U.S. Patent 4,175,114, 1979.
85. Araya, A., and Lowe, B. M., "Effect of Organic Species on the Synthesis and Properties of ZSM-5," *Zeolites*, (1986), 6, 111.
86. Lok, B. M., Cannan, T. R., and Messina, C. A., "The Role of Organic Molecules in Molecular Sieve Synthesis," *Zeolites*, (1983), 3, 282.
87. Grose, R. W., and Flanigen, E. M., "Zeolite Compositions and Using Same," U.S. Patent 4,257,885, 1982.
88. Narita, E., Sato, K., Yatabe, N., and Okabe, T., "Synthesis and Crystal Growth of Zeolite ZSM-5 from Sodium Aluminosilicate Systems free of Organic Templates," *Ind. Eng. Chem. Prod. Res. Dev.*, (1985), 24, 507.
89. Rollmann, L. D., "ZSM-5 Particle Containing Aluminum-free Shells on its Surface," U.S. Patent 4,148,713, 1979.
90. Kokotailo, G. T., "Crystalline Zeolite Product Constituting ZSM-5/ZSM-11 Intermediates," U.S. Patent 4,229,424, 1980.
91. Derouane, E. G., Detremmerie, S., Gabelica, Z., and Blom, N., "Synthesis and Characterization of ZSM-5 Type Zeolites I. Physico-chemical Properties of Precursors and Intermediates," *Appl. Catal.*, (1981), 1, 201.

92. Kokotailo, G. T., "Catalytic Conversion with Crystalline Zeolite Product Constituting ZSM-5/ZSM-11 Intermediates," U.S. Patent 4,289,607, 1981.
93. Jablonski, G. A., Gard, J. A., and Sand, L. B., "Synthesis and Identification of ZSM-5/ZSM-11 Pentasil Intergrowth Structures," *Zeolites*, (1986), 6, 396.
94. Doelle, H.-J., Heering, J., and Rieckert, L., "Sorption and Catalytic Reaction in Pentasil Zeolites. Influence of Preparation and Crystal Size on Equilibria and Kinetics," *J. Catal.*, (1981), 71, 27.
95. Suzuki, K., Kiyozumi, Y., Shin, S., Fujisawa, K., Watanabe, H., Saito, K., and Noguchi, K., "Zeolite Synthesis in the System Pyrrolidine- Na_2O - Al_2O_3 - SiO_2 - H_2O ," *Zeolites*, (1986), 6, 290.
96. Rollmann, L. D., "Synthesis of Zeolites, an Overview," in Zeolites: Science and Technology; Ribeiro, F. R., Rodrigues, A. E., Rollmann, L. D., and Naccache, C., Ed.; NATO ASI Series, Martinus Nijhoff Publishers, Boston, 1984, p. 109.
97. Flanigen, E. M., "Molecular Sieve Zeolite Technology - The First Twenty-five Years," in Proceedings of the Fifth International Conference on Zeolites; Rees, L. V., Ed.; Heyden, Philadelphia, 1980, p. 760.
98. Flanigen, E. M., Bennett, J. M., Grose, R. W., Cohen, J. P., Patton, R. L., Kirchner, R. M., and Smith, J. V., "Silicalite, A New Hydrophobic Crystalline Silica Molecular Sieve," *Nature*, (1978), 271, 512.
99. Kerr, G. T., "The Synthesis and Properties of Two Catalytically Important Zeolites," *Catal. Rev.-Sci. Eng.*, (1981), 23, 281.
100. Taramasso, M., Perego, G., and Notari, B., "Molecular Sieve Borosilicates," in Proceedings of the Fifth International Conference on Zeolites; Rees, L. V., Ed.; Heyden, Philadelphia, 1980, p. 40.
101. Klotz, M. R., and Ely, S. R., "Crystalline Borosilicate with a Metallic Cation Deficit," U.S. Patent 4,285,919, 1981.
102. Scholle, K. F. M. G. J., Kentgens, A. P. M., Veeman, W. S., Frenken, P. and van der Velden, G. P. M., "Proton Magic Angle Spinning Nuclear Magnetic Resonance and Temperature Programmed Desorption Studies of Ammonia on the Acidity of the Framework Hydroxyl Groups in the Zeolite H-ZSM-5 and in H-Boralite," *J. Phys. Chem.*, (1984), 88, 5.
103. Holderich, W., Eichorn, H., Lehnert, R., Marosi, L., Mross, W., Reinke, R., Ruppel, W., and Schlimper, H., "Aluminosilicate and Borosilicate Zeolites and Their Use in the Conversion of Methanol to Olefins," in Proceedings of the Sixth International Zeolite Conference; Olson, D., and Bisio, A., Ed.; Butterworths, UK, 1984, p. 545.

104. Gabellica, Z. B., Nagy, J., Bodart, P., and Debras, G., "High Resolution Solid State MAS Boron-11 NMR Evidence of Boron Incorporation in Tetrahedral Sites of Zeolites," *Chem. Lett.*, (1984), 7, 1059.
105. Bolton, A. P., "Molecular Sieve Zeolites," in Experimental Method in Catalytic Research, Vol. 2; Anderson, R. B., and Dawson, P. T., Ed.; Academic Press, New York, 1976, p. 43.
106. Beyer, H. K., and Belenykaja, I., "A New Method for the Dealumination of Faujasite-type Zeolites," *Stud. Surf. Sci. Catal.*, (1980), 5, 203.
107. Klinowski, J., Thomas, J. M., Audier, M., Vasudevan, S., Fyfe, C. A., and Hentman, J. S., "Solid-state Silicon-29 NMR and High Resolution Electron Microscopic Studies of a Silicate Analog of Faujasite," *J. Chem. Soc. Chem. Commun.*, (1981), 11, 570.
108. Chang, C. D., "Dealumination of Aluminosilicates," U.S. Patent 4,273,753, 1981.
109. Namba, S., Inaka, A., and Yashima, T., "Effect of Selective Removal of Aluminum from External Surfaces of HZSM-5 Zeolite on Shape Selectivity," *Zeolites*, (1986), 6, 107.
110. Baerlocher, C., "Zeolite Structure Refinements Using Powder Data," *Zeolites*, (1986), 6, 325.
111. Thomas, J. M., Millward, G. R., Ramadas, S., and Audier, M., "New Approaches to the Structural Characterization of Zeolites: High Resolution Electron Microscopy and Optical Diffractometry," in Intrazeolite Chemistry; Stucky, G. D., and Dwyer, F. G., Ed.; ACS Symposium Series 218, Washington, D. C., 1983, p. 181.
112. Auroux, A., Dexpert, H., Leclercq, C., and Vedrine, J., "Chemical, Physical and Catalytic Properties of ZSM-5 and ZSM-11 Zeolites: A Study by Electron Microscopy, EDX-STEM and XPS," *Appl. Catal.*, (1983), 6, 95.
113. Lechert, H., "The Physical Characterization of Zeolites," in Zeolite: Science and Technology; Ribeiro, F. R., Rodrigues, A. E., Rollmann, L. D., and Naccache, C., Ed.; Elsevier, New York, 1984, p. 151.
114. Ballmoos, V., and Meier, W., "Zoned Aluminium Distribution in Synthetic Zeolite ZSM-5," *Nature*, (1981), 289, 782.
115. Auroux, A., Dexpert, H., Leclercq, C., and Vedrine, J., "Chemical, Physical and Catalytic Properties of ZSM-5 and ZSM-11 Zeolites: A Study by Electron Microscopy, EDX-STEM and XPS," *Applied Catal.*, (1983), 6, 95.
116. Lyman, C. E., Betteridge, P. W., and Moran, E. F., "Compositional Variations Across Zeolite Particles," in Intrazeolite Chemistry; Stucky, G. D., and Dwyer, F. G., Ed.; ACS Symposium Series 218, Washington, D. C., 1983, p. 199.

117. Anderson, J. R., Foger, K., Mole, T., Radahyaksha, R. A., and Sander, J. V., "Reactions on ZSM-5-type Zeolite Catalysts," *J. Catal.*, (1979), 58, 114.
118. Topsoe, N., Pedersen, K., and Derouane, E. G., "Infrared and Temperature-programmed Desorption Study of the Acidic Properties of ZSM-5 Type Zeolites," *J. Catal.*, (1981), 70, 41.
119. Post, J. G., and van Hooff, J. H. C., "Acidity and Activity of H-ZSM-5 Measured with NH_3 -t.p.d. and n-Hexane Cracking," *Zeolites*, (1984), 4, 9.
120. Kurschner, U., Parltitz, E., Schreier, E., Ohlmann, G., and Volter, J., "Effect of Thermal Treatments on Shape Selectivity and Acidity of ZSM-5 Type Zeolite Catalysts," *Appl. Catal.*, (1987), 30, 159.
121. Haag, W. O., "Acid Catalysis with Medium Pore Zeolites," in Proceedings of the Sixth International Zeolite Conference; Olson, D., and Bisio, A., Ed.; Butterworth & Co., UK, 1984, p. 466.
122. Flanigen, E. M., "Structural Analysis by Infrared Spectroscopy," in Zeolite Chemistry and Catalysis; Rabo, J. A., Ed.; ACS Monograph 171, American Chemical Society, Washington, D.C., 1976, p. 80.
123. Jacobs, P. A., "Evidence for X-ray-amorphous Zeolites," *J. Chem. Soc. Comm.*, (1981), 501.
124. Kazansky, V. B., Kustov, L. M., and Borovkov, V. Y., "Near Infrared Diffuse Reflectance Study of High Silica Containing Zeolites," *Zeolites*, (1983), 3, 77.
125. Lok, B. M., Marcus, B. K., and Angell, C. L., "Characterization of Zeolite Acidity. II. Measurement of Zeolite Acidity by Ammonia Temperature Programmed Desorption and FTIR Spectroscopy Techniques," *Zeolites*, (1986), 6, 185.
125. Aronson, M. T., Gorte, R. J., and Farneth, W. E., "An Infrared Spectroscopy Study of Simple Alcohols Adsorbed on H-ZSM- 5," *J. Catal.*, (1987), 105, 455.
127. Ison, A., and Gorte, R., "The Adsorption of Methanol and Water on H-ZSM-5," *J. Catal.*, (1984), 89, 150.
128. Aronson, M. T., Gorte, R. J., and Farneth, W. E., "The influence of Oxonium ion and Carbonium ion Stability on the Alcohol/H-ZSM-5 Interaction," *J. Catal.*, (1986), 98, 434.
129. Sayed, M. B., Kydd, R. A., and Cooney, R. P., "A Fourier-transform Infrared Spectral Study of H-ZSM-5 Surface Sites and Reactivity Sequences in Methanol Conversion," *J. Catal.*, (1984), 88, 137.
130. Datka, J., and Tuznik, E., "Infrared Spectroscopic Studies of Acid Properties of NaHZSM-5 Zeolites," *J. Catal.*, (1986), 102, 43.

131. Datka, J., and Tuznik, E., "Hydroxyl Groups and Acid Sites in Na-ZSM-5 Zeolites Studied by IR Spectroscopy," *Zeolites*, (1985), 5, 230.
132. Vedrine, J. C., Auroux, A., Bolis, V., Dejaifve, P., Naccache, C., Wierzchowski, P., Derouane, E. G., Nagy, J. B., Gilson, J., van Hooff, J. H. C., van den Berg, J. P., and Wolthuizen, J., "Infrared, Microcalorimetric, and Electron Spin Resonance Investigations of the Acidic properties of the H-ZSM-5 Zeolite," *J. Catal.*, (1979), 59, 248.
133. Topsøe, N., Pedersen, K., and Derouane, E. G., "Infrared and Temperature-Programmed Desorption Study of the Acidic properties of ZSM-5-type Zeolites," *J. Catal.*, (1981), 70, 41.
134. Jacobs, P. T., and von Ballmoos, R., "Framework Hydroxyl Groups of H-ZSM-5 Zeolites," *J. Phy. Chem.*, (1982), 86, 3050.
135. Qin, G., Zheng, L., Xie, Y., and Wu, C., "On the Framework Hydroxyl Groups of H-ZSM-5 Zeolites," *J. Catal.*, (1985), 95, 609.
136. Lippmaa, E., Alla, M. A., Pehk, T. J., and Engelhardt, G., "Solid-state High Resolution NMR Spectroscopy of Spin 1/2 Nuclei (^{13}C , ^{29}Si , ^{119}Sn) in Organic Compounds," *J. Am. Chem. Soc.*, (1978), 100, 1929.
137. Lippmaa, E., Magi, M., Samoson, A., Engelhardt, G., and Grimmer, A., "Structural Studies of Silicates by Solid-state High-resolution ^{29}Si NMR," *J. Am. Chem. Soc.*, (1980), 102, 4889.
138. Lippmaa, E., Magi, M., Samoson, A., Tarmak, M., and Engelhardt, G., "Investigation of the Structure of Zeolites by Solid-state High Resolution ^{29}Si NMR Spectroscopy," *J. Am. Chem. Soc.*, (1981), 103, 4992.
139. Klinowski, J., Thomas, J. M., Fyfe, C. A., and Hartman, J. S., "Application of Magic-Angle-Spinning Silicon-29 Nuclear Magnetic Resonance Evidence for Two Different Kinds of Silicon-Aluminium Ordering in Zeolite Structures," *J. Phy. Chem.*, (1981), 85, 2590.
140. Ramdas, S., Thomas, J. M., Klinowski, J., Fyfe, C. A., and Hartman, J. S., "Ordering of Aluminium and Silicon in Synthetic Faujasites," *Nature*, (1981), 292, 228.
141. Klinowski, J., Carpenter, T. A., and Gladden, L. F., "High-resolution Solid-state NMR Studies of Temperature-induced Phase Transitions in Silicalite (Zeolite ZSM-5)," *Zeolites*, (1987), 7, 73.
142. Engelhardt, G., Jerschke, H., Lohse, U., Sarv, P., Samoson, A., and Lippmaa, E., "500 MHz ^1H -MAS NMR Studies of Dealuminated HZSM-5 Zeolites," *Zeolites*, (1987), 7, 289.
143. Hunger, M., Freude, D., Frohlich, T., Pfeifer, H. and Schwieger, W., " ^1H -MAS NMR Studies of ZSM-5 Type Zeolites," *Zeolites*, (1987), 7, 108.

144. Scherzer, J., "The Preparation and Characterization of Aluminum-deficient Zeolites," in Catalytic Materials: Relationship between Structure and Reactivity; Whyte, T. E., Jr., Dalla Betta, R. A., Derouane, E. G., and Baker, R. T., Ed.; Am. Chem. Soc., Washington, D. C., 1984, p.157.
145. Engelhardt, G., Lohse, U., Magi, M., and Lippmaa, E., "Solid State ^{29}Si and ^{27}Al NMR Studies of Deactionized and Dealuminated Zeolites," in Structure and Reactivity of Modified Zeolites; Jacobs, P. A., Jaeger, N. I., Jiru, P., Kazansky, V. B., and Schulz-Ekloff, G., Ed.; Elsevier, New York, 1984, p. 23.
146. Kokotailo, G. T., Fyfe, C. A., Kennedy, G. J., Gobbi, G. C., Strobl, H., Pasztor, C. T., Barlow, G.E., and Bradley, S., "Zeolite Structural Investigations by High Resolution Solid State MAS NMR," in New Developments in Zeolite Science and Technology; Murakami, Y., Lijima, A., and Ward, J. W., Ed.; Elsevier, New York, 1986, p.361.
147. Jacobs, P. A., Tielen, M., Nagy, J. B., Debras, G., Derouane, E. G., and Gabelica, Z., "Study of the Dealumination and Realumination of ZSM-5 Type Zeolites by ^{29}Si and ^{27}Al High Resolution Magic Angle Spinning NMR Spectroscopy," in Proceedings of the Sixth International Zeolite Conference; Olson, D., and Bisio, A., Ed.; Butterworths, UK, 1984, p. 783.
148. Gabeliva, Z., Nagy, J. B., Bodart, P., Debras, G., Derouane, E. G., and Jacobs, P. A., "Structural Characterization of Zeolites by High Resolution Magic-Angle-Spinning Solid State ^{29}Si -NMR Spectroscopy," in Zeolites: Science and Technology; Ribeiro, F. R., Rodrigues, A. E., Rollmann, L. D., and Naccache, C., Ed.; NATO ASI Series, Martinus Nijhoff Publishers, Boston, 1984, p. 193.
149. Thomas, J. M., Klinowski, J., Fyfe, C. A., Gobbi, G. C., Ramadas, S., and Anderson, M. W., "New Approaches to the Structural Characterization of Zeolites: Magic-angle Spinning NMR (MASNMR)," in Intrazeolite Chemistry; Stucky, G. D., and Dwyer, F. G., Ed.; ACS Symposium Series 218, Washington, D. C., 1983, p. 159.
150. Miale, J. N., Chen, N. Y., and Weisz, P. B., "Catalysis by Crystalline Aluminosilicativity: IV. Attainable Catalytic Cracking Rate Constants, and Superactivity," *J. Catal.*, (1966), 6, 278.
151. Weisz, P. B., and Miale, J. N., "Superactive Crystalline Aluminosilicate," *J. Catal.*, (1965), 4, 527.
152. Miale, J. N., Chen, N. Y., and Weisz, P. B., "Catalysis by Crystalline Aluminosilicates. IV Attainable Catalytic Cracking Rate Constants, and Superacidity," *J. Catal.*, (1966), 6, 278.
153. Olson, D. H., Haag, W. O., Lago, R. M., "Chemical and Physical Properties of the ZSM-5 Substitutive Series," *J. Catal.*, (1980), 61, 390.
154. Hilaireau, P., Bearez, C., Chevalier, F., Perot, G., and Guisnet, M., "Transition-state Selectivity on HZSM-5 Zeolite Evidenced by Isobutane Conversion," *Zeolites*, (1982), 2, 69.

155. Csicsery, S. M., "Catalysis by Shape-selective Zeolites - Science and Technology," *Pure & Appl. Chem.*, (1986), 58(6), 841.
156. Vedrine, J. C., Auroux, A., Bolix, V., Dejaifve, P., Naccache, C., Wierzchowski, P., Derouane, E. G., Nagy, J., Gilson, J. P., Van Hoof, J. H. C., Van den Berg, J. P., and Wolthuizen, J., "Infrared, Microcalorimetric, and Electron Spin Resonance Investigations of the Acidic Properties of the H-ZSM-5 Zeolite," *J. Catal.*, (1979), 59, 248.
157. Haag, W. O., and Dessau, R. M., "Duality of Mechanism for Acid-catalyzed Paraffin Cracking," in Proceeding of the Eighth Int. Congr. Catalysis; Berlin, Dechema, Verlag Chemie, 1984, p. 305.
158. Gilson, J. P. and Derouane, E. G., "On the External and Intracrystalline Surface Catalytic activity of Pentasil Zeolites," *J. Catal.*, (1984), 88, 538.
159. Inomata, M., Yamada, M., Okada, S., Niwa, M., and Murakami, Y., "Benzene-filled Pore Method: A Method of Measuring External Surface Areas Applicable to Zeolites with Low-to-high Si-to-Al Ratios," *J. Catal.*, (1986), 100, 264.
160. Breck, D. W., Zeolite Molecular Sieves, Wiley, New York, 1974, p. 671.
161. Barrer, R. M., Zeolites and Clay Minerals, Academic Press, New York, 1978, p. 287.
162. Weisz, P. B., "Zeolites - New Horizons in Catalysis," *CHEMTECH*, 3, 498 (1973).
163. Weisz, P. B., "Molecular Shape Selective Catalysis," *Pure & Appl. Chem.*, (1980), 52, 2091.
164. Derouane, E. G., "Diffusion and Shape-selective Catalysis in Zeolites," in Intercalation Chemistry; Whittingham, M. S., and Jacobson, A. J., Ed.; Academic Press, New York, 1982, p. 101.
165. Chen, N. Y. and Weisz, P. B., "Molecular Engineering of Shape-selective Catalysts," *Chem. Eng. Prog., Symp. Ser.*, (1967), 63(73), 86.
166. Csicsery, S. M., "Shape-selective Catalysis in Zeolites," *Zeolites*, (1984), 4, 202.
167. Derouane, E. G., "Molecular Shape-selective Catalysis by Zeolites," in Zeolites: Science and Technology; Ribeiro, F. R., Rodrigues, A. E., Rollmann, L. D., and Naccache, C., Ed.; NATO ASI Series, Martinus Nijhoff Publishers, Boston, 1984, p. 317.
168. Derouane, E. G., and Gabelica, Z., "A Novel Effect of Shape Selectivity: Molecular Traffic Control in Zeolite ZSM-5," *J. Catal.*, (1980), 65, 486.
169. Derouane, E. G., Gabelica, Z. and Jacobs, P. A., "Molecular Traffic Control in Zeolite ZSM-5," *J. Catal.*, (1981), 70, 238.

170. Lowe, B. M., Whan, D. A., and Spencer, M. S., "Molecular Traffic Control in Zeolite ZSM-5," *J. Catal.*, (1981), 70, 237.
171. Rollmann, L. D., "Systematics of Shape Selectivity in Common Zeolites," *J. Catal.*, (1977), 47, 113.
172. Rollmann, L. D., and Walsh, D. E., "Shape Selectivity and Carbon Formation in Zeolites," *J. Catal.*, (1979), 56, 139.
173. Walsh, D. E., and Rollmann, L. D., "Radiotracer Experiments on Carbon Formation in Zeolites," *J. Catal.*, (1979), 56, 195.
174. Langner, B. E., "Reactions of Methanol on Zeolite with Different Pore Structures," *Appl. Catal.*, (1982), 2, 289.
175. Derouane, E. G., "Factors Affecting the Deactivation of Zeolites by Coking," in Catalysis by acids and Bases; Imelik, B., Naccache, C., Coudurier, G., Taarit, Y. B., and Vedrine, J. C., Ed.; Elsevier, New York, 1985, p. 221.
176. Bibby, D. M., Milestone, N. B., Patterson, J. E., and Aldridge, L. P., "Coke Formation in Zeolite ZSM-5," *J. Catal.*, (1986), 97, 493.
177. McLellan, G. D., Howe, R. F., Parker, L. M., and Bibby, D. M., "Effects of Coke Formation on the acidity of ZSM-5," *J. Catal.*, (1986), 99, 486.
178. Thedorou, D., and Wei, J., "Diffusion and Reaction in Blocked and High Occupancy Zeolite Catalysts," *J. Catal.*, (1983), 83, 205.
179. Langer, B. E., "Reactions of Methanol on Zeolites with Different Pore Structures," *Appl. Catal.*, (1982), 2, 289.
180. Dejaive, P., Auroux, A., Gravelle, P. C., and Vedrine, J. C., "Methanol Conversion on Acidic ZSM-5, Offretite, and Mordenite Zeolites: A Comparative Study of the Formation and Stability of Coke Deposits," *J. Catal.*, (1981), 70, 123.
181. Meisel, S. L., McCullough, J. P., Lechthaler, C. H., and Weisz, P. B., "Gasoline from Methanol in One Step," *CHEMTECH*, (1976), 2, 86.
182. Liederman, D., Yurchak, S., Kuo, J. C. W., and Lee W., "Mobil Methanol-to-Gasoline," *J. Energy*, (1982), 6, 340.
183. Sayed, M. B., and Cooney, R. P., "A Mechanism for Methanol Conversion over HZSM-5 Catalyst," *Aust. J. Chem.*, (1982), 35, 2483.
184. Espinoza, R. L., Stander, C. M., and Mandersloot, W. G. B., "Catalytic Conversion of Methanol to Hydrocarbons over Amorphous or Zeolitic Silica-alumina," *Appl. Catal.*, (1983), 6, 11.

185. Nayak, V. S., and Choudhary, V. R., "Selective Poisoning of Stronger Acid Sites on HZSM-5 in the Conversion of Alcohols and Olefins to Aromatics," *Appl. Catal.*, (1984), 9, 251.
186. Haag, W. O., Lago, R. M., and Rodewald, P. G., "Aromatics, Light Olefins and Gasoline from Methanol: Mechanistic Pathways with ZSM-5 Zeolite catalyst," *J. Mol. Catal.*, (1982), 17, 161.
187. Choudhary, V. R., and Nayak, V. S., "Conversion of Alcohols to Aromatics on H-ZSM-5: Influence of Si/Al Ratio and Degree of Cation Exchange on Product Distribution," *Zeolites*, (1985), 5, 325.
188. Anderson, J. R., Fogar, K., Mole, T., Rajadhyaksha, R. A., and Sanders, J. V., "Reactions on ZSM-5-type Zeolite Catalysts," *J. Catal.*, (1979), 58, 114.
189. Dejaifve, P., Viedrine, J. C., Bolis, V., and Derouane, E. G., "Reaction Pathways for the Conversion of methanol and Olefins on H-ZSM-5 Zeolite," *J. Catal.*, (1980), 63, 331.
190. Chang, C. D., and Silvestri, A. J., "The Conversion of Methanol and Other O-compounds to Hydrocarbons over Zeolite Catalysts," *J. Catal.*, (1977), 47, 249.
191. Chen, N. Y., and Reagan, W. J., "Evidence of Autocatalysis in Methanol to Hydrocarbon Reactions over Zeolite Catalysts," *J. Catal.*, (1979), 59, 123.
192. Kaeding, W. W., and Butter, S. A., "Production of Chemicals from Methanol," *J. Catal.*, (1980), 61, 155.
193. Ione, K. G., Echevskii, G. V., and Nosyreva, G. N., "Study of Stability and Selectivity of Catalytic Action of ZSM-type Zeolites in Methanol Transformation," *J. Catal.*, (1984), 85, 287.
194. (a) Chang, C. D., Chu, C. T., and Socha, R. F., "Methanol Conversion to Olefins over ZSM-5," *J. Catal.*, (1984), 86, 289. (b) Chang, C. D., Lang, W. H., and Bell W. K., "Molecular Shape-selective Catalysis in Zeolites," in Moser, W. R., Catalysis of Organic Reactions, Marcel Dekker, New York, 1981, p. 73.
195. Dass, D. V., Martin, R. W., and Odell, A. L., "Studies on the Conversion of Methanol and Other Small Molecules over H-ZSM-5: Yield Studies and the Use of ^3H NMR in a Reexamination of Routes to Ethylene Production," *J. Catal.*, (1987), 108, 153.
196. Hagg, W. O., "Catalysis by Intermediate Pore Zeolites," in Heterogeneous Catalysis; Shapiro, B. L., Ed.; Published for the IUCCP by Texas A & M Univ. Press, Texas, 1984, p. 95.
197. Pines, H., The Chemistry of Catalytic Hydrocarbon Conversions, Academic Press, New York, 1981, p. 284.

198. van den Berg, J. P., Wolthuizen, J. P., and van Hooff, J. H. C., "The Conversion of Dimethylether to Hydrocarbons on Zeolite H-ZSM-5 - The Reaction Mechanism for Formation of Primary Olefins," in Proceedings of the Fifth International Conference on Zeolites; Rees, L. V., Ed.; Heyden, Philadelphia, 1980, p. 649.
199. Vaughan, D. E. W., "Industrial Uses of Zeolite Catalysts," in Townsend, R. P., The Properties and Applications of Zeolites; Townsend, R. P., Ed.; Whitstable Litho, Kent, England, 1980, p. 294.
200. Garwood, W. E., "Conversion of C₂-C₁₀ to Higher Olefins over Synthetic Zeolite ZSM-5," in Intrazeolite Chemistry; Stucky, G. D., and Dwyer, F. G., Ed.; ACS Sym. Series 218, Am. Chem. Soc., Washington, D. C., 1983, p. 383.
201. Derouane, E. G., "New Aspects of Molecular Shape Selectivity: Catalysis by Zeolite ZSM-5," in Catalysis by Zeolites; Imelik, B., Naccache, C., Taarit, Y. B., Vedrine, J. C., Coudurier, G., and Praliaud, H., Ed.; Elsevier, New York, 1980, p. 5.
202. Inui, T., Suzuki, T., Inoue, M., Murakami, Y., and Takegami, Y., "Relation between Acidic Properties of ZSM-5 and Catalyst Performance of Methanol Conversion to Gasoline," in Structure and Reactivity of Modified Zeolites; Jacobs, P. A., Jaeger, N. I., Jiru, P., Kazansky, V. B., and Schulz-Ekloff, G., Ed.; Elsevier, New York, 1984, p. 201.
203. Dwyer, F. G., Chester, W., and F. V. Hanson, "Conversion of Methanol to Gasoline Product," Patent 4,035,430, 1977.
204. Kaeding, W.W., and Butter, S. A., "Production of Chemicals from Methanol. I. Low Molecular Weight Olefins," *J. Catal.*, (1980), 61, 155.
205. Holderich, W., Eichron, H., Lehnert, R., Marosi, L., Mross, W. D., Reinke, R., Ruppel, W., and Schlimper, H., "Aluminosilicate and Borosilicate Zeolites and Their Use in the Conversion of Methanol to Olefins," in Proceedings of the Sixth International Zeolite Conference; Olson, D., and Bisio, A., Ed.; Butterworths, UK, 1984, p. 545.
206. Tabak, S. A., and Krambeck, F. J., "Shaping Process Makes Fuels," *Hydrocarbon Processing*, (1985), September, 72.
207. Chen, N. Y., Schlenker, L. L., Garwood, W. E., and Kokotailo, G. T., "TMA-offretite Relationship between Structural and Catalytical Properties," *J. Catal.*, (1984), 86, 24.
208. Chen, N. Y., Goring, R. L., Ireland, H. R., and Stein, T. R., "New Process Cuts Pour Points of Distillates," *Oil Gas J.*, (1977), 75(23), 165.
209. Chen, N. Y., and Garwood, W. E., "Selective Hydrocracking of n-Paraffins in Jet Fuels," *Ind. Eng. Chem. Pro. Des. Dev.*, (1978), 17(4), 513.
210. Ireland, H. R., Redini, C., Raff, A. S., and Fava, L., "Distillate Dewaxing in Operation," *Hydrocarbon Processing*, (1979), 58(5), 119.

211. Smith, K. W., Starr, W. C., and Chen, N. Y., "New Process Dewaxes Lube Base Stocks," Oil Gas J., (1980), 78(21), 75.
212. Bennett, R. N., Elkes, G. J., and Wanless, G. J., "New Process produces Low-pour Oils," Oil Gas J., (1975), 73(1), 69.
213. Chen, N. Y., Maziuk, J., Schwartz, A. B., and Weisz, P. B., "Selectoforming, A New Process to Improve Octane and Quality," Oil Gas J., (1968), 66(47), 154.
214. Garwood, W. E., and Chen, N. Y., "Octane Boosting Potential of Catalytic Processing of Reformate over Shape Selective Zeolites," Am. Chem. Soc. Div. Pet. Chem. Prep., (1980), 25(1), 84.
215. Holderich, W., and Gallei, E., "Industrial Use of Zeolite Catalysts in Petrochemical Processes," Ger. Chem. Eng., (1985), 8, 337.
216. Kaeding, W. W., and Butler, S. A., "Conversion of Methanol and Dimethylether," U.S. Patent 3,911,041, 1975.
217. Kaeding, W. W., "Zeolite Catalyst Containing Oxide of Boron or Magnesium," U.S. Patent 4,049,573, 1977.
218. Kaeding, W. W., and Young, L. B., "Selective Production of p-Xylene," U.S. Patent 4,034,053, 1977.
219. Kaeding, W. W., Chu, C., Young, L.B., and Butler, S. A., "Selective Alkylation of Toluene with Methanol to Produce para-Xylene," J. Catal., (1981), 67, 159.
220. Kaeding, W. W., Chu, C., Young, L.B., and Butler, S. A., "Shape-selective Reactions with Zeolite Catalyst. II. Selective Disproportionation of Toluene to Produce Benzene and p-Xylene," J. Catal., (1981), 69, 392.
221. Grandio, P., Schneider, F. H., Schwartz, A. B., and Wise, J. J., "Toluene Disproportion over Zeolite catalysts," Am. Chem. Soc. Div. Petrol. Chem. Prepr., (1971), 16(3), B70.
222. Grandio, P., Schneider, F. H., Schwartz, A. B., and Wise, "Toluene for Benzene and Xylenes," Hydrocarbon Process, (1972), 51(8), 85.
223. Olson, D. H., and Haag, W. O., "Structure-selectivity Relationship in Xylene Isomerization and Selective Toluene Disproportionation," in Catalytic Materials: Relationship between Structure and Reactivity; Whyte, T. E., Jr., Dalla Betta, R. A., Derouane, E. G., and Baker, R. T. K., Ed.; Am. Chem. Soc., Washington, D. C., 1984, p.275.
224. Grandio, P., Schneider, F. H., Schwartz, A. B., and Wise, J. J., "Xylene Isomerization over Zeolite catalysts," Am. Chem. Soc. Div. Petrol. Chem. Prepr., (1971), 16(3), B70.

225. Guisnet, M., and Gnep, N. S., "Zeolites as Catalysts in Xylene Isomerization Processes," in Zeolites: Science and Technology; Ribeiro, F. R., Rodrigues, A. E., Rollmann, L. D., and Naccache, C., Ed.; NATO ASI Series, Martinus Nijhoff Publishers, Boston, 1984, p. 571.
226. Derouane, E. G., "Factors Affecting the Deactivation of Zeolite by Coking," *Stud. Surf. Sci. Cat.*, (1985), 20, 221.
227. Niwa, M., Kato, S., Hattori, T., and Murakami, Y., "Fine Control of The Pore-opening Size of the Zeolite Mordenite by Chemical Vapor Desorption of Silicon Alkoxide," *J. Chem. Soc. Faraday Trans. I*, (1984), 80, 3135.
228. Rodewald, P. G., "Selective Production of p-Dialkyl-substituted Benzenes," U.S. Patent 4,100,219, 1978.
229. Morrison, R. A., and Tabak, S. A., "Aromatic Compounds Having Six to Eight Carbon Atoms," U.S. Patent 4,224,141, 1980.
230. Dwyer, F. G., and Chu, P., "ZSM-4 Crystallization via Faujasite Metamorphosis," *J. Catal.*, (1979), 59, 263.
231. Flanigen, E. M., Szymanski, H. A., and Khatami, H., "Infrared Structural Studies of Zeolite Framework," in Molecular Sieve Zeolite I. Advances in Chemistry; Gould, R. F., Ed.; series 101, Am. Chem. Soc., Washington D. C., 1976, p. 206.
232. Mirodatos, C., and Barthomeuf, D., "A New Concept in Zeolite-catalyzed Reactions: Energy Gradient Selectivity," *J. Catal.*, (1985), 93, 246.
233. Weitkamp, A.W., "Stereochemistry and Mechanism of Hydrogenation of Naphthalenes on Transition Metal Catalysts and Conformational Analysis of the Products," Adv. Catal. Relat. Subj., 18, 110 (1968).
234. Hanson, F.V., and Pugmire, R.J., Private Communication.
235. Anderson, J.R., "Structure of Metallic Catalysts," Academic Press, NY (1975).
236. Taylor, H.S., "A Theory of the Catalytic Surface," *Proc. Royal Soc. Series A*, 108, 105 (1925).
237. Boudart, M., "Kinetics of Chemical Processes," p. 189, Prentice-Hall, Englewood Cliffs, New Jersey, 1968.
238. Benton, A.F.J., "The Adsorption of Gases by Platinum Black," *J. Am. Chem. Soc.* 48 1850 (1926).
239. Spenadel, L., and Boudart, M., "Dispersion of Platinum on Supported Catalysts," *J. Phys. Chem.* 64, 204 (1960).

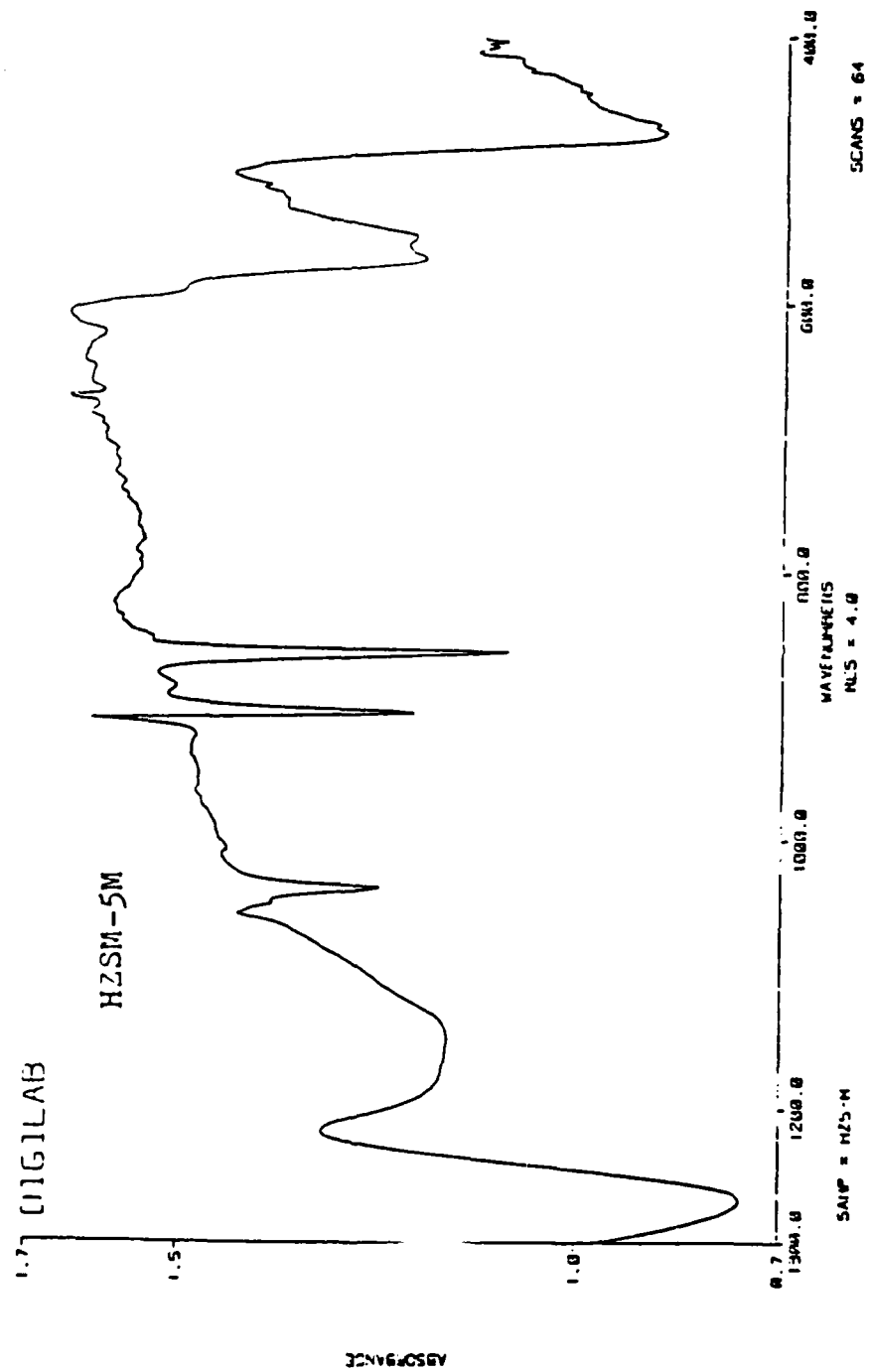
240. Adams, C.R., Benesi, H.A., Curtis, R.M., and Meisenheimer, R.G., "Particle Size Determination of Supported Catalytic Metals: Platinum on Silica Gel," *J. Catal.* **1**, 336 (1962).
241. Poltorak, O.M., and Boronin, V.S., "Chemisorption and Catalysis on Platinized Silica Gels. I. Degree of Dispersion of the Platinum from Chemisorption Data," *Zh. Fiz. Khim.* **39**, 1476 (1965).
242. Borekov, G.K., and Karnaukhov, A.P., "An Adsorption Method for Measuring the Surface Area of the Platinum in Platinum-Impregnated Silica Oils," *Zh. Fiz. Khim.* **26**, 1814 (1952).
243. Yates, D.J.C., and Sinfelt, J.H., "The Catalytic Activity of Rhodium in Relation to its State of Dispersion," *J. Catal.* **8**, 348 (1967).
244. Brooks, C.S., "Characterization of Iridium Catalyst Surfaces by Gas Chemisorption," *J. Colloid Interface Sci.* **34**, 419 (1970).
245. Beeck, O., "Catalysis and the Adsorption of Hydrogen on Metals," *Advan. Catal. Relat. Subj.*, **2**, 151 (1950).
246. Benson, J.E., and Boudart, M., "Hydrogen-Oxygen Titration Method for the Measurement of Supported Platinum Surface Areas," *J. Catal.* **4**, 704 (1965).
247. Mears, D.E., and Hansford, R.C., "The Stoichiometry for Hydrogen Titration of Oxygen on Supported Platinum," *J. Catal.* **9**, 125 (1967).
248. Wilson, G.R., and Hall, W.K., "Studies of the Hydrogen Held by Solids. XIX. H_2 and O_2 Chemisorption on Silica-Supported Platinum," *J. Catal.* **24**, 306 (1972).
249. Wanke, S.E., and Dougharty, N.A., "Interaction of Hydrogen, Oxygen, and Carbon Monoxide with Supported Rhodium," *J. Catal.* **24**, 367 (1972).
250. Benson, J.E., Hwang, H.S., and Boudart, M., "Hydrogen-Oxygen Titration Method for the Measurement of Supported Palladium Surface Areas," *J. Catal.* **30**, 146 (1973).
251. Kaeding, W. W., Chu, C., Young, L. B., Weinstein, B. and Butter, S. A., "Selective Alkylation of Toluene with Methanol to Produce para-Xylene," *J. Catal.*, (1981), **67**, 159.
252. Yanik, Stephen J., Demmel, Edward J., Humphries, Adrian P. and Campagna, Robert J., "FCC Catalysts Containing Shape-Selective Zeolites", *Oil & Gas J.*, (1985), **83**, (19), 108.
253. Csicsery, Sigmund M., "Types of Shape Selectivities," *Pure & Appl. Chem.*, (1986), **58**, (6), 841.
254. Bezouhanova, C. P., Dimitrov, Chr., Nenova, V., Dimitrov, L. and Lechert, L., "Cracking of Paraffins on Pentasils with Different Si/Al Ratios," *Appl. Catal.*, (1985), **19**, 101.

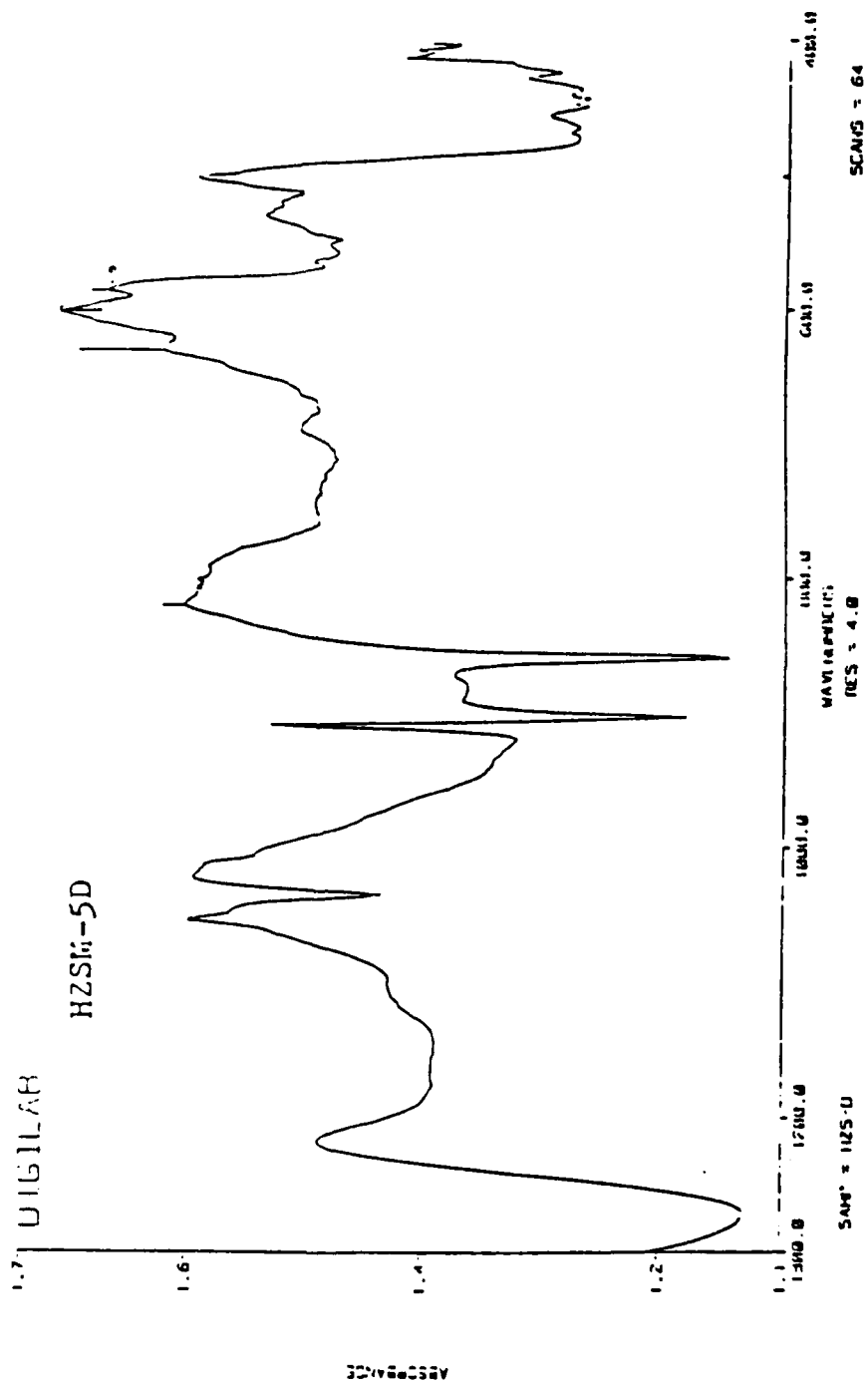
255. Weitkamp, Jens, Jacobs, Peter A. and Martens, Johan A. "Isomerization and Hydrocracking of C₉ Through C₁₆ n-Alkanes on Pt/HZSM-5 Zeolite," Appl. Catal., (1983), 8, 123.
256. Vedrine, Jacques C., Auroux, Aline, Bolis, Vera, Dejaifve, Pierre, Naccache, Claude, Wierzchowski, Pierre, Derouane, Eric G., Nagy, Janos B., Gilson, Jean-Pierre, Van Hooff, Jan H. C., Van Den Burg, Jan P. and Julius Wolthuizen, "Infrared, Microcalorimetric, and Electron Spin Resonance Investigations of the Acidic Properties of the H-ZSM-5 Zeolite," J. Catal., (1979), 59, 248.
257. Corma, A., Monton, J.B., and Orchilles, A.V., "Cracking of n-Heptane on a HZSM-5 Zeolite. The Influence of Acidity and Pore Structure," Appl. Catal., (1985), 16, 59.
258. Greensfelder, B.S., Voge, H.H., and Good, G.M., "Catalytic and Thermal Cracking of Pure Hydrocarbons: Mechanisms of Reaction," Ind. Eng. Chem., (1949), 41, 2573.
259. Brunauer, Stephen, Emmett, P.H., and Teller, Edward, "Adsorption of Gases in Multimolecular Layers," J. Am. Chem. Soc., (1930), 60, 309.
260. Thomas, J.M., and Thomas, W.J., Introduction to the Principles of Heterogeneous Catalysis, Academic Press, Inc., London, 1967, p. 75.
261. Breck, Donald W., Zeolite Molecular Sieves, John Wiley and Sons, Inc., New York, (1974), p. 595.
262. Derouane, Eric G., Detremmerie, Serge, Gabelica, Zelimir, and Blom, Niels, "Synthesis and Characterization of ZSM-5 Type Zeolites. I. Physico-Chemical Properties of Precursors and Intermediates," Appl. Catal., (1981), 1, 201.
263. Reid, Robert C., Prausnitz, John M., and Sherwood, Thomas K., The Properties of Gases and Liquids, 3rd Ed., McGraw-Hill Book Co., Inc., New York, 1977, p. 630.
264. Suzuki, Isao, Namba, Seitaro, and Yashima, Tatsuaki, "Determination of External Surface Area of ZSM-5 Type Zeolite," J. Catal., (1983), 81, 485.
265. Thomas, J.M., and Thomas, W.J., Introduction to the Principles of Heterogeneous Catalysis, Academic Press, Inc., London, 1967, p. 199.
266. Moffat, J.B., "Microporosity in Heteropoly Oxometalate Catalysts," Tenth N. Amer. Mtg., The Catal. Soc., San Diego, Ca., 1987, in print.
267. Wang, H. Paul, "The Production of Methyl Substituted Aromatics Via Novel Zeolite Catalyst Process Routes," Ph.D. Dissertation, University of Utah, Salt Lake City, Utah, 1988.
268. Thomas, J.M., and Thomas, W.J., Introduction to the Principles of Heterogeneous Catalysis, Academic Press, Inc., London, 1967, p. 204.

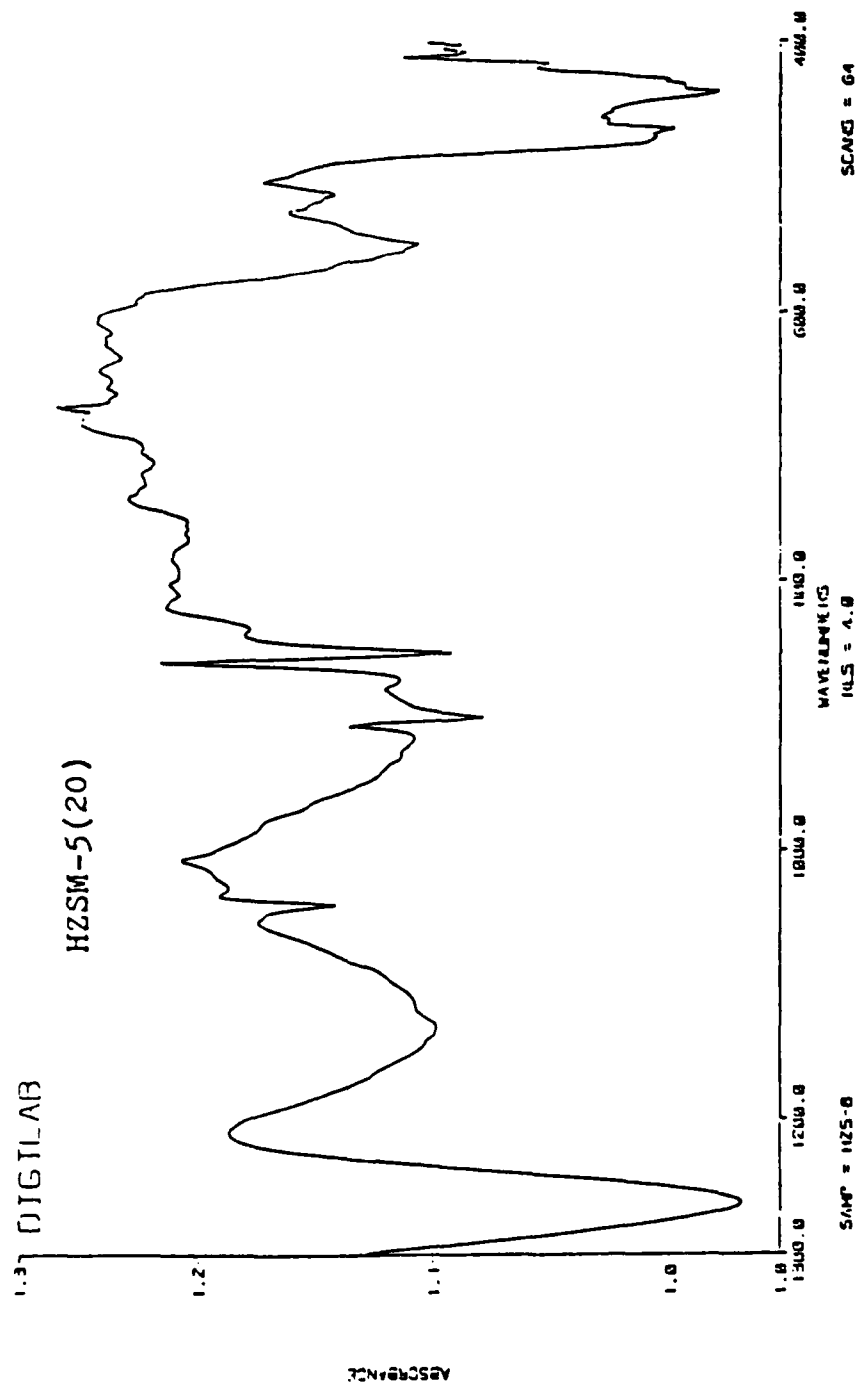
APPENDIX A

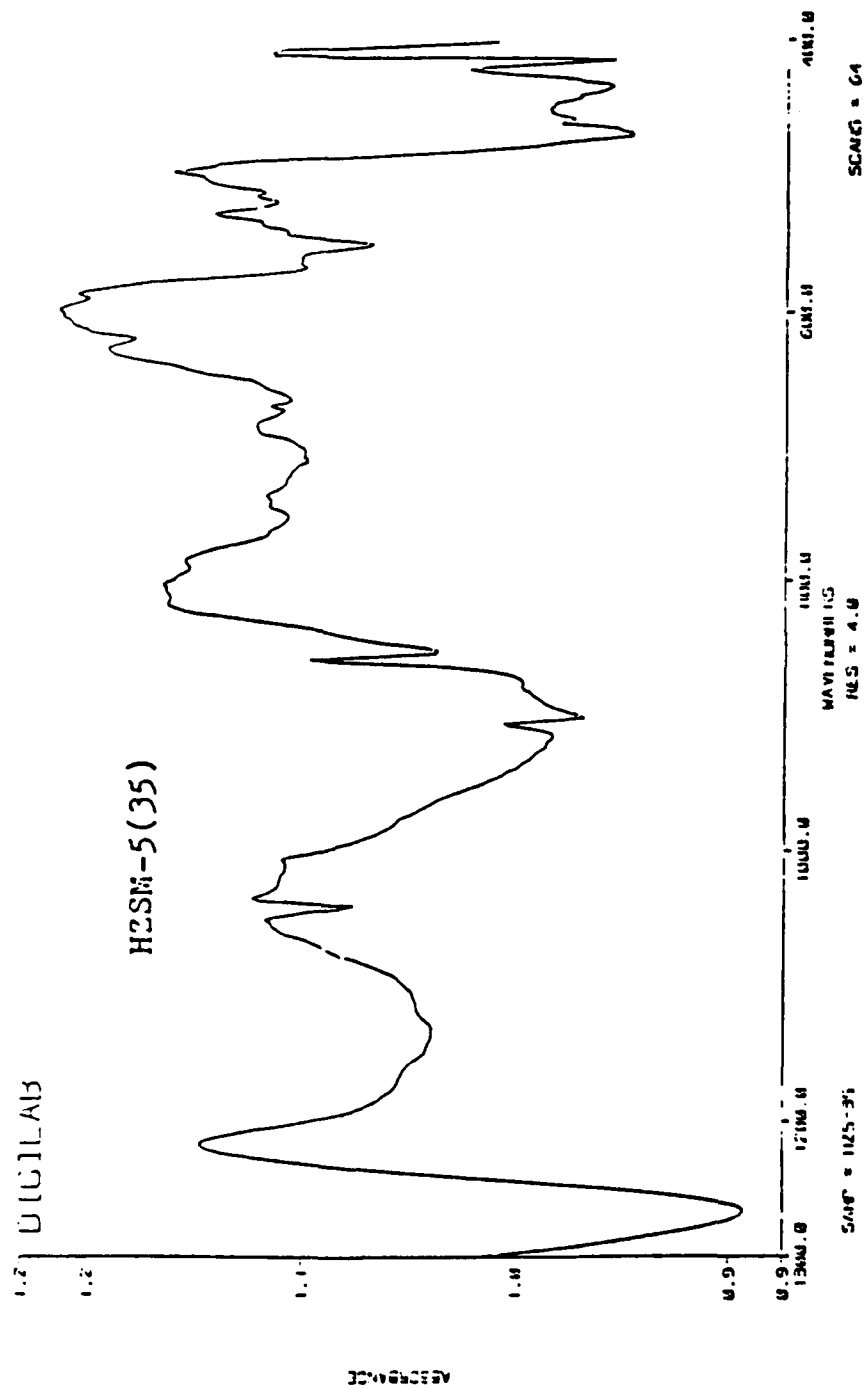
STRUCTURAL FTIR SPECTRA OF SYNTHESIZED ZEOLITES

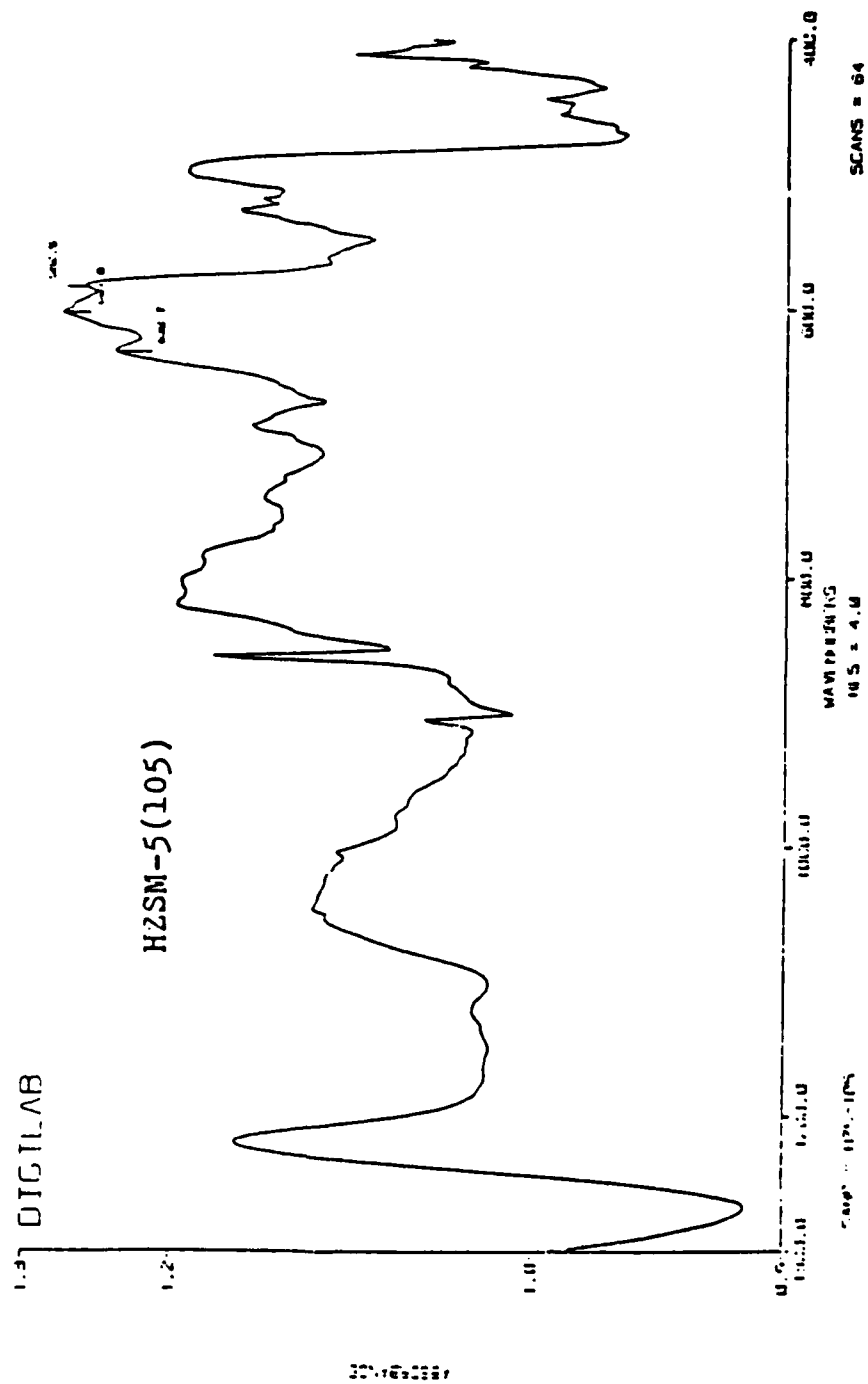
IR spectra of synthetic zeolites were measured by the use of diffuse reflectance FTIR spectroscopy. The IR spectra in the lattice vibrational mode region are presented in this Appendix. Furthermore, a criterion (optical density ratio) for determining the structural characteristics of the zeolite frameworks was established using the data derived from these spectra.









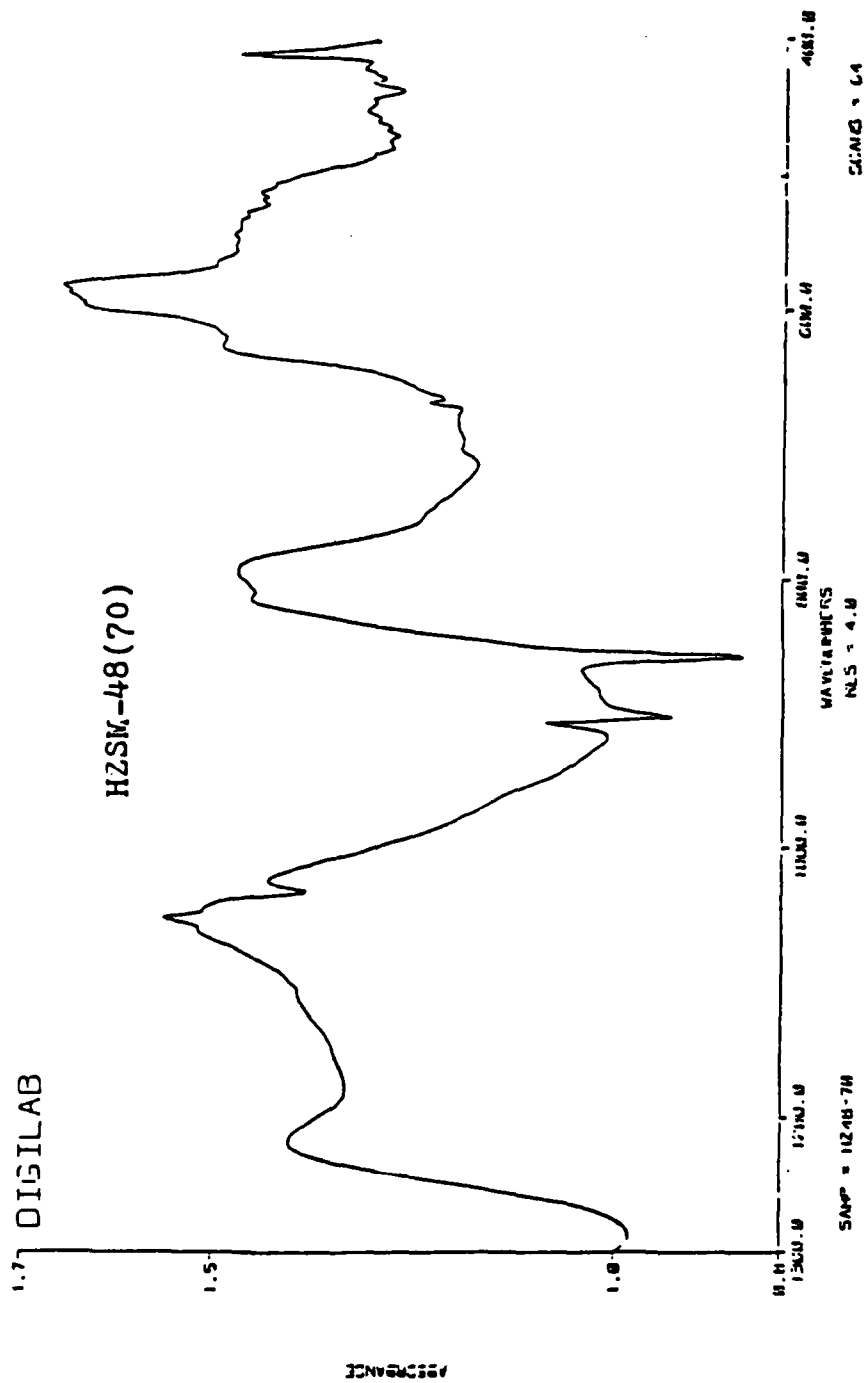


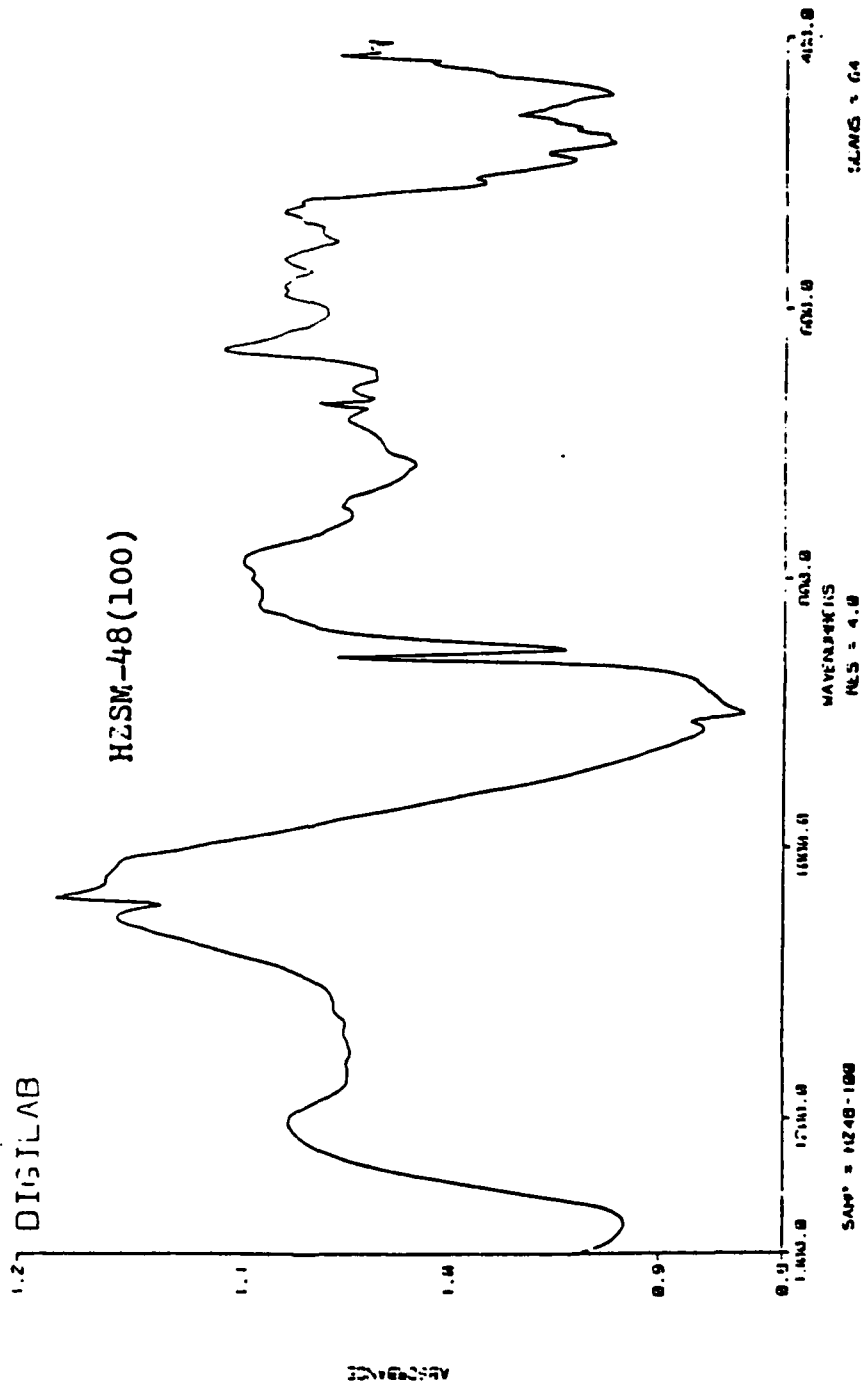
H2SM-5(105)

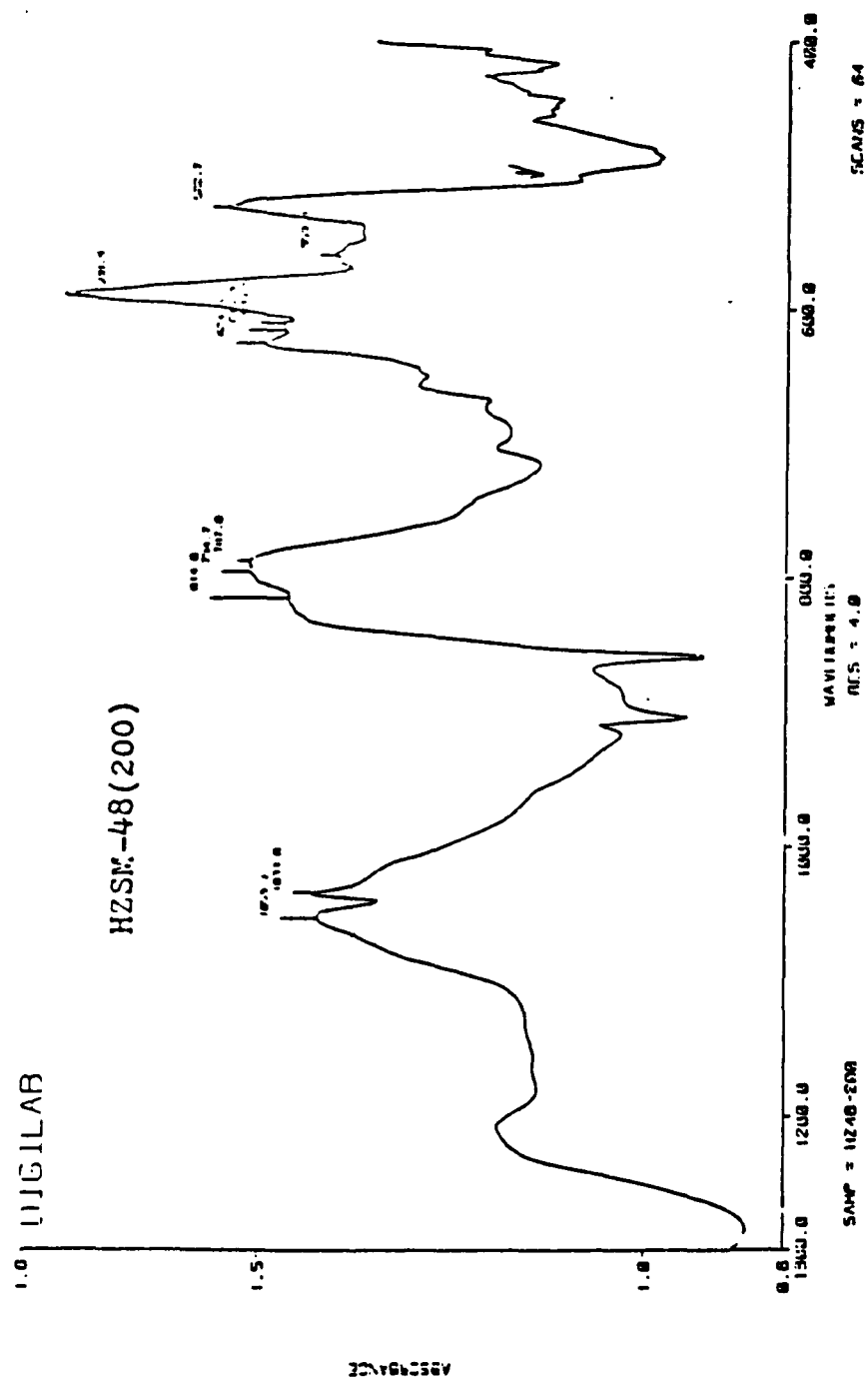
SCANS = 64

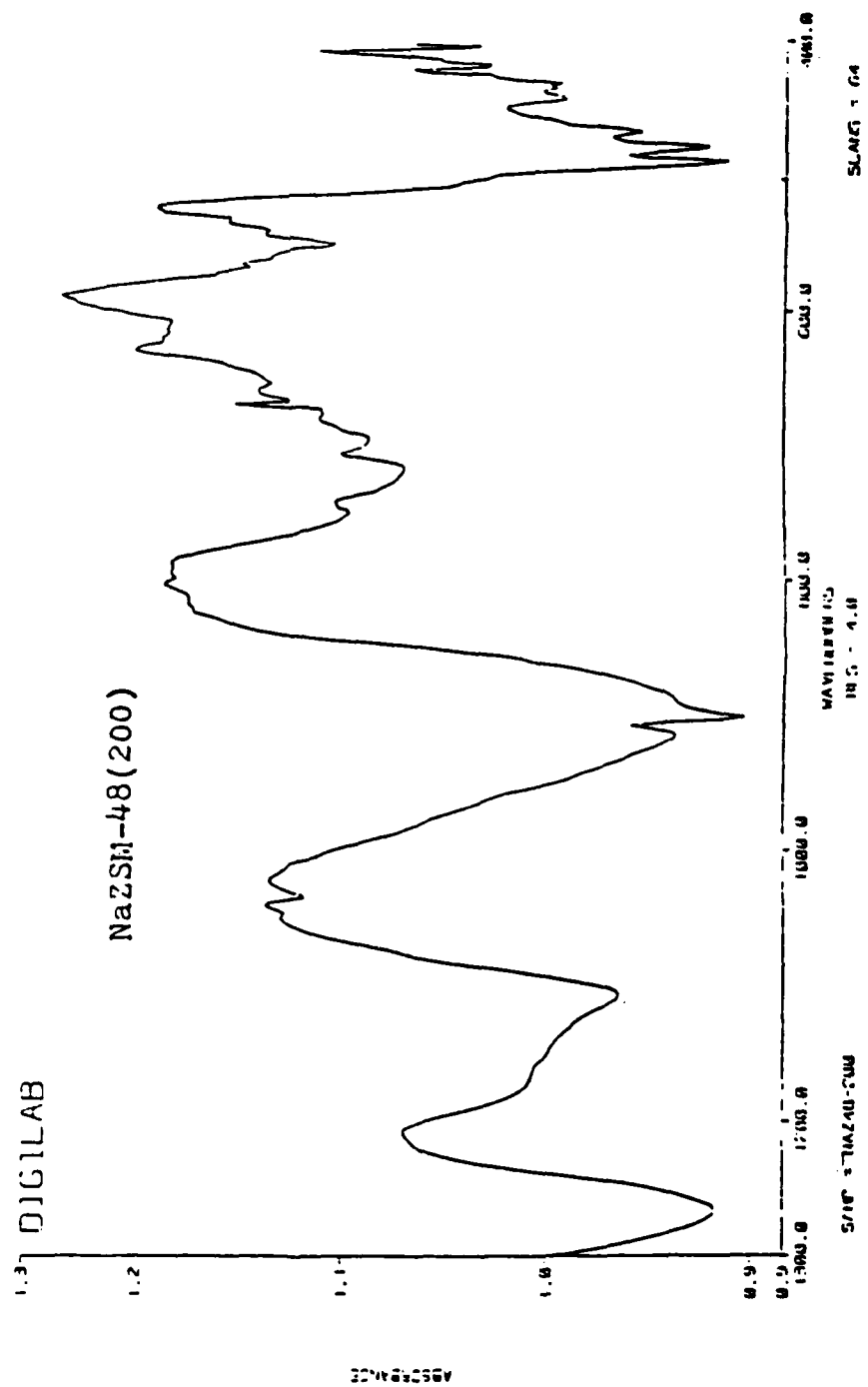
MS = 4.0
SILFADLAW
MM

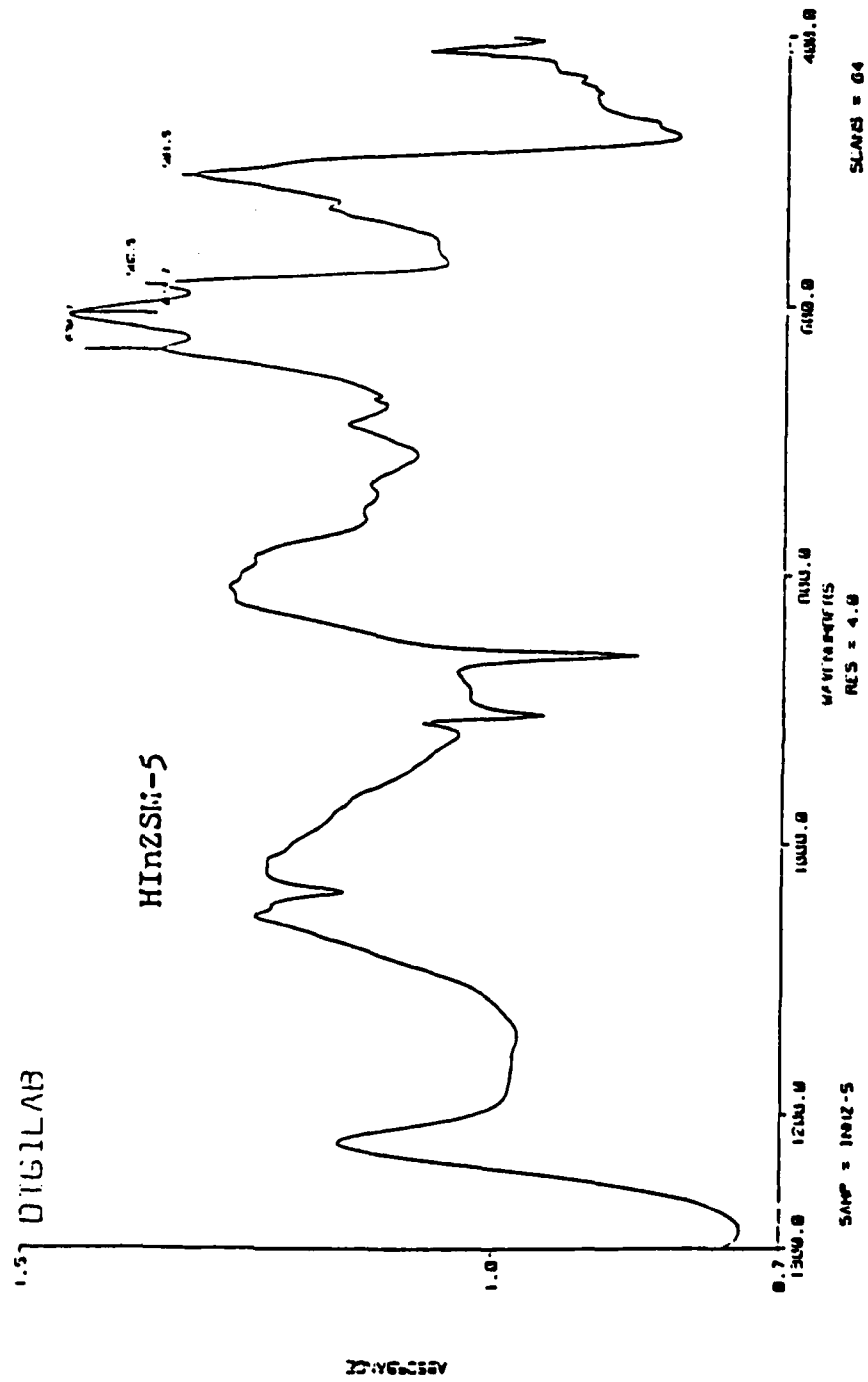
١١٦٠ - ١١٦١

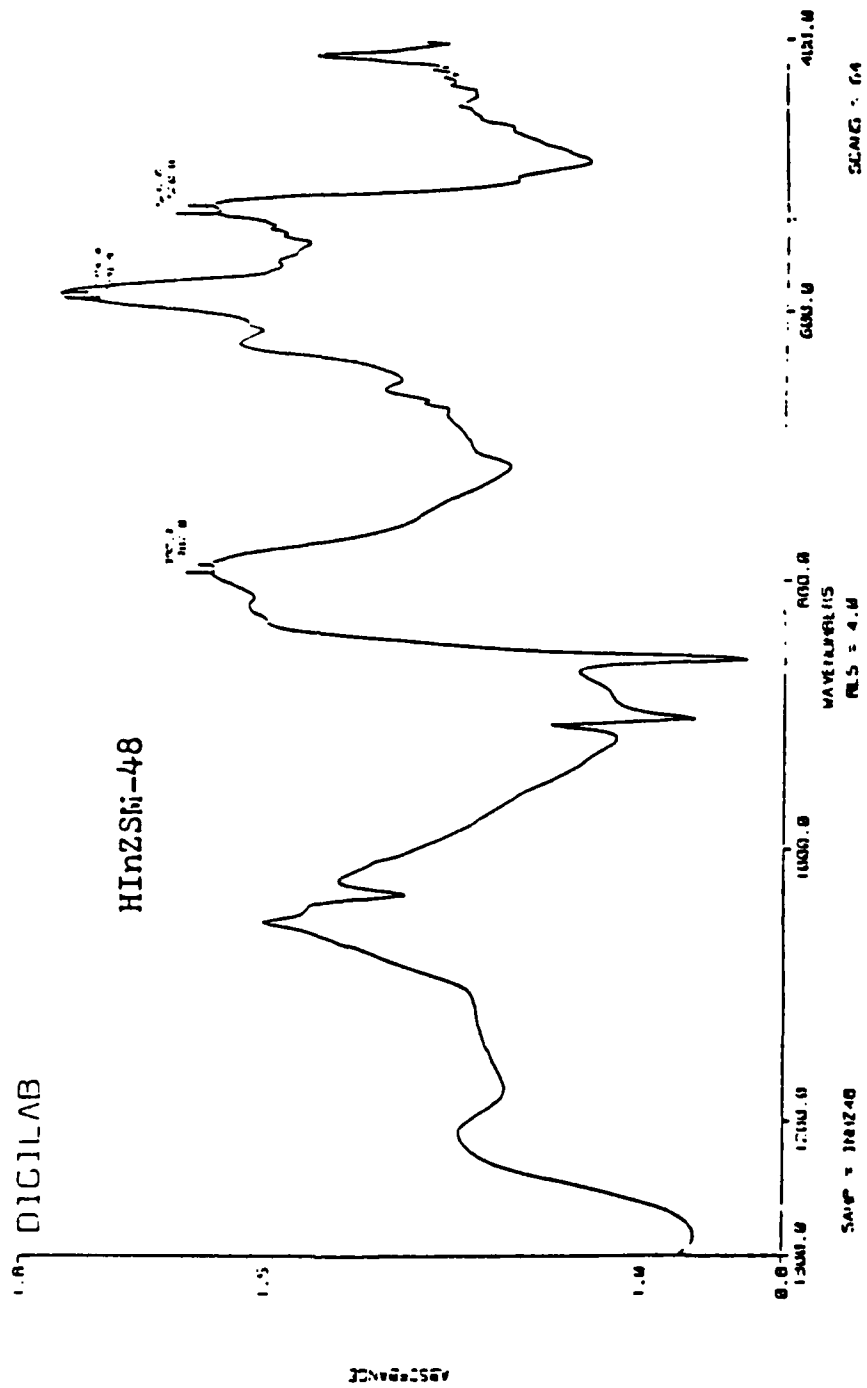


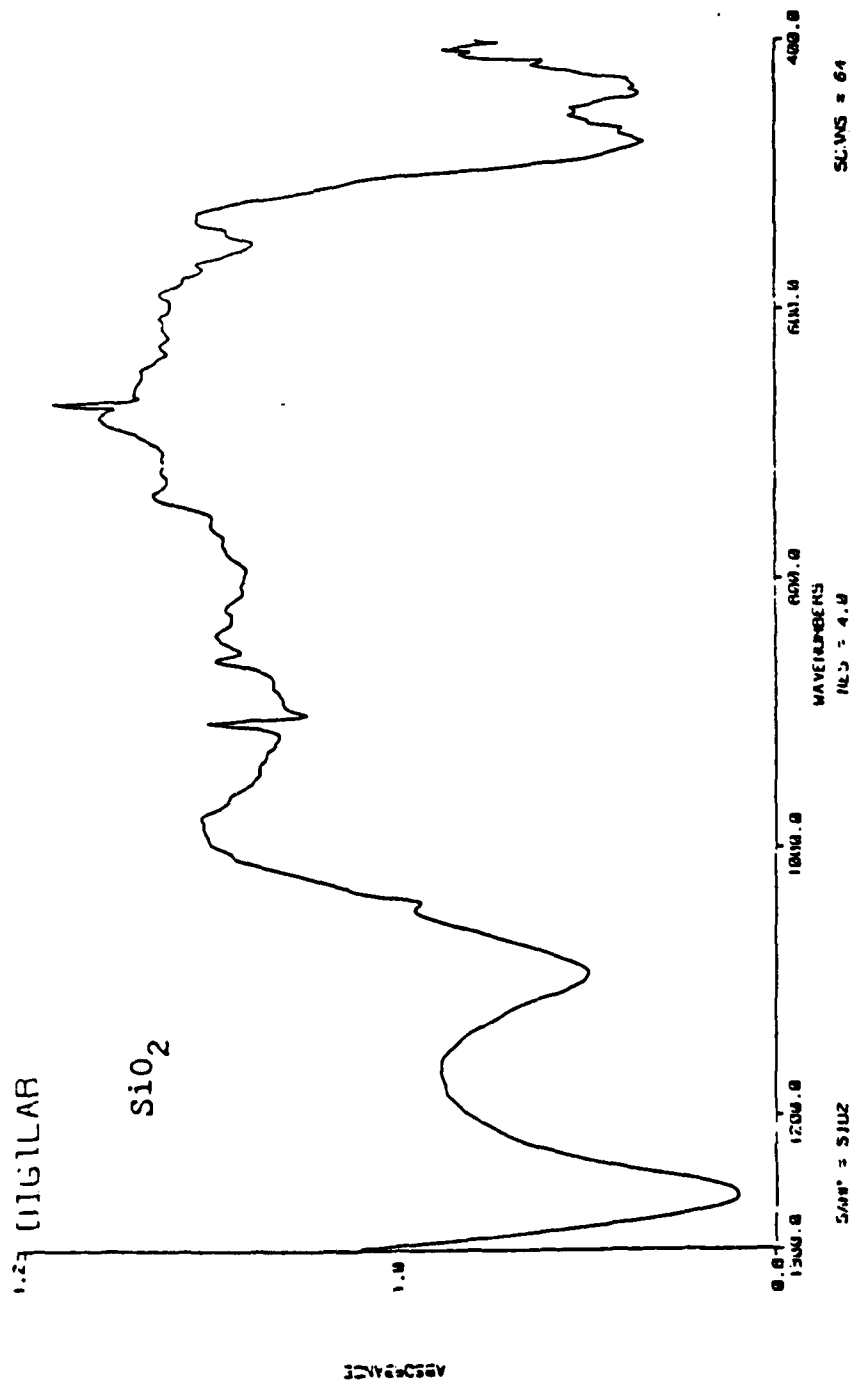


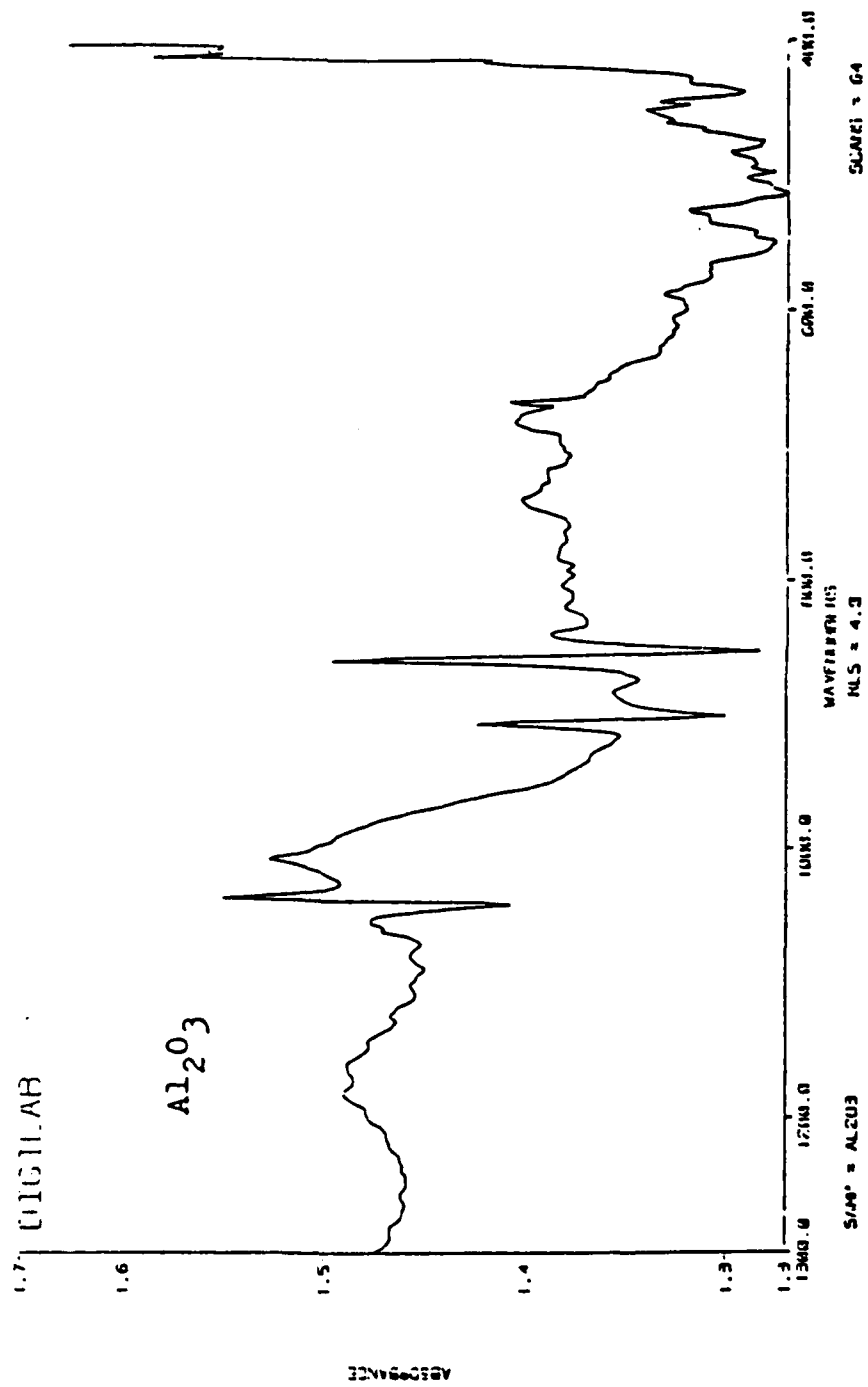












349/350

APPENDIX B

PRODUCT DISTRIBUTION FOR NORMAL-HEXANE CRACKING OVER SYNTHESIZED ZEOLITES

Cracking of normal-hexane over synthesized zeolites was studied using a fixed-bed continuous flow microreactor operating at atmospheric pressure. Normal-hexane was transported into the reactor from a saturator by means of the helium carrier gas. Product distributions were recorded after ten minutes on stream.

The objective of these experiments was to determine the acidity of the synthesized zeolites. The product distribution obtained with the catalysts used in this study is presented in Table 32.

Table 32
Normal-hexane Cracking over Synthesized Zeolites

	Amorphous SiO ₂ Al ₂ O ₃	ZSM-5	ZSM-48	ZSM-48/5
SiO ₂ /Al ₂ O ₃	-4	70	200	70
Reaction Temp., K	805	481	627	585
Conversion	0.12	0.12	0.17	0.17
Product Distribution, wt%				
C ₁ + C ₂	2.1	1.7	1.4	0.7
C ₃	7.7	2.8	6.4	4.0
C ₄	2.2	4.5	6.3	7.6
C ₅	0.3	3.1	2.6	4.7

APPENDIX C

PRODUCT DISTRIBUTION FOR ALCOHOL REACTIONS OVER SYNTHESIZED ZEOLITES

The reaction of alcohols was studied using a fixed-bed continuous flow microreactor operating at atmospheric pressure. Alcohols were transported into the reactor from a saturator by means of the helium carrier gas. Product distributions were recorded after 40 minutes on stream.

The objective of these experiments was to determine the effect of acidity on the selectivity and activity and to determine the influence of channel structure on selectivity.

Alcohols/He/HZSM-5(35), Temperature - 643 K

Product Distribution, wt. %				
	CH ₃ OH	Reactant		
		C ₂ H ₅ OH	C ₃ H ₇ OH	C ₄ H ₉ OH
C ₁ + C ₂	8.9	11.5	9.0	11.4
C ₃	21.3	23.1	27.6	29.5
C ₄	29.7	29.3	29.4	24.9
C ₅	10.2	6.9	5.5	3.5
C ₆	8.1	4.7	3.8	3.9
C ₇ ⁺ Aliphatics	11.4	9.5	9.1	5.6
A ₆	1.4	2.1	2.3	1.8
A ₇	4.9	5.9	6.4	4.8
A ₈	10.0	8.5	7.9	7.7
A ₉ ⁺	0.8	1.2	0.6	1.1

Alcohols/He/HZSM-5(70), Temperature - 643 K

Product Distribution, wt. %				
	CH ₃ OH	Reactant		
		C ₂ H ₅ OH	C ₃ H ₇ OH	C ₄ H ₉ OH
C ₁ + C ₂	11.1	27.8	10.4	15.2
C ₃	22.1	22.2	31.3	34.0
C ₄	29.7	25.9	31.5	29.6
C ₅	12.7	9.6	8.5	6.5
C ₆	6.3	2.8	4.1	2.1
C ₇ ⁺ Aliphatics	4.1	4.3	3.3	2.0
A ₆	1.1	1.0	1.4	1.6
A ₇	5.5	3.2	5.2	5.5
A ₈	6.8	2.8	4.1	3.3
A ₉ ⁺	0.6	0.4	0.2	0.2

Alcohols/He/HZSM-5(105), Temperature = 643 K

Product Distribution, wt. %				
	CH ₃ OH	Reactant		C ₄ H ₉ OH
		C ₂ H ₅ OH	C ₃ H ₇ OH	
C ₁ + C ₂	12.0	40.0	8.1	-
C ₃	22.3	20.0	35.8	-
C ₄	27.1	18.5	29.0	-
C ₅	8.3	2.8	3.8	-
C ₆	8.6	6.1	6.3	-
C ₇ ⁺ Aliphatics	4.9	2.7	3.4	-
A ₆	1.1	1.0	1.5	-
A ₇	4.6	2.6	4.6	-
A ₈	9.8	4.9	6.2	-
A ₉ ⁺	1.3	1.5	1.2	-

Alcohols/He/HZSM-5D, Temperature = 643 K

Product Distribution, wt. %				
	CH ₃ OH	Reactant		C ₄ H ₉ OH
		C ₂ H ₅ OH	C ₃ H ₇ OH	
C ₁ + C ₂	9.9	17.8	10.4	13.6
C ₃	22.1	23.1	29.8	27.8
C ₄	29.7	26.4	28.7	18.4
C ₅	9.9	6.0	5.0	2.4
C ₆	7.4	5.2	4.6	8.4
C ₇ ⁺ Aliphatics	3.6	3.2	2.4	0.7
A ₆	1.2	1.9	2.4	6.1
A ₇	5.8	7.1	8.8	13.8
A ₈	9.6	8.1	7.4	8.6
A ₉ ⁺	0.8	1.2	0.5	0.2

Alcohols/He/HZSM-48(70), Temperature = 643 K

	Product Distribution, wt. %			
	CH ₃ OH	Reactant		C ₄ H ₉ OH
		C ₂ H ₅ OH	C ₃ H ₇ OH	
C ₁ + C ₂	18.2	70.5	8.0	-
C ₃	23.8	11.9	34.3	-
C ₄	24.2	6.5	31.0	-
C ₅	8.3	0.9	5.0	-
C ₆	7.6	1.9	5.4	-
C ₇ ⁺ Aliphatics	2.9	0.7	1.9	-
A ₆	0.8	0.1	1.4	-
A ₇	4.8	2.1	6.6	-
A ₈	8.7	4.6	5.9	-
A ₉ ⁺	0.7	0.9	0.0	-

Alcohols/He/HZSM-48(200), Temperature = 643 K

	Product Distribution, wt. %			
	CH ₃ OH	Reactant		C ₄ H ₉ OH
		C ₂ H ₅ OH	C ₃ H ₇ OH	
C ₁ + C ₂	14.4	75.7	2.7	3.6
C ₃	23.7	12.3	52.1	29.8
C ₄	26.4	5.2	28.2	42.1
C ₅	9.4	0.8	2.4	4.7
C ₆	13.1	1.9	6.6	11.1
C ₇ ⁺ Aliphatics	6.4	0.7	3.3	3.5
A ₆	0.9	0.4	0.9	1.6
A ₇	1.2	0.9	0.9	1.3
A ₈	3.8	2.1	1.9	1.7
A ₉ ⁺	0.7	0.0	0.0	0.6

Methanol/He/HZSM-5(70)

	Product Distribution, wt. %			
	Reaction Temperature, K			
	594	648	710	752
C ₁ + C ₂	23.3	15.4	21.7	33.6
C ₃	17.5	27.6	34.1	34.3
C ₄	0.0	17.8	16.0	11.2
C ₅	23.0	15.2	9.4	4.2
C ₆ ⁺ Aliphatics	32.6	13.0	6.2	2.3
A ₆	0.6	1.1	1.6	1.4
A ₇	0.9	4.3	4.8	4.7
A ₈	1.8	5.0	5.7	7.6
A ₉ ⁺	0.3	0.6	0.5	0.7

Methanol/He/HZSM-48(200)

	Product Distribution, wt. %			
	Reaction Temperature, K			
	597	648	710	759
C ₁ + C ₂	17.9	16.9	19.6	34.5
C ₃	31.8	36.1	50.3	44.1
C ₄	0.0	8.2	4.1	0.0
C ₅	14.1	9.8	0.5	1.8
C ₆ ⁺ Aliphatics	33.7	23.7	18.6	7.9
A ₆	1.4	0.9	1.0	1.1
A ₇	0.5	1.2	1.5	2.5
A ₈	0.6	3.1	4.2	7.6
A ₉ ⁺	0.0	0.1	0.2	0.5
Conversion, wt. %	87.0	95.0	95.2	96.0

Methanol/H₂/HZSM-5(70)

	Product Distribution, wt. %			
	Reaction Temperature, K			
	597	648	710	762
C ₁ + C ₂	21.5	15.6	27.1	37.8
C ₃	22.4	36.9	46.2	43.8
C ₄	0.0	0.0	0.1	0.1
C ₅	23.8	21.1	10.8	5.0
C ₆ ⁺ Aliphatics	29.6	16.1	4.0	1.3
A ₆	0.0	1.3	1.5	1.6
A ₇	1.5	4.6	5.0	5.0
A ₈	1.1	3.8	5.1	5.2
A ₉ ⁺	0.1	0.6	0.2	0.2

Methanol/H₂/HZSM-48(200)

	Product Distribution, wt. %			
	Reaction Temperature, K			
	598	649	711	769
C ₁ + C ₂	19.2	19.7	20.9	29.5
C ₃	30.2	34.3	40.3	39.9
C ₄	0.0	18.1	20.2	15.7
C ₅	21.6	11.2	8.3	4.4
C ₆ ⁺ Aliphatics	26.7	14.2	7.2	4.3
A ₆	1.4	0.0	0.8	1.1
A ₇	0.4	0.9	0.9	2.3
A ₈	0.4	1.5	1.4	2.8
A ₉ ⁺	0.0	0.1	0.0	0.0

APPENDIX D

INTERPOLATION OF CAPSULE CALIBRATION AND CHEMISORPTION ISOTHERM COMPUTER PROGRAM

It was convenient to calculate the isotherms on the computer whenever a large number of adsorption isotherms were determined for a single catalyst. However, the use of the computer required interpolation of the precision pressure gage capsule calibration data in a form readily usable in the program.

Interpolation of Capsule Calibration Data

The pressure was calculated using the following equations. For angles of rotation in the range

$$0 < \text{Deg} < 1$$

the pressure was calculated from the following expression

$$\text{Pressure} = \text{B1L} * \text{Deg} \quad (\text{D-1})$$

where B1L is the tube constant in Torr deg⁻¹ supplied by Texas Instruments, Incorporated, for the pressure range 0 to 40 Torr. For angles of rotation in the range

$$1 < \text{Deg} < 999.9$$

the pressure was calculated from the following expression

$$\text{Pressure} = \text{C} + \text{B1} * \text{Deg} + \text{B2} * (\text{Deg})^2 \quad (\text{D-2})$$

where C, B1, and B2 are constants. The calibration data supplied by Texas Instruments, Incorporated, was fit by least-squares polynomials using an orthogonal polynomial method. The data were fit to second through fifth order polynomials with an index of determination of 0.9999992

and a standard error of estimate for y (i.e., pressure) of 0.2258019.

The precision pressure gage was purchased with two quartz Bourdon tube capsules. The cell and least squares constants were as follows:

Bourdon tube serial number	4741	5083
B1L	8.05082	8.14762
C	-0.0859211	-0.4245883
B1	8.086858	8.160982
B2	0.00008718	-0.0001544

A program was written in IBM Fortran IV language to generate a table of pressures as a function of degrees of rotation for use in hand calculating adsorption isotherms. The program is reproduced below with appropriate comment cards to explain its use.

\$WATFIV

```

C THIS PROGRAM GENERATED A TABULATION OF PRESSURES IN UNITS OF CM OF
C HG AS A FUNCTION OF THE DEGREES OF ROTATION READ FROM TI PRECISION
C PRESSURE GAGE. THE CALIBRATION DATA SUPPLIED BY TEXAS INSTRUMENTS,
C INC FOR THE QUARTZ SPIRAL BOURDON TUBES WERE FIT BY A LEAST SQUARE
C POLYNOMIAL METHOD. THE SECOND ORDER POLYNOMIAL FIT WAS SELECTED TO
C CORRELATE THE DATA FROM 1.0 TO 102.0 DEGREES, THAT IS,  $P(I) = C +$ 
C  $B1*DEG + B2*DEG*DEG$  WHERE C WAS THE INTERCEPT, B1 WAS COEFFICIENT
C OF THE FIRST ORDER TERM AND B2 WAS COEFFICIENT OF THE SECOND ORDER
C TERM. THE PRESSURE FROM 0.0 TO 1.0 WAS CORRELATED BY  $P(I) = B1L*$ 
C  $DEG$  WHERE B1L WAS THE TUBE CONSTANT IN TORR PER DEG FROM THE ORIG-
C INAL CALIBRATION. THE PRESSURES WERE PRINTED OUT FOR EVERY 0.002
C DEGREES OF ROTATION. QUARTZ SPIRAL BOURDON CAPSULE NO. 5083.
1 DIMENSION H(20),PRESS(20)
2 CK=0.000000
C CARD 3 INTERCEPT C WAS READ
3 C = -0.4245883
C CARD 4 COEFFICIENT OF FIRST ORDER TERM B1 WAS READ
4 B1 = 8.160982
C CARD 5 COEFFICIENT OF SECOND ORDER TERM B2 WAS READ
5 B2 = -0.0001544
C CARD 6 TUBE CONSTANT B1L WAS READ
6 B1L = 8.14762
7 DO 20 I=1,10
8 H(I)=0.0+0.002000*FLOAT(I-1)
9 20 PRESS(I)= 0.0000
10 DO 90 N=1,203
11 35 WRITE(6,40)N
12 400FORMAT(20X,'TEXAS GAGE CALIBRATION, F. V. HANSON, 27 FEBRUARY 1987
13 4',30X,'PAGE',17///)
14 WRITE(6,45) (H(N1),N1=1,10)
15 45 FORMAT(29X,F8.3,9F9.3)
16 WRITE(6,47)
17 470FORMAT(23X,'*****')
18 4*****')
19 DO 80 K=1,25
20 DEGI = FLOAT(N-1)*0.5000+FLOAT(K-1)*0.0200
21 DO 62 I=10
22 DEG = D*91 + H(I)
23 IF(DEG-1.0)64,65,65
24 64 PRESS(I)=B1L*DEG
25 GO TO 62
26 65 PRESS(I)= C+DEG*B1+DEG*DEG*B2
27 62 CONTINUE
28 660WRITE(6,67)DEGI,PRESS(1),PRESS(2),PRESS(3),PRESS(4),PRESS(5),PRESS
29 4(6),PRESS(7),PRESS(8),PRESS(9),PRESS(10)
30 67 FORMAT(20X,F7.3,' ',F8.3,9F9.3/)
31 80 CONTINUE
32 WRITE(6,85)
33 85 FORMAT(1H1)
34 90 CONTINUE

```

35	STOP
36	END
37	\$DATA
38	\$STOP
39	/*

Adsorption Isotherm Computer Program

The adsorption isotherm computer program was also written in IBM Fortran IV language and was based on the isotherm calculation procedure outlined in Section VII. The program was adapted from an original program written by Dalla Betta.⁵² The input data included helium calibration pressures, P_1 , P_2 , and P_3 , and temperatures T_1 , T_2 , and T_3 , and isotherm data points, that is, pressures $P_1(n)$ and $P_2(n)$ and temperatures $T_1(n)$. The mass of catalyst was also included to permit calculation of the amount adsorbed per unit mass of catalyst; however, isotherms computed on this basis must be corrected to a dry catalyst basis. The program will accept up to 10 calibration data points and up to 20 isotherm data points. As many as five isotherms can be calculated in a single computation.

The program is reproduced below and the use of the various options are explained on the comment cards. A typical adsorption isotherm printout for the 0.53 percent platinum on silica gel catalyst is presented following the program.

\$WATFIV

C THIS PROGRAM CALCULATED THE DOSER AND CELL VOLUMES AND THE ADSORP-
C TION ISOTHERM FROM PRESSURE DATA, IN UNITS OF DEGREES, OBTAINED
C WITH A TEXAS INSTRUMENTS PRECISION PRESSURE GAGE IN A CONSTANT VOL-
C UME ADSORPTION APPARATUS. THE PROGRAM CONVERTED THE DATA TO PRESS-
C URE IN CM OF HG, THEN CALCULATED THE VOLUME ADSORBED IN CC / GRAM
C AND THE AMOUNT ADSORBED IN MICROMOLES PER GRAM. THE PROGRAM CALCU-
C LATED UP TO FIVE ISOTHERMS AT A TIME. QUARTZ SPIRAL BOURDON CAP-
C SULE NO 5083.

C DATA DECK WAS ARRANGED AS FOLLOWS

C 1ST CARD EXPERIMENT IDENTIFICATION INCLUDING LSAC CATALYST
C CODE AND ISOTHERMS OBTAINED - UP TO 80 ALPHANUMERIC
C CHARACTERS

C 2ND CARD N YY.YYYY ZZ.ZZ
C WHERE N WAS AN INTEGER-0, 1 OR 2 THAT DEFINES THE
C STATUS OF THE CALIBRATED BULB, VBULB.
C N=0 STANDARD BULB WAS CLOSED TO THE DOSER VOLUME,
C N=1 STANDARD BULB WAS OPEN TO THE DOSER VOLUME AND
C WAS INCLUDED AS PART OF THE DOSER VOLUME
C N=2 STANDARD BULB WAS VARIABLE, THAT IS, EITHER
C OPENED OR CLOSED FOR EACH ISOTHERM POINT.

C Y (FREE FORM) WAS THE MASS OF THE CATALYST CHARGED
C TO ADSORPTION CELL, GRAMS

C Z (FREE FORM) WAS CELL TEMPERATURE IN DEG CENTIGRADE
C 3RD CARD CELL VOLUME CALIBRATION DATA, P1, T1, P2, T2, P3, T3
C (FREE FORM, SEPARATED BY A SINGLE SPACE) IN THE FORM
C UUU.UUU VV.VV WWW.WW XX.XX YYY.YYY ZZ.ZZ
C WHERE U=P1 WAS THE PRESSURE IN CALIBRATED DOSER
C VOLUME MEASURED AT THE AMBIENT TEMPERATURE V=T1,
C W = P2 WAS THE PRESSURE IN THE CALIBRATED DOSER VOL-
C UME PLUS THE CONNECTING STOPCOCK VOLUME AFTER EXPAN-
C SION MEASURED AT THE AMBIENT TEMPERATURE X = T2, Y =
C P3 WAS THE PRESSURE IN THE DOSER VOLUME PLUS THE
C CELL AFTER THE SECOND EXPANSION MEASURED AT THE AM-
C BIENT TEMPERATURE Z = T3 WITH THE CELL IMMersed IN
C THE CONSTANT TEMPERATURE BATH, P1, P2, AND P3 WERE IN
C DEGREES AND T1, T2, AND T3 WERE IN DEGREES CENTIGRADE
C 4TH CARD LAST CARD OF CALIBRATION DATA, SAME FORM AS DATA EX-
C CEPT UUU.UUU WAS 999.9 OR LARGER, THAT IS, FINAL
C CARD SHOULD READ

C 999.9 999.9 999.9 999.9 999.9 999.9

C 5TH CARD ISOTHERM TITLE - UP TO 80 ALPHANUMERIC CHARACTERS

C 6TH CARD ADSORPTION ISOTHERM DATA, P1, T1, P2, T2
C (FREE FORM, SEPARATED BY A SINGLE SPACE) IN THE FORM
C WWW.WWW XX.XX YYY.YYY ZZ.ZZ

C WHERE W = P1 WAS THE PRESSURE IN THE DOSER VOLUME AT
C AMBIENT TEMPERATURE X = T1, Y = P2 WAS THE PRESSURE
C IN THE DOSER VOLUME PLUS THE CELL AFTER EXPANSION AT
C AMBIENT TEMPERATURE Z = T2.

C THE PROGRAM ACCEPTED 1 TO 20 SETS OF ISOTHERM DATA
C 7TH CARD LAST CARD OF ISOTHERM DATA, SAME FORM AS DATA EXCEPT

```

C      UUU.UUU WAS USED TO TERMINATE ISOTHERM CALCULATION
C      OR TO SET THE MODE FOR CONTINUATION OF CALCULATION
C      OF SUBSEQUENT ISOTHERM, THE FORM OF FINAL CARD WAS
C      UUU.UUU 999.9 999.9 999.9
C      WHERE IF UUU.UUU = 999.9 TERMINATION OF CALCULATION
C      IF UUU.UUU = 1002.0 ANOTHER ISOTHERM TO FOLLOW
C      WHICH INCLUDED A NEW SET
C      OF CELL VOLUME CALIBRATION
C      DATA
C      IF N WAS EQUAL TO 2 ON SECOND CARD (STANDARD BULB IN
C      VARIABLE MODE) THEN THE ADSORPTION ISOTHERM DATA,
C      6TH CARD WAS OF FORM
C      WWW.WWW XX.XX YYY.YY ZZ.ZZ M
C      WHERE W, X, Y, AND Z WERE THE SAME AS ABOVE
C      IF M = 0, STANDARD BULB WAS NOT INCLUDED IN DOSER
C      VOLUME
C      IF M = 1, STANDARD BULB WAS INCLUDED IN DOSER VOLUME
1      DIMENSION TIT(80),CP1(10),CP2(10),CP3(10)
2      DIMENSION PISOI(100),PISOF(100),DCP1(100),DCP2(100),DCP3(100)
3      DIMENSION RSC(10),RCCELL(10),TIC(100),TFC(100),TI(100),TF(100)
4      DIMENSION T1(10),T2(10),T3(10),TK1(10),TK2(10),TK3(10)
5      DIMENSION DPISOF(100),TIT2(80,5),DPISOI(100),NVSB(100),L(5)
6      1 CONTINUE
C      THE QUARTZ BOURDON TUBE CALIBRATION CONSTANTS C, B1, B2 AND B1L
C      WERE READ AT THIS POINT. THE PRESSURE FROM 1.0 TO 102.0 DEGREES
C      WAS CALCULATED FROM THE EQUATION  $P(I) = C + B1*DEG + B2*DEG*DEG$ 
C      WHERE THE CONSTANTS WERE DEFINED AS FOLLOWS, C WAS THE INTERCEPT,
C      B1 WAS THE COEFFICIENT OF THE FIRST ORDER TERM AND B2 WAS THE
C      COEFFICIENT OF THE SECOND ORDER TERM. THE PRESSURE FROM 0.0 TO 1.0
C      DEGREE WAS CALCULATED FROM THE EQUATION  $P(I) = B1L*DEG$  WHERE B1L
C      WAS THE TUBE CONSTANT IN TORR DEGREE FROM THE ORIGINAL CALIBRATION
C      IT WAS NECESSARY TO CHANGE THESE CARDS WHEN CAPSULE WAS CHANGED.
C      ALSO THE CALIBRATED DOSER VOLUME WAS RECALIBRATED WHEN CAPSULE WAS
C      CHANGED, THAT IS, NEW VALUE OF V1 REQUIRED (PROGRAM CARD NO. 12)
7      B1 = 8.160982
8      B2 = -0.0001544
9      C = -0.4245883
10     B1L = 8.14762
11     VBULB = 49.0548
12     V1 = 6.2890
13     MODE=1
14     NK=0
15     XMULT=0.0
16     ARSC=0.0
17     ARCELL=0.0
18     READ(5,25) (TIT(I),I=1,80)
19     25 FORMAT(80A1)
20     READ, IFSB, WTSAMP, TCELL
21     TC= 273.16 + TCELL
22     N=0
23     3 N=N+1

```

```

24      READ, DCP1(N), T1(N), DCP2(N), T2(N), DCPE(N), T3(N)
25      TK1(N) = 273.16 + T1(N)
26      TK2(N) = 273.16 + T2(N)
27      TK3(N) = 273.16 + T3(N)
28      IF(DCP1(N)-999.9)100,5,5
29      100 CP1(N) = (C + B1*DCP1(N) + B2*DCP1(N)*DCP1(N))/10.0
30      CP2(N) = (C + B1*DCP2(N) + B2*DCP2(N)*DCP2(N))/10.0
31      CP3(N) = (C + B1*DCP3(N) + B2*DCP3(N)*DCP3(N))/10.0
32      RSC(N) = (CP1(N)/TK1(N) - CP2(N)/TK2(N))*TK2(N)/CP2(N)
33      RCELL(N) = (CP2(N)/TK2(N) - CP3(N)/TK3(N))*TC/CP3(N)
34      ARSC = ARSC + RSC(N)
35      ARCELL = ARCELL + RCELL(N)
36      GO TO 3
37      5 N = N - 1
38      ARSC = ARSC / FLOAT(N)
39      ARCELL = ARCELL / FLOAT(N)
40      AVSC = ARSC * V1
41      AVCELL = ARCELL * (V1 + AVSC)
42      NIFSB = IFSB + 1
43      152 NK = NK + 1
44      L(NK) = 20 * (NK - 1)
45      153 READ(5,25) (TIT2(I,NK), I=1,80)
46      9 L(NK) = L(NK) + 1
47      M = L(NK)
48      GO TO (55,55,56), NIFSB
49      56 CONTINUE
50      READ, DPISOI(M), DPISOF(M), NVSB(M)
51      GO TO 59
52      55 CONTINUE
53      READ, DPISOI(M), TIC(M), DPISOF(M), TFC(M)
54      59 IF(DPISOI(M) - 999.9)15,20,20
55      20 IF(DPISOI(M) - 1000.0)53,53,21
56      21 MODE = IFIX(DPISOI(M) - 1000.0)
57      GO TO (53,152,53), MODE
58      15 IF(DPISOI(M) - 1.0)16,17,17
59      16 PISOI(M) = B1L*DPISOI(M)/10.0
60      GO TO 18
61      17 PISOI(M) = (C + B1*DPISOI(M) + B2*DPISOI(M)*DPISOI(M))/10.0
62      18 CONTINUE
63      TI(M) = 273.16 + TFC(M)
64      TF(M) = 273.16 + TIC(M)
65      22 IF(DPISOF(M) - 1.0)23,24,24
66      23 PISOF(M) = B1L*DPISOF(M)/10.0
67      GO TO 51
68      24 PISOF(M) = (C + B1*DPISOF(M) + B2*DPISOF(M)*DPISOF(M))/10.0
69      51 CONTINUE
70      52 GO TO 9
71      53 VDOSER = V1 + AVSC + BULB*FLOAT(IFS)
72      WRITE (6,27)
73      27 FORMAT ('1')
74      WRITE(6,28)(TIT(I), I=1,80)

```

```

75      28 FORMAT(1X,80A1)
76      WRITE(6,10)
77      10 FORMAT(/43H          P(DEG)          P(CM)          RATIO)
78      DO 6 I=1,N
79      60WRITE(6,7) DCP1(I),CP1(I),TK1(I),DCP2(I),CP2(I),TK2(I),RSC(I),DCP3
      4(I),CP3(I),TK3(I),RCELL(I)
80      70FORMAT(F10.3,F13.3,1H(,F6.2,1H)/F10.3,F13.3,1H(,F6.2,1H),F14.6/
      4F10.3,F13.3,1H(,F6.2,1H),F14.6/)
81      WRITE(6,32)ARSC,ARCELL
82      32 FORMAT(35X,9H-----/30X,F14.6/30X,F14.6)
83      WRITE(6,8)AVSC,AVCELL
84      8 FORMAT(1X,12HAVE FSC      =,F10.4/1X,12HAVE VCELL =,F10.4)
85      GO TO (70,70,71),NIFSB
86      70 WRITE(6,80)VDOSER
87      GO TO 72
88      71 WRITE(6,81)
89      80 FORMAT(1X,12HVDOSER      =,F10.4)
90      81 FORMAT(1X,22HVDOSER      = VARIABLE)
91      72 IF(WTSAMP)154,154,34
92      34 XMULT = 1.0/(76.0*WTSAMP)
93      WRITE(6,31)WTSAMP
94      31 FORMAT(1X,12H DRY WEIGHT =,F10.4)
95      154 DO 155 NL=1,NK
96      SPVADS=0.0
97      SUMADS=0.0
98      OPVLEF=0.0
99      35 WRITE(6,28) (TIT2(I,NL),I=1,80)
100     IF(NL-1)98,98,99
101     98 WRITE(6,11)
102     110 FORMAT(/77H P(DEG)          P(CM)          PV(ADSORB)  V ADS(CC/G)
      4SUM VADS      MOLES E-6)
103     99 L(NL)=L(NL)-1
104     M1=L(NL)-(NL-1)*20
105     DO 13 I1=1,M1
106     I=I1+(NL-1)*20
107     PRINT,VDOSER,AVCELL
108     PVLEFT=PISOF(I)*AVCELL
109     GO TO (60,60,58),NIFSB
110     58 VDCSER=V1+AVSC+VBULB*FLOAT(NIFSB(1))
111     60 PVADS = ((PISOI(I)/TI(I)-PISOF(I)/TF(I))*VDOSER + OPVLEF/TC-
      4PVLEFT/TC)*273.16
112     PRINT,PISOI(I),TI(I),PISOF(I),TF(I),VDOSER,OPVLEF,PVLEFT
113     SPVADS=SPVADS+PVADS
114     OPVLEF=PVLEFT
115     30 AD SG=PVADS*XMULT
116     33 SUMADS=SUMADS+ADSG
117     XMOLES=SUMADS/0.022414
118     GO TO (64,64,62),NIFSB
119     62 WRITE(6,63)I1,DPISOI(I),PISOI(I),VDOSER
120     63 FORMAT(13,1H),F7.3,F9.3,4X,8HVDOSER =,F10.4)
121     GO TO 13

```

```

122      64 WRITE(6,19)I1,DPISOI(I),PISOI(I),TI(I)
123      19 FORMAT(13,1H),F7.3F9.3,1H(F6.2,1H)
124      13 WRITE(6,26) DPISOF(I),PISOF(I),TF(I),PVADS,ADSG,SUMADS,XMOLES
125      26 FORMAT(F11.3,F9.3,1H(,F6.2,1H),4(F12.4)/)
126      155 CONTINUE
127      GO TO (150,150,1),MODE
128      150 CONTINUE
129      STOP
130      END
131  $DATA
132  $STOP
133  /*

```


TAR-11---H2, O2, AND TITRATION ISOTHERMS, PLATINUM/SILICA GEL CATALYST

P(DEG)	P(CM)	RATIO
83.593	68.070(27.00)	
76.633	62.407(27.05)	0.090921
31.235	25.433(27.10)	1.419770
84.266	68.617(24.95)	
77.248	62.907(25.05)	0.091132
31.357	25.533(25.15)	1.439332
84.560	68.856(25.45)	
77.507	63.118(25.50)	0.091097
31.636	25.760(25.60)	1.423842
83.386	67.901(26.10)	
76.457	62.264(26.20)	0.090909
31.159	25.371(26.30)	1.424306

		0.091015
		1.426812

AVE VSC = 0.5724

AVE VCFL = 9.7899

VDOSER = 6.8614

DRY WIGHT = 0.5030

OXYGEN ADSORPTION ISOTHERM AT 20 C--400 C RED, 400 C EVAC 8 HOUR(REPEAT)

	P(DEG)	P(CM)	PV(ADSORB)	V ADS(CC/G)	SUM VADS	MOLES E-6
1)	8.845	7.175(25.7)				
	3.199	2.568(26.35)	5.3662	0.1404	0.1404	6.2666
2)	13.342	10.843(26.3)				
	7.260	5.882(26.70)	0.7369	0.0193	0.1597	7.1272
3)	20.140	16.387(26.8)				
	12.452	10.117(26.95)	0.4799	0.0126	0.1722	7.6877
4)	25.676	20.901(26.9)				
	17.765	14.451(27.40)	0.5617	0.0147	0.1869	8.3437
5)	30.126	24.529(27.4)				
	22.724	18.495(27.70)	0.5906	0.0154	0.2023	9.0333
6)	36.289	29.553(27.6)				
	28.183	22.945(27.80)	0.4518	0.0118	0.2142	9.5610

CORE USAGE OBJECT CODE = 6552 BYTES, ARRAY AREA= 7130 BYTES, TOTAL
 COMPILE TIME= 0.57 SEC, EXECUTION TIME = 0.18 SEC, WATFIV - VERSION 1

APPENDIX E

REACTOR MASS BALANCE COMPUTER PROGRAMS

A. Program for Product Analysis for the Catalytic Cracking of Kerosene

The Fortran program, MASSBAL2, was written to process the data from the analyses of the products produced in the catalytic cracking of kerosene. A sample input and output are included. The input data was taken from the analyses of the gas and liquid products produced in Run number 44.

Table E-1

Program Listing for MASSBAL2

C Program to calculate the product yield from the cracking of
C kerosene. The program can be easily modified to calculate
C product yield for the cracking of diesel boiling range material,
C simply by increasing the product slate to include the highest
C boiling carbon number below the initial boiling point of diesel. The
C highest boiling point carbon number which boiled below the initial
C boiling point of the kerosene for which this program was written was
C C₉.
C The input is obtained from gas chromatographic analyses of the
C gas and liquid products. The gas product data is cast in the
C form of adjusted weight percents (the sum of all the weight
C percents must equal 100 %). The liquid product data is input as
C relative weight percents, obtained directly from the analyses of the
C liquid product. The mass of the liquid, the mass of the gas and the
C average molecular weight are input in free formatted form. The
C names of each chemical species and the amounts in the liquid and gas
C products are also input in a set format.
C The program calculates the weight percent and mole percent for
C each species present in the products. The program also
C calculates the number of moles of each product produced per
C 100 moles of feed converted. In addition the program also
C computes the following:
C 1) the weight percent of the feed that was converted,
C 2) the weight percent yield to aromatics,
C 3) the number of moles of double bonds in aromatics,
C 4) the number of moles of double bonds in monounsaturates
C (olefins + naphthenes),
C 5) the ratio of accounted double bonds to theoretical
C double bonds based on the change of the number of moles
C during the reaction, this value should equal unity when
C there is no hydrogenation or dehydrogenation and the
C product analysis is accurate,
C 6) the hydrogen to carbon ratio of the products, and

C 7) the number of moles of product produced for every
 C hundred moles of feed converted.
 C

C Variables

C MLIQ-----mass of liquid product
 C MVAP-----mass of vapor product
 C MWAVGF-----average molecular weight of feed
 C FRAC-----ratio of accounted unsaturations to theoretical
 C unsaturations
 C HSUM-----the number of moles of hydrogen present in the
 C products
 C CSUM-----the number of moles of carbon present in the
 C products
 C HCRAT-----hydrogen to carbon ratio of the products
 C CENSUM-----number of moles of product produced for every
 C hundred moles of feed converted
 C MOLEO-----the number of moles of feed into the reactor
 C MOLEFN-----the number of moles of product
 C TUNSAT-----the theoretical number of unsaturations produced
 C = MOLEFN - MOLEO
 C OUNSAT-----the number of moles of unsaturations present as
 C olefins and naphthenes
 C AUNSAT-----the number of unsaturations present in aromatics
 C

C Arrays

C NAME-----contains the names of each species in the
 C reactor products
 C MW-----molecular weight of each species
 C WT-----relative weight percent of products in liquid
 C feed replaced by absolute weight percent of
 C products in the total liquid and gas product
 C WTG-----absolute weight percent of products in gas
 C product
 C H-----moles of hydrogen atoms/mole of each species
 C C-----moles of carbon atoms/mole of each species
 C MOL-----mole percent of each species in the products
 C CEN-----moles of each product produced per one hundred
 C moles of feed cracked
 C

C -----
 C Variable and array declarations
 C

REAL MLIQ,MVAP,SUMWT,SUM,SUMOL,MWAVGF,FRAC
 REAL WT(42),ADJWT(42),WTLIQ(42),WTG(42),MW(42)
 REAL AUNSAT,OUNSAT,TUNSAT,MOLEO,MOLEFN,H(42),C(42)
 REAL MOL(42),MOLIQ(42),MOLGAS(42),WTGAS(42),FEED(22)
 REAL HSUM,CSUM,HCRAT,CENSUM,CEN(42)

```

INTEGER I
CHARACTER*14, NAME(42)
C
C Input the data
  PRINT *, ' Input names of species and molecular wts,',
  # ' wt. % of liquid products, wt. % of gas products,',
  # ' moles of H and moles of C in mole of species.'
  DO 10 I=1,42
    READ(5,11)NAME(I),MW(I),WT(I),WTG(I),H(I),C(I)
    WRITE(6,11)NAME(I),MW(I),WT(I),WTG(I),H(I),C(I)
11    FORMAT(1X,A14,1X,F5.0,1X,F7.3,1X,F7.3,1X,F4.0,1X,F4.0)
10  CONTINUE
C
  PRINT *, ' Input the total wt. of liquid product (g.).'
  READ *, MLIQ
  WRITE(6,12)MLIQ
12  FORMAT(2X,F7.2)
  PRINT *, ' Input average molecular weight of feed.'
  READ *, MWAVGF
  WRITE(6,12)MWAVGF
  PRINT *, ' Input the total wt. of gas product (g.).'
  READ *, MVAP
  WRITE(6,12)MVAP
C
C Normalize the adjusted weight percents in the liquid to
C absolute weight percents, and determine the number of moles
C of each species in the product stream.
  SUM= 0.
  DO 14 I=1,42
    SUM= SUM + WT(I)/100.
14  CONTINUE
C
C
  DO 20 I=1,42
    ADJWT(I)=WT(I)/SUM
    WTLIQ(I)= ADJWT(I)*MLIQ/100.
    MOLIQ(I)= WTLIQ(I)/MW(I)
20  CONTINUE
  DO 21 I=1,13
    WTGAS(I)=WTG(I)*MVAP/100.
    MOLGAS(I)=WTGAS(I)/MW(I)
21  CONTINUE
C Determine absolute weight and liquid fractions.
C
  SUMOL= 0.
  DO 25 I=1,42
    MOL(I)= MOLGAS(I) + MOLIQ(I)

```

```

SUMOL= SUMOL + MOL(I)
WT(I)= MOL(I)*MW(I)*100./(MLIQ+MVAP)
25 CONTINUE
DO 26 I=1,42
    MOL(I)= MOL(I)*100./SUMOL
26 CONTINUE
C
C Calculate conversions (based on weight percent of product).
C Xa is a dummy variable initially, then it becomes the
C total conversion. Xd is conversion to aromatics.
XA= 0.
DO 28 I=1,19
    XA= XA + WT(I)
28 CONTINUE
XD= 0.
DO 30 I=36,42
    XD= XD + WT(I)
30 CONTINUE
XA= (XA+XD)
C Calculate moles of unsaturations.
C Aunsat is moles of unsaturations in aromatics.
C Ounsat is number of unsaturations in naphthenes and
C olefins (assuming no cycloolefins or diolefins).
AUNSAT= SUMOL/100.*(4.*(MOL(36)+MOL(37)+MOL(38)
# + MOL(39)+MOL(40)+MOL(41) + MOL(42)) )
OUNSAT= SUMOL/100.*(MOL(2)+MOL(4)+MOL(8)+MOL(11)+MOL(13)
# + MOL(15)+MOL(17)+MOL(19)+MOL(21)+MOL(23)+MOL(25) )
C
C Calculate number of theoretical unsaturations by delta
C moles during reaction.
MOLEO= (MLIQ+MVAP)/MWAVGF
MOLEFN= SUMOL
TUNSAT= MOLEFN - MOLEO
C
C Calculate actual unsaturations/theoretical unsaturations
FRAC= (AUNSAT+OUNSAT)/TUNSAT
C
C Calculate H/C ratio of products.
HSUM= 0.
CSUM= 0.
DO 35 I=1,19
    HSUM= HSUM + MOL(I)*H(I)
    CSUM= CSUM + MOL(I)*C(I)
35 CONTINUE
DO 36 I=36,42
    HSUM= HSUM + MOL(I)*H(I)
    CSUM= CSUM + MOL(I)*C(I)

```

```

36  CONTINUE
    HCRAT=HSUM/CSUM
C   Calculate the number of moles of each species for every one
C   hundred moles cracked.
C
    CENSUM = 0.
    TMOL= (MLIQ+MVAP)*(XA)/(100.*MWAVGF)
    DO 37 I=1,42
        IF( (I.GE.20).AND.(I.LE.35) )GO TO 37
        CEN(I)= WT(I)*(MLIQ+MVAP)/(MW(I)*TMOL)
        CENSUM= CENSUM + CEN(I)
37  CONTINUE
    WRITE(6,39)
39  FORMAT('1',1X)
    PRINT *, '-----',
# '-----'
    PRINT *, ' Product      Mole percent  Wt. percent  Moles/',
# '100 Moles'
    PRINT *, '-----',
# '-----'
    DO 40 I=1,42
        WRITE(6,41) NAME(I),MOL(I),WT(I),CEN(I)
41  FORMAT(2X,A14,2X,F5.2,3X,F5.2,8X,F7.2)
40  CONTINUE
    PRINT *, '-----',
# '-----'
    WRITE(6,42)XA,XD
42  FORMAT(1X,' Total conversion = ',F6.2,/,1X,
# ' Conversion to aromatics = ',F6.2,/)
    WRITE(6,51)OUNSAT,AUNSAT,FRAC
51  FORMAT(1X, ' Olefinic and naphthenic unsaturations ',
# F6.4,/,1X, ' Aromatic unsaturations ', F6.4,/,1X,
# ' Accounted Unsaturations/Theoretical Unsaturations =',
# 1X,F6.4,/)
    WRITE(6,52)HCRAT
52  FORMAT(1X,' Hydrogen/Carbon Ratio =',1X,F5.2)
    WRITE(6,53)CENSUM
53  FORMAT(1X,' Number of moles produced per 100 moles of,
# ' feed cracked = ',F7.2)
    PRINT *, '-----',
# '-----'
    STOP
    END

```

Table E-2

Sample Input For MASSBAL2

Since the input for MASSBAL2 is formatted, this data must be input exactly as it appears here. The data in the first column are the names of each species, the data in the second column are their molecular weights, the data in the third column are the relative weight percents of each species in the liquid product and the data in the fourth column are the absolute weight percent of each species in the gas product. The final three numbers in the table are the mass of liquid product collected from the run, the average molecular weight of the feed and the mass of the gas collected from the run, respectively.

C1	16	0	0.07	4	1
C2 olefin	28	0	1.03	4	2
C2	30	0	0.70	6	2
C3 olefin	42	0.0	6.57	6	3
C3	44	0.333	25.14	8	3
Iso C4	58	0.339	20.07	10	4
C4	58	1.727	22.02	10	4
C4 olefin	56	0.524	8.91	8	4
Iso C5	72	3.622	0.15	12	5
C5	72	2.343	5.49	12	5
C5 olefin	70	1.917	8.06	10	5
C6	86	1.878	1.01	14	6
C6 olefin	84	3.406	0.78	12	6
C7	100	0.41	0	16	7
C7 olefin	98	2.05	0	14	7
C8	114	1.07	0	18	8
C8 olefin	112	1.074	0	16	8
C9	128	0.905	0	20	9
C9 olefin	126	0.77	0	18	9
C10	142	4.153	0	22	10
C10 olefin	140	0.0	0	20	10
C11	156	9.795	0	24	11
C11 olefin	154	0.0	0	22	11
C12	170	18.041	0	26	12
C12 olefin	168	0.0	0	24	12
C13	184	14.546	0	28	13
C14	198	11.168	0	30	14
C15	212	6.653	0	32	15
C16	226	3.23	0	34	16
C17	240	3.173	0	36	17
C18	254	1.13	0	38	18
C19	268	0.0	0	40	19
C20	282	0.0	0	42	20
C21	296	0.0	0	44	21
C22	310	0.0	0	46	22
Benzene	78	0.551	0	6	6
Toluene	92	0.76	0	8	7
Xylenes	106	1.081	0	10	8
C9 aromatics	120	0.995	0	12	9
C10 aromatics	134	0.0	0	14	10
C11 aromatics	142	0.0	0	16	11
C12 aromatics	156	0.0	0	18	12
21.95					
181.6					
4.30					

Table E-3**Sample Output from MASSBAL2**

This is a sample output resulting from the input data listed in Table B-5. The first page is an output of the input data. The second page presents the results that are calculated from the input data.

Input names of species and molecular wts, wt percent of liquid products, wt percent of gas products, moles of H and moles of C in mole of species.

C1	16	0.000	0.070	4	1
C2 olefin	28	0.000	1.030	4	2
C2	30	0.000	0.700	6	2
C3 olefin	42	0.000	6.570	6	3
C3	44	0.333	25.140	8	3
Iso C4	58	0.339	20.070	10	4
C4	58	1.727	22.020	10	4
C4 olefin	56	0.524	8.910	8	4
Iso C5	72	3.622	0.150	12	5
C5	72	2.343	5.490	12	5
C5 olefin	70	1.917	8.060	10	5
C6	86	1.878	1.010	14	6
C6 olefin	84	3.406	0.780	12	6
C7	100	0.410	0.000	16	7
C7 olefin	98	2.050	0.000	14	7
C8	114	1.070	0.000	18	8
C8 olefin	112	1.074	0.000	16	8
C9	128	0.905	0.000	20	9
C9 olefin	126	0.770	0.000	18	9
C10	142	4.153	0.000	22	10
C10 olefin	140	0.000	0.000	20	10
C11	156	9.795	0.000	24	11
C11 olefin	154	0.000	0.000	22	11
C12	170	18.041	0.000	26	12
C12 olefin	168	0.000	0.000	24	12
C13	184	14.546	0.000	28	13
C14	198	11.168	0.000	30	14
C15	212	6.653	0.000	32	15
C16	226	3.230	0.000	34	16
C17	240	3.173	0.000	36	17
C18	254	1.130	0.000	38	18
C19	268	0.000	0.000	40	19
C20	282	0.000	0.000	42	20
C21	296	0.000	0.000	44	21
C22	310	0.000	0.000	46	22
Benzene	78	0.551	0.000	6	6
Toluene	92	0.760	0.000	8	7
Xylenes	106	1.081	0.000	10	8
C9 aromatics	120	0.995	0.000	12	9

C10 aromatics	134	0.000	0.000	14	10
C11 aromatics	142	0.000	0.000	16	11
C12 aromatics	156	0.000	0.000	18	12

Input the total wt. of liquid product (g.).
21.95

Input average molecular weight of feed.
181.60

Input the total wt. of gas product (g.).
4.30

Product Species	Mole (%)	Weight (%)	<u>Moles Produced</u> 100 Moles Cracked
C1	0.08	0.01	0.34
C2 olefin	0.65	0.17	2.85
C2	0.42	0.11	1.81
C3 olefin	2.78	1.08	12.11
C3	10.87	4.40	47.28
Iso C4	6.70	3.58	29.15
C4	9.53	5.09	41.43
C4 olefin	3.70	1.91	16.10
Iso C5	4.72	3.13	20.52
C5	4.38	2.91	19.07
C5 olefin	4.60	2.96	19.99
C6	2.24	1.77	9.74
C6 olefin	3.94	3.04	17.12
C7	0.38	0.35	1.66
C7 olefin	1.95	1.76	8.46
C8	0.87	0.92	3.80
C8 olefin	0.89	0.92	3.88
C9	0.66	0.78	2.86
C9 olefin	0.57	0.66	2.47
C10	2.72	3.56	0.00
C10 olefin	0.00	0.00	0.00
C11	5.84	8.39	0.00
C11 olefin	0.00	0.00	0.00
C12	9.87	15.45	0.00
C12 olefin	0.00	0.00	0.00
C13	7.35	12.46	0.00
C14	5.25	9.56	0.00
C15	2.92	5.70	0.00
C16	1.33	2.77	0.00
C17	1.23	2.72	0.00
C18	0.41	0.97	0.00
C19	0.00	0.00	0.00
C20	0.00	0.00	0.00
C21	0.00	0.00	0.00
C22	0.00	0.00	0.00
Benzene	0.66	0.47	2.86
Toluene	0.77	0.65	3.34
Xylenes	0.95	0.93	4.13
C9 aromatics	0.00	0.00	0.00
C10 aromatics	0.00	0.00	0.00
C11 aromatics	0.00	0.00	0.00
C12 aromatics	0.00	0.00	0.00

Total conversion = 38.44

Conversion to aromatics = 2.90

Olefinic and naphthenic unsaturations 0.0461

Aromatic unsaturations 0.0304

Accounted Unsaturations/Theoretical Unsaturations = 0.7880

Hydrogen/Carbon Ratio = 2.21

Number of moles produced per 100 moles of feed cracked = 274.32

APPENDIX F
DERIVATION OF THE BET EQUATIONS

In order to better understand the nature of the BET equation and its limitations, the equations obtained by Brunauaer, Emmett and Teller²⁵⁹ are derived here. In addition to the derivation of the BET (A) ('the BET equation'), the derivations of the BET (B), BET (C) and BET (D) equations are also provided.

The Derivation of the BET (A) Equation

The derivation of the BET (A) equation incorporates several basic assumptions:

- 1) the properties of the adsorptive in the second and higher monolayers are equivalent to the properties of adsorptive in the liquid phase, and;
- 2) an infinite number of monolayers can be formed.

In the derivation that follows $s_1, s_2, s_3, \dots, s_i$ represent the area covered by the 1st, 2nd, 3rd, ..., ith layers of adsorptive adsorbed on the surface of the adsorbent. The term s_0 will represent the bare or uncovered surface of the adsorbent.

At equilibrium the area of uncovered surface, s_0 , remains constant. That is, the rate of uncovering of bare surface by desorption from the first monolayer is equivalent to the rate of bare surface being covered by adsorption from the gas phase.

First equate the rate of adsorption in the first monolayer on the bare adsorbent surface and the rate of desorption from the first monolayer which exposes the bare adsorbent surface:

$$a_1 p s_0 = b_1 s_1 \exp \left(\frac{-E_1}{RT} \right) \quad (F-1)$$

where

- a_1 is the rate constant for adsorption;
 p is the partial pressure of adsorptive;
 s_0 is the area of adsorbent surface available for adsorption;
 b_1 is the rate constant for desorption;
 s_1 is the surface area covered by the first monolayer; and
 E_1 is the heat of adsorption of adsorptive in the first monolayer.

A similar expression can be written for the second adsorbed monolayer at equilibrium.

$$a_2 p s_1 + b_1 s_1 \exp\left(\frac{-E_1}{RT}\right) = b_2 s_2 \exp\left(\frac{-E_2}{RT}\right) + a_1 p s_0 \quad (F-2)$$

where:

- a_2 is the rate constant for adsorption of the second adsorbed monolayer;
 b_2 is the rate constant for desorption of the second adsorbed monolayer;
 s_2 is the surface area covered by the second adsorbed monolayer; and
 E_2 is the heat of adsorption of adsorptive in the second adsorbed monolayer.

The first term on the left represents the rate of adsorption on the first monolayer as it is covered with adsorptive to form the second adsorbed monolayer. The second term is the rate of desorption from the first monolayer to uncover the bare adsorbent surface. The first term on the right is the rate of formation of the first monolayer due to desorption from the second adsorbed monolayer, the second term on the right is the rate of formation of the first monolayer due to adsorption of adsorptive on the bare surface. If Equation (F-1) is subtracted from Equation (F-2) we obtain the following expression:

$$a_2 p s_1 = b_2 s_2 \exp \left(\frac{-E_2}{RT} \right) \quad (F-3)$$

This procedure can be extended to an infinite number of monolayers to generate the following set of equations:

$$\begin{aligned} a_3 p s_2 &= b_3 s_3 \exp \left(\frac{-E_3}{RT} \right) \\ &\vdots \\ &\vdots \\ a_i p s_{i-1} &= b_i s_i \exp \left(\frac{-E_i}{RT} \right) \end{aligned} \quad (F-4)$$

The total surface area of the adsorbent is obtained from the summation of the exposed surface areas of all the monolayers formed from the bare surface or zeroth monolayer up to the highest monolayer:

$$A = \sum_{i=0}^{\infty} s_i \quad (F-5)$$

The total volume of adsorptive adsorbed in all monolayers is given by Equation F-6.

$$V = V_0 \sum_{i=0}^{\infty} i s_i \quad (F-6)$$

where:

- V_0 is the volume of gas required to cover a unit area of the bare surface, cm^3 ;
- s_i is the surface area covered by the i^{th} monolayer, m^2 ; and

i in the summation represents the sum of the monolayers covered by the i^{th} monolayer.

It follows that:

$$\frac{v}{Av_0} = \frac{v}{v_m} = \frac{\sum_{i=0}^{\infty} i s_i}{\sum_{i=0}^{\infty} s_i} \quad (\text{F-7})$$

where:

v_m is the volume of gas adsorbed when the entire adsorbent surface is covered with a complete unimolecular monolayer of adsorptive.

It is assumed that the heats of adsorption of the second and higher monolayers of adsorbent are identical to the latent heat of condensation of the adsorptive. It is also assumed that the adsorption/desorption properties of the second and higher monolayers are equal. These two assumptions can be expressed as follows:

$$E_2 = E_3 = \dots E_i = E_L \quad (\text{F-8})$$

and

$$\frac{b_2}{a_2} = \frac{b_3}{a_2} = \dots \frac{b_i}{a_i} = g \quad (\text{F-9})$$

The fraction of the surface covered by the first monolayer, s_1 , can be calculated from Equation (F-1):

$$s_1 = \frac{a_1}{b_1} p s_0 \exp \left(-\frac{E_1}{RT} \right) \quad (\text{F-10})$$

or

$$s_1 = y s_0 \quad \text{where } y = \frac{a_1}{b_1} p \exp \left(-\frac{E_1}{RT} \right) \quad (\text{F-11})$$

The fraction of the surface covered by the second monolayer, s_2 , can be calculated from Equation (F-3).

$$s_2 = \frac{a_2 p s_1}{b_2} \exp \left(-\frac{E_2}{RT} \right) = \frac{p s_1}{g} \exp \left(-\frac{E_L}{RT} \right) \quad (\text{F-12})$$

or

$$s_2 = x s_1 \quad \text{where } x = \frac{p}{g} \exp \left(-\frac{E_L}{RT} \right) \quad (\text{F-13})$$

This analysis can be extended to subsequent monolayers:

$$s_3 = x s_2 = x^2 s_1 \quad (\text{F-14})$$

or for the i^{th} monolayer we have:

$$s_i = x s_{i-1} = x^{i-1} s_1 = x^{i-1} y s_0 = c x^i s_0 \quad (\text{F-15})$$

where

$$c = \frac{y}{x} \quad (\text{F-16})$$

$$c = \frac{a_1}{b_1} g \exp \left[\frac{(E_1 - E_L)}{RT} \right] \quad (\text{F-17})$$

The substitution of Equation (F-15) into Equation (F-7) gives:

$$\frac{v}{v_m} = \frac{\sum_{i=0}^{\infty} i s_i}{\sum_{i=0}^{\infty} s_i} = \frac{\sum_{i=0}^{\infty} i (c x^i s_0)}{s_0 + \sum_{i=1}^{\infty} (c x^i s_0)} \quad (\text{F-18})$$

Since c and s_0 are constant, they can be moved out of the summations. When $i = 0$, the first term in the upper summation vanishes, thus,

$$\frac{v}{v_m} = \frac{c s_0 \sum_{i=1}^{\infty} i x^i}{s_0 + c s_0 \sum_{i=1}^{\infty} x^i} = \frac{c \sum_{i=1}^{\infty} i x^i}{1 + c \sum_{i=1}^{\infty} x^i} \quad (\text{F-19})$$

When x is less than 1, the summation in the denominator can be written as:

$$\sum_{i=1}^{\infty} x^i = \frac{x}{1-x} \quad (\text{F-20})$$

Equation (F-20) may be substituted into Equation (F-19) to obtain:

$$\frac{v}{v_m} = \frac{c \sum_{i=1}^{\infty} i x^i}{\left[1 + \frac{c x}{(1-x)} \right]} \quad (\text{F-21})$$

Consider the expansion of the summation in the numerator:

$$i x^i = x + 2x^2 + 3x^3 + 4x^4 \dots \quad (\text{F-22})$$

which may be rewritten as:

$$\sum_{i=1}^{\infty} ix^i = x \frac{d(x)}{dx} + x \frac{d(x^2)}{dx} + x \frac{d(x^3)}{dx} + \frac{d(x^4)}{dx} \dots \quad (\text{F-23})$$

We can rewrite Equation (F-23) as:

$$\sum_{i=1}^{\infty} ix^i = x \frac{d}{dx} \left(\sum_{i=1}^{\infty} x^i \right) \quad (\text{F-24})$$

Substituting Equation (F-20), for the summation reduces the summation to an algebraic expansion:

$$\sum_{i=1}^{\infty} ix^i = x \frac{d}{dx} \left(\frac{x}{(1-x)} \right) = x \left(\frac{x}{(1-x)^2} \right) \quad (\text{F-25})$$

$$\sum_{i=1}^{\infty} ix^i = \frac{x}{(1-x)^2} \quad (\text{F-26})$$

If we substitute Equation (F-26) into Equation (F-21), we obtain:

$$\frac{v}{v_m} = \frac{\frac{cx}{(1-x)^2}}{1 + \frac{cx}{(1-x)}} = \frac{cx}{(1-x)^2 \left(1 + \frac{cx}{(1-x)} \right)} \quad (\text{F-27})$$

$$\frac{v}{v_m} = \frac{cx}{(1-x)(1-x+cx)} \quad (\text{F-28})$$

Adsorption on a free surface at the saturation pressure of the adsorptive, p_0 , results in the formation of an infinite number of monolayers. If $v = \infty$ and $p = p_0$, then:

$$\frac{v}{v_m} = \frac{cx}{(1-x)(1-x+cx)} \quad (\text{F-29})$$

which requires $x = 1$ for finite values of c .

Then

$$x = 1 = \frac{p_0}{g} \exp\left(\frac{E_L}{RT}\right) \quad (\text{F-30})$$

or

$$\frac{1}{g} \exp\left(\frac{E_L}{RT}\right) = \frac{1}{p_0}$$

and

$$\frac{p}{p_0} = p \frac{1}{g} \exp\left(\frac{E_L}{RT}\right) \quad \text{for all } p$$

$$\frac{p}{p_0} = x \quad (\text{F-31})$$

The substitution of Equation (F-31) into Equation (F-29) gives:

$$\frac{v}{v_m} = \frac{c\left(\frac{p}{p_0}\right)}{\left(1 - \frac{p}{p_0}\right) \left(1 + \frac{p}{p_0} + \frac{cp}{p_0}\right)}$$

$$v = \frac{v_m cp}{(p_0 - p) \left[1 + (c-1)\frac{p}{p_0}\right]} \quad (\text{F-32})$$

$$\frac{1}{v_m c} \left[1 + (c-1) \frac{p}{p_0} \right] = \frac{p}{v(p_0 - p)}$$

$$\frac{p}{v(p_0 - p)} = \frac{1}{v_m c} + \frac{(c-1)p}{v_m c p_0} \quad (\text{F-33})$$

Equation (F-33) is known as the BET (A) equation.

There are three other BET equations which relieve assumptions that were included as part of the derivation of the BET (A) equation. The BET (B) equation relieves the assumption that an infinite number of monolayers form. Adsorption in the pores of solid adsorbents permits the formation of a limited number of monolayers. Consequently, at higher dimensionless pressures, the pores of the catalyst limit the formation of additional monolayers and the actual adsorption is less than the adsorption predicted by the BET (A) equation. This normally occurs above dimensionless pressures greater than $x = p/p_0$ greater than 0.35, but it can occur at lower dimensionless pressures in materials with small pore diameters.

The BET (C) equation relieves the assumption that $E_2 = E_L$, that is, that the heat of adsorption of the second monolayer is equal to the heat of condensation of liquid adsorptive.

The BET (D) equation relieves the assumption in the BET (B) equation that the pores are all of equal size.

Each of the equations are derived below.

The Derivation of the BET (B) Equation

The BET (B) equation assumes that an infinite number of monolayers is formed. The derivation of the BET (A) equation and the BET (B) equations are identical until that assumption is applied in the derivation of the BET (A) equation. Equation (F-19) is the starting point for

the derivation of the BET (B) equation. Since only n monolayers are formed, the maximum limit of the summation is n and not infinity.

$$\frac{v}{v_m} = \frac{c \sum_{i=1}^n i x^i}{1 + c \sum_{i=1}^n x^i} \quad (\text{F-19})$$

The summations can be expanded as follows:

$$\frac{v}{v_m} = \frac{c \left[\sum_{i=1}^{\infty} i x^i - \sum_{i=n+1}^{\infty} i x^i \right]}{1 + c \left[\sum_{i=1}^{\infty} x^i - \sum_{i=n+1}^{\infty} x^i \right]} \quad (\text{F-34})$$

Substituting Equation (F-26) for the first summation that appears in Equation (F-34) and substituting Equation (F-20) for the first summation in the denominator of Equation (F-34) yields:

$$\frac{v}{v_m} = \frac{c \frac{x}{(1-x)^2} - \sum_{i=n+1}^{\infty} i x^i}{\left[1 + \frac{cx}{(1-x)} - c \sum_{i=n+1}^{\infty} x^i \right]} \quad (\text{F-35})$$

The summations with limits of $n+1$ and infinity must be converted to closed algebraic expressions.

The summation in the denominator can be converted to a closed algebraic expression by factoring out x^n so that its lower limit is one. The resulting summation has the closed algebraic form that appeared in the derivation of the BET (A) equation.

$$\sum_{i=n+1}^{\infty} x^i = x^n \sum_{i=1}^{\infty} x^i = x^n \frac{x}{(1-x)^2} = \frac{x^{n+1}}{(1-x)^2} \quad (\text{F-36})$$

or:

$$\sum_{i=n+1}^{\infty} x^i = \frac{x^{n+1}}{(1-x)^2} \quad (\text{F-37})$$

The summation in the numerator of Equation (F-35) can be converted to a closed algebraic form by the same method with which the equivalent summation was converted in the derivation of the BET (A) equation. The summation in the numerator of Equation (F-35) can be expressed as the following:

$$\sum_{i=n+1}^{\infty} ix^i = x \frac{d}{dx} \left[\sum_{i=n+1}^{\infty} x^i \right]$$

Substituting Equation (F-37) for the summation term yields:

$$\sum_{i=n+1}^{\infty} ix^i = x \frac{d}{dx} \left[\frac{x^{n+1}}{(1-x)} \right]$$

$$\sum_{i=n+1}^{\infty} ix^i = x \frac{[(n+1)x^n - nx^{n+1}]}{(1-x)^2}$$

$$\sum_{i=n+1}^{\infty} ix^i = \frac{(n+1)x^{n+1} - nx^{n+2}}{(1-x)^2} \quad (\text{F-38})$$

Substituting (F-38) and (F-37) into (F-35) gives the following:

$$\frac{v}{v_m} = c \frac{\left[\frac{x}{(1-x)^2} - \frac{(n+1)x^{n+1}}{(1-x)^2} - \frac{nx^{n+2}}{(1-x)^2} \right]}{1 + c \left[\frac{x}{(1-x)} - \frac{x^{n+1}}{(1-x)} \right]} \quad (\text{F-39})$$

Factoring and cancelling give:

$$\frac{v}{v_m} = \frac{cx [1 - (n+1)x^n + nx^{n+1}]}{(1-x)(1 - x + cx - cx^{n+1})}$$

or:

$$v = \frac{cv_m x [1 - (n+1)x^n + nx^{n+1}]}{(1-x) [1 + (c-1)x - cx^{n+1}]} \quad (\text{F-40})$$

Equation (F-40) is known as the BET (B) equation. For the special case of $n = 1$, this equation reduces to the Langmuir equation by the following transformation:

$$v = \frac{cv_m x (1 - 2x + x^2)}{(1-x) [1 + (c-1)x - cx^2]}$$

Factoring yields:

$$v = \frac{cv_m x (1-x)^2}{(1-x)(1-x)(1+cx)}$$

Cancelling terms yields:

$$v = \frac{cv_m x}{(1 + cx)} \quad (\text{F-41})$$

If c/p_0 is set equal to b , the result is:

$$\frac{v}{v_m} = \frac{\left[\frac{c}{p_0}\right] p}{\left(1 + \frac{cp}{p_0}\right)} = \frac{bp}{(1 + bp)} \quad (\text{F-42})$$

which is the Langmuir equation.

The Derivation of the BET (C) Equation

The derivation of the BET (C) equation relaxes two assumptions employed in the derivation of the BET (A) equation, that is:

- (1) the heat of adsorption of the second monolayer is equal to the heat of condensation of the liquid adsorptive; and
- (2) the packing of the molecules in the first monolayer is the same as the packing of the molecules in the liquid state.

The derivation of the BET (C) equation is the same as the derivation of the BET (A) equation up until the point that assumptions 1 and 2 above are applied. Starting with Equation (F-7):

$$\frac{v}{Av_0} = \frac{v}{v_m} = \frac{\sum_{i=0}^{\infty} i s_i}{\sum_{i=0}^{\infty} s_i} \quad (\text{F-7})$$

When $i = 0$, the first term in the upper summation is equal to 0, which yields:

$$\frac{v}{Av_0} = \frac{v}{v_m} = \frac{\sum_{i=1}^{\infty} i s_i}{\sum_{i=0}^{\infty} s_i} \quad (\text{F-43})$$

The heats of adsorption of the third and higher monolayers are assumed to be equal to the heat of condensation of the adsorptive, so the following is true,

$$E_3 = E_4 = \dots = E_i = E_L \quad (\text{F-44})$$

and

$$\frac{b_3}{a_3} = \frac{b_4}{a_4} \dots = \frac{b_i}{a_i} = g \quad (\text{F-45})$$

From Equation (F-11), the following is known:

$$s_1 = y s_0 \quad \text{where } y = \frac{a_1}{b_1} p \exp \left(\frac{E_1}{RT} \right) \quad (\text{F-11})$$

Since $E_2 = E_L$, a new quantity, z , is defined:

$$s_2 = z s_1 = z y s_0; \quad \text{where } z = \frac{a_2}{b_2} p \exp \left[\frac{E_2}{RT} \right] \quad (\text{F-46})$$

$$s_3 = x s_2 = x z s_1 = x z y s_0; \quad \text{where } x = \frac{a_3}{b_3} p \exp \left[\frac{E_3}{RT} \right] \quad (\text{F-47})$$

or:

$$x = \frac{p}{g} \exp \left[-\frac{E_L}{RT} \right]$$

For the fourth monolayer:

$$s_4 = xs_3 = x^2s_2 = x^2zs_1 = x^2zys_0 \quad (F-48)$$

For the i^{th} monolayer:

$$s_i = xs_{i-1} = x^{i-2}zs_1 = x^{i-2}zys_0 \quad i \geq 2 \quad (F-49)$$

Equation (F-49) does not apply for $i=1$. However, for s_1 , the following is true:

$$s_1 = cxs_0 \quad (F-50)$$

The variable c is defined as it was in Equation (F-16) in the derivation of the BET (A) equation. Since $E_2 = E_L$, an additional variable, b , is also defined as follows:

$$b = \frac{z}{x} = \frac{a_2}{b_1} g \exp \left[-\frac{(E_2 - E_L)}{RT} \right] \quad (F-51)$$

Substituting (F-16) and (F-51) into (F-49) gives:

$$s_i = x^{i-2}zys_0 = x^{i-2}bcs_0 \quad (F-52)$$

Equation (F-44) can be rewritten as:

$$\frac{v}{v_m} = \frac{s_1 + \sum_{i=2}^{\infty} s_i}{s_0 + s_1 + \sum_{i=2}^{\infty} s_i} \quad (F-53)$$

δ is defined as the ratio of the volume of adsorptive required to form the first monolayer to the volume of adsorptive required to form subsequent monolayers:

$$\delta = \frac{v_{m,1}}{v_m} \quad (F-54)$$

δ allows for the possibility that molecules of adsorptive packed into the first monolayer are in an adsorbed state which is packed more densely than adsorptive molecules in the liquid phase but less densely than adsorptive molecules in the solid phase. Since $v_{m,1}$, the volume of adsorptive required to form a monolayer on the bare surface, is greater than v_m for any other subsequent monolayer δ should be greater than one, but it should not exceed the ratio of the solid density to the liquid density raised to the $2/3$ power.

Substituting (F-11) and (F-52) into (F-53) gives:

$$\begin{aligned} \frac{v}{v_m} &= \frac{\delta y s_0 + \sum_{i=2}^{\infty} b c s_0 (i x^i)}{s_0 + c s_0 x + \sum_{i=2}^{\infty} b c s_0 (x^i)} \\ \frac{v}{v_m} &= \frac{\delta c x s_0 + b c s_0 \sum_{i=2}^{\infty} i x^i}{s_0 + c s_0 x + b c s_0 \sum_{i=2}^{\infty} x^i} \end{aligned} \quad (55)$$

s_0 and c can be factored out of the numerator to give:

$$\frac{v}{v_m} = \frac{cs_0 (\epsilon x + b \sum_{i=2}^{\infty} ix^i)}{s_0 (1 + cx + bc \sum_{i=2}^{\infty} x^i)} \quad (F-56)$$

The summations with the limits 2 and infinity can be converted to summations with limits of 1 and infinity.

$$\frac{v}{v_m} = \frac{c (\epsilon x + b \sum_{i=1}^{\infty} ix^i - bx)}{(1 + cx + bc \sum_{i=1}^{\infty} x^i - bcx)} \quad (F-57)$$

Substituting (F-20) and (F-22) into (F-57) yields:

$$\frac{v}{v_m} = \frac{c (\epsilon x + b \frac{x}{(1-x)^2} - bx)}{(1 + cx + \frac{bcx}{(1-x)} - bcx)} \quad (F-58)$$

Factoring $\frac{x}{(1-x)^2}$ out of the numerator and $\frac{1}{(1-x)}$ out of the denominator yields:

$$\frac{v}{v_m} = \frac{\frac{cx}{(1-x)^2} [\epsilon(1-x)^2 + b - b(1-x)^2]}{\frac{1}{(1-x)} [(1-x) + cx(1-x) + \frac{bcx}{(1-x)} - bcx(1-x)]}$$

Expanding and distributing yields:

$$\frac{v}{v_m} = \frac{cx}{(1-x)} \left[\frac{\epsilon(1-2x+x^2) + b - b(1-2x+x^2)}{1 - x + cx - cx^2 + bcx - bcx + bcx^2} \right]$$

Consolidation of terms in the numerator finally yields:

$$v = \frac{v_m cx}{(1-x)} \left[\frac{s + (b-s)(2x-x^2)}{1 + (c-1)x + (b-1)cx^2} \right] \quad (F-59)$$

Equation (F-59) is the BET (C) equation.

The BET (D) equation requires no lengthy derivation, but it is included here for purposes of completeness. The BET (D) equation results from the derivation of the BET (B) equation. In the derivation of the BET (B) equation, it was assumed that the pores were all of uniform size so that only n monolayers could form in any pore. When there is a wide distribution of pore sizes, the BET (B) equation will not suitably predict the data.

Equation (F-40) is the BET (B) equation:

$$v = \frac{cv_m x [1 - (n+1)x^n + nx^{n+1}]}{(1-x) [1 + (c-1)x - cx^{n+1}]} \quad (F-40)$$

The left hand term of the right hand side is not a function of the pore size distribution and it will not be manipulated to derive the BET (D) equation. The right hand term of the right hand side is a function of the pore size distribution as manifest in the variable n . Each set of pores with the same pore size distribution has the same diameter and consequentially the same value for n . For each set of pores with the same pore size, the right hand term of the right hand side can be written as follows:

$$\frac{1 - (n+1)x^n + nx^{n+1}}{1 + (c-1)x - cx^{n+1}} \quad (F-60)$$

The fraction of the surface that is contained in each set of pores can be multiplied in the front of each expression equivalent to Equation (F-60). Summing for all pores gives the BET (D) equation.

$$v = \frac{v_m c x}{(1-x)} \sum_{i=1}^{\infty} \beta_n \left[\frac{1 - (n+1)x^n + nx^{n+1}}{1 + (c-1)x - cx^{n+1}} \right] \quad (\text{F-61})$$

β_n here is the fraction of the total surface contained in pores that can contain no more than n monolayers.

The procedure for using the BET (B), BET (C), and BET (D) equations is to first use the BET (A) equation to determine v_m and c , and then to use subsequent equations to determine the respective variables that give the best fit of a plot of the curve with the data.

The BET (A) equation is used far more often than the other three equations combined, but they are useful in various applications and can provide insights to the nature of an adsorbent.

APPENDIX G

BET SURFACE AREA COMPUTER PROGRAM

A. Program for the Calculation of BET Surface Areas

BET1 is a Fortran program written to process data obtained from the BET equipment described in Section VII. Sample input and output for this program are included here. The data presented was taken from run number 7 in which a complete adsorption/desorption isotherm was determined for a sample of HZSM-5 catalyst (sample 6).

Table G-1

Program Listing for BET1

C A program to calculate Vadsorbed from BET data, and to
C perform a linear regression on the data to determine the surface
C area and the heat of adsorption, (E_1-E_L).
C Inputs include the vapor pressure of nitrogen at the
C temperature of the cell, the temperature of the cell, the
C temperature of the doser manifold, the volume of the doser
C manifold, the volume of the cell at liquid nitrogen
C temperature, the volume of the cell at ambient temperature,
C the mass of the sample and the number of data points that were
C taken. Additional information includes the number of points to
C be used to determine the monolayer volume and whether or not
C to use the Langmuir or BET equation to determine the monolayer
C volume. Finally the data points obtained from the adsorption
C equipment are needed. With each set of data points the volume
C of the dosing manifold is needed. If zero is input then the
C volume that is used in the mass balance is the volume that was
C used in the last step of the mass balance. This allows for the
C possibility that the operator of the adsorption/desorption equipment
C can use different dosing volumes to facilitate the determination of
C the adsorption/desorption isotherm.
C The method is to calculate the amount of gas adsorbed at
C each adsorptive pressure and to fit a set of points to a straight
C line by least squares. The slope and y-intercept of the line will
C be related to the monolayer volume and the heat of adsorption
C of adsorbate on the surface. Data points below a dimensionless
C pressure of P/P_o of 0.01-0.05 are not included in the least
C squares because such points do not fit the theory of the
C Langmuir or BET equations very well. Since this program was
C used almost exclusively to calculate the surface area of
C zeolites, $P/P_o \leq 0.01$ were not used. For larger pore adsorbents
C the higher value than $P/P_o = 0.01$ should be used in this program.

C Outputs are the surface area per unit mass of sample, the
 C monolayer volume, the slope and y-intercept of the line that
 C was used in the least squares approximation. A coefficient is
 C also printed which is the average percentage deviation of each
 C point from the least squares approximation. The points used
 C for the least squares method are also printed.

C If the Langmuir equation is used to determine the monolayer
 C volume then the straight line is generated from it and the 'b-
 C value' is included in the output. If the BET equation is used
 C then the 'c-value' is included in the output. Output includes
 C the volume (STP) of adsorbent adsorbed at various pressures
 C and dimensional pressures (P/Po).

C

C

Variables

C

C

C

C

C

C

C

C

C

C

C

C

C

C

C

C

C

C

C

C

C

C

C

C

C

C

C

C

C

C

C

C

C

C

PO-----the partial pressure of nitrogen at the
 temperature of the sample in the cell
 TM-----the temperature of the dosing manifold
 TC-----the temperature of the cryogenic portion of the
 cell
 VCC-----the volume of the cell at cryogenic temperature
 VCH-----the volume of the cell at ambient temperature
 NAVAN2----the surface area covered by a mole of nitrogen
 molecules, in m2
 C-----the 'c-value' of the BET equation or the 'b-
 value' of the Langmuir equation
 E1-----the (E1-EL) of the BET equation, or the heat of
 adsorption of the Langmuir equation
 R-----Gas Constant, 1.9869 cal./gmol.K.
 ASMPL-----surface area of sample per unit mass
 VMONO-----monolayer volume
 BETA1,BETA2,ALPHA1,ALPHA2----quantities of the least
 squares method
 S-----fit coefficient, average percentage deviation
 from least squares approximation
 M-----slope of line generated by least squares method
 B-----y-intercept of the line generated by least
 squares
 N-----the number of data points corresponding to the
 number of points taken to determine the
 adsorption/desorption isotherm
 NO-----the number of points to be disregarded for the
 linear regression because they were taken at
 too low of a pressure, see 'the BET paper'.
 NBET-----the cutoff of points to be considered for the
 linear regression
 ASKM-----character work variables for asking questions to
 the user

```

C           Arrays
C   P1-----contains the initial pressures of the dosing
C           volume before it was opened to the sample
C   P2-----contains the equilibrium pressures in the
C           dosing manifold and sample cell
C   PE-----contains the pressure in the sample cell
C           which is equal to P2 of the previous data
C           point
C   VADS-----contains the volume of adsorbent (STP) adsorbed
C           on the sample at each data point in cc./unit
C           mass
C   X,Y-----contains the points to be used for the least
C           squares approximation
C   VM-----the volume of the dosing manifold for each point
C   VMAYBE---work array used with VM
C
C Variable declarations
C   REAL P1(60),P2(60),PE(60),VADS(60),X(60),Y(60)
C   REAL PO,TM,TC,VCC,VCH
C   INTEGER I,N,NO
C   CHARACTER*1 ASKM
C
C   REAL BETA1,BETA2,ALPHA1,ALPHA2,S,M,B
C   INTEGER NBET
C
C   REAL NAVAN2,VM(60),VMAYBE(60)
C   REAL C,E1,R,ASMPL,MSMPL,VMONO
C
C Input data
5   PRINT *, 'Input PO,VCH,VCC.'
    READ *, PO,VCH,VCC
    WRITE(6,6)PO,VCH,VCC
6   FORMAT(2X,F5.1,', ',F6.3,', ',F6.3)
    PRINT *, ' Input TM and TC.'
    READ *, TM,TC
    WRITE(6,7)TM,TC
7   FORMAT(2X,F6.2,', ',F6.2)
    PRINT *, ' Mass of sample?'
    READ *, MSMPL
    WRITE(6,8)MSMPL
8   FORMAT(2X,F8.5)
C
C Initialize data
C   NAVAN2= 9.7556 *(10**4)
C   R= 1.9869
C
C Input data

```

```

PRINT *, 'No. of points?'
READ *, N
WRITE(6,9)N
9  FORMAT(2X,I2)
C
PRINT *, ' Use BET or Langmuir equation? '
READ(5,70)ASKM
70  FORMAT(1X,A1)
WRITE(6,21)ASKM
21  FORMAT(2X,A2)
C
PRINT *, ' Input P1''s and P2''s, and VM.'
DO 10 I=1,N
  READ *, P1(I),P2(I),VMAYBE(I)
  IF(VMAYBE(I) .NE. 0.)THEN
    VM(I)= VMAYBE(I)
  ELSE
    VM(I)= VM(I-1)
  ENDIF
10  CONTINUE
C
C Calculate mass balance
PE(1)= 0.
VADS(1)= (273.15/760.)*( VM(1)/TM*(P1(1)-P2(1)) +
# (VCC/TC+VCH/TM)*(PE(1)-P2(1)) )/MSMPL
C
DO 20 I=2,N
  PE(I)= P2(I-1)
  VADS(I)= VADS(I-1) + (273.15/760.)*( VM(I)/TM*
# (P1(I)-P2(I)) + (VCC/TC+VCH/TM)*(PE(I)-P2(I)) )/MSMPL
20  CONTINUE
C
C Send data from mass balance to be put in the particular
C equation to get points for least squares approximation
IF( ASKM .EQ. 'L' )THEN
  CALL LANGMU(VADS,P2,N,X,Y)
ELSE
  CALL BET(VADS,P2,PO,N,NO,X,Y)
ENDIF
C
DO 40 I=1,N
  WRITE(6,41) P1(I),P2(I),VADS(I),X(I),Y(I)
41  FORMAT(2X,F8.2,2X,F8.2,2X,F8.3,2X,F7.4,2X,F12.8)
40  CONTINUE
C
C Perform linear regression using the least squares method
PRINT *, ' How many points for the BET? '

```

```

READ *, NBET
WRITE(6,42)NBET
42  FORMAT(1X,I2)
    IF( NBET .LE. (NO+2))THEN
        PRINT *, ' ERROR!, More points are needed for the',
#         ' linear regression.'
        STOP
    ENDIF
    WRITE(6,9)
C
    BETA1= 0.
    BETA2= 0.
    ALPHA1= 0.
    ALPHA2= 0.
    DO 60 I= NO+1, NBET
        BETA1= BETA1 + X(I)*Y(I)
        BETA2= BETA2 + (X(I)**2)
        ALPHA1= ALPHA1 + X(I)
        ALPHA2= ALPHA2 + Y(I)
    (d) CONTINUE
C
    B= (ALPHA2- ALPHA1*(BETA1/BETA2))/( REAL(NBET) -
#     (ALPHA1**2)/BETA2 )
    M= (BETA1-B*ALPHA1)/BETA2
C
    S= 0.
    DO 61 I= NO+1, NBET
        S= S + ( ((Y(I) - (M*X(I) + B))**2)**0.5 )/
#     (M*X(I)+B)
    61 CONTINUE
    S= 100.*S/REAL(NBET-NO)
C
C Calculate monolayer volume, heat of adsorption, and surface
C area
C IF(ASKM .EQ. 'L')THEN
    VMONO= 1./M
    C= 1./(VMONO*B)
    E1= 0.
ELSE
    VMONO= 1./(M+B)
    C= (M+B)/B
    IF( C .LE. 0. )THEN
        PRINT *, ' ERROR! Intercept is less than zero.'
        E1= -1.
        GO TO 63
    ENDIF
    E1= R*TC*ALOG(C)

```

```

63  ENDIF
    ASMPL= VMONO*NAVAN2/22400.
    IF( ASKM .EQ. 'L' )THEN
        VMONO= 1./M
        C= (M+B)/B
        IF( C .LE. 0. )THEN
            PRINT *, ' ERROR! Intercept is less than zero. '
            GO TO 64
        ENDIF
        E1= R*TC*ALOG(C)
64  ENDIF
    ASMPL= VMONO*NAVAN2/22400.
C  Print results
    WRITE(6,65)ASMPL,VMONO
65  FORMAT(2X,'ASMPL= ',F7.2,2X,'Monolayer volume cc.,(STP)=',
# F7.2)
    WRITE(6,67)C,E1
67  FORMAT(2X,'C= ',F8.2,2X,'E1-EL= ',F8.2)
    WRITE(6,68)M,B,S
68  FORMAT(6X,'Linear Equation from Least Squares',
# ' Approximation',/,2X,'y = ',1PE11.4,'x + ',1PE11.4,/,
# 2X,'S= ',G10.4,' %')
    STOP
    END
C
C
C
    SUBROUTINE LANGMU(VADS,P,N,X,Y)
    REAL VADS(60),P(60),X(60),Y(60)
    INTEGER I,NLANG
C
    PRINT *, ' No. of points for the Langmuir eqn.?'
    READ *, NLANG
C
    DO 10 I=1,NLANG
        Y(I)= P(I)/VADS(I)
        X(I)= P(I)
10  CONTINUE
    PRINT *, '      P1      P2      VADS      P',
# '      P/V'
    PRINT *, '-----',
# '-----'
    DO 20 I=2,NLANG
        DELTA= (Y(I)-Y(I-1))/(X(I)-X(I-1))
        PRINT *, DELTA
20  CONTINUE
    RETURN

```



```

      END
C
C
C
      SUBROUTINE BET(VADS,P,PO,N,NO,X,Y)
      REAL VADS(60), P(60), X(60), Y(60), PO
      INTEGER I,N,NO
C
      NO= 1
      DO 10 I=1,N
        X(I)= P(I)/PO
        IF( X(I).LE. 0.001 )THEN
          NO= I
        ENDIF
        Y(I)= P(I)/( VADS(I)*(PO-P(I)) )
10  CONTINUE
      PRINT *, '      P1      P2      VADS      P/PO',
#      '      P/V(PO-P)'
      PRINT *, '-----',
#      '-----'
      RETURN
      END

```

Table G-2

Sample Input for BET1

This table contains a sample input for Fortran program BET1. Since the program is free formatted it does not require that the data be input in a specific format.

The first line of data contains the vapor pressure of nitrogen at the temperature of the sample, the volume of the sample cell at ambient temperature and the volume of the sample cell at liquid nitrogen temperatures. The volumes must be input in units of cubic centimeters. The terms in the second line are the ambient temperature and the temperature of the cryogenic bath, both must be in degrees Kelvin. The third line is the mass of the sample in grams. The fourth line is the number of sets of data points for which the mass balance is to be calculated. The fifth line tells the computer that the BET (A) equation is to be used to calculate the surface area. The other choice is 'L' which tells the computer to use the Langmuir equation to calculate the surface area. The following lines each contain three data points. The first data point is the initial pressure in the dosing manifold before the dosing volume and the sample cell were allowed to come to equilibrium. The second data point is the pressure in the dosing volume after the dosing volume and the sample cell pressure had come to equilibrium. The final point is the volume of the dosing volume if the dosing volume is different than in the taking of the previous data point, if not, the third data point is zero. The very last point tells the program how many points are to be used for calculating the BET surface area. BET1 automatically eliminates points taken at pressures less than $p/p_0 < 0.01$. then it does the linear regression up to the n^{th} data point taken. Where n is the integer specified in the last data point.

655.8,2.512,4.981
299.6,76.1
.06045
42
B
410.6,0.06,9.57
31.5,0.12,0.
33.9,1.,0.
37.5,5.2,0.
9.2,5.9,0.
23.3,9.1,0.
35.7,14.5,0.
38.5,19.7,0.
54.7,27.7,0.
70.,37.6,0.
80.4,47.7,0.
112.7,63.4,0.
154.,86.2,0.
284.5,138.5,0.
323.5,189.1,0.
365.7,238.2,0.
374.7,276.2,0.
455.6,326.3,0.
518.5,379.1,0.
516.4,415.8,0.
605.3,465.3,0.
658.1,512.9,0.
589.5,563.1,60.84
652.3,621.5,0.
706.3,640.0,9.57
677.9,646.8,0.
672.8,650.4,0.
685.5,651.9,0.
684.4,654.,0.
717.2,655.3,0.
721.2,655.7,0.
510.2,650.1,0.
490.0,628.4,0.
269.1,530.7,0.
344.5,477.3,0.
243.4,410.4,0.
199.7,350.6,0.
137.1,304.9,0.
63.1,264.6,0.
112.9,157.5,60.84
1.5,115.6,9.57
22.2,91.3,0.
9

Table G-3

Sample Output from BET1

This table contains a sample output from BET1. The output is clearly explained except the very last term, 'S', which is the average percentage deviation of all the points used in the linear regression from the value predicted based on the slope and y-intercept of the least squares fit of those points.

Input PO,VCH,VCC.

655.8, 2.512, 4.981

Input TM and TC.

299.60, 76.10

Mass of sample?

0.06045

No. of points?

42

Use BET or Langmuir equation?

B

Input P1's and P2's, and VM (manifold volume).

P1	P2	VADS	P/PO	P/V(PO-)
410.60	0.06	77.942	0.0001	0.00000117
31.50	0.12	83.875	0.0002	0.00000218
33.90	1.00	89.737	0.0015	0.00001702
37.50	5.20	94.027	0.0079	0.00008500
9.20	5.90	94.347	0.0090	0.00009622
23.30	9.10	95.639	0.0139	0.00014713
35.70	14.50	97.294	0.0221	0.00023239
38.50	19.70	98.582	0.0300	0.00031415
54.70	27.70	100.198	0.0422	0.00044014
70.00	37.60	102.005	0.0573	0.00059626
80.40	47.70	103.781	0.0727	0.00075583
112.70	63.40	106.251	0.0967	0.00100725
154.00	86.20	109.118	0.1314	0.00138688
284.50	138.50	113.886	0.2112	0.00235091
323.50	189.10	117.197	0.2884	0.00345730
365.70	238.20	119.856	0.3632	0.00475905
374.70	276.20	121.881	0.4212	0.00596984
455.60	326.30	124.443	0.4976	0.00795779
518.50	379.10	127.737	0.5781	0.01072572
516.40	415.80	130.731	0.6340	0.01325236
605.30	465.30	135.589	0.7095	0.01801416
658.10	512.90	142.268	0.7821	0.02522861
589.50	563.10	152.104	0.8586	0.03993594
652.30	621.50	163.653	0.9477	0.11071908
706.30	640.00	168.123	0.9759	0.24093276
677.90	646.80	171.044	0.9863	0.42016417
672.80	650.40	173.718	0.9918	0.69333816
685.50	651.90	179.441	0.9941	0.93153632
684.40	654.00	184.292	0.9973	1.97152102
717.20	655.30	195.477	0.9992	6.70461702
721.20	655.70	207.741	0.9998	31.57103160
510.20	650.10	183.630	0.9913	0.62109768
490.00	628.40	166.872	0.9582	0.13743640
269.10	530.70	160.081	0.8092	0.02650034

344.50	477.30	158.303	0.7278	0.01689130
243.40	410.40	155.957	0.6258	0.01072330
199.70	350.60	153.551	0.5346	0.00748125
137.10	304.90	141.746	0.4649	0.00613005
63.10	264.60	121.170	0.4035	0.00558209
112.90	157.50	114.339	0.2402	0.00276437
1.50	115.60	111.064	0.1763	0.00192678
22.20	91.30	108.608	0.1392	0.00148917

How many points for the BET?

9

ASMPL= 418.07 Monolayer volume cc.,(STP)= 95.99

C= 7677.11 E1-EL= 1352.66

Linear Equation from Least Squares Approximation

$y = 1.0416E-02x + 1.3569E-06$

S= 0.7458 %

C. Program for the Prediction of Adsorption Isotherms

Because of the narrow pores of ZSM-5 zeolite the BET(A) equation can only predict the amount of nitrogen adsorbed on the zeolite at dimensionless pressures $p/p_0 < 0.1$. The BET(B) equation relieves the infinite pore diameter assumption used in the derivation of BET(A) equation. The BET(D) equation relieves the homogenous pore diameter assumption used in derivation of the BET(B) equation. Consequently a Fortran language program was written to predict the adsorption of nitrogen (or any other adsorptive) on a adsorbent whose pore properties are known or estimated. This program was used to find the right combination of pore properties which would permit an estimation of the adsorption of nitrogen on ZSM-5 zeolite. The derivation of the various BET equations are found in Appendix A.

Table G-4

Program Listing for BETD

Program Listing for BETD

C Program to predict nitrogen adsorption data based on a
C special form of the BET (D) equation (below). The BET(D)
C equation is found in the original paper by Brunauer, Emmett
C and Teller. That equation has been modified here to allow c
C to vary according to pore size. For pores larger than 10-20
C angstroms the heat of adsorption of adsorbate which appears
C in c is fairly constant. While for micropores (less than
C 10-20 angstroms) the apparent heat of adsorption is higher.
C Since this program was written mainly for estimating the
C adsorption isotherms of zeolites which are microporous the
C above modification of the BET (D) equation was necessary.
C For each adsorbent, vm, the monolayer volume, needs to be
C input.
C The adsorption isotherm for an adsorbent with as many as
C five different pore sizes can be estimated here. For each
C type of pore the heat of adsorption (E1-EL) needs to be
C input. In addition the fraction of the total surface area in
C those pores needs to be input. The size of each pore is input
C as n which is the number of monolayers of adsorbent which can
C be adsorbed in that pore. n can be any real number.
C The amount of adsorption adsorbate is calculated for p/po
C from zero to (1-0.2delx) where delx is the increment by which
C p/po is increased along the curve of vadsorbed vs. p/po. delx
C is also an input variable.
C The output data are the points of the adsorption curve,
C vadsorbed vs. p/po.
C Variables
C VM monolayer volume
C R ideal gas constant
C T temperature of adsorbent, is set equal to 76.1 K
C in this program. It can be changed for other
C adsorbents than nitrogen
C X dimensionless pressure, p/po
C VADS the volume of adsorbent adsorbed at a given
C dimensionless pressure x. VADS is in the same units
C as VM
C I do variable
C K number of different pore types in the adsorbent,
C must not exceed five
C
C Arrays
C C contains the BET equation 'c-values' for each pore
C type

C BET the β -values in the BET(D) equation, that is, the
 C fraction of the total adsorbent surface that is
 C contained in the pores of a certain type
 C N the number of monolayers that can be formed in a
 C pore of a certain size
 C E1 the heat of adsorption of the first monolayer of
 C adsorbate minus the heat of condensation of liquid
 C adsorbate for each pore size. The values in the
 C array C are calculated from this value. BETD allows
 C this value to be different for different pore
 C sizes. E1 is to be in cal./gmole.
 C
 C
 C

REAL VM,C(5),BET(5),N(5),E1(5),R,T,VADS,X
 INTEGER I,K

C

R= 1.9869
 T= 76.1

1 WRITE(6,20)
 20 FORMAT(2X, ' Input number of types of pores and Vm.')

READ(5,*)K, VM
 IF(K .GT. 5)THEN
 PRINT *, ' ERROR! K cannot be greater than 5.'
 GO TO 1
 ENDIF
 WRITE(6,2) K,VM
 2 FORMAT(2X,I2,2X,F7.2)

C

DO 3 I=1,K
 WRITE(6,21)I
 21 FORMAT(2X,/, ' Input BETA and N for pore type ',I1)
 READ(5,*)BET(I),N(I)
 WRITE(6,4)BET(I),N(I)
 4 FORMAT(2X,F5.3,2X,F6.2)
 3 CONTINUE

C

DO 5 I=1,K
 WRITE(6,22)I
 22 FORMAT(2X,/, ' Input E1-EL for pore type ',I1)
 READ(5,*)E1(I)
 WRITE(6,6)E1(I)
 6 FORMAT(2X,F5.0)
 C(I)= EXP(E1(I)/(R*T))
 5 CONTINUE

C

WRITE(6,23)

```

23  FORMAT(2X,/, ' Input delta p/po.')
    READ(5,*)DELX
    WRITE(6,24)DELX
24  FORMAT(2X,F7.3)
    WRITE(6,25)
25  FORMAT('1','-----',/,
# 2X,'p/po',6X,'Vads',/)
C
    X= 0.
9   VADS= 0.
    DO 10 I=1,K
        VADS= VADS + BET(I)*C(I)*X/(1.-X) *
#      ( 1. - (N(I)+1.)*(X**N(I)) +
#      N(I)*(X**(N(I)+1.)) )/
#      ( 1. + (C(I)-1.)*X - C(I)*(X**(N(I)+1.)) )
10  CONTINUE
    VADS= VM*VADS
    IF(X .EQ. 0.)THEN
        WRITE(6,13)X,VADS
13  FORMAT('+',1X,F6.4,',',F7.2,',')
    ELSE
        WRITE(6,12)X,VADS
12  FORMAT(2X,F6.4,',',F7.2,',')
    ENDIF
    X= X + DELX
    IF( (X .GE. 1.) .AND. (Z .NE. 1.) )THEN
        Z= 1.
        X= X - 0.2*DELX
    ENDIF
    IF(X .GE. 1)STOP
    GO TO 9
END

```

Table G-5

Sample Input for BETD

This table contains a sample input for the Fortran program BETD, which estimates the amount of adsorptive that is adsorbed on a material, where adsorption on that material can be described by the BET(D) equation.

The first line contains the number of different pore diameters in the adsorbent and the monolayer volume of adsorptive on the sample, in $\text{cm}^3(\text{STP})/\text{g}$. The next three data points contain the fraction of surface area contained in each pore type and the number of monolayers that can be formed in each type of pore. Specifying the number of monolayers that can be formed in each type of pore is equivalent to specifying the diameter of pore type.

The next three lines are the differential heats of adsorption of adsorptive in each pore type. The last line states the increments for which data points are to be calculated in terms of dimensionless pressure, p/p_0 .

3,100.
0.47,1.2
0.50,1.95
0.03,30.
1500.
900.
800.
0.02

Table G-6

Sample Output from BETD

This table contains the output generated by BETD. It is obvious what each term represents.

The volume adsorbed is in cm^3 (STP)/g of adsorbent.

Input number of types of pores and V_m .

3 100.00

Input BETA and N for pore type 1

0.470 1.20

Input BETA and N for pore type 2

0.500 1.95

Input BETA and N for pore type 3

0.030 30.00

Input E1-EL for pore type 1

1500.

Input E1-EL for pore type 2

900.

Input E1-EL for pore type 3

800.

Input delta p/po.

0.020

p/po	Vads
0.0000,	0.00,
0.0200,	94.99,
0.0400,	99.32,
0.0600,	101.64,
0.0800,	103.35,
0.1000,	104.78,
0.1200,	106.05,
0.1400,	107.22,
0.1600,	108.31,
0.1800,	109.33,
0.2000,	110.31,
0.2200,	111.25,
0.2400,	112.15,
0.2600,	113.02,
0.2800,	113.86,
0.3000,	114.69,
0.3200,	115.49,
0.3400,	116.27,
0.3600,	117.04,
0.3800,	117.80,
0.4000,	118.55,
0.4200,	119.29,
0.4400,	120.02,
0.4600,	120.75,
0.4800,	121.48,
0.5000,	122.22,
0.5200,	122.95,
0.5400,	123.70,
0.5600,	124.46,
0.5800,	125.23,
0.6000,	126.02,
0.6200,	126.84,
0.6400,	127.69,
0.6600,	128.58,
0.6800,	129.53,
0.7000,	130.53,
0.7200,	131.62,
0.7400,	132.80,
0.7600,	134.11,
0.7800,	135.56,
0.8000,	137.21,
0.8200,	139.08,
0.8400,	141.24,
0.8600,	143.74,
0.8800,	146.62,
0.9000,	149.92,

0.9200, 153.67,
0.9400, 157.83,
0.9600, 162.33,
0.9800, 167.05,
0.9960, 172.59,

APPENDIX II

DATA BASE MANAGEMENT SYSTEM FOR THE SURVEYED LITERATURE FROM THE HIGH DENSITY AVIATION FUEL PROJECT

The LITERATURE DATABASE FILES are created to match the needs of the research project for which the literature survey is to be compiled. Then, each pertinent literature citation/reference can be stored as a record in the relative data files by utilizing the DATA TRANSITION function. The data transition process includes three independent modes: record addition, record editing, and record deletion. The MAINTENANCE routine is performed after each batch of citations has been transmitted, to confirm that no duplicated entries exist and to insure that the format of the input record is correct. Any error found in the records should be corrected by the use of the DATA TRANSITION routine. The literature in the database files can be searched and retrieved by using the author's name, journal name, year, or index as a search parameter in the SEARCHING routine. Multiple parameter searching is also included.

The structures of the related database files and the programs for the database management are already created and stored on the disk. The performance of the data (record) transition routine is supported by the general dBASE III software commands. The performance of searching and maintenance is supported by the 'SM' program.

Start Procedure

- 1 > Insert the system disk in disk drive A.
- 2 > Turn on power.
- 3 > Type the date and time; wait for the A> prompt.
- 4 > Insert dBASE III disk in drive A.
- 5 > Type dBASE ↵ (↵ means hit the return key).
- 6 > Wait until . prompt appears (The . prompt means the computer is under control of the dBASE III system).

Major Commands

- 1 > USE: open file.
- 2 > LIST: list all the files on the screen.
- 3 > DISPLAY: list the file or parts of the files on the screen.
- 4 > BROWSE: list the file and each record in one line.
- 5 > COPY: duplicate the structure or file to other file.
- 6 > APPEND: add the record at the end of file.
- 7 > EDIT: correct the existing record.
- 8 > DELETE: temporarily delete the record.
- 9 > PACK: permanently delete the record.
- 10 > GOTO: point to the desired record.
- 11 > SKIP: point to the next record.
- 12 > DO: execute the program.
- 13 > QUIT: return to DOS.

EXAMPLE:

USE TT

. LIST

Record#	AUTHOR1	AUTHOR2	AUTHOR3	AUTHOR4
AUTHOR5	AUTHOR6	YEAR INDEX1	JOURNAL INDEX2	VOL INDEX3
	INDEX4	INDEX5	TITLE	
1	Hanson, F.V.	Bensen, J.E.	J. Catal.	31, 471
	73	Pump	Gas Circulation	
			An Inexpensive Noncontaminat	
	ing Gas Recirculation Pump			
2	Hanson, F.V.	Boudart, M.	J. Catal.	53, 56
	78	Pt	Hydrogen	Oxygen
			The Reaction Between Hydroge	
	n and Oxygen over Supported Platinum Catalysts			
3	Hanson, F.V.	Miller, J.D.	Oblad, A.G.	
	82	Tar Sand	U.S. Pat.	4,3337,14
			Process for Obtaining Produc	
	ts from Tar Sand			
4			J. Catal.	53, 56
	78			

Record#	AUTHOR1	AUTHOR2	AUTHOR3	AUTHOR4	AUTHOR5
---------	---------	---------	---------	---------	---------

ing Gas Recirculation Pump

n and Oxygen over Supported Platinum Catalysts

ts from Tar Sand

Record#	AUTHOR1	AUTHOR2	AUTHOR3	AUTHOR4	AUTHOR5
---------	---------	---------	---------	---------	---------

4

. BROWSE

Record No. 2 TT
AUTHOR1----- AUTHOR2----- AUTHOR3----- AUTHOR4-----
Hanson, F.V. Bensen, J.E.
Hanson, F.V. Boudart, M.
Hanson, F.V. Miller, J.D. Oblad, A.G.

Record No. 2 TT
AUTHOR5----- AUTHOR6----- JOURNAL-----
J. Catal.
J. Catal.
U.S. Pat.
J. Catal.

Record No. 2 TT
VOL----- YEAR INDEX1----- INDEX2-----
31, 471 73 Pump Gas Circulation
53, 56 78 Pt Hydrogen
4,3337,143 82 Tar Sand
53, 56 78

After the BROWSE command, each record appears on the screen at one line. The right-side fields of the records can be seen by hitting the Control → keys. Screen editing can be done in the BROWSE mode; hit Control-End when complete.

Function Keys

The function keys at the left side of the keyboard can execute the special functions. They can be redefined by using some commands. (For details, see the dBASE III manual).

The function keys are defined as follows:

Function key F1:	help
Function key F2:	assist
Function key F3:	list
Function key F4:	dir
Function key F5:	display structure
Function key F6:	display status
Function key F7:	display memory
Function key F8:	display
Function key F9:	append
Function key F10:	edit

Data File Structure

The data file structures of the following are used for the surveyed literatures.

TT.DBF: database files of the surveyed literatures for practice purpose.

Structure for database : C:TT.dbf
Number of data records : 4
Date of last update : 01/01/80

Field	Field name	Type	Width	Dec
1	AUTHOR1	Character	15	
2	AUTHOR2	Character	15	
3	AUTHOR3	Character	15	
4	AUTHOR4	Character	15	
5	AUTHOR5	Character	25	
6	AUTHOR6	Character	25	
7	JOURNAL	Character	25	
8	VOL	Character	30	
9	YEAR	Character	2	
10	INDEX1	Character		20
11	INDEX2	Character		20
12	INDEX3	Character		20
13	INDEX4	Character		20
14	INDEX5	Character		20
15	TITLE	Character	120	
** Total **			388	

STDJOUR.DBF: database file for the standard journal name.

Structure for database : C:STDJOUR.dbf
Number of data records : 3
Date of last update : 01/01/80

Field	Field name	Type	Width	Dec
1	VJOUR	Character		25
** Total **			26	

Create Data File Structure

- 1 > Use the CREATE command to create the desired file. (For details, see the dBASE III manual.)
- 2 > Use the COPY command to create the file structure from the existing files.

Example:

XXX.DBF: existing file

YYY.DBF: created file

```
.USE XXX  ┘
```

```
.COPY STRUCTURE TO YYY.DBF  ┘
```

Then, YYY.DBF has the same structure as the XXX.DBF.

or

```
.USE XXX  ┘
```

```
.COPY TO YYY.DBF  ┘
```

Then YYY.DBF has the same structure and the same data as the XXX.DBF.

Data Transition

Make sure the database file is in 'USE' before data transition.

1 > Add Record:

APPEND

Record No.	5
AUTHOR1	
AUTHOR2	
AUTHOR3	
AUTHOR4	
AUTHOR5	
AUTHOR6	
JOURNAL	
VOL	
YEAR	
INDEX1	
INDEX2	
INDEX3	
INDEX4	
INDEX5	
TITLE	

The record appended at the current file appears on the screen. Input the data and hit Control-End when complete.

2 > Edit Record:

. EDIT 1

Record No.	1
AUTHOR1	Hanson, F. V.
AUTHOR2	Bensen, J. E.
AUTHOR3	
AUTHOR4	
AUTHOR5	
AUTHOR6	
JOURNAL	J. Catal.
VOL	31, 471
YEAR	73
INDEX1	Pump
INDEX2	Gas Circulation
INDEX3	
INDEX4	
INDEX5	
TITLE	An Inexpensive Noncontaminating Gas Recirculation Pump

The edited record appears on the screen. Correct the errors and hit Control-End when complete.

Screen editing can also be done if several records having errors are found. For details, see the example of the BROWSE command in the "Major Commands" section.

3 > Deleted Record:

Use the following commands:

GOTO n ┘

DELETE ┘

The record of record number 'n' is temporarily deleted from the file. The deleted record can be recalled. (For details, see the dBASE III manual.)

Use the commands

GOTO n ┘

DELETE ┘

PACK ┘

The record of record number 'n' is permanently deleted from the file.

You can use either the 'LIST' or the 'DISPLAY ALL' command to list the current file in order to confirm that the record has been deleted.

Data Searching and Maintenance

The searching and maintenance functions are executed with the 'SM' program as explained in the following figures.

An example performance of the 'SM' program is listed as follows.

```
*****
*
*   THIS IS A SEARCHING AND MAINTENANCE PROGRAM FOR THE   *
*LITERATURE SURVEY, FINISHED UNDER THE AIR FORCE PROJECT. *
*   Contract No. F33615-85-C-2567                         *
*
*   AUTHOR, JOURNAL NAME, YEAR, AND INDEX CAN BE USED AS  *
*   THE SEARCHING PARAMETERS; THE COMBINED SEARCHING ALSO *
*   CAN BE SELECTED.                                       *
*
*   THIS PROGRAM IS USED UNDER THE DBASE III SOFTWARE.    *
*
*   THE PROGRAM IS WRITTEN BY KIEN-RU CHEN                 *
*   NOVEMBER, 1985                                          *
*   FUELS ENGINEERING DEPT.                                *
*   UNIVERSITY OF UTAH                                     *
*
*****
```

Press any key to continue.

INPUT THE FILE NAME INCLUDING THE EXTENSION(.DBF) TT.DBF

```
***** MAIN MENU *****
*
* 1> AUTHOR          4> INDEX          *
* 2> JOURNAL        5> MULTIPLE       *
* 3> YEAR           6> MAINTENANCE    *
*
*                  type Q to quit    *
*
*****
```

INPUT THE SELECTION:


```

***** MAIN MENU *****
*
* 1> AUTHOR          4> INDEX          *
* 2> JOURNAL         5> MULTIPLE       *
* 3> YEAR            6> MAINTENANCE    *
*
*           type Q to quit             *
*
*****

```

INPUT THE SELECTION: 2

INPUT THE JOURNAL NAME: J. Catal.

SEARCHING PARAMETER: J. Catal.

Record#	AUTHOR1	AUTHOR2	AUTHOR3	AUTHOR4	AUTHOR5
	AUTHOR6	YEAR	INDEX1	JOURNAL	VOL
	INDEX4	INDEX5	INDEX2	TITLE	INDEX3
1	Hanson, F.V.	Bensen, J.E.		J. Catal.	31, 471
		73 Pump		Gas Circulation	
				An Inexpensive Noncontaminat	
	ing Gas Recirculation Pump				
2	Hanson, F.V.	Boudart, M.		J. Catal.	53, 56
		78 Pt		Hydrogen	Oxygen
				The Reaction Between Hydroge	
	n and Oxygen over Supported Platinum Catalysts				
3				J. Catal.	53, 56
		78			

JOURNAL NAME SEARCHING COMPLETE !

Press any key to continue...

```

***** MAIN MENU *****
*
* 1> AUTHOR          4> INDEX          *
* 2> JOURNAL        5> MULTIPLE        *
* 3> YEAR           6> MAINTENANCE      *
*
*           type Q to quit             *
*
*****

```

INPUT THE SELECTION: 3

```

***** YEAR SEARCHING MENU *****

```

```

1> EQUAL THE INPUT YEAR
2> BEFORE THE INPUT YEAR (INCLUDING THE YEAR)
3> AFTER THE INPUT YEAR (INCLUDING THE YEAR)

```

INPUT THE SELECTION: 1

INPUT THE YEAR: 78

TYPE SELECTION (1 =, 2 <=, 3 >=): 1
 SEARCHING PARAMETER: 78

Record#	AUTHOR1	AUTHOR2	AUTHOR3	AUTHOR4	AUTHOR5
	AUTHOR6	YEAR	JOURNAL		VOL
	INDEX4	INDEX1	INDEX2		INDEX3
		INDEX5	TITLE		
1	Hanson, F.V.	Boudart, M.	J. Catal. Hydrogen		53, 56 Oxygen
	78	Pt	The Reaction Between Hydroge		
n and Oxygen over Supported Platinum Catalysts					
2			J. Catal.		53, 56
	78				

YEAR SEARCHING COMPLETE !

Press any key to continue...

```

***** MAIN MENU *****
*
* 1> AUTHOR          4> INDEX          *
* 2> JOURNAL        5> MULTIPLE        *
* 3> YEAR           6> MAINTENANCE     *
*
*                  type Q to quit      *
*
*****

```

INPUT THE SELECTION: 4

INPUT THE INDEX NAME: Tar Sand

SEARCHING PARAMETER: Tar Sand

Record#	AUTHOR1	AUTHOR2	AUTHOR3	AUTHOR4	AUTHOR5
	INDEX4	YEAR INDEX1	JOURNAL		VOL
		INDEX5	INDEX2		INDEX3
			TITLE		
1	Hanson, F.V.	Miller, J.D.	Oblad, A.G.		
			U.S. Pat.		4,3337,14
3		82 Tar Sand			
					Process for Obtaining Produc
					ts from Tar Sand

INDEX SEARCHING COMPLETE !

Press any key to continue...

```

***** MAIN MENU *****
*
* 1> AUTHOR          4> INDEX          *
* 2> JOURNAL        5> MULTIPLE       *
* 3> YEAR           6> MAINTENANCE    *
*
*           type Q to quit           *
*
*****

```

INPUT THE SELECTION: 5

```

***** MULTIPLE SEARCHING MENU *****

```

```

1> AUTHOR          4> INDEX
2> JOURNAL        5> RETURN TO MAIN MENU
3> YEAR

```

INPUT THE SELECTION

***** MULTIPLE SEARCHING MENU *****

- | | |
|------------|------------------------|
| 1> AUTHOR | 4> INDEX |
| 2> JOURNAL | 5> RETURN TO MAIN MENU |
| 3> YEAR | |

INPUT THE SELECTION 1

INPUT THE AUTHOR NAME: Hanson, F.V.

SEARCHING PARAMETER: Hanson, F.V.

Record#	AUTHOR1	AUTHOR2	AUTHOR3	AUTHOR4	AUTHOR5
	AUTHOR6	YEAR	INDEX1	INDEX2	VOL
	INDEX4		INDEX5	TITLE	INDEX3
1	Hanson, F.V.	Bensen, J.E.		J. Catal.	31, 471
		73 Pump		Gas Circulation	
				An Inexpensive Noncontaminat	
	ing Gas Recirculation Pump				
2	Hanson, F.V.	Boudart, M.		J. Catal.	53, 56
		78 Pt		Hydrogen	Oxygen
				The Reaction Between Hydroge	
	n and Oxygen over Supported Platinum Catalysts				
3	Hanson, F.V.	Miller, J.D.	Oblad, A.G.		
			U.S. Pat.		4,3337,14
3		82 Tar Sand			
				Process for Obtaining Produc	
	ts from Tar Sand				

AUTHOR SEARCHING COMPLETE !

Press any key to continue...

***** MULTIPLE SEARCHING MENU *****

1> AUTHOR 4> INDEX
 2> JOURNAL 5> RETURN TO MAIN MENU
 3> YEAR

INPUT THE SELECTION 4

INPUT THE INDEX NAME: Tar Sand

SEARCHING PARAMETER: Tar Sand

Record#	AUTHOR1	AUTHOR2	AUTHOR3	AUTHOR4	AUTHOR5
	AUTHOR6	JOURNAL			VOL
	YEAR	INDEX1	INDEX2		INDEX3
	INDEX4	INDEX5	TITLE		
1	Hanson, F.V.	Miller, J.D.	Oblad, A.G.		
			U.S. Pat.		4,3337,14
3		82 Tar Sand			
					Process for Obtaining Produc
					to from Tar Sand

INDEX SEARCHING COMPLETE !

Press any key to continue...

```
***** MAIN MENU *****
*
* 1> AUTHOR          4> INDEX          *
* 2> JOURNAL        5> MULTIPLE       *
* 3> YEAR           6> MAINTENANCE    *
*
*           type Q to quit          *
*
*****
```

INPUT THE SELECTION: 6

```
***** MAINTENANCE MENU *****
```

```
1> DUPLICATE CHECK
2> VERIFY
3> RETURN TO MAIN MENU
```

INPUT THE SELECTION

***** MAINTENANCE MENU *****

- 1> DUPLICATE CHECK
- 2> VERIFY
- 3> RETURN TO MAIN MENU

INPUT THE SELECTION : 1

THE FOLLOWING TWO RECORDS ARE DUPLICATED

RECORD NO. = 4
RECORD NO. = 2

Record#	AUTHOR1	AUTHOR2	AUTHOR3	AUTHOR4	AUTHOR5
	AUTHOR6	JOURNAL			VOL
	YEAR INDEX1	INDEX2			INDEX3
	INDEX4	INDEX5	TITLE		
3			J. Catal.		53, 56
	78				

DUPLICATE CHECKING COMPLETE !

Press any key to continue...

***** MAINTENANCE MENU *****

- 1> DUPLICATE CHECK
- 2> VERIFY
- 3> RETURN TO MAIN MENU

INPUT THE SELECTION : 2

JOURNAL NAME OF THE FOLLOWING RECORD NOT IN THE STANDARD STYLE

RECORD NO. = 3
JOURNAL NAME = U.S. Pat.

VERIFY COMPLETE !

Press any key to continue...

***** MAINTENANCE MENU *****

- 1> DUPLICATE CHECK
- 2> VERIFY
- 3> RETURN TO MAIN MENU

INPUT THE SELECTION : 2

***** VERIFY MENU *****

- 1> CONTINUE VERIFY
- 2> DISCRETE VERIFY
- 3> RETURN TO MAINTENANCE MENU

INPUT THE SELECTION: 1

INPUT THE RECORD NUMBER: 1

JOURNAL NAME OF THE FOLLOWING RECORD NOT IN THE STANDARD STYLE

RECORD NO. = 3
JOURNAL NAME = U.S. Pat.

VERIFY COMPLETE !

Press any key to continue...

Printout Procedure

The hard copies from the printer can be obtained by two methods.

- 1 > hit Ctrl P
The printout can be obtained from the latter data appeared on the screen.
Hit Ctrl P to cancel the hard copies.
- 2 > hit Shift PrtSc
The printout will be the same as the data on the screen.

Stop Procedure

- 1 > .QUIT ↵, return to the DOS A > prompt.
- 2 > Insert the DATABASE FILE BACKUP disk into drive A.
- 3 > A > COPY C:*.DBF A: ↵
- 4 > Take the disk from drive A, and keep the disk inside the disk bank.
- 5 > Turn off power.

```

clear
set Talk off
store ' ' to nul
store 'T' to MORE
store ' ' to LI
CLEAR
@3,9 say '*****'
@4,9 say '* THIS IS A SEARCHING AND MAINTENANCE PROGRAM FOR THE *'
@5,9 SAY '* LITERATURE SURVEY, FINISHED UNDER THE AIR FORCE PROJECT. *'
@6,9 SAY '* Contract No. F33615-85-C-25867 *'
@7,9 say '* *'
@8,9 SAY '* AUTHOR, JOURNAL NAME, YEAR, AND INDEX CAN BE USED AS *'
@9,9 SAY '* THE SEARCHING PARAMETERS; THE COMBINED SEARCHING ALSO *'
@10,9 SAY '* CAN BE SELECTED. *'
@11,9 SAY '* *'
@12,9 SAY '* THE PROGRAM IS USED UNDER THE DBASE III SOFTWARE. *'
@13,9 SAY '* *'
@14,9 SAY '* THE PROGRAM IS WRITTEN BY KIEN-RU CHEN *'
@15,9 SAY '* NOVEMBER, 1985 *'
@16,9 SAY '* FUELS ENGINEERING DEPT. *'
@17,9 SAY '* UNIVERSITY OF UTAH *'
@18,9 SAY '******'
@23,5 SAY 'Press any key to continue' get nul
CLEAR
@ 9,3 SAY 'INPUT THE FILE NAME INCLUDING THE EXTENSION(.DBF)' GET LI
READ
Do while MORE = 'T'
clear
@4,16 SAY '***** MAIN MENU *****'
@5,16 SAY '* *'
@6,16 SAY '* 1> AUTHOR 4> INDEX *'
@7,16 SAY '* 2> JOURNAL 5> MULTIPLE *'
@8,16 SAY '* 3> YEAR 6> MAINTENANCE *'
@9,16 SAY '* *'
@10,16 SAY '* type Q to quit *'
@11,16 SAY '******'
store ' ' to CHOICE
@13,18 SAY 'INPUT THE SELECTION: ' GET CHOICE
READ
store ' ' TO AUTHOR
store ' ' TO JOUR
store ' ' TO IX
SET DELETE ON
Do case
case CHOICE = '1'
DO AR
case CHOICE = '2'
DO JR
case CHOICE = '3'
DO YR
CASE CHOICE = '4'

```

```
DO IN
CASE CHOICE = '5'
DO ML
CASE CHOICE = '6'
DO MN
case UPPER(CHOICE) = 'Q'
MORE = 'F'
ENDCASE CHOICE
USE $LI
SET DELETE OFF
RECALL ALL
ENDDO SEARCH
```

```

*THIS IS A SUB PROGRAM FOR AUTHOR SEARCHING
@15,18 SAY 'INPUT THE AUTHOR NAME: ' GET AUTHOR
READ
USE $LI
GOTO TOP
DO WHILE .NOT. EOF()
  IF ((AUTHOR = AUTHOR1) .OR. (AUTHOR = AUTHOR2)) . OR. AUTHOR = AUTHOR3
    SKIP
  ELSE
    IF ((AUTHOR=AUTHOR4) .OR. (AUTHOR = AUTHOR5)) . OR. AUTHOR = AUTHOR6
      SKIP
    ELSE
      DELETE
      SKIP
    ENDIF
  ENDIF
ENDDO
?
? '      SEARCHING PARAMETER: ', AUTHOR
?
?
COPY TO TP.DBF
USE TP
DISPLAY ALL
CLOSE DATABASE
ERASE TP.DBF
?
?
?
? 'AUTHOR SEARCHING COMPLETE !'
?
WAIT
RETURN
C>

```

```

*THIS IS A SUB PROGRAM FOR YEAR SEARCHING
clear
@5,10 say '***** YEAR SEARCHING MENU *****'
@7,10 SAY '      1> EQUAL THE INPUT YEAR'
@8,10 SAY '      2> BEFORE THE INPUT YEAR (INCLUDING THE YEAR)'
@9,10 SAY '      3> AFTER THE INPUT YEAR (INCLUDING THE YEAR)'
STORE ' ' TO YRSELECT
@ 12,12 SAY 'INPUT THE SELECTION: ' GET YRSELECT
Store ' ' to YRINPUT
@ 14,12 SAY 'INPUT THE YEAR: ' GET YRINPUT
READ
USE $LI
GOTO TOP
do case
  case YRSELECT = '1'
    DO WHILE .NOT. EOF()
      IF YRINPUT = YEAR
        SKIP
      ELSE
        DELETE
        SKIP
      ENDIF
    ENDOO
  CASE YRSELECT = '2'
    DO WHILE .NOT. EOF()
      IF YEAR >= YRINPUT
        SKIP
      ELSE
        DELETE
        SKIP
      ENDIF
    ENDDO
ENDCASE YRSELECT
?
?' TYPE SELECTION (1=, 2 <=, 3 >=): ', YRSELECT
?' YEAR SEARCHING PARAMETER: ', YRINPUT
?
?
copy to tp.dbf
use tp
DISPLAY ALL
CLOSE DATABASE
erase tp.dbf
?
?
?
? 'YEAR SEARCHING COMPLETE !'
?
WAIT
RETURN

```



```

*THIS IS A SUB PROGRAM FOR JOURNAL SEARCHING
@ 15,10 ^^^ 'INPUT THE JOURNAL NAME: ' GET JOUR
READ
USF -1
GO TO TOP
DO WHILE .NOT. EOF()
    IF JOUR = JOURNAL
        SKIP
    ELSE
        DELETE
        SKIP
    ENDIF
ENDDO
?
?'    SEARCHING PARAMETER: ', JOUR
?
?
copy to tp.dbf
use tp
DISPLAY ALL
CLOSE DATABASE
erase tp.dbf
?
?
?
? 'JOURNAL NAME SEARCHING COMPLETE !'
?
WAIT
RETURN

C>

```

```

*THIS IS A SUB PROGRAM FOR INDEX SEARCHING
@ 15,10 SAY 'INPUT THE INDEX NAME: ' GET IX
READ
USE $LI
GOTO TOP
DO WHILE .NOT. EOF()
    IF IX = INDEX1 .OR. IX = INDEX2 .OR. IX = INDEX3
        SKIP
    ELSE
        DELETE
        SKIP
    ENDIF
ENDDO
?
?'  SEARCHING PARAMETER: ', IX
?
?
copy to tp.dbf
use tp
DISPLAY ALL
CLOSE DATABASE
erase tp.dbf
?
?
?
? 'INDEX SEARCHING COMPLETE !'
?
WAIT
RETURN

C>

```

```

* THIS IS A MULTIPLE SEARCHING PROGRAM
STORE 'T' TO KEYING
STORE ' ' TO CBSEL
DO WHILE KEYING = 'T'
CLEAR
@4,18 SAY '***** MULTIPLE SEARCHING MENU *****'
@6,18 SAY ' 1> AUTHOR          4> INDEX'
@7,18 SAY ' 2> JOURNAL          5> RETURN TO MAIN MENU'
@8,18 SAY ' 3> YEAR'
@10,20 SAY '      INPUT THE SELECTION ' GET CBSEL
READ
DO CASE
CASE CBSEL = '1'
DO AR
CASE CBSEL = '2'
DO JR
CASE CBSEL = '3'
DO YR
CASE CBSEL = '4'
DO IN
CASE CBSEL = '5'
KEYING = 'F'
ENDCASE
ENDDO
RETURN

```

C>

```

*THIS IS A MAINTENANCE PROGRAM
*set up loop
SET TALK OFF
STORE 'T' To Morel
STORE ' ' TO Selectm
DO WHILE Morel = 'T'
  *set up screen
  clear
  @ 5,17 SAY  '***** MAINTENANCE MENU *****'
  @ 7,20 SAY  '  1> DUPLICATE CHECK'
  @ 8,20 SAY  '  2> VERIFY'
  @ 9,20 SAY  '  3> RETURN TO MAIN MENU'
  @ 11,18 SAY '    INPUT NUMBER TO SELECTION : ' GET Selectm
  READ
  *perform desired function
  do case
    case Selectm = '1'
      *check for duplicate
      do du
        case selectm = '2'
          *verify new records
          do vr
            case selectm = '3'
              *setup the loop to exit
              store 'F' to Morel
            endcase
          enddo
        RETURN
      enddo
    endcase
  enddo
  RETURN

```

C>

```

* THIS IS A DUPLICATE CHECKING PROGRAM
store '
store '
store ' ' to CYEAR
store 1 to CC
USE $1i
GOTO BOTTOM
STORE RECNO() TO ALPHA
GOTO CC
DO WHILE .NOT. EOF()
    CVOL = VOL
    CJOUR = JOURNAL
    CYEAR = YEAR
    SKIP
    DO WHILE .NOT. EOF()
        IF ((CVOL = VOL) .AND. (CYEAR = YEAR)) .AND. (CJOUR = JOURNAL)
            ?
            ? 'THE FOLLOWING TWO RECORDS ARE DUPLICATED'
            ?
            ? 'RECORD NO. = ', RECNO()
            ? 'RECORD NO. = ', CC
            ?
            DISPLAY
            SKIP
        ELSE
            SKIP
        ENDIF
    ENDDO
    IF CC < ALPHA
        CC = CC + 1
        GOTO CC
    ELSE
        ENDIF
    ENDDO
    ?
    ?
    ?
    ? ' DUPLICATE CHECKING COMPLETE !'
    ?
    WAIT
    RETURN

C>

```

```

*THIS IS A VERIFY PROGRAM
CLEAR
@6,18 SAY '***** VERIFY MENU *****'
@8,18 SAY ' 1> CONTINUE VERIFY'
@9,18 SAY ' 2> DISCRETE VERIFY'
@10,18 SAY ' 3> RETURN TO MAINTENANCE MENU'
STORE ' ' TO VERCHOI
@ 12,18 SAY 'INPUT THE SELECTION: ' GET VERCHOI
STORE ' ' TO PN
@ 14,18 SAY 'INPUT THE RECORD NUMBER: ' GET PN
READ
STORE 1 TO PT
PT = VAL(PN)
STORE ' ' TO JOURN
STORE 0 TO ALPHA
DO CASE
CASE VERCHOI = '1'
USE $LI
GOTO BOTTOM
STORE RECNO() TO ALPHA
GOTO PT
DO WHILE .NOT. EOF()
JOURN = JOURNAL
STORE 0 TO CC
SELECT 2
USE STDJOUR
GOTO TOP
DO WHILE .NOT. EOF()
IF (VJOUR = JOURN)
CC = CC+1
SKIP
ELSE
SKIP
ENDIF
ENDDO
IF CC = 0
?
? 'JOURNAL NAME OF THE FOLLOWING RECORD NOT IN THE STANDARD STYLE'
?
? 'RECORD NO. = ', PT
? 'JOURNAL NAME = ', JOURN
ENDIF
IF PT < ALPHA
PT = PT + 1
SELECT 1
GOTO PT
ELSE
SELECT 1
SKIP
ENDIF
ENDDO

```

```

CASE VERCHOI = '2'
  SELECT 1
  USE $LI
  GOTO PT
    JOURN = JOURNAL
    STORE 0 TO CC
    SELECT 2
    USE STDJOUR
    GOTO TOP
    DO WHILE .NOT. EOF()
      IF (VJOUR = JOURN)
        CC = CC+1
        SKIP
      ELSE
        SKIP
      ENDIF
    ENDDO
    IF CC = 0
      ?
      ? 'DISCRETE VERIFY'
      ? 'JOURNAL NAME OF THE FOLLOWING RECORD NOT IN THE STANDARD STYLE'
      ?
      ? 'RECORD NO. = ', PT
      ? 'JOURNAL NAME = ', JOURN
    ENDIF
    SELECT 1
  ENDCASE
?
?
?
? 'VERIFY COMPLETE !'
?
WAIT
RETURN
C>

```